10-23-2017 10:00 AM

# Bi-directional Cyclic Behaviour and Liquefaction Analysis of a silica-carbonate sand

Keyvan Mirbaha
*The University of Western Ontario*

Supervisor
Professor Abouzar Sadrekarimi
*The University of Western Ontario*

Graduate Program in Civil and Environmental Engineering
A thesis submitted in partial fulfillment of the requirements for the degree in Master of Engineering Science

# Abstract

The cyclic behavior and liquefaction behavior of reconstituted samples of a local silica-carbonate sand are examined by performing monotonic and cyclic simple shear tests in addition to bender element shear wave velocity measurements. Shear wave velocity was found to vary with effective overburden stresses by an average power of 0.25. Maximum shear modulus ($G_{max}$) was also computed from the shear wave velocity measurements and a correlation was developed between $G_{max}$, effective stress and void ratio. Small strain and cyclic strain dependent shear modulus of the soil were determined, and shear modulus reduction curves were obtained. The results show a slower degrading stiffness and damping ratio, compared to an average proposed for sands. A critical state line of the samples was developed by performing drained and constant-volume monotonic simple shear tests.

Cyclic resistance, shear wave velocity and rigidity factors of the sand samples were evaluated with the critical state approach. Circular, elliptical (oval) and figure-8 bi-directional cyclic load patterns were applied, in addition to mono-directional shearing modes and cyclic response of loose (25% relative density), medium dense (45% relative density), and dense samples (65% relative density) were investigated. Wide ranges of the generated excess pore water pressure ratio ($r_u$) were observed. Changing patterns of $r_u$ values were assessed based on the cyclic shear strength of multiple tests and number of cycles prior to liquefaction. Also, the test results showed up to 35% reduction in cyclic resistance of bi-directionally loaded samples relative to mono-directionally loaded ones, which is the least for an elliptical cyclic pattern and the most for a circular cyclic pattern. Bi-directional cyclic results are found to be dependent on the loading pattern, and confining stress, and under-estimated by currently proposed coefficients.

Critical state analysis was used for evaluating the cyclic resistance of the samples under different cyclic load patterns and the results were correlated to shear wave velocity parameter of samples. In addition, liquefaction susceptibility of the samples was evaluated and compared to previous research studies based on bi-directional cyclic tests, which suggests that current procedures may overestimate cyclic resistance of the soils based on shear wave velocity measurements.

Moreover, the behaviour of samples was investigated for multiple liquefaction occurrences by applying a second cyclic load to specimens after the occurrence of a first liquefaction. Densification of samples due to repeated cyclic load application was observed and evaluated. The cyclic resistance of samples was assessed in consecutive liquefaction events. Results show a general decreasing resistance for loose samples which is more significant for mono-directional load patterns rather than bi-directional patterns. The resistance changes of medium dense samples from first to a second liquefaction is negligible and almost consistent for all load patterns. For dense samples, there is a distinction in the behaviour of samples under mono-directional shear patterns and bi-directional patterns. Although the majority of samples get more resistant to a second liquefaction under mono-directional loads, more complicated behavior was observed for dense samples as well as medium dense samples in large consolidation stresses under bi-directional cyclic loads. It was found that when applied shear loads get larger, the resistance of the samples decreases (becomes more liquefiable); inversely, when shear loads get smaller, the behavior changes to an increasing resistance and less liquefiable response. Pore water pressure generation of the samples was also studied. The results showed the quicker development of pore water pressures during first cyclic loading compared to the second cyclic loading stage for almost entire cyclic load patterns regardless of soil initial relative density. However, pore water pressure generation was found to be dependant on initial consolidation stresses.

# Keywords

Direct simple shear test; soil liquefaction; re-liquefaction; earthquake; cyclic resistance; silica-carbonate sand; critical state; shear wave velocity; shear modulus; bi-directional cyclic load.

# Co-authorship statement

This thesis has been prepared in accordance with the regulations for an Integrated-Article format thesis stipulated by the School of Graduate and Postdoctoral Studies at the University of Western Ontario and has been co-authored as:

**Chapter 2: Characterization of a Silica-Carbonate Sand Based on Shear Wave Velocity Measurement and Cyclic Simple Shear Tests**

All experimental work was completed by Keyvan Mirbaha under the close supervision of Dr. Abouzar Sadrekarimi. A paper co-authored by Keyvan Mirbaha and Abouzar Sadrekarimi has been submitted to 3rd International Conference on Performance-Based Design in Earthquake Geotechnical Engineering (PBD III), Vancouver, 2017.

**Chapter 3: Cyclic Behavior and Liquefaction Analysis of a Silica-Carbonate Sand Based on Bi-directional Cyclic Simple Shear Tests**

All experimental work was completed by Keyvan Mirbaha under the close supervision of Dr. Abouzar Sadrekarimi. A paper co-authored by Keyvan Mirbaha and Abouzar Sadrekarimi will be submitted to the Soil Dynamics and Earthquake Engineering Journal.

**Chapter 4: Evaluating the Liquefaction and Re-liquefaction behavior of a Silica-Carbonate Sand**

All experimental work was completed by Keyvan Mirbaha under the close supervision of Dr. Abouzar Sadrekarimi. The abstract of this paper has been submitted to GeoOttawa conference 2017 and a paper co-authored by Keyvan Mirbaha and Abouzar Sadrekarimi will be submitted to the Canadian Geotechnical Journal.

# Acknowledgments

I want to deliver my most sincere appreciations to my supervisor Dr. Abouzar Sadrekarimi who advised and supported me consistently in reaching our research objectives and helped me to learn a lot in the field of our research.

I would also like to thank my wife and daughter who encouraged me and supported me in my research path and my father and mother who always gave me strength by giving their words and wishes.

Many gratitude's to technical and laboratory staff who facilitated testing procedures. Special thanks to Melodie Richards, Erol Tas, and Osama Abuhajar and my best wishes for my friends and colleagues for helping me by their words or by their works.

# Table of Contents

Abstract ..... i

Keywords ..... iii

Co-authorship statement ..... iv

Acknowledgments ..... v

List of tables ..... x

List of Appendices ..... xvi

List of nomenclatures ..... xvii

1. Introduction ..... 1

1.1. Problem overview ..... 1

1.2. Purpose of research and thesis outline ..... 3

2. Characterization of a silica-carbonate sand based on shear wave velocity measurement ..... 6

2.1. Introduction ..... 6

2.2. Experimental plan ..... 11

2.2.1. Tested material ..... 11

2.2.2. Specimen preparation ..... 13

2.2.3. Consolidation ..... 17

2.2.4. Monotonic simple shear tests ..... 17

2.2.5. Critical state approach ..... 20

2.2.6. Cyclic DSS tests ..... 22

2.2.7. Shear wave velocity measurement ..... 24

2.3. Test results ..... 26

2.3.1. Monotonic drained and constant-volume simple shear tests ..... 26

2.3.2. Critical state line location ..... 29

2.3.3. Shear wave velocity measurement ..... 30

2.3.4. Evaluation of maximum shear modulus ($G_{max}$) ..... 36

2.3.5. Mono-directional cyclic simple shear test results ..... 38

2.3.6. Evaluation of large strain modulus (G) and degradation curves for Boler sand ..... 41

2.3.7. Particle crushing verification ..... 45

2.4. Conclusions ..... 46

2.5. References ..... 47

3. Cyclic behavior and liquefaction analysis of a silica-carbonate sand based on bi-directional cyclic simple shear tests ..... 52

3.1. Introduction ..... 52

3.2. Experimental plan ..... 54

3.2.1. Soil characteristics and specimen preparation ..... 54

3.2.2. Testing apparatus ..... 55

3.2.3. Testing plan and parameter definitions ..... 56

3.3. Test results ..... 62

3.3.1. Introducing resultant shear strain and cyclic stress ratio ..... 62

3.3.2. Mechanism of strength reduction under cyclic loads ..... 65

3.4. Analysis of results ..... 67

3.4.1. Cyclic shear resistance characterization ..... 67

3.4.2. Bi-directional to mono-directional load adjustment ratio....83
3.4.3. Pore water pressure generation....90
3.4.4. Critical state analysis approach to cyclic behavior....92
3.4.5. Evaluating CRR variation based on $V_S$ measurements....93
3.4.6. Liquefaction susceptibility analysis....95
3.5. Conclusions....102
3.6. References....103
4. Evaluating the liquefaction and re-liquefaction behavior of a silica-carbonate sand 110
4.1. Introduction....110
4.2. Experimental plan....112
4.2.1. Tested material....112
4.2.2. Specimen preparation....112
4.2.3. Cyclic DSS tests....113
4.3. Test results....115
4.3.1. Critical state line approach....115
4.3.2. First stage of cyclic loading (liquefaction)....115
4.3.3. Second stage of cyclic loading (re-liquefaction)....115
4.4. Analysis of results....124
4.4.1. Densification effect of pre-shearing....124
4.4.2. Effect of relative density and consolidation stress on a re-liquefaction event....126
4.4.3. Pore water pressure generation pattern....133

4.4.4. Cyclic resistance variation due to re-liquefaction ..... 136

4.5. Conclusions ..... 140

4.6. References ..... 141

5. Summary and conclusions ..... 145

Appendices ..... 148

# List of tables

Table 2.1: $G_{max}$ correlations of cohesionless Soils (Sawangsuriya, 2012).....10

Table 2.2: HCL dissolution test results of Boler sand for determining carbonate content.....13

Table 2.3: Uniformity check for two dense samples.....14

Table 2.4: Summary of monotonic drained simple shear tests of Boler sand.....19

Table 2.5: Summary of monotonic constant-volume simple shear tests of Boler sand.....20

Table 2.6: Summary of mono-directional cyclic simple shear tests.....24

Table 2.7: Summary of characteristics for shear wave velocity measurement tests.....25

Table 2.8: Summary of selected monotonic DSS tests (for CSL establishment).....29

Table 3.1: Summary of cyclic tests for loose samples .....60

Table 3.2: Summary of cyclic tests for medium dense samples.....60

Table 3.3: Summary of cyclic tests for dense samples .....61

Table 3.4: CSR regression parameters for power function of $CSR = \alpha.NC^{-\beta}$ used for calculation of CRR (CSR at 15 number of cycles) for loose ($D_{rc}$ = 25%) samples .....78

Table 3.5: CSR regression parameters for power function of $CSR = \alpha.NC^{-\beta}$ used for calculation of CRR (CSR at 15 number of cycles) for medium dense ($D_{rc}$ = 45%) samples .79

Table 3.6: CSR regression parameters for power function of $CSR = \alpha.NC^{-\beta}$ used for calculation of CRR (CSR at 15 number of cycles) for dense ($D_{rc}$ = 65%) samples.....80

Table 3.7: Summary of factors for shear wave velocity and CRR correlation.....95

Table 4.1: Summary of cyclic DSS tests for both stages of liquefaction.....114

Table 4.2: Results for liquefaction / re-liquefaction at $D_{rc}$ = 25% / mono-directional .....118

Table 4.3: Results for liquefaction / re-liquefaction at $D_{rc}$ = 25% / bi-dir. (circular).....118

Table 4.4: Results for liquefaction / re-liquefaction at $D_{rc}$ = 25% / bi-dir. (elliptical).....119

Table 4.5: Results for liquefaction / re-liquefaction at $D_{rc}$ = 25% / bi-dir. (figure-8) .....119

Table 4.6: Results for liquefaction / re-liquefaction at $D_{rc}$ = 45% / mono-directional .....120

Table 4.7: Results for liquefaction / re-liquefaction at $D_{rc}$ = 45% / bi-dir. (circular).....120

Table 4.8: Results for liquefaction / re-liquefaction at $D_{rc}$ = 45% / bi-dir. (elliptical).....121

Table 4.9: Results for liquefaction / re-liquefaction at $D_{rc}$ = 45% / bi-dir. (figure-8) .....121

Table 4.10: Results for liquefaction / re-liquefaction at $D_{rc}$ = 65% / mono-directional .....122

Table 4.11: Results of liquefaction / re-liquefaction at $D_{rc}$ = 65% / bi-dir. (circular).....122

Table 4.12: Results liquefaction / re-liquefaction at $D_{rc}$ = 65% / bi-dir. (elliptical).....123

Table 4.13: Results of liquefaction / re-liquefaction at $D_{rc}$ = 65% / bi-dir. (figure-8) .....123

# List of figures

Figure 2.1: Strain-dependent stiffness properties of soils (Sawangsuriya, 2012) .....7

Figure 2.2: Stress-strain loop of soil under cyclic loading and related parameters.....8

Figure 2.3: Average grain size distribution of Boler sand.....12

Figure 2.4: X-Ray diffraction analysis for Boler sand .....12

Figure 2.5: Uniformity control with frozen sample .....15

Figure 2.6: Sample uniformity check (left: cut of frozen / right: tin filled) .....15

Figure 2.7: Sample setup after preparation (up-left) and after mounting on DSS machine (up-right) and loading mechanism a) after consolidation b) shearing c) constant-volume boundary condition and shear strain illustration d) 3D deformed shape (Yao Li et al. 2017).....16

Figure 2.8: Characteristic response of sands under undrained static loading (Chern, 1985)18

Figure 2.9: Critical state line introduction and overview of parameters for Boler sand .....21

Figure 2.10: Typical respons of Boler sand in mono-directional cyclic simple shear tests....23

Figure 2.11: Monotonic constant-volume simple shear test results for Boler sand.....27

Figure 2.12: Monotonic drained simple shear test results for Boler sand.....28

Figure 2.13: Critical state lines of Boler (from this study), Hokksund (Castro, 1969), and Monterey #0 (Jefferies and Been, 2006) sands .....30

Figure 2.14: Shear wave (S wave) propagation in soil sample .....31

Figure 2.15: Shear wave signals for specimens (top to bottom; $D_{rc}$ = 25, 45, 65%).....32

Figure 2.16: Variation of $V_S$ with normalized $\sigma'_{vc}$ for Boler sand.....34

Figure 2.17: Variation of F(e) with consolidation void ratio ($e_c$) from this study for Boler sand and comparison with the correlation derived by Hardin and Richart (1963) .....35

Figure 2.18: Shear wave velocity ($V_S$) versus state parameter ($\Psi$) from the DSS tests .....35

Figure 2.19: Variation of $G_{max}$ with $\sigma'_{vc}$ for Boler sand at $D_{rc}$ = 25, 45, and 65%.....37

Figure 2.20: Variations of AF'(e) with $e_c$ for Boler sand and suggested values by several other studies (Hardin 1978; Iwasaki et al. 1978; Kokusho 1980) for clean sands .....37

Figure 2.21: Cyclic test results for a specimen (Drc = 65%, σ'vc = 100 kPa, CSR = 0.1).....38

Figure 2.22: CSR VS no. of cycles to trigger liquefaction of Boler sand at $\sigma'_{vc}$ = 100 kPa....39

Figure 2.23: Comparison of $CRR_1$ (at $\sigma'_{vc}$ = 100 kPa) and $V_{S1}$ for Boler sand with liquefaction triggering curves of Andrus and Stokoe (2000) and Robertson et al. (1992).....40

Figure 2.24: Shear modulus curves for Boler sand samples with $D_{rc}$ = 25, 45, and 65%, $\sigma'_{vc}$ = 50, 100, 200, 400, and 600 kPa .....42

Figure 2.25: Damping ratio variation for Boler sand samples with $D_{rc}$ = 25, 45, and 65%, $\sigma'_{vc}$ = 50, 100, 200, 400, and 600 kPa .....42

Figure 2.26: $G/G_{max}$ degradation curves for Boler sand samples with $D_{rc}$ = 25, 45, and 65%, $\sigma'_{vc}$ = 50, 100, 200, 400, and 600 kPa.....44

Figure 2.27: $G/G_{max}$ curves for Boler sand compared to lower and upper bands proposed by Seed et al. (1984, 1986) and Iwasaki et al. (1978) for sands.....45

Figure 2.28: Gradation of a sample before and after shearing to a CSR = 0.152 for a sample with $D_{rc}$ = 65% and $\sigma'_{vc}$ = 600 kPa.....46

Figure 3.1: Different applicable bi-directional loading patterns (Yang et al., 2016).....58

Figure 3.2: Comparing cyclic response of medium dense samples ($D_{rc}$ = 45%) to cyclic

Figure 3.3: Response of a sample to mono-directional cyclic load with $D_{rc}$ = 63.1%, .....63

$\sigma'_{vc}$ = 50 kPa, CSR = 0.071 and frequency of f = 0.1 Hz .....63

Figure 3.4: Response of a sample to bi-directional / circular pattern cyclic load with .....63

Figure 3.5: Response of a sample to bi-directional / elliptical pattern cyclic load with $D_{rc}$ = 65.9%, $\sigma'_{vc}$ = 50 kPa, $CSR_{resultant}$ = 0.073 and frequency of $f_X = f_Y$ = 0.1 Hz .....64

Figure 3.6: Response of a sample to bi-directional / figure-8 pattern cyclic load with $D_{rc}$ = 66.9%, $\sigma'_{vc}$ = 50 kPa, $CSR_{resultant}$ = 0.065 and frequency of $f_X$ = 0.1 Hz, $f_Y$ = 0.2 Hz .....64

Figure 3.7: CSR (and CRR) variation for mono-directional tests at different relative densities ($D_{rc}$ = 25%, 45%, 65% ± 3%) and .....68

under vertical effective stress of $\sigma'_{vc}$ = 400 kPa .....68

Figure 3.8: CSR versus $N_C$ for mono-directional cyclic loads at liquefaction .....69

Figure 3.9: CSR versus $N_C$ for mono-directional cyclic loads at re-liquefaction.....70

Figure 3.10: CSR versus $N_C$ for bi-directional / circular loads at liquefaction .....71

Figure 3.11: CSR versus $N_C$ for bi-directional / circular loads at re-liquefaction .....72

Figure 3.12: CSR versus $N_C$ for bi-directional / elliptical loads at liquefaction .....73

Figure 3.13: CSR versus $N_C$ for bi-directional / elliptical loads at re-liquefaction.....74

Figure 3.14: CSR versus $N_C$ for bi-directional / figure-8 loads at liquefaction.....75

Figure 3.15: CSR versus $N_C$ for bi-directional / figure-8 loads at re-liquefaction .....76

Figure 3.16: Effect of the relative density changes on $K_\sigma$ factor for Fraser delta river sand specimens (Idriss and Boulanger 2008) .....77

Figure 3.17: Overburden correction factor ($K_\sigma$) factor variation with effective stress for Boler sand (liquefaction) at three different relative densities ($D_{rc}$ = 25%, 45%, and 65%).....81

Figure 3.18: Comparison of $K_\sigma$ factor variation with $\sigma'_{vc}$ for various research studies.....83

Figure 3.19: CRR variation for one and two directional loaded samples ($\sigma'_{vc}$ = 50 kPa)

Figure 3.20: CRR variation for one and two directional loaded samples ($\sigma'_{vc}$ = 100 kPa).....85

Figure 3.21: CRR variation for one and two directional loaded samples ($\sigma'_{vc}$ = 200 kPa).....86

Figure 3.22: CRR variation for one and two directional loaded samples ($\sigma'_{vc}$ = 400 kPa).....87

Figure 3.23: CRR variation for one and two directional loaded samples ($\sigma'_{vc}$ = 600 kPa).....88

Figure 3.24: Reduction factors to convert bi-directional to mono-directional CRR .....89

Figure 3.25: Pore water pressure ratio at liquefaction ($r_{u\text{-}limit}$) variation with cyclic stress ratio (CSR) for cyclic DSS tests of Boler sand.....91

Figure 3.26: Pore water pressure ratio at liquefaction ($r_{u\text{-}limit}$) variation with number of loading cycles ($N_C$) for cyclic DSS tests of Boler sand .....92

Figure 3.27: CRR versus state parameter ($\Psi$) for cyclic DSS tests of Boler sand.....93

Figure 3.28: Cyclic resistance ratio (CRR) versus shear wave velocity ($V_S$) correlations from cyclic DSS tests and bender element tests of this study for Boler sand.....94

Figure 3.29: SPT test based liquefaction triggering curves for M = 7.5 and $\sigma'_{vc}$ =100 kPa ...96

Figure 3.30: CPT test based liquefaction triggering curves for M = 7.5 and $\sigma'_{vc}$ =100 kPa ...96

Figure 3.31: Vs based liquefaction triggering curves for M = 7.5 and $\sigma'_{vc}$ =100 kPa.....97

Figure 3.32: Vs based liquefaction triggering curves for M = 7.5 and $\sigma'_{vc}$ =100 kPa for Boler sand compared to same curves by Andrus & Stokoe and Kayen et al. .....100

Figure 3.32 (continued): Vs based liquefaction triggering curves for M = 7.5 and $\sigma'_{vc}$ =100 kPa for Boler sand compared to Andrus & Stokoe and Kayen et al. results. .....101

Figure 4.1: Definition of cyclic load patterns in this study.....113

Figure 4.2: Liquefaction stage results at $D_{rc}$ = 25%, $\sigma'_{vc}$ = 100 kPa and CSR=0.07 .....116

Figure 4.3: Re-liquefaction stage results at $D_{rc}$ = 25%, $\sigma'_{vc}$ = 100 kPa and CSR=0.07 .....116

Figure 4.4: Void ratio changes VS number of cycles at consecutive liquefaction stages....124

Figure 4.5: Volumetric strain changes VS initial state parameter (Ψ).....125

Figure 4.6: Variable trend of cyclic resistance (CSR) VS number of cycles at consecutive liquefaction events for mono-directional loading patterns .....127

Figure 4.7: Comparison of cyclic resistance (CSR) vs number of cycles with consecutive liquefaction occurrence in multiple studies and results of current study for dense samples .....128

Figure 4.8: Variable trend of (CSR) VS ($N_{CL}$) for loose samples ($D_{rc}$ = 25%).....130

Figure 4.9: Variable trend of (CSR) VS ($N_{CL}$) for medium dense samples ($D_{rc}$ = 45%).....131

Figure 4.10: Variable trend of (CSR) VS ($N_{CL}$) for dense samples ($D_{rc}$ = 65%).....132

Figure 4.11: Comparison of pore water pressure ratio ($r_u$) variation by relative density for two stages of liquefaction in different cyclic load patterns .....134

($D_{rc}$ = 25% left column and $D_{rc}$ = 65% right column) .....134

Figure 4.12: Comparison of pore water pressure ratio ($r_u$) variation by consolidation stresses for two stages of liquefaction in different cyclic load patterns.....135

($\sigma'_{vc}$= 50 kPa left column and 600 kPa right column) .....135

Figure 4.13: Calculating CRR values for liquefaction and re-liquefaction of Boler sand in mono-directional cyclic tests at $\sigma'_{vc}$ = 400 kPa and in different relative densities .....136

Figure 4.14: CRR VS initial state parameter for mono-directional cyclic loads.....138

Figure 4.15: CRR VS initial state parameter for bi-directional (circular) cyclic loads .....139

Figure 4.16: CRR VS initial state parameter for bi-directional (elliptical) cyclic loads .....139

Figure 4.17: CRR VS initial state parameter for bi-directional (figure-8) cyclic loads.....140

# List of Appendices

**Appendix 1:** Mono-directional cyclic simple shear test results

This appendix includes plots (shear stress VS shear strain – pore water pressure ratio VS shear strain – pore water pressure ratio VS number of cycles – shear stress VS vertical effective stress) for individual test results of samples with 25%, 45%, and 65% relative densities and consolidated to vertical effective stress of 50, 100, 200, 400, and 600 kPa under mono-directional cyclic simple shear loads.

**Appendix 2:** Bi-directional / circular cyclic simple shear test results

This appendix includes plots (shear stress path – pore water pressure ratio VS shear strain – pore water pressure ratio VS number of cycles – shear stress VS vertical effective stress) for individual test results of samples with 25%, 45%, and 65% relative densities and consolidated to vertical effective stress of 50, 100, 200, 400, and 600 kPa under bi-directional / circular cyclic simple shear loads.

**Appendix 3:** Bi-directional / elliptical cyclic simple shear test results

This appendix includes plots (shear stress path – pore water pressure ratio VS shear strain – pore water pressure ratio VS number of cycles – shear stress VS vertical effective stress) for individual test results of samples with 25%, 45%, and 65% relative densities and consolidated to vertical effective stress of 50, 100, 200, 400, and 600 kPa under bi-directional / elliptical cyclic simple shear loads.

**Appendix 4:** Bi-directional / figure-8 cyclic simple shear test results

This appendix includes plots (shear stress path – pore water pressure ratio VS shear strain – pore water pressure ratio VS number of cycles – shear stress VS vertical effective stress) for individual test results of samples with 25%, 45%, and 65% relative densities and consolidated to vertical effective stress of 50, 100, 200, 400, and 600 kPa under bi-directional / figure-8 cyclic simple shear loads.

# List of nomenclatures

| | |
|---|---|
| **A ($A_X$, $A_Y$)** | Amplitude of cyclic loading |
| **$a_{max}$** | Maximum ground acceleration, [$m/s^2$] |
| **CSL** | Critical state line |
| **CSR** | Cyclic stress ratio |
| **CRR** | Cyclic resistance ratio |
| **D** | Damping ratio of a sample in cyclic loading, [%] |
| **$D_{rc}$** | Relative density at the end of consolidation, [%] |
| **$D_{50}$** | Particle size corresponding to 50% finer soil-size particles, [mm] |
| **$e_{max}$** | Maximum void ratio |
| **$e_{min}$** | Minimum void ratio |
| **e** | Void ratio |
| **$e_c$** | Void ratio at the end of consolidation |
| **$e_{cs}$** | Void ratio at the critical state |
| **f(e), F(e)** | Void ratio function |
| **f** | Frequency, [Hz] |
| **g** | Gravitational acceleration, [$m/s^2$] |
| **$G_{max}$** | Small-strain shear modulus, [MPa] |
| **h** | Height of specimen, [mm] |
| **$K_o$** | Coefficient of lateral earth pressure at rest |
| **$K_\sigma$** | Overburden pressure correction factor |
| **$L_{tt}$** | Tip-to-tip distance between bender elements, [mm] |
| **$M_w$** | Earthquake magnitude |
| **$N_C$** | Number of cycles |
| **$N_{CL}$** | Number of cycles to trigger liquefaction |
| **n** | Stress exponent |
| **Pa** | Atmospheric pressure, [kPa] |
| **$P_L$** | Plasticity limit |
| **$r_u$** | Excess pore water pressure ratio |
| **$r_{u\text{-}limit}$** | Excess pore water pressure ratio at liquefaction |
| **$r_d$** | Shear stress reduction factor |

| | |
|---|---|
| $S_u$ | Undrained shear strength, [kPa] |
| $S_{u(critical)}$ | Critical undrained shear strength, [kPa] |
| $V_S$ | Shear wave velocity, [m/s] |
| $V_{S1}$ | Shear wave velocity at overburden pressure of 100 kPa, [m/s] |
| $W_D$ | Energy dissipated in one cycle of loading, [J] |
| $W_S$ | Maximum strain energy stored in a cycle, [J] |
| $\sigma_v$ | Total vertical (normal) stress, [kPa] |
| $\sigma'_v$ | Vertical effective stress, [kPa] |
| $\sigma'_{vc}$ | Vertical Effective stress at consolidation, [kPa] |
| $\sigma'_{cs}$ | Vertical effective stress at critical state, [kPa] |
| $\psi$ | Critical state parameter |
| $\Phi'$ | Effective friction angle, [degree] |
| $\Phi'_{cs}$ | Critical state (effective) friction angle, [degree] |
| $\Phi$ | Phase offset in cyclic loading, [degree] |
| $\gamma$ | Shear Strain, [%] |
| $\gamma_{DA}$ | Double amplitude shear strain, [%] |
| $\gamma_L$ | Shear Strain at liquefaction, [%] |
| $\Delta u$ | Excess pore water pressure, [kPa] |
| $\rho$ | Mass density, [kg/m$^3$] |
| $\tau$ | Shear stress, [kPa] |
| $\tau_{cyc}$ | Cyclic shear stress, [kPa] |
| $\lambda_{cs}$ | Slope of the critical state line, [mm] |
| $\lambda$ | Wavelength (Bender tests) |
| $\Gamma_{cs}$ | Critical state void ratio at 1 kPa |
| $\varepsilon_a$ | Axial strain, [%] |
| $\varepsilon_v$ | Volumetric strain, [%] |

# Chapter 1

## 1. Introduction

## 1.1. Problem overview

Liquefaction of saturated sandy soils is the among major causes of destruction to structures and infrastructure in earthquake events. When cyclic loads are applied on saturated loose sands, they are likely to contract and hence impose stress from the sand matrix to the surrounding pore water. Due to increased pore water pressure and consequently decreased effective confining stress on the soil, strength, and stiffness of the soil would drop. Because of a reduced stiffness, soil deposits experience small to large deformations. Some of the most significant damages to man-made construction facilities or natural grounds were observed after earthquakes in high seismic hazard zones of the world. For example, after the 1964 Niigata (Japan) earthquake and the 1964 Prince William Sound (Alaska) earthquake, liquefaction was identified to have considerable consequences. Liquefaction also demolished the Nerlerk (Canada) artificial island, which resulted in more than $100 million financial loss. As another instance, liquefaction of the Lower San Fernando Dam (California) required a population of 80,000 to immediately leave the downstream area. Extensive failures of reclaimed lands and man-made islands due to this phenomenon were reported after the 1995 Kobe earthquake which is one of the largest ports in the world (Idriss and Boulanger 2008).

Evaluation of soil undrained shear strength plays an important role in liquefaction assessment. Correct estimation of undrained shear strength is particularly necessary for the design of earth structures to protect them against failures during earth shaking. Undrained shear strength of soil in liquefaction could be either determined through empirical correlations based on field test results of earlier failure cases (Seed and Harder 1990; Stark and Mesri 1992; Baziar and Dobry 1995; Olson and Stark 2002; Idriss and Boulanger 2008), or laboratory cyclic shear tests on undisturbed samples obtained from the field by ground freezing (Robertson et al. 2000) or high-quality tube sampling techniques corrected for sample disturbance effects (Poulos et al. 1985). Each of the addressed approaches has some advantages and some limitations. Particularly, the empirical methods based on in-situ tests are subject to significant uncertainties with lots of assumptions (mostly based on observations), applied to them. Accordingly, our

knowledge of soil behavior is based upon a limited range of soils that have been tested in the laboratory or those encountered in past field failures. Several factors (e.g. density, shear and consolidation stress levels, compressibility, and testing device and procedure) significantly affect the response of sands. The separate and mixed roles of these factors on sand behavior needs to be accurately identified to formulate and regulate soil behavior for analysis and design purposes. Extensive investigation both in the filed and laboratories are required to complete previous studies and existing knowledge on an accurate assessment of soil behavior under cyclic loads and build evaluation methods to analyze, predict and design soil interacted facilities and infrastructures with the maximum factor of safety and minimum economical requirements and consequences.

Soil cyclic and liquefaction susceptibility demands precise evaluation of cyclic loads and soil response to applied loads. Liquefaction is mainly a consequence of the earthquake, which is the main dynamic load resource in nature. The movement of ground in an earthquake is an unpredictable event due to unlimited eventual combinations of deformations and accelerations in different directions. The variable parameters of an earthquake could be mainly divided into three categories: amplitude, pattern, and frequency. Ground accelerations are usually measured and recorded in vertical and two perpendicular horizontal directions by accelerograms. A peak horizontal ground acceleration (PGA) is usually selected as the higher individual record, the mean value or the resultant value. In the structural analysis and design practice, depending on the importance of structure and location (seismic hazard) of the structure, combination of two perpendicular seismic loads have been proposed to consider this multidirectional load effect. For example, American ASCE code or Canadian NBCC provision, persuade the combination of 100% seismic loads in one direction in addition to 30% seismic loads in a perpendicular direction.

However, in geotechnical engineering, the effect of multidirectional cyclic loads has been rarely considered in practice. A great portion of codes and provisions, only consider a unidirectional effect. Moreover, the majority of code instructions are based on the cyclic response of soils in one directional cyclic tests. Earthquake and specifically liquefaction are addressed in Canadian Foundation Engineering Manual and Canadian Highway Bridge Design Code, based on responses and analysis of soil behavior under one directional cyclic loads.

## 1.2. Purpose of research and thesis outline

In the current study, the bi-directional cyclic response of a silica-carbonate sand is verified by applying different two directional cyclic load combinations to help to have a better understanding of soil behavior under dynamic loads such as earthquake and specifically focused on liquefaction behavior. Although some investigations have been performed in this area before, those studies have been mainly focused on the limited type of soils and in a limited domain of densities. Another purpose of this study is to compare the behavior of a silica-carbonate sand with the previously limited type of sands such as Monterey #0,30 and Fraser river which mainly composed of a silicate mineralogy. A wide range of void ratio (relative density) increments has been chosen by applying moist tamping method for preparing specimens to have a better understanding of the cyclic load's effect on different soil states.

For investigating cyclic load effects, in addition to a mono-directional load pattern, three different cyclic load patterns have been applied in this work which will be discussed in detail, later. As a brief explanation, bi-directional circular, elliptical and figure-8 load patterns have been chosen based on the limits of the test device. The reason for selection of these three patterns was to consider effective and variable factors of an actual cyclic load such as an earthquake (magnitude, frequency, and multi-directional nature). A circular pattern can represent the effect of a cyclic load with equal magnitudes in two directions but with a time lag between one direction relative to the other. An elliptical pattern can represent the effect of a cyclic load with un-equal magnitudes in two directions and with a time lag between one direction relative to the other. Finally, a figure-8 pattern can represent the effect of a cyclic load with un-equal frequencies in two perpendicular directions.

Factors such as cyclic resistance ratio (CRR) variation, shear strain changes, and pore water pressure generation patterns were studied for a wide range of soil states. Investigating reduction factor which incorporates multidirectional loading effect in liquefaction analysis (proposed 0.9 by Seed and colleagues) is another objective of this study. Currently, this factor is the most common way to account for multi-directional loading in liquefaction triggering. The magnitude of this factor was evaluated for different bi-directional loading patterns, comparing to mono-directional loads.

This study presents a framework for estimating the cyclic undrained shear strength for liquefaction triggering of a silica-carbonate sand by a critical-state soil mechanics approach and demonstrates the significance of cyclic load amplitudes, direction and pattern, sand compressibility, consolidation condition and density of samples in the failure of sandy soils during a liquefaction. Understanding the effects of these factors on sand cyclic shear behavior would be helpful for assessment, evaluation and prediction of liquefaction occurrence.

The critical state line of the soil was obtained to effectively characterize and correlate impacting parameters in liquefaction to soil state and formulate the factors that can let us predict soil behavior as precise as possible and correlate similar in-situ soil states to its performance during shaking. Shear wave velocity of samples under different densities and consolidation stresses was also measured and correlated to soil liquefaction parameters to account for soil rigidity factors effective in its behavior.

The main purpose of shear wave velocity measurement and its correlation to soil properties is that there are various in-situ methods of measuring shear wave velocity which could be a confident way to soil assessment when coupled to laboratory-based results and analysis, although questions around accounting for behavior variation between intact soil and re-constituted soil samples remains. Finally, due to the importance of soil post-liquefaction behaviour assessment, specifically in prediction of soil response after cyclic load events such as an earthquake, which is a very common phenomenon in seismic zones, soil samples were subjected to repeating cyclic loads for liquefaction triggering (re-liquefaction) to understand how they behave compared to a first-time liquefaction.

The characteristics which distinguish the current study from previous researches could be categorized in four main parts; The material (a silica-carbonate sand which has angular to sub-angular particle shapes), a wide range of density and consolidations stresses (precious studies mostly focused on cyclic load amplitude and patterns), variety of bi-directional cyclic load patterns and amplitudes, and finally post-liquefaction analysis of the samples by re-applying cyclic loads.

This thesis has been prepared in "Integrated-Article" format. It is organized into 5 chapters. A brief description of the following four chapters is as follows:

**Chapter 2** illustrates the shear wave velocity and shear modulus variation of reconstituted samples for a local silica-carbonate sand using a pair of bender elements. Shear modulus, damping ratio and stiffness reduction patterns were evaluated. The cyclic resistance of the samples was also assessed with constant volume cyclic simple shear tests. Moreover, critical state parameters of the soil were evaluated. The cyclic resistance of the specimens was correlated to shear wave velocity and shear modulus within a critical state framework.

**Chapter 3** investigates the cyclic resistance and liquefaction susceptibility of the local silica-carbonate sand under mono-directional and three different bi-directional cyclic load patterns. In this chapter, the liquefied undrained strength ratio is correlated to the shear wave velocity and the state parameter ($\Psi$) for several samples at different relative densities and a wide range of consolidation stresses. Moreover, cyclic resistance, pore water pressure generation and liquefaction susceptibility of the samples are verified and compared. Multi-directional by the one-directional cyclic resistance of a silica-carbonate sand is also studied in this chapter.

**Chapter 4** presents the post-cyclic response and liquefied shear strength of a silica-carbonate sand under different cyclic load patterns. Cyclic load pattern, pore water pressure generation, relative density, and consolidation pressure effects on a sample’s behavior in repeating occurrence of liquefaction were evaluated.

**Chapter 5** is a summary of the research work carried out and the conclusions from the work.

# Chapter 2

# 2. Characterization of a silica-carbonate sand based on shear wave velocity measurement

## 2.1. Introduction

Shear wave velocity ($V_S$) and shear modulus (G) are two of the most fundamental parameters for characterizing materials including soils and play a key role in engineering design practice. $V_S$ is used in several constitutive models to determine the small strain response of soils, to estimate the in-situ stress state of cohesionless soils (Robertson, et al., 1995), for ground deformation prediction, for seismic site classification in many design codes including the current National Building Code of Canada and the Canadian Highway Bridge Design Code, to characterize site-response for evaluating seismic hazard, and assessing the potential for liquefaction triggering of cohesionless soils (Andrus, et al., 2004, Clayton, 2011). $V_S$ can be measured both in the laboratory (e.g. bender elements or resonant column device) and in the field by down-hole, cross-hole, suspension logging and surface wave methods. Shear wave velocity ($V_s$) represents soil elasticity and provides a direct measure of the maximum (small-strain) shear modulus ($G_{max}$) of a soil as shown in Equation 2.1:

$$G_{max} = \rho V_S^2 \tag{2.1}$$

Where $G_{max}$ is in Pascal, $V_s$ is in m/s, and ρ is the total soil mass density in kg/m$^3$. Along with soil damping characteristics, $G_{max}$ is a useful parameter for the analysis of natural or man-made structures under dynamic or cyclic loads (e.g., caused by an earthquake, machine foundation, ocean waves, or blast). Several investigations have been performed on shear wave velocity and shear modulus of cohesionless soils and their correlations with soil characteristics such as relative density and confining pressure (Hardin and Black, 1966, Iwasaki, et al., 1978, Kokusho, 1980, Lo Presti, et al., 1997, Robertson, et al., 1995). These studies have been mostly carried out on sands predominantly composed of silica and quartz particles. For example,

Hardin and Black (1966) and Robertson, et al. (1995) studied dynamic characteristics of Ottawa sand while Kokusho (1980) focused on the behavior of Toyoura sand. Both types of sands are composed of silica particles. This paper studies the dynamic behavior of a silica-carbonate sand using bender element measurements and cyclic direct simple shear (DSS) tests. Bender elements provide soil dynamic modulus at very small shear strains ($< 10^{-5}$), while cyclic DSS tests are employed to augment the $V_S$ measurements from bender elements at higher cyclic shear strains (between 0.1 – 4%). The plane-strain boundary condition and simple shearing mode applied in a DSS test provide a closer representation of in-situ conditions than a triaxial test. Furthermore, a soil specimen is subjected to repeated abrupt 90$^o$ rotations of principal stresses in a cyclic triaxial test. This is very different from the smooth rotation of principal stress directions, which occurs during an actual seismic event or in a cyclic DSS tests. As shown in Figure 2.1, stiffness (shear modulus and in a similar way, damping properties) of a soil is strain dependent. Shear wave velocity measurement provides estimates of stiffness characteristics of a soil over small strain ranges, unlike cyclic shear tests which are used to evaluate soil stiffness properties at higher strain levels.

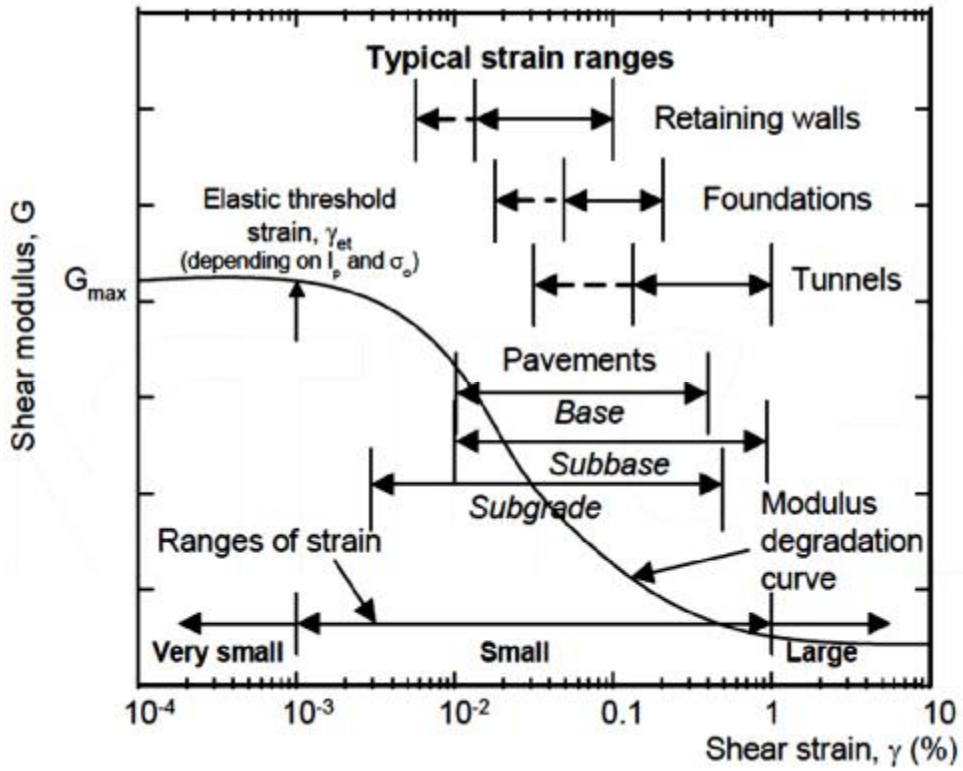


**Figure 2.1: Strain-dependent stiffness properties of soils (Sawangsuriya, 2012)**

Soil subjected to symmetric cyclic loading has a non-linear behavior which results in dissipating energy in each hysteresis loop of cyclic load, illustrated in Figure 2.2. For a wave propagating through the soil, this dissipated energy will cause a decrease in the amplitude of the wave as it travels away from the source (Kramer, 1996). Increasing shear strain amplitude from dynamic loading results in more dissipated energy, and an increasing damping ratio. As the damping ratio increases, the shear stiffness of the soil decreases, weakening the material (Kramer, 1996).

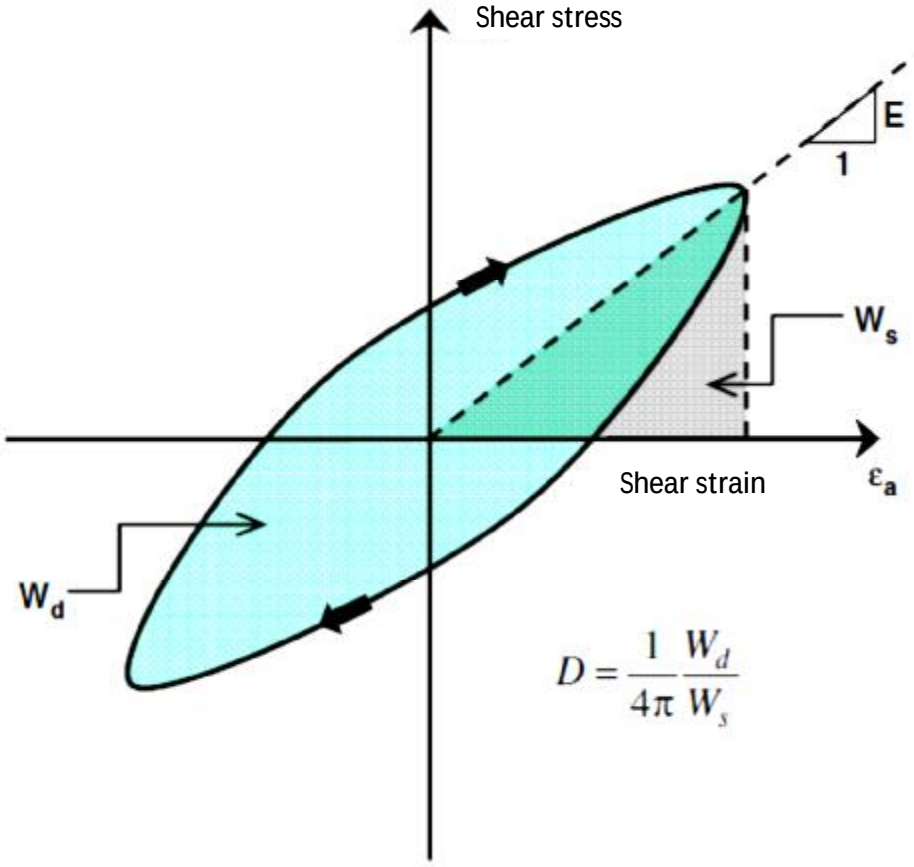


**Figure 2.2: Stress-strain loop of soil under cyclic loading and related parameters**

Regarding past liquefaction research studies, shear wave velocity is an important parameter that is used for identification of liquefaction both in the field (in-situ) and in the laboratory. SPT, CPT and shear wave velocity are the main three in-situ tests that are currently used for field liquefaction assessment, characterization, and identification.

Among those tests, shear wave velocity is the only parameter which could be measured in the laboratory as well and thus be correlated to in-situ properties of a soil. Bender element (BE), resonant-column (RC) and Ultrasonic pulse test are the principal devices of measuring shear wave velocity in the laboratory. The RC test is relatively expensive and time-consuming in terms of preparation and calibration. Short-circuiting and loss of signal, depolarization at high voltages and small thicknesses have been noted as some of the shortcomings of BE tests. There are also several different methods for measuring shear wave velocity in situ (e.g., cross-hole, downhole, seismic CPT, and spectral analysis of surface waves (SASW)). A general advantage of shear wave velocity tests is that they can be used for sites underlain by soils that are difficult to penetrate or sample (e.g., gravels, cobbles, and boulders).

The general disadvantage of shear wave velocity tests, like other in-situ tests such as SPT and CPT, is that they provide very limited spatial distribution for characterizing site stratigraphy, e.g. they measure an average velocity over relatively large volumes (Idriss and Boulanger, 2012). Shear wave velocities have been identified to increase with increasing effective confining stress. Also, it is usual to use normalized shear wave velocity in studies. The normalization is based on overburden ($\sigma'_{vc}$) and atmospheric ($P_a$ = 100 kPa) pressures and a normalized shear wave velocity ($V_{S1}$) is defined as below in which the overburden normalization for shear wave velocity values follows from the experimental observation that the maximum (low-strain) shear modulus ($G_{max}$) in sand is approximately proportional to the square root of the effective confining stress (Idriss and Boulanger, 2008):

$$V_{S1} = V_S \left(\frac{P_a}{\sigma'_{vc}}\right)^{0.25} \tag{2.2}$$

There are a couple of empirical correlations between shear wave velocity and maximum shear modulus of a soil and other basic soil properties. The general format of correlation between factors in soil stiffness parameters could be summarized as below (Kallioglu et al. (2008) and Sawangsuriya (2012):

$$G_{max} = A\, f(e)\sigma'^{n}_{a} P_a^{1-n} g(OCR, PI) \quad (2.3)$$

Where A is a constant, f (e) is the void ratio function, $\sigma'_a$ (kPa) is the applied mean confining stress, n is the stress exponent, $P_a$ is the atmospheric pressure ($P_a \approx 100$ kPa), and g (OCR, PI) is a function of over-consolidation ratio (OCR) and plasticity index (PI) estimation of soils. These factors are shown in Table 2.1 for some of the previous studies. The Vs-based liquefaction triggering has improved significantly in recent years, with more advanced correlations and more complete databases, as recently summarized by Andrus and Stokoe (2000) and Andrus et al. (2003). One of their principal research results is used to identify sands cyclic resistance ratios in liquefaction analysis and is based on shear wave velocity measurement in the fields with observed liquefaction symptoms. It appears that shear wave velocity measurements would be the least sensitive for distinguishing among different types of in-situ tests (e.g. SPT and CPT) (Idriss and Boulanger, 2012). Developed curves and equations for correlating in-situ test results to cyclic resistance factors of different soils are called liquefaction triggering curves and will be discussed completely and compared to current study results, in upcoming chapters.

**Table 2.1: $G_{max}$ correlations of cohesionless Soils (Sawangsuriya, 2012)**

| Type of materials | A | f ( e ) | n | Reference |
|---|---|---|---|---|
| Round-grained | 6900 | (2.17-e)2/(1+e) | 0.5 | Hardin and Black (1968) |
| Ottawa sand / Angular-grained / Crushed quartz | 3270 | (2.97-e)2/(1+e) | 0.5 | Hardin and Black (1968) |
| Clean sand | 41600 | (0.67-e)/(1+e) | 0.5 | Shibata and Soelarno (1975) |
| Clean sand (Cu < 1.8) | 14100 | (2.17-e)2/(1+e) | 0.4 | Iwasaki and Tatsuoka (1977) |
| Clean sand | 9000 | (2.17-e)2/(1+e) | 0.4 | Iwasaki et al. (1978) |
| Toyoura sand | 8400 | (2.17-e)2/(1+e) | 0.5 | Kokusho (1980) |
| Clean sand | 7000 | (2.17-e)2/(1+e) | 0.5 | Yu and Richart (1984) |
| Ticino sand | 7100 | (2.27-e)2/(1+e) | 0.4 | Lo Presti et al. (1993) |
| Clean sand | 9300 | 1/(e1.3) | 0.45 | Lo Presti et al. (1997) |
| Several soils | 5700 | 1/e | 0.5 | Biarez and Hicher (1994) |

## 2.2. Experimental plan

### 2.2.1. Tested material

A local silica-carbonate sand is tested in the experiments of this study. This sand was collected from Boler Mountain in London, Ontario (called "Boler sand" hereafter). The natural Boler sand contains about 11% fine particles. However, for the experiments of this study, the fines were removed to focus on the behavior of a clean sand and compare its dynamic behavior with those of other clean sands. A specific gravity ($G_S$) of 2.67, and maximum ($e_{max}$) and minimum ($e_{min}$) void ratios of respectively 0.845 and 0.525 were determined following ASTM standard procedures. Particle size distribution of Boler sand is presented in Figure 2.3 with $D_{50}$ = 0.25 mm. Accordingly, Boler sand is classified as a poorly-graded (SP) sand according to the Unified Soil Classification System (USCS).

Scanning electron microscopic images and X-Ray diffraction analyses were carried out to determine particle shape and mineralogy. X-ray diffraction test (XRD) is a fast technique used for analysis and identification of different phases of a crystalline material. The results of this test can provide quantitative information on minerals. This test is based on interference of X-rays radiation and crystalline of samples. The interaction of the emitted X-rays with the sample produces interference and a diffracted ray which satisfy Bragg's Law ($n.\lambda = 2d \sin\theta$). This law relates the wavelength of radiation ($\lambda$) to the diffraction angle ($\theta$) and the spacing in a crystalline sample (d). By scanning the sample through a range of angles ($\theta$), all possible diffraction directions could be attained due to the random orientation of the crystals. Conversion of the diffraction peaks to spacings (d) allows identification of the mineral since each mineral has a set of unique spacings (d). (Barbara L Dutrow, Christine M. Clark). Based on the results of this test, it was found that the Boler sand is mainly composed of carbonate ($CaCO_3$), dolomite ($MgCa(CO_3)_2$), and quartz ($SiO_2$) minerals with sub-angular to angular particle shapes. X-ray diffraction test (XRD) result for Boler sand is shown in Figure 2.4. Quantitative analysis is another method of identifying different minerals and the quantity of contents in a sample. There are different methods, but chemical methods are more useful ones. Acid dissolution method was used to determine the amount of carbonate content of Boler sand.

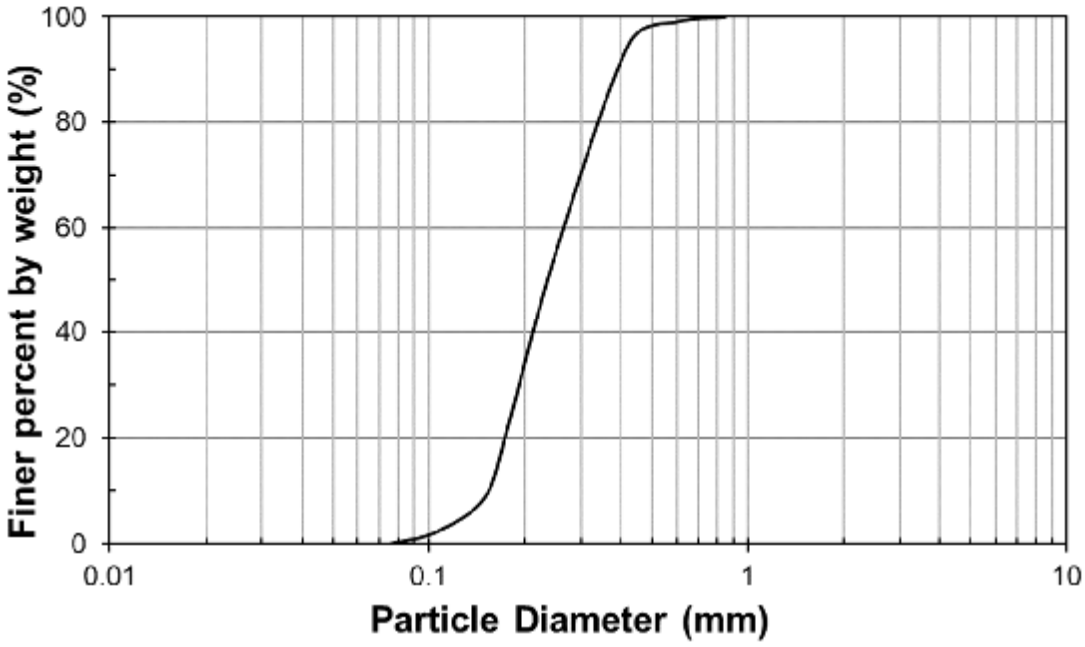


**Figure 2.3: Average grain size distribution of Boler sand**

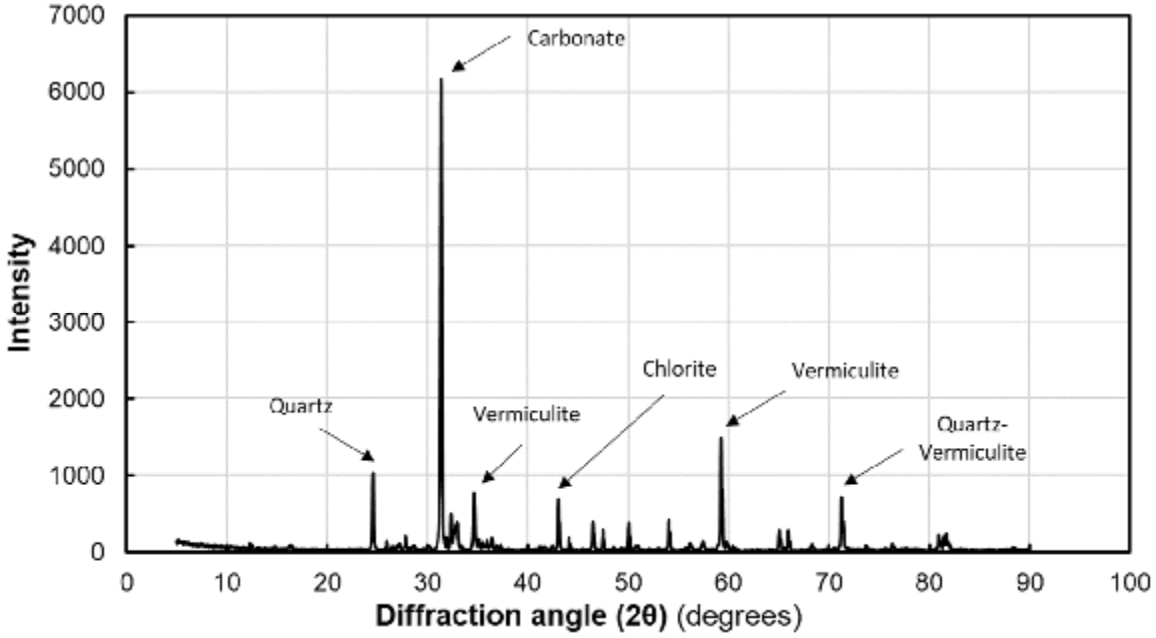


**Figure 2.4: X-Ray diffraction analysis for Boler sand**

The solubility of carbonate (mostly $CaCO_3$) in acid could help quantifying the amount of carbonate minerals. The results of the acid dissolution test are demonstrated in table 2.2. It is shown that two tests confirm a quantity of almost 11.8% carbonate in Boler sand.

**Table 2.2: HCL dissolution test results of Boler sand for determining carbonate content**

| Container Weight | Soil Initial Weight | Container W (After) | Soil Final W | Lost Percentage |
|---|---|---|---|---|
| gr | gr | gr | gr | % |
| 50.04 | 2 | 51.82 | 1.78 | 11.0 |
| 49.99 | 1.99 | 51.73 | 1.74 | 12.6 |
| | | | | **11.8 (Average)** |

### 2.2.2. Specimen preparation

Simple shear tests were carried out using an advanced computer-controlled cyclic simple shear apparatus (Model VDDCSS) manufactured by GDS Instruments (UK). For specimen preparation, a latex membrane was first placed around the bottom cap of the DSS apparatus and secured with an O-ring. A series of 1 mm-thick Teflon-coated stainless-steel rings were then stacked around the membrane. Two supporting retainers were used to hold the stacked rings in place during sample preparation and the membrane was then folded over the stacked steel rings. Specimens were prepared at loose ($D_{rc}$ = 25%), medium dense ($D_{rc}$ = 45%), and dense ($D_{rc}$ = 65%) relative densities using the moist tamping method. The height and diameter of the specimens were respectively 20 mm and 70.7 mm in cyclic DSS tests. This corresponds to an aspect ratio of 0.28, which is less than (0.4) that is recommended by the ASTM D6528 standard method for simple shear testing. In regular moist-tamping, the density of the lower sublayers is increased by compacting the overlying layers. This would produce a non-uniform specimen. In order to improve specimen uniformity, the under-compaction (Ladd, 1978) method was used in this study. In this method, over-dried sand was thoroughly mixed with 5% moisture. The specimen was then prepared by compacting moist sand in three sublayers. The first and second sublayers were compacted to dry densities of respectively 5% and 2.5% (“under-compacted”) lower than the target dry density of the specimen. After compacting the third overlying sublayer, the final density of these sublayers was hence compacted closer to the target density of the specimen. The dry density was adjusted by changing the mass of soil placed in each sublayer, while all sublayers were compacted to equal heights. Except for the

final sublayer, the surface of each sublayer was also scarified to improve the bonding between sublayers. The top cap of the DSS apparatus was subsequently lowered on the sand surface, the membrane was folded back on the top cap and then secured with an O-ring. The retainer plates were also removed. The small amount of moisture content (5%) imparts a small amount of matric suction to a moist-tamped specimen and helps to stabilize the specimen during preparation. However, since this matric suction was not measured here, it was removed by saturating the specimens after specimen preparation. A small seating vertical stress of 5 kPa was first applied to stabilize the specimen and prevent piping. Saturation was then carried out by flushing the specimens with $CO_2$ gas, followed by de-aired water through drainage ports on the specimen endcaps. Carbone dioxide ($CO_2$) was used to enhance specimen saturation as it is heavier than air (so it replaces air during flushing) and it is many times more soluble in water than air. Specimen height was carefully recorded during this process to determine the precise initial void ratio of the specimen. For samples uniformity check, two relatively dense samples were prepared, frozen, cut in two halves (dividing the cylindrical specimens to top and bottom layers) and their volume and oven dried weight measured. The results are shown in Table 2.3.

**Table 2.3: Uniformity check for two dense samples**

| | SAMPLE 1 | | | | SAMPLE 2 | | | |
|---|---|---|---|---|---|---|---|---|
| | Top layer | | Bot. layer | | Top layer | | Bot. layer | |
| | D | H | D | H | D | H | D | H |
| | mm | mm | mm | mm | mm | mm | mm | mm |
| Avg. Dim. | 67.23 | 10.08 | 68.48 | 11.21 | 49.50 | 15.00 | 49.50 | 15.00 |
| Weight | $W_{dry}$ | $W_{bowl}$ | $W_{dry}$ | $W_{bowl}$ | $W_{dry}$ | $W_{bowl}$ | $W_{dry}$ | $W_{bowl}$ |
| | gr | gr | gr | gr | gr | gr | gr | gr |
| | 255.47 | 205.80 | 254.51 | 196.65 | 242.40 | 198.94 | 234.70 | 192.33 |
| V | 35753.3 | $mm^3$ | 41248.6 | $mm^3$ | 28851.7 | $mm^3$ | 28851.7 | $mm^3$ |
| W | 49.67 | gr | 57.86 | gr | 43.46 | gr | 42.37 | gr |
| $\rho_{dry}$ | 1389.2 | $Kg/m^3$ | 1402.7 | $Kg/m^3$ | 1506.3 | $Kg/m^3$ | 1468.5 | $Kg/m^3$ |
| Uniformity | 99.04 | | % | | 97.49 | | % | |

The samples which were used to control the uniformity, are shown in Figure 2.5 and 2.6. Based on the results, samples are distributed by a uniformity degree of 97% and 99% which is expected for very thin layers of sands.

**Figure 2.5: Uniformity control with frozen sample**

**Figure 2.6: Sample uniformity check (left: cut of frozen / right: tin filled)**

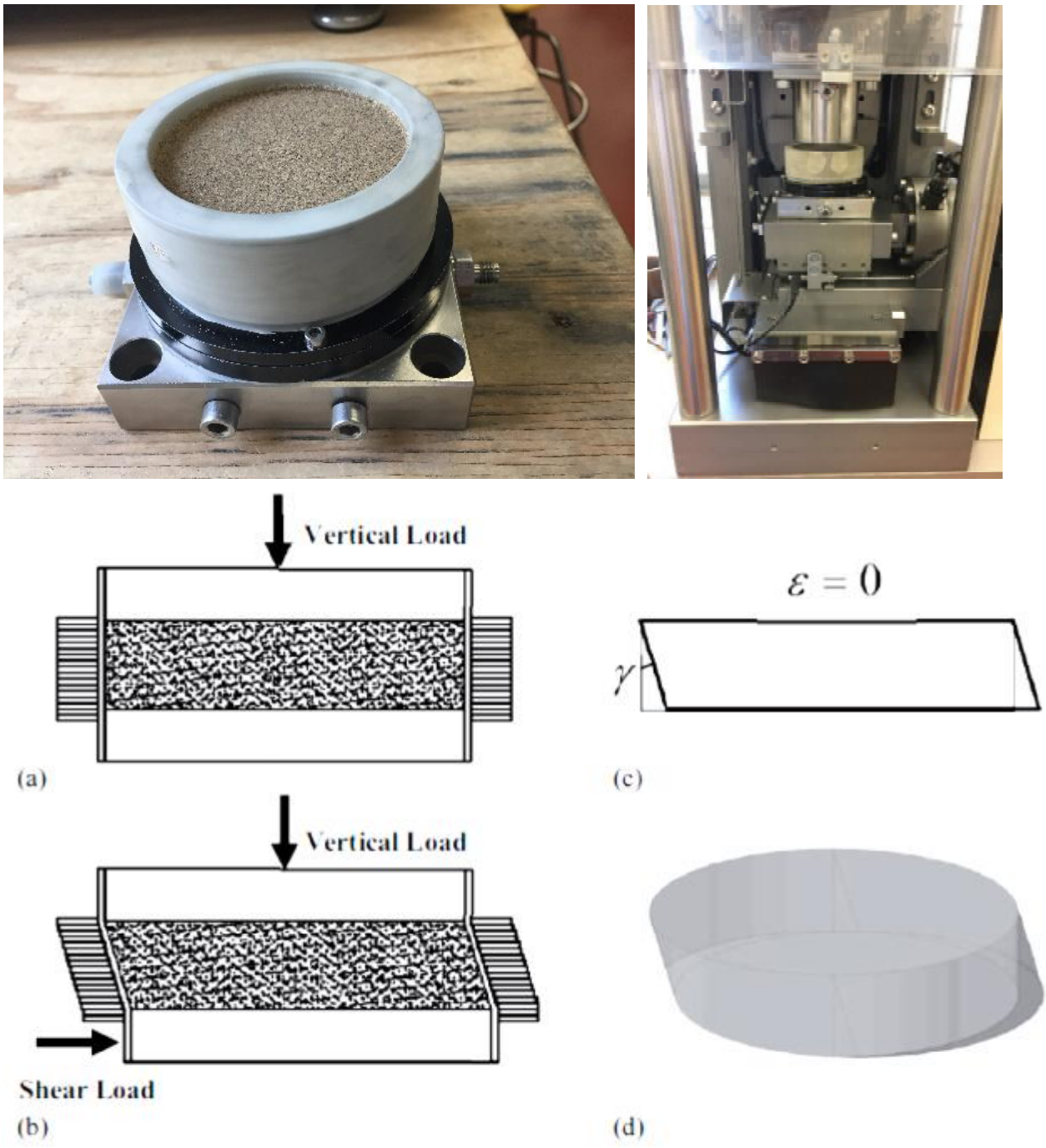


**Figure 2.7: Sample setup after preparation (up-left) and after mounting on DSS machine (up-right) and loading mechanism a) after consolidation b) shearing c) constant-volume boundary condition and shear strain illustration d) 3D deformed shape (Yao Li et al. 2017)**

### 2.2.3. Consolidation

Following with saturation, the specimens were consolidated to an effective vertical stress ($\sigma'_{vc}$) of 50, 100, 200, 400, or 600 kPa. The top drainage port was open during consolidation to allow excess pore pressure dissipation. Specimens void ratio after consolidation ($e_c$) was subsequently calculated from changes in the specimen height.

### 2.2.4. Monotonic simple shear tests

Assessment of sands behavior under monotonic undrained loading has been mostly developed from triaxial tests on reconstituted samples. Based early test results (Castro, 1969; Lee and Seed, 1970; Castro et al., 1982; Vaid and Chern, 1985; Vaid and Thomas, 1992; and Ishihara, 1993), responses of samples are mostly dependant on void ratio changes (relative density) as well as confining stress.

Three types of behavior were mainly recognized in sand samples when a monotonic shear load is applied. In type 1 response which is a typical characteristic of loose sands, (Shown in Figure 2.8) by the progress of shear deformation, the strength of soil reaches its maximum value and then decreases to a stable or critical state. This flow like deformations after reaching the peak of stress-strain curve (undrained yield strength, $S_u$) is the major cause of in-situ failures. This strain softening type of response was called "static liquefaction" by Castro (1969), Casagrande (1975), and Seed (1979). Nonetheless, some of the materials, demonstrate partial or limited flow deformations. In this type of response, pore water pressure increases gradually and reaches its maximum value and decreases again towards the end of shearing (shown in Figure 2.8). This type of behavior is a full contractive behavior.

In type 2 response, which is characteristic of medium dense samples, strain softening behavior is observed in early stages and the material starts to experience a second-time strain hardening after softening and reaching the minimum strength (e.g. maximum pore water pressure). The changing state from softening and flow deformation to a hardening state which depicts a changing behaviour from contraction to dilation, was called "phase transformation" (PT) by Ishihara (1975), a "limited liquefaction" by Castro, 1969 and Vaid and Chern, 1985 and "partial liquefaction" by Lee and Seed (1970).

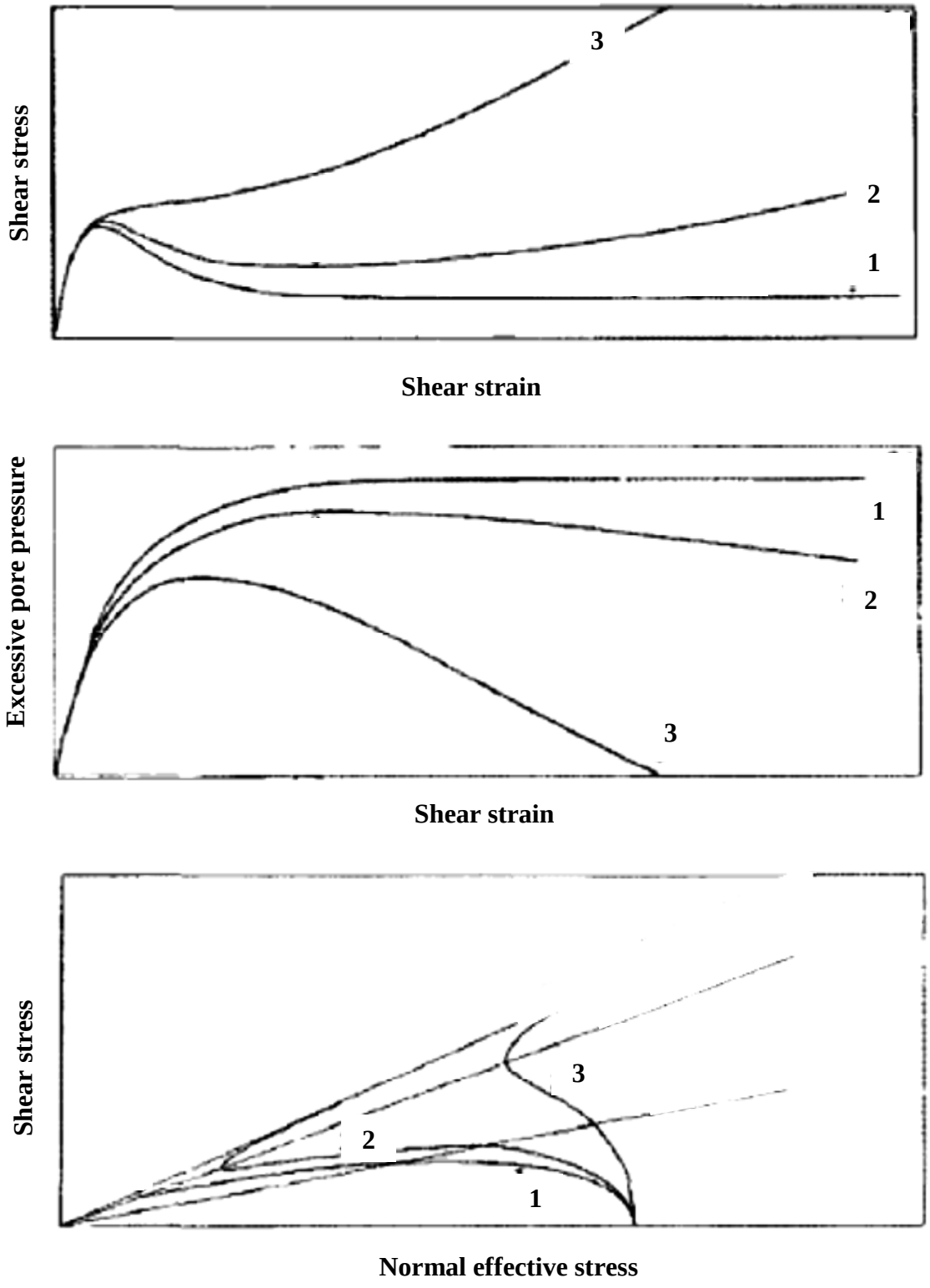


**Figure 2.8: Characteristic response of sands under undrained static loading (Chern, 1985)**

There is a general agreement between researchers that some of the soil characteristics such as friction angle (strength) mobilised at critical state (type 1) or phase transformation (type 2) state, are unique material properties (Castro, 1969; Vaid and Chern, 1985; Vaid and Sivathayalan, 2000) irrespective of void ratio, initial state, mode of loading, sample preparation method, intermediate principal stress values and rotation of principal stress axis.

At a constant vertical effective stress, the behaviour of the soil changes from contractive to dilative while relative density increases (Bishop, 1971; Been et al., 1991; Vaid and Thomas, 1995; Vaid and Sivathayalan, 1996; Vaid and Uthaykumar, 1998). On the other hand, at a constant relative density, increasing confining stress, amplifies the contractive response of the samples. In the current study, monotonic drained and constant-volume simple shear tests were carried out to determine liquefaction susceptibility, static shear behavior, and the critical state line of Boler sand. A summary of tests is shown in Tables 2.4 and 2.5.

**Table 2.4: Summary of monotonic drained simple shear tests of Boler sand**

| ID | $\sigma'_{vc}$ | $e_c$ | $D_{rc}$ | $e_{cs}$ | $\sigma'_{vc,s}$ |
|---|---|---|---|---|---|
| | kPa | | % | | kPa |
| D1 | 50 | 0.812 | 10.3 | 0.782 | 50 |
| D2 | 300 | 0.793 | 16.3 | 0.745 | 300 |
| D3 | 50 | 0.795 | 15.6 | 0.802 | 50 |
| D4 | 100 | 0.753 | 28.8 | 0.753 | 100 |
| D5 | 400 | 0.756 | 27.8 | 0.733 | 400 |
| D6 | 100 | 0.697 | 46.3 | 0.698 | 100 |
| D7 | 400 | 0.699 | 45.6 | 0.697 | 400 |
| D8 | 50 | 0.621 | 70.0 | 0.626 | 50 |
| D9 | 80 | 0.77 | 23.4 | 0.758 | 80 |
| D10 | 200 | 0.771 | 23.1 | 0.767 | 200 |
| D11 | 400 | 0.749 | 30.0 | 0.727 | 400 |
| D12 | 500 | 0.732 | 35.3 | 0.709 | 500 |
| D13 | 600 | 0.74 | 32.8 | 0.721 | 600 |

**Table 2.5: Summary of monotonic constant-volume simple shear tests of Boler sand**

| ID | $\sigma'_{vc}$ | $e_c$ | $D_{rc}$ | $e_{cs}$ | $\sigma'_{vc,s}$ |
|---|---|---|---|---|---|
| | kPa | | % | | kPa |
| CV1 | 100 | 0.812 | 10.3 | 0.812 | 59 |
| CV2 | 300 | 0.778 | 20.9 | 0.778 | 42 |
| CV3 | 200 | 0.809 | 11.3 | 0.809 | 20 |
| CV4 | 400 | 0.750 | 29.7 | 0.750 | 87 |
| CV5 | 300 | 0.763 | 25.6 | 0.763 | 72 |
| CV6 | 150 | 0.697 | 46.3 | 0.697 | 56 |
| CV7 | 100 | 0.802 | 13.4 | 0.802 | 11 |
| CV8 | 400 | 0.621 | 70.0 | 0.621 | 96 |
| CV9 | 800 | 0.728 | 36.6 | 0.728 | 187 |
| CV10 | 100 | 0.762 | 25.9 | 0.762 | 41 |
| CV11 | 400 | 0.749 | 30.0 | 0.749 | 213 |
| CV12 | 800 | 0.732 | 35.3 | 0.732 | 432 |
| CV13 | 1000 | 0.706 | 43.4 | 0.706 | 346 |
| CV14 | 1200 | 0.697 | 46.3 | 0.697 | 421 |
| CV15 | 100 | 0.629 | 67.5 | 0.629 | 36 |
| CV16 | 400 | 0.631 | 66.9 | 0.631 | 93 |

### 2.2.5. Critical state approach

Been and Jefferies (1985) introduced the state parameter (Ψ) to describe the shearing behavior of a soil based on the combination of void ratio, effective stress and their relation to the critical state void ratio at same effective stress. The critical state line (CSL) represents a boundary between strain-softening (or contractive) and strain-hardening (or dilative) behaviors of a soil where ψ is the difference between the current void ratio (e) and the critical-state void ratio ($e_{cs}$) for certain value of stress. Denser soils have negative ψ, and loose contractive soils have positive ψ. Monotonic drained and undrained simple shear tests could be applied to extract soil critical state line which is a unique characteristic of a soil. An equation of critical state line, correlating void ratio and vertical effective stress characteristics of a soil is defined as:

$$e_{CS} = \Gamma_{CS} - \lambda_{CS}\, Log\, (\sigma'_{VC}) \qquad (2.4)$$

In which, $\Gamma_{CS}$ is the soil critical void ratio at $\sigma'_{vc}$ (vertical effective stress) = 1 kPa and $\lambda_{cs}$ is the slope of the critical state line in an e - log $\sigma'_{vc}$ plane. This is also shown in Figure 2.9.

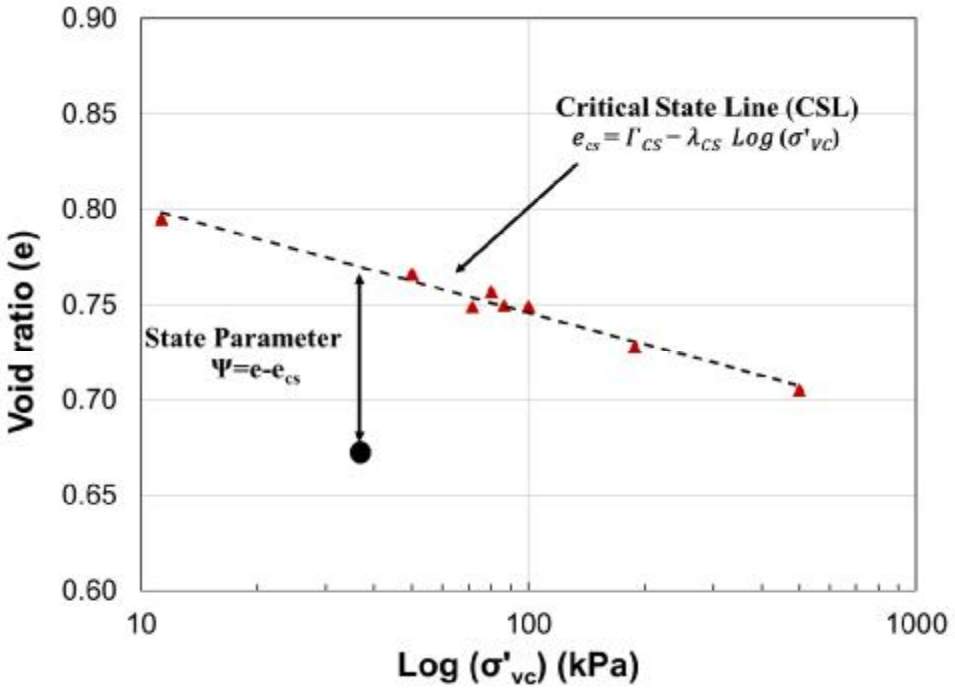


**Figure 2.9: Critical state line introduction and overview of parameters for Boler sand**

Undrained shear strength at the critical state is termed "undrained critical shear strength", $S_{u(critical)}$, which is also the minimum undrained shear strength mobilized in liquefaction flow failures. Sadrekarimi (2013) suggests characterization of $S_{u(critical)}$ by using $S_{u(critical)}/ \sigma'_{vc}$. For strain-hardening sands ($\Psi < 0$), $S_{u(critical)}$ exceeds the drained shear strength due to negative excessive pore-water pressure (suction) generation, whereas in real field conditions cavitation will occur (Brandon et al. 2006) and limits $S_{u(critical)}$ to the drained critical strength ratio (= tan $\Phi'cs$, $\Phi'cs$ = Critical state friction angle). Sadrekarimi (2013) illustrates that $\Psi$ has a considerable impact on $S_{u(critical)}/ \sigma'_{vc}$. Therefore, beside e-$e_c$, also N ($e_c$ at $\sigma'_{vc}$ = 1 kPa) has a large impact on $S_{u(critical)}/ \sigma'_{vc}$. The magnitude of N depends on sand fabric developed during specimen preparation in the laboratory, or in-situ (Sadrekarimi, 2013). He collected numerous data from case histories of field liquefaction flow failures and laboratory experimental data and verified critical state soil mechanics application in sandy soils liquefaction. He also proposed a correlation between sands state parameters and their strength parameters (friction

angle and undrained strength) at liquefaction. Sands compressibility, critical state parameters, and effective stress were reported the most effective parameters on soil undrained strength in the critical state, unlike soil variation of soil critical state friction angle that seems to be less impacting (Sadrekarimi, 2013). In another research study, Sadrekarimi and Olson demonstrated the effects of initial soil fabric and particle characteristics by testing a variety of samples under different sample preparation methods (Sadrekrimi and Olson, 2013).

### 2.2.6. Cyclic DSS tests

Similar mechanisms that were identified in monotonic loading, can be identified in cyclic loading as well. A progressive increment of pore water pressure and deformation could be observed with increasing number of shearing cycles. A contractive (strain softening) behaviour for loose samples which may be followed by cyclic mobility for medium dense sands (called phase transformation) and finally a complete dilative behavior and cyclic mobility as a response of denser sands have been realized in several past researches.

In the current study, constant-volume cyclic simple shear tests were carried out to determine the cyclic response and liquefaction behavior of Boler sand. Similar to the constant-volume monotonic tests, a constant-volume condition was imposed in these tests by precisely adjusting the vertical stress. Stress-controlled shearing was performed by cycling shear stress within a certain range of stresses at a frequency of 0.1 Hz. Cyclic stress ratio (CSR) is determined as the ratio of the peak shear stress ($_{max}$) to $\sigma'_{vc}$.

Figure 2.10 illustrates the stress-strain response and effective stress path of typical obtained results for mono-directional cyclic loading. Gradual drop in vertical effective stress which is equivalent to rise in pore water pressure in low strain cycles and jumping shear strain with dissipating vertical effective stress is observed in samples. This is a typical result for both dense and loose samples under undrained cyclic shear loads. The number of cycles before undergoing large shear strains differ for various samples depending on their relative density and initial vertical effective stress which will be discussed in the results.

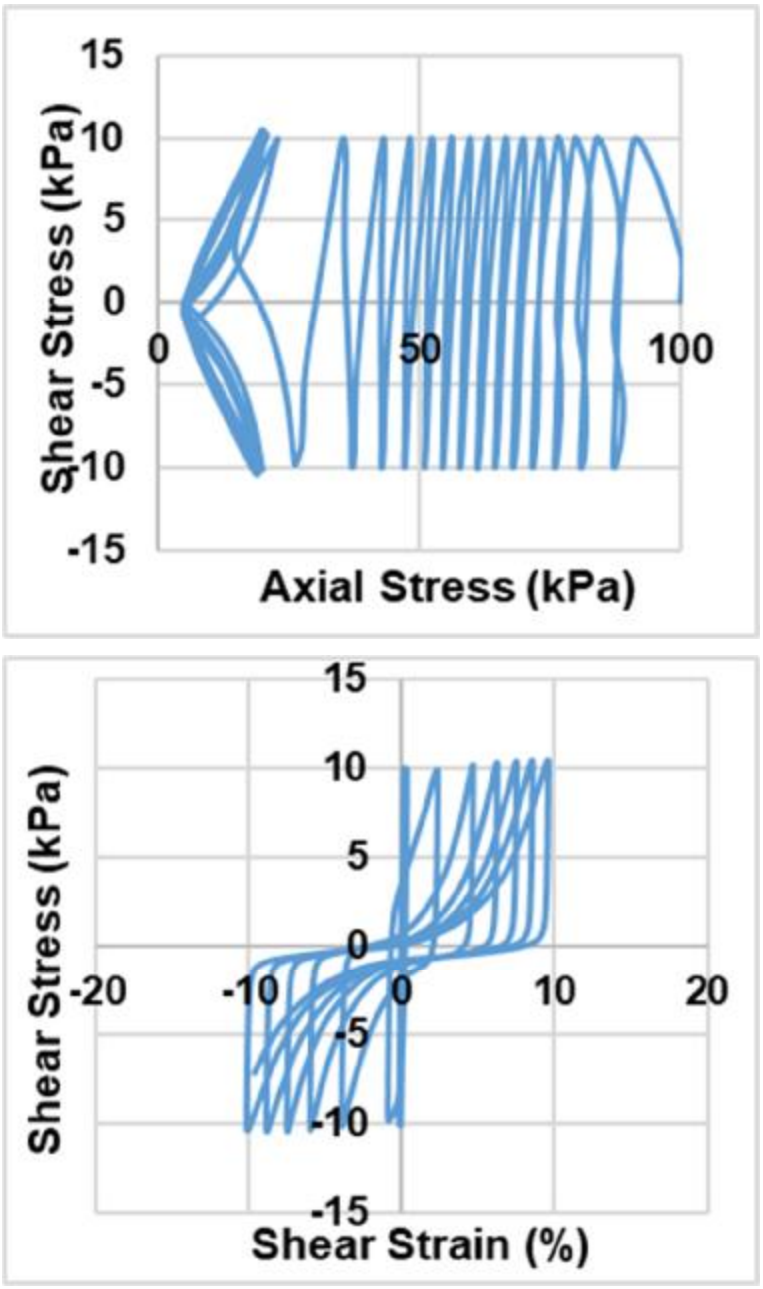


**Figure 2.10: Typical respons of Boler sand in mono-directional cyclic simple shear tests**

Table 2.6 summarizes the characteristics of mono-directional cyclic simple shear tests which was used for analysis of this chapter. Further cyclic test results (including diverse bi-directional cyclic load patterns) which are not applicable in this chapter, will be completely introduced and discussed in next chapter of the thesis.

**Table 2.6: Summary of mono-directional cyclic simple shear tests**

| $\sigma'_{vc}$ (kPa) | Avg. $e_c$ | Avg. $D_{rc}$ (%) | Test Type | Freq. (Hz) | CSR values |
|---|---|---|---|---|---|
| 50 | 0.764 | 25.3 | M | 0.1 | 0.062 - 0.071 - 0.080 |
| 100 | 0.764 | 25.3 | M | 0.1 | 0.067 - 0.080 - 0.090 |
| 200 | 0.768 | 24.1 | M | 0.1 | 0.080 - 0.090 - 0.100 |
| 400 | 0.769 | 23.8 | M | 0.1 | 0.090 - 0.100 - 0.110 |
| 600 | 0.763 | 25.6 | M | 0.1 | 0.100 - 0.110 - 0.125 |
| 50 | 0.701 | 45.0 | M | 0.1 | 0.073 - 0.082 - 0.094 |
| 100 | 0.700 | 45.3 | M | 0.1 | 0.083 - 0.097 - 0.103 |
| 200 | 0.706 | 43.4 | M | 0.1 | 0.08 - 0.102 - 0.112 |
| 400 | 0.709 | 42.5 | M | 0.1 | 0.122 - 0.131 - 0.151 |
| 600 | 0.694 | 47.2 | M | 0.1 | 0.131 - 0.141 - 0.161 |
| 50 | 0.643 | 63.1 | M | 0.1 | 0.047 - 0.071 - 0.093 |
| 100 | 0.635 | 65.6 | M | 0.1 | 0.079 - 0.095 - 0.105 |
| 200 | 0.639 | 64.4 | M | 0.1 | 0.104 - 0.118 - 0.132 |
| 400 | 0.634 | 65.9 | M | 0.1 | 0.122 - 0.137 - 0.151 |
| 600 | 0.633 | 66.3 | M | 0.1 | 0.141 - 0.152 - 0.191 |

### 2.2.7. Shear wave velocity measurement

Shear wave velocity of the specimens was measured by a pair of piezoelectric bender elements embedded with epoxy into the platens of the DSS apparatus. The epoxy-coated bender elements protruded 1 mm into the specimen. Marjanovic and Germaine (2013) show that this bender element setup (shorter and wider tips) produces the best shear waves without significant interference from compression waves. A sinusoidal pulse was applied to the transmitting bender element, which provides high versatility in selecting a signal frequency and amplitude (compared to square waves). A high voltage of ±14 Volts was chosen to improve the signal to noise ratio. Taller specimens of 30 mm high were prepared for measuring shear wave velocity ($V_S$) to increase $V_S$ travel distance and improve signal resolution. Shear wave velocity was measured after allowing about 30 minutes of consolidation at $\sigma'_{vc}$. Earlier studies (Lee and Santamarina, 2005, Sanchez-Salinero, et al., 1986, Viggiani and Atkinson, 1995) have often recommended wavelengths ($\lambda$) of at least twice the distance between the bender element tips

($L_{tt}$) to reduce near-field effects and allow for the development and propagation of shear waves. Besides preparing taller specimens (= 30 mm), a high frequency (36 kHz) signal was also used to produce short wavelengths and generate at least 2 wavelengths between the bender elements ($L_{tt}/\lambda > 2$). The high signal frequency used in the bender element tests further minimized dispersion from wave reflections at specimen boundaries (Alvarado and Coop 2012). Table 2.7 summarizes the characteristics of shear wave velocity measurement samples of this study. Total of 15 samples in 3 different relative densities under 5 different consolidation stresses was used for analysis. Three different frequencies were applied for bender elements to obtain the most accurate results. Although the difference of result for different frequencies were negligible, wavelength ratio criteria of $L_{tt}/\lambda > 2$ was met in all of the experiments and a 50-kHz frequency was selected for results.

**Table 2.7: Summary of characteristics for shear wave velocity measurement tests**

| $\sigma'_{vc}$ (kPa) | Avg. $D_{rc}$ (%) | Freq. 1 (kHz) | Freq. 2 (kHz) | Freq. 3 (kHz) |
|---|---|---|---|---|
| 50 | 25 | 35.7 | 50 | 83.3 |
| 50 | 45 | 35.7 | 50 | 83.3 |
| 50 | 65 | 35.7 | 50 | 83.3 |
| 100 | 25 | 35.7 | 50 | 83.3 |
| 100 | 45 | 35.7 | 50 | 83.3 |
| 100 | 65 | 35.7 | 50 | 83.3 |
| 200 | 25 | 35.7 | 50 | 83.3 |
| 200 | 45 | 35.7 | 50 | 83.3 |
| 200 | 65 | 35.7 | 50 | 83.3 |
| 400 | 25 | 35.7 | 50 | 83.3 |
| 400 | 45 | 35.7 | 50 | 83.3 |
| 400 | 65 | 35.7 | 50 | 83.3 |
| 600 | 25 | 35.7 | 50 | 83.3 |
| 600 | 45 | 35.7 | 50 | 83.3 |
| 600 | 65 | 35.7 | 50 | 83.3 |

## 2.3. Test results

### 2.3.1. Monotonic drained and constant-volume simple shear tests

Constant-volume shear was replicated by maintaining a constant specimen volume. This was performed using the electronic feedback and control system of the DSS apparatus by precisely adjusting the vertical stress to prevent any volume change during shearing. Volume change resulted from changes in specimen height as the area of the specimen was kept constant by the stainless-steel rings. Since pore water pressure was not measured in the DSS apparatus, the top drainage port was left open during shearing. Changes in total vertical stress during constant-volume shear were considered as an equivalent excess pore water pressure which would have developed in an undrained shear test (Dyvik, et al., 1987).

Monotonic shearing was carried out at a shear strain rate of 3% / hour up to a shear strain of 30%. Both strain hardening (dilative) and softening (contractive) behavior could be diagnosed from the results of constant-volume tests which is shown in plots of Figure 2.11. As it is clearly shown in Axial stress plot, the majority the tests terminated in a critical state in the range of applicable strains and regarding their state (relative density and initial consolidation stress). The majority of tests display a significant strain-softening and static liquefaction behavior. A reduction in vertical effective stress $\sigma'_{vc}$ is assumed to be equivalent to the shear-induced pore pressure generated in an undrained condition for each test. In drained shear tests, a constant effective vertical stress (= $\sigma'_{vc}$) was maintained while changes in specimen height were carefully recorded to determine void ratio changes. The results of drained shear tests are shown in Figure 2.12. Both strain hardening (dilative) and softening (contractive) behavior could be diagnosed from the results which are shown in plots. As it is clearly shown in volumetric strain plot, a few of the tests terminated in a critical state in the range of applicable strains and regarding their state (relative density and initial consolidation stress).

Shearing under strain rate of 0.1 - 0.2 mm/min has been reported in several studies as the maximum shearing rate to prevent pore water pressure generation resulting in a partially drained condition in soils (Horn, 1964). A high possibility of undrained condition in the rates equal and above 0.5 mm/min shearing strain rate has been reported (Thermann et al., 2006). Also, according to ASTM D6528, (Standard test method for consolidated undrained direct

simple shear testing of fine grain soils) most of the practical direct simple shear experiences are based on strain rate of 5% / hour. In the current study, although higher drainage rate is expected from a sand compared to a clayey soil, small rate of shearing (0.01 mm/min) was selected in performing tests to prevent any eventual generation of pore water pressure and undrained condition. Drained water could be directed out of samples by the performance of porous platens enclosing the soil sample from top and bottom and considering a relatively small height (20 mm) to large diameter (70.1 mm) of samples.

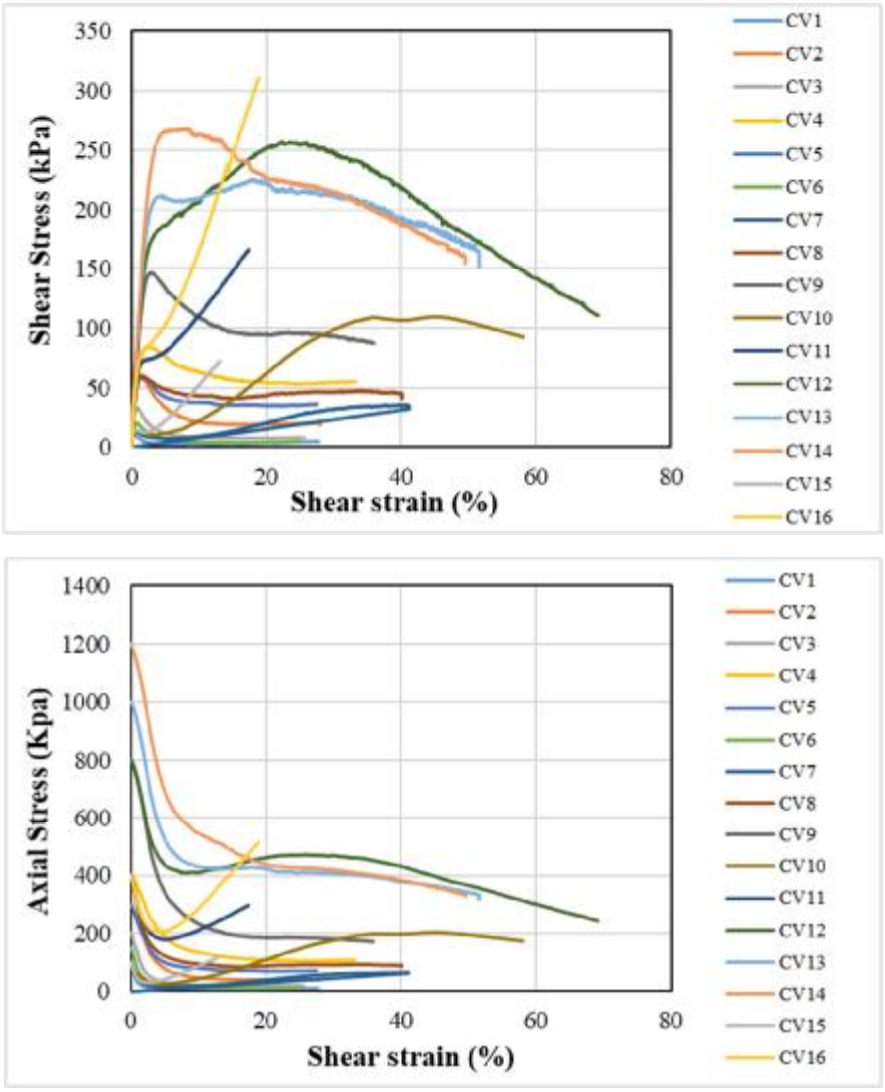


**Figure 2.11: Monotonic constant-volume simple shear test results for Boler sand**

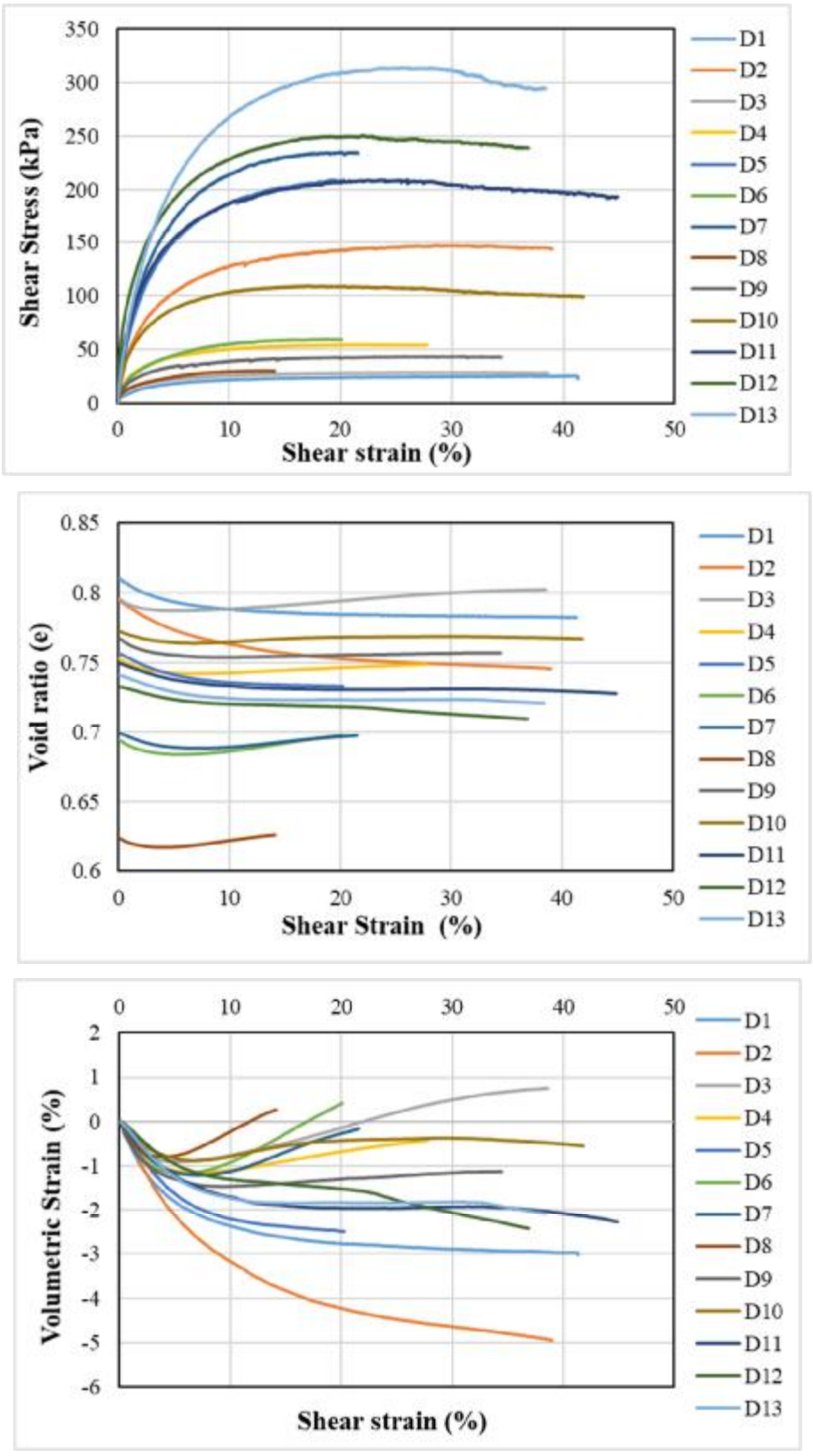


**Figure 2.12: Monotonic drained simple shear test results for Boler sand**

### 2.3.2. Critical state line location

As it was discussed in previous sections, only some of the samples reached a critical state point for the range of applied strains and according to their initial state. Table 2.8, summarizes the tests which were clearly reaching a critical state and were selected for the establishment of the critical state line of Boler sand.

**Table 2.8: Summary of selected monotonic DSS tests (for CSL establishment)**

| $\sigma'_{vc}$ (kPa) | $e_c$ | $D_{rc}$ (%) | $e_{cs}$ | $\sigma'_{v,cs}$ (kPa) | Drainage |
|---|---|---|---|---|---|
| 100 | 0.762 | 26 | 0.762 | 40.8 | Constant Volume |
| 100 | 0.802 | 13 | 0.802 | 11.3 | |
| 200 | 0.809 | 11 | 0.809 | 19.6 | |
| 300 | 0.778 | 21 | 0.778 | 41.5 | |
| 300 | 0.763 | 26 | 0.763 | 71.8 | |
| 400 | 0.75 | 30 | 0.75 | 86.6 | |
| 800 | 0.728 | 37 | 0.728 | 187 | |
| 1000 | 0.706 | 43 | 0.706 | 346 | |
| 1200 | 0.697 | 46 | 0.697 | 421 | |
| 50 | 0.812 | 10 | 0.782 | 50 | Drained |
| 80 | 0.77 | 23 | 0.758 | 80 | |
| 100 | 0.753 | 29 | 0.753 | 100 | |
| 400 | 0.699 | 46 | 0.697 | 400 | |

The critical state is taken at the minimum shear stress reached after failure, although some tests displayed “phase transformation” (Ishihara, 1993) to a strain-hardening (or dilative) behavior after an extended range of constant volume, shear, and effective vertical stresses. An overall frictional angle of $\Phi'_{cs} = 30^{o}$ is determined at the critical state from both constant-volume and drained tests. Table 2.8 shows void ratio ($e_{cs}$) and effective vertical stress ($\sigma'_{v,cs}$) at the critical state of both drained and constant-volume shear tests. These data are plotted in Figure 2.13 to establish the CSL for Boler sand as below:

$$e_{CS} = 0.888 - 0.071\ Log\ (\sigma'_{VC}) \quad (2.5)$$

This equation suggests a critical void ratio of 0.888 at an effective stress of $\sigma'_{vc}$ = 1 kPa and a critical state line slope of 0.071. CSL of Boler sand is comparable to those for Monterey #0 sand (Jefferies and Been, 2006) and Hokksund sand (Castro, 1969) determined from isotropically-consolidated triaxial compression shear tests. These are compared in Figure 2.13 assuming a horizontal stress ratio of $K_o$ = 0.5 for the converting isotropic effective confining stress (in triaxial tests) to $\sigma'_{vc}$.

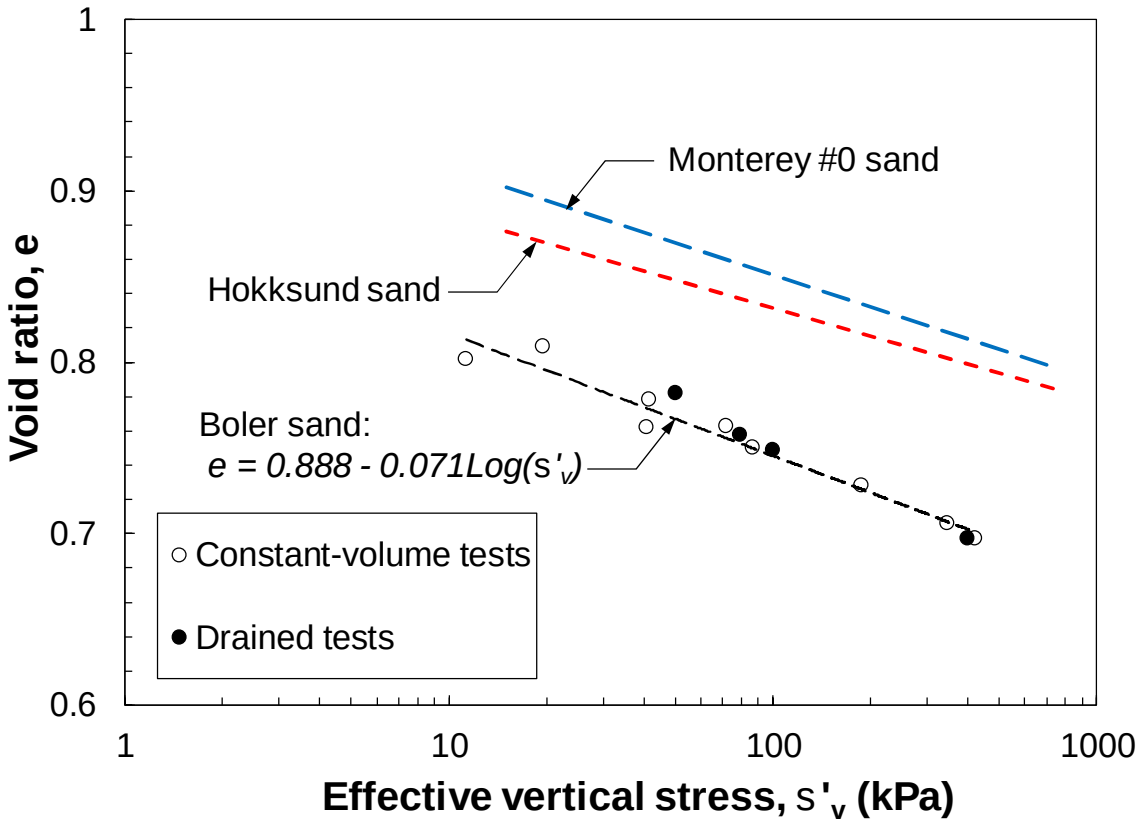


**Figure 2.13: Critical state lines of Boler (from this study), Hokksund (Castro, 1969), and Monterey #0 (Jefferies and Been, 2006) sands**

### 2.3.3. Shear wave velocity measurement

Bender elements are piezoelectric cantilever beam-shaped transducers which either bend by an applied voltage or produce a voltage when it is bent. Despite their simple operation, the interpretation of bender element pules can be complicated. While the wave travel distance can be confidently taken as the tip-to-tip distance ($L_{tt}$) between the bender elements (Brignoli, et

al., 1996, Viggiani and Atkinson, 1995), identifying the correct travel time is often challenging. Various time and frequency domain methods (Jovicic, et al., 1996, Lee and Santamarina, 2005) are suggested by different researchers to determine travel time. Shear wave propagation through soil sample from a source to a receiver bender element is shown in Figure 2.14.

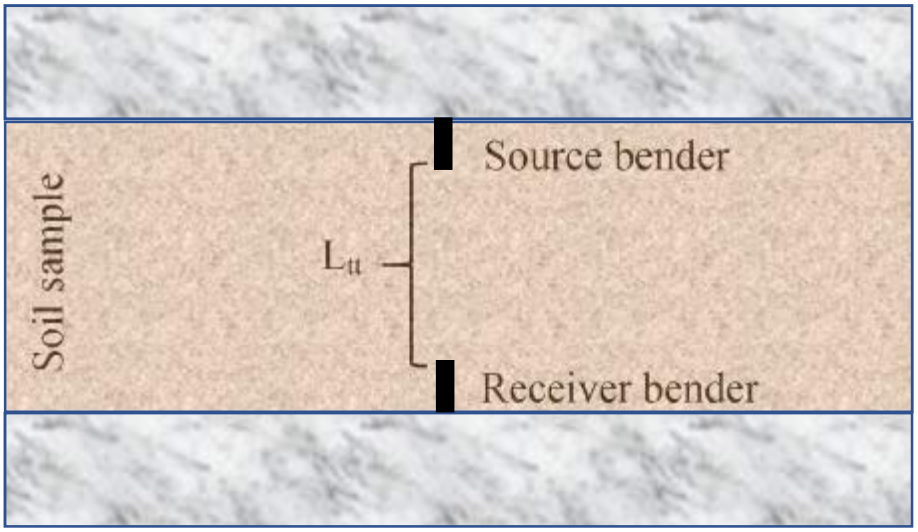


**Figure 2.14: Shear wave (S wave) propagation in soil sample**

Figure 2.15 illustrates the transmitted and received shear waves for the experiments. The reverse polarity of the initial small bumps is a characteristic of near-field effects and compression waves generated from the lateral vibration of the bender elements. These compression-wave signals travel faster and reach the receiving bender element earlier than a shear wave, but rapidly decay in subsequent reflections from the endcaps (Camacho-Tauta, et al., 2015).

Low amplitude pulses in the received signal have been observed in other bender-element studies (Arulnathan, et al., 1998, Brandenberg, et al., 2008, Brignoli, et al., 1996), which are often associated with distorted compression waves reflected from the specimen boundaries. These were thus disregarded. The tip-to-tip distance between the bender elements ($L_{tt}$) was measured by subtracting the height of the bender elements from the specimen height.

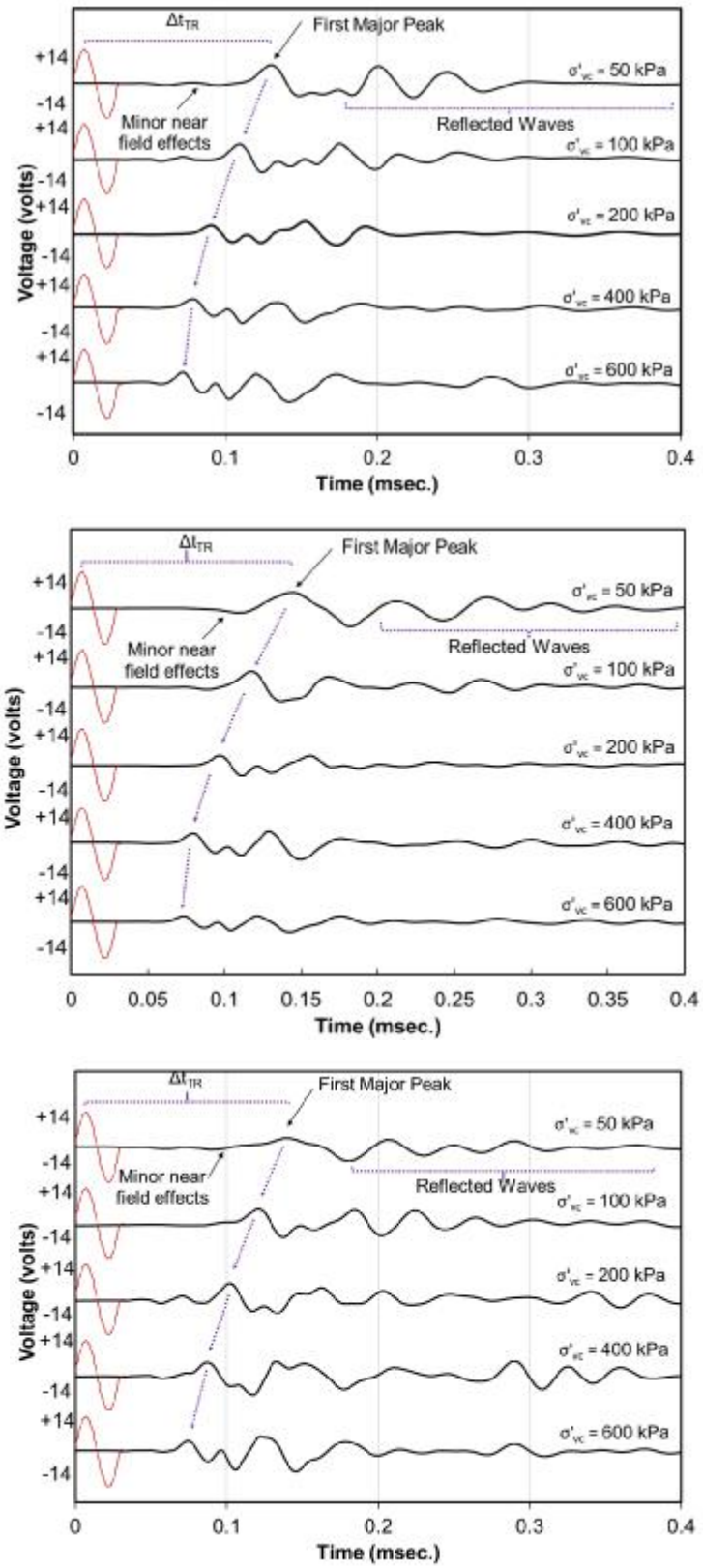


**Figure 2.15: Shear wave signals for specimens (top to bottom; $D_{rc}$ = 25, 45, 65%)**

Almost all obtained output signals in the present study exhibited a clear major peak (shear-wave). Hence, the peak-to-peak time of the first transmitted and received signals was used to measure travel time ($\Delta t_{TR}$) and determine $V_S$. Several investigators suggest that this approach can provide an accurate measurement of $V_S$ (Brignoli, et al., 1996, Camacho-Tauta, et al., 2015, Jovicic, et al., 1996, Lee and Santamarina, 2005, Viggiani and Atkinson, 1995, Yamashita, et al., 2009) which match well with $V_S$ measured by other laboratory techniques (e.g., resonant column tests, acceleration measurements, etc). For example, Yamashita et al. (2009) found that the peak-to-peak time difference between transmitted and received signals provided the most consistent determination of $V_S$ travel time using bender elements among 23 different laboratories around the world. Accordingly, $V_S$ was determined as $\Delta t_{TR}/L_{tt}$.

Measurements carried out at higher input frequencies (50 & 83 kHz) results in similar travel times and $V_S$, suggesting that $V_S$ remains unaltered by changes in input frequency. Shear wave velocity is often expressed as a function of void ratio, F(e) and effective confining pressure ($\sigma'_c$) as below (Hardin and Richart Jr., 1963):

$$Vs\left(\frac{m}{s}\right) = F(e).{\sigma'_C}^{\beta} \tag{2.6}$$

Where exponent $\beta$ is a material constant which reflects the nature of inter-particle contacts (Santamarina, et al., 2001). For the $K_o$-consolidated simple shear samples of this study, $\sigma'_c$ can be approximated as $(1+2K_o)\ \sigma'_{vc}$. Because of the difficulties in determining $K_o$ in the field, it is simpler to express $V_S$ as a function of $\sigma'_{vc}$. The influence of effective stress on any soil parameter is usually considered in geotechnical engineering practice by normalization to $\sigma'_{vc}$ = 100 kPa. Like the overburden stress correction used for SPT or CPT penetration resistances, Equation (2.7) is used to account for the effect of overburden pressure on $V_S$.

A normalized shear wave velocity ($V_{S1}$) corresponding to $\sigma'_{vc}$ = 100 kPa is often calculated as equation 2.7 where $P_a \approx 100$ kPa. According to Figure 2.16, irrespective of $D_{rc}$ the typical stress exponent of $\beta = 0.25$ (Hardin and Richart Jr., 1963, Kayen, et al., 2013, Robertson, et al., 1992) fits $V_S$ profile for Boler sand quite well. Several studies (Hardin and Richart Jr., 1963,

Robertson, et al., 1995) suggest a linear variation of F(e) with the void ratio. As shown in Figure 2.17, the $V_S$ data of this study also indicate an approximately linear relationship for F(e) which is quite close to the relationship derived by Hardin and Richart Jr. (1963). Figure 2.17 further suggests a slightly decreasing trend of F(e) and thus $V_S$ with increasing void ratio (like Hardin and Richart 1963). Similar to Boler sand, some other studies also report a narrow range of $V_S$ for a wide range of void ratios (Cha, et al., 2014, Roe, 1981, Santamarina, et al., 2001). According to Figures 2.16 and 2.27, Equation 2.8 is a proper fit for Boler sand to correlate shear wave velocity variation with void ratio and vertical effective stress.

$$V_{S1} = V_S.\left(\frac{P_a}{\sigma'_{VC}}\right)^{\beta} \tag{2.7}$$

$$V_S\left(\frac{m}{s}\right) = (89.4 - 26.6e_C)\sigma'^{0.25}_{VC} \tag{2.8}$$

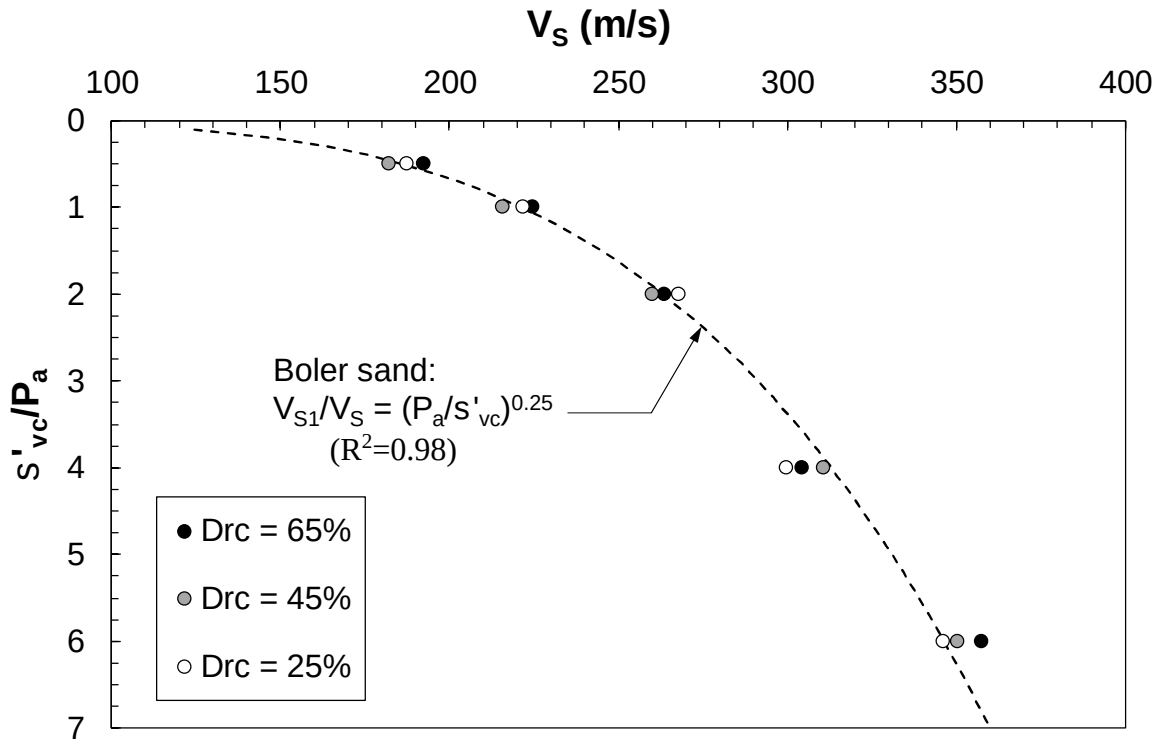


**Figure 2.16: Variation of $V_S$ with normalized $\sigma'_{vc}$ for Boler sand**

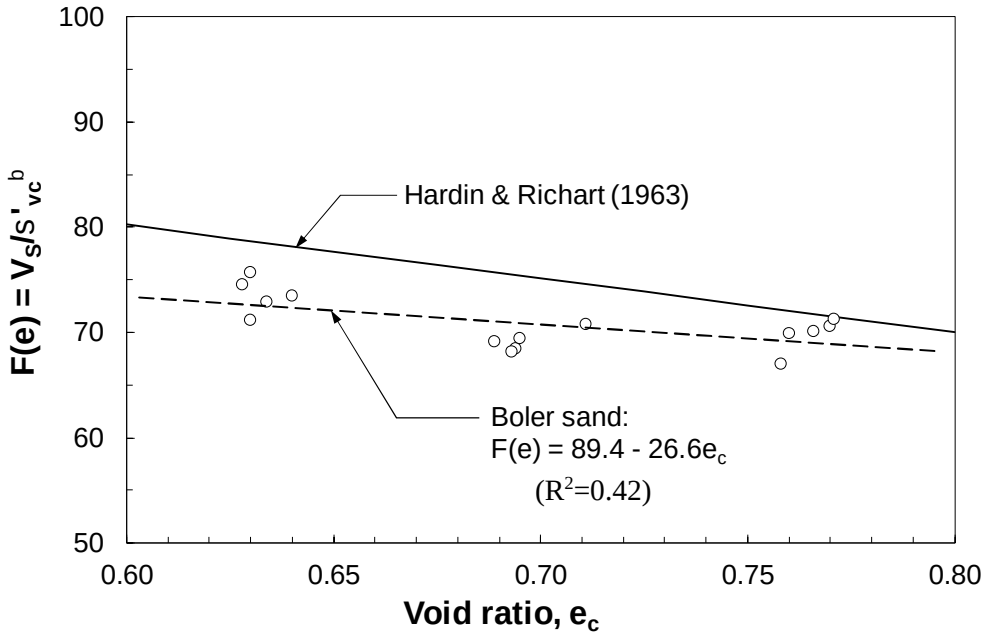


**Figure 2.17: Variation of F(e) with consolidation void ratio ($e_c$) from this study for Boler sand and comparison with the correlation derived by Hardin and Richart (1963)**

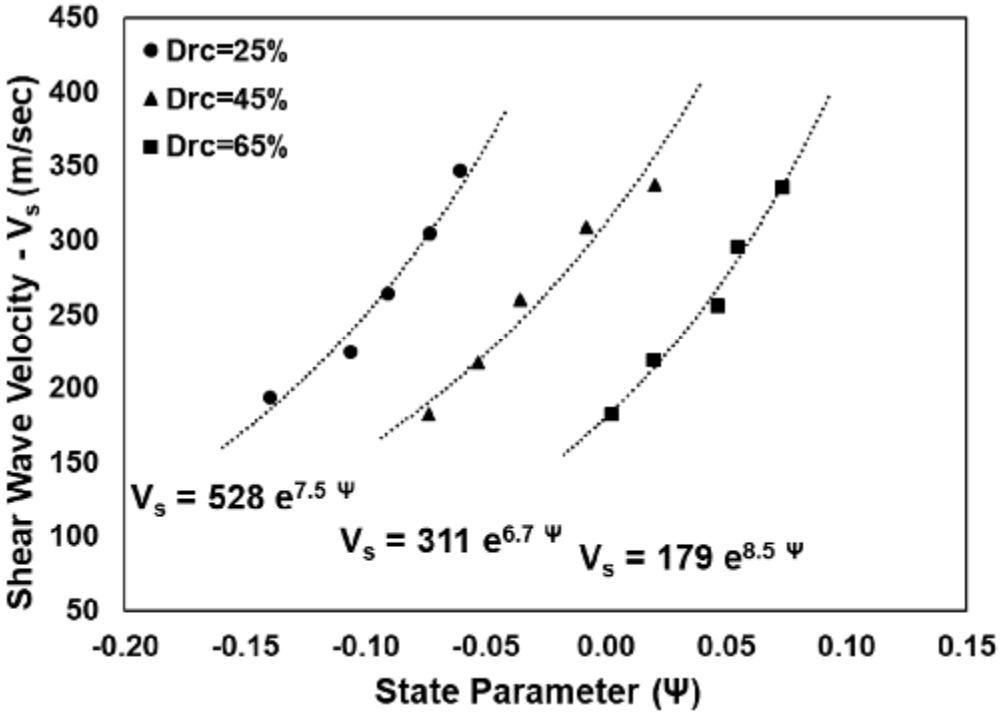


**Figure 2.18: Shear wave velocity ($V_S$) versus state parameter (Ψ) from the DSS tests**

As both the shearing behavior (e.g. in Fig. 2.12) and $V_S$ (in Figs. 2.17 & 2.18) of Boler sand are affected by $e_c$ and $\sigma'_{vc}$, $V_S$ can be used to determine the liquefaction susceptibility and strain-softening potential of Boler sand. Figure 2.18 presents the variations in state parameter (determined from Eq. 2.5 and definition given in Figure 2.9) with $V_S$ data for the specimens tested in this study.

### 2.3.4. Evaluation of maximum shear modulus ($G_{max}$)

As discussed in the introduction, calculation of small-strain or maximum shear modulus of a soil is one of the main purposes of measuring shear wave velocity. $G_{max}$ is a useful and practical parameter for engineering design purposes which correlates soil deformation properties to applied stress. $G_{max}$ is calculated for the specimens of this study using Equation 2.1.

As shown in Figure 2.19, $G_{max}$ largely increases with increasing $\sigma'_{vc}$ for a particular $e_c$, whereas the effect of $e_c$ seems to be secondary. It can be explained that increasing $\sigma'_{vc}$ not only raises $\rho$ but also decreases the propagation distance between the bender elements ($L_{tt}$), resulting in a greater $V_S$ and hence $G_{max}$. Several empirical correlations have been developed for $G_{max}$ characterization, all of which consider void ratio and effective stress as in the following form (Hardin and Richart Jr., 1963, Jamiolkowski, et al., 1991):

$$\frac{G_{max}}{P_a} = AF'(e).\left(\frac{\sigma'_{VC}}{P_a}\right)^n \tag{2.9}$$

Where n is a stress exponent often equal to 0.5 (= 2β). Equation 2.9 and in particular F'(e) have been fitted to experimental data by many investigators. Similar to $V_S$, a linear relationship appears to fit F'(e) for the experiments of this study in Figure 2.20. For the normally-consolidated DSS specimens, $K_o = 0.5$ is used for converting $\sigma'_{vc}$ to $\sigma'_c$. According to Figure 2.20, the normalized $G_{max}$ ($= G_{max}/\sigma'^{n}_{c}P_a^{1-n}$) data are within the ranges of AF'(e) relationships proposed by several other studies (Hardin, 1978, Iwasaki, et al., 1978, Kokusho, 1980) for clean sands.

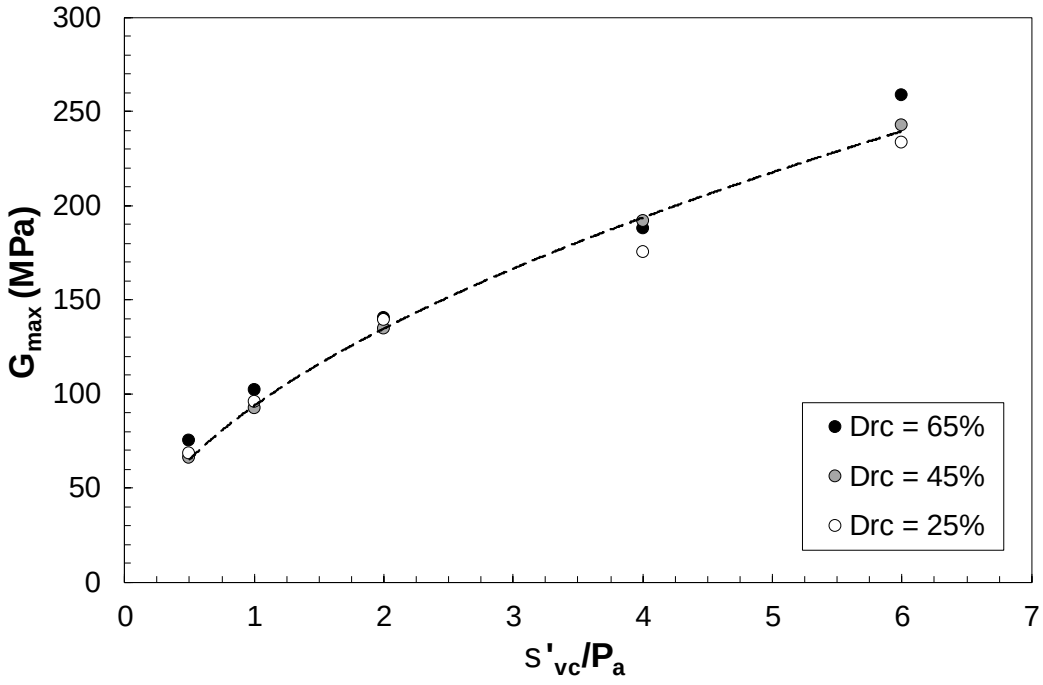


**Figure 2.19: Variation of $G_{max}$ with $\sigma'_{vc}$ for Boler sand at $D_{rc}$ = 25, 45, and 65%**

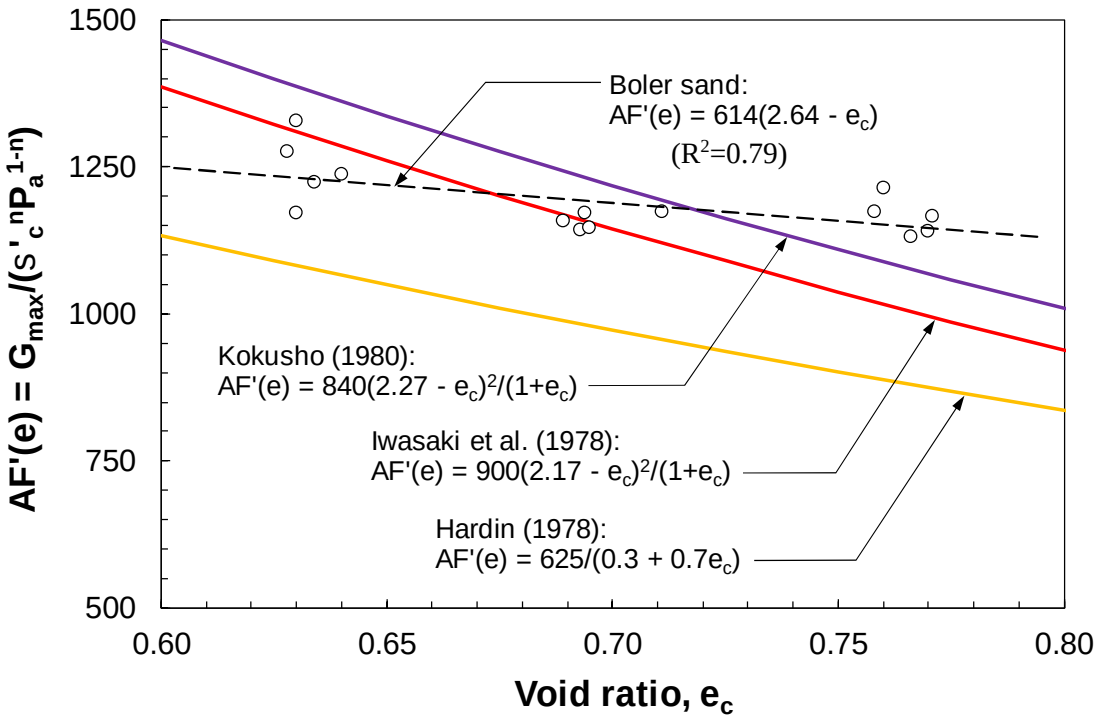


**Figure 2.20: Variations of AF'(e) with $e_c$ for Boler sand and suggested values by several other studies (Hardin 1978; Iwasaki et al. 1978; Kokusho 1980) for clean sands**

### 2.3.5. Mono-directional cyclic simple shear test results

Mono-directional cyclic simple shear tests were carried out to determine the cyclic liquefaction behavior of Boler sand. Figure 2.21 shows typical results of the cyclic DSS tests of this study. According to these plots, liquefaction is triggered when excess pore pressure ratio ($r_u$) exceeds 90%. This corresponded to reaching a double-amplitude cyclic shear strain of 7.5% in the DSS tests. This is essentially equivalent to the liquefaction definition (Vaid and Sivathayalan, 1996) of 5% double-amplitude axial strain in a triaxial test. Liquefaction triggering is followed by a much larger increase in cyclic shear strain and loss of shear stiffness in Figure 2.21.

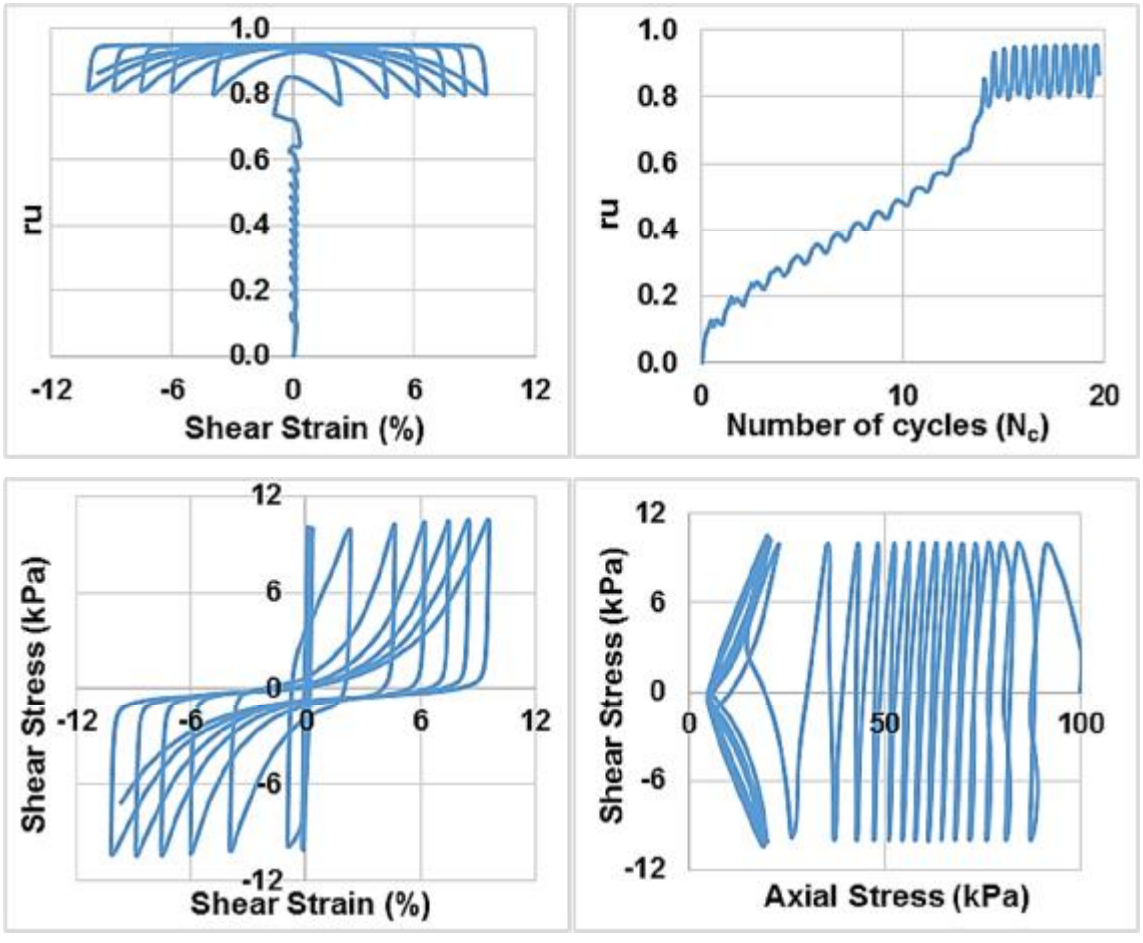


**Figure 2.21: Cyclic test results for a specimen (Drc = 65%, σ'vc = 100 kPa, CSR = 0.1)**

The cyclic stress ratio (= $t_{cyc}/\sigma'_{vc}$) required for liquefaction occurrence in a specified number of loading cycles is called the "Cyclic Resistance Ratio (CRR)". Figure 2.22 shows the number of cycles to triggering liquefaction ($N_L$) at different CSR for specimens consolidated to $\sigma'_{vc}$ = 100 kPa. For an earthquake magnitude of 7.5, CRR is defined as the CSR to cause liquefaction in 15 uniform cycles of shear stress (Seed and Idriss, 1971). In the simplified stress-based approach for liquefaction analysis, seismic demand is calculated as the cyclic shear stress ratio applied by an earthquake (CSR) and the cyclic resistance ratio (CRR) of the soil (capacity) is estimated from a correlation with an in-situ test. Earthquake-induced CSR can be estimated using the Seed and Idriss (1971) simplified procedure or numerical methods such as finite element method based seismic response analysis. The simplified procedure provides CRR of a level-ground (no shear stress bias) for an effective overburden pressure of 100 kPa.

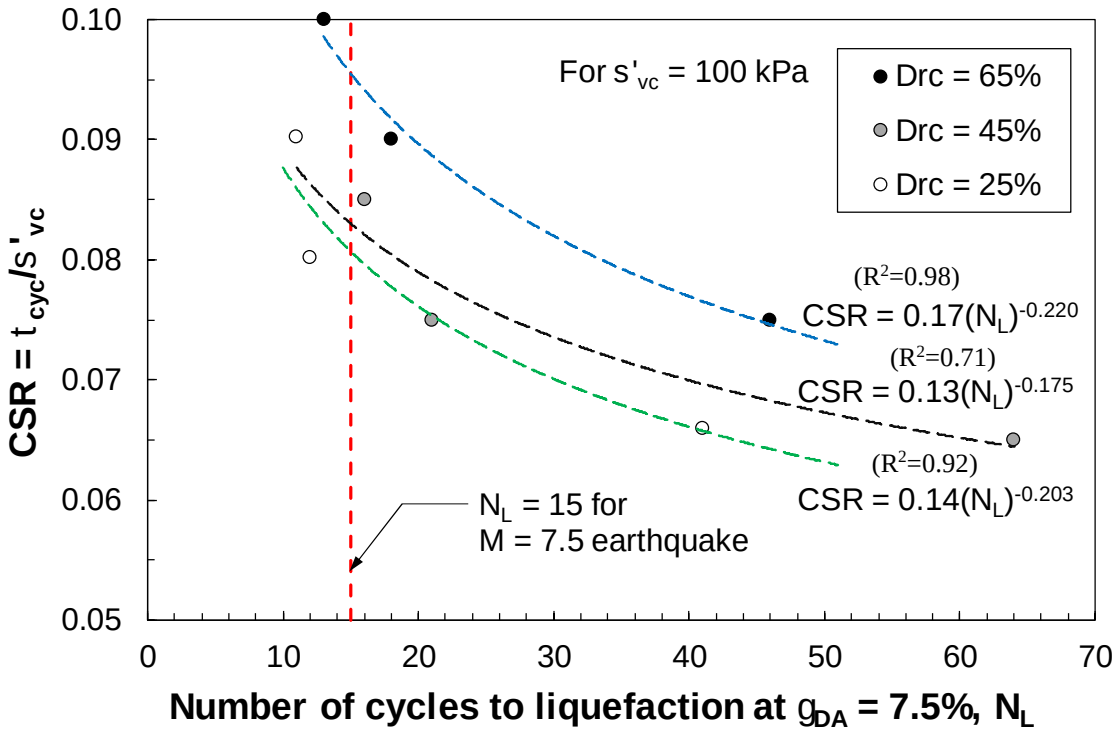


**Figure 2.22: CSR VS no. of cycles to trigger liquefaction of Boler sand at $\sigma'_{vc}$ = 100 kPa**

Cyclic liquefaction is deemed to occur when CSR exceeds CRR. Semi-empirical relationships between CRR and SPT or CPT penetration resistance have been extensively studied by many researchers. Determining CRR from in-situ shear wave velocity measurement can be a particularly useful alternative for sites underlain by soils that are difficult to penetrate or extract

undisturbed samples. Robertson, et al. (1992) present one of the earliest boundary curves between liquefaction and non-liquefaction cases using a limited field database. Based on cases of liquefaction and non-liquefaction for 26 earthquakes and more than 70 different sites, Andrus and Stokoe (2000) developed relationships between CRR and $V_{S1}$ which are the current state of practice for evaluating liquefaction potential using $V_{S1}$. Pairs of shear wave velocity ($V_{S1}$) and $CRR_1$ measured from the experiments of this study at $\sigma'_{vc}$ = 100 kPa are compared with these $V_S$-based liquefaction trigging boundaries in Figure 2.23. As illustrated in this plot, Boler sand exhibits lower liquefaction resistance than the field-based liquefaction triggering curves. In other words, the current methods for estimating liquefaction resistance could largely overestimate CRR of Boler sand. This would lead to an unsafe liquefaction analysis. The lower CRR of Boler sand compared to that from field-based CRR curves is possibly associated with the carbonaceous composition of Boler sand as well as differences in the triggering of liquefaction in the laboratory and in the field. Because of the effects of excess pore pressure redistribution and upward flow of water, the triggering of cyclic liquefaction could occur at much smaller cyclic shear strains (≈ 0.06 – 0.12%) in the field (Dobry, et al., 2015). Whereas, liquefaction is determined at a single-amplitude shear strain of 3.75% in laboratory DSS tests.

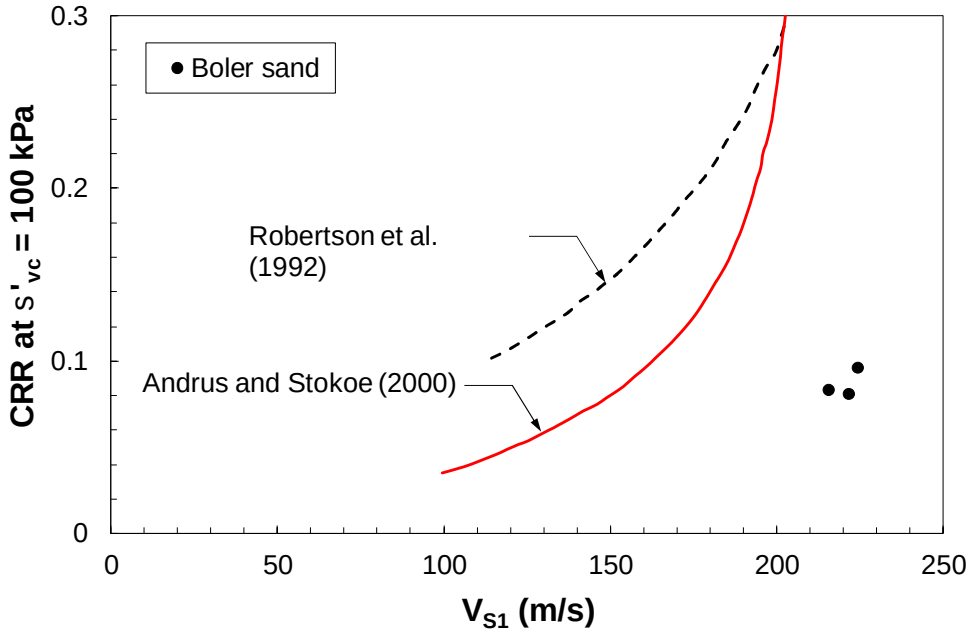


**Figure 2.23: Comparison of $CRR_1$ (at $\sigma'_{vc}$ = 100 kPa) and $V_{S1}$ for Boler sand with liquefaction triggering curves of Andrus and Stokoe (2000) and Robertson et al. (1992)**

### 2.3.6. Evaluation of large strain modulus (G) and degradation curves for Boler sand

As discussed in the previous section, shear wave velocity measurements yield the maximum possible rigidity characteristic of soils (shear modulus, $G_{max}$) which is an important practical property of a soil. This parameter is also called small strain shear modulus which would reflect soil behavior in a very small range of deformations. A general characteristic of a soil which is highly effective in practice relies on variable nature of shear modulus based on the magnitude of deformations (strains) which is called shear modulus degradation (Kramer, 1996).

According to this characteristic, the soil will lose rigidity with increasing deformations which normally happens in the majority of loading such as transferred loads to a foundation from wind or earthquake sources. As defined in section 2.1 of this chapter, secant shear modulus of a soil in each cycle of a cyclic loading and unloading could be generated by calculating the slope of a line, connecting the pick points of a load-deformation curve when the direction of load changes. Damping ratio D (as also shown in Figure 2.2) is also defined as an area enclosed by the first closed hysteresis loop and computed as below (Matasovic and Vucetic, 1993):

$$G_{\gamma_0} = \frac{\tau_0}{\gamma_0} \tag{2.10}$$

$$D = \frac{W_D}{4\pi W_S} \tag{2.11}$$

Where $W_D$ is the energy dissipated in one cycle of loading (the area inside hysteresis loop) and $W_S$ is the maximum strain energy stored in a cycle (area of the triangle). Maximum shear modulus ($G_{max}$) of Boler sand at different states was obtained from the results of bender element tests presented in section 2.34. Based on mono-directional cyclic simple shear tests of this study which were introduced in section 2.3.5, shear modulus (G) and damping ratio (D) of samples under applied cyclic loads were calculated as shown in Figure 2.24 and 2.25.

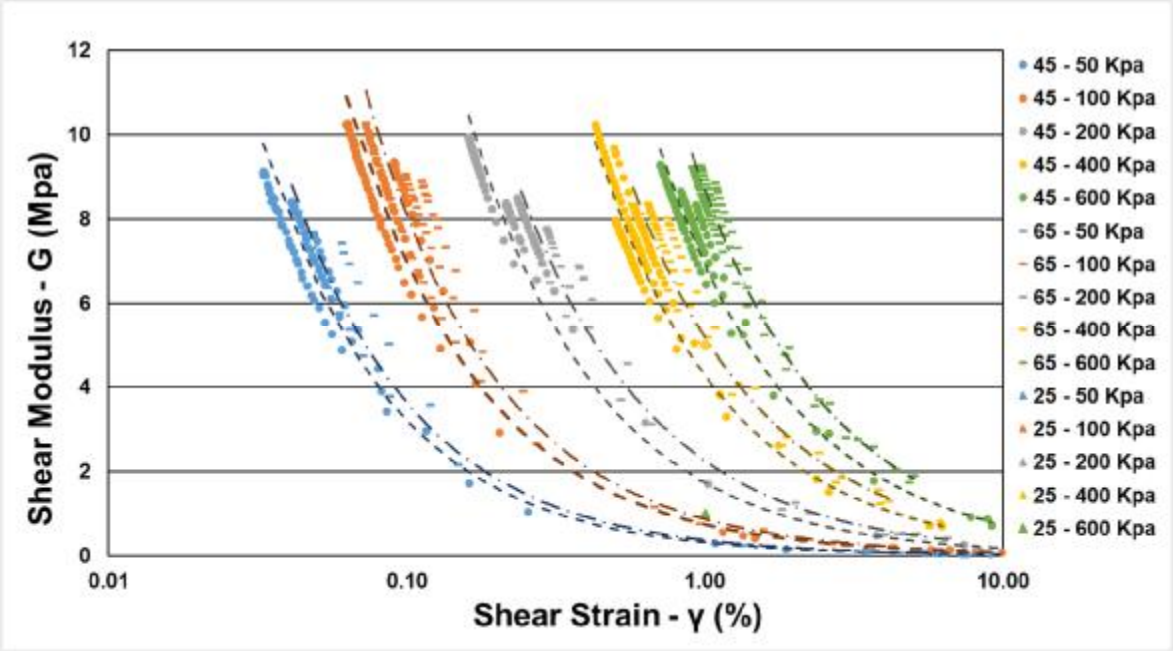


**Figure 2.24: Shear modulus curves for Boler sand samples with $D_{rc}$ = 25, 45, and 65%, $\sigma'_{vc}$ = 50, 100, 200, 400, and 600 kPa**

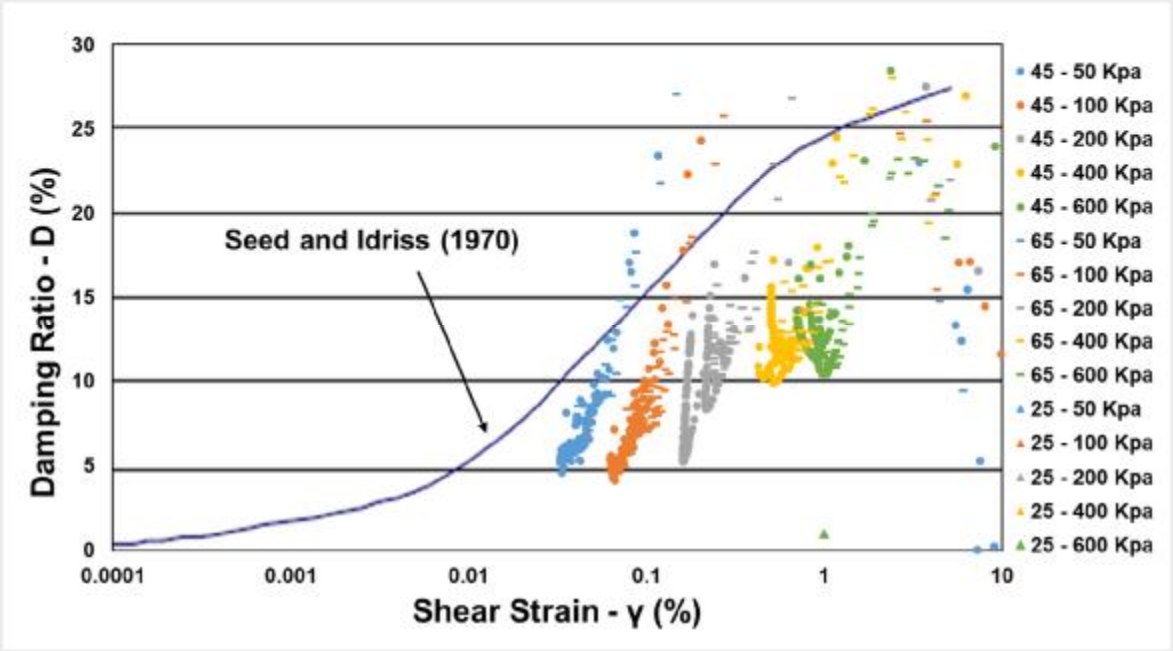


**Figure 2.25: Damping ratio variation for Boler sand samples with $D_{rc}$ = 25, 45, and 65%, $\sigma'_{vc}$ = 50, 100, 200, 400, and 600 kPa**

In Figures 2.24 and 2.25, the increase of damping ratio (D) and decrease (degradation) of shear modulus (G) with increasing strain amplitudes is clearly shown. Relative density and consolidation effective stress dissipation during cyclic loading play the most effective role in shear stiffness degradation and damping ratio of Boler sand samples. Based on the results, shear modulus and damping ratio are stress dependant as shear modulus declines with decreasing effective stresses from 600 kPa (green plotted area) to 50 kPa (blue plotted area) while damping ratio shows an inverse change. Comparing the damping ratio amplification curves with an average curve proposed by Seed and Idriss (1970) for sands, shows lower values in general.However, for shear strains larger than 0.5% (for samples under lower confining stresses $\sigma'_{vc}$ = 50 kPa) to 1.5% (for samples under lower confining stresses $\sigma'_{vc}$ = 600 kPa), there is an increased scatter in data. El Naggar et al. (2007) reported similar scatter in results of centrifuge tests for shear strains larger than 0.5% due to higher frictional energy loss in the soil skeleton as samples experience more contact at larger shear strains.

Relative density is another parameter that controls the range of variation. When samples get denser from 25% to 65%, larger shear moduli are obtained, and degradation curves slightly shift to high shear moduli. These findings are in good accordance with previously reported results by many researchers as Hardin and Kalinsky (2005), Matasovic and Vucetic (1993), Zhang et al. (1993 and 2005), Guzman et al. (1989). Also normalized shear modulus factor ($G/G_{max}$) shown in Figure 2.26, exhibits a close trend to previous studies by Seed et al. (1986), Vucetic and Dobry (1991), and Ishibashi and Zhang (1993). Iwasaki et al. (1978) and Kokoshu (1980) reported influence of effective confining pressure, particularly for low-plastic soils. Slower reduction curve with increasing confining stresses were concluded, which is also schematically shown in Figure 2.26. Under stress-controlled cyclic shear loads, pore water pressure generation and structural changes can cause the stiffness reduction and thus increase in shear strain amplitude due to increasing number of cycles (Kramer, 1996).

It is observed for current study results that at higher consolidation stresses, changes in $G/G_{max}$ reduction is smaller which depicts the fact that, soil sensitivity to stiffness and damping changes gets larger in lower stresses. Iwasaki et al. (1978) and Kokusho et al. (1982) reported a similar conclusion. Also, Ishibashi et al. (1993) and Stokoe et al. (1999) showed that $G/G_{max}$ decreases less with effective stress increases. Although denser samples show stiffer responses relative to looser ones, effect of a density change is relatively small compared to the effect of

consolidation stresses. This could be verified by comparing sample's when consolidation stress or relative density increases. Variations of shear modulus and damping ratio as Drc increases from 25% to 65% is limited to narrow clusters, unlike the change of same parameters when consolidation stress increases.

The current study results are also compared to lower band and upper band curves by Seed et al. (1984, 1986) and Iwasaki et al. (1978) for sands in Figure 2.26 proposed for sands. In this plot, increasing consolidation stress effects for their test results are also shown. Due to the stress-controlled tests of this study, the results only cover strains larger than 0.01% and $G/G_{max}$ less than 0.15. As represented in Figure 2.27 for the portion of test results in this part, a smaller than lower band values relative to suggested bands by Seed et al. (1984, 1986) and Iwasaki et al. (1978) for sands, are visible. A fast-degrading modulus ratio of Boler sand could be verified based on test results which makes this sand more susceptible to pore water pressure generation, confining pressure reduction and finally, a liquefaction occurrence, comparing to empirical correlations proposed by previous studies.

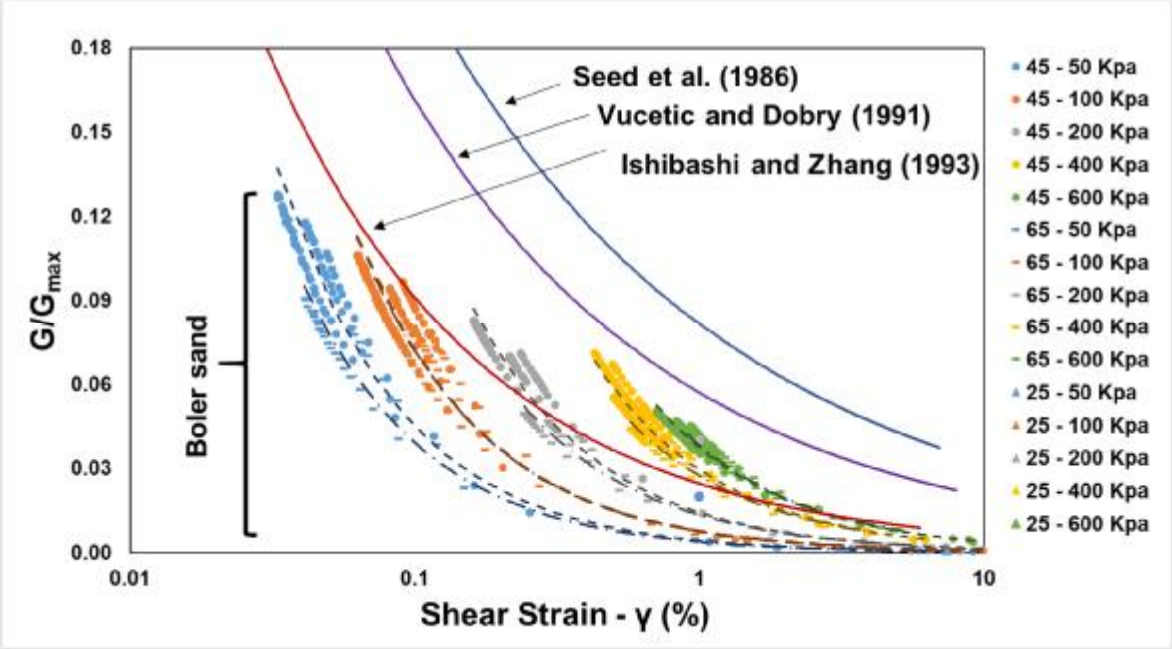


**Figure 2.26: $G/G_{max}$ degradation curves for Boler sand samples with $D_{rc}$ = 25, 45, and 65%, $\sigma'_{vc}$ = 50, 100, 200, 400, and 600 kPa**

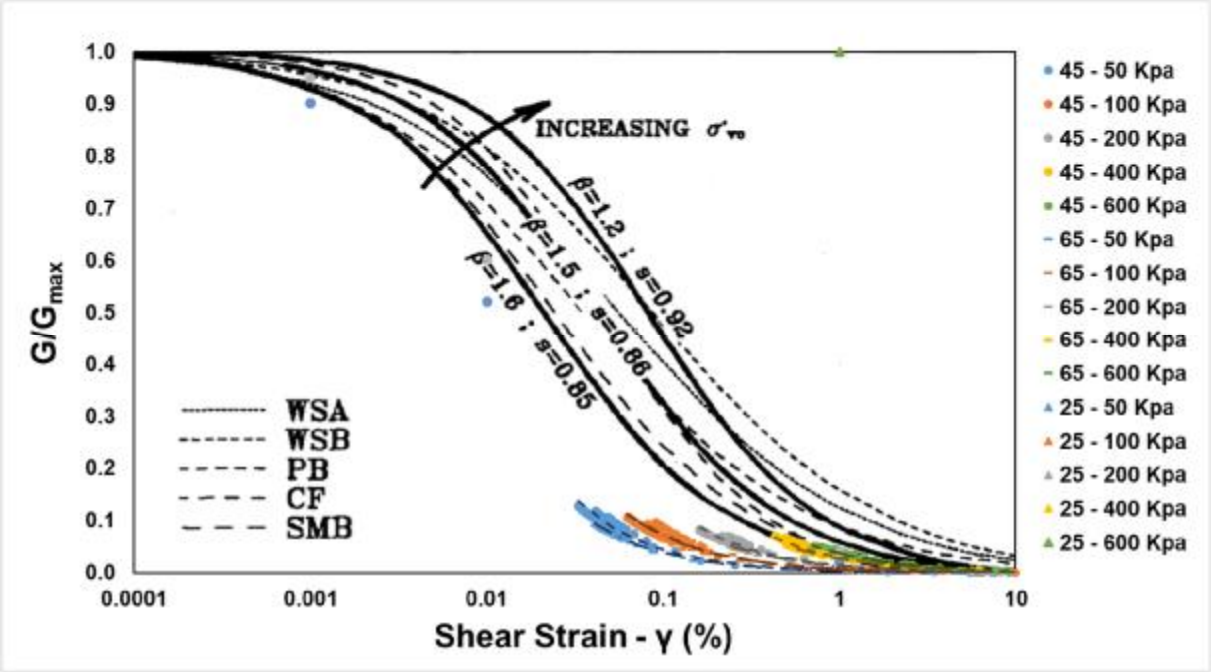


**Figure 2.27: $G/G_{max}$ curves for Boler sand compared to lower and upper bands proposed by Seed et al. (1984, 1986) and Iwasaki et al. (1978) for sands**

### 2.3.7. Particle crushing verification

Particle crushing can be one of the consequences of shearing carbonate soils. This could change particle size distribution and thus the behavior of a soil which is significantly related to soil gradation characteristics. Some studies in this area show that crushability of carbonate soils is affected significantly by confining pressure and applied loads. Due to the importance of soil crushability on changing the behavior of a soil under the cyclic shear loads, particle distribution of samples was examined occasionally under different loading conditions.

The result of sand gradation before and after shearing a sample cyclic simple shear test is shown in Figure 2.28. It is shown that there is not a significant change in particles distribution after shearing to a double-amplitude shear strain of 7.5% under a relatively large cyclic load. This procedure was repeated for a few times without observing a considerable change in particles size distribution. This can be due to a relatively small carbonate content and dominance of silica content in Boler sand.

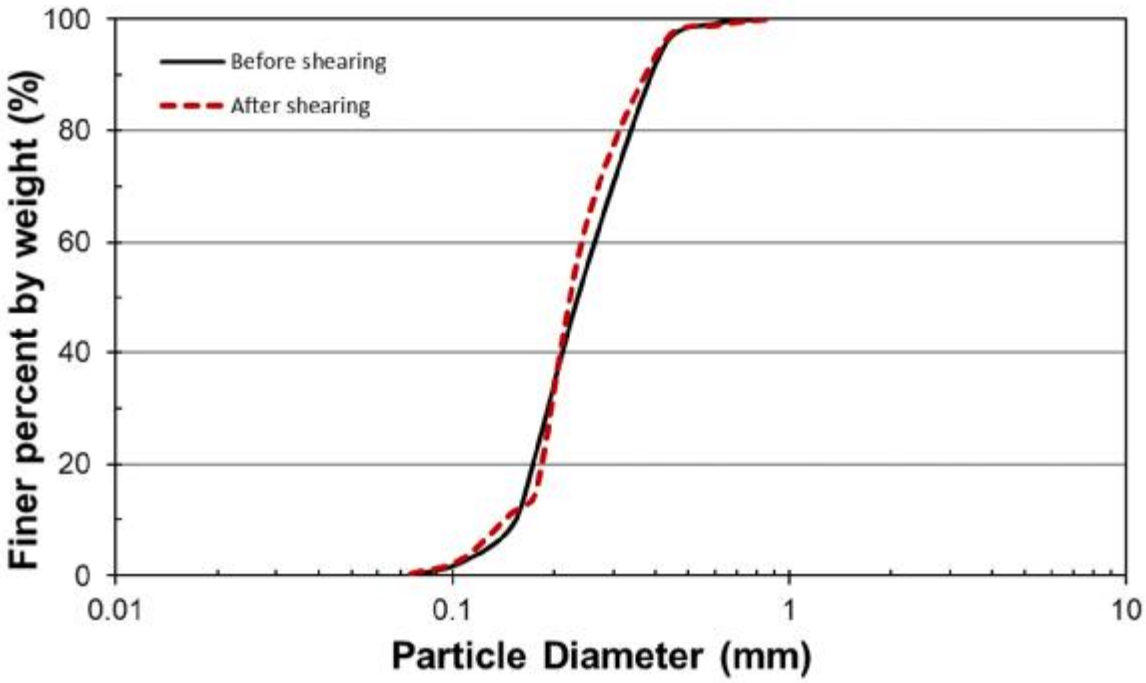


**Figure 2.28: Gradation of a sample before and after shearing to a CSR = 0.152 for a sample with $D_{rc}$ = 65% and $\sigma'_{vc}$ = 600 kPa**

## 2.4. Conclusions

This chapter presented the monotonic and cyclic behavior of a silica-carbonate sand ("Boler sand") from London Ontario. Shear wave velocity ($V_S$) and small-strain stiffness ($G_{max}$) were also measured using bender element tests. Power functions were used to fit $V_S$ and $G_{max}$ data with effective vertical stress with exponents of 0.25 and 0.50, respectively. Both $V_S$ and $G_{max}$, however, displayed a much weaker variation with the void ratio. Despite the weak effect, linear functions were used to describe the effect of void ratio on $V_S$ and $G_{max}$.

The critical state line of Boler sand, determined from the monotonic shear tests, was found to be similar to those of some other clean sands. State parameters ($\Psi$) of the specimens were subsequently calculated using the critical state line and initial states of the specimens. Separate relationships were found between $\Psi$ and $V_S$ at different relative densities, suggesting that $\Psi$ is not a suitable parameter to combine the effects of void ratio and effective stress on $V_S$.

Cyclic liquefaction behavior of Boler sand was also determined from cyclic DSS tests. It was found that the current liquefaction triggering method could significantly overestimate the liquefaction resistance of Boler sand, leading to unsafe liquefaction analysis. This could be associated with the carbonaceous composition of Boler sand as well as differences in the triggering of liquefaction in the laboratory and in the field.

Shear modulus, damping ratio, and shear modulus degradation curves of Boler sand were computed based on small strain shear modulus ($G_{max}$) obtained from shear wave velocity measurements and shear modulus and damping ratio calculations from cyclic simple shear tests. Although both shear modulus and damping ratio depend on strain levels, relative densities and overburden effective stress, they exhibit a considerable sensitivity to consolidation stress changes rather than other parameters. It was also observed that $G/G_{max}$ curves degrade faster than those proposed by previous studies, which confirms that, $G/G_{max}$ curves are material dependent properties and would be affected by testing method and conditions. The damping ratio of tests was observed to be lower than previously proposed patterns for sands, which could be attributed to lower frictional energy loss due to less particle contact as a matter of particle angular shapes.

## 2.5. References

Andrus, R. D., and Stokoe, K. H. (2000). "Liquefaction resistance of soils from shear-wave velocity." Journal of Geotechnical and Geoenvironmental Engineering, 126(11), 1015-1025.

Andrus, R. D., Stokoe, K. H., and Juang, C. H. (2004). "Guide for shear-wave-based liquefaction potential evaluation." Earthquake Spectra, 20(2), 285-308.

Arulnathan, R., Boulanger, R. W., and Riemer, M. F. (1998). "Analysis of bender element tests." Geotechnical Testing Journal, ASTM, 21(2), 120 - 131.

Brandenberg, S. J., Kutter, B. L., and Wilson, D. W. (2008). "Fast stacking and phase corrections of shear wave signals in a noisy environment." Journal of Geotechnical and Geoenvironmental Engineering, 134(8), 1154-1165.

Brignoli, E. G. M., Gotti, M., and Stokoe II, K. H. (1996). "Measurement of shear waves in laboratory specimens by means of piezoelectric transducers." Geotechnical Testing Journal, ASTM, 19(4), 384 - 397.

Camacho-Tauta, J., Cascante, G., Fonseca, V. D., and Santos, J. (2015). "Time and frequency domain evaluation of bender element systems." Geotechnique, 65(7), 548 - 562.

Castro, G. (1969). "Liquefaction of sands." Ph.D., Harvard University, Cambridge, Massachusetts.

Cha, M., Santamarina, J., Kim, H., and Cho, G. (2014). "Small-strain stiffness, shear-wave velocity, and soil compressibility." Journal of Geotechnical and Geoenvironmental Engineering, ASCE, 140(10).

Clayton, C. R. I. (2011). "Stiffness at small strain: research and practice." Geotechnique, 61(1), 5 - 37.

Drnevich, V. P. & Richart, F. E. (1970). Dynamic pre-straining of dry sand. J. Soil Mech. Found. Div. ASCE 96, No. SM2, 453 –469.

Dobry, R., Abdoun, T., Stokoe II, K. H., Moss, R. E. S., Hatton, M., and El Ganainy, H. (2015). "Liquefaction potential of recent fills versus natural sands located in high-seismicity regions using shear-wave velocity." Journal of Geotechnical and Geoenvironmental Engineering, ASCE, 141(3), 1 - 13.

Dyvik, R., Berre, T., Lacasse, S., and Raadim, B. (1987). "Comparison of truly undrained and constant volume direct simple shear tests." Geotechnique, 37(1), 3 - 10.

Hardin, B. O. (1978). "The nature of the stress-strain behavior of soils." ASCE Geotechnical Engineering Division Speciality Conference on Earthquake Engineering and Soil Dynamics, Pasadena, California, 3 - 90.

Hardin, B. O., and Black, W. L. (1966). "Sand stiffness under various triaxial stresses." Journal of the Soil Mechanics and Foundations Division, ASCE, 92(2), 27 - 42.

Hardin, B. O., and Richart Jr., F. E. (1963). "Elastic wave velocities in granular soils." Journal of Soil Mechanics and Foundation Division, American Society of Civil Engineers, 89(1), 33 - 65.

Ishihara, K. (1993). "Liquefaction and flow failure during earthquakes." Geotechnique, 43(3), 351 - 415.

HORN, A. 1964. The shear strength of silt. Forschungsberichte des Landes Nordrhein-Westfalen Nr. 1346, Westdeutscher Verlag, Köln (in German).

Iwasaki, T., Tatsuoka, F., and Takagi, Y. (1978). "Shear moduli of sands under cyclic torsional shear loading." Soils and Foundations, 18(1), 39 - 56.

Jamiolkowski, M., Leroueil, S., and Lo Presti, D. C. F. (1991). "Design parameters from theory to practice." Proceedings of the International Conference on Geotechnical Engineering for Coastal Development: GeoCoast 1991, Yokohama, Japan, 877 - 917.

Jefferies, M. G., and Been, K. (2006). Soil liquefaction - a critical state approach, Taylor & Francis, New York.

Jovicic, V., Coop, M. R., and Simic, M. (1996). "Objective criteria for determining Gmax from bender element tests." Geotechnique, 46(2), 357 - 362.

KARSTEN THERMANN, CHRISTIAN GAU & JOACHIM TIEDEMANN. (2006). “Shear strength parameters from direct shear tests - influencing factors and their significance” Geological Society, London, Engineering Geology Special Publications.

Kallioglou, P., Tika, Th. and Pitilakis, K. (2008). “Shear Modulus and Damping Ratio of Cohesive Soils.” Journal of Earthquake Engineering. 12(6), 879 – 913.

Kayen, R. E. et al., 1992. "Evaluation of SPT-, CPT-, and shear wave-based methods for liquefaction potential assessment using Loma Prieta Data". Honolulu, Proceedings of the 4th U.S. Workshop on Earthquake Resistance Design of Lifeline Facilities and Countermeasures Against Soil Liquefaction.

Kayen, R. et al., 2013. "Shear-wave velocity-based probabilistic and deterministic assessment of seismic soil liquefaction potential". Journal of Geotechnical and Geoenvironmental Engineering, 139(3), pp. 407-419.Kokusho, T. (1980). "Cyclic triaxial test of dynamic soil properties for wide strain range." Soils and Foundations, 20(2), 45-60.

Kokusho T, Yoshida Y, Esashi Y (1982) Dynamic properties of soft clay for wide strain range. Soils Found 22(4):1–18

Ladd, R. S. (1978). "Preparing test specimen using under compaction." Geotechnical Testing Journal, ASTM, 1(1), 16 - 23.

Lee, J.-S., and Santamarina, J. C. (2005). "Bender elements: performance and signal interpretation." Journal of Geotechnical and Geoenvironmental Engineering, ASCE, 131(9), 1063 - 1070.

Lo Presti, D. C. F., Jamiolkowshi, M., Pallara, O., Cavallaro, A., and Pedroni, S. (1997). "Shear modulus and damping of soils." Geotechnique Symposium in Print, 43(3), 603 - 617.

M.A. Pando, E.A. Sandoval, and J. Catano. 2012. "Liquefaction Susceptibility and Dynamic Properties of Calcareous Sands from Cabo Rojo, Puerto Rico”. 15th world conference on earthquake engineering.

Marjanovic, J., and Germaine, J. T. (2013). "Experimental study investigating the effects of setup conditions on bender element velocity results." Geotechnical Testing Journal, ASTM, 36(2).

N. Matasovic and M. Vucetic, (1993), "Cyclic characterization of liquefiable sands", ASCE Journal of Geotechnical Engineering, 1993.119:1805-1822.

Rayhani MHT, El Naggar MH (2008) Dynamic Properties of Soft Clay and Loose Sand from Seismic Centrifuge Tests. Geotechnical and Geological Engineering Journal, DOI 0.1007/s10706-008-9192-5

Robertson, P. K., Sasitharan, S., Cunning, J. C., and Sego, D. C. (1995). "Shear-wave velocity to evaluate the in-situ state of Ottawa sand. ." Journal of Geotechnical Engineering, ASCE, 121(3), 262 - 273.

Robertson, P. K., Woeller, D. J., and Finn, W. D. L. (1992). "Seismic Cone Penetration Test for Evaluating Liquefaction Potential under Cyclic Loading." Canadian Geotechnical Journal, 29(4), 686-695.

Roe, G. V. (1981). "An acoustic method for identifying sand fabric and liquefaction potential." Ph.D., University of New Hampshire, New Hampshire.

Sadrekarimi, A. 2013. Influence of state and compressibility on the liquefied strength of sands, Can. Geotech. J. 50: 1–10.

Sadrekarimi A, Olson SM. A new ring shear device to measure the large displacement shearing behavior of sands. Geotech Test J ASTM 2009; 32:197–208.

Sadrekarimi A, Olson SM. Yield strength ratios, critical strength ratios, and brittleness of sandy soils from laboratory tests. Can Geotech J 2011; 48:493–510.

Sadrekarimi A, Olson SM. Shear band formation observed in ring shear tests on sandy soils. J Geotech Geoenviron 2010; 136:366–75.

Sadrekarimi A, Olson SM. Particle damage observed in ring shear tests on sands. Can Geotech J 2010; 47:497–515.

Sanchez-Salinero, I., Roesset, J. M., and Stokoe, I. I. (1986). "Analytical studies of body wave propagation and attenuation.", The university of Texas, Geotechnical Engineering Center, Texas, Austin, 272.

Santamarina, J. C., Klein, K. A., and Fam, M. A. (2001). Soils and Waves: Particulate Materials Behavior, Characterization, and Process Monitoring, Wiley, New York.

Sawangsuriya, A., (2012). “Wave Propagation Methods for Determining Stiffness of

Geomaterials.” INTECH Open Access Publisher.

Seed, H. B., and Idriss, I. M. (1971). "Simplified procedure for evaluating soil liquefaction potential." Journal of the Soil Mechanics and Foundations Division, ASCE, 97(SM9), 1249 - 1273.

Sun, J. I., Goleskorkhi, R., and Seed, H. B. (1988). “Dynamic moduli and damping ratios for cohesive soils.” Rep. No. UCB/EERC-88/15, Univ. of California at Berkeley, Berkeley, Calif.

Vaid, Y. P., and Sivathayalan, S. (1996). "Static and cyclic liquefaction potential of Fraser River delta sand in simple shear and triaxial tests." Canadian Geotechnical Journal, 33(2), 281-289.

Viggiani, G., and Atkinson, J. H. (1995). "Interpretation of bender element tests." Geotechnique, 45(1), 149 - 154.

Vucetic M, Dobry R (1991) Effect of soil plasticity on the cyclic response. J Geotech Eng ASCE 117(1):89–107

Yamashita, S., Kawaguchi, T., Nakata, Y., Mikami, T., Fujiwara, T., and Shibuya, S. (2009). "Interpretation of International Parallel Test on the Measurement of G(Max) Using Bender Elements." Soils and Foundations, 49(4), 31-650.

Yao Li, Yunming Yang, Hai-Sui Yu, and Gethin Roberts, 2017. “Monotonic Direct Simple Shear Tests on Sand under Multidirectional Loading”. 10.1061/(ASCE)GM.1943-5622.0000673.

# Chapter 3

# 3. Cyclic behavior and liquefaction analysis of a silica-carbonate sand based on bi-directional cyclic simple shear tests

## 3.1. Introduction

Sands behavior have been widely studied under either monotonic or cyclic load tests. Assessment of sands response to monotonic undrained loading has been mostly developed by triaxial tests on reconstituted samples. Based on early test results (Castro, 1969; Lee and Seed, 1970; Castro et al., 1982; Vaid and Chern, 1985; Vaid and Thomas, 1992; and Ishihara, 1993), responses of samples considered to be mostly dependent on void ratio changes (relative density) and stress levels. Similar mechanisms that were identified in monotonic loading, could be identified in cyclic loading as well. A progressive increment of increasing pore water pressure and shear deformation development could be observed with increasing number of shearing cycles. At a constant vertical effective stress, denser materials show higher cyclic resistance. Large deformations during a liquefaction mostly develop in loose deposits and are called flow failure unlike more limited deformations in denser samples which are called cyclic mobility.

Before development of first multi-directional direct simple shear apparatus by Casagrande and Rendon (1978) and later by Ishihara and Yamazaki (1980), single axis loading was the only method of performing cyclic simple shear tests. Unlike mono-directional cyclic simple shear tests, combination of two independent and perpendicular directions of loading could create a wide range of cyclic patterns. Rotational (circular and elliptical) and alternate (plus shape) loading were the patterns which Ishihara and Yamazaki applied on their sand samples. They found that stress rotation can decrease sample resistance to liquefaction and as a general conclusion, adding an extra direction of loading would lower the resistance to liquefaction. They also noted that, in some of their tests, the maximum pore pressure (pore pressure limit) was lower than theoretical expectations. They reported that the number of cycles before liquefaction (at an equal shear stress) compared to unidirectional loading dropped up to a maximum of 35% for elliptical patterns and 25% for alternate patterns. In addition, Seed et al.

(1975) performed shaking table tests on Monterey # 0 sand. One of their most outstanding test results was proposing for a reduction factor of 0.9 applicable to incorporate the effect of multi-directional loading in liquefaction analysis. Other outstanding study based on the multi-directional cyclic direct simple shear test, was performed by Degroot (1989) to simulate the cyclic stress condition at the foundation of an offshore arctic gravity structure. A decade later, Boulanger and Seed (1995) and Boulanger et al. (1993) conducted some tests on fully saturated sands. They tested samples under initial static shear stresses which was resembling sloped soil conditions. Kammerer et al. (2002) also performed extensive tests on Monterey # 0/30 sand under various types of multi-directional cyclic loads. Parts of conclusions to their extensive research depicts that, the behavior of soils under multi-directional loading is far more complex than anticipated and compared to mono-directional test results. In general, resulting shear strains are larger than equivalent mono-directional cyclic loaded samples.

The main factors affecting their complex response could be summarized as excess pore water pressure attainment and magnitude of imposed shear stress. Multi-directional cyclic loading would cause a quicker attainment of pore pressure ratio and fewer liquefaction cycles, comparing to equivalent mono-directional loads, although the behavior is more complicated. At low values of average shear stresses, additional shear stresses would result in higher cyclic shear strains unlike high values of average shear stresses which increasing stress values result in much lower cyclic shear strains. The magnitude of shear stress affects both the limiting pore pressure and the resulting strain levels. Also, they found, initial static shear stresses can have enormous effects on both, pore pressure generation and strains. Larger initial static shear stress ratio can increase resistance to liquefaction by reducing the potential for excess pore pressure generation. Smaller initial static shear stresses increase the shear strains compared to equivalent condition but without initial static shear stress. Results of both studies done by Kammerer et al. and Ishihara et al. are in good agreement. One of the main results of both research teams depicts the reduction factor for compensating liquefaction resistance regarding a multi-directional behavior compared to mono-direction. Adjustment ratios of 0.8 and 0.9 verified to be an underestimation. A wide range of 0.6 to 1.3 is introduced by both research teams. Been and Jefferies (1985) introduced the state parameter ($\psi$) to describe the shearing behavior of a soil based on the combination of void ratio, effective stress and their relation to the critical state void ratio at same effective stress. The critical state line (CSL) represents a

boundary between strain-softening (or contractive behavior) and strain-hardening (or dilative behavior) of a soil where ψ (state parameter) is the difference between the current void ratio (e) and the critical-state void ratio ($e_{cs}$) for certain value of stress. Vaid and Sivathayalan (1996) noted that the cyclic resistance ratio (CRR) of a sand specimen can be expressed as an approximately unique function of state parameter. Earlier studies were mostly focused on limited types of silica sands (mostly Monterey sand), for medium to dense saturated samples and consolidated to small range of vertical effective stresses, less than 180 kPa.

## 3.2. Experimental plan

### 3.2.1. Soil characteristics and specimen preparation

A clean local carbonate-silica sand (Boler sand) with the specific gravity ($G_S$) of 2.67, maximum ($e_{max}$) and minimum ($e_{min}$) void ratios of respectively 0.845 and 0.525, and $D_{50}$ = 0.25 mm (classified as a poorly-graded) is tested in the experiments of this study. Sand specimens of this study were prepared at loose ($D_{rc}$ = 25% ± 3%), medium dense ($D_{rc}$ = 45% ± 3%), and dense ($D_{rc}$ = 65% ± 3%) relative densities using the moist tamping method. The height and diameter of the specimens were respectively 20 mm and 70.7 mm in cyclic DSS tests based on the geometry of platens. This corresponds to an aspect ratio of 0.28, which is less than (0.4) and recommended by the ASTM D6528 standard method for simple shear testing.

In regular moist-tamping, the density of the lower sublayers is increased by compacting the overlying layers. This would produce a non-uniform specimen. To improve specimen uniformity, the under-compaction (Ladd, 1978) method was used in this study. In this method, over-dried sand was thoroughly mixed with 5% moisture. The specimen was then prepared by compacting moist sand in three sublayers. The first and second sublayers were compacted to dry densities of respectively 5% and 2.5% (“under-compacted”) lower than the target dry density of the specimen. After compacting the third overlying sublayer, the final density of these sublayers was hence compacted closer to the target density of the specimen. The dry density was adjusted by changing the mass of soil placed in each sublayer, while all sublayers were compacted to equal heights. Except for the final sublayer, the surface of each sublayer was also scarified in order to improve the bonding between sublayers. The top cap of the DSS

apparatus was subsequently lowered on the sand surface, the membrane was folded back on the top cap and then secured with an O-ring. The retainer plates were also removed. The small amount of moisture content (5%) imparts a small amount of matric suction to a moist-tamped specimen and helps to stabilize the specimen during preparation. However, since this matric suction was not measured here, it was removed by saturating the specimens after specimen preparation. A small seating vertical stress of 5 kPa was first applied to stabilize the specimen and prevent piping. Saturation was then carried out by flushing the specimens with $CO_2$ gas, followed by de-aired water through drainage ports on the specimen endcaps. Specimen height was carefully recorded during this process to determine the precise initial void ratio of the specimen. Following saturation, the specimens were consolidated to effective vertical stresses ($\sigma'_Z$) of 50, 100, 200, 400, or 600 kPa. The top drainage port was open during consolidation in order to allow excess pore pressure dissipation. Specimen void ratio after consolidation ($e_c$) was subsequently calculated from changes in specimen height.

### 3.2.2. Testing apparatus

Rendon (1978) and later Ishihara and Yamazaki (1980) were the pioneers of bi-directional test developers. Although their developed devices were designed for investigating soil liquefaction behavior, each of them had their limitations. Some of the limitations engaged with the use of these devices are; rocking of top and bottom caps, out of control back-pressure while testing, considerable or not measurable friction between the horizontal loading plates, and limited load and frequency capacity. The limits of apparatus designed by Casagrande and Rendon is the possibility to apply only constant shear forces during a test and thus preventing the researcher to perform undrained shear tests at constant strain rates. Also, Ishihara and Yamazaki (1980) developed another major apparatus at the University of Tokyo which could help them to apply two horizontal cyclic shear loads at the top of circular samples and in two perpendicular directions. The shortcoming of this device was the possibility of applying very limited loading patterns. Later, Boulanger et al. (1993) conducted a new research study and significantly overcame previous issues. Their developed device, not only reduced the problem engaging with cap rocking, it could provide with the back-pressure controlled saturation of the main chamber. However, because of a pneumatic loading technology, it was not possible to apply high-frequency loads which are characteristics of earthquake actual loads.

In the current study, simple shear tests were carried out using an advanced computer-controlled apparatus (VDDCSS) manufactured by GDS Instruments (UK). The GDS Variable Direction Dynamic Cyclic Simple Shear is a laboratory system that can apply direct simple shear loads in any horizontal shearing direction to soil specimens via three electro-mechanical loading actuators. A pair of bender element mounted platens are considered to perform shear wave velocity measurements by this device. The GDS Bender Elements enables measurement of the maximum shear modulus of a soil at small strains. The source and receiver pair of bender elements can send S waves or P waves through a soil specimen with computerized control on triggering and recording data. Bender elements are made from piezoelectric ceramic bimorphs. Two sheets are attached together with a metal shim. An excitation voltage is applied to produce a displacement in the source bender side, resulting in a wave being sent through the sample. This wave generates a displacement in the receiver bender side, which induces a voltage that can be recorded.

The first type of body waves is a primary or P wave. This is a longitudinal wave in which the direction of motion of the particles is in the direction of wave propagation introducing the $V_P$ speed. The P waves exert volumetric strains in the soil, and hence $V_P$ is controlled by the bulk modulus of the specimen. Body waves can also be secondary or S wave which is a transverse wave and the direction of motion of the particles is perpendicular to the direction of wave propagation introducing shear wave velocity $V_S$. The $V_S$ is constant regardless of the rate of applied loading. Since $V_P > V_S$, the first waves to arrive from any disturbance will always be P waves. P waves can be transmitted through a fluid such as a pore water or through the soil solid, hence the saturation of the media may influence $V_P$ significantly. The bulk modulus of water could be up to 50 times the value in the soil. Shear waves, however, are almost completely unaffected by saturation of the media due to the negligible shear modulus of water.

### 3.2.3. Testing plan and parameter definitions

Drained and undrained (constant volume) static simple shear tests, mono-directional and bi-directional cyclic tests and shear wave velocity measurement tests were carried out at different void ratios and consolidation stresses to characterize and identify soil behavior in different states. As discussed in Chapter 2, part of several monotonic shear tests at wide ranges of consolidation stresses ($\sigma'_{vc}$) and relative densities ($D_{rc}$) were chosen to establish critical state line (CSL) of the Boler sand. Constant volume tests and few drained tests were chosen to

extract the required data in the adjustment of CSL since critical state line is a unique characteristic of a sand and could be derived based on both drained and undrained test results. Also, as shown in Tables 3.3, 3.4, and 3.5, a comprehensive set of experiments were planned on cyclic simple shear testing of Boler sand samples. Similar to static simple shear tests, constant volume cyclic tests were performed for loose ($D_{rc}$ = 25%), medium dense ($D_{rc}$ = 45%), and dense ($D_{rc}$ = 65%) sand samples under consolidation pressures of 50, 100, 200, 400, and 600 kPa. Dynamic tests include mono-directional (one dimension) and bi-directional cyclic load tests. Cyclic loads are applied in a sinusoidal format of $F_{cyc} = A.Sin(2\pi.f.t)$ in which, the applied load (F) is a function of time (t). In a sinusoidal format, f is the frequency of loading and A is load amplitude. In a two-dimensional cyclic load with the sinusoidal formats shown in equals 3.1 and 3.2 (for X and Y direction respectively), one of the directions (for instance Y here) could be programmed to start loading, a portion of a full cycle later than the other (X direction) that is called phase difference (Φ).

$$F_{cyc-x} = A_x.Sin(2\pi.f_x.t) \tag{3.1}$$

$$F_{cyc-y} = A_y.Sin(2\pi.f_y.t + \Phi) \tag{3.2}$$

Most usual bi-directional cyclic loading patterns (paths) which have been applied by previous researchers through multi-directional cyclic simple shear tests are shown in Figure 3.1. When the amplitude of loading in two perpendicular directions is equal ($A_x = A_Y$), load frequencies are equal ($f_x = f_Y$), and phase offset is 90 degrees (Φ = 90), this loading pattern is called circular (Figure 3.1 – a). When $A_x \neq A_Y$, $f_x = f_Y$, and Φ = 90, this load pattern is called elliptical or oval (Figure 3.1 – a,b). When $A_x = A_Y$ and $f_x = f_Y$ but stress in different directions are programmed to be applied separately at different times, then the load pattern is called alternate (Figure 3.1 – c). Finally, when $A_x = A_Y$ and Φ = 0 but, $f_x \neq f_Y$, the load pattern is named figure-8 (Figure 3.1 – d).

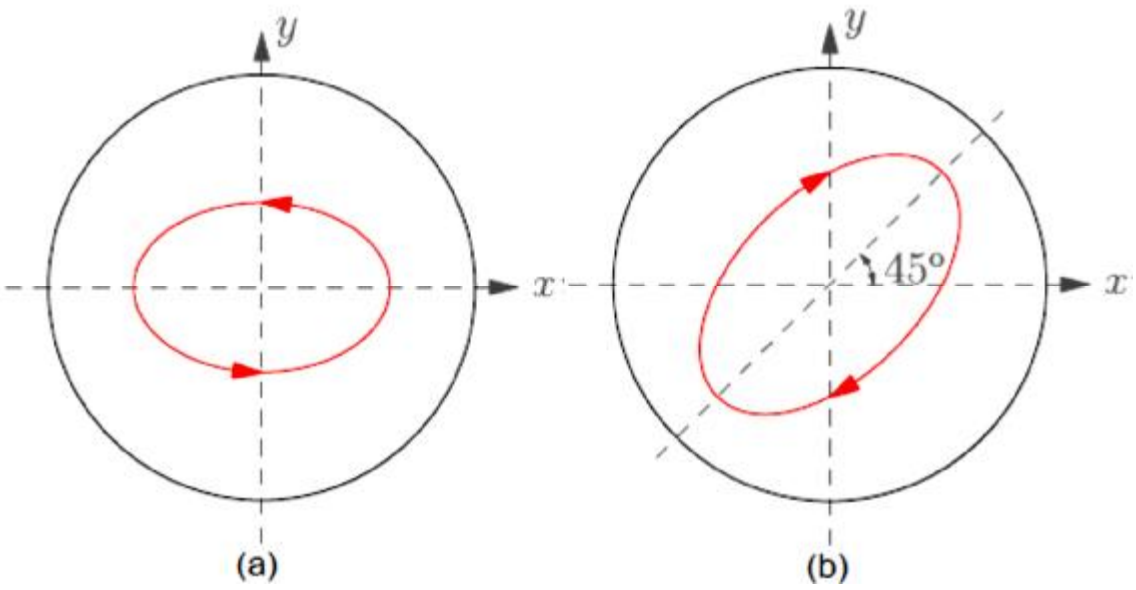


**a) Circular / Elliptical (Oval)** **b) Rotated Elliptical**

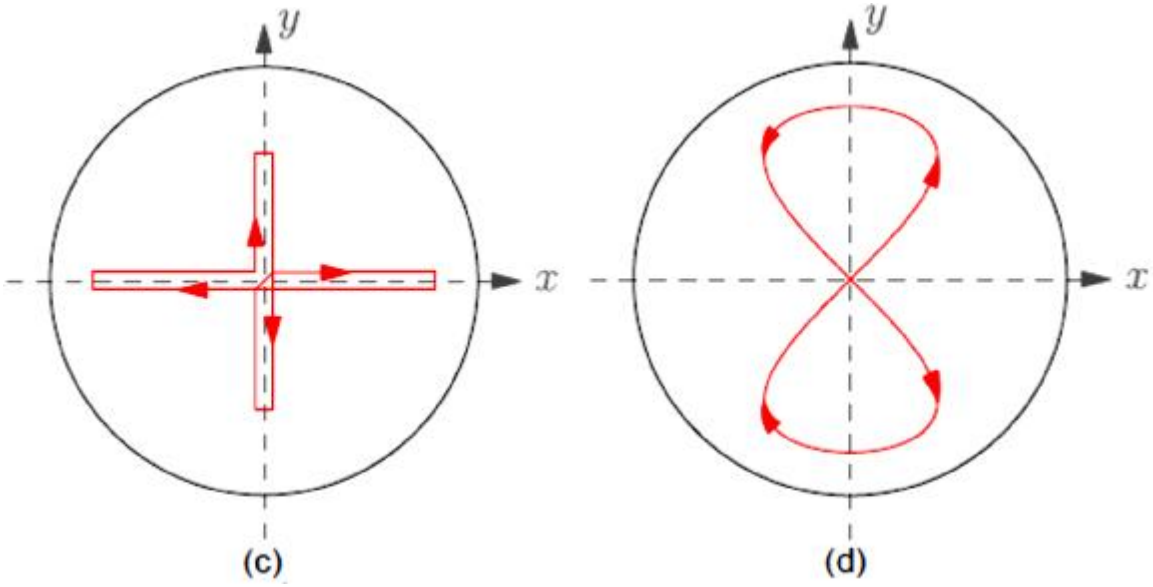


**c) Alternate path** **d) figure-8 path**

**Figure 3.1: Different applicable bi-directional loading patterns (Yang et al., 2016)**

For standard cyclic simple shear tests, excess pore water pressure ratio ($r_u$) is computed from pore water pressure changes to vertical effective consolidation stress ratio ($\sigma'_{vc}$) at any vertical stress ($\sigma'_v$):

$$r_u = \frac{\Delta u}{\sigma'_{vc}} = \frac{\sigma'_{vc} - \sigma'_v}{\sigma'_{vc}} \quad (3.3)$$

Liquefaction in current study corresponds to reaching a double-amplitude cyclic shear strain of 7.5%. This is essentially equivalent to the liquefaction definition of 5% double-amplitude axial strain in a triaxial test (Vaid and Sivathayalan, 1996). Liquefaction susceptibility under cyclic loads is normally characterized by the cyclic stress ratio (CSR). CSR is defined as applied cyclic shear stress ($\tau_{cyc}$) in horizontal planes divided by the vertical effective consolidation stress:

$$CSR = \frac{\tau cyc}{\sigma' vc} \quad (3.4)$$

The value of CSR which is required to exceed 3.75% single-amplitude shear strain in 15 number of cycles (corresponding to an earthquake magnitude of M = 7.5), is defined cyclic resistance ratio (CRR) in this study as well as most experimental research studies. Summary of cyclic test parameters for loose to dense samples are shown in Tables 3.1 to 3.3. Loading frequency of 0.1 Hz was applied to all samples except loads of a second direction for figure-8 loading pattern (0.2 Hz). Application of higher frequency (1 Hz) on samples was also assessed. The results of tests on medium dense samples ($D_{rc}$ = 45%) is shown in Figure 3.2. As it is shown for a range of 100 kPa to 400 kPa loaded samples, Boler sand samples response does not change significantly. This is in good agreement with previous studies such as Jong and Seed (1988) who depicted that frequency of loading does not affect sands behavior in liquefaction which is mostly a deformation-based phenomenon.

**Table 3.1: Summary of cyclic tests for loose samples**

| $\sigma'_{vc}$ (kPa) | Avg. $e_c$ | Avg. $D_{rc}$ (%) | Test Type | Freq. (Hz) | CSR values |
|---|---|---|---|---|---|
| 50 | 0.764 | 25.3 | M | 0.1 | 0.062 - 0.071 - 0.080 |
| 100 | 0.764 | 25.3 | M | 0.1 | 0.067 - 0.080 - 0.090 |
| 200 | 0.768 | 24.1 | M | 0.1 | 0.080 - 0.090 - 0.100 |
| 400 | 0.769 | 23.8 | M | 0.1 | 0.090 - 0.100 - 0.110 |
| 600 | 0.763 | 25.6 | M | 0.1 | 0.100 - 0.110 - 0.125 |
| 50 | 0.763 | 25.6 | C | 0.1 | 0.042 - 0.057 - 0.067 |
| 100 | 0.763 | 25.6 | C | 0.1 | 0.053 - 0.071 - 0.082 |
| 200 | 0.763 | 25.6 | C | 0.1 | 0.061 - 0.081 - 0.091 |
| 400 | 0.763 | 25.6 | C | 0.1 | 0.081 - 0.091 - 0.101 |
| 600 | 0.768 | 24.1 | C | 0.1 | 0.081 - 0.091 - 0.101 |
| 50 | 0.766 | 24.7 | E | 0.1 | 0.056 - 0.073 - 0.091 |
| 100 | 0.760 | 26.6 | E | 0.1 | 0.073 - 0.081 - 0.091 |
| 200 | 0.766 | 24.7 | E | 0.1 | 0.08 - 0.100 - 0.111 |
| 400 | 0.772 | 22.8 | E | 0.1 | 0.090 - 0.100 - 0.110 |
| 600 | 0.762 | 25.9 | E | 0.1 | 0.090 - 0.100 - 0.110 |
| 50 | 0.766 | 24.7 | F | 0.1-0.2 | 0.057 - 0.076 - 0.100 |
| 100 | 0.761 | 26.3 | F | 0.1-0.2 | 0.055 - 0.077 - 0.101 |
| 200 | 0.757 | 27.5 | F | 0.1-0.2 | 0.064 - 0.089 - 0.114 |
| 400 | 0.761 | 26.3 | F | 0.1-0.2 | 0.076 - 0.101 - 0.126 |
| 600 | 0.760 | 26.6 | F | 0.1-0.2 | 0.101 - 0.0113 - 0.138 |

**M**: mono-directional, **C**: circular, **E**: elliptical, **F**: figure-8

**Table 3.2: Summary of cyclic tests for medium dense samples**

| $\sigma'_{vc}$ (kPa) | Avg. | Avg. $D_{rc}$ (%) | Test Type | Freq. (Hz) | CSR values |
|---|---|---|---|---|---|
| 50 | 0.701 | 45.0 | M | 0.1 | 0.073 - 0.082 - 0.094 |
| 100 | 0.700 | 45.3 | M | 0.1 | 0.083 - 0.097 - 0.103 |
| 200 | 0.706 | 43.4 | M | 0.1 | 0.08 - 0.102 - 0.112 |
| 400 | 0.709 | 42.5 | M | 0.1 | 0.122 - 0.131 - 0.151 |
| 600 | 0.694 | 47.2 | M | 0.1 | 0.131 - 0.141 - 0.161 |
| 50 | 0.705 | 43.8 | C | 0.1 | 0.053 - 0.063 - 0.077 |
| 100 | 0.705 | 43.8 | C | 0.1 | 0.053 - 0.076 - 0.087 |
| 200 | 0.699 | 45.6 | C | 0.1 | 0.072 - 0.091 - 0.101 |
| 400 | 0.705 | 43.8 | C | 0.1 | 0.101 - 0.113 - 0.121 |
| 600 | 0.698 | 45.9 | C | 0.1 | 0.091 - 0.111 - 0.121 |
| 50 | 0.701 | 45.0 | E | 0.1 | 0.062 - 0.071 - 0.091 |
| 100 | 0.702 | 44.7 | E | 0.1 | 0.081 - 0.091 - 0.111 |
| 200 | 0.706 | 43.4 | E | 0.1 | 0.100 - 0.110 - 0.120 |
| 400 | 0.698 | 45.9 | E | 0.1 | 0.110 - 0.120 - 0.130 |
| 600 | 0.704 | 44.1 | E | 0.1 | 0.120 - 0.130 - 0.140 |
| 50 | 0.702 | 44.7 | F | 0.1-0.2 | 0.067 - 0.077 - 0.089 |
| 100 | 0.705 | 43.8 | F | 0.1-0.2 | 0.077 - 0.089 - 0.102 |
| 200 | 0.705 | 43.8 | F | 0.1-0.2 | 0.101 - 0.126 - 0.138 |
| 400 | 0.704 | 44.1 | F | 0.1-0.2 | 0.083 - 0.101 - 0.126 |
| 600 | 0.699 | 45.6 | F | 0.1-0.2 | 0.114 - 0.139 - 0.163 |

**M**: mono-directional, **C**: circular, **E**: elliptical, **F**: figure-8

**Table 3.3: Summary of cyclic tests for dense samples**

| $\sigma'_{vc}$ (kPa) | Avg. | Avg. $D_{rc}$ (%) | Test Type | Freq. (Hz) | CSR values |
|---|---|---|---|---|---|
| 50 | 0.643 | 63.1 | M | 0.1 | 0.047 - 0.071 - 0.093 |
| 100 | 0.635 | 65.6 | M | 0.1 | 0.079 - 0.095 - 0.105 |
| 200 | 0.639 | 64.4 | M | 0.1 | 0.104 - 0.118 - 0.132 |
| 400 | 0.634 | 65.9 | M | 0.1 | 0.122 - 0.137 - 0.151 |
| 600 | 0.633 | 66.3 | M | 0.1 | 0.141 - 0.152 - 0.191 |
| 50 | 0.637 | 65.0 | C | 0.1 | 0.037 - 0.067 - 0.073 |
| 100 | 0.638 | 64.7 | C | 0.1 | 0.067 - 0.082 - 0.096 |
| 200 | 0.637 | 65.0 | C | 0.1 | 0.081 - 0.096 - 0.111 |
| 400 | 0.640 | 64.1 | C | 0.1 | 0.081 - 0.111 - 0.121 |
| 600 | 0.634 | 65.9 | C | 0.1 | 0.111 - 0.131 - 0.150 |
| 50 | 0.633 | 66.3 | E | 0.1 | 0.073 - 0.081 - 0.101 |
| 100 | 0.632 | 66.6 | E | 0.1 | 0.081 - 0.091 - 0.110 |
| 200 | 0.639 | 64.4 | E | 0.1 | 0.08 - 0.100 - 0.110 |
| 400 | 0.636 | 65.3 | E | 0.1 | 0.120 - 0.130 - 0.140 |
| 600 | 0.641 | 63.8 | E | 0.1 | 0.130 - 0.140 - 0.150 |
| 50 | 0.634 | 65.9 | F | 0.1-0.2 | 0.065 - 0.077 - 0.090 |
| 100 | 0.642 | 63.4 | F | 0.1-0.2 | 0.064 - 0.090 - 0.114 |
| 200 | 0.632 | 66.6 | F | 0.1-0.2 | 0.089 - 0.101 - 0.113 |
| 400 | 0.638 | 64.7 | F | 0.1-0.2 | 0.088 - 0.126 - 0.151 |
| 600 | 0.638 | 64.7 | F | 0.1-0.2 | 0.101 - 0.126 - 0.176 |

**M**: mono-directional, **C**: circular, **E**: elliptical, **F**: figure-8

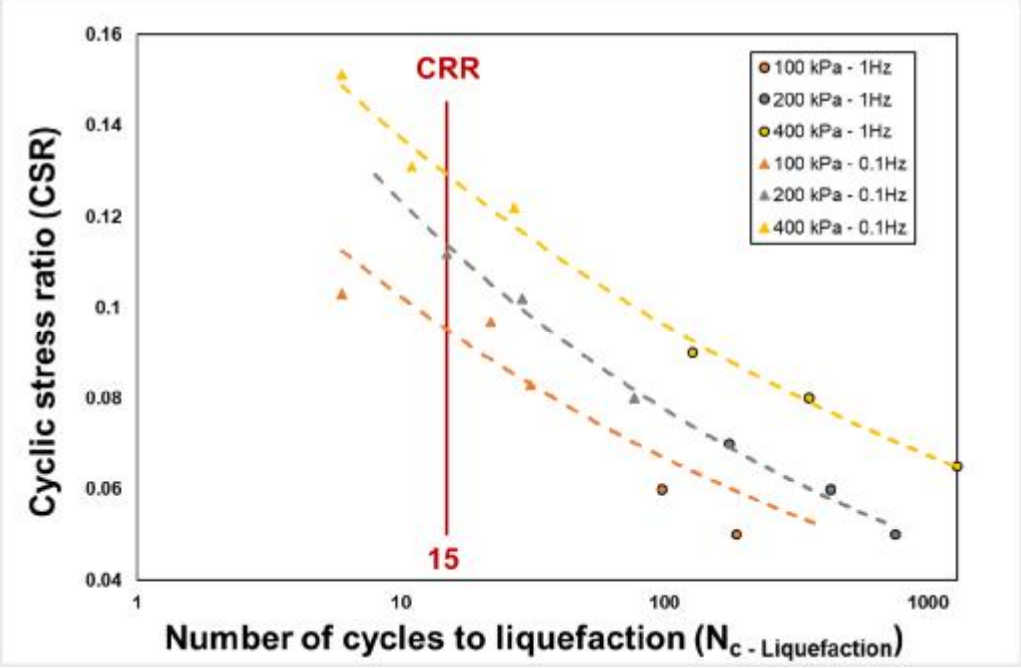


**Figure 3.2: Comparing cyclic response of medium dense samples ($D_{rc}$ = 45%) to cyclic loads of different frequencies (0.1 Hz and 1 Hz)**

## 3.3. Test results

### 3.3.1. Introducing resultant shear strain and cyclic stress ratio

Investigating cyclic simple shear behavior of samples based on plans shown in Tables 3.1, 3.2, and 3.3, was followed by considering four cyclic patterns including mono-directional, and bi-directional (circular, elliptical and figure-8). Typical results for four different shearing modes are demonstrated in Figures 3.3, 3.4, 3.5 and 3.6. Illustrated results present, excess pore water generation, stress path and shear strain development with increasing number of cycles. In a certain level of generated pore water pressure, specimens become unstable and both pore water pressure ratio ($r_u$) and shear strain ($\gamma_L$) exhibit a bouncing increase in further load cycles. The shear load pattern of bi-directional loaded samples is also illustrated in Figures 3.3, to 3.6. For bi-directional cyclic tests, resultant values of both shear strain and cyclic stress ratio (CSR) are calculated and considered in the analysis because, unlike the mono-directional tests, samples in bi-directional tests experience the actual combined effect of both horizontal and perpendicular loads. Although, each individual direction may respond like a mono-directional test, the combined effect of two directions are not necessarily similar. For this purpose, resultant shear strains and CSR values are calculated as below:

$$\gamma_{L-Resultant} = \sqrt{{\gamma_x}^2 + {\gamma_y}^2} \tag{3.5}$$

$$CSR_{Resultant} = \sqrt{{CSR_x}^2 + {CSR_y}^2} \tag{3.6}$$

The detailed results of individual tests are presented in Appendices 1, 2, 3, and 4 for mono-directional, bi-directional / circular, bi-directional / elliptical, and bi-directional / figure-8 loading patterns, respectively.

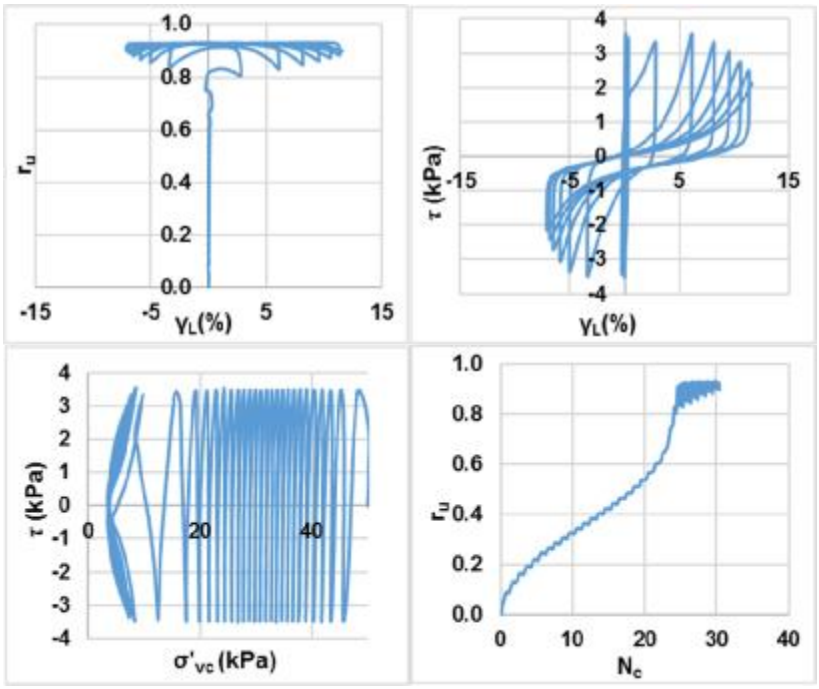


**Figure 3.3: Response of a sample to mono-directional cyclic load with $D_{rc}$ = 63.1%, $\sigma'_{vc}$ = 50 kPa, CSR = 0.071 and frequency of f = 0.1 Hz**

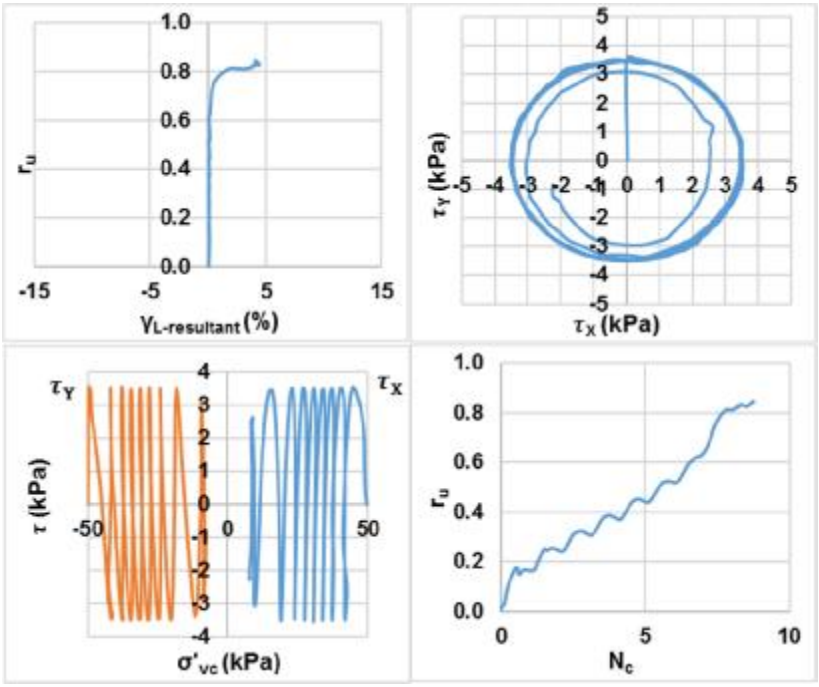


**Figure 3.4: Response of a sample to bi-directional / circular pattern cyclic load with $D_{rc}$ = 64.1%, $\sigma'_{vc}$ = 50 kPa, CSR $_{resultant}$ = 0.067 and frequency of $f_X$ = $f_Y$ = 0.1 Hz**

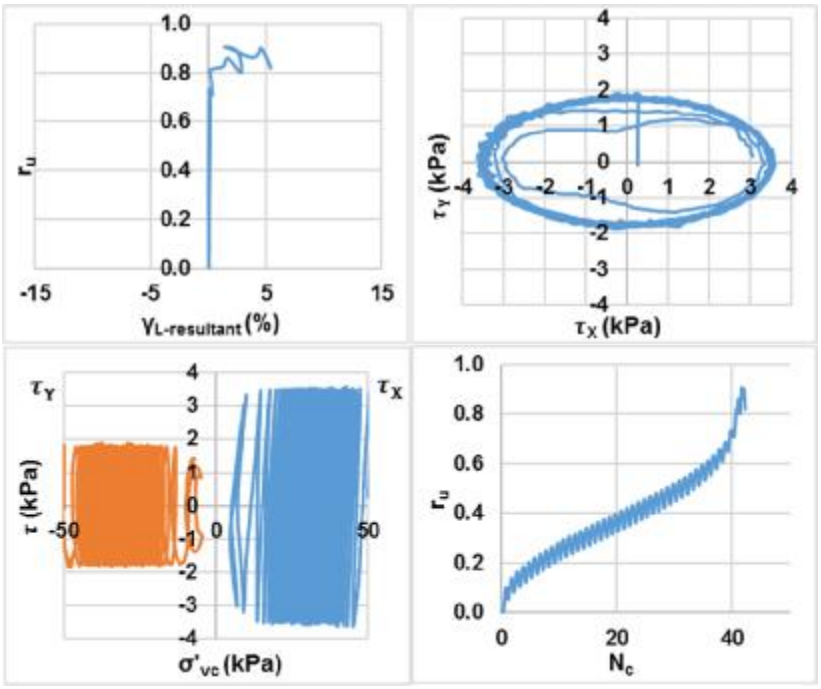


**Figure 3.5: Response of a sample to bi-directional / elliptical pattern cyclic load with $D_{rc}$ = 65.9%, $\sigma'_{vc}$ = 50 kPa, CSR $_{resultant}$ = 0.073 and frequency of $f_X = f_Y$ = 0.1 Hz**

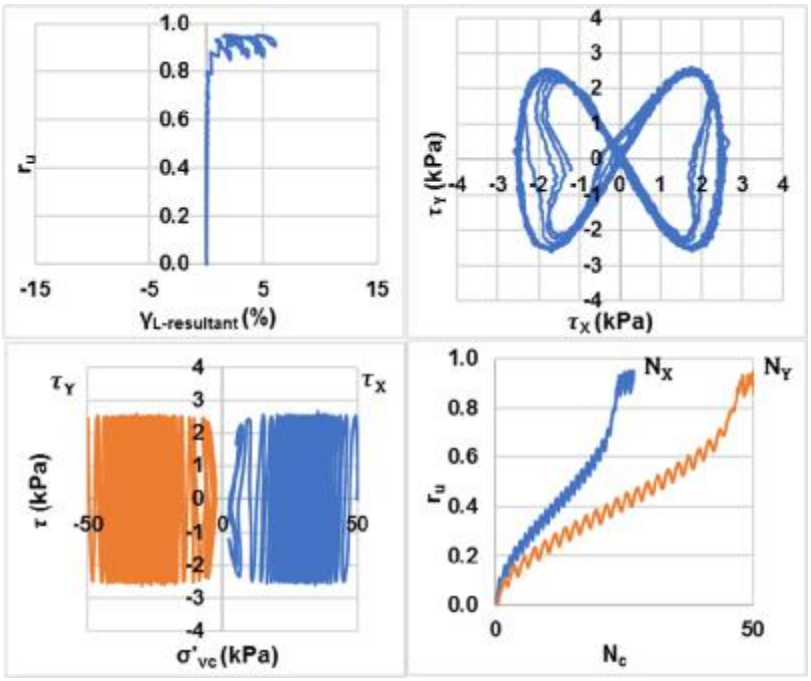


**Figure 3.6: Response of a sample to bi-directional / figure-8 pattern cyclic load with $D_{rc}$ = 66.9%, $\sigma'_{vc}$ = 50 kPa, CSR $_{resultant}$ = 0.065 and frequency of $f_X$ = 0.1 Hz, $f_Y$ = 0.2 Hz**

### 3.3.2. Mechanism of strength reduction under cyclic loads

Because of any applied cyclic stress or strain in an undrained condition, the structure of a cohesionless soil tends to become more compact, with a resulting transfer of stress to the pore water pressure and a reduction in vertical effective stress on the soil grains. As a result of a reduction in vertical effective stress, the soil grain structure tends to deform to the extent required to keep the volume constant. This tendency of soil to volume change on successive cycles determines the magnitude of the increase in pore water pressure in the soil. It could be observed in examples shown in Figures 3.3 to 3.6 that, during shear cycling, axial stress begins to decrease (corresponding to pore water pressure increase). The pore water pressure ratio ($r_u$) denotes the generation of pore water pressure and represents the ratio of pore water pressure to total vertical stress. At liquefaction, pore water pressure ratio gets close to 1. This phenomenon coincides with an increasing shear strain as there is little resistance with the soil to applied cyclic shear loading. Liquefaction, weather-induced by a natural earthquake event or by a laboratory test equipment, is caused by an excess pore water pressure generation during repeated cyclic shear loading. Pyke, Seed, and Chan (1974) performed extensive tests and introduced a model based on the mechanism explained above that correlates the settlement of a dry sand sample to their potential of pore water generation in an undrained saturated test. By introducing above model, they performed cyclic mono-directional and bi-directional shaking table tests on Monterey sand and compared the results regarding their stress-settlement correlation. Two basic patterns of motion were used in these tests. The first was a combination of two sinusoidal components with a phase difference of 90 degrees so that a circular resultant motion, termed gyratory shear, was obtained. The second was a pair of randomly generated motions which could be run with the peaks of the two components either in or out of phase. They observed that settlement of dry sand is greater (approximately double) under multidirectional shaking than under one-directional shaking of similar amplitude and thus, it appears that the liquefaction potential of a saturated sand will be increased if this factor is considered. Because the stress-settlement relationship is non-linear, the stress ratio causing a given settlement for the combined motions was typically only about 20 percent less than the stress ratio which causes the same settlements under a single component.

It was verified later by Seed (1978) that, the combination of cyclic stresses in two or more directions, induces greater volume contractions of a sand sample than individual components

do. In another study, Horie (2000) performed two-directional simple shear tests on dense samples. Typically, he was starting the test with shearing in one direction. Sand samples were showing a dilatant (expanding) behavior. As soon as starting to shear in an excessive direction, a significant extent of volume contraction was observed. This transition from positive dilatancy to contraction corresponds to a higher potential for pore water pressure generation in an undrained shear. It could be observed in previous examples that during shear cycling, axial stress begins to decrease (corresponding to pore water pressure increase). The pore water pressure ratio ($r_u$) denotes the generation of pore water pressure and represents the ratio of pore water pressure to total vertical stress. At liquefaction, pore water pressure ratio gets close to 1. This phenomenon coincides with an increasing shear strain as there is little resistance with the soil to applied cyclic shear loading. Liquefaction, weather-induced by a natural earthquake event or by a laboratory test equipment, is caused by an excess pore water pressure generation during repeated cyclic shear loading. Consequently, two main liquefaction criteria are defined. As first criteria, when a specimen reaches a value of $r_u = 1$, it indicates that the pore water pressure is completely equal to total vertical stress and the specimen has undergone liquefaction. This liquefaction criterion, however, is not always applicable in cyclic shear tests and is often reliant on certain conditions such as in loose soils, on level ground, and those that are loaded mono-directionally (Kammerer 2002). A second or deformation based criterion for liquefaction is often used for both cyclic triaxial and direct simple shear tests as a substitute to classify the occurrence of liquefaction. There have been various studies on the exact point of shear deformation required to classify a specimen as liquified. Ishihara (1996) stated that developed pore water pressure across all densities becomes equal to normal stress when a shear strain value of about 3% is reached. Seed & Idriss (1971) found that for triaxial tests, once a single amplitude axial strain of 2.5% was reached, the stress conditions on the specimen became uncontrolled and strain measurements unreliable. The deformation failure criteria used in this study, which has been used in many previous studies, including on Fraser River sand (Wijewickreme et al. 2005), was that of a single amplitude shear strain value of 3.75% or a double amplitude value of 7.5%. This deformation criterion for cyclic simple shear tests has been proposed as the shear strain value for which liquefaction is triggered and is equivalent to a single amplitude axial strain of 2.5% in cyclic triaxial tests (Committee on Earthquake Engineering 1985; Harder & Boulanger 1997).

## 3.4. Analysis of results

### 3.4.1. Cyclic shear resistance characterization

As was discussed in previous chapters, several cyclic simple shear tests were performed at various initial vertical effective stresses and respective different cyclic stress ratio (CSR) for loose, medium dense, and dense samples. These tests were repeated in different shearing modes as well. The cyclic stress ratio (CSR) required for liquefaction occurrence in a specified number of loading cycles (15 number of cycles in this study) which causes a double-amplitude cyclic shear strain of 7.5% is called Cyclic Resistance Ratio (CRR). Evaluating CRR variation of a soil is important since in the simplified stress-based approach for liquefaction analysis, seismic demand is calculated as the cyclic shear stress ratio applied by an earthquake (CSR) and the cyclic resistance ratio (CRR) of the soil (capacity) is estimated from a correlation with an in-situ test. Earthquake-induced CSR can be estimated using empirical correlations or numerical methods such as finite element analysis. The empirical correlations provide CRR of a level-ground (no shear stress bias) for an effective overburden pressure of 100 kPa.

Cyclic liquefaction is deemed to occur when CSR exceeds CRR. Semi-empirical relationships between CRR and SPT or CPT penetration resistance have been extensively studied by many researchers. Based on the results of previous studies, correlations between on-site measurements and cyclic resistance parameters of soils have been developed (called liquefaction triggering curves). Liquefaction triggering curves will be discussed later in this chapter in a separate section. Prior to further discussing the results, details of the calculation and individual curves taken from the results would be presented.

Based on the procedure described previously in this chapter, a number of cycles to liquefaction of various samples were examined in different shear stresses and loading patterns which the results are shown in Figures 3.8 to 3.15. Two consecutive and similar shearing load and boundary conditions were applied to each sample of this study to liquefy which the first (earlier) one is called “liquefaction” and the second (later) one is called “re-liquefaction”. Each sample was unloaded, re-consolidated and the second cycle of shear loads was applied. The details and incentives of a re-liquefaction analysis will be discussed in chapter 4. An example for a number of resisting cycles to produce liquefaction at various applied CSR values based

on the results of this study is shown in Figure 3.7 for mono-directional cyclic simple shear tests at $\sigma'_{vc}$ = 400 kPa and in three different relative densities. Cyclic resistance of samples increases with increasing relative density from $D_{rc}$ = 25% (loose) to $D_{rc}$ = 65% (dense) samples. It is also visually shown that how a CRR value could be computed.

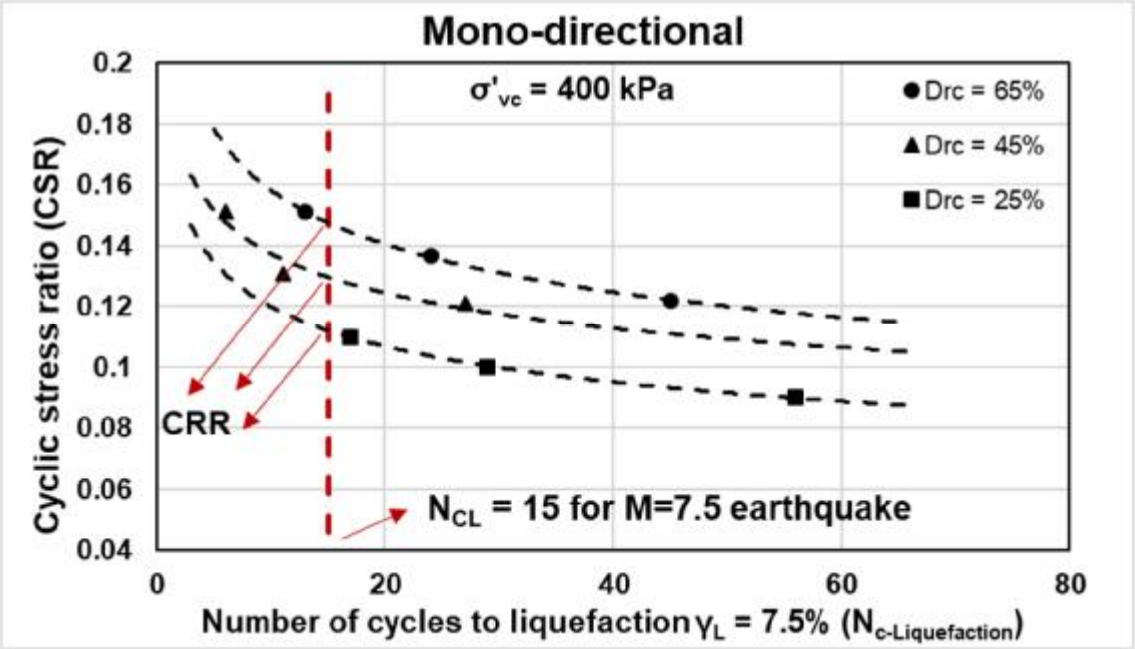


**Figure 3.7: CSR (and CRR) variation for mono-directional tests at different relative densities ($D_{rc}$ = 25%, 45%, 65% ± 3%) and under vertical effective stress of $\sigma'_{vc}$ = 400 kPa**

The relationship between the CSR and $N_C$ can generally be approximated with a power function as shown in equation 3.7 and plotted in Figures 3.8 to 3.15 for various samples.

$$CSR = \alpha . N_C^{-\beta} \tag{3.7}$$

The parameters α and β are normally are determined by regression of experimental data.

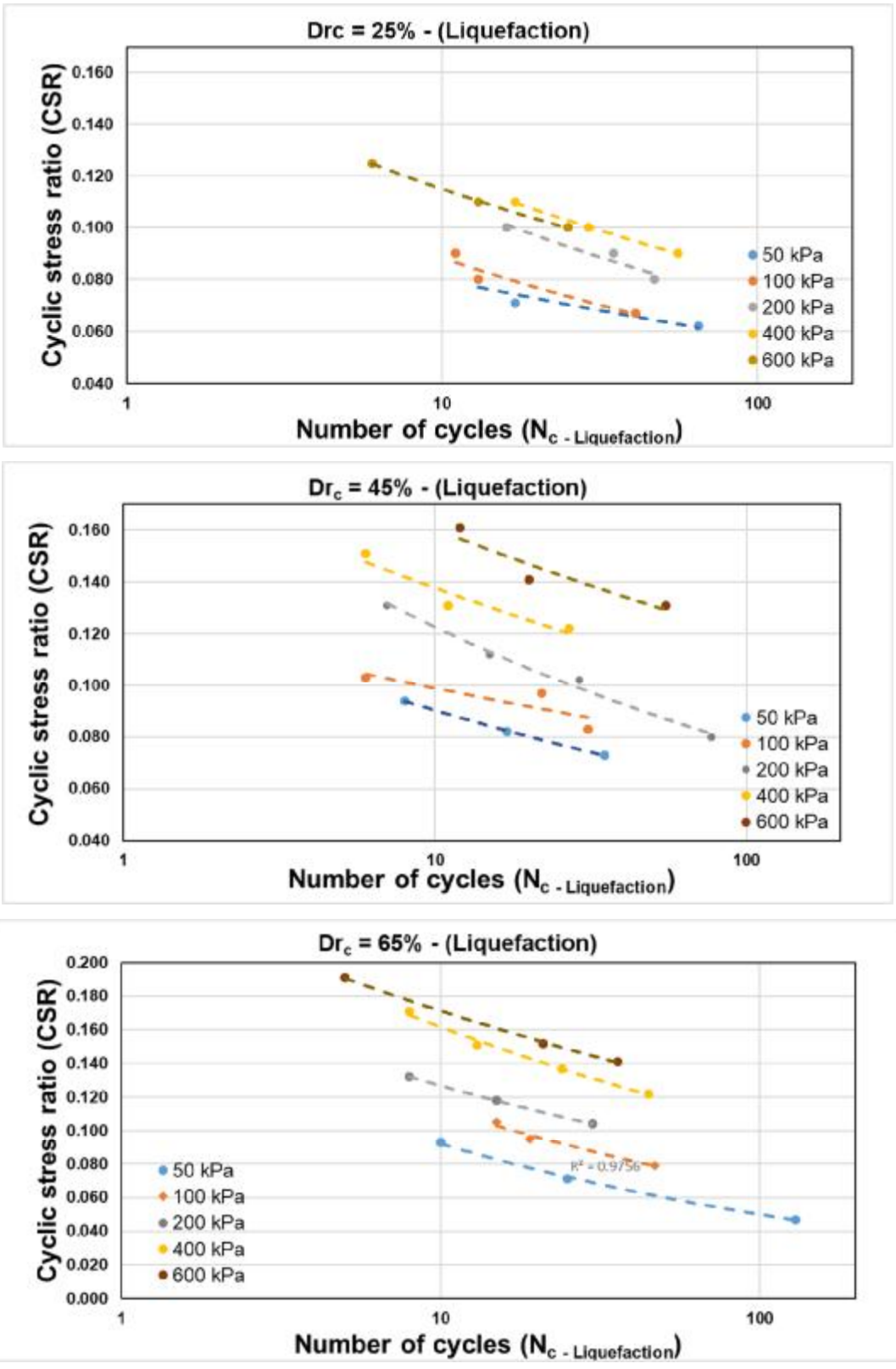


**Figure 3.8: CSR versus $N_C$ for mono-directional cyclic loads at liquefaction**

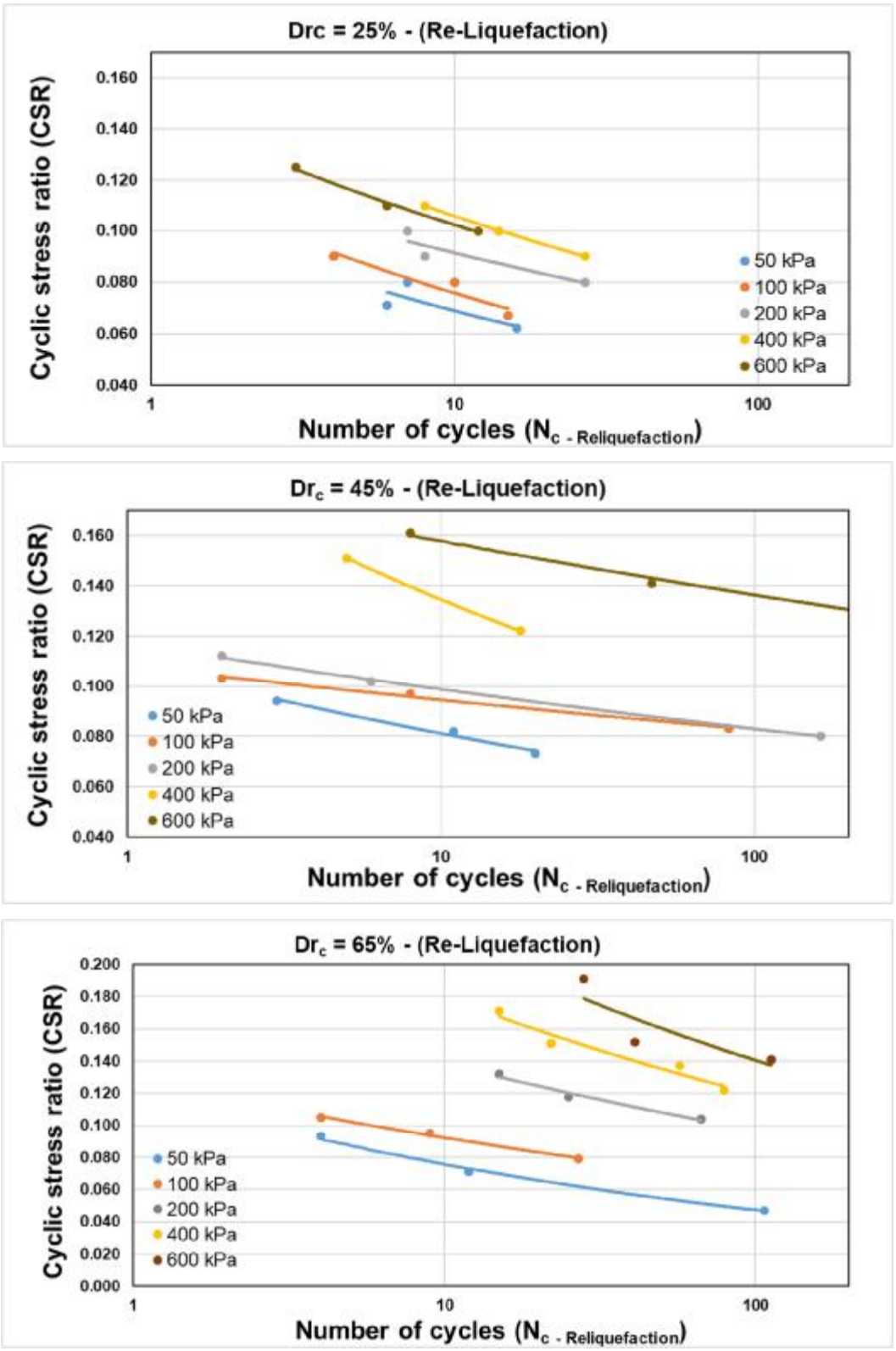


**Figure 3.9: CSR versus $N_C$ for mono-directional cyclic loads at re-liquefaction**

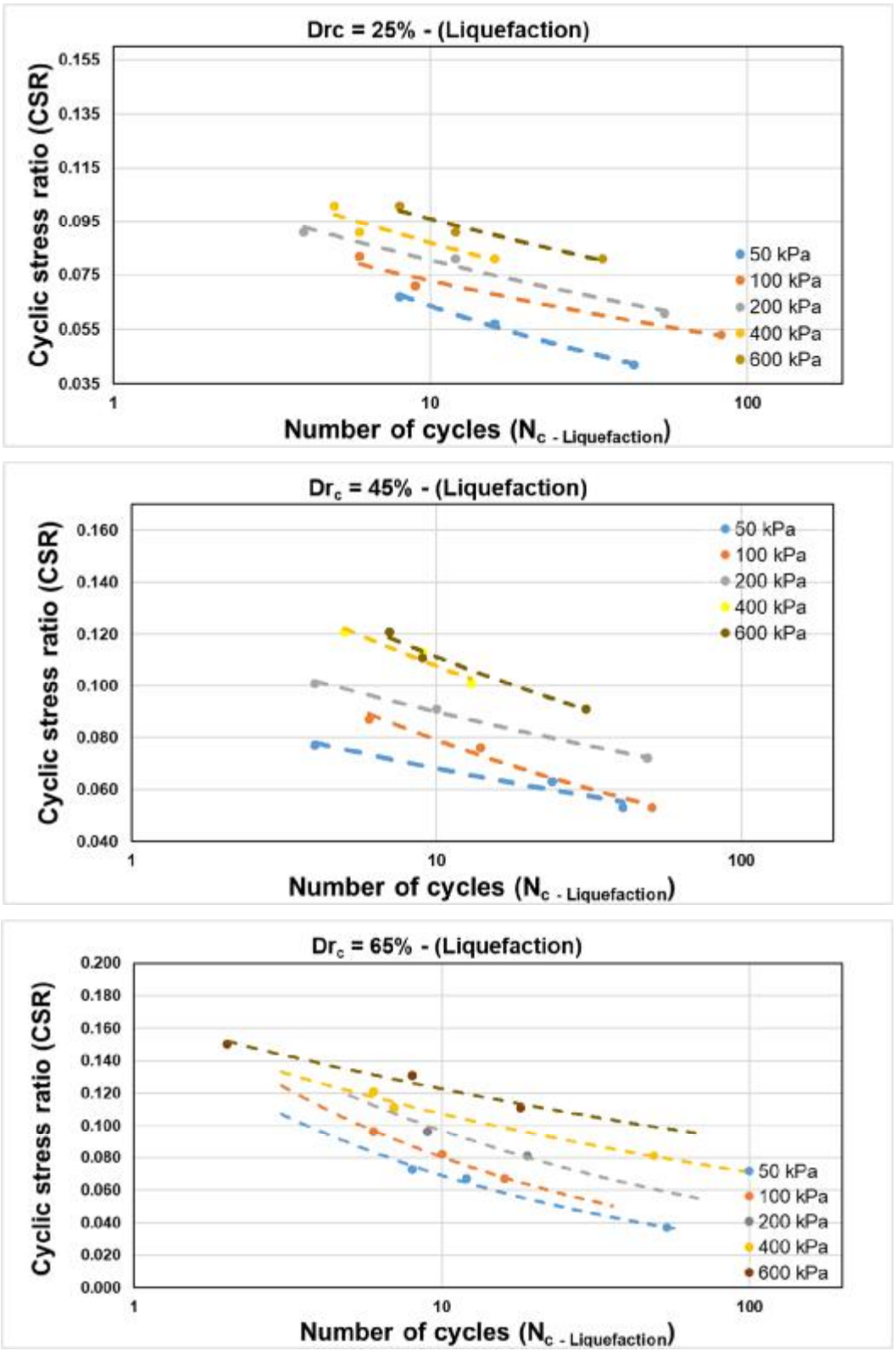


**Figure 3.10: CSR versus $N_C$ for bi-directional / circular loads at liquefaction**

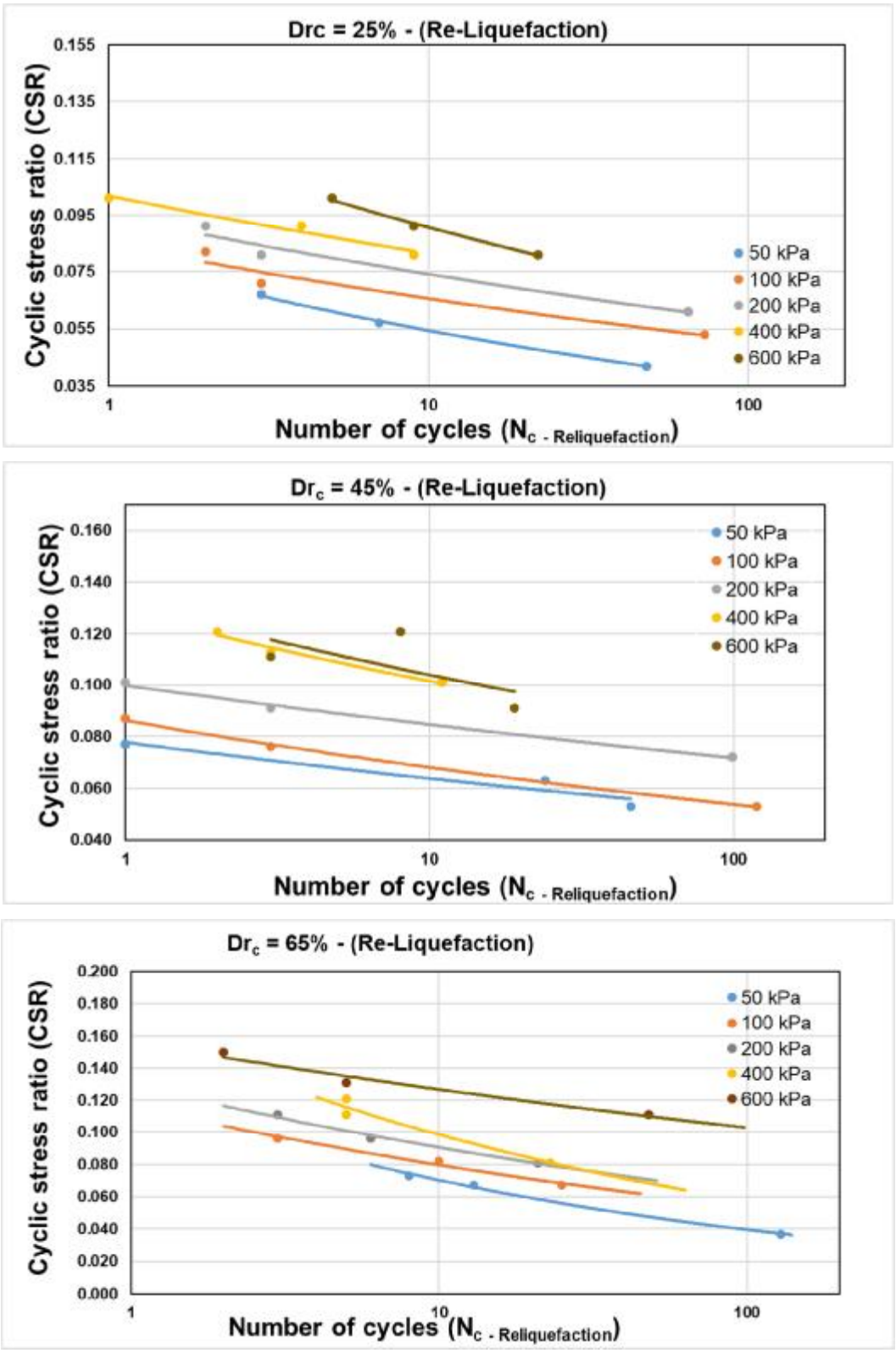


**Figure 3.11: CSR versus $N_C$ for bi-directional / circular loads at re-liquefaction**

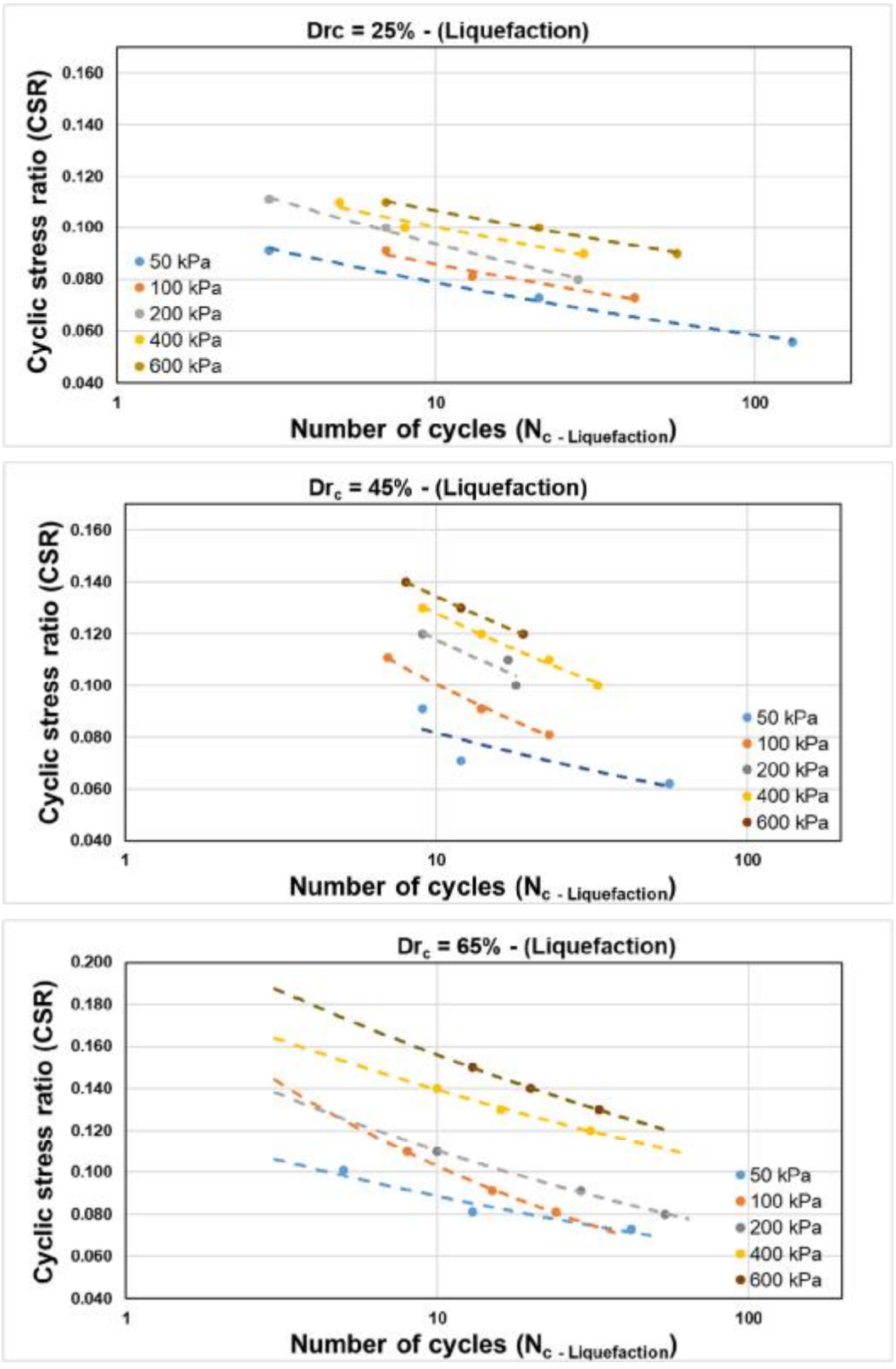


**Figure 3.12: CSR versus $N_C$ for bi-directional / elliptical loads at liquefaction**

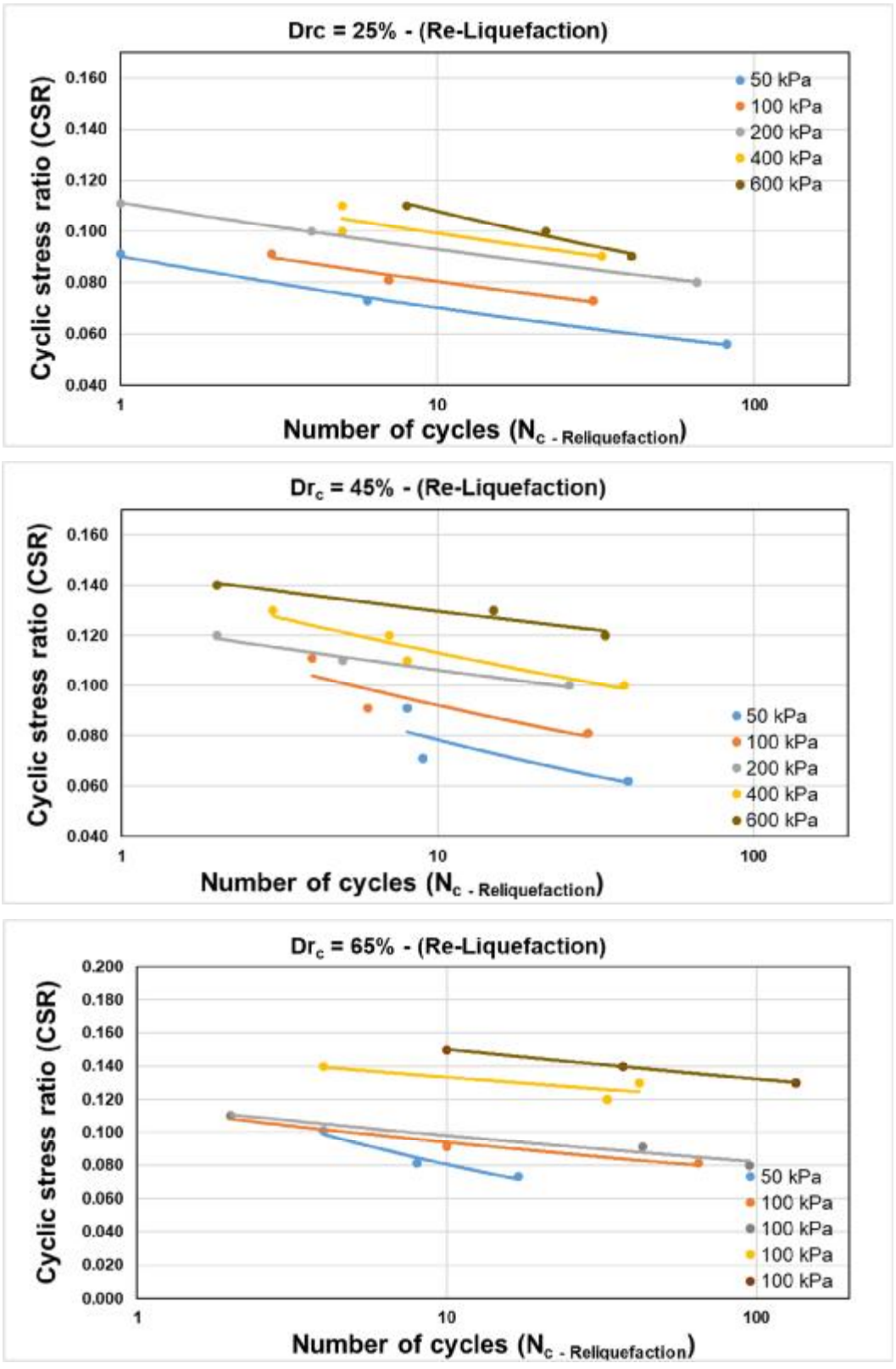


**Figure 3.13: CSR versus $N_C$ for bi-directional / elliptical loads at re-liquefaction**

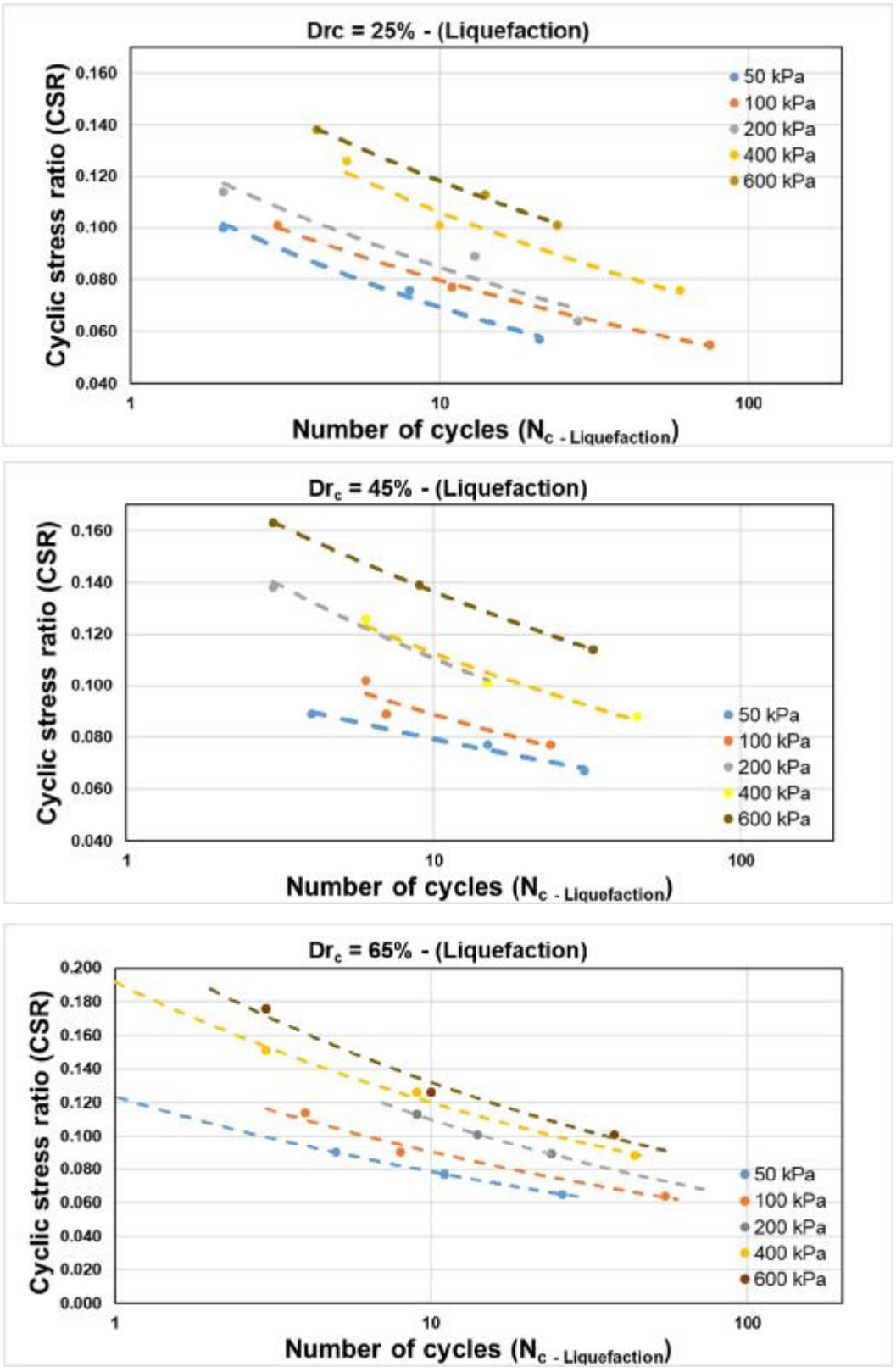


**Figure 3.14: CSR versus $N_C$ for bi-directional / figure-8 loads at liquefaction**

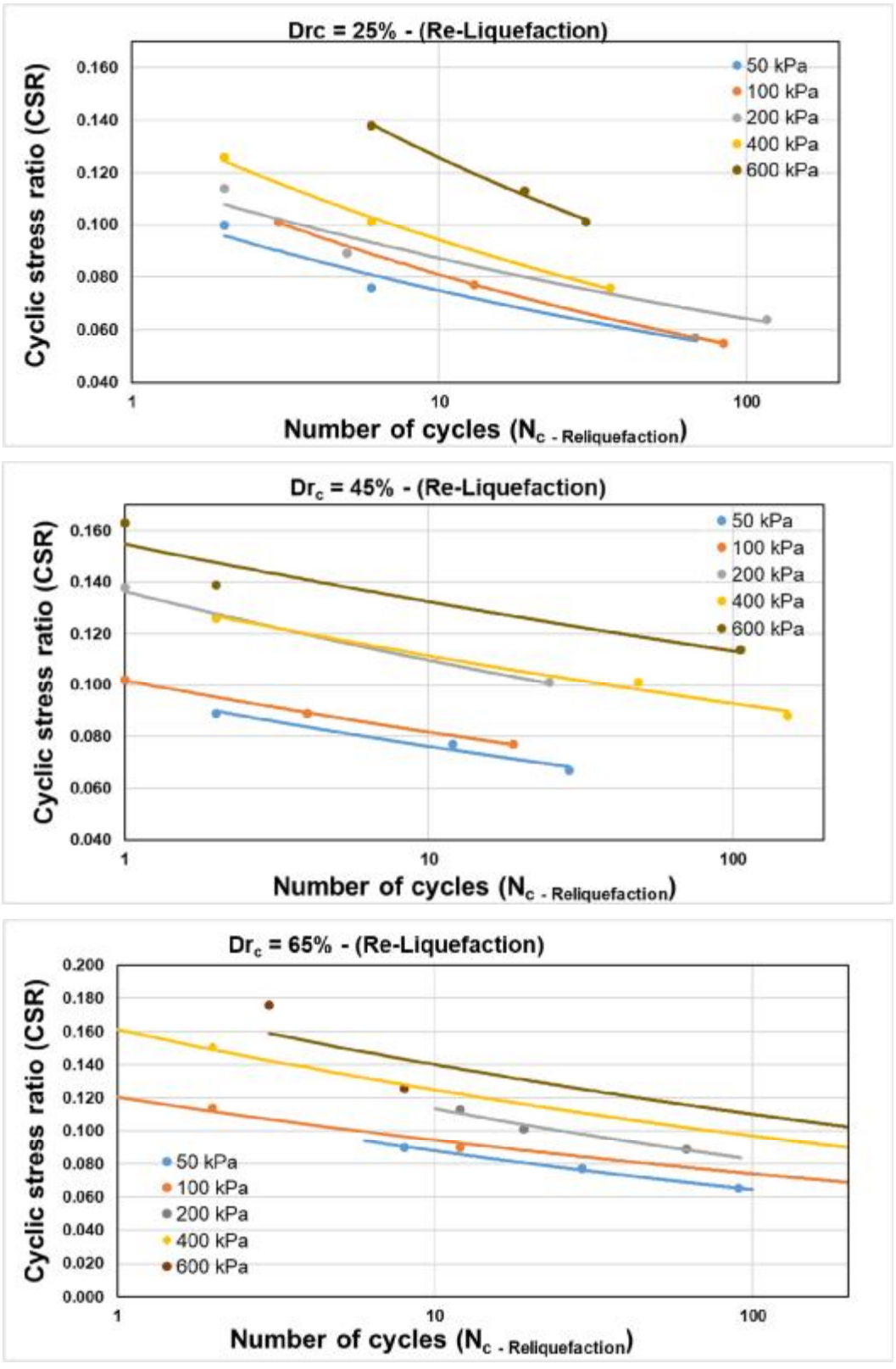


**Figure 3.15: CSR versus $N_C$ for bi-directional / figure-8 loads at re-liquefaction**

As shown in Figures 3.8 to 3.15 for various cyclic load patterns of this study, CSR values depend on effective stress (confining stress) in addition to relative density. Seed (1983) proposed an overburden correction factor ($K_\sigma$) to show how CRR values relate consolidations stress of the soil. Based on this definition:

$$K_\sigma = \frac{CRR_{\sigma' vc}}{CRR_{\sigma' vc=100\ kPa}} \tag{3.8}$$

Where $CRR_{\sigma'_{vc}}$ and $CRR_{\sigma'_{vc}=1atm}$ are the cyclic resistance ratios (CRR) at a given $\sigma'_{vc}$ and at $\sigma'_{vc}$ = 1 atm (≈ 100 kPa), respectively for the level ground condition. It was also shown by Vaid and Sivathayalan (1996) that $K_\sigma$ factor changes in variable relative densities as shown in Figure 3.16 for Fraser Delta sand specimens.

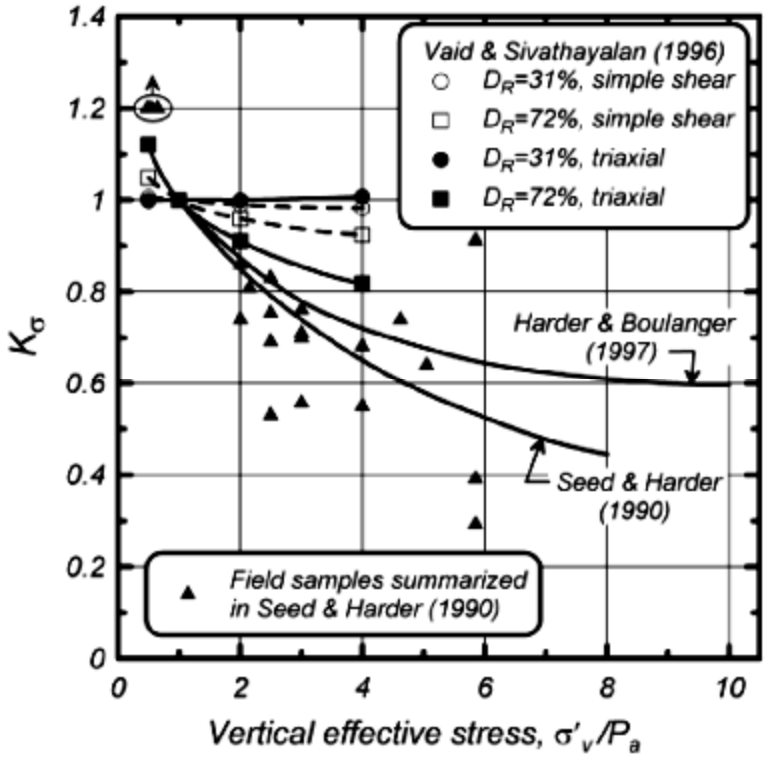


**Figure 3.16: Effect of the relative density changes on $K_\sigma$ factor for Fraser delta river sand specimens (Idriss and Boulanger 2008)**

**Table 3.4: CSR regression parameters for power function of $CSR = \alpha . N_C^{-\beta}$ used for calculation of CRR (CSR at 15 number of cycles) for loose ($D_{rc}$ = 25%) samples**

| Mono | | | | | | |
|---|---|---|---|---|---|---|
| | Liquefaction | | Re-liquefaction | | | |
| σ'vc | α | β | α | β | $CRR_1$ | $CRR_2$ |
| 50 | 0.1103 | -0.140 | 0.1078 | -0.195 | 0.075 | 0.064 |
| 100 | 0.1393 | -0.199 | 0.1220 | -0.207 | 0.081 | 0.070 |
| 200 | 0.1720 | -0.192 | 0.1256 | -0.138 | 0.102 | 0.086 |
| 400 | 0.1767 | -0.168 | 0.1548 | -0.165 | 0.112 | 0.099 |
| 600 | 0.1651 | -0.157 | 0.1484 | -0.161 | 0.108 | 0.096 |

| Circular | | | | | | |
|---|---|---|---|---|---|---|
| | Liquefaction | | Re-liquefaction | | | |
| σ'vc | α | β | α | β | $CRR_1$ | $CRR_2$ |
| 50 | 0.1203 | -0.276 | 0.0798 | -0.167 | 0.057 | 0.051 |
| 100 | 0.1042 | -0.155 | 0.0845 | -0.110 | 0.068 | 0.063 |
| 200 | 0.1150 | -0.155 | 0.0946 | -0.106 | 0.076 | 0.071 |
| 400 | 0.1275 | -0.166 | 0.1019 | -0.098 | 0.081 | 0.078 |
| 600 | 0.1328 | -0.141 | 0.1272 | -0.147 | 0.091 | 0.085 |

| Eliptical | | | | | | |
|---|---|---|---|---|---|---|
| | Liquefaction | | Re-liquefaction | | | |
| σ'vc | α | β | α | β | $CRR_1$ | $CRR_2$ |
| 50 | 0.1058 | -0.128 | 0.0902 | -0.110 | 0.075 | 0.067 |
| 100 | 0.1127 | -0.119 | 0.0991 | -0.092 | 0.082 | 0.077 |
| 200 | 0.1317 | -0.148 | 0.1112 | -0.078 | 0.088 | 0.090 |
| 400 | 0.1283 | -0.107 | 0.1195 | -0.081 | 0.096 | 0.096 |
| 600 | 0.1329 | -0.096 | 0.1422 | -0.120 | 0.102 | 0.103 |

| Figure 8 | | | | | | |
|---|---|---|---|---|---|---|
| | Liquefaction | | Re-liquefaction | | | |
| σ'vc | α | β | α | β | $CRR_1$ | $CRR_2$ |
| 50 | 0.1196 | -0.236 | 0.1064 | -0.153 | 0.063 | 0.070 |
| 100 | 0.1229 | -0.188 | 0.1232 | -0.182 | 0.074 | 0.075 |
| 200 | 0.1351 | -0.203 | 0.1183 | -0.133 | 0.078 | 0.083 |
| 400 | 0.1662 | -0.195 | 0.1404 | -0.173 | 0.098 | 0.088 |
| 600 | 0.1757 | -0.172 | 0.1948 | -0.190 | 0.110 | 0.116 |

$CRR_1$: CRR for liquefaction

$CRR_2$: CRR for liquefaction

$\sigma'_{vc}$: Vertical effective stress (kPa)

**Table 3.5: CSR regression parameters for power function of $CSR = \alpha . N_C^{-\beta}$ used for calculation of CRR (CSR at 15 number of cycles) for medium dense ($D_{rc}$ = 45%) samples**

| Mono | | | | | | |
|---|---|---|---|---|---|---|
| | Liquefaction | | Re-liquefaction | | | |
| σ'vc | α | β | α | β | $CRR_1$ | $CRR_2$ |
| 50 | 0.1339 | -0.171 | 0.1091 | -0.129 | 0.084 | 0.077 |
| 100 | 0.1267 | -0.108 | 0.1082 | -0.059 | 0.095 | 0.092 |
| 200 | 0.1953 | -0.202 | 0.1175 | -0.076 | 0.113 | 0.096 |
| 400 | 0.1888 | -0.137 | 0.1571 | -0.078 | 0.130 | 0.127 |
| 600 | 0.2146 | -0.127 | 0.1662 | -0.044 | 0.152 | 0.148 |

| Circular | | | | | | |
|---|---|---|---|---|---|---|
| | Liquefaction | | Re-liquefaction | | | |
| σ'vc | α | β | α | β | $CRR_1$ | $CRR_2$ |
| 50 | 0.0957 | -0.148 | 0.0778 | -0.087 | 0.064 | 0.061 |
| 100 | 0.1359 | -0.235 | 0.0861 | -0.102 | 0.072 | 0.065 |
| 200 | 0.123 | -0.136 | 0.0999 | -0.072 | 0.085 | 0.082 |
| 400 | 0.164 | -0.182 | 0.1283 | -0.101 | 0.100 | 0.098 |
| 600 | 0.1691 | -0.182 | 0.1320 | -0.103 | 0.103 | 0.100 |

| Eliptical | | | | | | |
|---|---|---|---|---|---|---|
| | Liquefaction | | Re-liquefaction | | | |
| σ'vc | α | β | α | β | $CRR_1$ | $CRR_2$ |
| 50 | 0.1205 | -0.169 | 0.1176 | -0.176 | 0.076 | 0.073 |
| 100 | 0.1856 | -0.266 | 0.1251 | -0.132 | 0.090 | 0.088 |
| 200 | 0.1913 | -0.211 | 0.1248 | -0.07 | 0.108 | 0.103 |
| 400 | 0.2018 | -0.198 | 0.1427 | -0.1 | 0.118 | 0.109 |
| 600 | 0.2026 | -0.178 | 0.1460 | -0.051 | 0.125 | 0.127 |

| Figure 8 | | | | | | |
|---|---|---|---|---|---|---|
| | Liquefaction | | Re-liquefaction | | | |
| σ'vc | α | β | α | β | $CRR_1$ | $CRR_2$ |
| 50 | 0.1083 | -0.135 | 0.0965 | -0.102 | 0.075 | 0.073 |
| 100 | 0.1314 | -0.170 | 0.1019 | -0.095 | 0.083 | 0.079 |
| 200 | 0.1741 | -0.196 | 0.1365 | -0.094 | 0.102 | 0.106 |
| 400 | 0.1685 | -0.174 | 0.1341 | -0.08 | 0.105 | 0.108 |
| 600 | 0.1923 | -0.149 | 0.1548 | -0.068 | 0.128 | 0.129 |

$CRR_1$: CRR for liquefaction

$CRR_2$: CRR for liquefaction

$\sigma'_{vc}$: Vertical effective stress (kPa)

**Table 3.6: CSR regression parameters for power function of $CSR = \alpha . N_C^{-\beta}$ used for calculation of CRR (CSR at 15 number of cycles) for dense ($D_{rc}$ = 65%) samples**

| Mono | | | | | | |
|---|---|---|---|---|---|---|
| | Liquefaction | | Re-liquefaction | | | |
| σ'vc | α | β | α | β | $CRR_1$ | $CRR_2$ |
| 50 | 0.169 | -0.264 | 0.1214 | -0.205 | 0.083 | 0.070 |
| 100 | 0.1953 | -0.236 | 0.1303 | -0.150 | 0.103 | 0.087 |
| 200 | 0.1922 | -0.18 | 0.1983 | -0.155 | 0.118 | 0.130 |
| 400 | 0.2509 | -0.191 | 0.2715 | -0.178 | 0.150 | 0.168 |
| 600 | 0.2447 | -0.155 | 0.3364 | -0.190 | 0.161 | 0.201 |

| Circular | | | | | | |
|---|---|---|---|---|---|---|
| | Liquefaction | | Re-liquefaction | | | |
| σ'vc | α | β | α | β | $CRR_1$ | $CRR_2$ |
| 50 | 0.1608 | -0.366 | 0.1244 | -0.249 | 0.060 | 0.063 |
| 100 | 0.1867 | -0.366 | 0.117 | -0.168 | 0.069 | 0.074 |
| 200 | 0.1913 | -0.295 | 0.1303 | -0.159 | 0.086 | 0.085 |
| 400 | 0.162 | -0.179 | 0.1691 | -0.235 | 0.100 | 0.089 |
| 600 | 0.1666 | -0.133 | 0.1563 | -0.091 | 0.116 | 0.122 |

| Eliptical | | | | | | |
|---|---|---|---|---|---|---|
| | Liquefaction | | Re-liquefaction | | | |
| σ'vc | α | β | α | β | $CRR_1$ | $CRR_2$ |
| 50 | 0.1251 | -0.15 | 0.1345 | -0.223 | 0.083 | 0.074 |
| 100 | 0.196 | -0.28 | 0.1149 | -0.087 | 0.092 | 0.091 |
| 200 | 0.1699 | -0.188 | 0.1169 | -0.077 | 0.102 | 0.095 |
| 400 | 0.1904 | -0.135 | 0.1489 | -0.048 | 0.132 | 0.131 |
| 600 | 0.2221 | -0.153 | 0.1705 | -0.055 | 0.147 | 0.147 |

| Figure 8 | | | | | | |
|---|---|---|---|---|---|---|
| | Liquefaction | | Re-liquefaction | | | |
| σ'vc | α | β | α | β | $CRR_1$ | $CRR_2$ |
| 50 | 0.1236 | -0.197 | 0.1196 | -0.134 | 0.072 | 0.083 |
| 100 | 0.147 | -0.211 | 0.1204 | -0.106 | 0.083 | 0.090 |
| 200 | 0.1924 | -0.243 | 0.1559 | -0.138 | 0.100 | 0.107 |
| 400 | 0.1916 | -0.203 | 0.1611 | -0.110 | 0.111 | 0.120 |
| 600 | 0.2181 | -0.218 | 0.1667 | -0.093 | 0.121 | 0.130 |

CRR values of the current study were calculated and shown in Tables 3.4, 3.5, and 3.6. To compare overburden pressure correction factors of this study with existing experimental results, the variation of $K_\sigma$ at different stress ratio (relative to 100 kPa), is plotted and shown in Figure 3.17. Similar plots were obtained for re-liquefied samples.

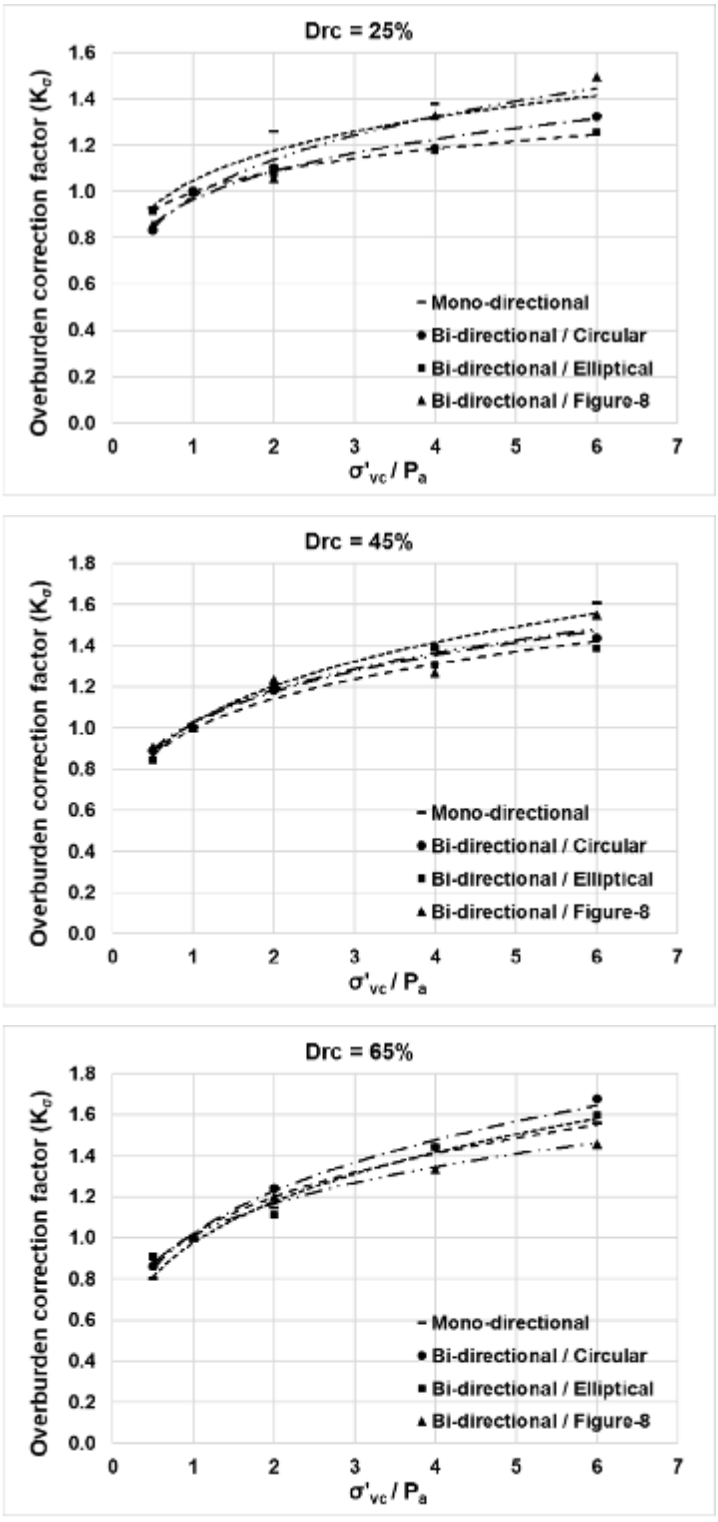


**Figure 3.17: Overburden correction factor ($K_\sigma$) factor variation with effective stress for Boler sand (liquefaction) at three different relative densities ($D_{rc}$ = 25%, 45%, and 65%)**

Based on the findings, at looser samples ($D_{rc}$ = 25%), mono-directionally loaded tests exhibit a larger increase in $K_\sigma$ with increasing $\sigma'_{vc}$ relative to bi-directionally loaded tests while figure-8 pattern loaded samples show a closer behavior to unidirectional and circular or elliptical pattern loaded samples experience a smaller increase. This would suggest that different loading conditions would play a role in the increase of cyclic resistance with increasing soil depth. In addition, some of the previous studies, report for a decreasing trend of $K_\sigma$ with increasing $\sigma'_{vc}$ (Idriss & Boulanger 2006; Hynes & Olsen 1998) unlike to the results of the current study which shows an increasing trend, regardless of load pattern and relative density. Robertson et al. (2000) and Wijewickreme et al. (2005) (for water pluviated specimens) demonstrated declining and flat CRR values with increasing $\sigma'_{vc}$ respectively. A common practice to investigate the changing trend of $K_\sigma$ in variable stress levels has begun. There is evidence of a flattened trend in many of recent researches (Idriss and Boulanger 2008). On the other hand, the studies of Sadrekarimi (2016) and Wijewickreme et al. (2005) show results for Fraser River sand that demonstrate the increase of CRR with increasing consolidation stress. Viana Da Fonseca et al. (2015) also performed cyclic simple shear tests on two types of sands (Algeria and Coimbra) to observe the CRR variation of these sands at different densities and consolidation stresses. Both sands are poorly-graded silica-based fine-grained sands, similar to Fraser river sand. The comparison of the results by Sadrekarimi (2016), Wijewickreme et al. (2005), and Viana Da Fonseca et al. (2015) with the current study, is shown in Figure 3.18. Based on their findings, CRR values gets larger with increasing consolidation stress, like results of this study. The common point of current study and the previous studies which show similar trends on CRR variation with increasing stress is the grading and particle sizes distribution. As it was mentioned in the previous chapter, Boler sands grading was adjusted exactly similar to Fraser river sand. This could be a point of further research, that how grading may affect sands controlled behavior in cyclic loading events. Also, the use of overburden correction factor correlations proposed by Idriss & Boulanger (2006) and Hynes & Olsen (1998) is under question as they do not appear to represent a comprehensive response for all type of sands. Although some of the past studies report for sample preparation effect on the cyclic response of the samples in laboratory tests, grading and particle size distribution seems to be another high impacting factor which could be investigated in future studies.

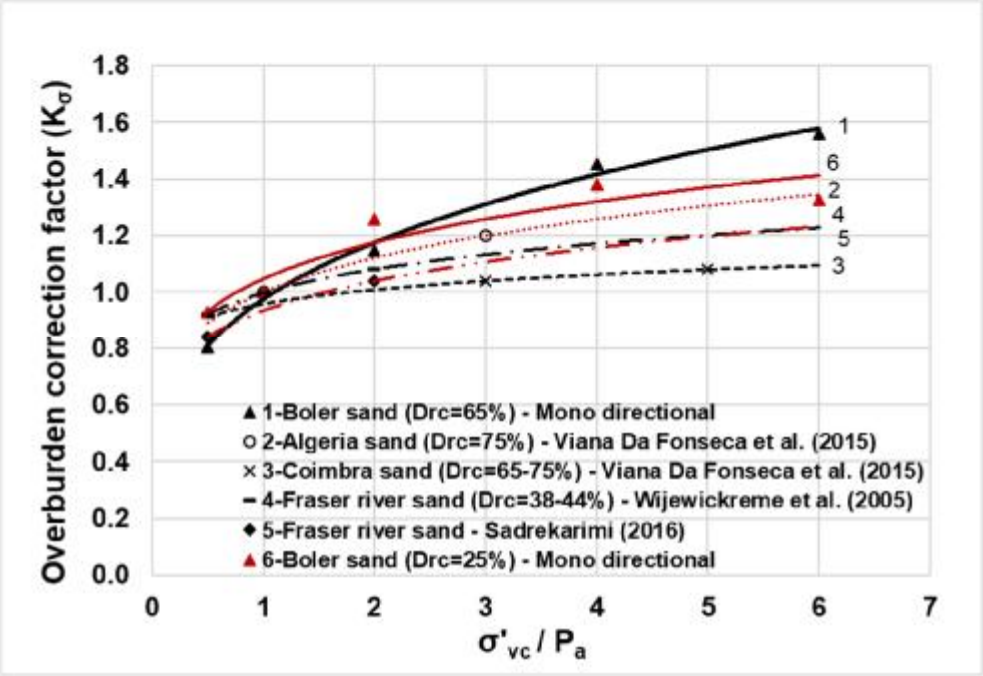


**Figure 3.18: Comparison of $K_\sigma$ factor variation with $\sigma'_{vc}$ for various research studies**

3.4.2. Bi-directional to mono-directional load adjustment ratio

As discussed previously, Seed et al. (1975) proposed a reduction factor of 0.8 to 0.9 applicable to calculated cyclic resistance ratios (CRR) to account for the effect of multi-directional loading relative to mono-directional loading, in liquefaction analysis. Ishihara et al. (1980) and later Kammerer et al. (2004) suggested based on various cyclic tests that, adjustment ratios of 0.8 and 0.9 are an underestimation while introducing a wider range of 0.6 to 1.3 for this ratio. Smaller CSR values in individual directions of a multi-directional loading combined with rotation of stress path in horizontal plane along with releasing of loads which affects both interlock of particles and pore pressure generation variation during load application and removal cycles, creates diverse scenarios which are supposed to be the reason for such a wide range of CRR adjustment ratios. It is shown in Figure 3.19, 3.20, 3.21, 3.22, and 3.23 that, how cyclic resistance ratio (CRR) of similar samples at same relative density, changes for bi-directionally loaded samples comparing to mono-directionally loaded ones in the current study. Normally, there is a dropping resistance and in very few cases, an equal resistance or small increase in resistance of samples loaded in two directions relative to the same sample loaded in one direction is observed.

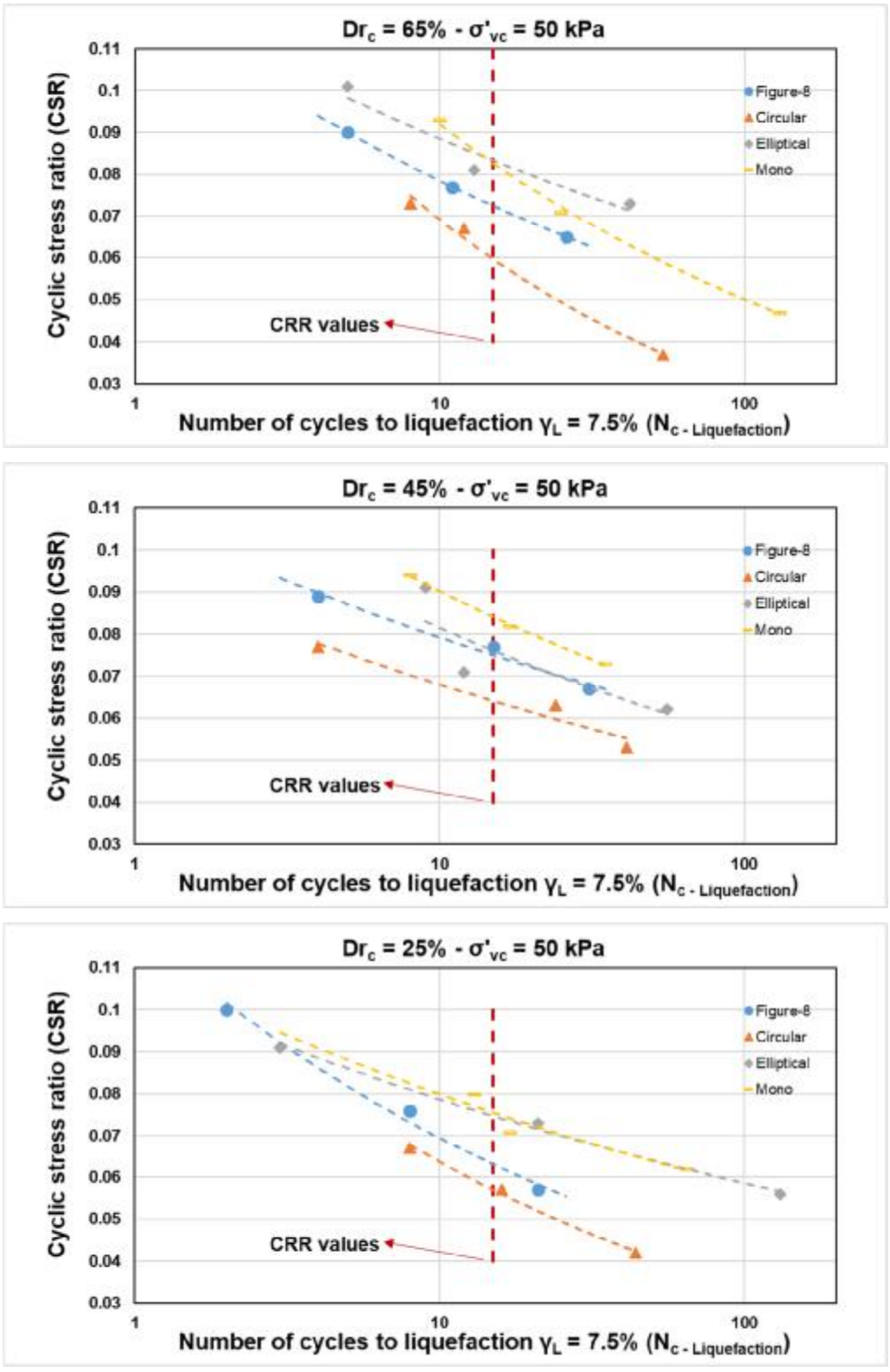


**Figure 3.19: CRR variation for one and two directional loaded samples (σ'$_{vc}$ = 50 kPa)**

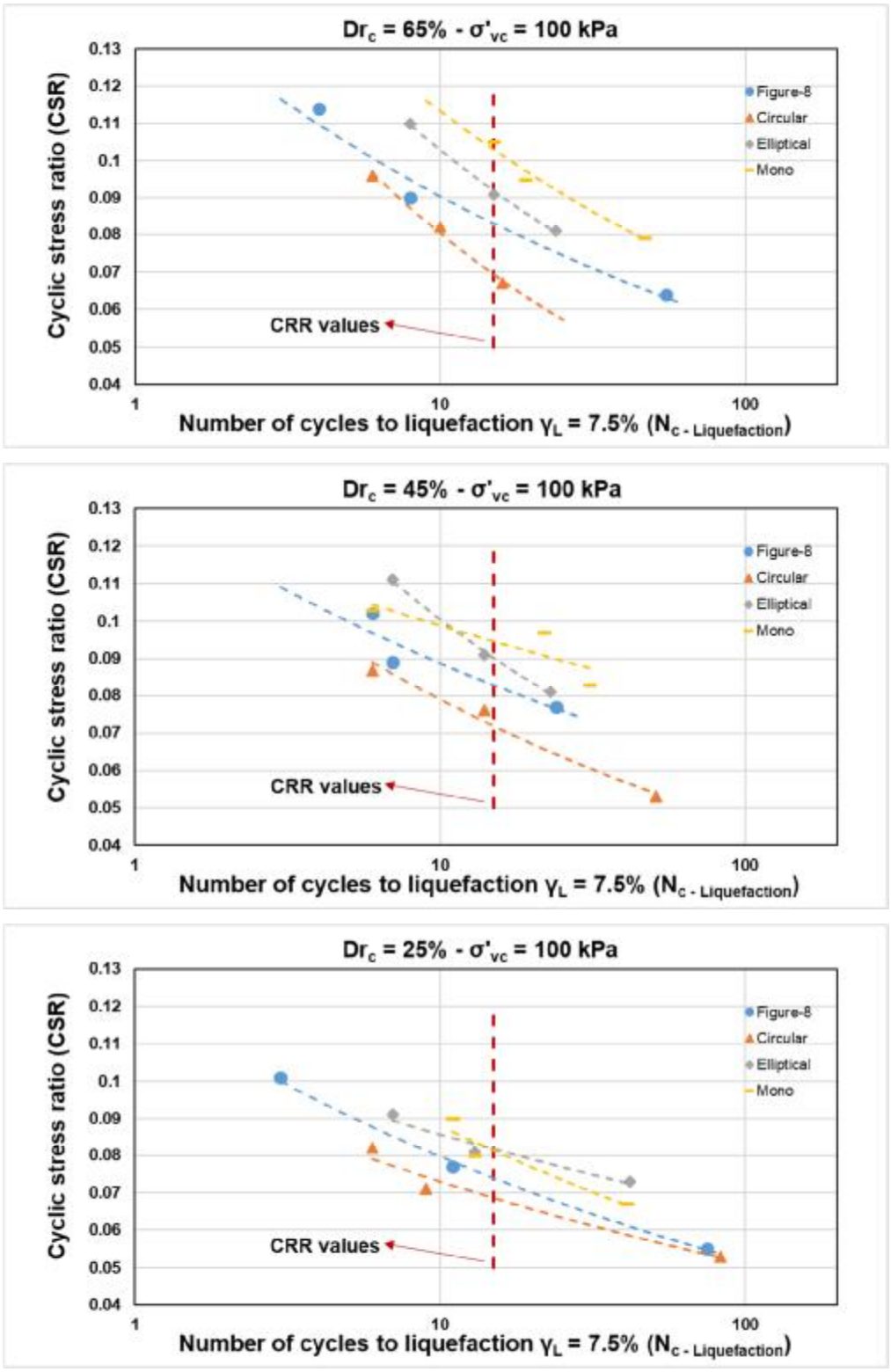


**Figure 3.20: CRR variation for one and two directional loaded samples (σ'$_{vc}$ = 100 kPa)**

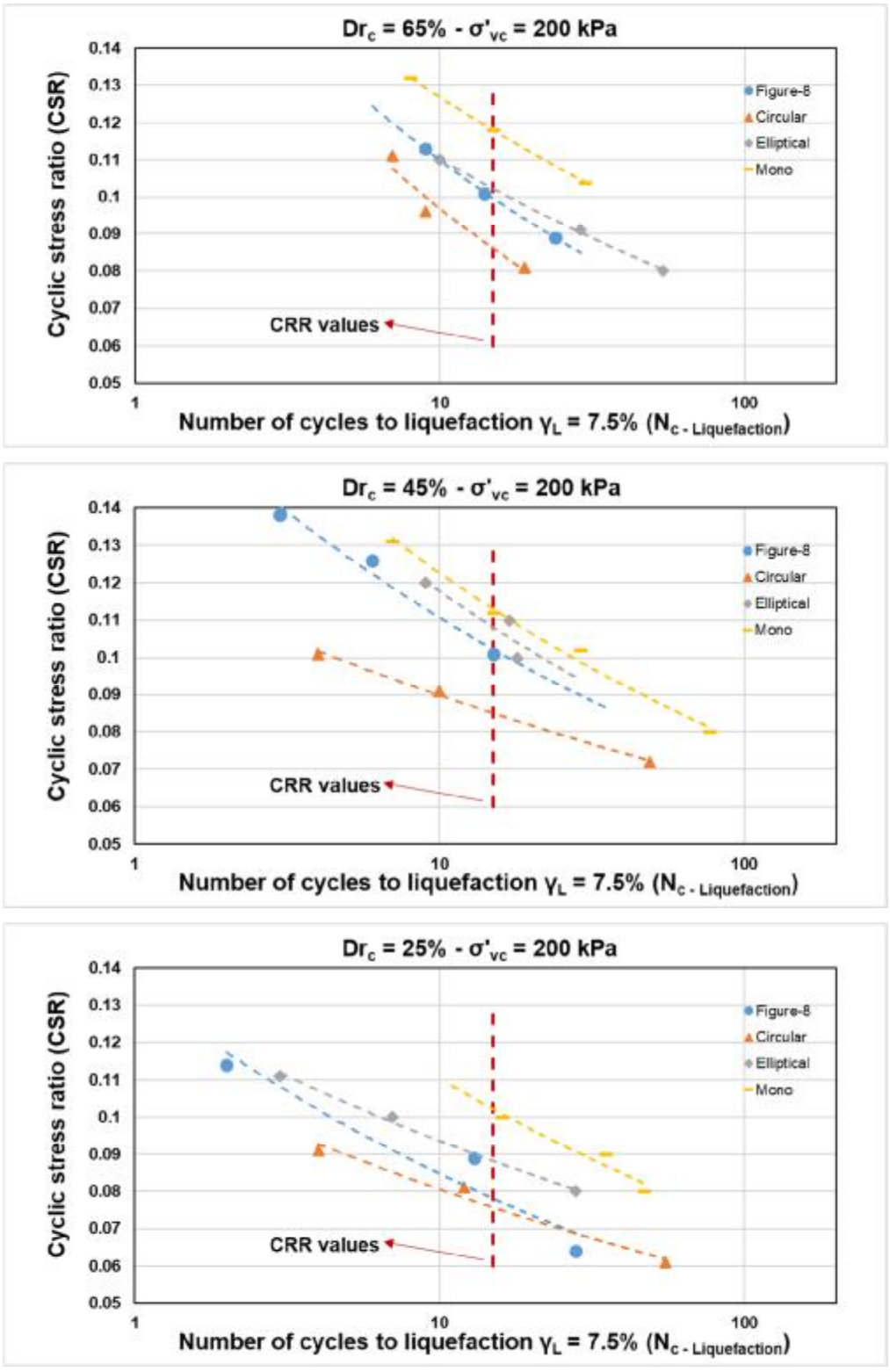


**Figure 3.21: CRR variation for one and two directional loaded samples (σ'$_{vc}$ = 200 kPa)**

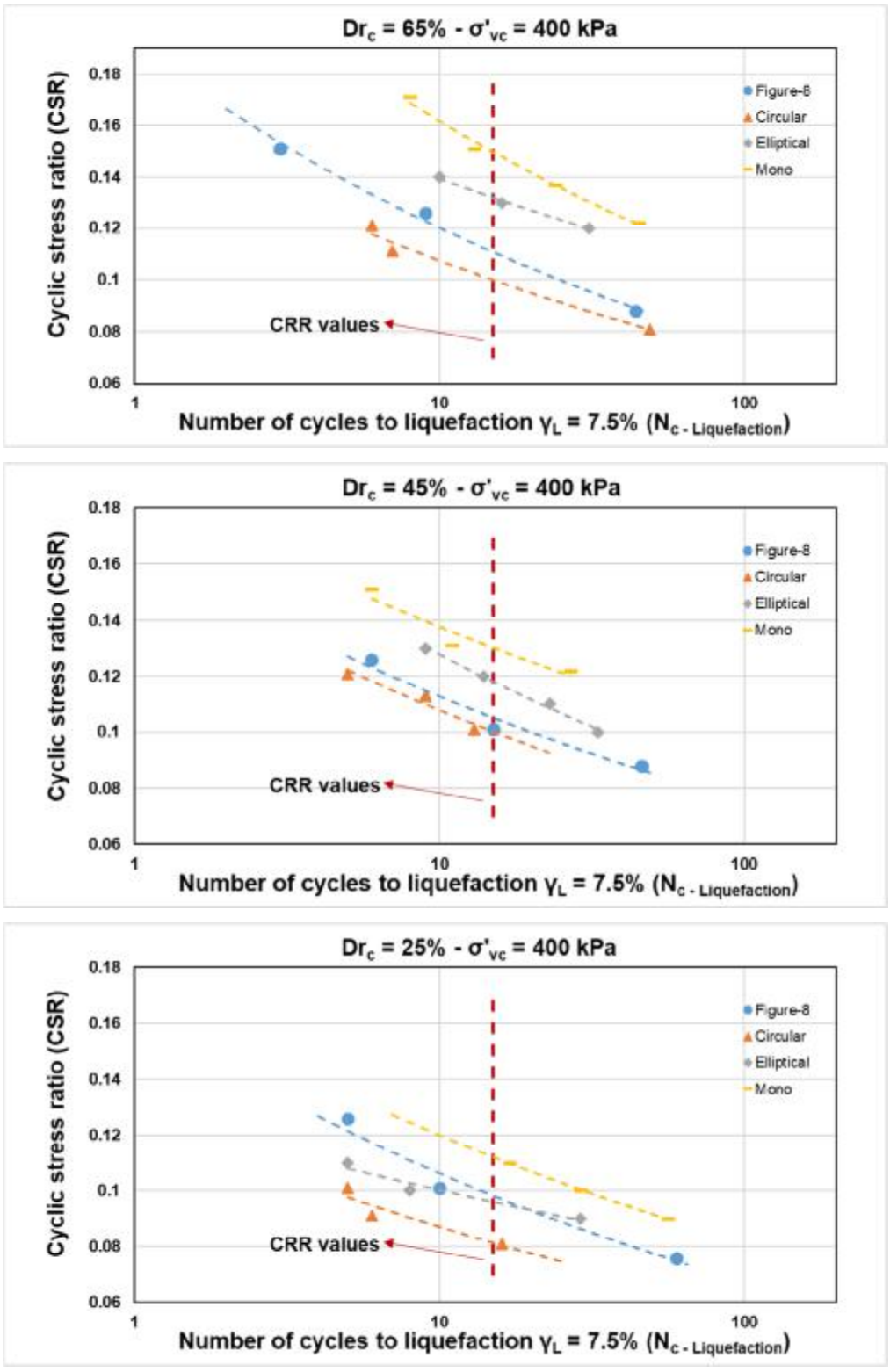


**Figure 3.22: CRR variation for one and two directional loaded samples (σ'$_{vc}$ = 400 kPa)**

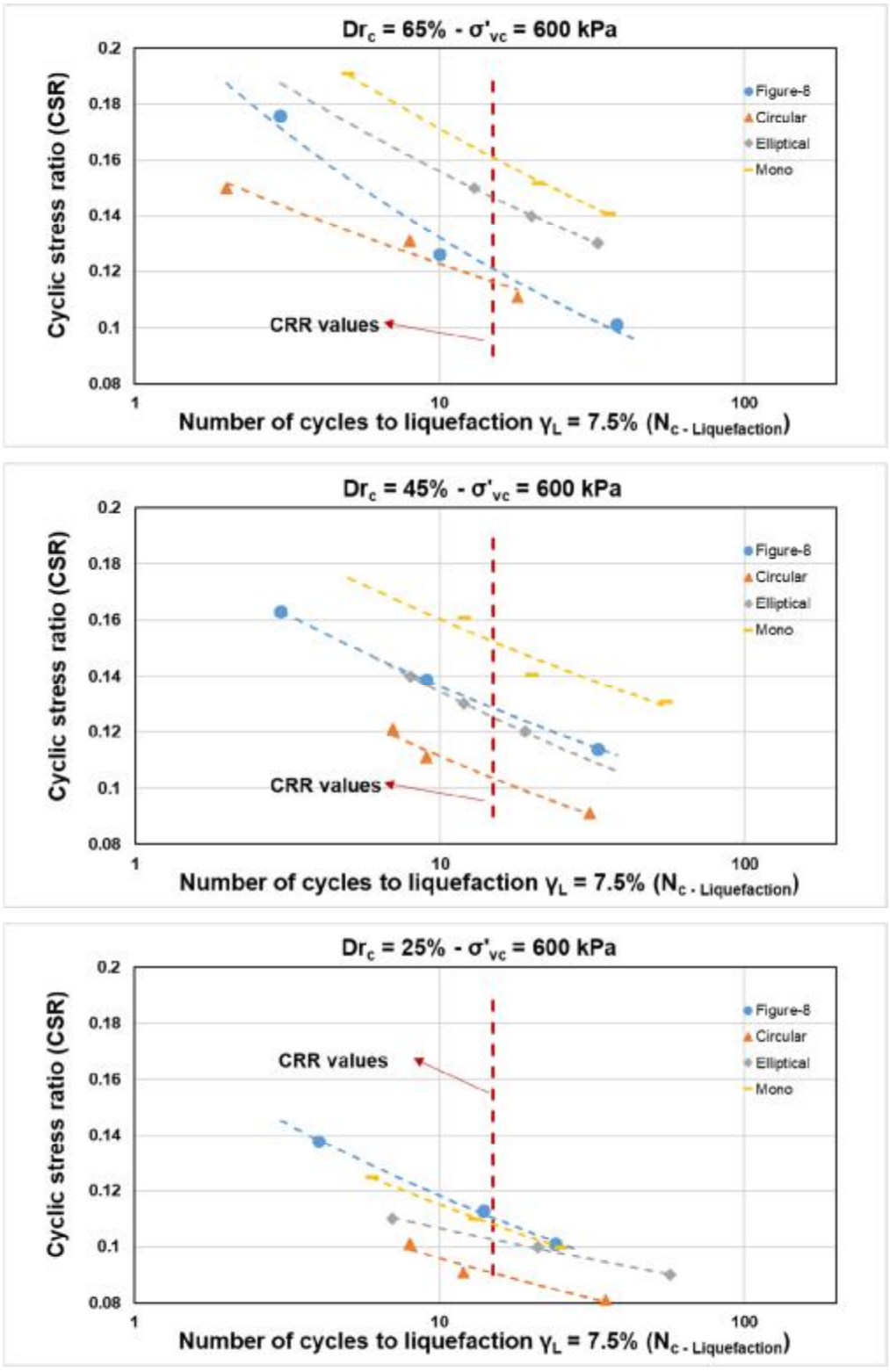


**Figure 3.23: CRR variation for one and two directional loaded samples (σ'$_{vc}$ = 600 kPa)**

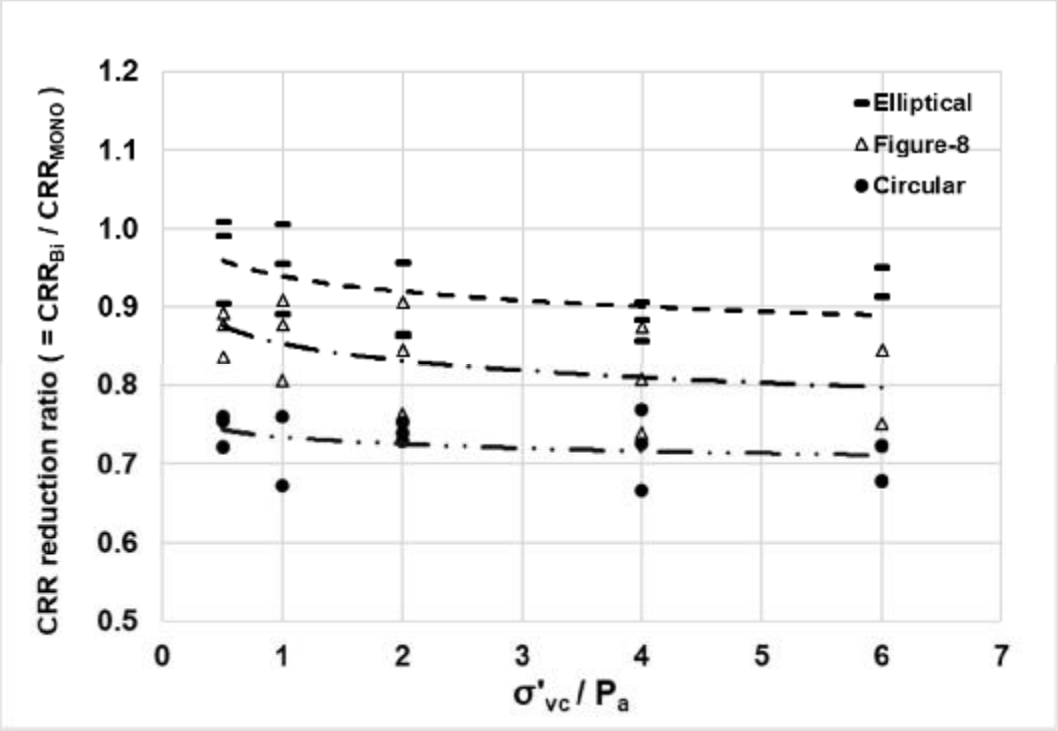


**Figure 3.24: Reduction factors to convert bi-directional to mono-directional CRR**

Based on the results of this study (Figures 3.19 to 3.23), the ratio of bi-directional to mono-directional CRR for 3 different bi-directional patterns varies as summarized in Figure 3.24.

A recent study on the effect of bi-directional cyclic loading was carried out by Kammerer (2002) on Monterey #30 sand. CRR for bi-directional loading in level ground conditions were found to be about 30 to 40% lower than those in mono-directional cyclic loads. This is greater than what is found in most other studies (Seed et al. 1976; Ishihara 1996; Pyke et al. 1974; Idriss & Boulanger 2008). Kammerer (2002) also noted that bi-directional loading using a circular shear stress path produced consistently larger reductions in CRR in comparison to oval- and "figure-8"-shaped cyclic stress paths. As demonstrated in Figure 3.24, cyclic resistance reduction factor for bi-directional to mono-directional cyclic loads varies between 0.67 to 1.03 in different load patterns which is in good agreement with Ishihara et al. (1980) and later Kammerer et al. (2004) research results on Fuji river sand and Monterey sand, although their results covered a wider range of almost 0.6 to 1.3 in some cases. Also, it is shown that there is a slight decrease in reduction factor with increasing stress level which is described as rather smaller impact of this effect at higher stress levels. Although the average of 0.85 for test results confirms Seed's early test results (0.8-0.9), a wider range of results could

not be ignored which makes it inevitable to consider other effective parameters to achieve more precise evaluations. Respectively, a smaller value of 0.67 recalls that previously suggested values by Seed et al. are underestimating the effect of adding a second direction of cyclic loading on soil response. It is also shown in Figure 3.24 that, among three main categories of bi-directional cyclic shear loads, the elliptical pattern causes the samples to experience the least resistance reduction in proportion to mono-directional loading and the circular pattern causes the largest drop. Reduction ratio due to a figure-8 pattern is between two other patterns. This is a very similar finding to results reported by Kammerer. Ishihara and Yamazaki also noted that circular pattern bi-directional loads, cause the highest resistance factor relative to a mono-directional load which current study is another confirmation. This, mainly depicts that, predicting the actual response of a soil to dynamic loads is not simple and affected by many factors which loading pattern could be one of them. It is recommended to consider a smaller value of CRR to cover all unpredictable cyclic load patterns. Average factors of 0.75, 0.85, and 0.95 are suggested in this study for reduction effect of the circular, figure-8 and elliptical loading patterns but a minimum factor of 0.65 is proposed for actual design purposes, because actual earthquake load patterns are quite unpredictable, in terms of directions and combined effect of individual direction.

### 3.4.3. Pore water pressure generation

The increased pore water pressure generated due to a cyclic shear load is the major cause of liquefaction in saturated sands and investigating pore water pressure attainment, plays an important role in assessment of this phenomenon. Many of past researchers performed experiments and monitored variation of this parameter during monotonic or cyclic loads. For example, Ishihara and Yamazaki reported a maximum pore water pressure attainment of 65% in elliptical cyclic pattern of loading and 75% for alternate pattern before liquefaction occurrence. Also, Boulanger and seed (1995) and Boulanger et al. (1993) investigated limitations for definition of liquefaction as reaching 100% excess pore pressure ratio and focused on soil conditions associated with dams. Kammerer et al. (2002) performed some cyclic tests on Monterey sand, which reported in lower than 100% generated excess pore water pressures at liquefaction. Boulanger (1993) reported formerly that, based on his bi-directional cyclic test results, pore water pressure attainment of samples at liquefaction was not necessarily 100%. Moreover, he proposed a linear correlation between applied cyclic shear values and

pore water pressure ratio at liquefaction as shown in Figure 3.25. Based on the results of current research, pore water pressure limit of samples at state of reaching liquefaction for each cyclic test is correlated to cyclic stress ratio of the same sample which is shown in Figure 3.25 and compared to proposed trend by Boulanger on Sacramento River sand. This plot illustrates that $r_{u\text{-}limit}$ ($r_u$ at liquefaction or double strain of 7.5%) variation with CSR changes in this study, is in good agreement with Boulanger test results. The Linear equation could formulate this correlation. As it is shown, pore water pressure generated at liquefaction decreases with increasing cyclic shear loads (CSR). This inverse relationship can be explained by the number of cycles to respond to a certain CSR. For a larger CSR, less number of cycles is required to reach liquefaction criterion (7.5% DA strain) and according to Figure 3.26, this leads to lower $r_u$. Figure 3.26 shows that the number of cycles to liquefy is proportional to pore water pressure attainment. Based on the results, pore water pressure ratio in liquefaction, for several tests of this study ranges between 70% to 90% which confirms previous cyclic test results on reaching a less than 100% $r_u$ at liquefaction under bi-directional shearing modes. It is also illustrated that a 100% pore water pressure generation only could happen in very high number of loading cycles which corresponds to very low cyclic stress.

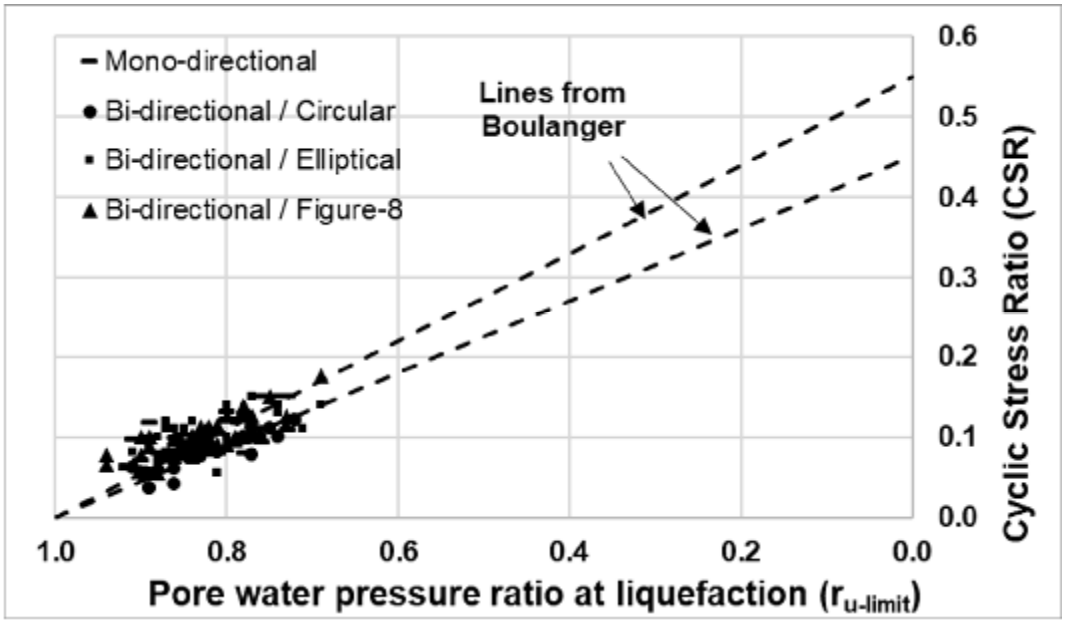


**Figure 3.25: Pore water pressure ratio at liquefaction ($r_{u\text{-}limit}$) variation with cyclic stress ratio (CSR) for cyclic DSS tests of Boler sand**

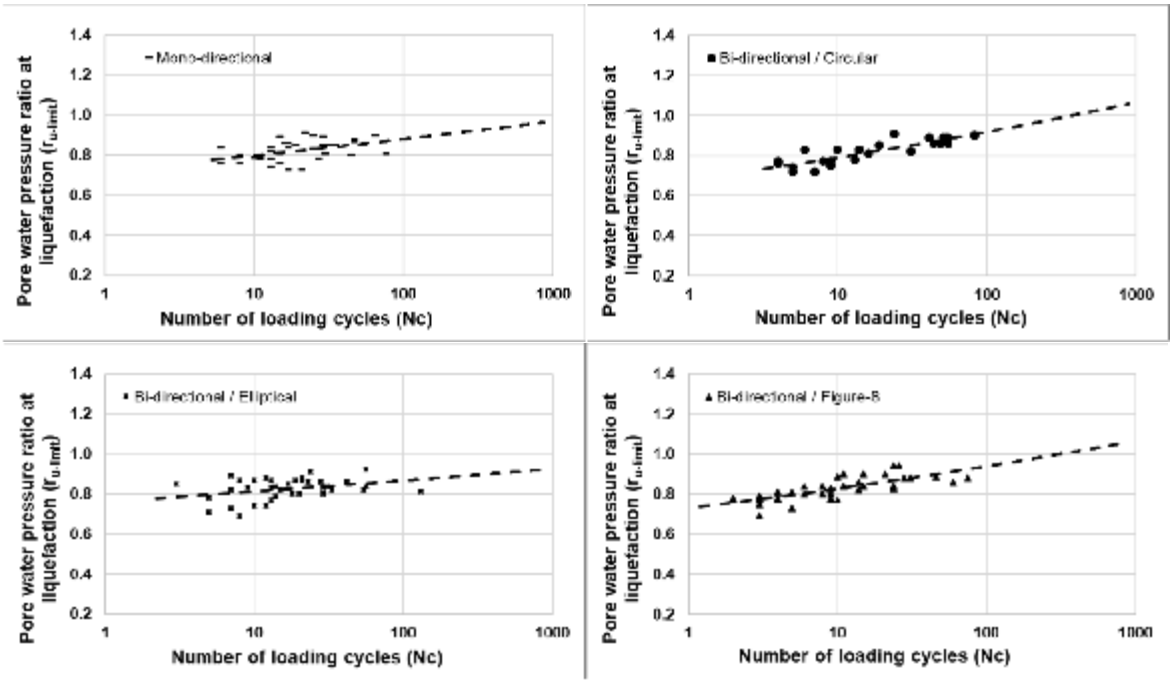


**Figure 3.26: Pore water pressure ratio at liquefaction ($r_{u\text{-}limit}$) variation with number of loading cycles ($N_C$) for cyclic DSS tests of Boler sand**

3.4.4. Critical state analysis approach to cyclic behavior

Cyclic behavior and liquefaction characteristics of a sand could be coupled to its state parameter variation. Vaid and Sivathayalan (1996) noted that the cyclic resistance ratio (CRR) of a sand specimen for a given test type can be expressed as an approximately unique function of state parameter. Critical state analysis approach is used to generalize the behavior of soil by correlating a response to soil state and considering both, effective stresses under which the soil is consolidated and soil void ratio of same soil. Based on the critical state parameters introduced in previous chapters, cyclic resistance ratio of the soil samples is correlated to their state at the onset of shearing. Figure 3.27 illustrates a changing trend for cyclic resistance ratio (CRR) values of loose to dense samples by state parameters (Ψ). Separate equations are found for different relative densities as an exponential function.

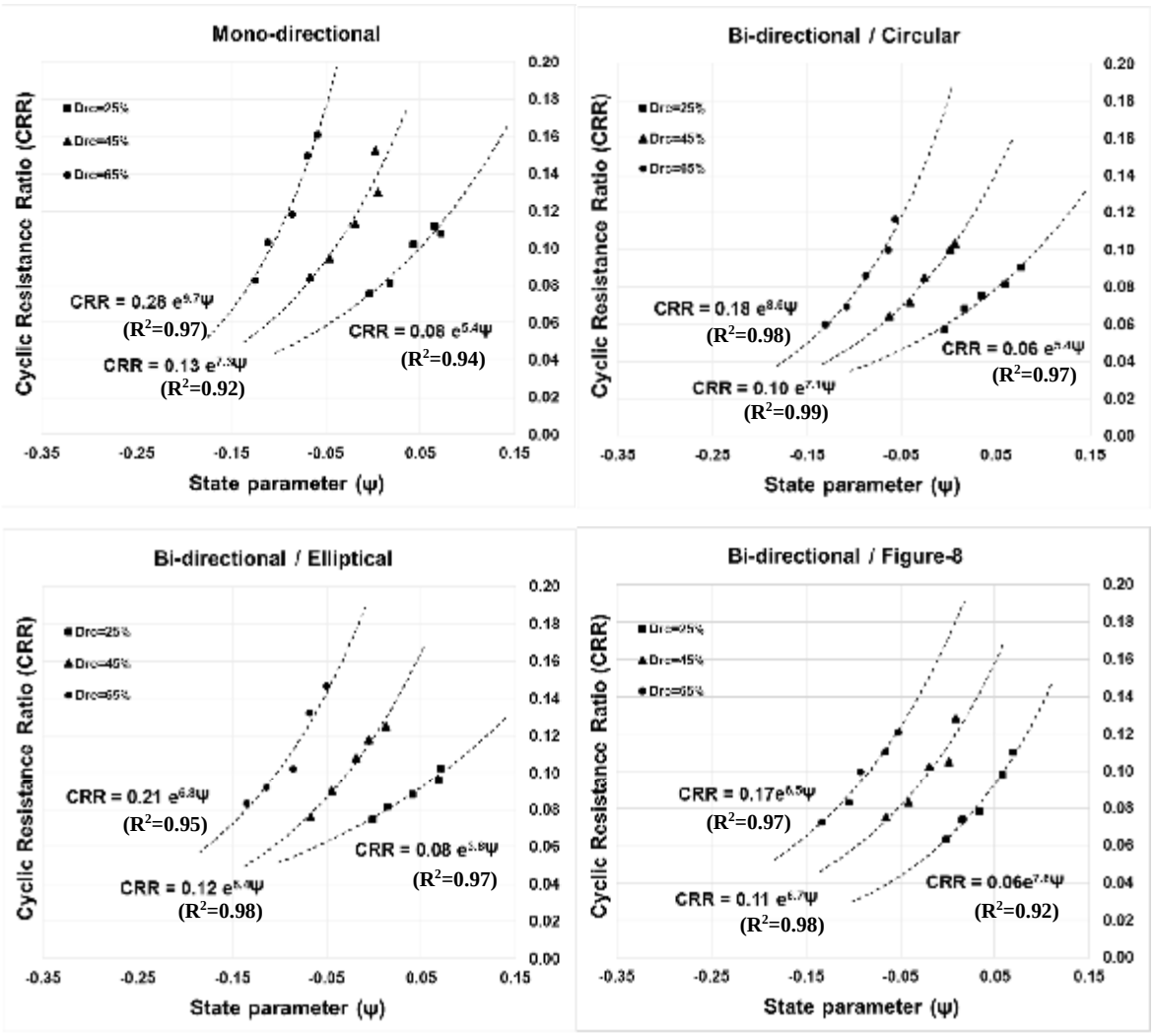


**Figure 3.27: CRR versus state parameter (Ψ) for cyclic DSS tests of Boler sand**

### 3.4.5. Evaluating CRR variation based on $V_S$ measurements

Although a critical state approach is a comprehensive approach to characterize and evaluate soil cyclic resistance by estimating soil state, this method is most beneficial when there is enough evidence about soil density (void ratio) and effective stress under which the soil is consolidated. It is more advantageous for laboratory reconstituted or undisturbed samples analysis. It could be difficult to evaluate soil in-situ states, specifically in deeper soil masses. Penetration tests (CPT, SPT, BPT, and LPT) are among the most conventional in-situ test that is used for predicting soil cyclic behavior. Shear wave velocity measurement is another method for in-situ liquefaction analysis and it has its own advantages over other methods since previous

methods are not useful when stiff layers with penetration difficulties exist. For evaluating cyclic resistance of Boler sand based on shear wave velocities, shear wave velocities of samples at various states were measured as was discussed in chapter 2. Figure 3.28 demonstrates how cyclic resistance ratio (CRR) of Boler sand is correlated with shear wave velocity measurements at similar states.

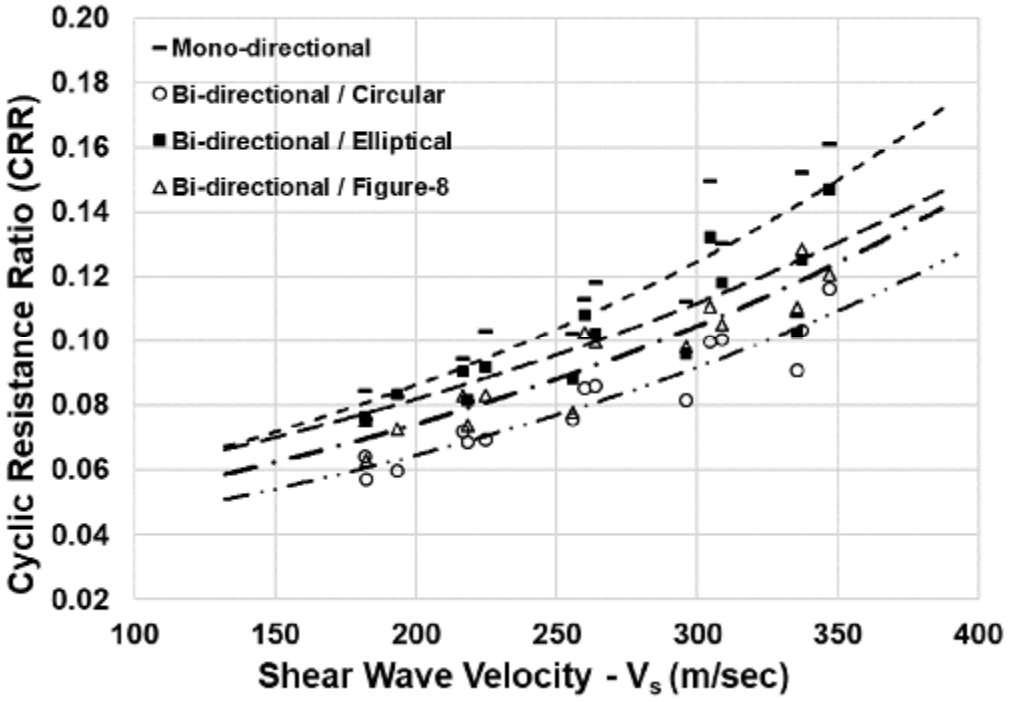


**Figure 3.28: Cyclic resistance ratio (CRR) versus shear wave velocity (Vs) correlations from cyclic DSS tests and bender element tests of this study for Boler sand**

General exponential equations could be developed for shear wave velocity and cyclic resistance ratio correlation of the Boler sand as shown in Equation 3.9. In Table 3.7, the most compatible exponential characterization factors of the equation are summarized.

$$CRR = a.e^{b.(V_S)} \tag{3.9}$$

**Table 3.7: Summary of factors for shear wave velocity and CRR correlation**

| Load pattern | a | b | $R^2$ |
|---|---|---|---|
| Mono-directional | 0.041 | 0.0037 | 0.79 |
| Bi-directional / Circular | 0.032 | 0.0035 | 0.89 |
| Bi-directional / Elliptical | 0.044 | 0.0031 | 0.78 |
| Bi-directional / Figure-8 | 0.037 | 0.0034 | 0.88 |

Although the correlations exhibit close trends and average set of factors could be used for prediction of cyclic resistance of soil deposits based on their measured shear wave velocity, it would be more conservative and recommended to consider the lowest resistance factors which are obtained based on circular pattern bi-directional cyclic tests in this study.

### 3.4.6. Liquefaction susceptibility analysis

Observing the consequences of liquefaction in earthquake events, caused researchers to investigate methods for correlating soil characteristics which could be mainly measured in the field (in-situ parameters) to soil cyclic resistance. The correlations are normally called “liquefaction triggering” curves and provide boundaries between the cases which have been observed as liquefied or not liquefied. The correlations have been developed based on the most conventional in-situ tests such as SPT, CPT, and Vs (shear wave velocity) measurement tests. Seed and Idriss (1970) are among the pioneers of researchers who proposed SPT based liquefaction triggering curves with case histories of previous earthquake events. This database considers for parameters such as SPT blow counts, relative density, and effective overburden stress to likelihood of a liquefaction event occurring (Seed & Idriss 1970). The most important outcoming of liquefaction triggering curves is cyclic resistance ratio (CRR) parameter which was introduced previously. A couple of proposed curves for clean sands and based on SPT, CPT, and Vs measurements, are shown in Figures 3.29, 3.30, and 3.31. Robertson and Wride (1997), Suzuki et al. (1997), Idriss and Boulanger (2004), Youd et al. (2001), Seed et al. (1979, 1982, 1997), Cetin et al. (2004), Shibata and Teparaksa (1988), Moses et al. (2006), Andrus and Stokoe (2000), Kayen et al. (2013), and Juang et al. (2001) are among the researchers who studied earthquake case histories and liquefaction triggering evidences and proposed correlations based on filed SPT, CPT or Vs measurements.

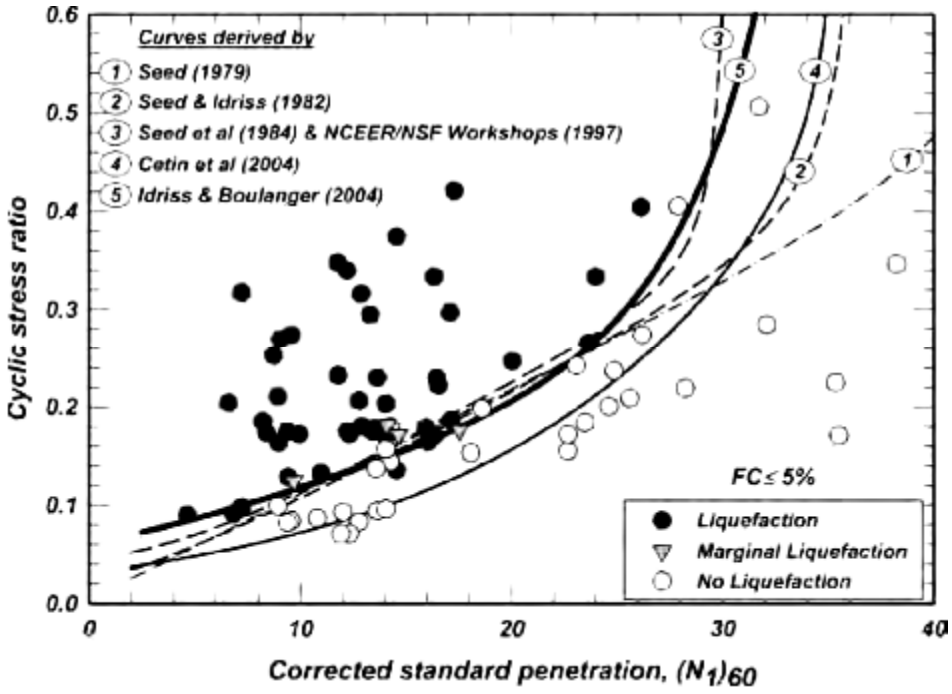


**Figure 3.29: SPT test based liquefaction triggering curves for M = 7.5 and $\sigma'_{vc}$ =100 kPa**

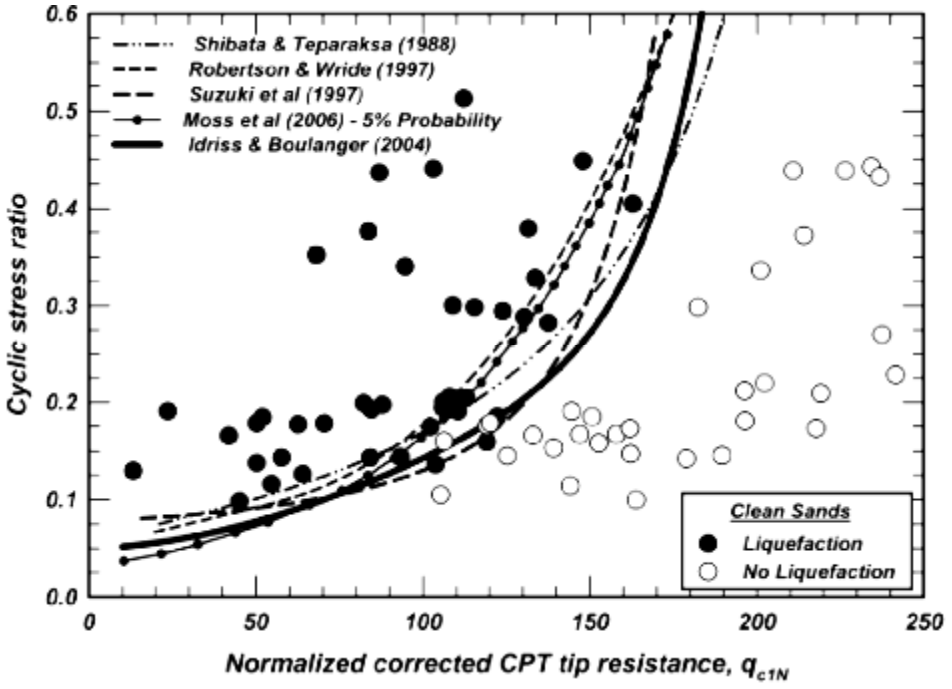


**Figure 3.30: CPT test based liquefaction triggering curves for M = 7.5 and $\sigma'_{vc}$ =100 kPa**

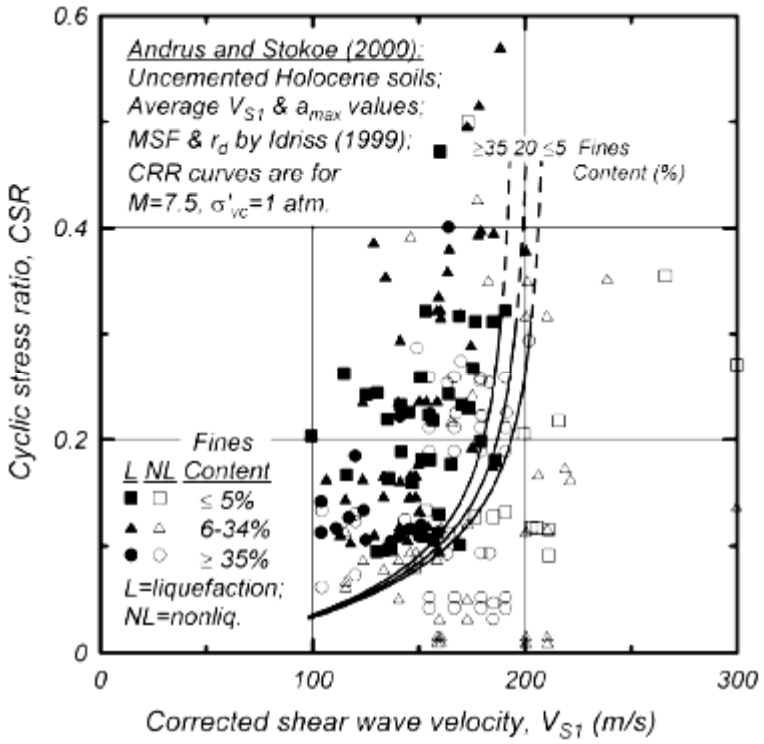


**Figure 3.31: Vs based liquefaction triggering curves for M = 7.5 and σ'$_{vc}$ =100 kPa**

One of the most conventional methods of liquefaction analysis based on experimental principals was developed by Seed and Idriss (1970). They introduced a simplified procedure for estimating earthquake-induced stresses or cyclic stress ratio (CSR) for an earthquake magnitude of M = 7.5 that would produce 15 loading cycles (Idriss 1999; Seed & Idriss 1982). This equation (Equation 3.10), determines the cyclic stress ratio (induced shear stress) applied by a specific earthquake.

$$CSR = 0.65 \frac{\tau_{max}}{\sigma'_{vc}} = 0.65 \frac{\sigma_{vc}}{\sigma'_{vc}} \frac{a_{max}}{g} r_d \qquad (3.10)$$

Where $\tau_{max}$ is the amplitude of the cyclic shear stress generated by a certain earthquake magnitude, $\sigma_{vc}$ and $\sigma'_{vc}$ are the total and effective overburden stresses respectively, $a_{max}$ is the ground surface acceleration, 'g' is the gravitational acceleration (= 9.81 m/s$^2$), and $r_d$ is a shear

stress reduction factor. The value of 0.65 compensates an average shear stress loading cycle relative to a peak shear stress loading cycle in an irregular pattern of seismic loading pattern (Seed & Idriss 1970). The shear stress reduction factor, $r_d$, which is based on reductions in site response for deep deposits, was originally developed by Seed and Idriss (1970). Correction factors have also been proposed to account for aging, $K_{DR}$ (Andrus et al. 2007; Andrus et al. 2009), overburden stress, $K_S$ (Harder & Boulanger 1997; Montgomery et al. 2010), and earthquake magnitude, MSF (Idriss 1999; Seed & Idriss 1982). The factor of safety against liquefaction triggering (equation 3.11), could be computed as the ratio of cyclic resistance ratio (CRR) obtained from historical case studies (liquefaction triggering curves) to earthquake-induced stress (CSR) calculated from empirical correlations like the one introduced in equation 3.10.

$$Factor\ of\ Safety = \frac{CRR}{CSR} \tag{3.11}$$

In previous sections, cyclic resistance ratios (CRR) values obtained from laboratory cyclic DSS tests, were correlated to measured shear wave velocities and general exponential equations were proposed for different cyclic load patterns. Both shear wave velocities and CRR parameters were also evaluated by soil state parameters in chapters 2 and 3. In this section, laboratory-based results of this study would be compared to existing liquefaction triggering curves. Among three main in-situ obtainable parameters, shear wave velocity is the parameter measured in laboratory for various soil states and thus is chosen to be compared with existing literature. $V_S$-based liquefaction triggering curves were first proposed in the early 1980's based on correlations with SPT data and subsequent implementation of a CRR-$V_s$ triggering curve (Seed et al. 1983). With the development of low-strain in-situ geophysical techniques, several direct $V_S$ databases were created using field measurements (Kayen et al. 1992; Robertson et al. 1992). Two of the most recent and commonly used $V_S$-based liquefaction triggering curves are Kayen et al. (2013) and Andrus & Stokoe (2000) which encompass $V_S$ data from hundreds of case histories located around the world. Shear wave velocity measurements should also be corrected for overburden stress (Andrus & Stokoe 2000) to a reference value ($\sigma'_v$ = 1 atm). Also, like the approach of Boulanger & Idriss (2016), the method of Kayen et al. (2013)

employs a probabilistic approach which includes confidence intervals to provide conservative curves that are more applicable to design practice. The on-site observations and measurements (such as Vs measurement) could always incorporate potential errors and misinterpretations. Visual liquefaction identification, determining the exact depth of liquefaction occurrence to calculate for accurate overburden stress factors and ground acceleration recordings are among the principal issues with on-site observations. Laboratory-based analysis, not only mitigates the issues with on-site observations but could be extended to a variety of controlled parameters such as consolidation stresses and relative densities. Based on the results of this study, $V_S$ values are normalized to provide comparison between values at different effective consolidation stresses which is defined as the '$V_{S1}$' value. Equations 3.12 and 3.13, present the correlations developed by Andrus & Stokoe (2000) and Kayen et al. (2013) methods, respectively.

$$CRR = a\left(\frac{V_{s1}}{100}\right)^2 + b\left(\left(\frac{1}{V_{s1}^* - V_{s1}}\right) - \left(\frac{1}{V_{s1}^*}\right)\right) \tag{3.12}$$

$$CRR = \exp\frac{\left((0.0073 * V_{s1})^{2.8011} - 2.6168 * ln(M_w) - 0.0099 * ln(\sigma'_{vc}) + 0.0028 * FC - 0.4809 * \varphi^{-1}(P_L)\right)}{1.946} \tag{3.13}$$

Where 'a' and 'b' are curve fitting parameters with suggested values of 0.022 and 2.8 respectively, $M_w$ is the moment magnitude earthquake, and f '(P) is the cumulative normal distribution function for model probability. To avoid any possible error engaged with overburden stress correction, only part of the results obtained for effective consolidation stress of $\sigma'_{vc}$ =100 kPa, are included in this section for comparison. As shown in Figure 3.32, the laboratory-based results obtained for Boler sand are plotted and show very close to curves proposed by Kayen et al. (2013) and more deviated form curves introduced by Andrus & Stokoe (2000).

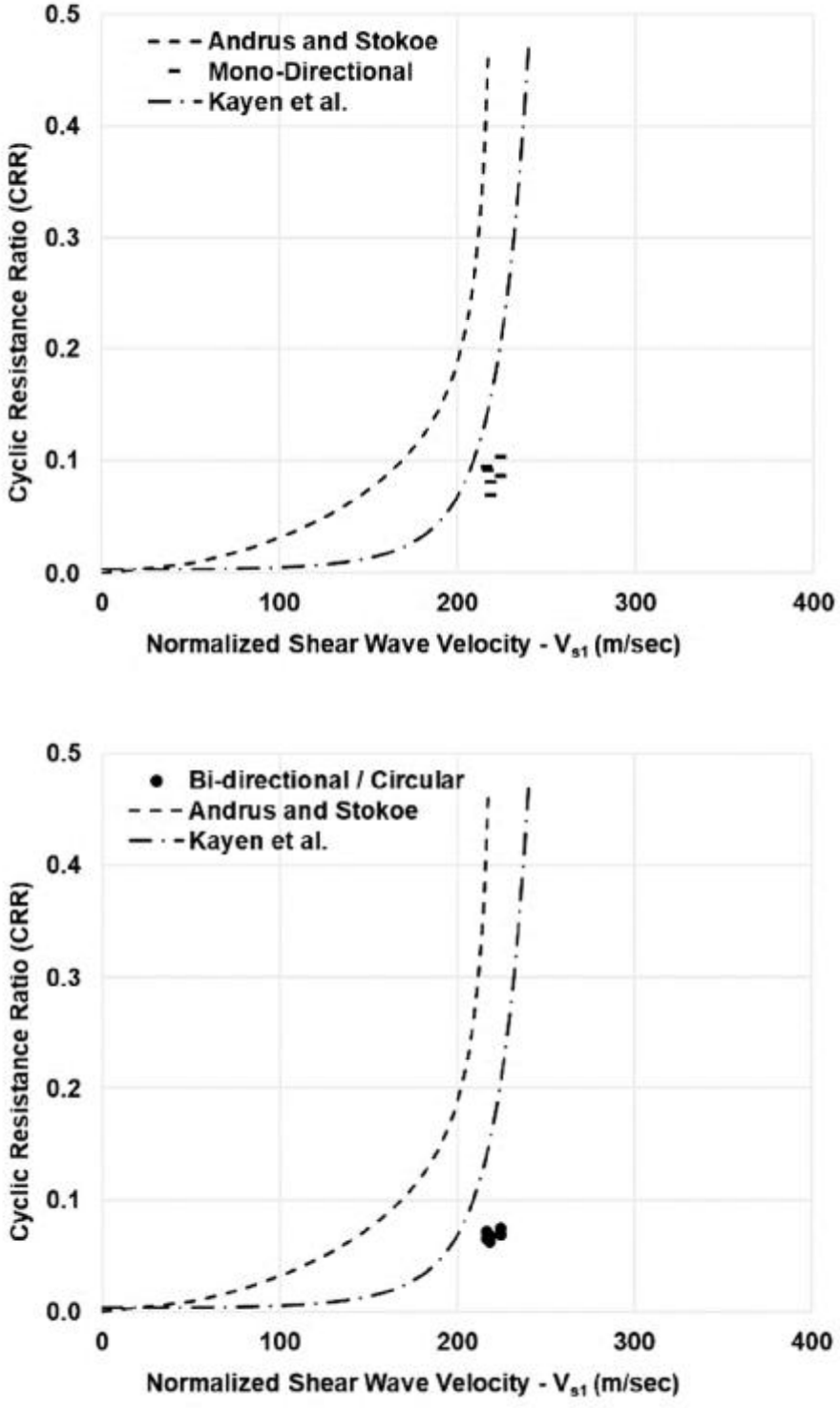


**Figure 3.32: Vs based liquefaction triggering curves for M = 7.5 and $\sigma'_{vc}$ =100 kPa for Boler sand compared to same curves by Andrus & Stokoe and Kayen et al.**

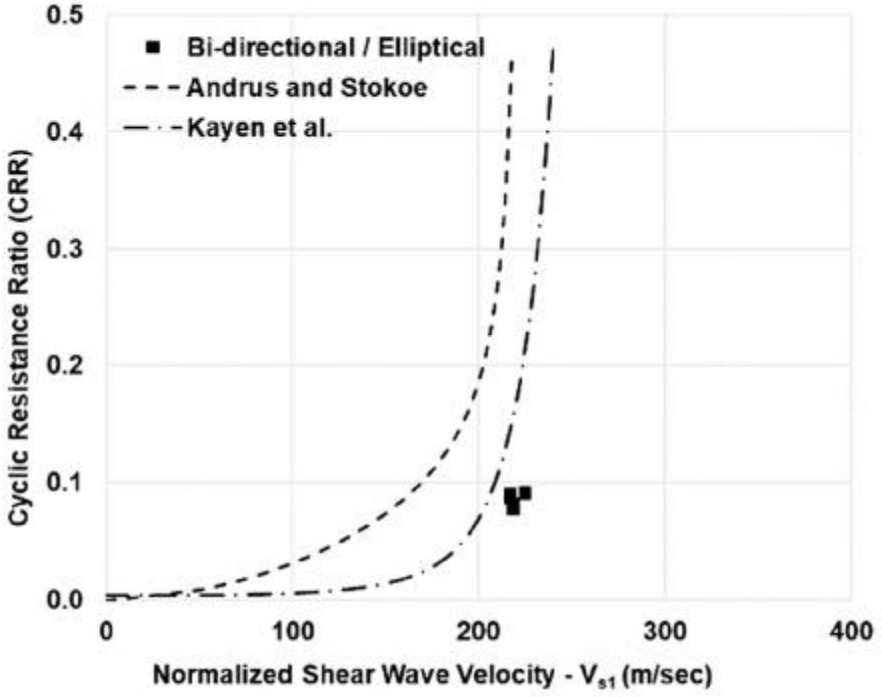


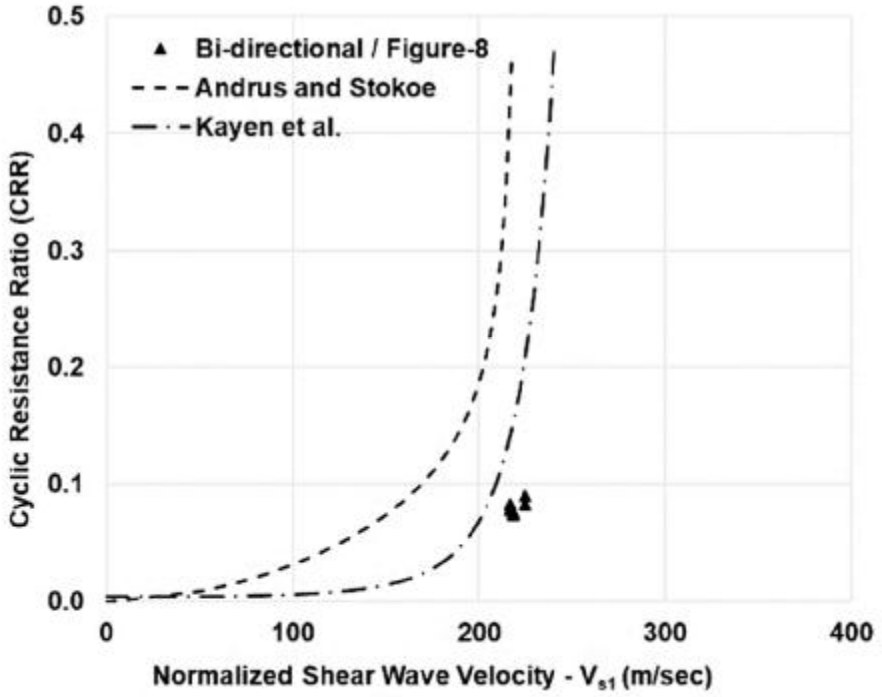


**Figure 3.32 (continued): Vs based liquefaction triggering curves for M = 7.5 and $\sigma'_{vc}$ =100 kPa for Boler sand compared to Andrus & Stokoe and Kayen et al. results.**

The slight shift of the curves to larger Vs values, confirms that on-site based observation and measurements in addition to applied correction factors to un-disturbed soil condition is not necessarily yielding the same results to laboratory controlled tests on re-constituted samples. Each of the methods has their own advantages and disadvantages. Engineering judgment and clear evidence of site condition in addition to laboratory test results could be a good combination for a more accurate soil assessment. The results of this study for various bi-directional and mono-directional cyclic loading and different soil states, show that current cyclic resistance evaluation practice, proposed by previous research studies, are overestimating sands cyclic response based on shear wave velocity measurements and further investigation or individual case studies are required for characterization of sands behaviour under cyclic load events.

## 3.5. Conclusions

The response of a local sand to liquefaction triggering under constant-volume static and various dynamic load patterns in loose to dense states were examined by an advanced cyclic simple shear test device. Bender element tests were also applied to measure shear wave velocities at similar states. For cyclic behavior assessment of the samples, mono-directional and three different patterns of bi-directional cyclic shear modes were applied. Liquefaction behavior of the samples was investigated according to multiple magnitudes and cyclic loading scenarios. Overburden correction factors ($K_\sigma$) showed an increase with increasing consolidation stresses which is in general agreement with recent studies but does not comply with some past studies. Also, the results exhibit a reduction in cyclic resistance of samples under bi-directional cyclic loads in comparison to similar samples under mono-directional cyclic loads.

A wide range of 0.67 to 1.03 dropped resistance was observed in the ratio of samples' resistance between bi-directional and unidirectional cyclic loading, which was most severe for a circular cyclic load pattern and the least for an elliptical cyclic load pattern. Median reductions were observed for figure-8 cyclic load pattern. Based on the above relative resistance reductions, a conservative multiplier of 0.65 is proposed for design purposes due to unpredictable loading patterns. Pore water pressure generation of samples in liquefaction occurrence was assessed and correlated to cyclic shear loads (CSR) and the number of cycles to liquefaction. It was found that pore water pressure ratio in current study never reaches to

100% at occurrence of liquefaction and lies in a range between 0.7 to 0.9 for multiple tests. This value decreases with cyclic shear addition, which corresponds to lower number of cycles. Moreover, exponential correlations were introduced between soil state and shear wave velocity measurements (Vs) and also cyclic resistance (CRR) of the soil in liquefaction based on critical state analysis. Separate exponential equations were proposed for both variations and different load patterns. Ultimately, liquefaction triggering curves were developed based on laboratory measurements and compared to literature proposed by past research, which shows a small deviation from existing curves. Cyclic resistance variation with shear wave velocity changes is in good accordance with Kayen et al.'s (2013) proposed curves.

## 3.6. References

A.M. Kammerer, J. M. Pestana, R. B. Seed. (2002). The undrained response of Monterey 0/30 sand under multidirectional simple shear loading conditions. Department of civil and environmental engineering, University of California.

Abouzar Sadrekarimi. (2013). "Influence of state and compressibility on liquefied strength of sands." Canadian Geotechnical Engineering Journal. 50: 1-10.

Annie Kammerer, Jiaer Wu, Michael Reimer, Juan Pestana and Raymond Seed. (2004). "Shear strain development in liquefiable soil under bi-directional loading conditions. 13th World Conference on Earthquake Engineering Vancouver, B.C., Canada. August 1-6, 2004 Paper No. 2081.

Andrus, R. D., and Stokoe, K. H. (2000). "Liquefaction resistance of soils from shear-wave velocity." Journal of Geotechnical and Geoenvironmental Engineering, 126(11), 1015-1025.

Andrus, R. D., Stokoe, K. H., and Juang, C. H. (2004). "Guide for shear-wave-based liquefaction potential evaluation." Earthquake Spectra, 20(2), 285-308.

Arango I. (1996). "Magnitude scaling factors for soil liquefaction evaluations". J. Geotechnical Eng. ASCE 122(11), 929–36, 1996.

Arulnathan, R., Boulanger, R. W., and Riemer, M. F. (1998). "Analysis of bender element tests." Geotechnical Testing Journal, ASTM, 21(2), 120 - 131.

ASTM, 2007. D6528-07 - "Standard test method for consolidated undrained direct simple shear testing of cohesive soils", West Conshohocken, PA: ASTM International.

ASTM, 2014. D854-14 - "Standard test methods for specific gravity of soil solids by water pycnometer", West Conshohocken, PA: ASTM International.

ASTM, 2016. D4254-16 - "Standard methods for minimum index density and unit weight of soils and calculation of relative density", West Conshohocken, PA: ASTM International.

ASTM, 2017. D6913/D6913M-17 - "Standard test methods for particle-size distribution (gradation) of soils using sieve analysis", West Conshohocken, PA: ASTM International.

Boulanger, R. W., Seed, R. B., Chan, C. K., Seed, H. B., and Sousa, J. B., (1991). “Liquefaction Behavior of Saturated Sands under Uni-Directional and Bi-Directional Monotonic and Cyclic Simple Shear Loading”. Geotechnical Engineering Report No. UCB/GT/91-08, University of California, Berkeley, August.

Boulanger, R. W., and Truman, S. P. (1996). “Void redistribution in sand under post-earthquake loading”. Canadian Geotechnical J.33, 829–34.

Boulanger, R. W. & Seed, R. B., 1995. Liquefaction of sand under bidirectional monotonic and cyclic loading. Journal of Geotechnical Engineering, 121(12), pp. 870-878.

Brandenberg, S. J., Kutter, B. L., and Wilson, D. W. (2008). "Fast stacking and phase corrections of shear wave signals in a noisy environment." Journal of Geotechnical and Geoenvironmental Engineering, 134(8), 1154-1165.

Brignoli, E. G. M., Gotti, M., and Stokoe II, K. H. (1996). "Measurement of shear waves in laboratory specimens by means of piezoelectric transducers." Geotechnical Testing Journal, ASTM, 19(4), 384 - 397.

Camacho-Tauta, J., Cascante, G., Fonseca, V. D., and Santos, J. (2015). "Time and frequency domain evaluation of bender element systems." Geotechnique, 65(7), 548 - 562.

Casagrande, A., (1976). “Liquefaction and Cyclic Deformation of Sands–a Critical Review” Harvard Soil Mechanics Series No. 88, Harvard University, Cambridge, MA.

Castro, G. (1969). "Liquefaction of sands." Ph.D., Harvard University, Cambridge, Massachusetts.

Castro, G., (1975). Liquefaction and cyclic mobility of saturated sands, J. Geotechnical Eng. Div., ASCE 101(GT6), 551–69.

Castro, G., and Poulos, S. J. (1977). Factors affecting liquefaction and cyclic mobility, J. Geotechnical Eng. Div., ASCE 103(GT6), 501–06.

Cha, M., Santamarina, J., Kim, H., and Cho, G. (2014). "Small-strain stiffness, shear-wave velocity, and soil compressibility." Journal of Geotechnical and Geoenvironmental Engineering, ASCE, 140(10).

Clayton, C. R. I. (2011). "Stiffness at small strain: research and practice." Geotechnique, 61(1), 5 - 37.

Dharma Wijewickereme, Maria Sanin. (2004). “Cyclic shear loading response of Frase Delta silt”. 13th World Conference on Earthquake Engineering Vancouver, B.C., Canada August 1-6, 2004 Paper No. 499.

Degroot, D. J., Germaine, J. T. & Ladd, C. C., 1993. "The multidirectional direct simple shear apparatus". Geotechnical Testing Journal, 16(3), pp. 283-295.

Dharma Wijewickreme, Somasundaram Sriskandakumar, and Peter Byrne. (2005). “Cyclic loading response of loose air-pluviated Fraser River sand for validation of numerical models simulating centrifuge tests”. Can. Geotech. J. 42: 550–561.

Dobry, R., Abdoun, T., Stokoe II, K. H., Moss, R. E. S., Hatton, M., and El Ganainy, H. (2015). "Liquefaction potential of recent fills versus natural sands located in high-seismicity regions using shear-wave velocity." Journal of Geotechnical and Geoenvironmental Engineering, ASCE, 141(3), 1 - 13.

Drnevich, V. P., 1972. "Undrained cyclic shear of saturated sand". Journal of the Soil Mechanics and Foundations Division, 98(8), pp. 807-825.

Dyvik, R., Berre, T., Lacasse, S., and Raadim, B. (1987). "Comparison of truly undrained and constant volume direct simple shear tests." Geotechnique, 37(1), 3 - 10.

El Take, A., Sadrekarimi, A. & El Naggar, H., 2016. "Cyclic resistance and liquefaction behavior of silts and sandy silts". Journal of Soil Dynamics and Earthquake Engineering, Volume 83, pp. 98-109.

Finn, W. D. L., Liam, J. J., Emery & Gupta, Y. P., 1970. "A shaking table study of the liquefaction of saturated sands during earthquakes". Sofia, Proceedings of the 3rd European Symposium on Earthquake Engineering.

Finn, W. D. L., Bransby, P. L. & Pickering, D. J., 1970. "Effect of strain history on liquefaction of sand". Journal of the Soil Mechanics and Foundations Division, 96(6), pp. 1917-1934.

Green, R. A., and Terri, G. A.. (2005). The number of equivalent cycles concept for liquefaction evaluations—revisited. J. Geotechnical and Geoenvironmental Eng., ASCE 131(4), 477–88.

Hardin, B. O. (1978). "The nature of stress-strain behavior of soils." ASCE Geotechnical Engineering Division Speciality Conference on Earthquake Engineering and Soil Dynamics, Pasadena, California, 3 - 90.

Hardin, B. O., and Black, W. L. (1966). "Sand stiffness under various triaxial stresses." Journal of the Soil Mechanics and Foundations Division, ASCE, 92(2), 27 - 42.

Hardin, B. O., and Richart Jr., F. E. (1963). "Elastic wave velocities in granular soils." Journal of Soil Mechanics and Foundation Division, American Society of Civil Engineers, 89(1), 33 - 65.

Hynes, M. E., and Olsen, R. (1998). “Influence of confining stress on liquefaction resistance, in Proceedings”. International Symposium on the Physics and Mechanics of Liquefaction, Balkema, Rotterdam. pp. 145–52.

Idriss, I. M., 1999. "An update to the Seed-Idriss simplified procedure for evaluating liquefaction potential". Washington D.C., Proceedings of Workshop on New Approaches to Liquefaction, Federal Highway Administration.

Idriss, I. M. & Boulanger, R. W., 2006. "Semi-empirical procedures for evaluating liquefaction potential during earthquakes". Soil Dynamics and Earthquake Engineering, Volume 26, pp. 115-130.

Idriss, I. M. & Boulanger, R. W., 2008. "Soil liquefaction during earthquakes". Oakland: Earthquake Engineering Research Institute.

Ishihara, K., 1996. "Soil behavior in earthquake geotechnics". New York: Oxford University Press.

Ishihara, K. & Li, S., 1972. "Liquefaction of saturated sand in triaxial torsion shear test". Soils and Foundations, 12(2), pp. 19-39.

Ishihara, K. & Okada, S., 1982. "Effect of large pre-shearing on cyclic behavior of sand". Soils and Foundations, 22(3), pp. 109-125.

Ishihara, K. & Yamazaki, F., 1980. "Cyclic simple shear tests on saturated sand in multi-directional loading". Japanese Society of Soil Mechanics and Foundation Engineering, 20(1), pp. 45-59.Iwasaki, T., Tatsuoka, F., and Takagi, Y. (1978). "Shear moduli of sands under cyclic torsional shear loading." Soils and Foundations, 18(1), 39 - 56.

J. Montgomery, R.W. Boulanger and L.F. Harder. JR. (2012). "Examination of overburden correction factor on liquefaction resistance." Department of civil and environmental engineering, University of California.

Jamiolkowski, M., Leroueil, S., and Lo Presti, D. C. F. (1991). "Design parameters from theory to practice." Proceedings of the International Conference on Geotechnical Engineering for Coastal Development: GeoCoast 1991, Yokohama, Japan, 877 - 917.

Jefferies, M. G., and Been, K. (2006). Soil liquefaction - a critical state approach, Taylor & Francis, New York.

Jovicic, V., Coop, M. R., and Simic, M. (1996). "Objective criteria for determining Gmax from bender element tests." Geotechnique, 46(2), 357 - 362.

Kammerer, A. M., 2002. Ph.D. Thesis - "Undrained response of Monterey 0/30 sand under multidirectional cyclic simple shear loading conditions", Berkeley: University of California.

Kayen, R., Moss, R. E. S., Thompson, E. M., Seed, R. B., Cetin, K. O., Der Kiureghian, A. K., Tanaka, Y., and Tokimatsu, K. (2013). "Shear-wave velocity-based probabilistic and deterministic assessment of seismic soil liquefaction potential." Journal of Geotechnical and Geoenvironmental Engineering, ASCE, 139(3), 407-419.

Kenji Ishihara and Fumio Yamazaki. (1980). “Cyclic simple shear tests on saturated sand in multi-directional loading.” Soils and foundations. Vol. 20 No. 1.

Kokusho, T. (1980). "Cyclic triaxial test of dynamic soil properties for wide strain range." Soils and Foundations, 20(2), 45-60.

Ladd, R. S. (1978). "Preparing test specimen using under compaction." Geotechnical Testing Journal, ASTM, 1(1), 16 - 23.

Lee, J.-S., and Santamarina, J. C. (2005). "Bender elements: performance and signal interpretation." Journal of Geotechnical and Geoenvironmental Engineering, ASCE, 131(9), 1063 - 1070.

Lo Presti, D. C. F., Jamiolkowshi, M., Pallara, O., Cavallaro, A., and Pedroni, S. (1997). "Shear modulus and damping of soils." Geotechnique Symposium in Print, 43(3), 603 - 617.

Marjanovic, J., and Germaine, J. T. (2013). "Experimental study investigating the effects of setup conditions on bender element velocity results." Geotechnical Testing Journal, ASTM, 36(2).

Mike Jefferies and Ken Been. (2016). "Soil liquefaction, a critical state approach." Taylor and Francis Group LLC.

Robertson, P. K., Sasitharan, S., Cunning, J. C., and Sego, D. C. (1995). "Shear-wave velocity to evaluate in-situ state of Ottawa sand. ." Journal of Geotechnical Engineering, ASCE, 121(3), 262 - 273.

Robertson, P. K., Woeller, D. J., and Finn, W. D. L. (1992). "Seismic Cone Penetration Test for Evaluating Liquefaction Potential under Cyclic Loading." Canadian Geotechnical Journal, 29(4), 686-695.

Roe, G. V. (1981). "An acoustic method for identifying sand fabric and liquefaction potential." Ph.D., University of New Hampshire, New Hampshire.

Sanchez-Salinero, I., Roesset, J. M., and Stokoe, I. I. (1986). "Analytical studies of body wave propagation and attenuation.", The University of Texas, Geotechnical Engineering Center, Texas, Austin, 272.

Rudolph, C., Grabe, J. & Albrecht, I., 2014. "Simple shear tests with a varying shearing direction during cyclic shearing". Géotechnique Letters, 4(2), pp. 102-107.

Rutherford, C. J., 2012. Ph.D. Thesis - "Development of a multi-directional direct simple shear testing device for characterization of the cyclic shear response of marine clays", College Station: Texas A&M University.

Sadrekarimi, A., 2016. "Cyclic shear response of Fraser River sand using cyclic ring shear. Chicago, Proceedings of Geo-Chicago 2016 Conference: Sustainability, Energy, and the Geoenvironment.

Santamarina, J. C., Klein, K. A., and Fam, M. A. (2001). Soils and Waves: Particulate Materials Behavior, Characterization and Process Monitoring, Wiley, New York.

Seed, H. B., Arango, I. & Chan, C. K., 1976. "Evaluation of soil liquefaction potential for level ground during earthquakes: A summary report", Washington D.C.: U.S. Nuclear Regulatory Commission.

Seed, H. B. & Idriss, I. M., 1971. "Simplified procedure for evaluating soil liquefaction potential". Journal of Geotechnical Engineering, 97(9), pp. 1249-1273.

Seed, H. B. & Idriss, I. M., 1982. "Ground motions and soil liquefaction during earthquakes", Earthquake Engineering Research Institute: Oakland.

Seed, H. B., Idriss, I. M., Makdisi, F. I. & Banerjee, N. G., 1975. "Representation of irregular stress time histories by equivalent uniform stress series in liquefaction analysis", Berkeley: Earthquake Engineering Research Center.

Seed, H. B., Mori, K. & Chan, C. K., 1977. "Influence of seismic history on liquefaction of sands". Journal of Geotechnical Engineering, 103(4), pp. 257-270.

Seed, R. B. & Harder, L. F., 1990. "SPT-based analysis of cyclic pore pressure generation and undrained residual strength". Berkeley, Proceedings of the Memorial Symposium of H. B. Seed.

Sivathayalan, S., 1994. M.ASc. Thesis - "Static, cyclic and post-liquefaction simple shear response of sands", Vancouver: University of British Columbia.

Sriskandakumar, S., Wijewickreme, D. & Byrne, P. M., 2012. "Multiple cyclic loading responses of loose air-pluviated Fraser River sand". Lisbon, Proceedings of the World Conference on Earthquake Engineering.

Vaid, Y. P., and Sivathayalan, S. (1996). "Static and cyclic liquefaction potential of Fraser River delta sand in simple shear and triaxial tests." Canadian Geotechnical Journal, 33(2), 281-289.

Viana Da Fonseca, A., Soares, M. & Fourie, A. B., 2015. "Cyclic DSS tests for the evaluation of stress densification effects in liquefaction assessment". Soil Dynamics and Earthquake Engineering, Volume 75, pp. 98-111.

Viggiani, G., and Atkinson, J. H. (1995). "Interpretation of bender element tests." Geotechnique, 45(1), 149 - 154.

Whitman, R. V., 1970. "Summary of results from shaking table tests at the University of Chile using a medium sand", Cambridge: Massachusetts Institute of Technology.

Wijewickreme, D., Sriskandakumar, S. & Byrne, P., 2005. "Cyclic loading response of loose air-pluviated Fraser River sand for validation of numerical models simulating centrifuge tests". Canadian Geotechnical Journal, 42(2), pp. 550-561.

Yamada, S., Tomoko, T. & Sato, K., 2010. "Effects on reliquefaction resistance produced by changes in anisotropy during liquefaction". Soils and Foundations, 50(1), pp. 9-25.

Yamamoto, T. et al., 2000. "Reliquefaction potential of cement-treated sandy soils". Auckland, Proceedings of the World Conference on Earthquake Engineering.

# Chapter 4

# 4. Evaluating the liquefaction and re-liquefaction behavior of a silica-carbonate sand

## 4.1. Introduction

Evaluating and predicting sandy soils behavior in cyclic liquefaction plays a key role in engineering design and practice. In current Canadian foundation design manual and the Canadian highway bridge design code, a special care is given to characterizing potential for liquefaction triggering of cohesionless soils. Several investigations have been performed on cyclic liquefaction assessment of cohesionless soils and their correlations with soil characteristics such as relative density and confining pressure. These studies have been mostly carried out on sands mainly composed of silica and quartz particles.

Although several pieces of research have been developed on liquefaction behavior of sands, a few of them have taken repeating liquefaction analysis into consideration. The importance of soil behavior assessment in repeating cyclic liquefaction is due to a variety of geotechnical design cases which involve repeated dynamic loading condition specifically in seismic zones. Porcino et al. (2009) evaluated the effect of pre-shearing on the behavior of sand samples by performing cyclic simple shear tests. They investigated, how shear strain development in a first cyclic shear loading can influence on soil resistance at a repeated cyclic shear load. They found that small strain pre-shearing brings about hardening of both loose and dense samples. On the other hand, larger developed strains in the first cycle of loads could have a hardening effect on dense samples but conversely, softening effect on loose ones.

Large strains can cause a decrease in repetitive liquefaction resistance of samples irrespective of the soil state. They also reported about different responses for different sands. In particular, they reported for grain crushing in carbonate sands, as one of the main reasons for their different behavior. In another research program at the University of Tokyo, S. Wahyudi, J. Koseki, and T. Sato (2014) studied the re-liquefaction behavior of sands with ring-shear tests. Their results, confirm the previous results found by the Italian team. They concluded that increasing density before a re-liquefaction occurrence is less important than the pre-shearing

history of the samples. Increasing resistance to small pre-shearing strains and decreasing resistance after large pre-shear strains were reported by them and co-related to soil structure and re-arrangement of soil particles. Some researchers point to the weakening of soil fabric during a liquefaction event which would correspond to cyclic resistance drop in successive liquefaction events (Finn et al. 1970) whereas others point to the increased densification of soils in succeeding liquefaction events which may show a greater resistance value relative to first liquefaction events (Seed et al. 1977; Sriskandakumar et al., 2012). Wahyudi et al. (2014) looked at the effects of the number of cycles at failure for repeated liquefaction events where failure deformation criteria ranged from 2% to 10% double amplitude shear strain. While it was found that the number of cycles at failure showed a general increase for each succeeding liquefaction event using all deformation criteria, the increasing resistance was particularly significant in tests where a smaller deformation criterion was used, i.e. maximum double amplitude shear strain of 2% (Wahyudi et al. 2014).

In the current study, cyclic liquefaction behavior of a carbonate sand under plane-strain boundary condition and a simple shearing mode is investigated. Dynamic shear loads are applied in a cyclic direct simple shear machine to provide a closer representation to in-situ conditions. Liquefaction criteria for attaining a double-amplitude cyclic shear strain of 7.5% in DSS tests is followed in this study. This is essentially equivalent to the liquefaction definition (Vaid and Sivathayalan, 1996) of 5% double-amplitude axial strain in a triaxial test. When the sample liquefies following with above criteria, cyclic loading is stopped, the sample is unloaded from shear loads, re-consolidated to initial axial stress prior to cyclic load application and finally, a second cyclic shear load equivalent to the first stage is applied. Soil state changes after re-liquefaction. Pore water pressure generation and cyclic resistance before and after repeating liquefaction are analyzed for various soil samples. Effect of cyclic load pattern is evaluated as well. Four different cyclic load pattern including mono-directional shearing and three bi-directional loading patterns are applied by an advanced multi-directional cyclic simple shear apparatus.

## 4.2. Experimental plan

### 4.2.1. Tested material

A clean carbonate-silica sand collected from Boler Mountain in London, Ontario (Boler sand) is used for experiments of this study which was discussed in previous chapters and any repeating description is avoided in this chapter.

### 4.2.2. Specimen preparation

Simple shear tests were carried out using an advanced computer-controlled cyclic simple shear apparatus. For specimen preparation, a latex membrane was first placed around the bottom cap of the DSS apparatus and secured with an O-ring. Series of 1 mm-thick Teflon-coated stainless-steel rings were then stacked around the membrane. Two supporting retainers were used to hold the stacked rings in place during sample preparation and the membrane was then folded over the stacked steel rings. Specimens were prepared at loose ($D_{rc}$ = 25%), medium dense ($D_{rc}$ = 45%), and dense ($D_{rc}$ = 65%) relative densities using the moist tamping method. The height and diameter of the specimens were respectively 20 mm and 70.7 mm in cyclic DSS tests. Under-compaction (Ladd, 1978) method was used in this study to improve the uniformity of specimens. In this method, over-dried sand was thoroughly mixed with 5% moisture. The specimen was then prepared by compacting moist sand in three sublayers.

The dry density was adjusted by changing the mass of soil placed in each sublayer, while all sublayers were compacted to equal heights. The top cap of the DSS apparatus was subsequently lowered on the sand surface, the membrane was folded back on the top cap and then secured with an O-ring. A small seating vertical stress of 5 kPa was first applied to stabilize the specimen and prevent piping. Saturation was then carried out by flushing the specimens with $CO_2$ gas, followed by de-aired water through drainage ports on the specimen endcaps. Specimen height was carefully recorded during this process to determine the precise initial void ratio of the specimen. Following saturation, the specimens were consolidated to effective vertical stresses ($\sigma'_{vc}$) of 50, 100, 200, 400, or 600 kPa. The top drainage port was open during consolidation to allow excess pore pressure dissipation.

### 4.2.3. Cyclic DSS tests

Constant-volume cyclic shear tests were carried out to determine the cyclic liquefaction and re-liquefaction behavior of Boler sand. Stress-controlled one directional and two directional shearing loads were applied within a wide range of stresses at a frequency of 0.1 Hz. Cyclic load patterns of this study, are defined and summarized in Figure 4.1 and Table 4.1. In "Test Type" column of Table 4.1, "M" stands for mono-directional, "C" stands for circular, "E" stands for elliptical (oval), and "F" stands for figure-8 cyclic load patterns.

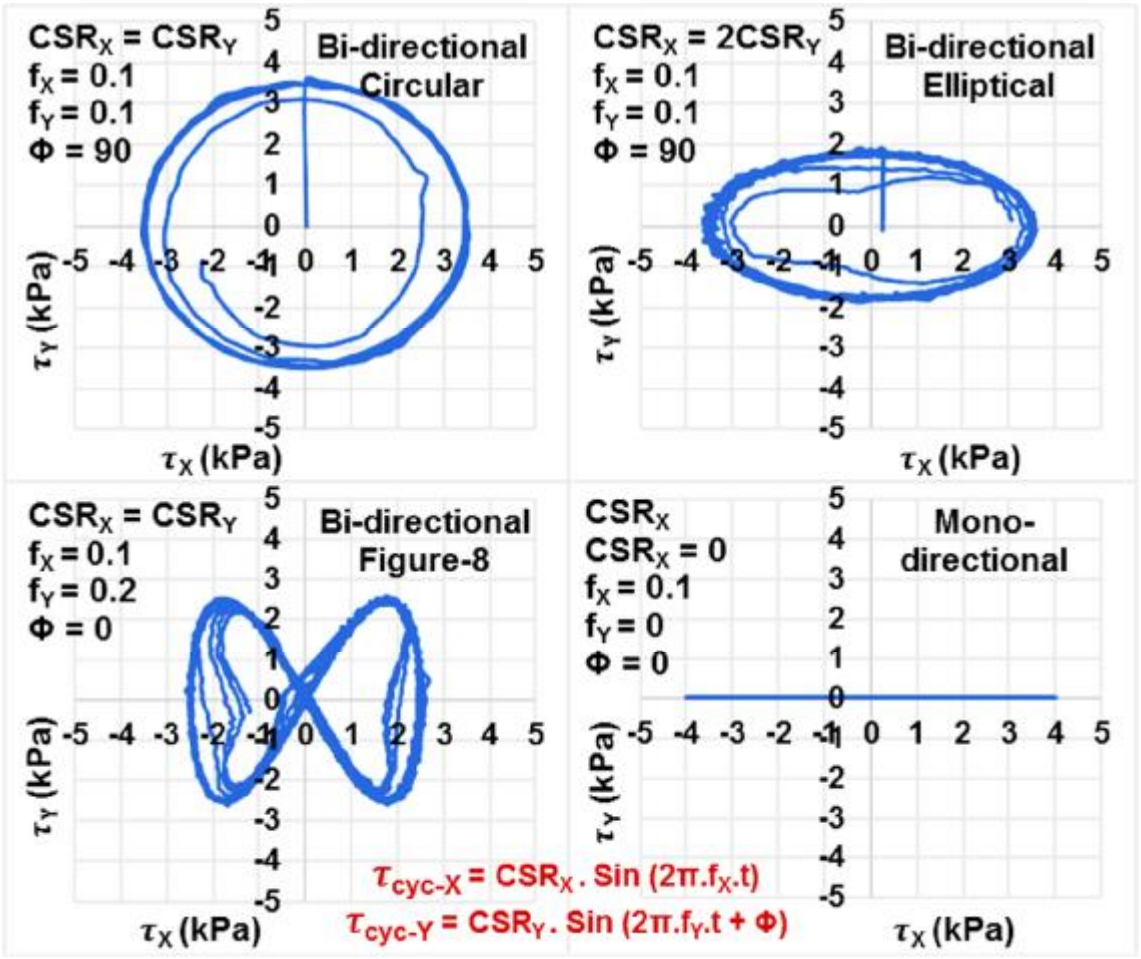


**Figure 4.1: Definition of cyclic load patterns in this study**

Specimens were consolidated to stress levels of $\sigma'_{vc}$ = 50, 100, 200, 400 and 600 kPa before applying cyclic loads and each stage of liquefaction. Table 4.1 summarize the characteristics

of the cyclic simple shear tests of this study. Cyclic stress ratio (CSR) is determined as the ratio of the peak shear stress to vertical stress ($_{max}$ / $\sigma'_{vc}$). In Table 4.1, the average void ratio (relative density) of the specimens at the time of applying shear loads (after the consolidation of the first stage) are shown. Three increments of relative densities at each consolidation stress level were examined under various CSR values. In bi-directional load patterns, resultant values of cyclic stress ratio (CSR) are considered in the analysis because, unlike the mono-directional tests, samples in bi-directional tests experience the actual combined effect of both horizontal loads. This was shown in equation 3.6. The same procedure is considered for shear strains. When the sample liquefies (reaching the strain limit), cyclic loading is stopped, the shear load is removed, the sample is re-consolidated to initial axial stress prior to cyclic load application and finally, a second cyclic shear load equivalent to the first stage is applied (re-liquefaction). All boundary condition and loading patterns are maintained similar to the first stage (liquefaction).

**Table 4.1: Summary of cyclic DSS tests for both stages of liquefaction**

| $\sigma'_{vc}$ (kPa) | Avg. $D_{rc}$ (%) | Test Type | Freq. (Hz) | CSR values 25% | CSR values 45% | CSR values 65% |
|---|---|---|---|---|---|---|
| 50 | 25 - 45 - 65 | M | 0.1 | 0.062 - 0.071 - 0.080 | 0.073 - 0.082 - 0.094 | 0.047 - 0.071 - 0.093 |
| 100 | 25 - 45 - 65 | M | 0.1 | 0.067 - 0.080 - 0.090 | 0.083 - 0.097 - 0.103 | 0.079 - 0.095 - 0.105 |
| 200 | 25 - 45 - 65 | M | 0.1 | 0.080 - 0.090 - 0.100 | 0.08 - 0.102 - 0.112 | 0.104 - 0.118 - 0.132 |
| 400 | 25 - 45 - 65 | M | 0.1 | 0.090 - 0.100 - 0.110 | 0.122 - 0.131 - 0.151 | 0.122 - 0.137 - 0.151 |
| 600 | 25 - 45 - 65 | M | 0.1 | 0.100 - 0.110 - 0.125 | 0.131 - 0.141 - 0.161 | 0.141 - 0.152 - 0.191 |
| 50 | 25 - 45 - 65 | C | 0.1 | 0.042 - 0.057 - 0.067 | 0.053 - 0.063 - 0.077 | 0.037 - 0.067 - 0.073 |
| 100 | 25 - 45 - 65 | C | 0.1 | 0.053 - 0.071 - 0.082 | 0.053 - 0.076 - 0.087 | 0.067 - 0.082 - 0.096 |
| 200 | 25 - 45 - 65 | C | 0.1 | 0.061 - 0.081 - 0.091 | 0.072 - 0.091 - 0.101 | 0.081 - 0.096 - 0.111 |
| 400 | 25 - 45 - 65 | C | 0.1 | 0.081 - 0.091 - 0.101 | 0.101 - 0.113 - 0.121 | 0.081 - 0.111 - 0.121 |
| 600 | 25 - 45 - 65 | C | 0.1 | 0.081 - 0.091 - 0.101 | 0.091 - 0.111 - 0.121 | 0.111 - 0.131 - 0.150 |
| 50 | 25 - 45 - 65 | E | 0.1 | 0.056 - 0.073 - 0.091 | 0.062 - 0.071 - 0.091 | 0.073 - 0.081 - 0.101 |
| 100 | 25 - 45 - 65 | E | 0.1 | 0.073 - 0.081 - 0.091 | 0.081 - 0.091 - 0.111 | 0.081 - 0.091 - 0.110 |
| 200 | 25 - 45 - 65 | E | 0.1 | 0.08 - 0.100 - 0.111 | 0.100 - 0.110 - 0.120 | 0.08 - 0.100 - 0.110 |
| 400 | 25 - 45 - 65 | E | 0.1 | 0.090 - 0.100 - 0.110 | 0.110 - 0.120 - 0.130 | 0.120 - 0.130 - 0.140 |
| 600 | 25 - 45 - 65 | E | 0.1 | 0.090 - 0.100 - 0.110 | 0.120 - 0.130 - 0.140 | 0.130 - 0.140 - 0.150 |
| 50 | 25 - 45 - 65 | F | 0.2 | 0.057 - 0.076 - 0.100 | 0.067 - 0.077 - 0.089 | 0.065 - 0.077 - 0.090 |
| 100 | 25 - 45 - 65 | F | 0.2 | 0.055 - 0.077 - 0.101 | 0.077 - 0.089 - 0.102 | 0.064 - 0.090 - 0.114 |
| 200 | 25 - 45 - 65 | F | 0.2 | 0.064 - 0.089 - 0.114 | 0.101 - 0.126 - 0.138 | 0.089 - 0.101 - 0.113 |
| 400 | 25 - 45 - 65 | F | 0.2 | 0.076 - 0.101 - 0.126 | 0.083 - 0.101 - 0.126 | 0.088 - 0.126 - 0.151 |
| 600 | 25 - 45 - 65 | F | 0.2 | 0.101 - 0.0113 - 0.138 | 0.114 - 0.139 - 0.163 | 0.101 - 0.126 - 0.176 |

**M**: mono-directional, **C**: circular, **E**: elliptical (oval), **F**: figure-8

## 4.3. Test results

### 4.3.1. Critical state line approach

As discussed in previous chapters, monotonic simple shear tests were carried out at wide ranges of consolidation relative density ($D_{rc}$) and consolidation stresses ($\sigma'_{vc}$). These data were used to establish the critical state line (CSL) of Boler sand. A semi-logarithmic equation was obtained which fitted to a critical void ratio of 0.888 at an effective stress of $\sigma'_{vc}$ = 1 kPa and a critical state line slope of 0.071. Due to a previous discussion, repeated description of the monotonic test results and critical state line establishment is avoided in this chapter. However, the results of the tests would be used in the current chapter.

### 4.3.2. First stage of cyclic loading (liquefaction)

Cyclic simple shear tests were carried out to determine the cyclic liquefaction behavior of Boler sand. The shear load was applied in one or two perpendicular horizontal directions (introduced as X and Y) with a possible phase offset of 90 degrees which correspond to a quarter of cycle delay in the Y direction, relative to the X direction. Figure 4.2 shows typical results of a cyclic DSS test in this study. In this example specimen, cyclic shear load with the frequency of 0.1 Hz and amplitude of 7 kPa was applied under consolidation stress of 100 kPa (CSR=0.07). The specimen, for example, liquefies after 9 cycles of loading when reaches 3.75% shear strain in both directions based on simplified liquefaction evaluation (Seed and Idriss 1971 and Castro 1969).

### 4.3.3. Second stage of cyclic loading (re-liquefaction)

For purpose of investigating the behavior of samples in excessive shaking and liquefaction occurrence, the liquefied soil specimens of the previous stage were exposed to the second stage of cyclic loading. To simulate the second stage of liquefaction, cyclic shear loading at first stage were stopped after exceeding 3.75% shear strain in at least one of X or Y directions.

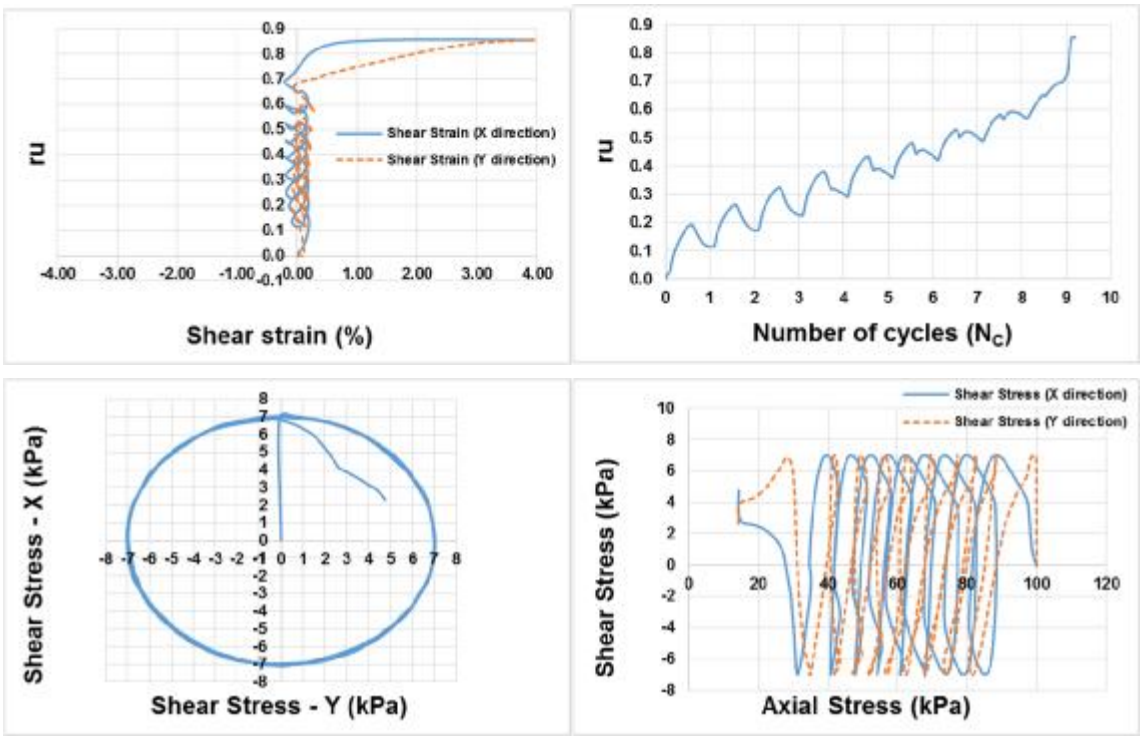


**Figure 4.2: Liquefaction stage results at $D_{rc}$ = 25%, $\sigma'_{vc}$ = 100 kPa and CSR=0.07**

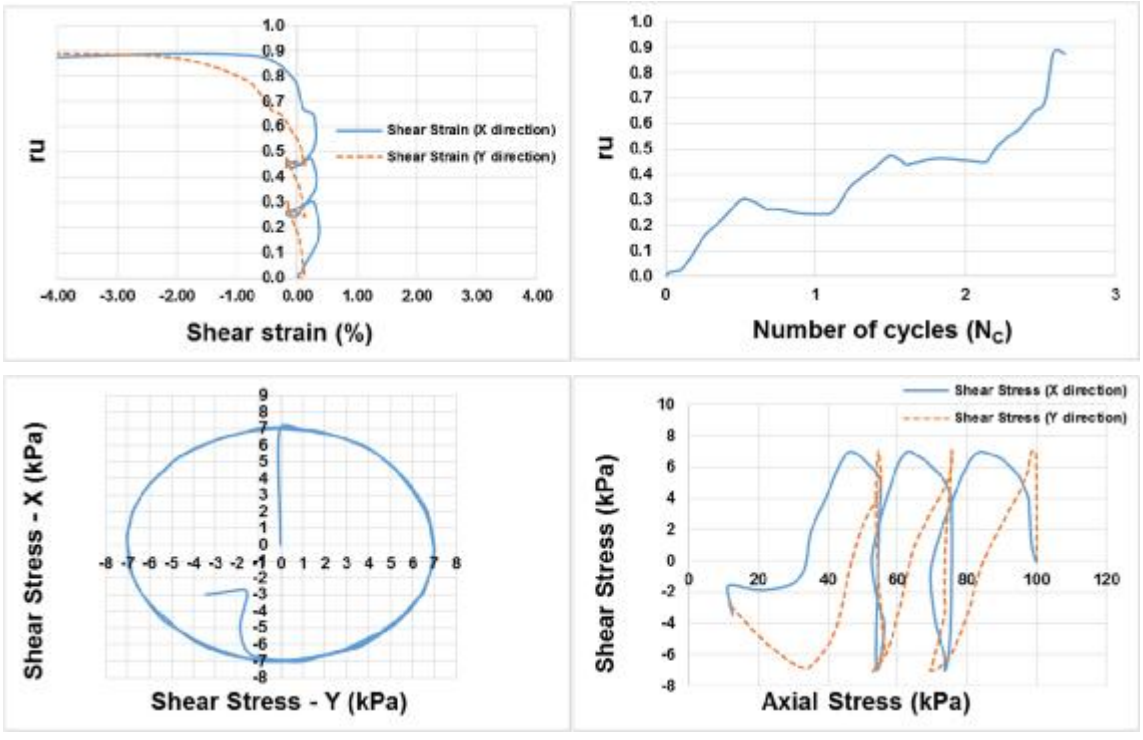


**Figure 4.3: Re-liquefaction stage results at $D_{rc}$ = 25%, $\sigma'_{vc}$ = 100 kPa and CSR=0.07**

Later, the shear loads in both directions were reduced to zero and then an equivalent consolidation axial stress to the first stage of the test was applied to samples. This procedure caused the soil samples to densify relative to the prior stage at the same boundary condition. Finally, similar cyclic loads as the first stage were applied to the samples. Reaching the shear strain of 3.75% is considered an occurrence of a second liquefaction too. In Figure 4.3 result of a re-liquefaction occurrence for the same sample in the previous example is shown. This time, the specimen of example liquefies after 3 cycles of loading when reaches 3.75% shear strain in both directions. Comparing the results of example experiment shown in Figures 4.2 and 4.3 shows that, at identical applied loads, number of cycles to liquefy, was dropped from 9 in first liquefaction stage to 3 in a second stage (re-liquefaction). It is also observed that, although pore water pressure attainment is much faster in the second stage, shear strains start to increase at a similar threshold of pore water pressure for both liquefaction stages. Despite a decrease in resistance observed in this example, dropping the number of resisting cycles is not a typical behavior and equal or increasing number of cycles from a first stage to the second stage of liquefaction was observed in other samples response to repeating liquefaction occurrence, as well. For a better comparison, the summary of consecutive liquefaction events is shown in Tables 4.2 to 4.13. As a result, it could be found that, in loose ($D_{rc}$ = 25%) samples, dropping number of cycles before liquefaction is more common than denser samples whereas it could be seen in densest samples ($D_{rc}$ = 65%) that they normally experience an increase in cyclic resistance or remain their first stage number of cycles at a second liquefaction. This could be related to the effect of relative density in attaining or losing cyclic resistance which will be further discussed in section 4.4. It was also observed that mono-directional loads would result in decreasing cyclic resistance in the majority of the tests while a greater part of samples gets more resistive after first liquefaction under bi-directional loads. Figure-8 cyclic load pattern seems to be the load pattern which causes the samples to attain higher cyclic resistance in the majority of tests. Another observation of the results reveals that, regardless of relative density, consolidation stress level, and even cyclic load pattern, at smaller cyclic shear loads (CSR), increasing resistance is a general behavior. This would declare the importance of applied cyclic shear load magnitudes in the future behavior of a soil which some researchers point to the weakening of soil fabric during a liquefaction event (Finn et al. 1970). All above observations will be further discussed and analyzed in the next section.

**Table 4.2: Results for liquefaction / re-liquefaction at $D_{rc}$ = 25% / mono-directional**

| Drc = 25% Mono-directional | | | | | | | |
|---|---|---|---|---|---|---|---|
| σvc = 50 kPa | | | | | | | |
| Liquefaction | | | | | Re-Liquefaction | | |
| CSR | Nc | $e_c$ | Dr | Δεv | Nc | $e_c$ | Dr |
| | | | % | | | | % |
| 0.062 | 65 | 0.764 | 25.3 | -2.86 | 16 | 0.713 | 41.3 |
| 0.071 | 17 | 0.760 | 26.6 | -3.47 | 6 | 0.699 | 45.6 |
| 0.080 | 13 | 0.769 | 23.8 | -2.76 | 7 | 0.72 | 39.1 |
| σvc = 100 kPa | | | | | | | |
| Liquefaction | | | | | Re-Liquefaction | | |
| CSR | Nc | $e_c$ | Dr | | Nc | $e_c$ | Dr |
| | | | % | | | | % |
| 0.067 | 41 | 0.770 | 23.4 | -3.97 | 15 | 0.700 | 45.3 |
| 0.080 | 13 | 0.758 | 27.2 | -4.15 | 10 | 0.685 | 50.0 |
| 0.090 | 11 | 0.764 | 25.3 | -2.57 | 4 | 0.719 | 39.4 |
| σvc = 200 kPa | | | | | | | |
| Liquefaction | | | | | Re-Liquefaction | | |
| CSR | Nc | $e_c$ | Dr | | Nc | $e_c$ | Dr |
| | | | % | | | | % |
| 0.080 | 47 | 0.769 | 23.8 | -2.69 | 27 | 0.722 | 38.4 |
| 0.090 | 35 | 0.767 | 24.4 | -3.09 | 8 | 0.713 | 41.3 |
| 0.100 | 16 | 0.768 | 24.1 | -2.59 | 7 | 0.720 | 39.1 |
| σvc = 400 kPa | | | | | | | |
| Liquefaction | | | | | Re-Liquefaction | | |
| CSR | Nc | $e_c$ | Dr | | Nc | $e_c$ | Dr |
| | | | % | | | | % |
| 0.090 | 56 | 0.766 | 24.7 | -2.82 | 27 | 0.716 | 40.3 |
| 0.100 | 29 | 0.770 | 23.4 | -3.58 | 14 | 0.707 | 43.1 |
| 0.110 | 17 | 0.770 | 23.4 | -2.92 | 8 | 0.718 | 39.7 |
| σvc = 600 kPa | | | | | | | |
| Liquefaction | | | | | Re-Liquefaction | | |
| CSR | Nc | $e_c$ | Dr | | Nc | $e_c$ | Dr |
| | | | % | | | | % |
| 0.100 | 25 | 0.765 | 25.0 | -3.27 | 12 | 0.707 | 43.1 |
| 0.110 | 13 | 0.764 | 25.3 | -3.73 | 6 | 0.697 | 46.3 |
| 0.125 | 6 | 0.760 | 26.6 | -3.59 | 3 | 0.697 | 46.3 |

**Table 4.3: Results for liquefaction / re-liquefaction at $D_{rc}$ = 25% / bi-dir. (circular)**

| Drc = 25% Bi-directional (Circular) | | | | | | | |
|---|---|---|---|---|---|---|---|
| σvc = 50 kPa | | | | | | | |
| Liquefaction | | | | | Re-Liquefaction | | |
| CSR | Nc | $e_c$ | Dr | Δεv | Nc | $e_c$ | Dr |
| | | | % | | | | % |
| 0.042 | 44 | 0.765 | 25.0 | -1.10 | 48 | 0.745 | 31.3 |
| 0.057 | 16 | 0.762 | 25.9 | -2.82 | 7 | 0.713 | 41.3 |
| 0.067 | 8 | 0.763 | 25.6 | -3.37 | 3 | 0.703 | 44.4 |
| σvc = 100 kPa | | | | | | | |
| Liquefaction | | | | | Re-Liquefaction | | |
| CSR | Nc | $e_c$ | Dr | | Nc | $e_c$ | Dr |
| | | | % | | | | % |
| 0.053 | 83 | 0.768 | 24.1 | -1.31 | 73 | 0.722 | 38.4 |
| 0.071 | 9 | 0.762 | 25.9 | -2.96 | 3 | 0.695 | 46.9 |
| 0.082 | 6 | 0.759 | 26.9 | -3.44 | 2 | 0.711 | 41.9 |
| σvc = 200 kPa | | | | | | | |
| Liquefaction | | | | | Re-Liquefaction | | |
| CSR | Nc | $e_c$ | Dr | | Nc | $e_c$ | Dr |
| | | | % | | | | % |
| 0.061 | 55 | 0.76 | 26.6 | -1.24 | 65 | 0.724 | 37.8 |
| 0.081 | 12 | 0.760 | 26.6 | -3.42 | 3 | 0.682 | 50.9 |
| 0.091 | 4 | 0.759 | 26.9 | -3.13 | 2 | 0.712 | 41.6 |
| σvc = 400 kPa | | | | | | | |
| Liquefaction | | | | | Re-Liquefaction | | |
| CSR | Nc | $e_c$ | Dr | | Nc | $e_c$ | Dr |
| | | | % | | | | % |
| 0.081 | 16 | 0.758 | 27.2 | -2.15 | 9 | 0.669 | 55.0 |
| 0.091 | 6 | 0.764 | 25.3 | -4.93 | 4 | 0.686 | 49.7 |
| 0.101 | 5 | 0.767 | 24.4 | -2.54 | 1 | 0.708 | 42.8 |
| σvc = 600 kPa | | | | | | | |
| Liquefaction | | | | | Re-Liquefaction | | |
| CSR | Nc | $e_c$ | Dr | | Nc | $e_c$ | Dr |
| | | | % | | | | % |
| 0.081 | 35 | 0.768 | 24.1 | -3.11 | 22 | 0.703 | 44.4 |
| 0.091 | 12 | 0.764 | 25.3 | -3.26 | 9 | 0.699 | 45.6 |
| 0.101 | 8 | 0.771 | 23.1 | -2.13 | 5 | 0.704 | 44.1 |

**Table 4.4: Results for liquefaction / re-liquefaction at $D_{rc}$ = 25% / bi-dir. (elliptical)**

| Drc = 25% Bi-directional (Eliptical) | | | | | | | |
|---|---|---|---|---|---|---|---|
| σvc = 50 kPa | | | | | | | |
| Liquefaction | | | | | Re-Liquefaction | | |
| CSR | Nc | $e_c$ | Dr | Δεv | Nc | $e_c$ | Dr |
| | | | % | | | | % |
| 0.056 | 131 | 0.771 | 23.1 | -1.15 | 82 | 0.751 | 29.4 |
| 0.073 | 21 | 0.771 | 23.1 | -1.55 | 6 | 0.743 | 31.9 |
| 0.091 | 3 | 0.757 | 27.5 | -1.51 | 1 | 0.73 | 35.9 |
| σvc = 100 kPa | | | | | | | |
| Liquefaction | | | | | Re-Liquefaction | | |
| CSR | Nc | $e_c$ | Dr | | Nc | $e_c$ | Dr |
| | | | % | | | | % |
| 0.073 | 42 | 0.764 | 25.3 | -3.48 | 31 | 0.703 | 44.4 |
| 0.081 | 13 | 0.758 | 27.2 | -1.42 | 7 | 0.733 | 35.0 |
| 0.091 | 7 | 0.759 | 26.9 | -1.32 | 3 | 0.736 | 34.1 |
| σvc = 200 kPa | | | | | | | |
| Liquefaction | | | | | Re-Liquefaction | | |
| CSR | Nc | $e_c$ | Dr | | Nc | $e_c$ | Dr |
| | | | % | | | | % |
| 0.080 | 28 | 0.768 | 24.1 | -2.43 | 66 | 0.725 | 37.5 |
| 0.100 | 7 | 0.759 | 26.9 | -1.68 | 4 | 0.729 | 36.3 |
| 0.111 | 3 | 0.770 | 23.4 | -1.27 | 1 | 0.747 | 30.6 |
| σvc = 400 kPa | | | | | | | |
| Liquefaction | | | | | Re-Liquefaction | | |
| CSR | Nc | $e_c$ | Dr | | Nc | $e_c$ | Dr |
| | | | % | | | | % |
| 0.090 | 29 | 0.771 | 23.1 | -1.63 | 33 | 0.742 | 32.2 |
| 0.100 | 8 | 0.767 | 24.4 | -1.69 | 5 | 0.737 | 33.8 |
| 0.110 | 5 | 0.778 | 20.9 | -2.04 | 5 | 0.742 | 32.2 |
| σvc = 600 kPa | | | | | | | |
| Liquefaction | | | | | Re-Liquefaction | | |
| CSR | Nc | $e_c$ | Dr | | Nc | $e_c$ | Dr |
| | | | % | | | | % |
| 0.090 | 57 | 0.753 | 28.8 | -2.19 | 41 | 0.715 | 40.6 |
| 0.100 | 21 | 0.758 | 27.2 | -1.88 | 22 | 0.725 | 37.5 |
| 0.110 | 7 | 0.774 | 22.2 | -2.62 | 8 | 0.727 | 36.9 |

**Table 4.5: Results for liquefaction / re-liquefaction at $D_{rc}$ = 25% / bi-dir. (figure-8)**

| Drc = 25% Bi-directional (figure-8) | | | | | | | |
|---|---|---|---|---|---|---|---|
| σvc = 50 kPa | | | | | | | |
| Liquefaction | | | | | Re-Liquefaction | | |
| CSRliq | Nc | $e_c$ | Dr | Δεv | Nc | $e_c$ | Dr |
| | | | % | | | | % |
| 0.057 | 21 | 0.763 | 25.6 | -1.11 | 68 | 0.744 | 31.6 |
| 0.076 | 8 | 0.770 | 23.4 | -0.95 | 6 | 0.753 | 28.8 |
| 0.100 | 2 | 0.765 | 25.0 | -1.71 | 2 | 0.735 | 34.4 |
| σvc = 100 kPa | | | | | | | |
| | Liquefaction | | | | Re-Liquefaction | | |
| CSR | Nc | $e_c$ | Dr | | Nc | $e_c$ | Dr |
| | | | % | | | | % |
| 0.055 | 75 | 0.759 | 26.9 | -1.77 | 84 | 0.728 | 36.6 |
| 0.077 | 11 | 0.768 | 24.1 | -1.31 | 13 | 0.745 | 31.3 |
| 0.101 | 3 | 0.757 | 27.5 | -0.96 | 3 | 0.740 | 32.8 |
| σvc = 200 kPa | | | | | | | |
| | Liquefaction | | | | Re-Liquefaction | | |
| CSR | Nc | $e_c$ | Dr | | Nc | $e_c$ | Dr |
| | | | % | | | | % |
| 0.064 | 28 | 0.759 | 26.9 | -1.48 | 116 | 0.733 | 35.0 |
| 0.089 | 13 | 0.756 | 27.8 | -4.15 | 5 | 0.683 | 50.6 |
| 0.114 | 2 | 0.757 | 27.5 | -1.63 | 2 | 0.728 | 36.6 |
| σvc = 400 kPa | | | | | | | |
| | Liquefaction | | | | Re-Liquefaction | | |
| CSR | Nc | $e_c$ | Dr | | Nc | $e_c$ | Dr |
| | | | % | | | | % |
| 0.076 | 60 | 0.772 | 22.8 | -2.55 | 36 | 0.727 | 36.9 |
| 0.101 | 10 | 0.757 | 27.5 | -1.96 | 6 | 0.723 | 38.1 |
| 0.126 | 5 | 0.755 | 28.1 | -1.76 | 2 | 0.724 | 37.8 |
| σvc = 600 kPa | | | | | | | |
| | Liquefaction | | | | Re-Liquefaction | | |
| CSR | Nc | $e_c$ | Dr | | Nc | $e_c$ | Dr |
| | | | % | | | | % |
| 0.101 | 24 | 0.76 | 26.6 | -1.92 | 30 | 0.726 | 37.2 |
| 0.113 | 14 | 0.757 | 27.5 | -1.88 | 19 | 0.724 | 37.8 |
| 0.138 | 4 | 0.764 | 25.3 | -1.61 | 6 | 0.736 | 34.1 |

**Table 4.6: Results for liquefaction / re-liquefaction at $D_{rc}$ = 45% / mono-directional**

| Drc = 45% Mono-directional | | | | | | | |
|---|---|---|---|---|---|---|---|
| σvc = 50 kPa | | | | | | | |
| Liquefaction | | | | | Re-Liquefaction | | |
| CSRliq | Nc | $e_c$ | Dr | Δεv | Nc | $e_c$ | Dr |
| | | | % | | | | % |
| 0.073 | 35 | 0.703 | 44.4 | -1.68 | 20 | 0.674 | 53.4 |
| 0.082 | 17 | 0.694 | 47.2 | -0.77 | 11 | 0.681 | 51.3 |
| 0.094 | 8 | 0.706 | 43.4 | -1.30 | 3 | 0.684 | 50.3 |
| σvc = 100 kPa | | | | | | | |
| Liquefaction | | | | | Re-Liquefaction | | |
| CSR | Nc | $e_c$ | Dr | | Nc | $e_c$ | Dr |
| | | | % | | | | % |
| 0.083 | 31 | 0.697 | 46.3 | -1.07 | 83 | 0.679 | 51.9 |
| 0.097 | 22 | 0.697 | 46.3 | -1.61 | 8 | 0.670 | 54.7 |
| 0.103 | 6 | 0.706 | 43.4 | -1.65 | 2 | 0.678 | 52.2 |
| σvc = 200 kPa | | | | | | | |
| Liquefaction | | | | | Re-Liquefaction | | |
| CSR | Nc | $e_c$ | Dr | | Nc | $e_c$ | Dr |
| | | | % | | | | % |
| 0.080 | 77 | 0.707 | 43.1 | -1.33 | 163 | 0.684 | 50.3 |
| 0.102 | 29 | 0.700 | 45.3 | -1.53 | 6 | 0.674 | 53.4 |
| 0.112 | 15 | 0.711 | 41.9 | -1.76 | 2 | 0.681 | 51.3 |
| 0.131 | 7 | 0.695 | 46.9 | | | | |
| σvc = 400 kPa | | | | | | | |
| Liquefaction | | | | | Re-Liquefaction | | |
| CSR | Nc | $e_c$ | Dr | | Nc | $e_c$ | Dr |
| | | | % | | | | % |
| 0.122 | 27 | 0.709 | 42.5 | -2.29 | 18 | 0.67 | 54.7 |
| 0.131 | 11 | 0.708 | 42.8 | -1.94 | | 0.675 | 53.1 |
| 0.151 | 6 | 0.697 | 46.3 | -2.16 | 5 | 0.66 | 57.8 |
| σvc = 600 kPa | | | | | | | |
| Liquefaction | | | | | Re-Liquefaction | | |
| CSR | Nc | $e_c$ | Dr | | Nc | $e_c$ | Dr |
| | | | % | | | | % |
| 0.131 | 55 | 0.693 | 47.5 | -1.38 | 212 | 0.67 | 54.7 |
| 0.141 | 20 | 0.694 | 47.2 | -1.41 | 47 | 0.67 | 54.7 |
| 0.161 | 12 | 0.694 | 47.2 | -2.01 | 8 | 0.66 | 57.8 |

**Table 4.7: Results for liquefaction / re-liquefaction at $D_{rc}$ = 45% / bi-dir. (circular)**

| Drc = 45% Bi-directional (Circular) | | | | | | | |
|---|---|---|---|---|---|---|---|
| σvc = 50 kPa | | | | | | | |
| Liquefaction | | | | | Re-Liquefaction | | |
| CSRliq | Nc | $e_c$ | Dr | Δεv | Nc | $e_c$ | Dr |
| | | | % | | | | % |
| 0.053 | 41 | 0.702 | 44.7 | -0.95 | 46 | 0.67 | 54.7 |
| 0.063 | 24 | 0.710 | 42.2 | -0.99 | 24 | 0.676 | 52.8 |
| 0.077 | 4 | 0.703 | 44.5 | -0.86 | 1 | 0.653 | 60.1 |
| σvc = 100 kPa | | | | | | | |
| | Liquefaction | | | | Re-Liquefaction | | |
| CSR | Nc | $e_c$ | Dr | | Nc | $e_c$ | Dr |
| | | | % | | | | % |
| 0.053 | 51 | 0.703 | 44.4 | -1.31 | 119 | 0.681 | 51.3 |
| 0.076 | 14 | 0.704 | 44.1 | -1.01 | 3 | 0.654 | 59.7 |
| 0.087 | 6 | 0.709 | 42.5 | -1.19 | 1 | 0.650 | 60.9 |
| σvc = 200 kPa | | | | | | | |
| | Liquefaction | | | | Re-Liquefaction | | |
| CSR | Nc | $e_c$ | Dr | | Nc | $e_c$ | Dr |
| | | | % | | | | % |
| 0.072 | 49 | 0.693 | 47.5 | -1.24 | 99 | 0.671 | 54.4 |
| 0.091 | 10 | 0.695 | 46.9 | -1.37 | 3 | 0.637 | 65.0 |
| 0.101 | 4 | 0.710 | 42.2 | -1.72 | 1 | 0.657 | 58.8 |
| σvc = 400 kPa | | | | | | | |
| | Liquefaction | | | | Re-Liquefaction | | |
| CSR | Nc | $e_c$ | Dr | | Nc | $e_c$ | Dr |
| | | | % | | | | % |
| 0.101 | 13 | 0.701 | 45.0 | -1.61 | 11 | 0.665 | 56.3 |
| 0.113 | 9 | 0.708 | 42.8 | -1.23 | 3 | 0.623 | 69.4 |
| 0.121 | 5 | 0.707 | 43.1 | -1.33 | 2 | 0.663 | 56.9 |
| σvc = 600 kPa | | | | | | | |
| | Liquefaction | | | | Re-Liquefaction | | |
| CSR | Nc | $e_c$ | Dr | | Nc | $e_c$ | Dr |
| | | | % | | | | % |
| 0.091 | 31 | 0.696 | 46.6 | -1.12 | 19 | 0.644 | 62.8 |
| 0.111 | 9 | 0.695 | 46.9 | -1.55 | 3 | 0.640 | 64.1 |
| 0.121 | 7 | 0.702 | 44.7 | -1.95 | 8 | 0.666 | 55.9 |

**Table 4.8: Results for liquefaction / re-liquefaction at $D_{rc}$ = 45% / bi-dir. (elliptical)**

| Drc = 45% Bi-directional (Eliptical) | | | | | | | |
|---|---|---|---|---|---|---|---|
| σvc = 50 kPa | | | | | | | |
| Liquefaction | | | | | Re-Liquefaction | | |
| CSRliq | Nc | $e_c$ | Dr | Δεv | Nc | $e_c$ | Dr |
| | | | % | | | | % |
| 0.062 | 56 | 0.700 | 45.3 | -1.35 | 40 | 0.677 | 52.5 |
| 0.071 | 12 | 0.703 | 44.4 | -1.59 | 9 | 0.676 | 52.8 |
| 0.091 | 9 | 0.700 | 45.3 | -1.35 | 8 | 0.677 | 52.5 |
| σvc = 100 kPa | | | | | | | |
| Liquefaction | | | | | Re-Liquefaction | | |
| CSR | Nc | $e_c$ | Dr | | Nc | $e_c$ | Dr |
| | | | % | | | | % |
| 0.081 | 23 | 0.699 | 45.6 | -1.17 | 30 | 0.679 | 51.9 |
| 0.091 | 14 | 0.703 | 44.4 | -1.31 | 6 | 0.680 | 51.6 |
| 0.111 | 7 | 0.703 | 44.4 | -1.21 | 4 | 0.682 | 50.9 |
| σvc = 200 kPa | | | | | | | |
| Liquefaction | | | | | Re-Liquefaction | | |
| CSR | Nc | $e_c$ | Dr | | Nc | $e_c$ | Dr |
| | | | % | | | | % |
| 0.100 | 18 | 0.710 | 42.2 | -1.44 | 26 | 0.685 | 50.0 |
| 0.110 | 17 | 0.705 | 43.8 | -1.18 | 5 | 0.685 | 50.0 |
| 0.120 | 9 | 0.703 | 44.4 | -1.35 | 2 | 0.680 | 51.6 |
| σvc = 400 kPa | | | | | | | |
| Liquefaction | | | | | Re-Liquefaction | | |
| CSR | Nc | $e_c$ | Dr | | Nc | $e_c$ | Dr |
| | | | % | | | | % |
| 0.100 | 33 | 0.697 | 46.3 | -1.80 | 39 | 0.663 | 56.9 |
| 0.110 | 23 | 0.701 | 45.0 | -1.80 | 8 | 0.67 | 54.7 |
| 0.120 | 14 | 0.695 | 46.9 | -1.56 | 7 | 0.669 | 55.0 |
| 0.130 | 9 | 0.702 | 44.7 | -1.50 | 3 | 0.676 | 52.8 |
| σvc = 600 kPa | | | | | | | |
| Liquefaction | | | | | Re-Liquefaction | | |
| CSR | Nc | $e_c$ | Dr | | Nc | $e_c$ | Dr |
| | | | % | | | | % |
| 0.120 | 19 | 0.707 | 43.1 | -2.12 | 34 | 0.671 | 54.4 |
| 0.130 | 12 | 0.7 | 45.3 | -1.58 | 15 | 0.673 | 53.8 |
| 0.140 | 8 | 0.705 | 43.8 | -1.82 | 2 | 0.674 | 53.4 |

**Table 4.9: Results for liquefaction / re-liquefaction at $D_{rc}$ = 45% / bi-dir. (figure-8)**

| Drc = 45% Bi-directional (figure-8) | | | | | | | |
|---|---|---|---|---|---|---|---|
| σvc = 50 kPa | | | | | | | |
| Liquefaction | | | | | Re-Liquefaction | | |
| CSRliq | Nc | $e_c$ | Dr | Δεv | Nc | $e_c$ | Dr |
| | | | % | | | | % |
| 0.067 | 31 | 0.709 | 42.5 | -0.98 | 29 | 0.692 | 47.8 |
| 0.077 | 15 | 0.692 | 47.8 | -1.36 | 12 | 0.669 | 55.0 |
| 0.089 | 4 | 0.706 | 43.4 | -1.49 | 2 | 0.681 | 51.3 |
| σvc = 100 kPa | | | | | | | |
| | Liquefaction | | | | Re-Liquefaction | | |
| CSR | Nc | $e_c$ | Dr | | Nc | $e_c$ | Dr |
| | | | % | | | | % |
| 0.077 | 24 | 0.701 | 45.0 | -1.12 | 19 | 0.682 | 50.9 |
| 0.089 | 7 | 0.704 | 44.1 | -1.16 | 4 | 0.684 | 50.3 |
| 0.102 | 6 | 0.711 | 41.9 | -1.55 | 1 | 0.684 | 50.3 |
| σvc = 200 kPa | | | | | | | |
| | Liquefaction | | | | Re-Liquefaction | | |
| CSR | Nc | $e_c$ | Dr | | Nc | $e_c$ | Dr |
| | | | % | | | | % |
| 0.101 | 15 | 0.71 | 42.2 | -1.27 | 25 | 0.688 | 49.1 |
| 0.126 | 6 | 0.700 | 45.3 | -2.07 | 2 | 0.665 | 56.3 |
| 0.138 | 3 | 0.706 | 43.4 | -1.52 | 1 | 0.68 | 51.6 |
| σvc = 400 kPa | | | | | | | |
| | Liquefaction | | | | Re-Liquefaction | | |
| CSR | Nc | $e_c$ | Dr | | Nc | $e_c$ | Dr |
| | | | % | | | | % |
| 0.088 | 46 | 0.702 | 44.7 | -1.65 | 152 | 0.674 | 53.4 |
| 0.101 | 15 | 0.707 | 43.1 | -1.24 | 49 | 0.686 | 49.7 |
| 0.126 | 6 | 0.704 | 44.1 | -2.60 | 2 | 0.66 | 57.8 |
| σvc = 600 kPa | | | | | | | |
| | Liquefaction | | | | Re-Liquefaction | | |
| CSR | Nc | $e_c$ | Dr | | Nc | $e_c$ | Dr |
| | | | % | | | | % |
| 0.114 | 33 | 0.693 | 47.5 | -1.84 | 106 | 0.661 | 57.5 |
| 0.139 | 9 | 0.696 | 46.6 | -1.37 | 2 | 0.673 | 53.8 |
| 0.163 | 3 | 0.709 | 42.5 | -3.84 | 1 | 0.643 | 63.1 |

**Table 4.10: Results for liquefaction / re-liquefaction at $D_{rc}$ = 65% / mono-directional**

| Drc = 65% Mono-directional | | | | | | | |
|---|---|---|---|---|---|---|---|
| σvc = 50 kPa | | | | | | | |
| Liquefaction | | | | Re-Liquefaction | | | |
| CSR | Nc | $e_c$ | Dr | Δεv | Nc | $e_c$ | Dr |
| | | | % | | | | % |
| 0.047 | 130 | 0.643 | 63.1 | -0.72 | 107 | 0.631 | 66.9 |
| 0.071 | 25 | 0.643 | 63.1 | -1.21 | 12 | 0.623 | 69.4 |
| 0.093 | 10 | 0.643 | 63.1 | -0.54 | 4 | 0.635 | 65.6 |
| σvc = 100 kPa | | | | | | | |
| Liquefaction | | | | Re-Liquefaction | | | |
| CSR | Nc | $e_c$ | Dr | | Nc | $e_c$ | Dr |
| | | | % | | | | % |
| 0.079 | 47 | 0.638 | 64.7 | -1.13 | 27 | 0.616 | 71.6 |
| 0.095 | 19 | 0.634 | 65.9 | -1.38 | 9 | 0.611 | 73.1 |
| 0.105 | 15 | 0.634 | 65.9 | -1.15 | 4 | 0.615 | 71.9 |
| σvc = 200 kPa | | | | | | | |
| Liquefaction | | | | Re-Liquefaction | | | |
| CSR | Nc | $e_c$ | Dr | | Nc | $e_c$ | Dr |
| | | | % | | | | % |
| 0.104 | 30 | 0.635 | 65.6 | -1.82 | 67 | 0.605 | 75.0 |
| 0.118 | 15 | 0.643 | 63.1 | -1.76 | 25 | 0.614 | 72.2 |
| 0.132 | 8 | 0.639 | 64.4 | -1.49 | 15 | 0.614 | 72.2 |
| σvc = 400 kPa | | | | | | | |
| Liquefaction | | | | Re-Liquefaction | | | |
| CSR | Nc | $e_c$ | Dr | | Nc | $e_c$ | Dr |
| | | | % | | | | % |
| 0.122 | 45 | 0.634 | 65.9 | -2.00 | 79 | 0.601 | 76.3 |
| 0.137 | 24 | 0.634 | 65.9 | -1.86 | 57 | 0.604 | 75.3 |
| 0.151 | 13 | 0.633 | 66.3 | -1.96 | 22 | 0.602 | 75.9 |
| 0.171 | 8 | 0.629 | 67.5 | -1.10 | 15 | 0.611 | 73.1 |
| σvc = 600 kPa | | | | | | | |
| Liquefaction | | | | Re-Liquefaction | | | |
| CSR | Nc | $e_c$ | Dr | | Nc | $e_c$ | Dr |
| | | | % | | | | % |
| 0.141 | 36 | 0.631 | 66.9 | -1.85 | 112 | 0.601 | 76.3 |
| 0.152 | 21 | 0.634 | 65.9 | -2.09 | 41 | 0.6 | 76.6 |
| 0.191 | 5 | 0.644 | 62.8 | -1.11 | 28 | 0.626 | 68.4 |

**Table 4.11: Results of liquefaction / re-liquefaction at $D_{rc}$ = 65% / bi-dir. (circular)**

| Drc = 65% Mono-directional | | | | | | | |
|---|---|---|---|---|---|---|---|
| σvc = 50 kPa | | | | | | | |
| Liquefaction | | | | Re-Liquefaction | | | |
| CSR | Nc | $e_c$ | Dr | Δεv | Nc | $e_c$ | Dr |
| | | | % | | | | % |
| 0.047 | 130 | 0.643 | 63.1 | -0.72 | 107 | 0.631 | 66.9 |
| 0.071 | 25 | 0.643 | 63.1 | -1.21 | 12 | 0.623 | 69.4 |
| 0.093 | 10 | 0.643 | 63.1 | -0.54 | 4 | 0.635 | 65.6 |
| σvc = 100 kPa | | | | | | | |
| Liquefaction | | | | Re-Liquefaction | | | |
| CSR | Nc | $e_c$ | Dr | | Nc | $e_c$ | Dr |
| | | | % | | | | % |
| 0.079 | 47 | 0.638 | 64.7 | -1.13 | 27 | 0.616 | 71.6 |
| 0.095 | 19 | 0.634 | 65.9 | -1.38 | 9 | 0.611 | 73.1 |
| 0.105 | 15 | 0.634 | 65.9 | -1.15 | 4 | 0.615 | 71.9 |
| σvc = 200 kPa | | | | | | | |
| Liquefaction | | | | Re-Liquefaction | | | |
| CSR | Nc | $e_c$ | Dr | | Nc | $e_c$ | Dr |
| | | | % | | | | % |
| 0.104 | 30 | 0.635 | 65.6 | -1.82 | 67 | 0.605 | 75.0 |
| 0.118 | 15 | 0.643 | 63.1 | -1.76 | 25 | 0.614 | 72.2 |
| 0.132 | 8 | 0.639 | 64.4 | -1.49 | 15 | 0.614 | 72.2 |
| σvc = 400 kPa | | | | | | | |
| Liquefaction | | | | Re-Liquefaction | | | |
| CSR | Nc | $e_c$ | Dr | | Nc | $e_c$ | Dr |
| | | | % | | | | % |
| 0.122 | 45 | 0.634 | 65.9 | -2.00 | 79 | 0.601 | 76.3 |
| 0.137 | 24 | 0.634 | 65.9 | -1.86 | 57 | 0.604 | 75.3 |
| 0.151 | 13 | 0.633 | 66.3 | -1.96 | 22 | 0.602 | 75.9 |
| 0.171 | 8 | 0.629 | 67.5 | -1.10 | 15 | 0.611 | 73.1 |
| σvc = 600 kPa | | | | | | | |
| Liquefaction | | | | Re-Liquefaction | | | |
| CSR | Nc | $e_c$ | Dr | | Nc | $e_c$ | Dr |
| | | | % | | | | % |
| 0.141 | 36 | 0.631 | 66.9 | -1.85 | 112 | 0.601 | 76.3 |
| 0.152 | 21 | 0.634 | 65.9 | -2.09 | 41 | 0.6 | 76.6 |
| 0.191 | 5 | 0.644 | 62.8 | -1.11 | 28 | 0.626 | 68.4 |

**Table 4.12: Results liquefaction / re-liquefaction at $D_{rc}$ = 65% / bi-dir. (elliptical)**

| Drc = 65% Bi-directional (Eliptical) | | | | | | | |
|---|---|---|---|---|---|---|---|
| σvc = 50 kPa | | | | | | | |
| Liquefaction | | | | | Re-Liquefaction | | |
| CSR | Nc | $e_c$ | Dr | Δεv | Nc | $e_c$ | Dr |
| | | | % | | | | % |
| 0.073 | 42 | 0.634 | 65.9 | -0.81 | 17 | 0.621 | 70.0 |
| 0.081 | 13 | 0.637 | 65.0 | -0.72 | 8 | 0.625 | 68.8 |
| 0.101 | 5 | 0.628 | 67.8 | -0.82 | 4 | 0.615 | 71.9 |
| σvc = 100 kPa | | | | | | | |
| Liquefaction | | | | | Re-Liquefaction | | |
| CSR | Nc | $e_c$ | Dr | | Nc | $e_c$ | Dr |
| | | | % | | | | % |
| 0.081 | 24 | 0.629 | 67.5 | -0.83 | 65 | 0.615 | 71.9 |
| 0.091 | 15 | 0.635 | 65.6 | -1.10 | 10 | 0.617 | 71.3 |
| 0.110 | 8 | 0.633 | 66.3 | -0.83 | 2 | 0.619 | 70.6 |
| σvc = 200 kPa | | | | | | | |
| Liquefaction | | | | | Re-Liquefaction | | |
| CSR | Nc | $e_c$ | Dr | | Nc | $e_c$ | Dr |
| | | | % | | | | % |
| 0.080 | 54 | 0.640 | 64.1 | -1.16 | 95 | 0.621 | 70.0 |
| 0.091 | 29 | 0.628 | 67.8 | -1.08 | 43 | 0.611 | 73.1 |
| 0.110 | 10 | 0.649 | 61.3 | -1.20 | 2 | 0.629 | 67.5 |
| σvc = 400 kPa | | | | | | | |
| Liquefaction | | | | | Re-Liquefaction | | |
| CSR | Nc | $e_c$ | Dr | | Nc | $e_c$ | Dr |
| | | | % | | | | % |
| 0.120 | 31 | 0.64 | 64.1 | -1.28 | 33 | 0.619 | 70.6 |
| 0.130 | 16 | 0.626 | 68.4 | -1.15 | 42 | 0.607 | 74.4 |
| 0.140 | 10 | 0.641 | 63.8 | -1.37 | 4 | 0.619 | 70.6 |
| σvc = 600 kPa | | | | | | | |
| Liquefaction | | | | | Re-Liquefaction | | |
| CSR | Nc | $e_c$ | Dr | | Nc | $e_c$ | Dr |
| | | | % | | | | % |
| 0.130 | 33 | 0.639 | 64.4 | -1.41 | 134 | 0.616 | 71.6 |
| 0.140 | 20 | 0.642 | 63.4 | -1.50 | 37 | 0.618 | 70.9 |
| 0.150 | 13 | 0.643 | 63.1 | -1.69 | 10 | 0.615 | 71.9 |

**Table 4.13: Results of liquefaction / re-liquefaction at $D_{rc}$ = 65% / bi-dir. (figure-8)**

| Drc = 65% Bi-directional (figure-8) | | | | | | | |
|---|---|---|---|---|---|---|---|
| σvc = 50 kPa | | | | | | | |
| Liquefaction | | | | | Re-Liquefaction | | |
| CSR | Nc | $e_c$ | Dr | Δεv | Nc | $e_c$ | Dr |
| | | | % | | | | % |
| 0.065 | 26 | 0.631 | 66.9 | -1.00 | 90 | 0.615 | 71.9 |
| 0.077 | 11 | 0.641 | 63.8 | -0.99 | 29 | 0.625 | 68.8 |
| 0.090 | 5 | 0.631 | 66.9 | -0.77 | 8 | 0.619 | 70.6 |
| σvc = 100 kPa | | | | | | | |
| Liquefaction | | | | | Re-Liquefaction | | |
| CSR | Nc | $e_c$ | Dr | | Nc | $e_c$ | Dr |
| | | | % | | | | % |
| 0.064 | 55 | 0.641 | 63.8 | -1.01 | 428 | 0.625 | 68.8 |
| 0.090 | 8 | 0.642 | 63.4 | -0.96 | 12 | 0.626 | 68.4 |
| 0.114 | 4 | 0.642 | 63.4 | -0.96 | 2 | 0.626 | 68.4 |
| σvc = 200 kPa | | | | | | | |
| Liquefaction | | | | | Re-Liquefaction | | |
| CSR | Nc | $e_c$ | Dr | | Nc | $e_c$ | Dr |
| | | | % | | | | % |
| 0.089 | 24 | 0.628 | 67.8 | -1.08 | 62 | 0.61 | 73.4 |
| 0.101 | 14 | 0.640 | 64.1 | -1.26 | 19 | 0.62 | 70.3 |
| 0.113 | 9 | 0.629 | 67.5 | -0.90 | 12 | 0.615 | 71.9 |
| σvc = 400 kPa | | | | | | | |
| Liquefaction | | | | | Re-Liquefaction | | |
| CSR | Nc | $e_c$ | Dr | | Nc | $e_c$ | Dr |
| | | | % | | | | % |
| 0.088 | 44 | 0.642 | 63.4 | -1.18 | 249 | 0.622 | 69.7 |
| 0.126 | 9 | 0.637 | 65.0 | -1.38 | 8 | 0.614 | 72.2 |
| 0.151 | 3 | 0.634 | 65.9 | -1.19 | 2 | 0.615 | 71.9 |
| σvc = 600 kPa | | | | | | | |
| Liquefaction | | | | | Re-Liquefaction | | |
| CSR | Nc | $e_c$ | Dr | | Nc | $e_c$ | Dr |
| | | | % | | | | % |
| 0.101 | 38 | 0.637 | 65.0 | -1.55 | 300 | 0.612 | 72.8 |
| 0.126 | 10 | 0.641 | 63.8 | -1.65 | 8 | 0.614 | 72.2 |
| 0.176 | 3 | 0.636 | 65.3 | -1.31 | 3 | 0.614 | 72.2 |

## 4.4. Analysis of results

### 4.4.1. Densification effect of pre-shearing

In Figures 4.2 and 4.3 as an example and later in Tables 4.2 to 4.13, liquefaction and re-liquefaction responses of samples were represented. An important result of the tests is the void ratio changes of samples in two stages. Before analysis of resisting cycles, void ratio (relative density) changes after first liquefaction stage, is discussed as the most important variable in sample properties after applying the first stage of shear loads. Based on the results, cyclic loading in the first stage and re-consolidation of samples prior to the second stage of cyclic loading causes their densification and thus, re-liquefied specimens are initially denser than liquefied samples. As a typical response, looser samples densify the most and denser ones tend to densify the least. Previously, particle re-arrangement after the first stage of shear loading was reported to be the most important reason of this densification (Wahyudi, J. Koseki, and T. Sato). As an example, the void ratio changes of various samples under bi-directional / figure-8 pattern cyclic loads are shown in Figure 4.4.

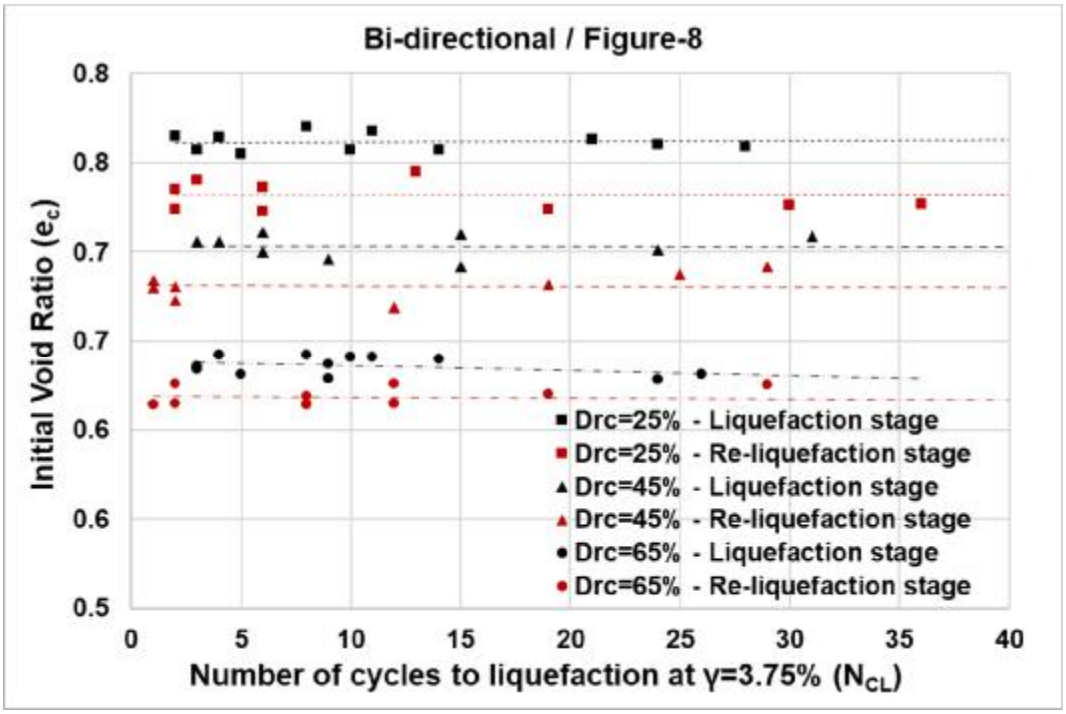


**Figure 4.4: Void ratio changes VS number of cycles at consecutive liquefaction stages**

Similar changes to the void ratio as observed in figure-8 pattern load occurs for the rest of cyclic load patterns. Considering all cyclic load patterns, an average increase in relative densities of 14%, 10% and 6% for specimens with average initial relative densities of 25%, 45%, and 65% were observed respectively. Furthermore, the densification of samples in this study is characterized by volumetric strain changes (Δεv) and correlated to their initial state parameters as shown in Figure 4.5. Initial state parameter could reflect both effects of relative density and effective stress at the same time and thus be a good means of comparison. Volumetric strain change (Δεv) is defined as the ratio of changes in sample volume to initial volume. Negative values represent a reduction in volume (densification). Based on sample geometry and lateral restraint supplied by metal rings, volumetric strain changes in this study is limited to axial strain changes only. As it is observed, volumetric strain changes due to first stage of shear loading and re-consolidation, is linearly proportional to initial state parameter and it gets smaller in larger negative state parameter values (depicts denser samples at equal vertical effective stresses) and increases in large positive values of state parameter (which addresses lower relative densities at similar consolidation stresses).

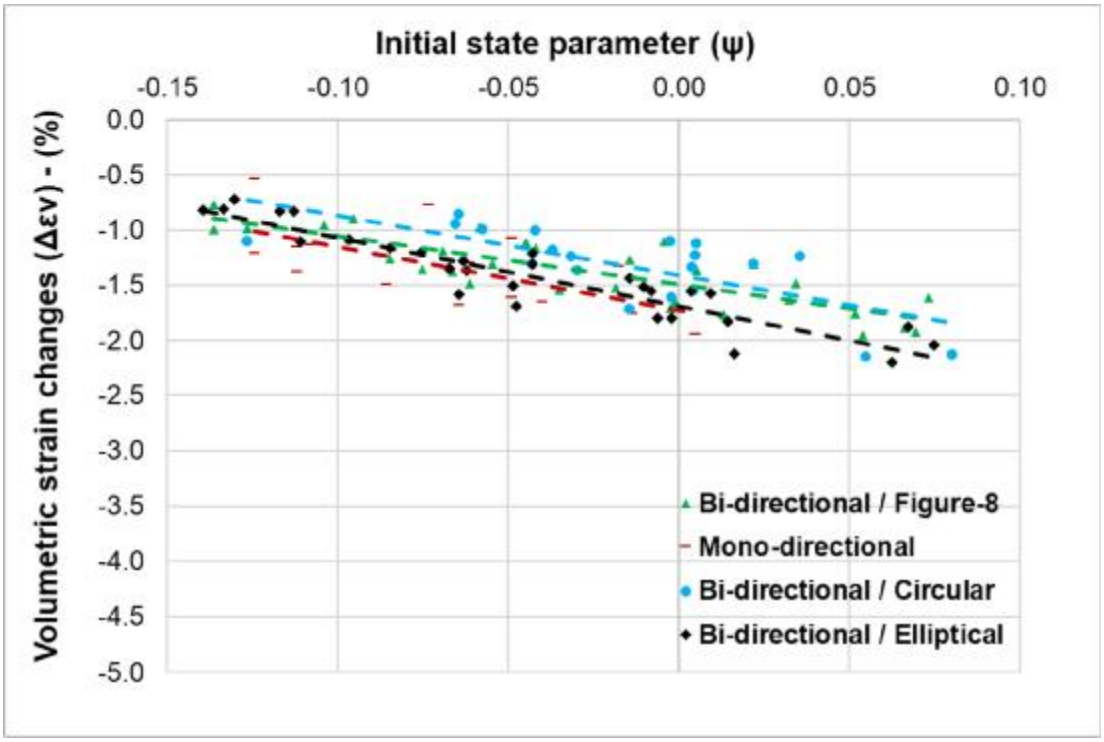


**Figure 4.5: Volumetric strain changes VS initial state parameter (Ψ)**

A linear correlation could be assigned to corresponding changes. Comparing the results of multiple loading patterns also shows very small deviation in behavior as the rate of changes (slope of the lines) are almost the same. Previous researchers focused on the effect of pre-shearing strain amplitudes on densification and post-liquefaction behavior of sand samples and did not investigate effects of shear loading details on their response. Since all samples of the current study were pre-sheared to shear strain of 3.75% to fulfill liquefaction criteria, it could be found that shear loading pattern is not more effective than the pre-shearing strain in densifying the samples. This, confirms the past observations which assign densification of sand samples to change in samples structure due to a pre-shearing and as a function of pre-shearing strain magnitudes.

### 4.4.2. Effect of relative density and consolidation stress on a re-liquefaction event

Porcino et. al. (2009) studied the effect of relative density in cyclic resistance of the soils and reported it as a controlling factor in the reduction or increase of a soil's cyclic resistance in subsequent liquefaction events. They found that denser samples appeared to exhibit a higher increase in resistance as compared to looser ones. This phenomenon of lower resistance values for re-liquefaction events in loose sands relative to dense sands is also observed for a silica-based Ticino sand, in the same study with a much higher ratio of resistance between first and second liquefaction events (Porcino et al. 2009).

Based on the results of this study discussed in section 3, relative density is a controlling factor in current research as well. Following up with the results, it is found that, the majority of denser samples experience an increase of their cyclic resistance (number of cycles at liquefaction increases) while many looser samples tend to undergo less resistance or sometimes maintain their resistance from the first stage to the second stage of liquefaction. As an example, results of consecutive liquefaction occurrence for loose to dense samples under mono-directional cyclic loads is shown in Figure 4.6. In this figure, solid lines show CRR trend following the first liquefaction event and dashed lines show CRR following the re-liquefaction loading. It is observed that, in loose samples ($D_{rc}$ = 25%), there is a severe decrease in resistance between two liquefaction stages at all stress levels (solid lines represent liquefaction trend and dashed lines represent re-liquefaction trends).

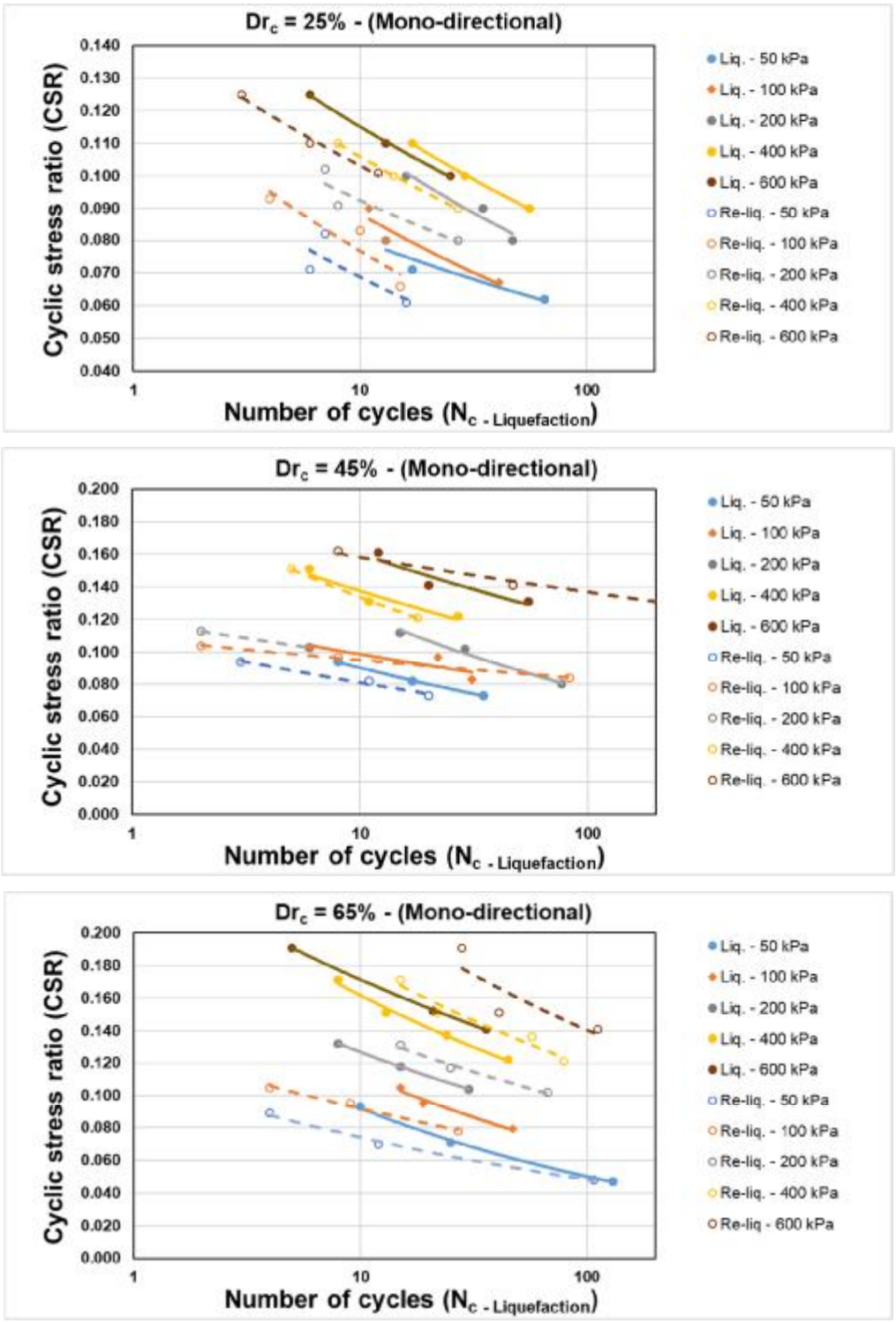


**Figure 4.6: Variable trend of cyclic resistance (CSR) VS number of cycles at consecutive liquefaction events for mono-directional loading patterns**

At the same time, there is a mild decrease in resistance of medium dense samples ($D_{rc}$ = 45%) in lower stresses and they remain almost constant in higher stresses. Unlikely, in dense samples ($D_{rc}$ = 65%), although there is a small drop in resistance to lower level stress, all the rest of the samples experience a severe increase in their resistance. Also, as it was illustrated that, when the consolidation stresses getting larger, soil samples tend to attain more cyclic resistance than before comparing to lower stresses. This depicts the idea that, the occurrence of repeating liquefaction events is more of a concern in a smaller depth of soils rather than deep soils, regardless of density. There are a couple of reported test results shown in Figure 4.7 which have mostly been reported for dense samples. A few results are available for medium dense and loose specimens. As illustrated in the plot, increasing resistance in dense samples of this study is in good accordance with past studies. Specifically, it is observed that ratio of changes in resistance amplifies when samples get denser and based on the current study when consolidation stresses get larger.

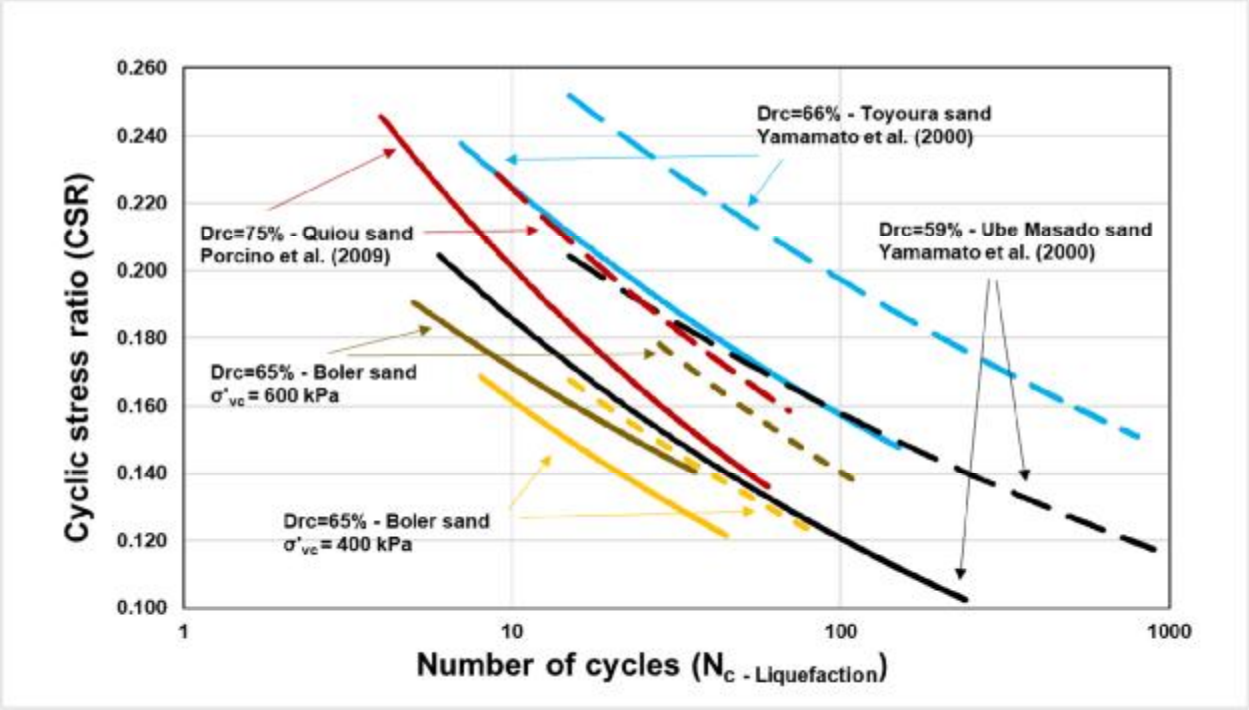


**Figure 4.7: Comparison of cyclic resistance (CSR) vs number of cycles with consecutive liquefaction occurrence in multiple studies and results of current study for dense samples**

Although mono-directional results of this study are in good agreement with past studies such as Porcino et. al. (2009), the behavior of samples under bi-directional load patterns, are more complicated, which would be further discussed. For a better comparison of results, cyclic stress (CSR) variation of samples with the number of cycles at liquefaction ($N_{CL}$) in similar relative densities are plotted and compared for different load patterns in Figures 4.8 to 4.10. Based on the results, it could be verified that decreasing resistance to liquefaction is a general behavior in loose samples ($D_{rc}$ = 25%). The resistance drop is more significant in mono-directional load patterns and impacting less in bi-directional loads. Among three different bi-directional load patterns, a figure-8 pattern seems to be the least effective pattern on changing the resistance of the samples in two consecutive liquefaction events, in most of the consolidation stresses ($\sigma'_{vc}$), resistance remains almost constant, except at larger effective stresses. Also based on the results, the resistance of the medium dense samples ($D_{rc}$ = 45%) does not significantly change from a first liquefaction to a second one. This is a typical behavior for all samples under different cyclic load patterns.

However, a change in exponential parameters of governing power function between CSR and $N_{CL}$ correlation in two liquefaction stages is observed, specifically in bi-directional load patterns and in larger stress levels ($\sigma'_{vc}$ = 400 and 600 kPa). It could be found that, in mentioned tests, CSR VS $N_{CL}$ curves, intersect each other and bring the idea that, when bi-directional cyclic loads are applied to samples under larger consolidation stresses, they may show different behaviors under different cyclic shear load amplitudes. When shear stresses (CSR) get larger, there is a drop, in resistance (soil gets more liquefiable) and when shear stresses (CSR) gets smaller, samples tend to get more resistant (less liquefiable) from a first to the second occurrence of liquefaction. Finally, it could be found about dense samples ($D_{rc}$ = 65%) that, although increasing resistance (especially in larger consolidation stresses) is observed in mono-directional load patterns, shear load magnitude dependent behavior of samples under bi-directional patterns is obvious. Similar to few results for medium dense samples mentioned above, almost majority of bi-directional pattern tests results for dense samples show the intersecting resistance trend in consecutive liquefaction occurrences, which increasing resistance when applied shear stresses get smaller, and decreasing resistance when applied shear stresses get larger, is a general behavior.

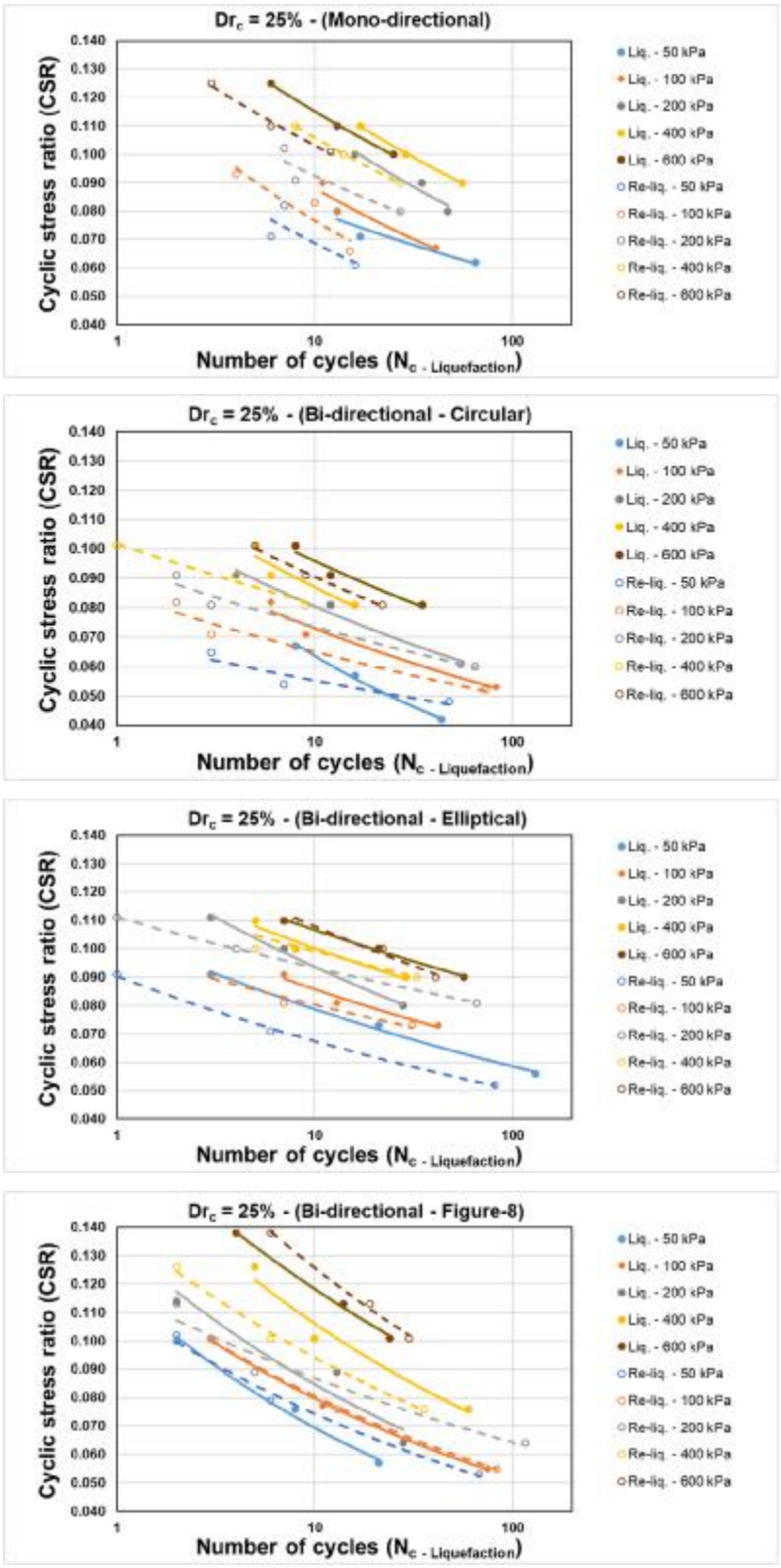


**Figure 4.8: Variable trend of (CSR) VS ($N_{CL}$) for loose samples ($D_{rc}$ = 25%)**

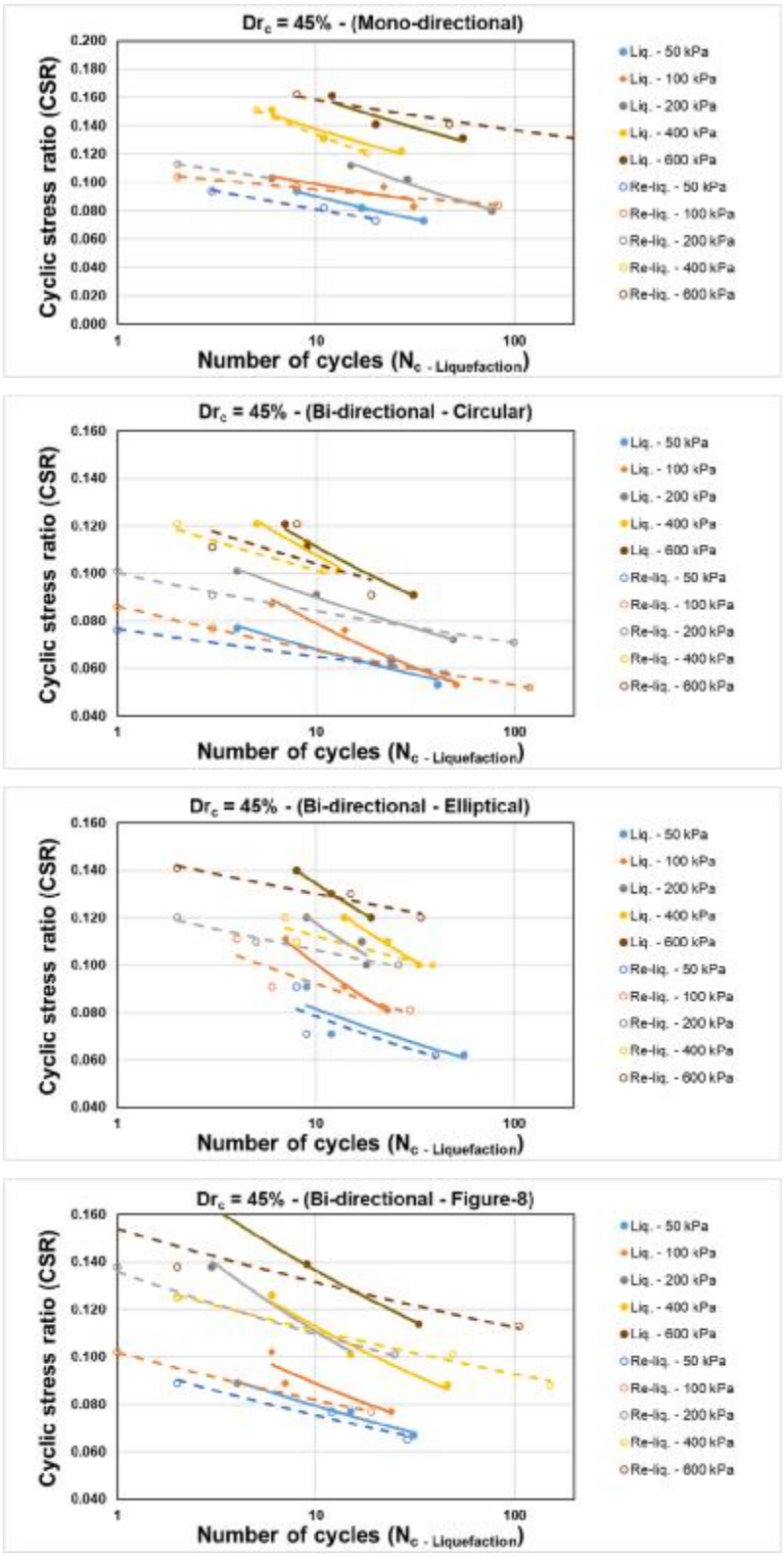


**Figure 4.9: Variable trend of (CSR) VS ($N_{CL}$) for medium dense samples ($D_{rc}$ = 45%)**

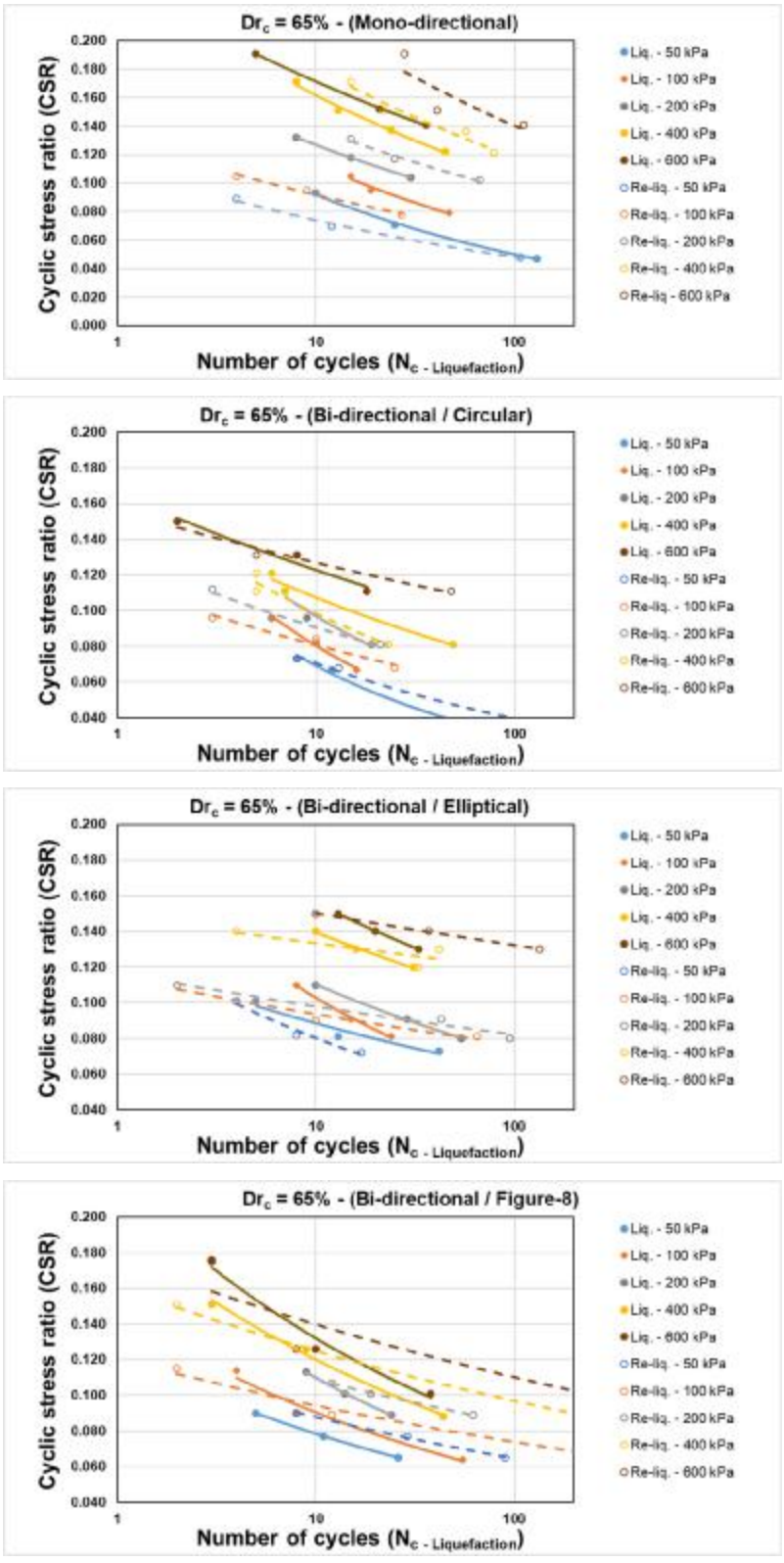


**Figure 4.10: Variable trend of (CSR) VS ($N_{CL}$) for dense samples ($D_{rc}$ = 65%)**

### 4.4.3. Pore water pressure generation pattern

Pore water pressure generation is considered the most influencing parameter of triggering a liquefaction and pattern and magnitude of generated pore water pressure is too different for various soil samples. Effect of relative density and consolidation stresses on pore water pressure ratio ($r_u$) changes in the occurrence of a re-liquefaction are investigated and compared to different cyclic load patterns. For a better comparison, test results for loose ($D_{rc}$ = 25%) and dense ($D_{rc}$ = 65%) samples are shown in plots of Figure 4.11. It is observed that $r_u$ develops more quickly during first cyclic loading compared to the second cyclic loading stage for almost entire cyclic load patterns and regardless of relative density changes. Also, as it is shown in the same figure, in a lower number of cycles corresponding to larger shear stresses, liquefaction, normally occurs in a lower pore water pressure ratio than re-liquefaction. This trend is inverse for the larger number of cycles (or smaller cyclic stresses). There is a boundary level of shear stress (and the number of cycles to liquefaction accordingly), which $r_u$ remains constant for both stages.

Another comparison is drawn for samples responses to a repeating liquefaction occurrence at different consolidation stresses and the results for two margins of $\sigma'_{vc}$= 50 kPa and $\sigma'_{vc}$= 600 kPa, is shown in Figure 4.12. Based on the results, development of pore water pressure ratio for two consecutive liquefaction follows a similar pattern in larger applied stresses ($\sigma'_{vc}$= 600 kPa), whereas in smaller applied stresses ($\sigma'_{vc}$= 50 kPa), faster development of pore water pressure in liquefaction and slower development in re-liquefaction is visible. Also, it is observed that a slightly larger generated pore water pressure in liquefaction, compared to re-liquefaction, is a general behavior of samples in this study at higher consolidation stress level of $\sigma'_{vc}$= 600 kPa with an exception to circular load pattern. In summary, stress levels play the most important role in pore water pressure generation pattern of Boler sand samples. Although there is a changing pattern in the response of samples when cyclic shear stress varies, any effect is limited to lower consolidation stress levels. In higher vertical effective stresses, soil samples respond more uniformly when they are under an extra liquefaction event.

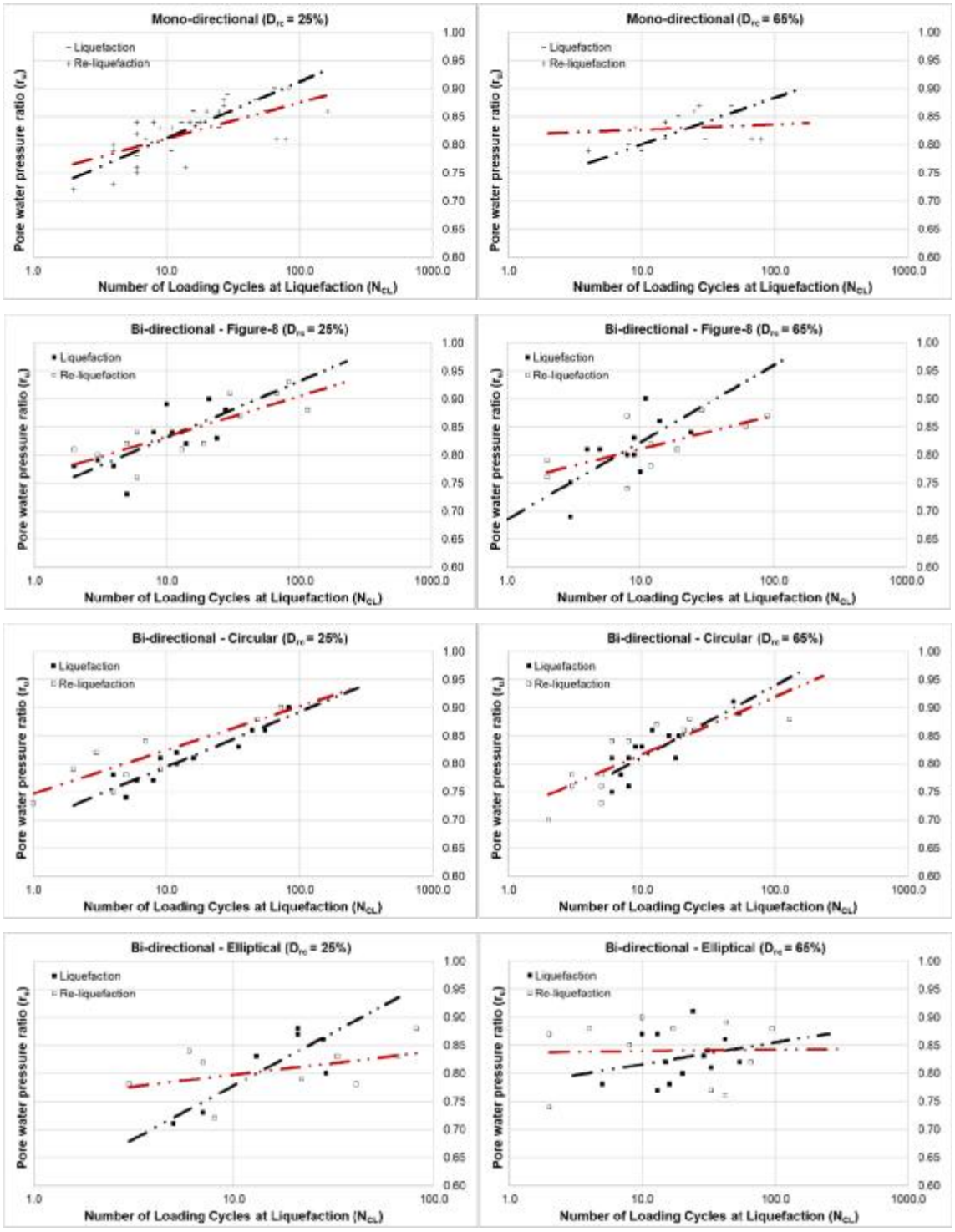


**Figure 4.11: Comparison of pore water pressure ratio ($r_u$) variation by relative density for two stages of liquefaction in different cyclic load patterns ($D_{rc}$ = 25% left column and $D_{rc}$ = 65% right column)**

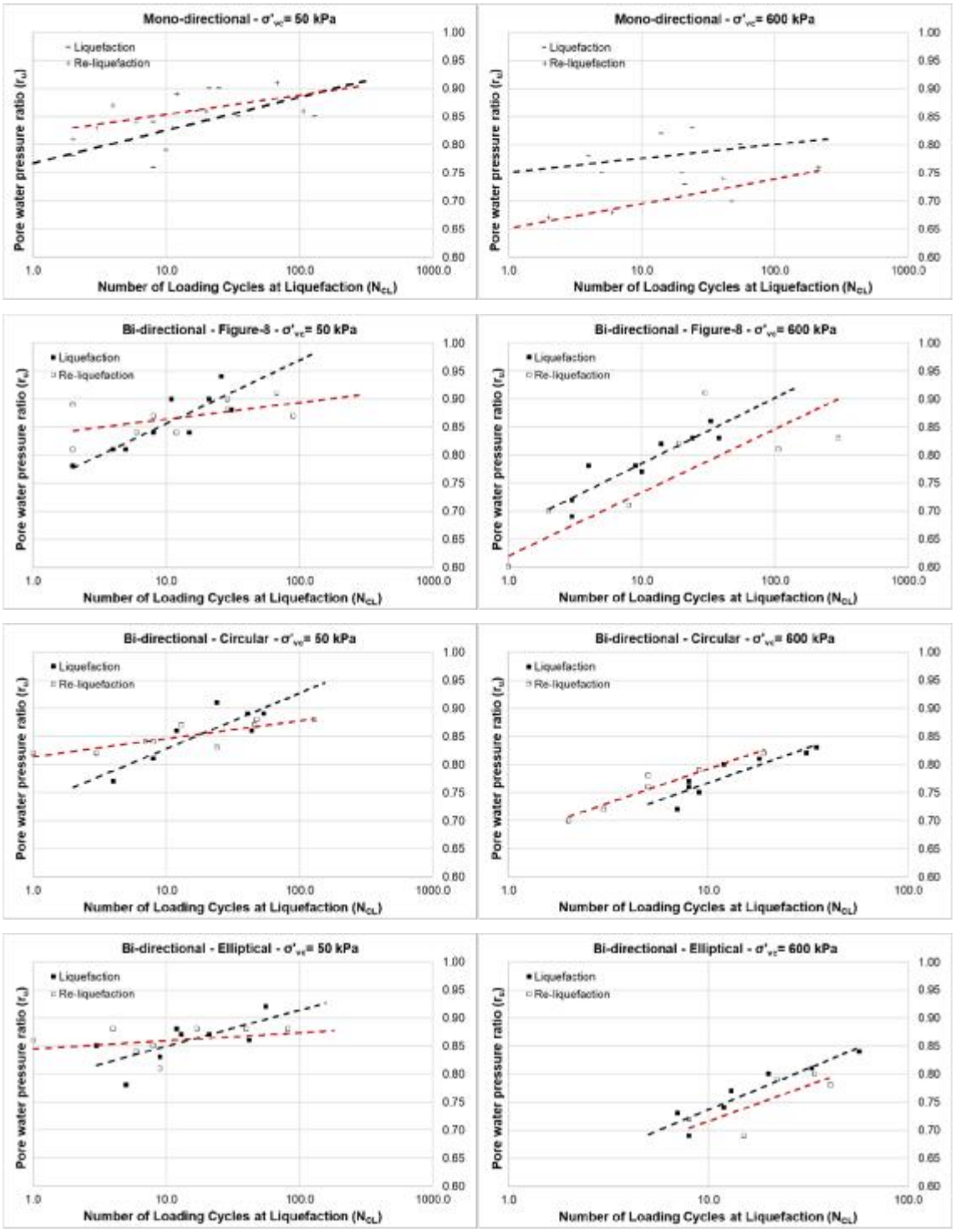


**Figure 4.12: Comparison of pore water pressure ratio ($r_u$) variation by consolidation stresses for two stages of liquefaction in different cyclic load patterns ($\sigma'_{vc}$= 50 kPa left column and 600 kPa right column)**

### 4.4.4. Cyclic resistance variation due to re-liquefaction

In few past studies, pre-shearing effects were investigated by assessing the effect of developed strain levels in the first stage of cyclic shearing, in resistance of a sample, after the second stage of cyclic loading. However, none of the studies focused on cyclic stress patterns and magnitudes in a repeating loading at similar developed strain levels. In the current study, a wide range of cyclic stresses was applied to multiple samples in two similar stages to investigate the occurrence of a repeated liquefaction. Cyclic resistance ratio (CRR) is used to evaluate and compare samples resistance to consecutive cyclic loads. The cyclic stress ratio (CSR) required for liquefaction occurrence in a specified number of loading cycles is called "Cyclic Resistance Ratio (CRR)". For an earthquake magnitude of 7.5, CRR is defined as the CSR to cause liquefaction in 15 uniform cycles of shear stress (Seed and Idriss, 1971). As an example, extracting CRR values for one test of this study is shown in Figure 4.13.

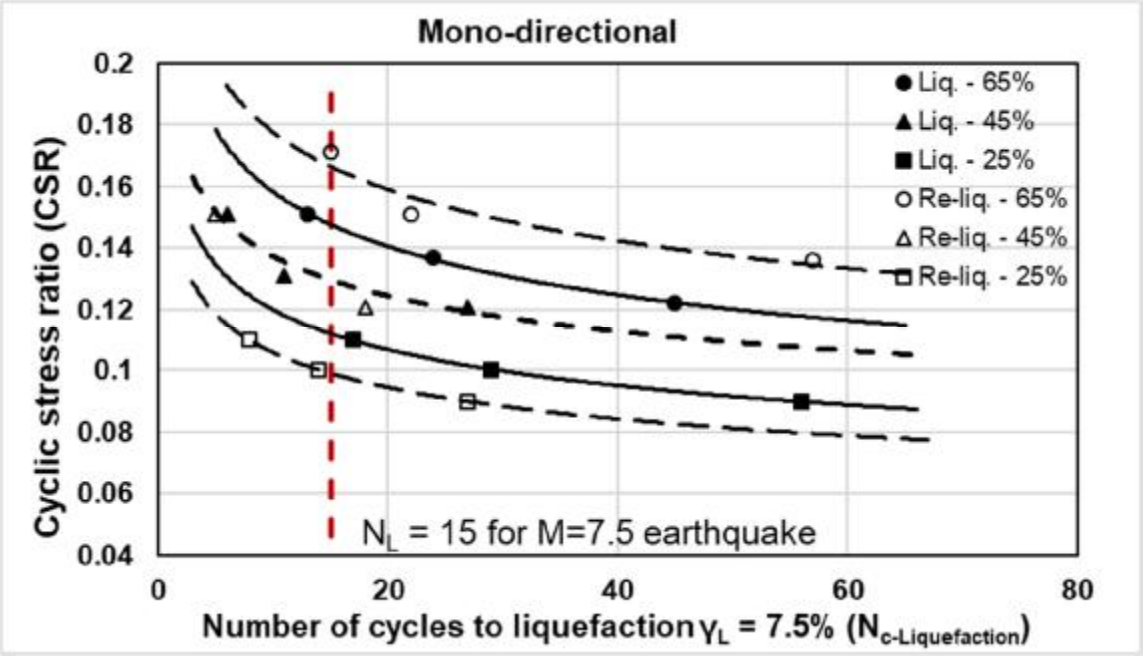


**Figure 4.13: Calculating CRR values for liquefaction and re-liquefaction of Boler sand in mono-directional cyclic tests at $\sigma'_{vc}$ = 400 kPa and in different relative densities**

In this example, variation of cyclic shear stress ratio (CSR) with the number of cycles for liquefaction and re-liquefaction of samples at $D_{rc}$ = 25%, 45%, 65% and in a vertical effective stress of $\sigma'_{vc}$ = 400 kPa are illustrated. As it is observed, and as a typical result of this study, change in the number of resisting cycles by variation of cyclic stresses (CSR), obeys the general, exponential function of $CSR = a.N^{-b}$ (which was discusses in previous chapters) for both liquefaction and re-liquefaction stages.

Also, it could be observed that, in equal number of cycles, resisting cyclic resistance (CRR) of mono-directional pattern loaded samples, increases for a denser sample ($D_{rc}$ = 65%), remains almost identical in medium dense sample ($D_{rc}$ = 45%), and drops in a loose sample ($D_{rc}$ = 25%) at this level of stress. Porcino et al. reported a very similar trend for Quiou sand samples tested under 40% and 75% of relative density. In the reported result, CRR value of tested specimens after re-liquefaction. Almost remains constant for $D_{rc}$=40% samples and increases significantly for $D_{rc}$=75% samples (Porcino et al. 2009). This phenomenon of lower CRR values for re-liquefaction events in loose sands relative to dense sands is also observed for a silica-based Ticino sand, in the studies of the same team (Porcino et al. 2009). This appears to be in agreement to the current study's findings on the effect of the relative density on increasing or decreasing of CRR for re-liquefaction events relative to first liquefaction events, for a wide range of consolidation stresses.

Majority of previous studies have focused specifically on the effect of the shear-strain history of a given soil and how much pre-shearing has occurred in each specimen (Ishihara & Okada 1982; Finn et al. 1970). Porcino et. al. (2009) studied the effects of both large (i.e. single amplitude shear strain value of 3.75%) and small (i.e. single amplitude shear strain value of 1.0 %) pre-shearing shear strains on CRR of succeeding liquefaction events. They found that small strain pre-shearing brings about hardening of both loose and dense samples. On the other hand, larger developed strains in the first cycle of loads could have a hardening effect on dense samples but conversely, softening effect on loose ones. Large strains can cause a decrease in repetitive liquefaction resistance of samples irrespective of the soil state. They also reported about different responses for different sands. In another research program at the University of Tokyo, S. Wahyudi, J. Koseki, and T. Sato (2014) studied the re-liquefaction behavior of sands with ring-shear tests. Their results, confirm the previous results found by the Italian team. They concluded that increasing density before a re-liquefaction occurrence is less important than the

pre-shearing history of the samples. Increasing resistance to small pre-shearing strains and decreasing resistance after large pre-shear strains were reported by them and co-related to soil structure and re-arrangement of soil particles. It should be considered that there are not enough reports on researchers which would cover a wide range of parameters including different levels of consolidation stresses. As discussed earlier, the behavior discussed mono-directional load patterns, is not a typical behavior for Boler sand. For a better comparison, calculated CRR values of multiple tests are correlated to their initial state parameters to find a numerical pattern between soil cyclic resistance and both its density and vertical effective stress at the same time (state of the soil). As illustrated in Figure 4.14 to 4.17, CRR changes for three different relative densities of are correlated to their initial state parameter. The initial state for re-liquefaction tests is after densification due to the first stage of liquefaction and re-consolidation. Exponential variation is found for individual curves and separated equations for liquefaction and re-liquefaction of samples in each relative density are introduced. This plots clearly show that initial state of a soil could be a better representative of cyclic resistance variation from one stage to the second stage of liquefaction. This is particularly important when both relative density and consolidation stresses affect the rate of resistance changes. Loading pattern and the shearing mode is shown to be another impacting factor.

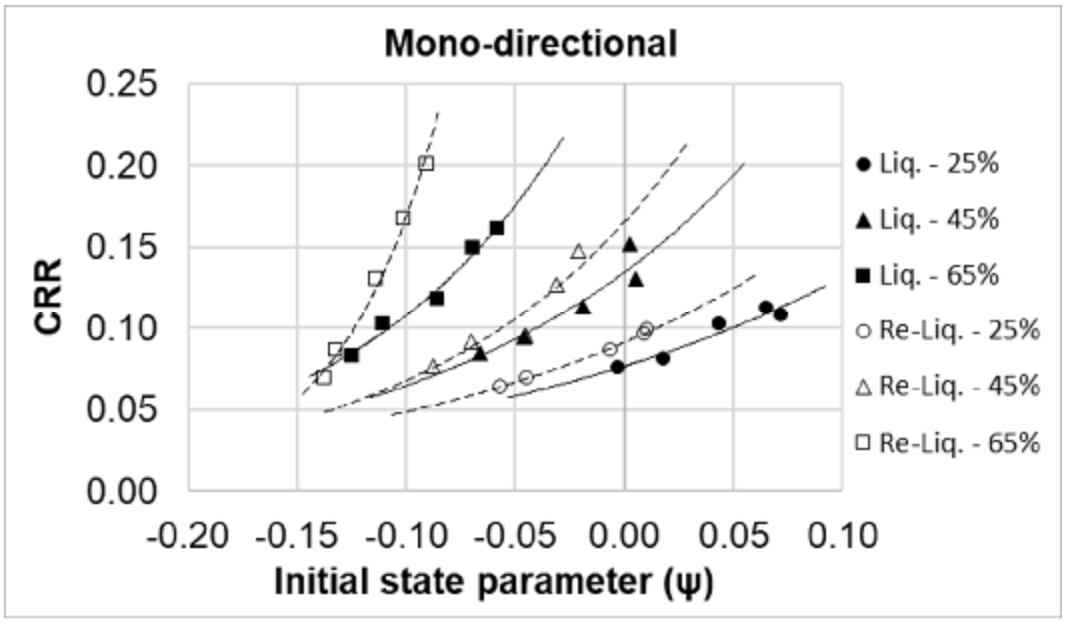


**Figure 4.14: CRR VS initial state parameter for mono-directional cyclic loads**

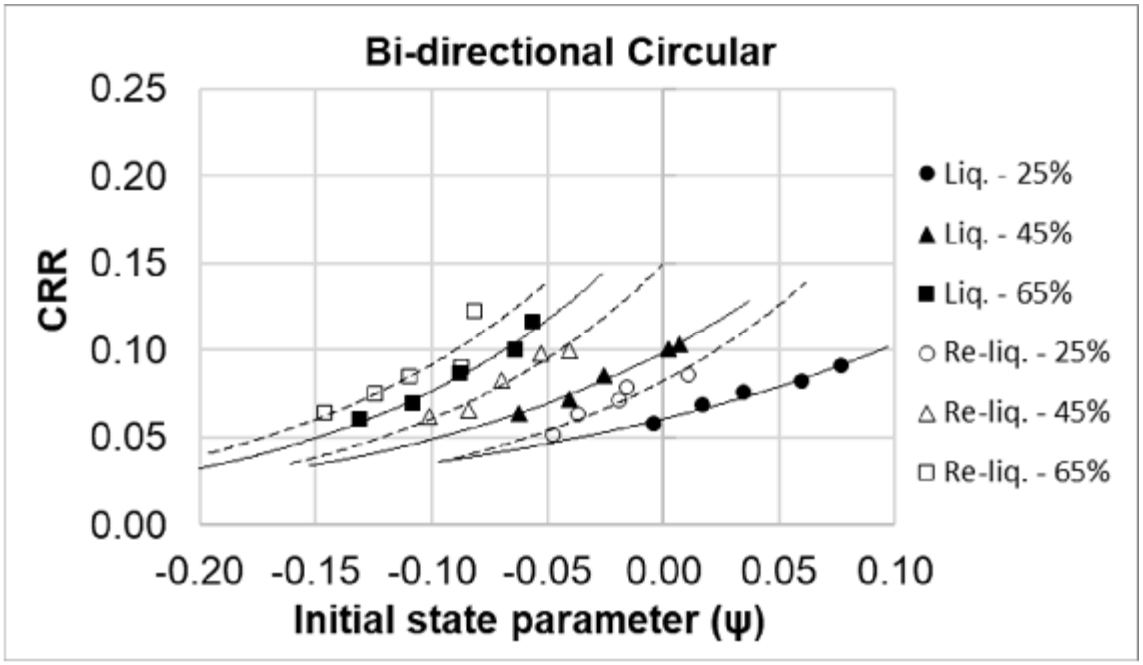


**Figure 4.15: CRR VS initial state parameter for bi-directional (circular) cyclic loads**

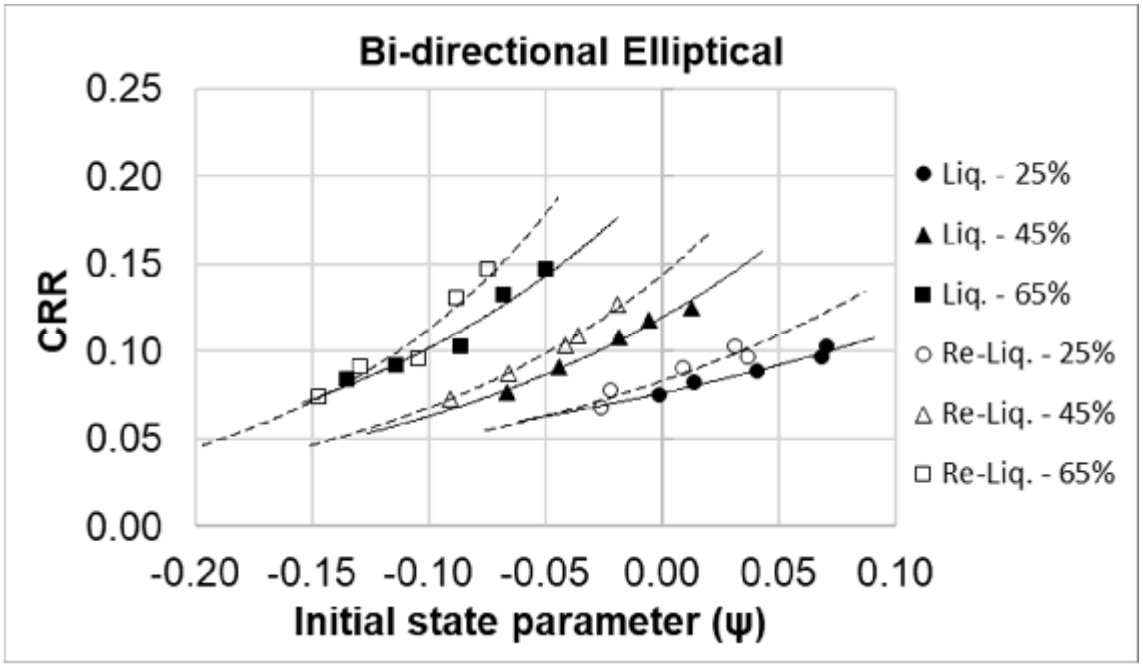


**Figure 4.16: CRR VS initial state parameter for bi-directional (elliptical) cyclic loads**

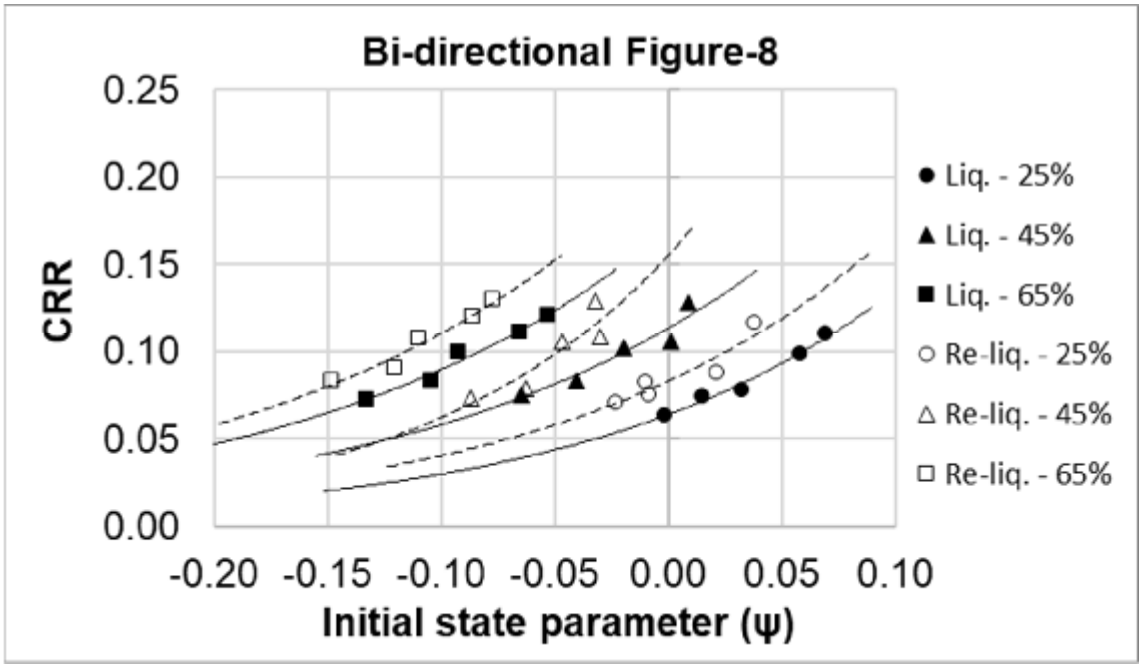


**Figure 4.17: CRR VS initial state parameter for bi-directional (figure-8) cyclic loads**

## 4.5. Conclusions

In this chapter, the liquefaction response of soil samples was investigated in two successive stages. The number of cycles to fulfill a liquefaction criterion of 3.75% cyclic shear strain and samples densification rates due to liquefaction were measured. Mono-directional and three different bi-directional cyclic patterns were applied to samples. It was found that specimens get denser when they are exposed to a cyclic liquefaction and then re-consolidated. They densify in a range between 6% for a dense sample (initial 65% relative density) to 14% for a loose specimen (initial 25% relative density).

Cyclic resistant of samples was assessed in consecutive liquefaction events. Results show a general decreasing resistance for loose samples, which is more significant for mono-directional load patterns rather than bi-directional patterns. The resistance changes of medium dense samples from first to a second liquefaction is negligible and almost consistent for all loading patterns. For dense samples, there is a distinction in the behaviour of samples under mono-directional shear patterns and bi-directional patterns. Although the majority of samples get more resistant in a second liquefaction under mono-directional loads, a more complicated

behavior is observed for dense samples as well as medium dense samples in large consolidation stresses, under bi-directional cyclic loads. It was found that when applied shear loads get larger, the resistance of the samples decreases (becomes more liquefiable); inversely, when shear loads get smaller, the behavior changes to a decreasing resistance and less liquefiable response. Pore pressure generation pattern of the samples was investigated. Unlike relative density changes, stress levels play the most important role in pore water pressure generation pattern of Boler sand samples. Quicker pore water pressure generation in the first liquefaction occurrence was a general behavior, regardless of load pattern and relative density, but confining stress dependent.

Finally, the cyclic resistance of the samples was numerically evaluated in repeating stages of liquefaction. Separate exponential correlations were found for liquefaction and re-liquefaction of samples in different relative densities, between cyclic resistance ratio (CRR) and initial state parameter (Ψ) of samples.

## 4.6. References

Airey, D. W. & Wood, D. M., 1986. "Pore pressures in simple shear. Soils and Foundations, 26(2), pp. 91-96.

A.M. Kammerer, J. M. Pestana, R. B. Seed. (2002). The undrained response of Monterey 0/30 sand under multidirectional simple shear loading conditions. Department of civil and environmental engineering, University of California.

Abouzar Sadrekarimi. (2013). "Influence of state and compressibility on the liquefied strength of sands." Canadian Geotechnical Engineering Journal. 50: 1-10.

Annie Kammerer, Jiaer Wu, Michael Reimer, Juan Pestana and Raymond Seed. (2004). “Shear strain development in liquefiable soil under bi-directional loading conditions. 13th World Conference on Earthquake Engineering Vancouver, B.C., Canada. August 1-6, 2004 Paper No. 2081.

Arango I. (1996). ”Magnitude scaling factors for soil liquefaction evaluations”. J. Geotechnical Eng. ASCE 122(11), 929–36, 1996.

Boulanger, R. W., Seed, R. B., Chan, C. K., Seed, H. B., and Sousa, J. B., (1991). “Liquefaction Behavior of Saturated Sands under Uni-Directional and Bi-Directional Monotonic and Cyclic

Simple Shear Loading". Geotechnical Engineering Report No. UCB/GT/91-08, University of California, Berkeley, August.

Boulanger, R. W., and Truman, S. P. (1996). "Void redistribution in the sand under post-earthquake loading". Canadian Geotechnical J.33, 829–34.

Byrne, P.M., and Beaty, M.H. (1997). "Post-liquefaction shear strength of granular soils: theoretical/conceptual issues, in Proceedings". Workshop on Post-Liquefaction Shear Strength of Granular Soils, Urbana-Champaign, IL, April 17–18, pp. 16–45.

Casagrande, A., (1976). "Liquefaction and Cyclic Deformation of Sands–a Critical Review" Harvard Soil Mechanics Series No. 88, Harvard University, Cambridge, MA.

Castro, G. (1969). "Liquefaction of sands." Ph.D., Harvard University, Cambridge, Massachusetts.

Castro, G., (1975). Liquefaction and cyclic mobility of saturated sands, J. Geotechnical Eng. Div., ASCE 101(GT6), 551–69.

Castro, G., and Poulos, S. J. (1977). Factors affecting liquefaction and cyclic mobility, J. Geotechnical Eng. Div., ASCE 103(GT6), 501–06.

Dharma Wijewickereme, Maria Sanin. (2004). "Cyclic shear loading response of Frase Delta silt". 13th World Conference on Earthquake Engineering Vancouver, B.C., Canada August 1-6, 2004 Paper No. 499.

Dharma Wijewickreme, Somasundaram Sriskandakumar, and Peter Byrne. (2005). "Cyclic loading response of loose air-pluviated Fraser River sand for validation of numerical models simulating centrifuge tests". Can. Geotech. J. 42: 550–561.

Dyvik, R., Berre, T., Lacasse, S., and Raadim, B. (1987). "Comparison of truly undrained and constant volume direct simple shear tests." Geotechnique, 37(1), 3 - 10.

Drnevich, V. P., 1972. "Undrained cyclic shear of saturated sand". Journal of the Soil Mechanics and Foundations Division, 98(8), pp. 807-825.

Finn, W. D. L., Bransby, P. L. & Pickering, D. J., 1970. "Effect of strain history on liquefaction of sand". Journal of the Soil Mechanics and Foundations Division, 96(6), pp. 1917-1934.

Goughari, M. S., 2012. M.ASc Thesis - "Effect of initial shear stress direction and stress history on the undrained behavior of sands under triaxial loading", Ottawa: Carleton University.

Green, R. A., and Terri, G. A.. (2005). The number of equivalent cycles concept for liquefaction evaluations—revisited. J. Geotechnical and Geoenvironmental Eng., ASCE 131(4), 477–88.

Hynes, M. E., and Olsen, R. (1998). “Influence of confining stress on liquefaction resistance, in Proceedings”. International Symposium on the Physics and Mechanics of Liquefaction, Balkema, Rotterdam. pp. 145–52.

Idriss, I. M., 1999. "An update to the Seed-Idriss simplified procedure for evaluating liquefaction potential". Washington D.C., Proceedings of Workshop on New Approaches to Liquefaction, Federal Highway Administration.

Ishihara, K. (1993). "Liquefaction and flow failure during earthquakes." Geotechnique, 43(3), 351 - 415.

Ishihara, K. & Okada, S., 1982. "Effect of large preshearing on cyclic behavior of sand". Soils and Foundations, 22(3), pp. 109-125.

J. Montgomery, R.W. Boulanger and L.F. Harder. JR. (2012). "Examination of overburden correction factor on liquefaction resistance." Department of civil and environmental engineering, University of California.

Jefferies, M. G., and Been, K. (2006). “Soil liquefaction - a critical state approach”, Taylor & Francis, New York.

Kenji Ishihara and Fumio Yamazaki. (1980). "Cyclic simple shear tests on the saturated sand in multi-directional loading." Soils and foundations. Vol. 20 No. 1.

Ladd, R. S. (1978). "Preparing test specimen using undercompacton." Geotechnical Testing Journal, ASTM, 1(1), 16 - 23.

Mike Jefferies and Ken Been. (2016). "Soil liquefaction, a critical state approach." Taylor and Francis Group LLC.

Peacock, W. H. & Seed, H. B., 1968. "Sand liquefaction under cyclic loading simple shear conditions". Journal of the Soil Mechanics and Foundations Division, 94(SM3), pp. 689-708.

Porcino, D., Marciano, V. & Ghionna, V. N., 2009. "Influence of cyclic pre-shearing on the undrained behavior of carbonate sand in simple shear tests". Geomechanics and Geoengineering: An International Journal, 4(2), pp. 151-161.

Seed, H. B., Arango, I. & Chan, C. K., 1976. "Evaluation of soil liquefaction potential for level ground during earthquakes: A summary report", Washington D.C.: U.S. Nuclear Regulatory Commission.

Seed, H. B. & Idriss, I. M., 1971. "Simplified procedure for evaluating soil liquefaction potential". Journal of Geotechnical Engineering, 97(9), pp. 1249-1273.

Seed, H. B. & Idriss, I. M., 1982. "Ground motions and soil liquefaction during earthquakes", Earthquake Engineering Research Institute: Oakland.

Seed, H. B., Idriss, I. M., Makdisi, F. I. & Banerjee, N. G., 1975. "Representation of irregular stress time histories by equivalent uniform stress series in liquefaction analysis", Berkeley: Earthquake Engineering Research Center.

Seed, H. B., Mori, K. & Chan, C. K., 1977. "Influence of seismic history on liquefaction of sands". Journal of Geotechnical Engineering, 103(4), pp. 257-270.

Seed, R. B. & Harder, L. F., 1990. "SPT-based analysis of cyclic pore pressure generation and undrained residual strength". Berkeley, Proceedings of the Memorial Symposium of H. B. Seed.

Sriskandakumar, S., Wijewickreme, D. & Byrne, P. M., 2012. "Multiple cyclic loading responses of loose air-pluviated Fraser River sand". Lisbon, Proceedings of the World Conference on Earthquake Engineering.

Vaid, Y. P., and Sivathayalan, S. (1996). "Static and cyclic liquefaction potential of Fraser River delta sand in simple shear and triaxial tests." Canadian Geotechnical Journal, 33(2), 281-289.

Wahyudi, S., Koseki, J. & Sato, T., 2014. "Characteristics of the re-liquified behavior of sand by means of image analysis and stacked-rings shear apparatus", University of Tokyo: Bulletin of Earthquake Resistant Structure Research Center.

Yamada, S., Tomoko, T. & Sato, K., 2010. "Effects on reliquefaction resistance produced by changes in anisotropy during liquefaction". Soils and Foundations, 50(1), pp. 9-25.

Yamamoto, T. et al., 2000. "Reliquefaction potential of cement-treated sandy soils". Auckland, Proceedings of the World Conference on Earthquake Engineering.

Yoshimi, Y., 1967. "An experimental study of the liquefaction of saturated sands. Soils and Foundations", 7(2), pp. 20-32.

# Chapter 5

## 5. Summary and conclusions

Numerous studies have been carried out on the dynamic behavior of sands. However, few studies have investigated the dynamic characteristics of silica-carbonate sands. This study presents series of laboratory simple shear tests on specimens of a local carbonate sand from London (ON). Besides monotonic and cyclic shearing, the dynamic behavior of the sand was also characterized by measuring the velocity of shear waves traveling through the specimens. Drained and undrained shearing behavior of specimens with a wide range of relative density and consolidation stresses were tested. Maximum shear modulus ($G_{max}$) was also computed from the shear wave velocity measurements and a correlation developed between $G_{max}$, effective stress, and void ratio for a carbonate sand.

The critical state line of the carbonate sand established from the simple shear tests was used for determining the state parameter of each specimen and this is related to the shear wave velocity measured in the same specimen. Such a relationship can be employed for measuring the in-situ state of this silica-carbonate sand. Cyclic resistances of the sand specimens were determined from cyclic shear tests.

Circular, elliptical (oval) and figure-8 bi-directional patterns were applied in addition to mono-directional cyclic shearing modes and cyclic resistance of loose (25% relative density), medium dense (45% relative density) and dense samples (65% relative density) are investigated. Changing pattern of pore water pressure ratio ($r_u$) values were assessed based on cyclic resistance (CSR) of multiple tests and number of cycles prior to liquefaction. Also, the test results showed up to 35% reduction in cyclic resistance of bi-directionally loaded samples relative to mono-directionally loaded ones.

Critical state analysis was developed equations were proposed for estimating the cyclic resistance of sand samples based on their initial state and correlated to their shear wave velocity ($V_s$) measured values as well. Samples were subjected to two consecutive cyclic loads and liquefaction behavior of the samples was examined and compared following both cyclic loads. Four different cyclic load patterns were applied to investigate load pattern effects on soil

response. Re-liquefaction were simulated by unloading the specimens after the first cyclic load and re-consolidating the specimen under the same initial vertical effective stress. A similar cyclic load was then re-applied on the sand specimen. The results showed a moderate increase in relative density after re-consolidation, which is greater for loose sand specimens. The summary of conclusions is listed below:

- Power functions were used to fit $V_S$ and $G_{max}$ data with effective vertical stress with exponents of 0.25 and 0.50, respectively.
- Linear functions were used to describe the effect of void ratio on $V_S$ and $G_{max}$.
- The critical state line of Boler sand, determined from the monotonic shear tests, was found to be similar to those of some other clean sands.
- Separate relationships were found between state parameter ($\Psi$) and shear wave velocity ($V_S$) at different relative densities.
- Correlating cyclic resistance ratio to shear wave velocity parameters of samples, it was found that the current liquefaction triggering method could overestimate the liquefaction resistance of Boler sand, leading to unsafe liquefaction analysis.
- Slow-degrading modulus reduction and lower damping ratio cluster of curves were observed for the Boler sand samples comparing to previously proposed band limits, which was highly affected by consolidation effective stress of samples.
- Power functions were developed and compared to various cyclic load patterns, including mono-directional and bi-directional modes.
- Overburden correction factor ($K_\sigma$) of tests increases with increasing confining stresses.
- The cyclic test results exhibit a reduction (0.67 to 1.03) in cyclic resistance of samples under bi-directional cyclic loads in comparison to similar samples under mono-directional cyclic loads.
- Reduction factors to compensate bi-directional to mono-directional cyclic load, increase with increasing confining stresses and are different for various cyclic load patterns.
- It was found that pore water pressure ratio in the current study never reaches to 100% in occurring a liquefaction and ranges between 0.7 to 0.9 for multiple tests. This value decreases with the cyclic shear addition which corresponds to a lower number of cycles.
- Exponential correlations were introduced between soil state and shear wave velocity values and also the cyclic resistance of the soil in liquefaction based on critical state analysis.

- Liquefaction susceptibility analysis of the results shows that current practice could overestimate soil resistance to cyclic loads by shear wave velocity measurements.
- It was found that specimens get denser when they are exposed to a cyclic liquefaction and then re-consolidated to a similar stress level. They densify in a range between 6% for a dense sample (initial 65% relative density) to 14% for a loose specimen (initial 25% relative density).
- Pore water pressure development is quicker for a first liquefaction occurrence compared to a second similar liquefaction event on same sample.
- Pore water pressure generation pattern is vertical effective stress dependant but regardless of relative density changes.
- Comparing the response of the samples under two stages of liquefaction occurrence, results show a general decreasing resistance for loose samples, which is more significant for mono-directional load patterns rather than bi-directional patterns.
- The resistance change of medium dense samples from first to a second liquefaction is negligible and almost consistent for all loading patterns.
- For dense samples, there is a distinction in the behaviour of samples under mono-directional shear patterns and bi-directional patterns.
- It was found that when applied shear loads get larger, the resistance of the samples decreases (becomes more liquefiable); inversely, when shear loads get smaller, the behavior changes to a decreasing resistance and less liquefiable response.
- Exponential correlations were found for liquefaction and re-liquefaction of samples in different relative densities, between cyclic resistance ratio (CRR) and initial state parameter ($\Psi$) of samples.

# Appendices

# Appendix 1

Mono-directional Cyclic Simple Shear Test Results

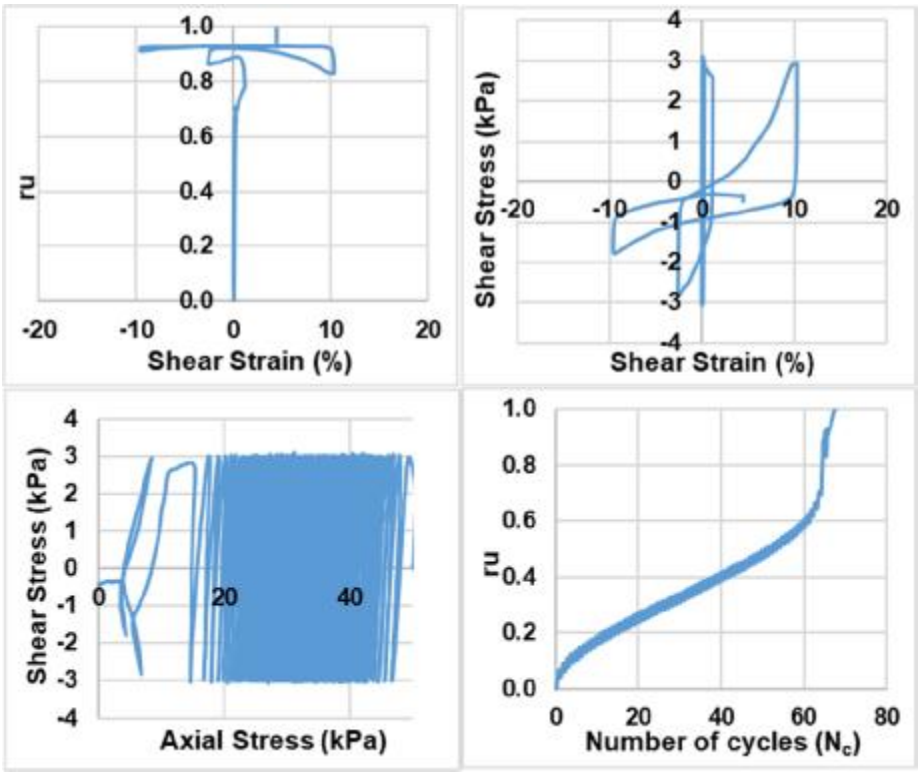


Monodirectional; $D_{rc}$ = 25%; $\sigma'_{vc}$ = 50 kPa; CSR = 0.06 (Liquefaction)

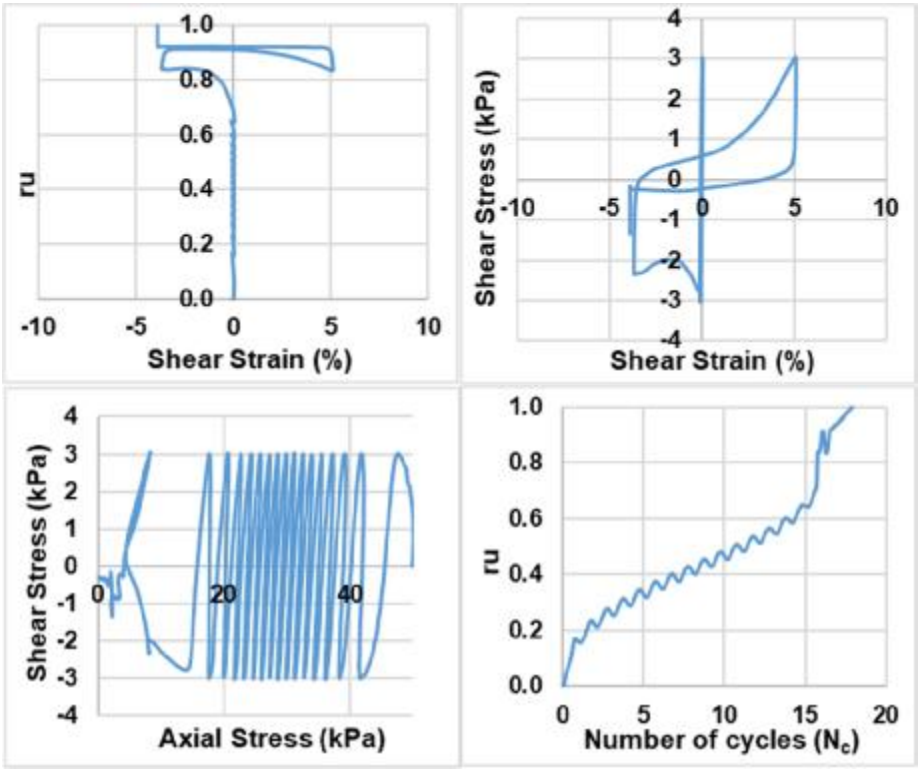


Monodirectional; $D_{rc}$ = 25%; $\sigma'_{vc}$ = 50 kPa; CSR = 0.06 (Re-liquefaction)

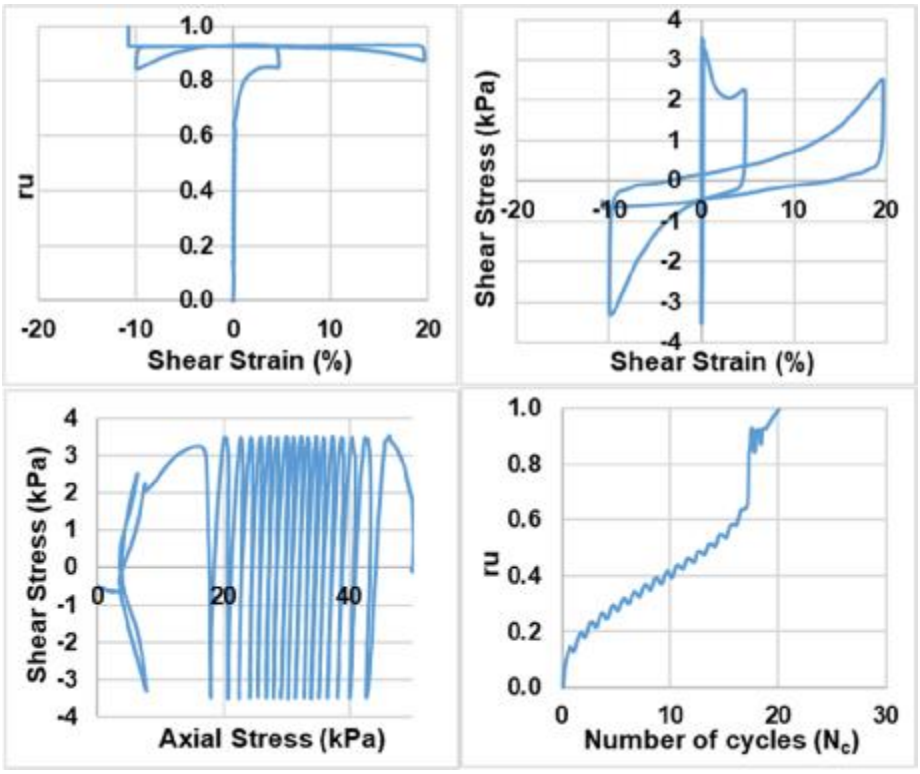


Monodirectional; $D_{rc}$ = 25%; $\sigma'_{vc}$ = 50 kPa; CSR = 0.07 (Liquefaction)

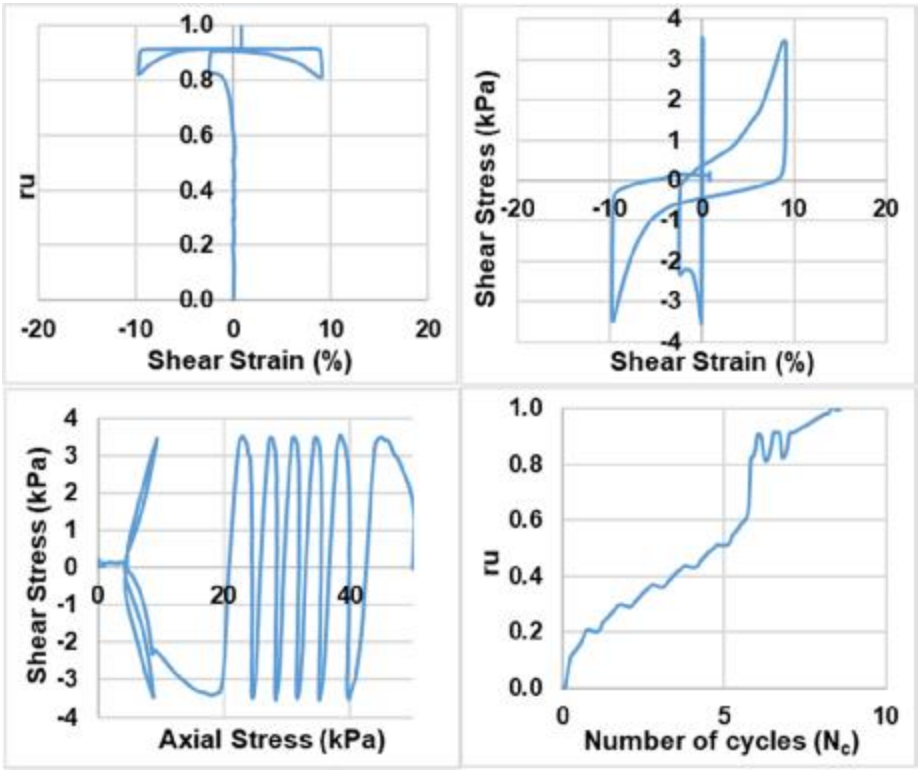


Monodirectional; $D_{rc}$ = 25%; $\sigma'_{vc}$ = 50 kPa; CSR = 0.07 (Re-liquefaction)

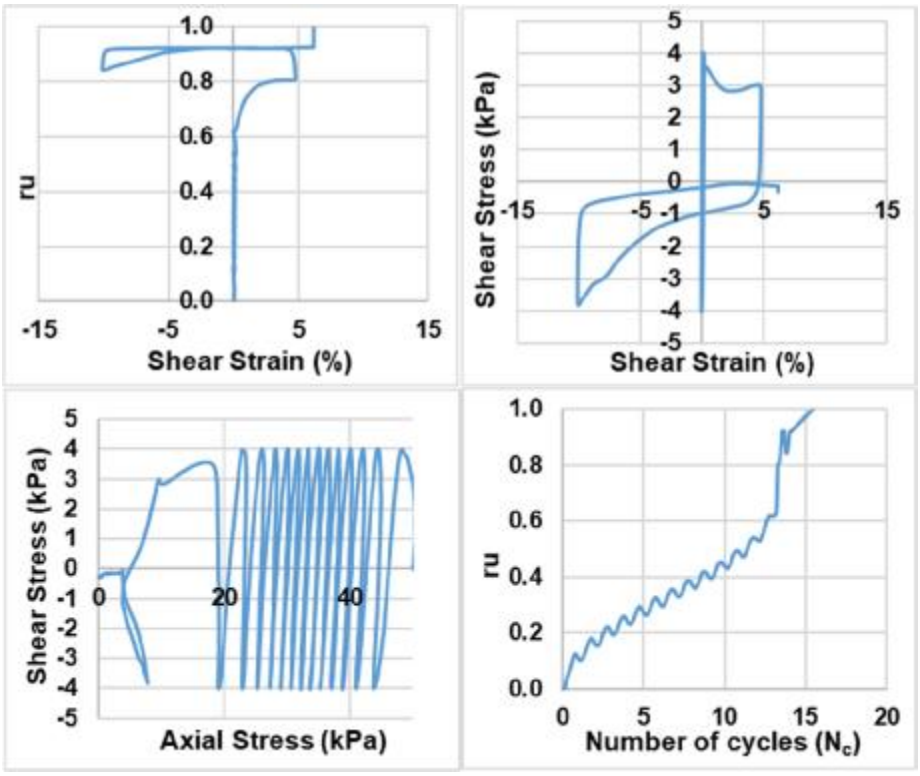


Monodirectional; $D_{rc}$ = 25%; $\sigma'_{vc}$ = 50 kPa; CSR = 0.08 (Liquefaction)

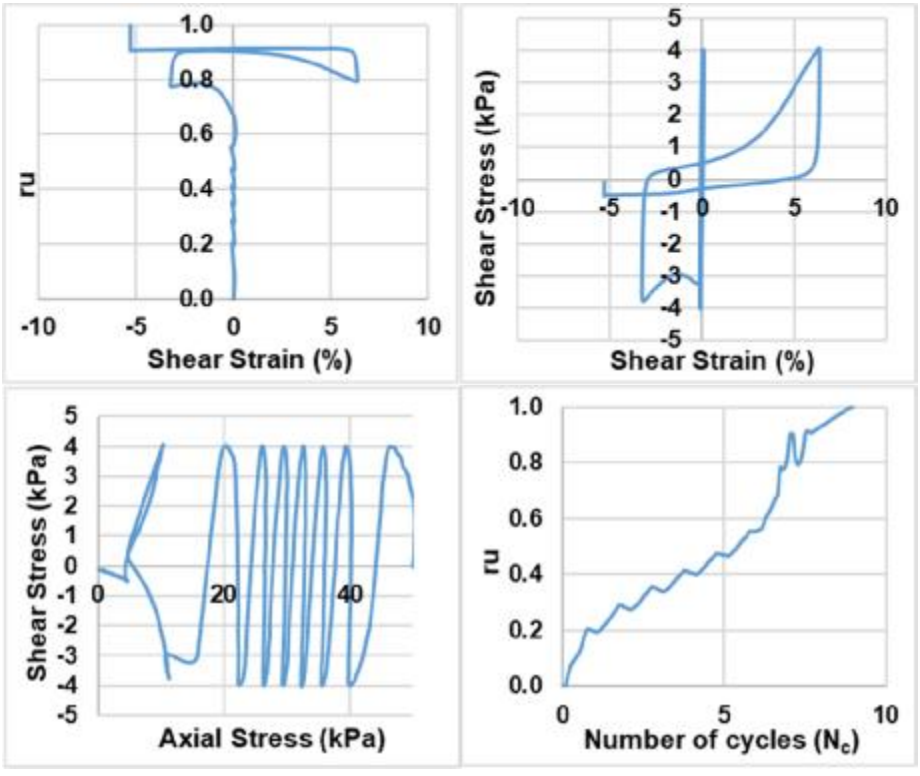


Monodirectional; $D_{rc}$ = 25%; $\sigma'_{vc}$ = 50 kPa; CSR = 0.08 (Re-liquefaction)

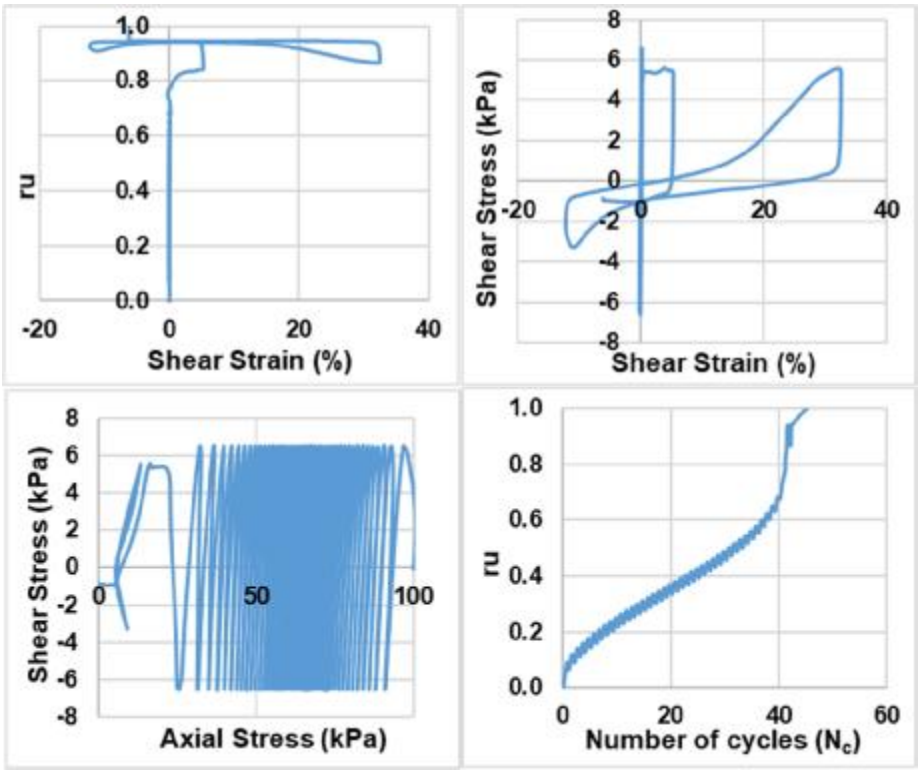


Monodirectional; $D_{rc}$ = 25%; $\sigma'_{vc}$ = 100 kPa; CSR = 0.07 (Liquefaction)

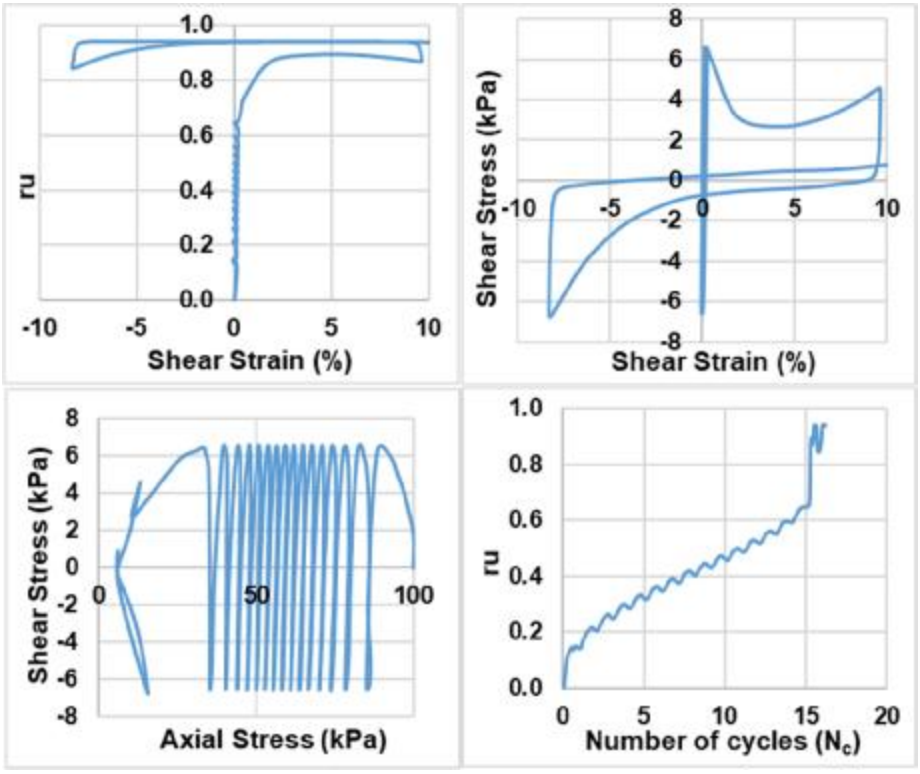


Monodirectional; $D_{rc}$ = 25%; $\sigma'_{vc}$ = 100 kPa; CSR = 0.07 (Re-liquefaction)

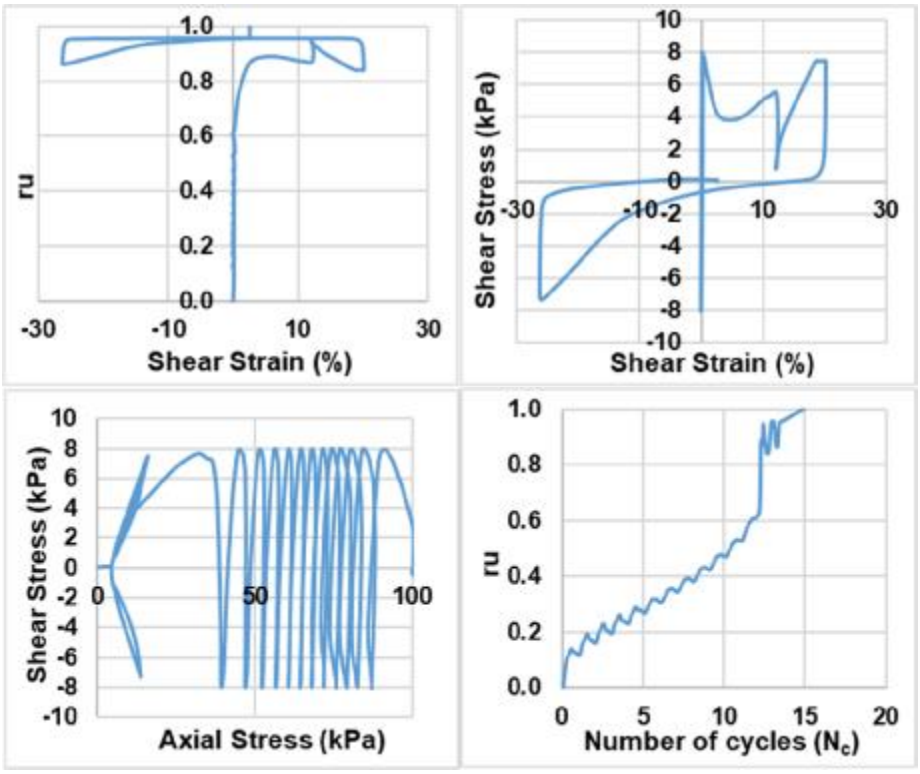


Monodirectional; $D_{rc}$ = 25%; $\sigma'_{vc}$ = 100 kPa; CSR = 0.08 (Liquefaction)

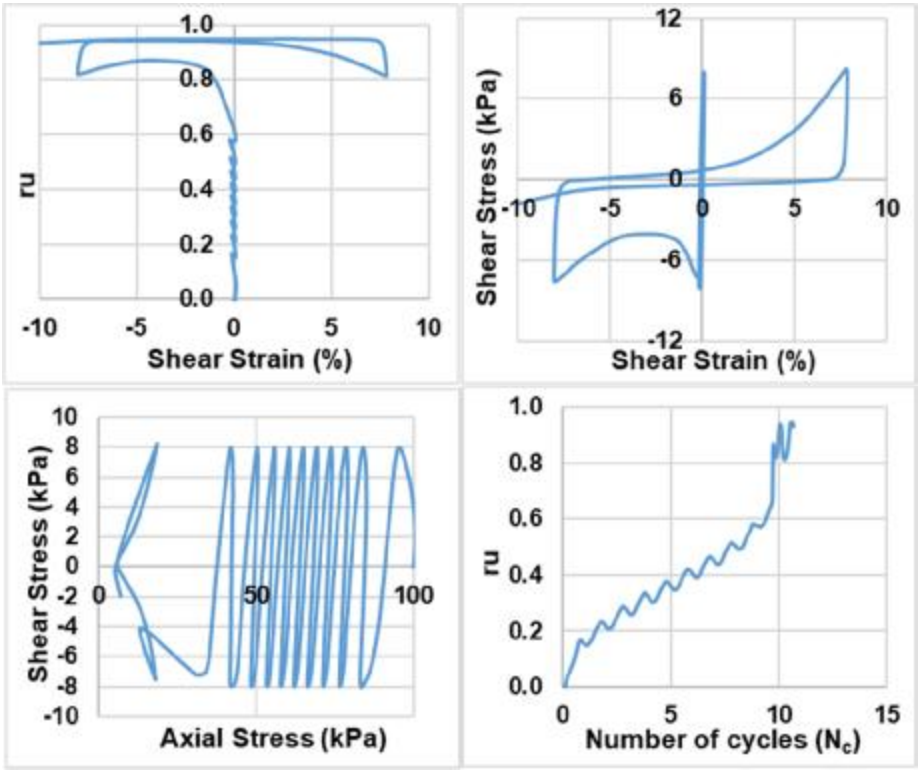


Monodirectional; $D_{rc}$ = 25%; $\sigma'_{vc}$ = 100 kPa; CSR = 0.08 (Re-liquefaction)

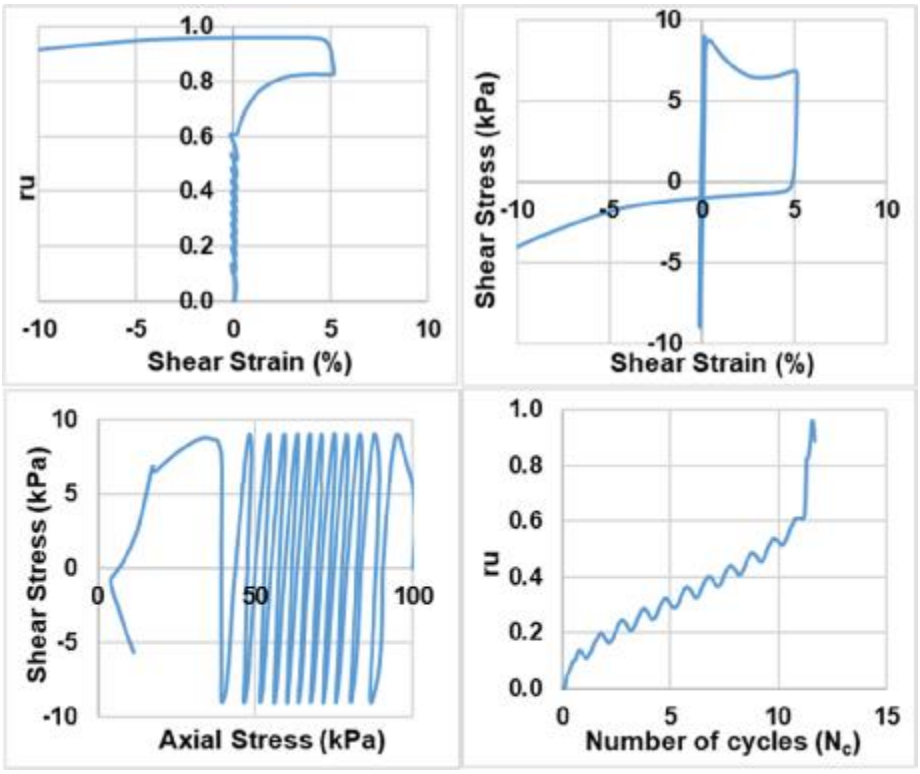


Monodirectional; $D_{rc}$ = 25%; $\sigma'_{vc}$ = 100 kPa; CSR = 0.09 (Liquefaction)

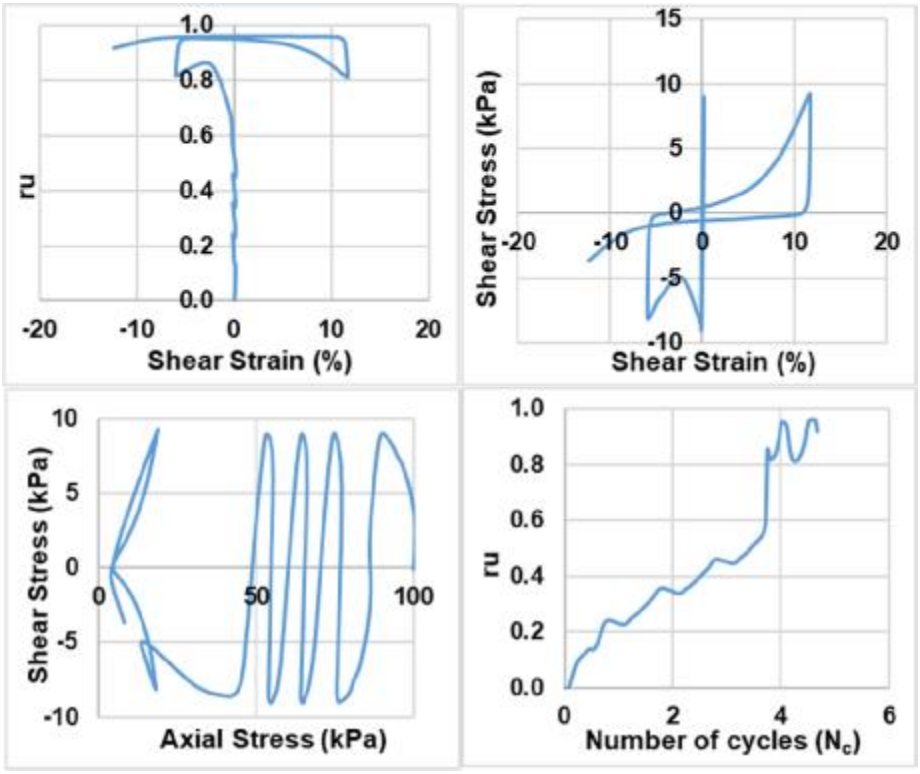


Monodirectional; $D_{rc}$ = 25%; $\sigma'_{vc}$ = 100 kPa; CSR = 0.09 (Re-liquefaction)

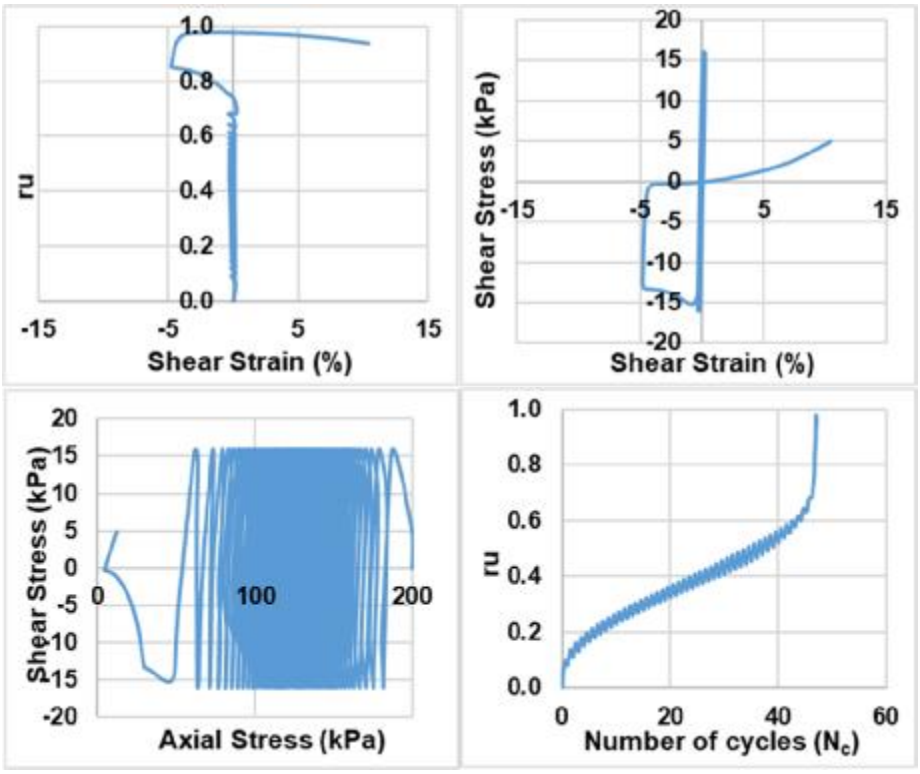


Monodirectional; $D_{rc}$ = 25%; $\sigma'_{vc}$ = 200 kPa; CSR = 0.08 (Liquefaction)

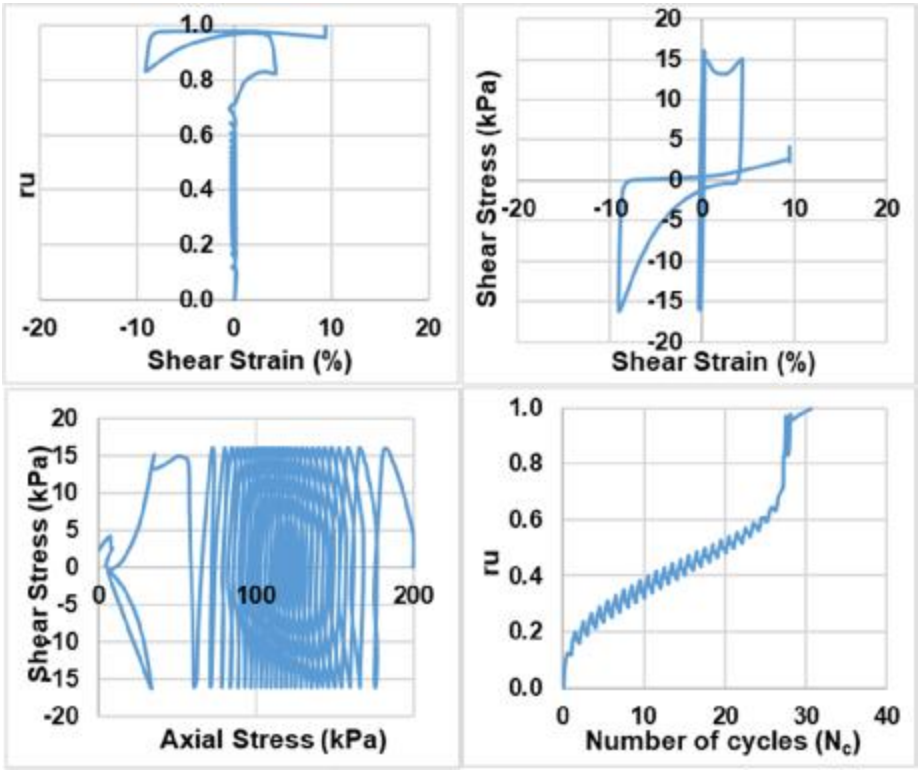


Monodirectional; $D_{rc}$ = 25%; $\sigma'_{vc}$ = 200 kPa; CSR = 0.08 (Re-liquefaction)

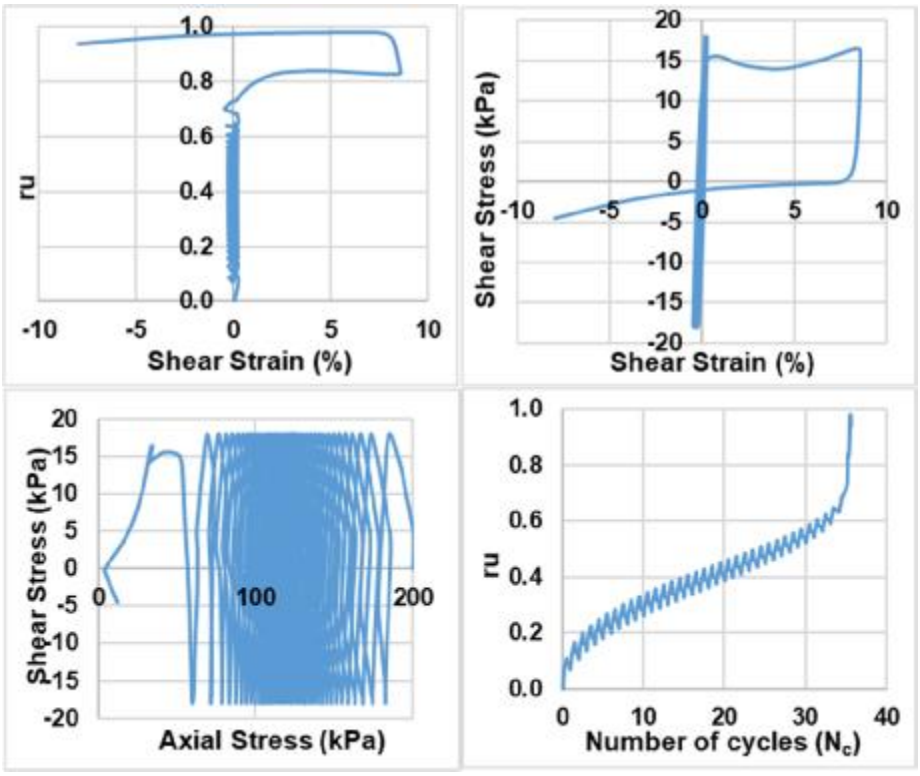


Monodirectional; $D_{rc}$ = 25%; $\sigma'_{vc}$ = 200 kPa; CSR = 0.09 (Liquefaction)

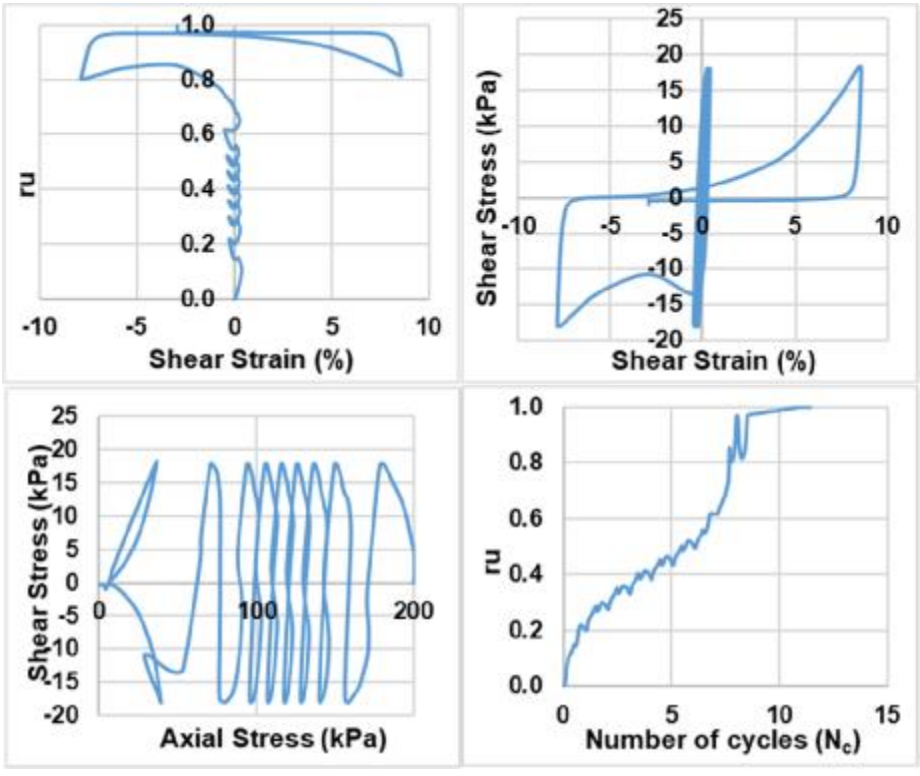


Monodirectional; $D_{rc}$ = 25%; $\sigma'_{vc}$ = 200 kPa; CSR = 0.09 (Re-liquefaction)

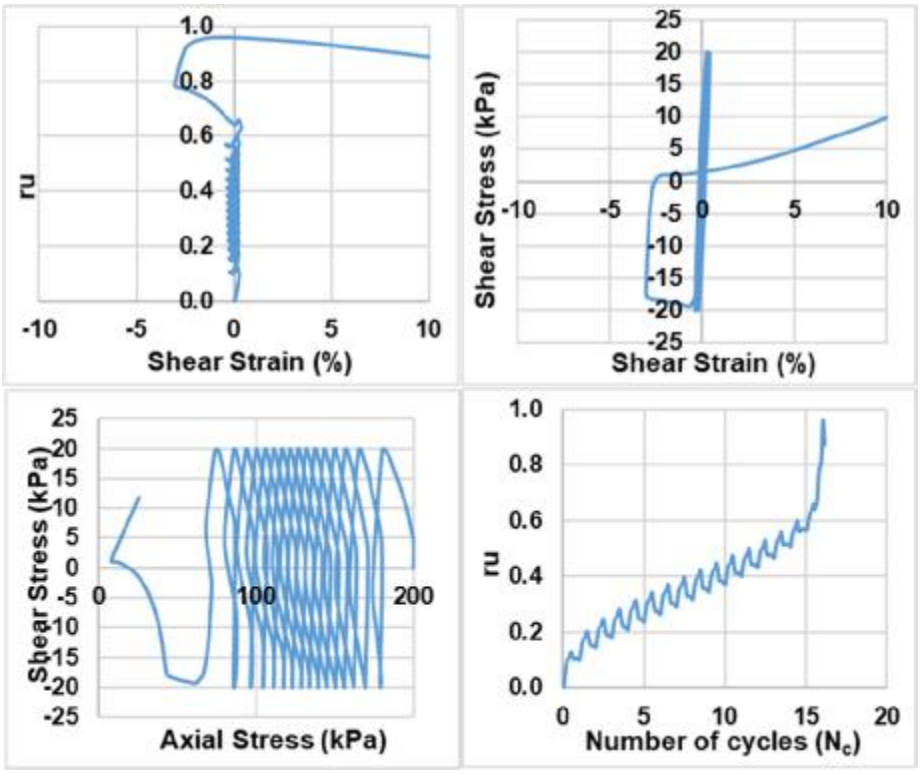


Monodirectional; $D_{rc}$ = 25%; $\sigma'_{vc}$ = 200 kPa; CSR = 0.1 (Liquefaction)

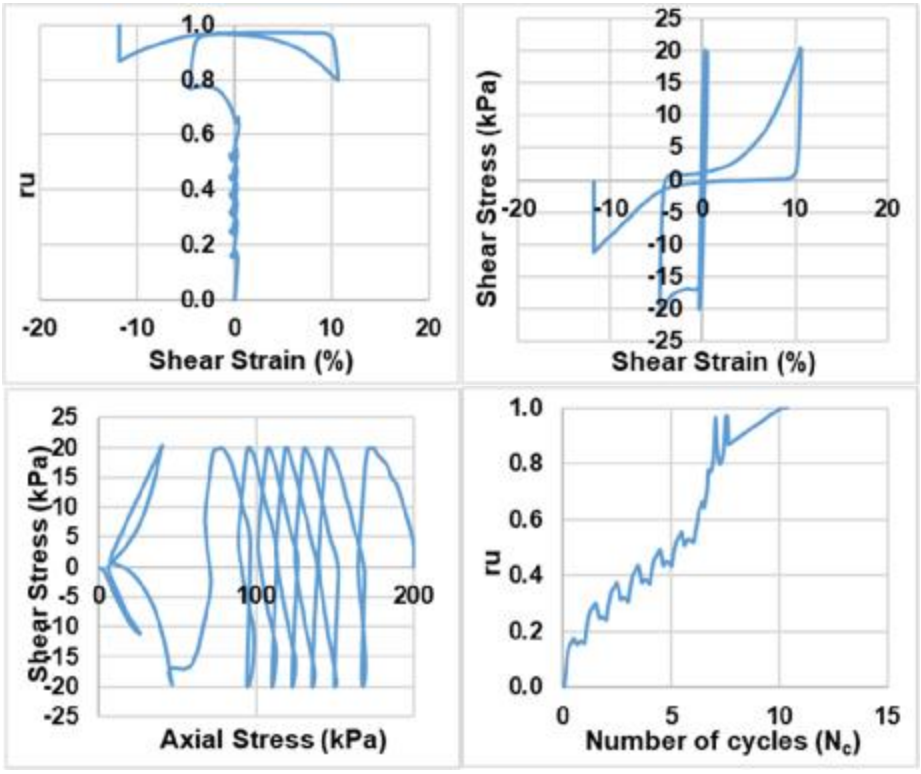


Monodirectional; $D_{rc}$ = 25%; $\sigma'_{vc}$ = 200 kPa; CSR = 0.1 (Re-liquefaction)

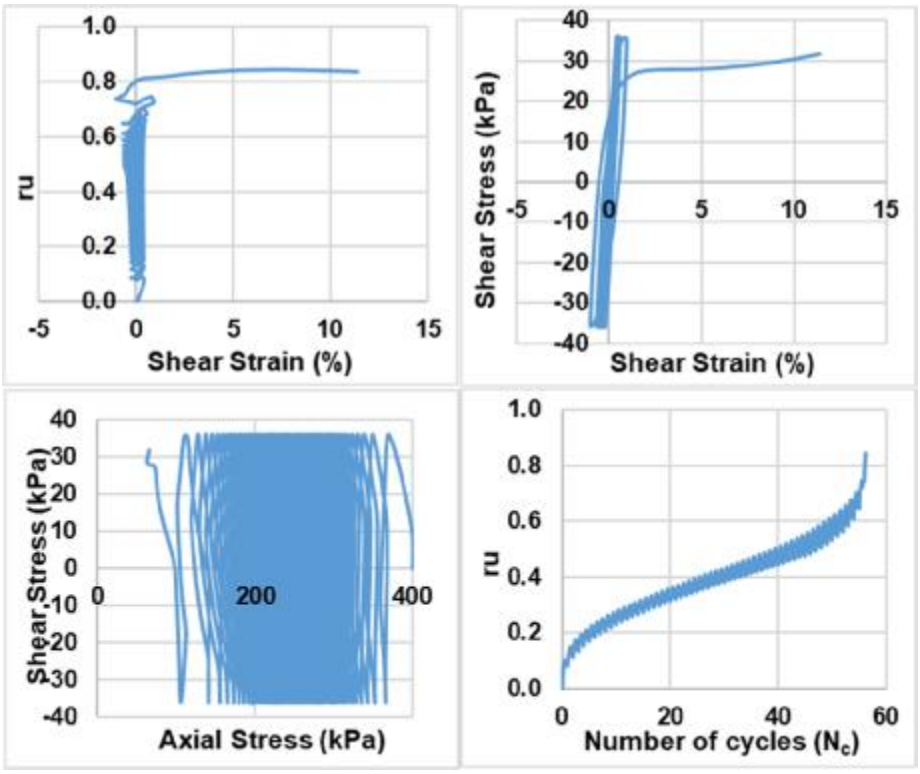


Monodirectional; $D_{rc}$ = 25%; $\sigma'_{vc}$ = 400 kPa; CSR = 0.09 (Liquefaction)

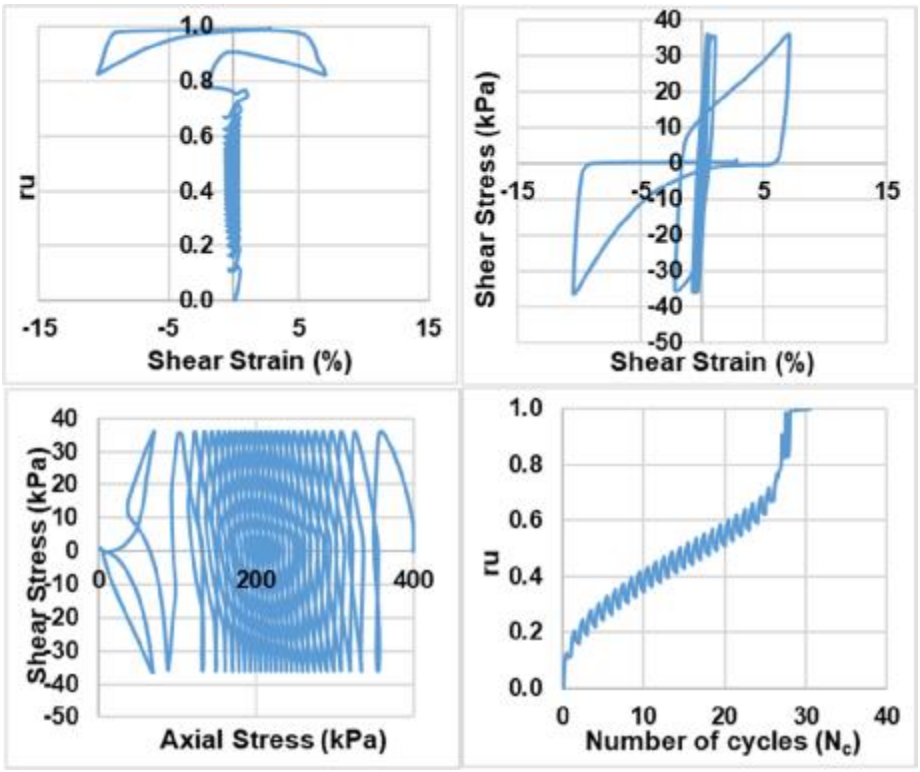


Monodirectional; $D_{rc}$ = 25%; $\sigma'_{vc}$ = 400 kPa; CSR = 0.09 (Re-liquefaction)

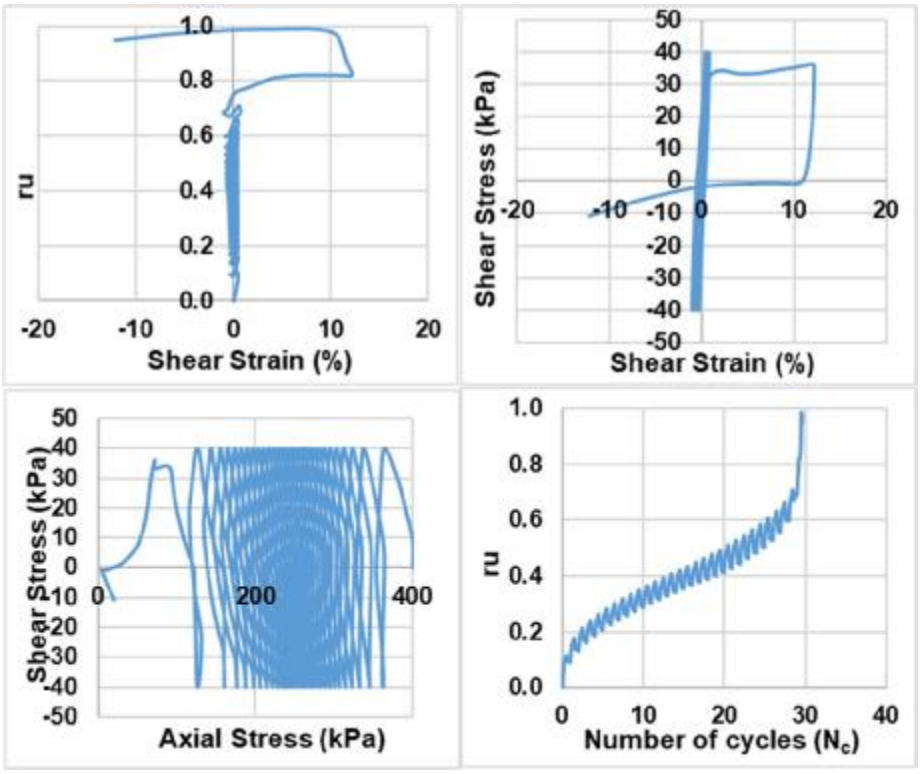


Monodirectional; $D_{rc}$ = 25%; $\sigma'_{vc}$ = 400 kPa; CSR = 0.1 (Liquefaction)

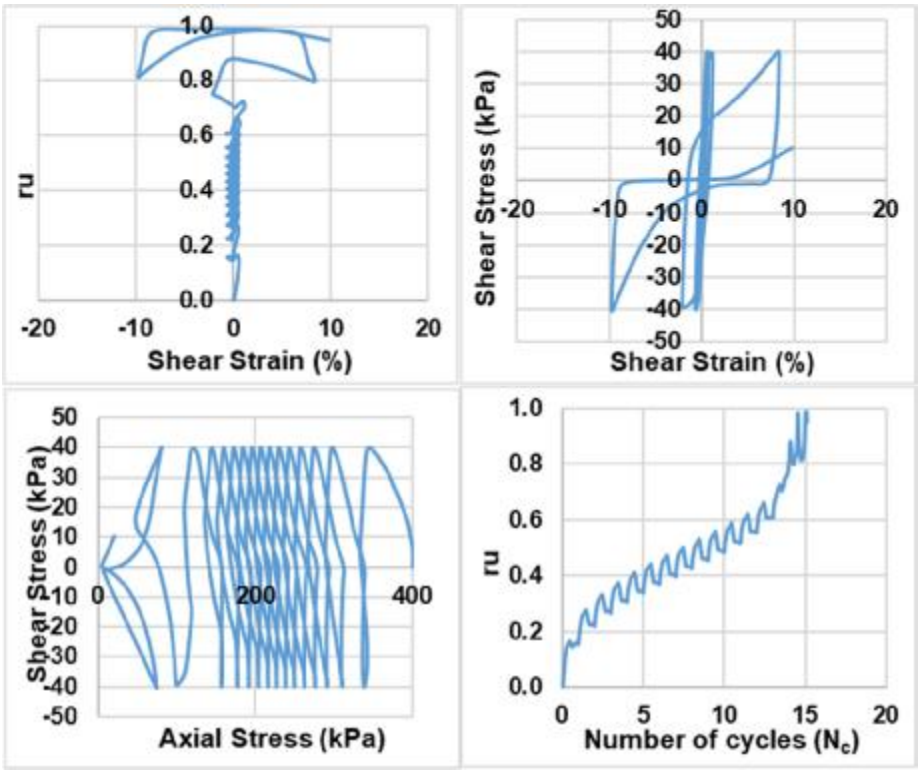


Monodirectional; $D_{rc}$ = 25%; $\sigma'_{vc}$ = 400 kPa; CSR = 0.1 (Re-liquefaction)

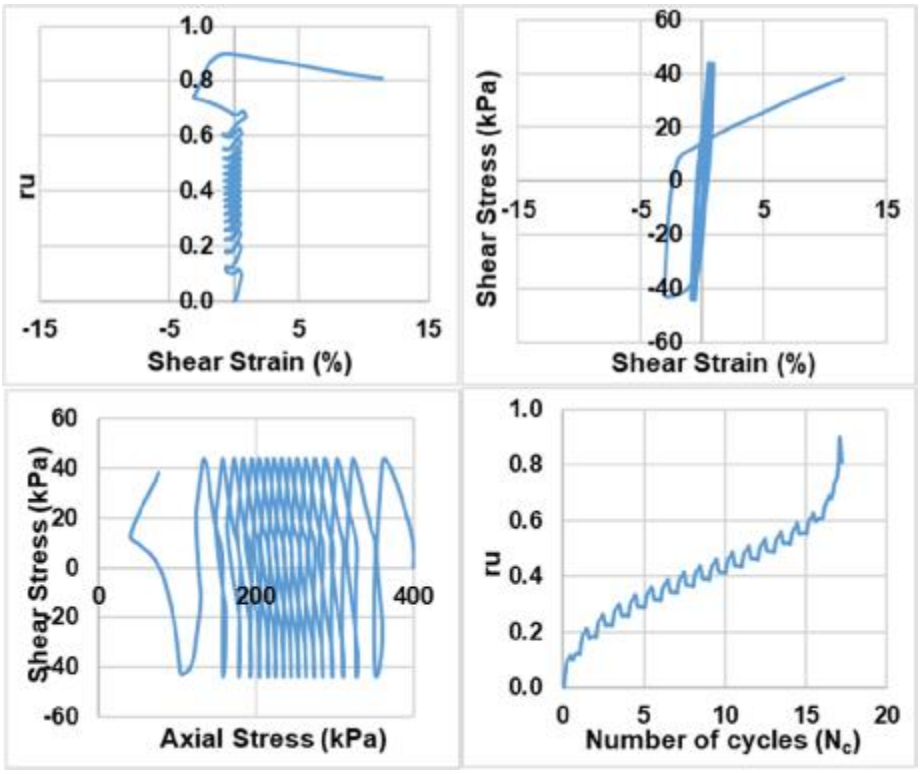


Monodirectional; $D_{rc}$ = 25%; $\sigma'_{vc}$ = 400 kPa; CSR = 0.11 (Liquefaction)

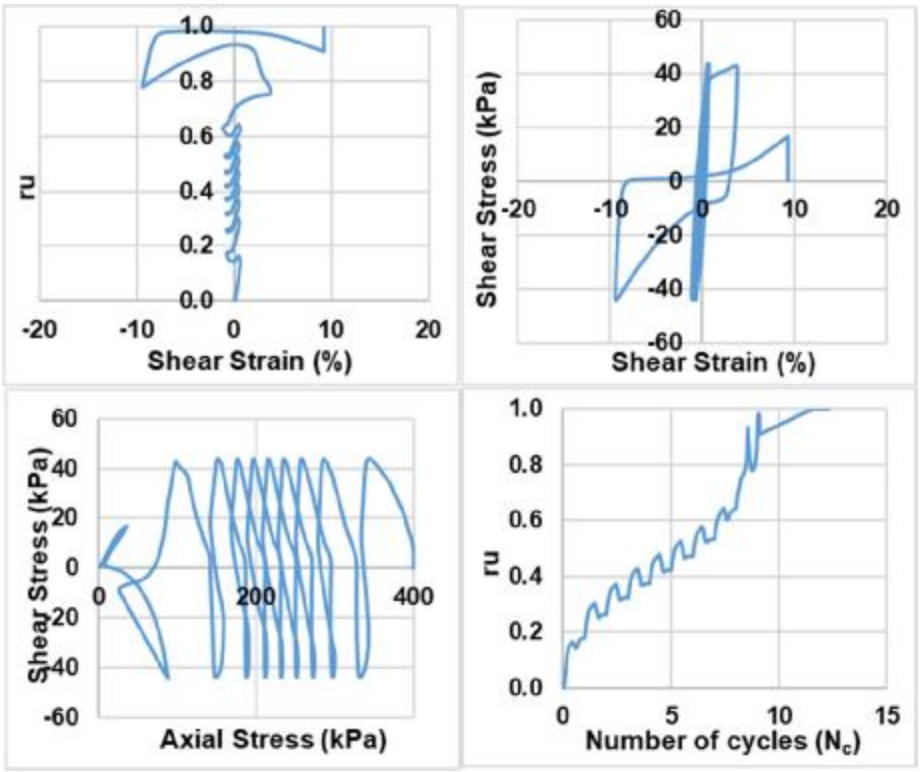


Monodirectional; $D_{rc}$ = 25%; $\sigma'_{vc}$ = 400 kPa; CSR = 0.11 (Re-liquefaction)

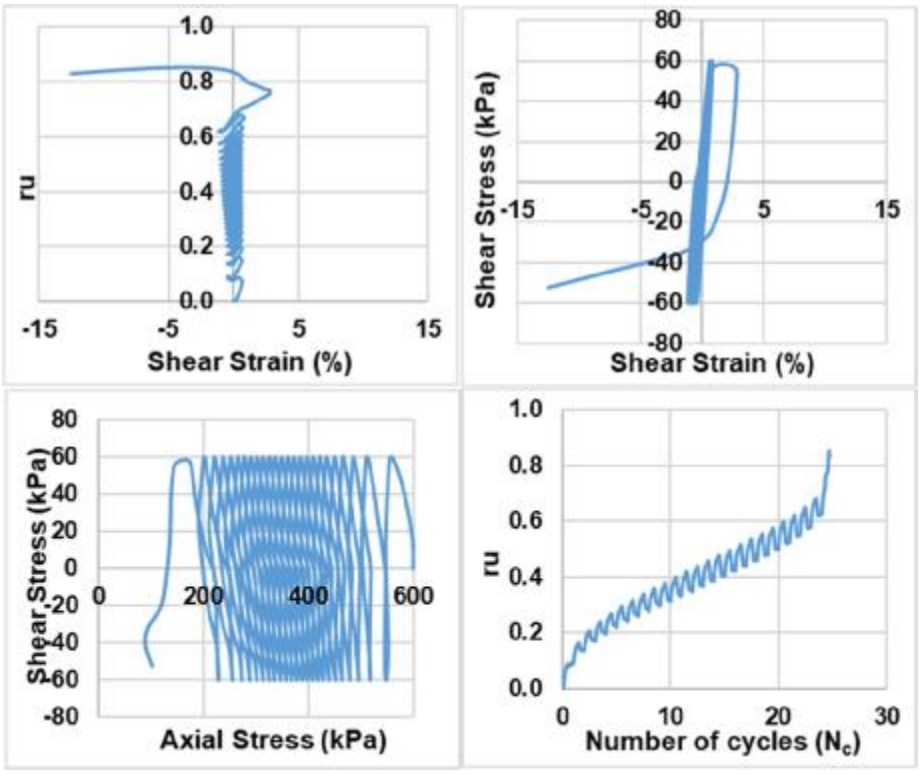


Monodirectional; $D_{rc}$ = 25%; $\sigma'_{vc}$ = 600 kPa; CSR = 0.1 (Liquefaction)

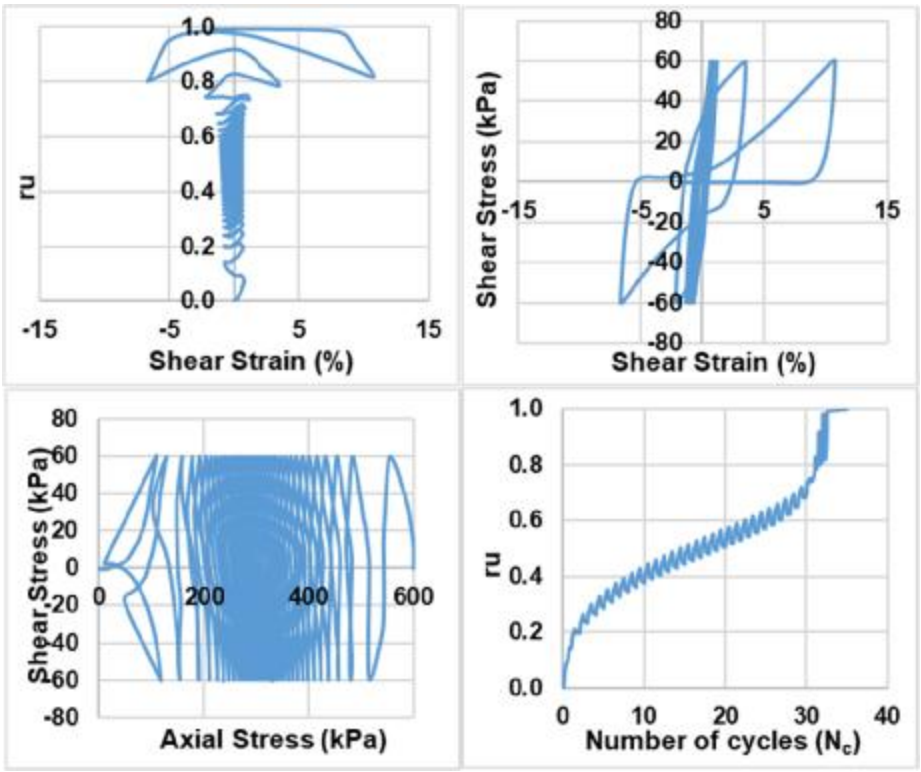


Monodirectional; $D_{rc}$ = 25%; $\sigma'_{vc}$ = 600 kPa; CSR = 0.1 (Re-liquefaction)

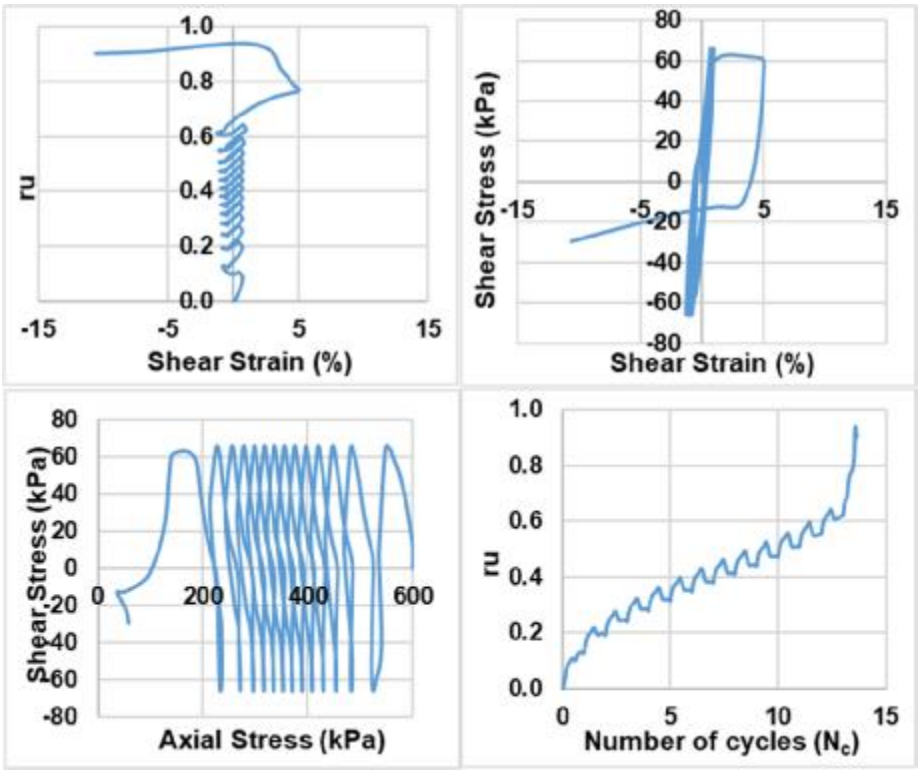


Monodirectional; $D_{rc}$ = 25%; $\sigma'_{vc}$ = 600 kPa; CSR = 0.11 (Liquefaction)

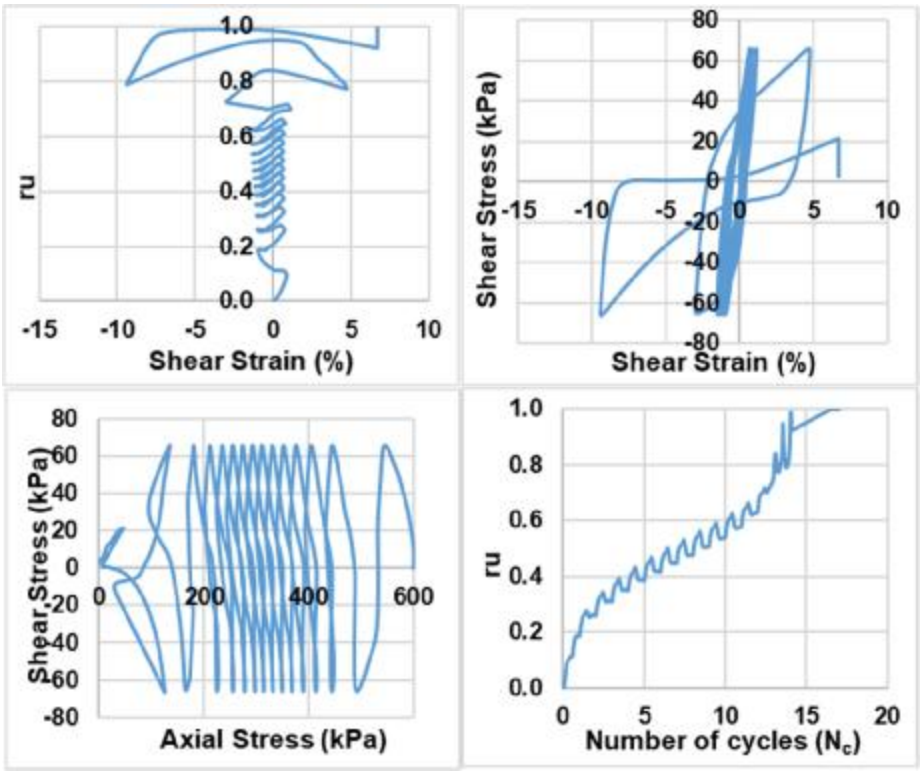


Monodirectional; $D_{rc}$ = 25%; $\sigma'_{vc}$ = 600 kPa; CSR = 0.11 (Re-liquefaction)

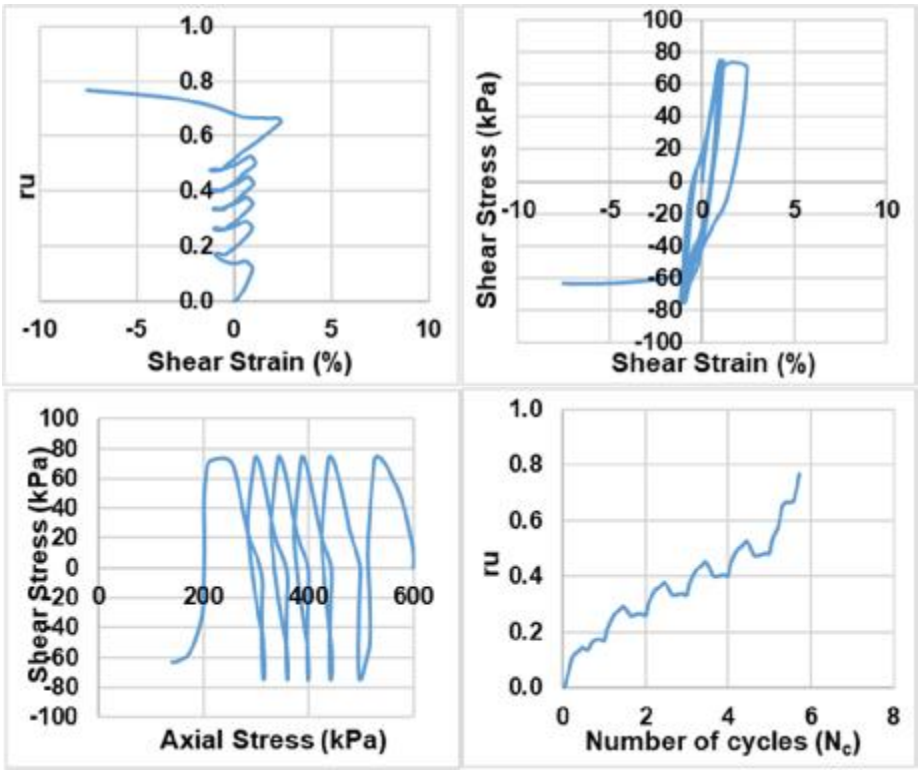


Monodirectional; $D_{rc}$ = 25%; $\sigma'_{vc}$ = 600 kPa; CSR = 0.125 (Liquefaction)

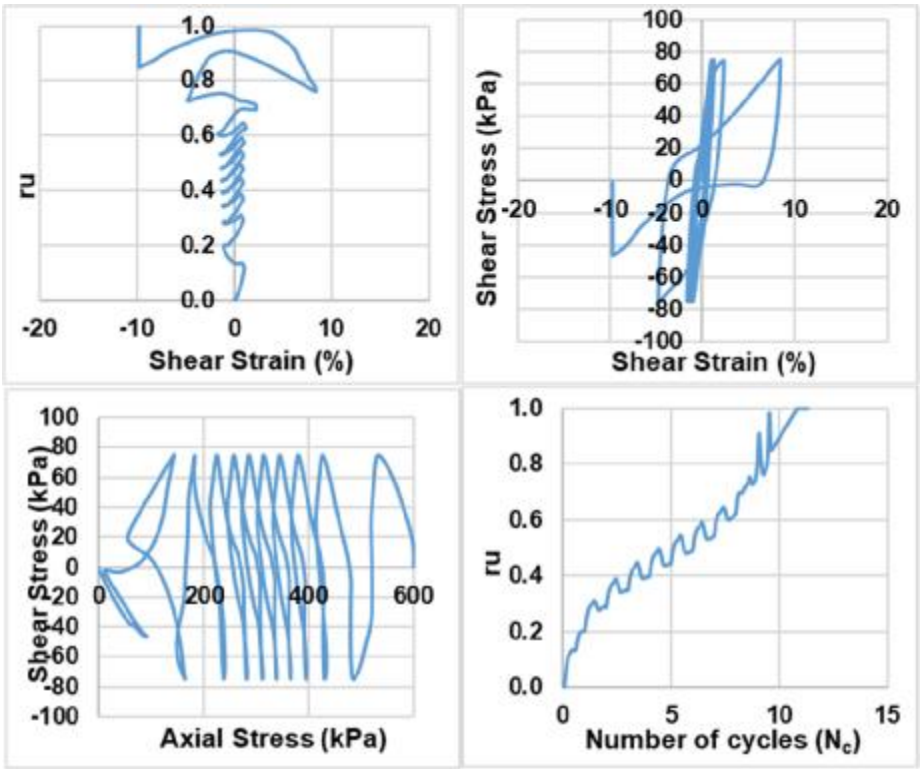


Monodirectional; $D_{rc}$ = 25%; $\sigma'_{vc}$ = 600 kPa; CSR = 0.125 (Re-liquefaction)

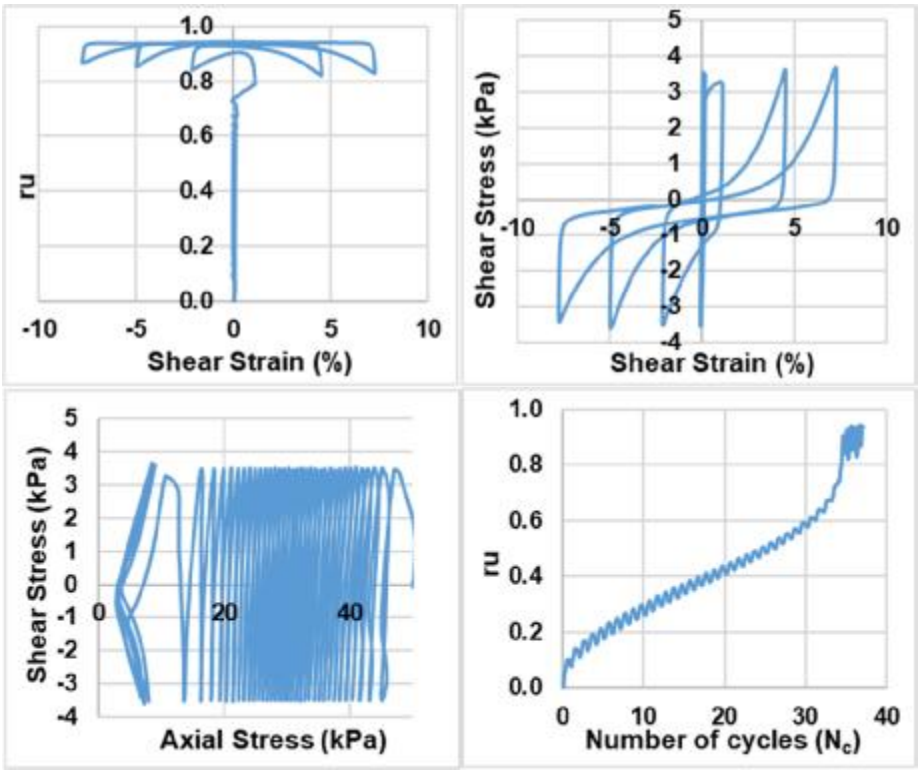


Monodirectional; $D_{rc}$ = 45%; $\sigma'_{vc}$ = 50 kPa; CSR = 0.07 (Liquefaction)

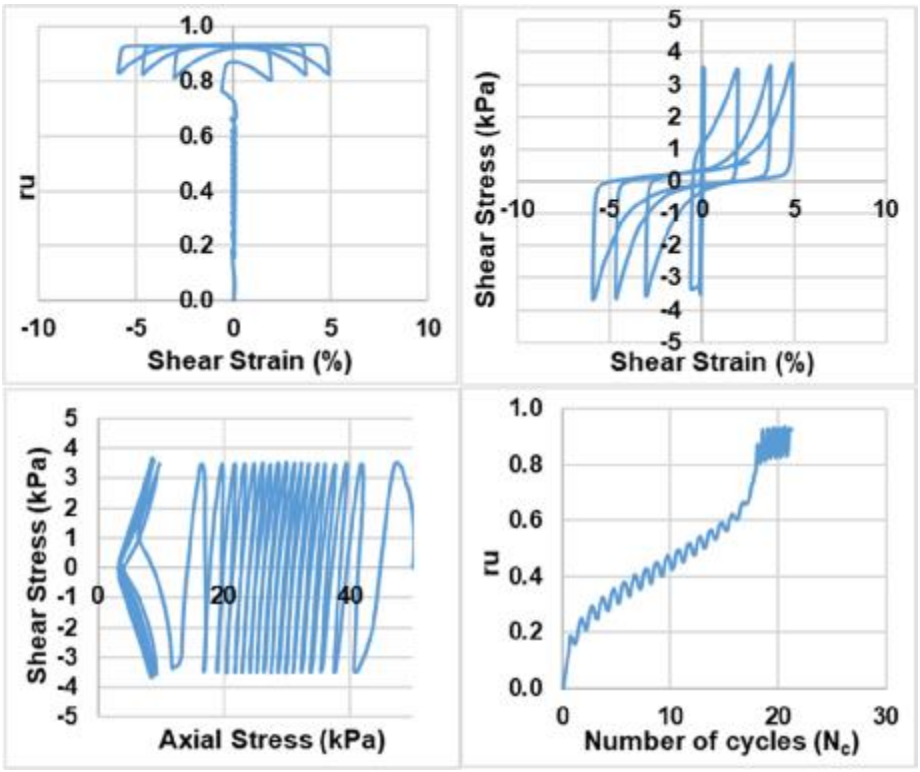


Monodirectional; $D_{rc}$ = 45%; $\sigma'_{vc}$ = 50 kPa; CSR = 0.07 (Re-liquefaction)

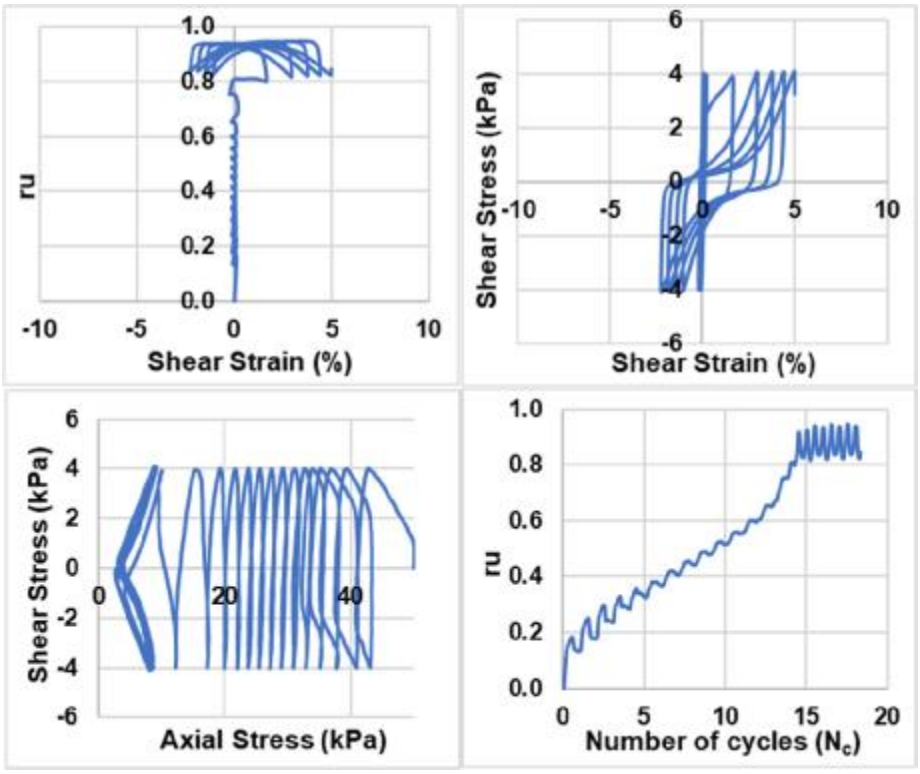


Monodirectional; $D_{rc}$ = 45%; $\sigma'_{vc}$ = 50 kPa; CSR = 0.08 (Liquefaction)

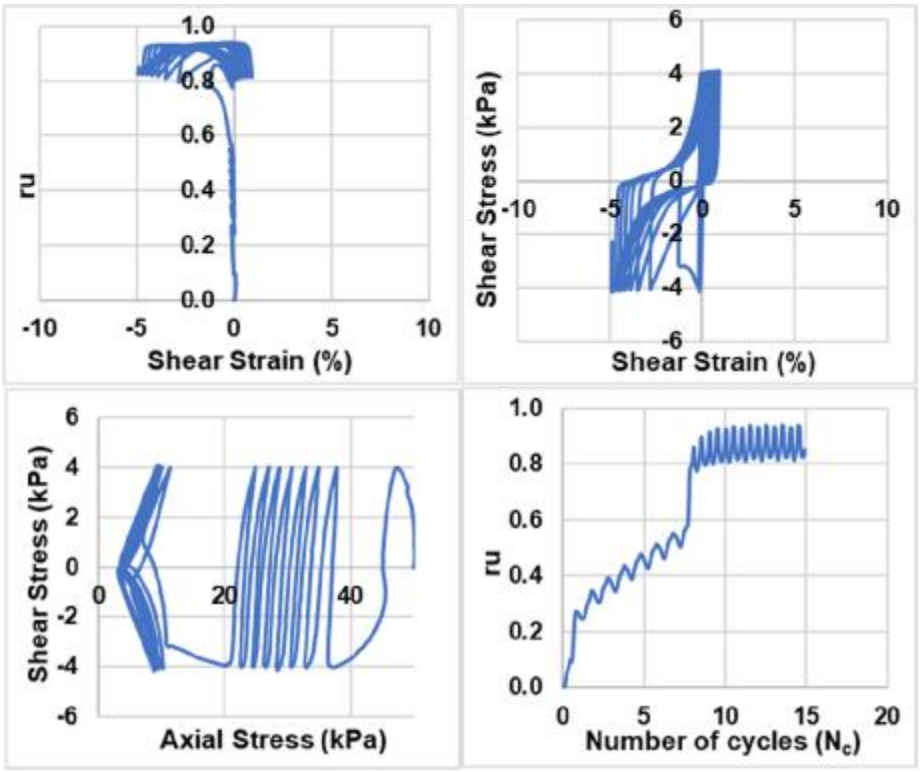


Monodirectional; $D_{rc}$ = 45%; $\sigma'_{vc}$ = 50 kPa; CSR = 0.08 (Re-liquefaction)

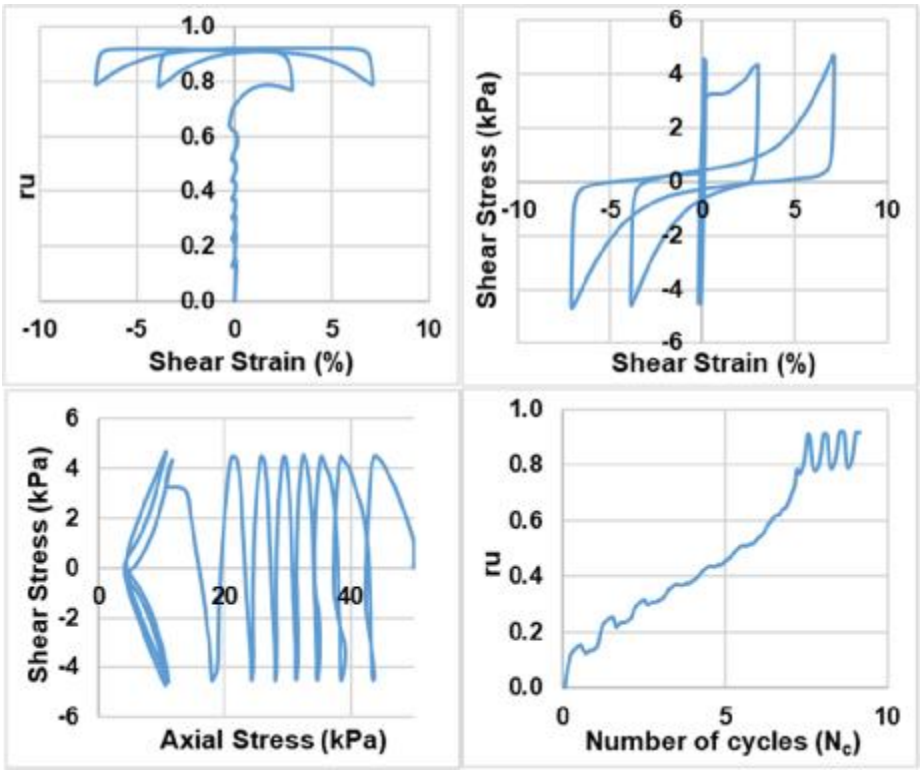


Monodirectional; $D_{rc}$ = 45%; $\sigma'_{vc}$ = 50 kPa; CSR = 0.09 (Liquefaction)

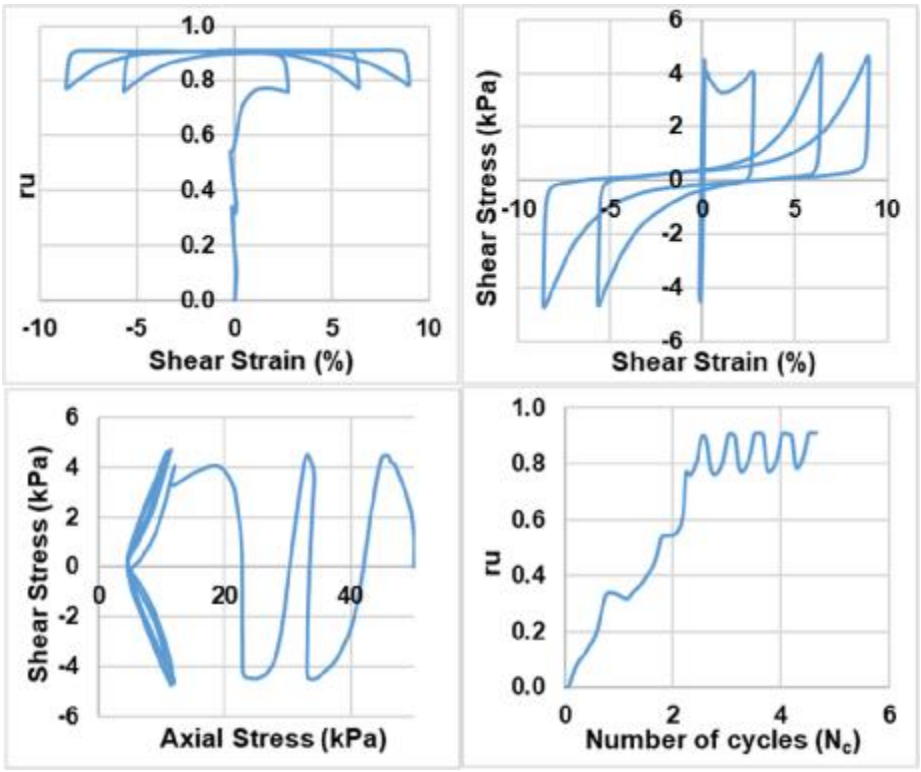


Monodirectional; $D_{rc}$ = 45%; $\sigma'_{vc}$ = 50 kPa; CSR = 0.09 (Re-liquefaction)

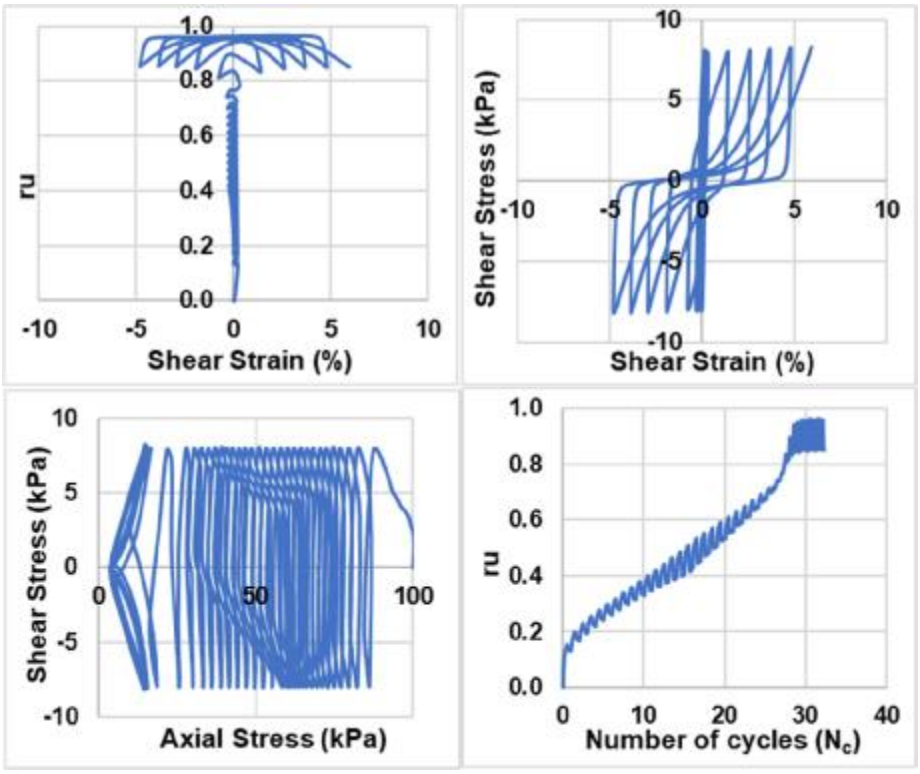


Monodirectional; $D_{rc}$ = 45%; $\sigma'_{vc}$ = 100 kPa; CSR = 0.08 (Liquefaction)

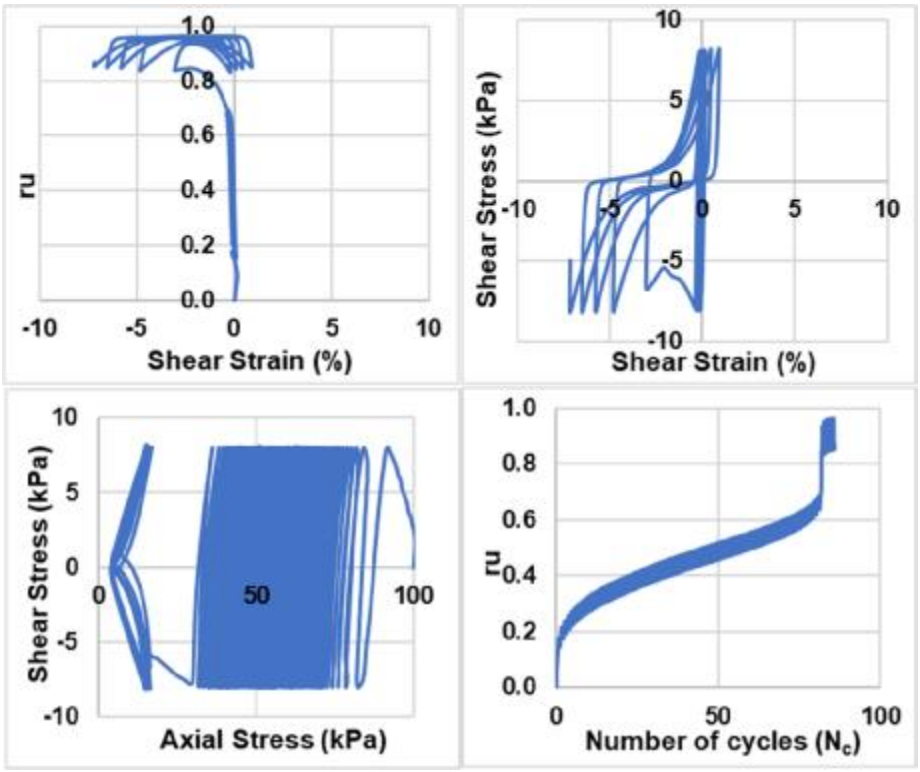


Monodirectional; $D_{rc}$ = 45%; $\sigma'_{vc}$ = 100 kPa; CSR = 0.08 (Re-liquefaction)

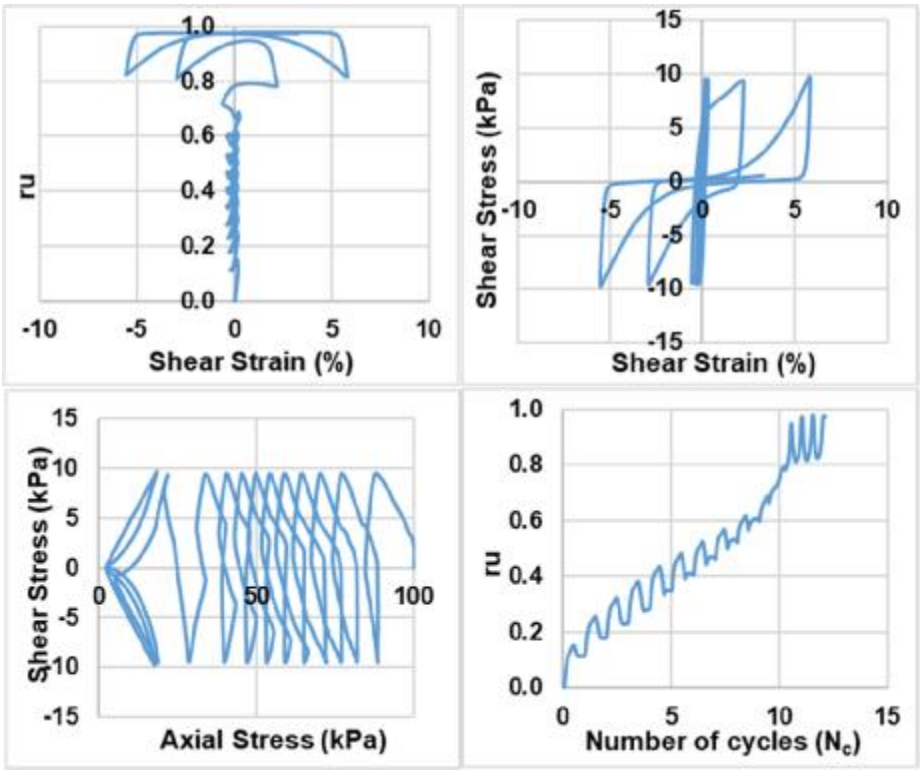


Monodirectional; $D_{rc}$ = 45%; $\sigma'_{vc}$ = 100 kPa; CSR = 0.095 (Liquefaction)

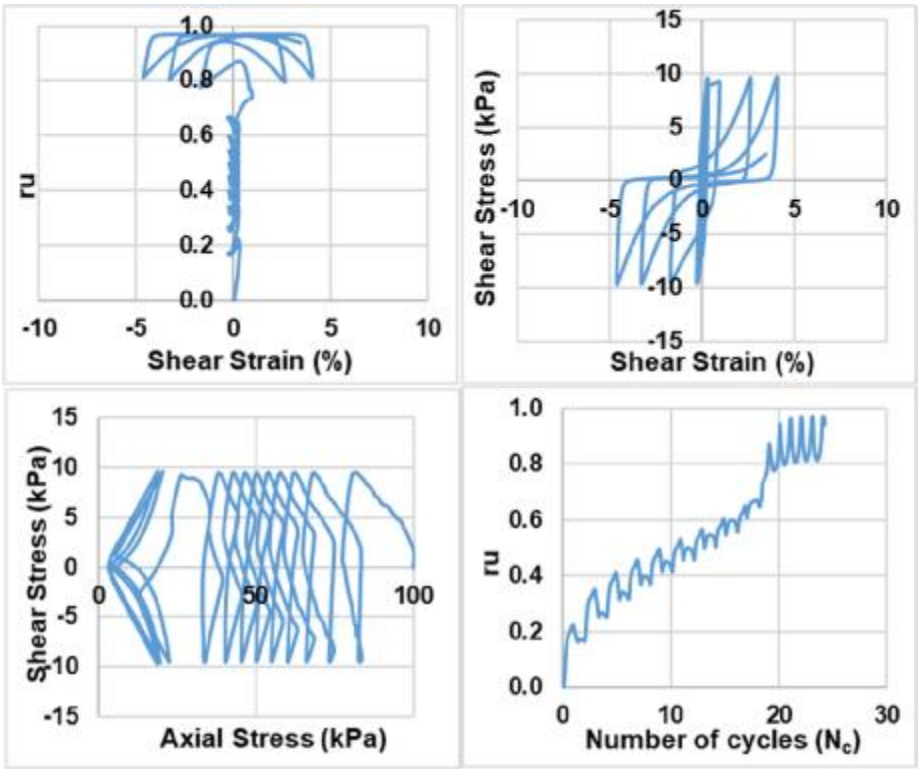


Monodirectional; $D_{rc}$ = 45%; $\sigma'_{vc}$ = 100 kPa; CSR = 0.095 (Re-liquefaction)

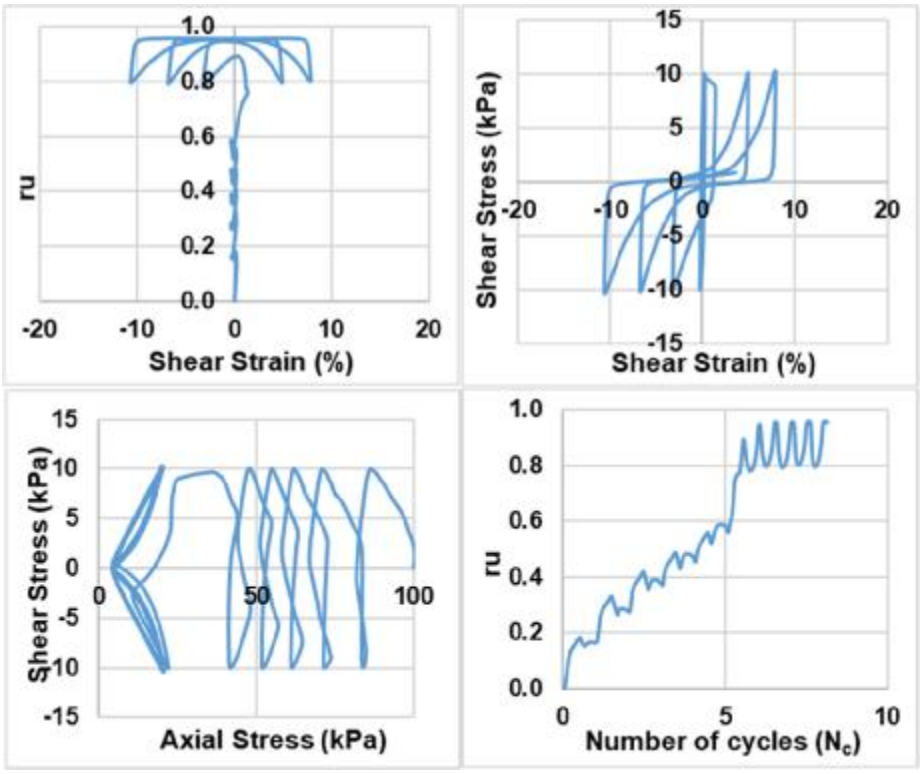


Monodirectional; $D_{rc}$ = 45%; $\sigma'_{vc}$ = 100 kPa; CSR = 0.1 (Liquefaction)

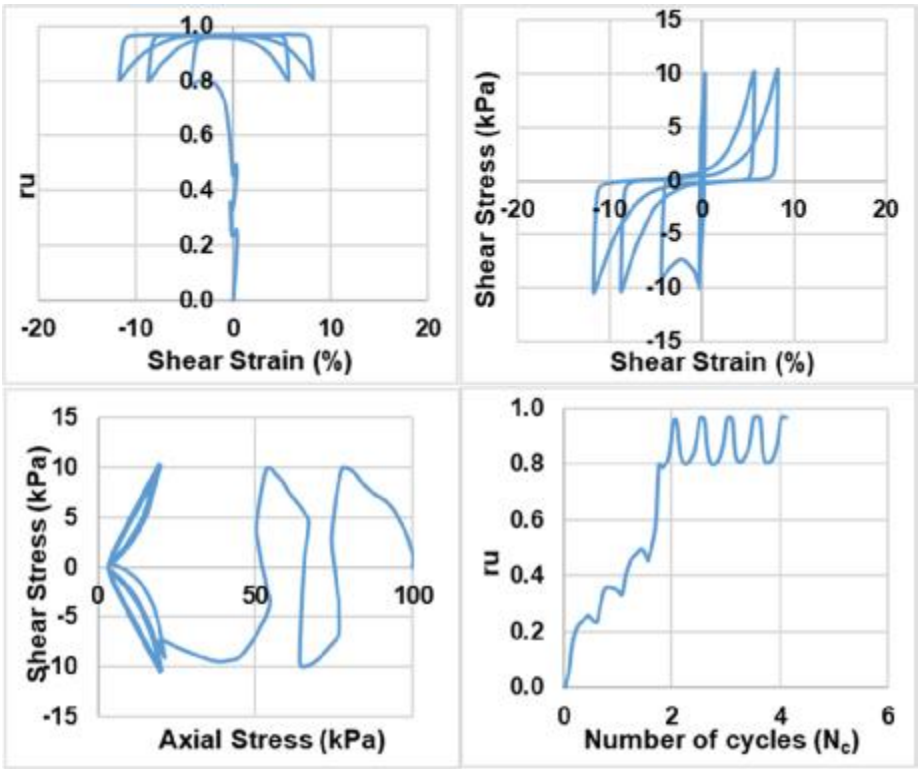


Monodirectional; $D_{rc}$ = 45%; $\sigma'_{vc}$ = 100 kPa; CSR = 0.1 (Re-liquefaction)

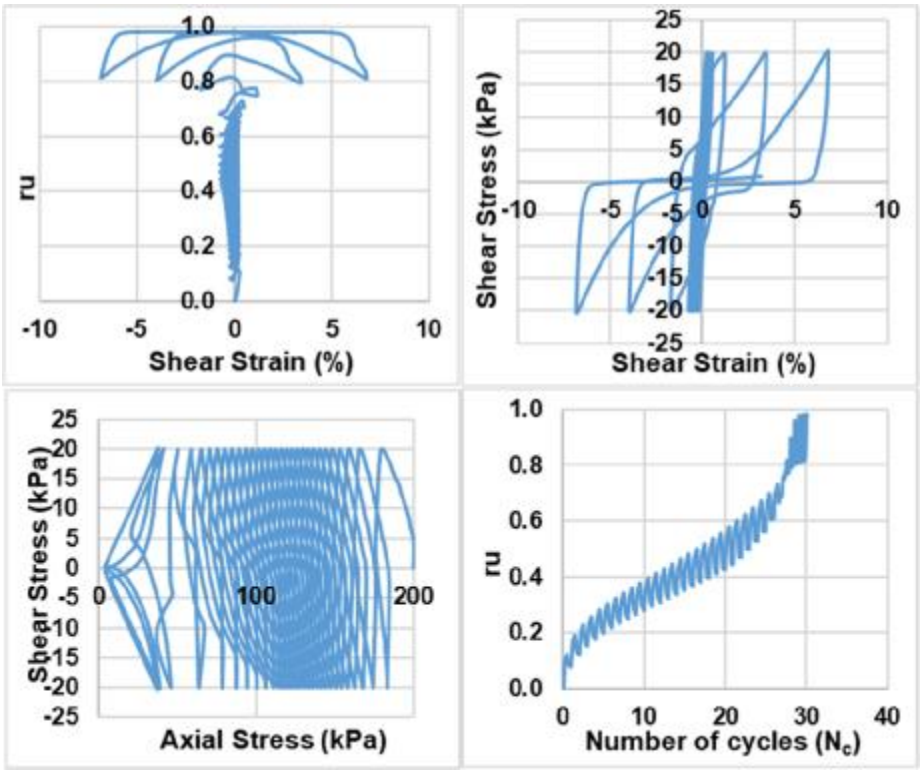


Monodirectional; $D_{rc}$ = 45%; $\sigma'_{vc}$ = 200 kPa; CSR = 0.1 (Liquefaction)

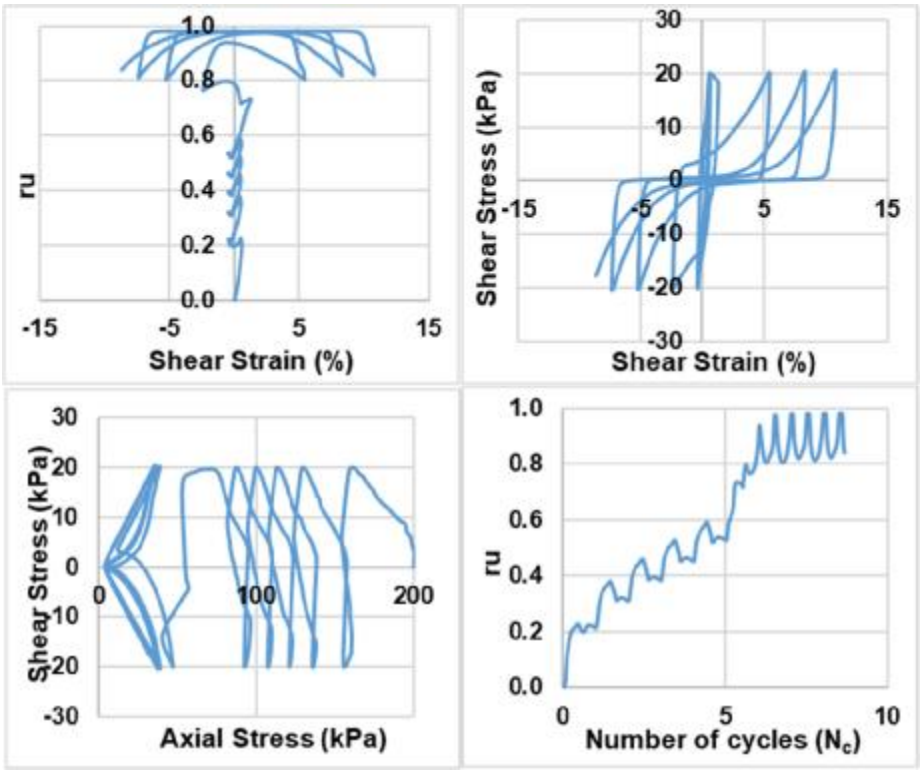


Monodirectional; $D_{rc}$ = 45%; $\sigma'_{vc}$ = 200 kPa; CSR = 0.1 (Re-liquefaction)

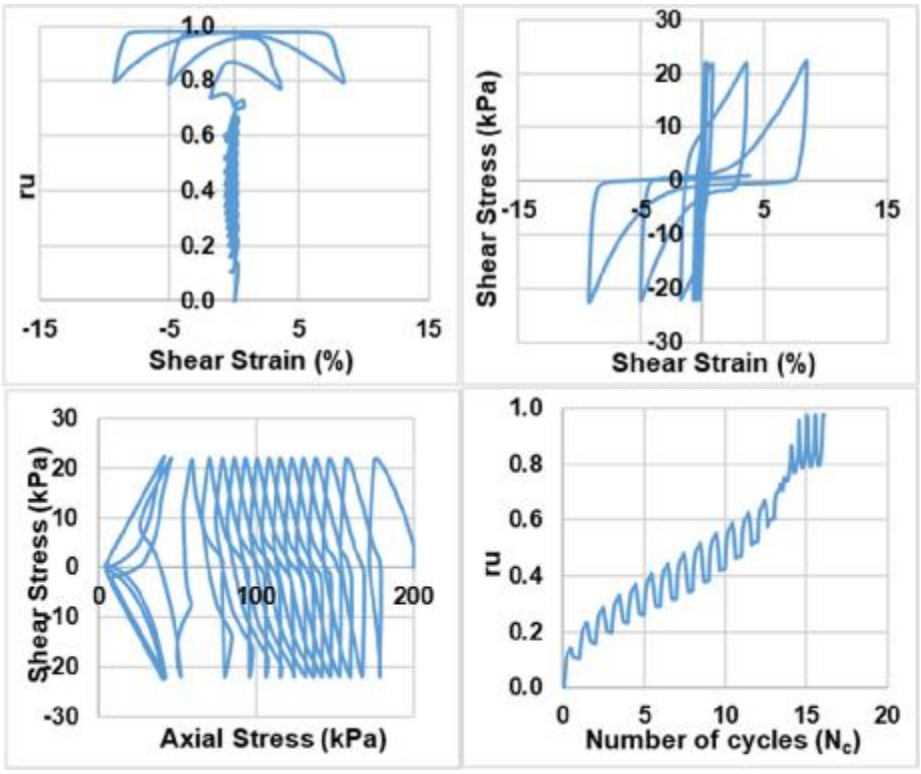


Monodirectional; $D_{rc}$ = 45%; $\sigma'_{vc}$ = 200 kPa; CSR = 0.11 (Liquefaction)

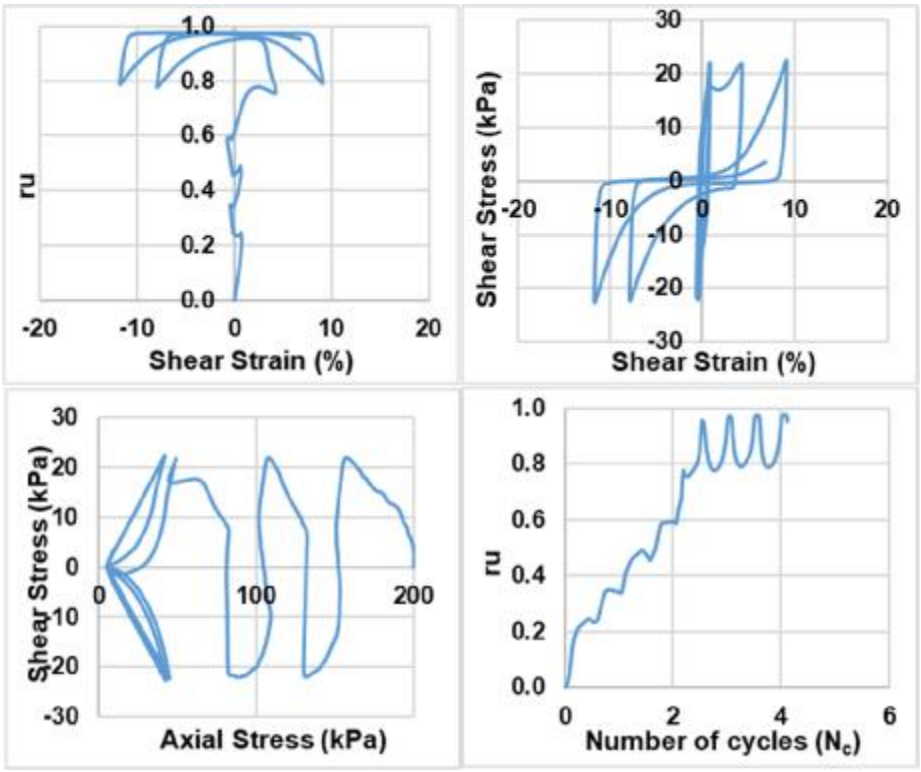


Monodirectional; $D_{rc}$ = 45%; $\sigma'_{vc}$ = 200 kPa; CSR = 0.11 (Re-liquefaction)

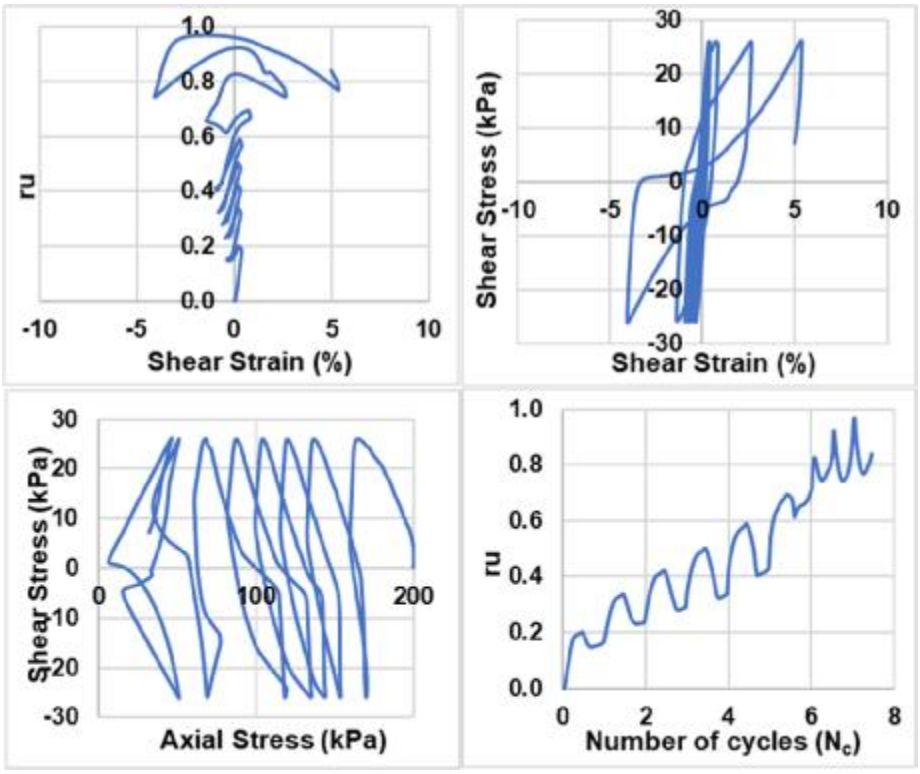


Monodirectional; $D_{rc}$ = 45%; $\sigma'_{vc}$ = 200 kPa; CSR = 0.13 (Liquefaction)

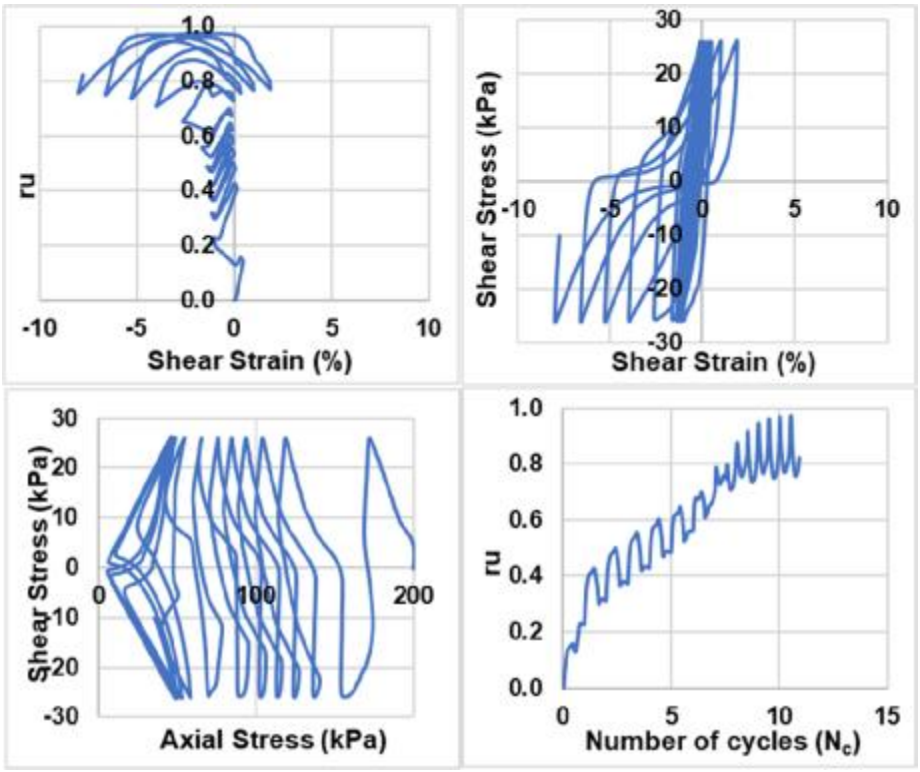


Monodirectional; $D_{rc}$ = 45%; $\sigma'_{vc}$ = 200 kPa; CSR = 0.13 (Re-liquefaction)

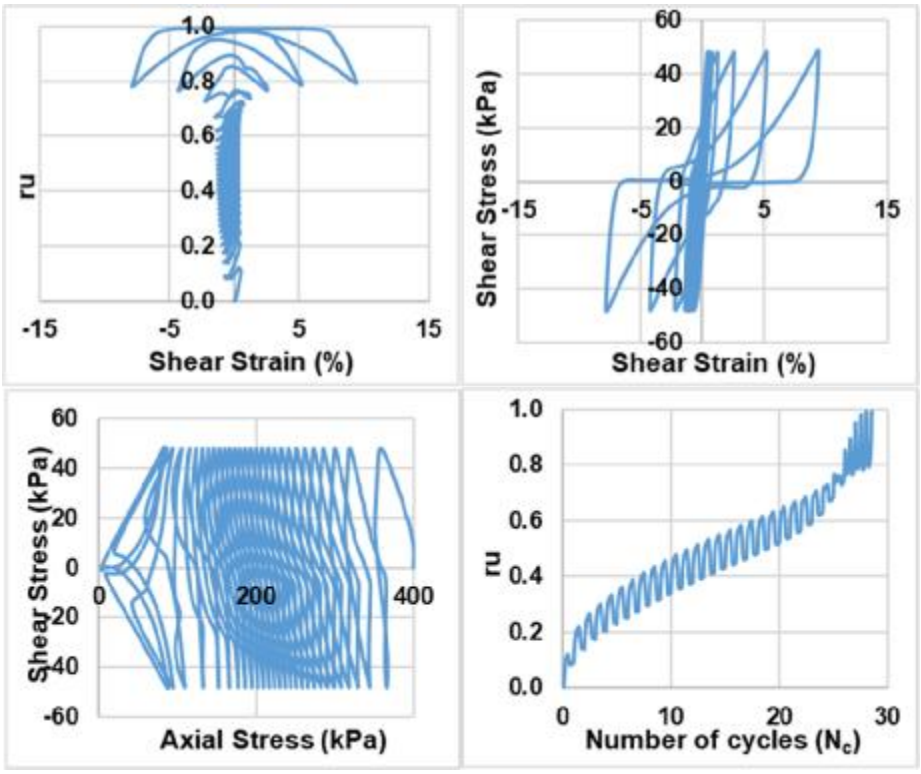


Monodirectional; $D_{rc}$ = 45%; $\sigma'_{vc}$ = 400 kPa; CSR = 0.12 (Liquefaction)

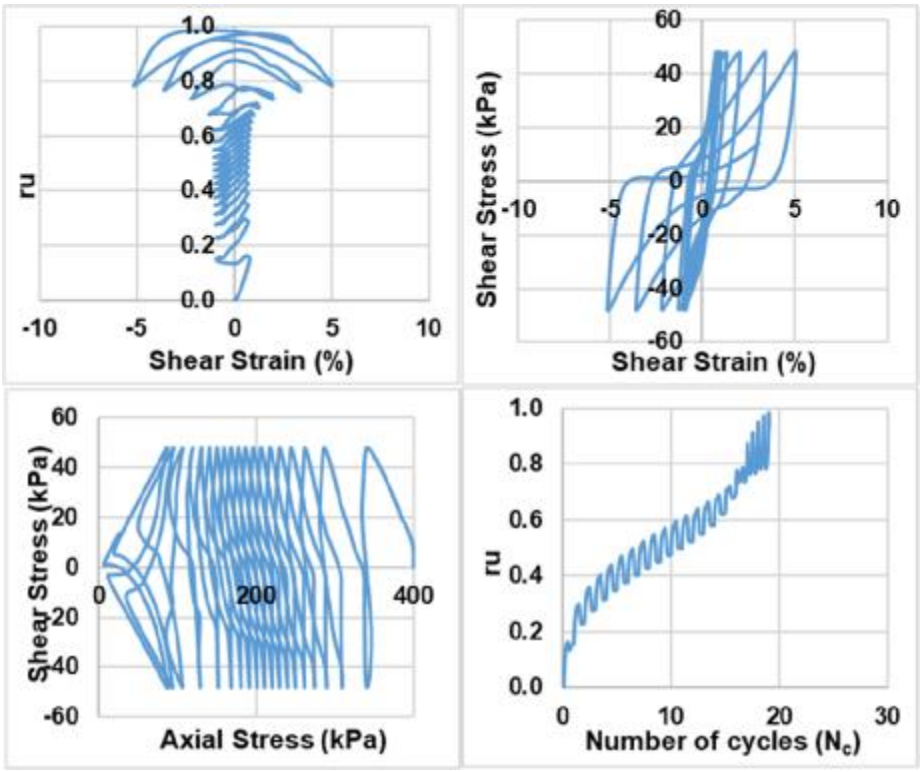


Monodirectional; $D_{rc}$ = 45%; $\sigma'_{vc}$ = 400 kPa; CSR = 0.12 (Re-liquefaction)

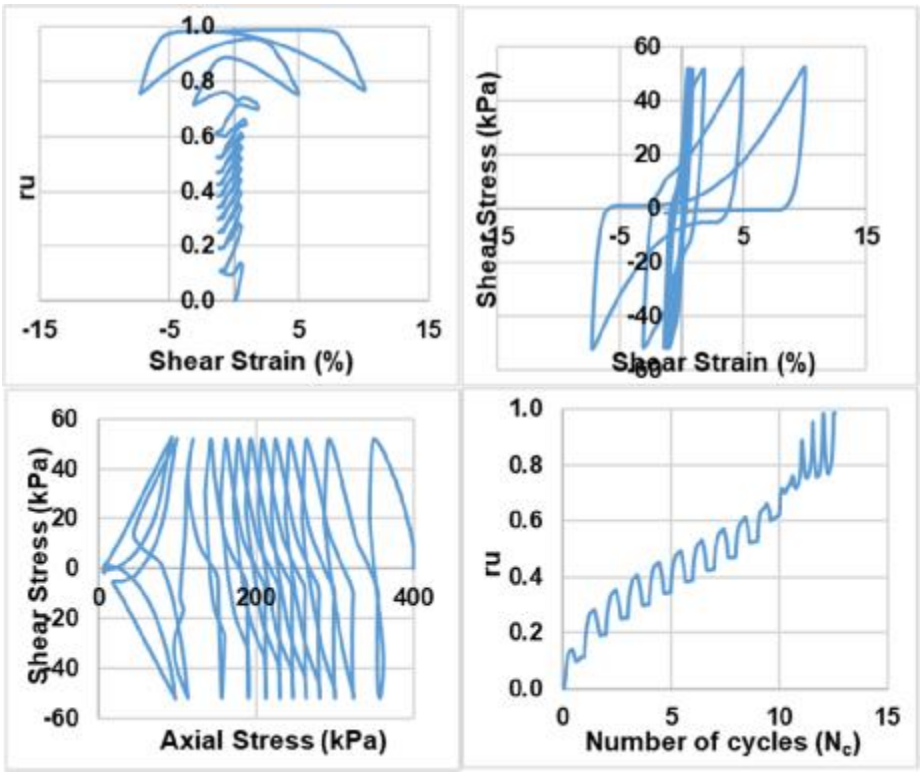


Monodirectional; $D_{rc}$ = 45%; $\sigma'_{vc}$ = 400 kPa; CSR = 0.13 (Liquefaction)

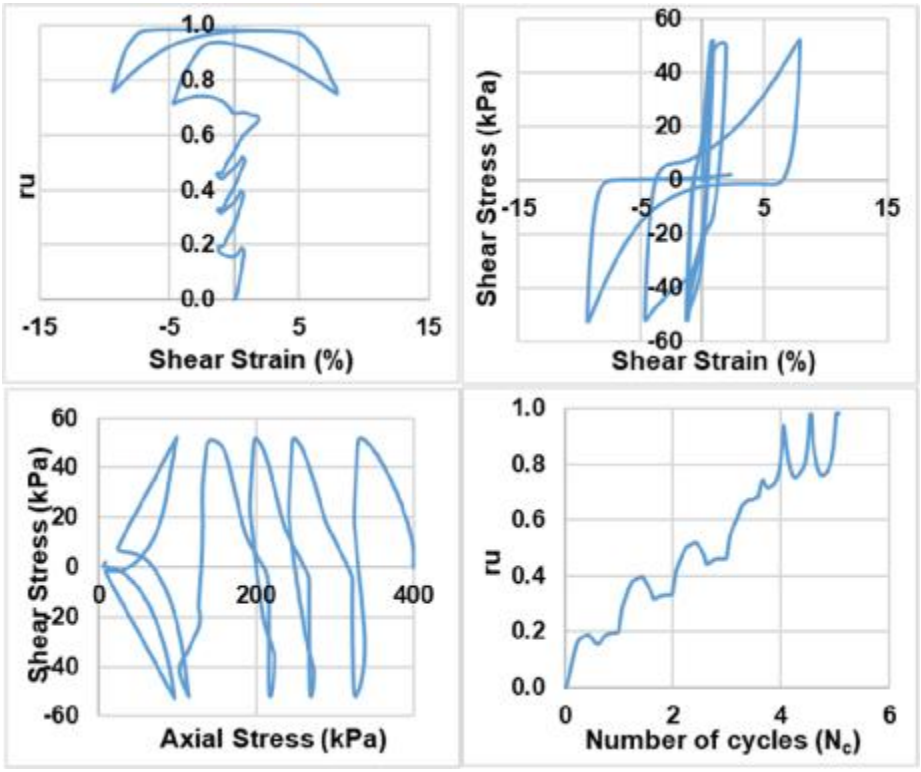


Monodirectional; $D_{rc}$ = 45%; $\sigma'_{vc}$ = 400 kPa; CSR = 0.13 (Re-liquefaction)

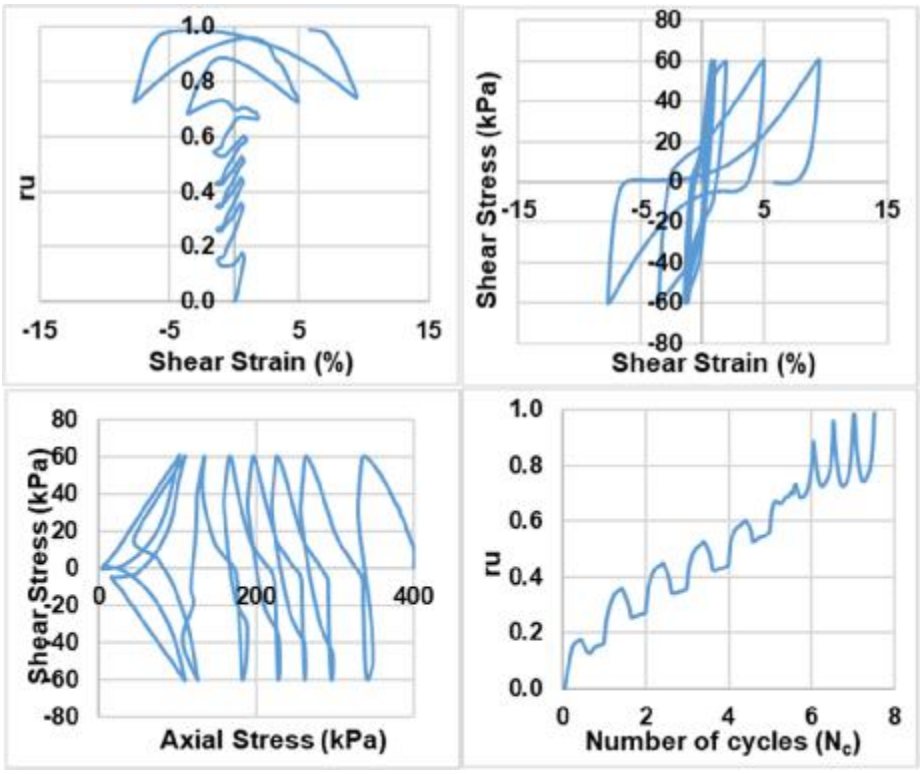


Monodirectional; $D_{rc}$ = 45%; $\sigma'_{vc}$ = 400 kPa; CSR = 0.15 (Liquefaction)

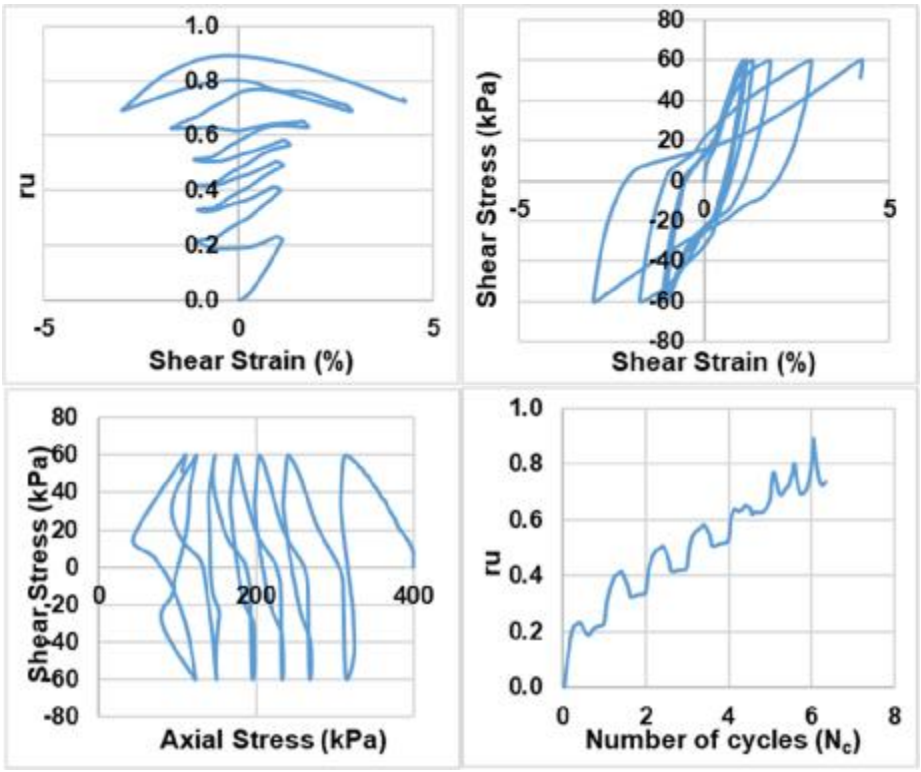


Monodirectional; $D_{rc}$ = 45%; $\sigma'_{vc}$ = 400 kPa; CSR = 0.15 (Re-liquefaction)

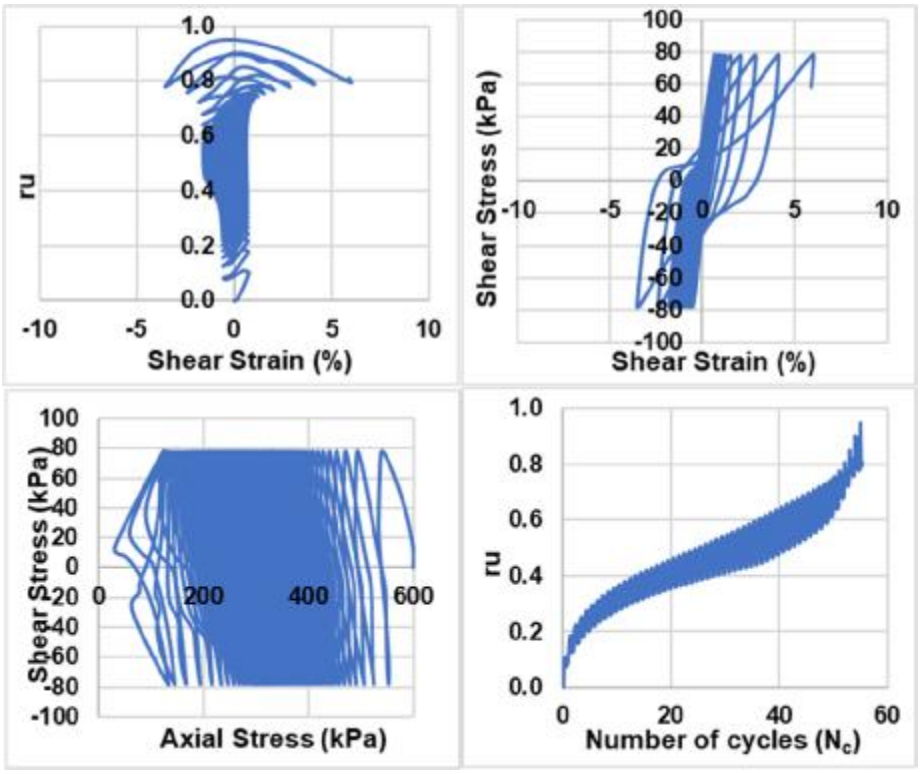


Monodirectional; $D_{rc}$ = 45%; $\sigma'_{vc}$ = 600 kPa; CSR = 0.13 (Liquefaction)

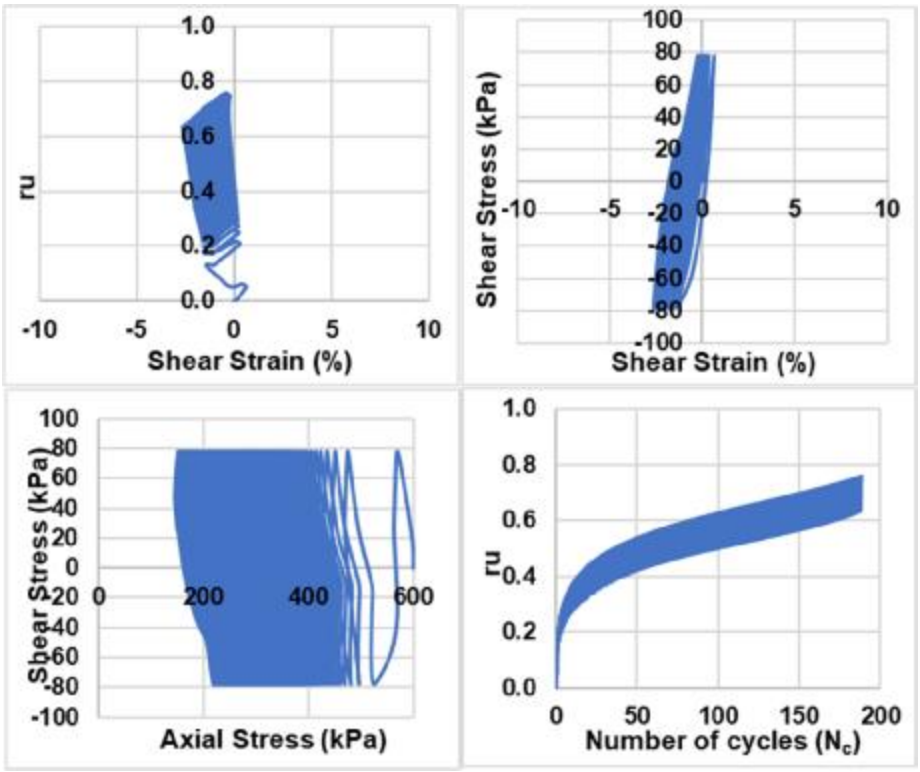


Monodirectional; $D_{rc}$ = 45%; $\sigma'_{vc}$ = 600 kPa; CSR = 0.13 (Re-liquefaction)

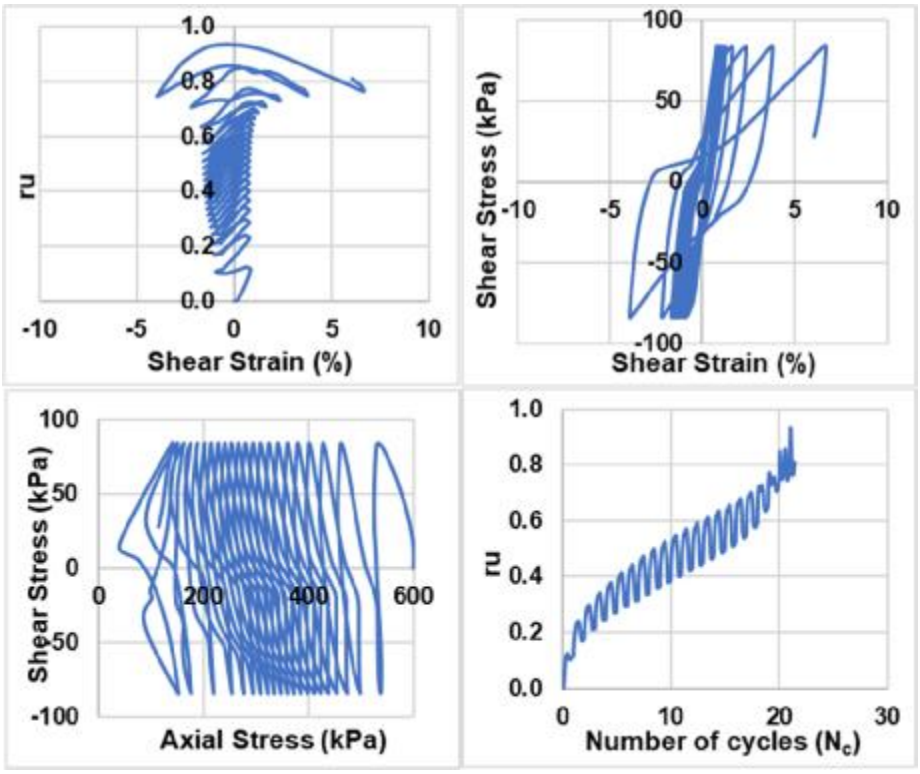


Monodirectional; $D_{rc}$ = 45%; $\sigma'_{vc}$ = 600 kPa; CSR = 0.14 (Liquefaction)

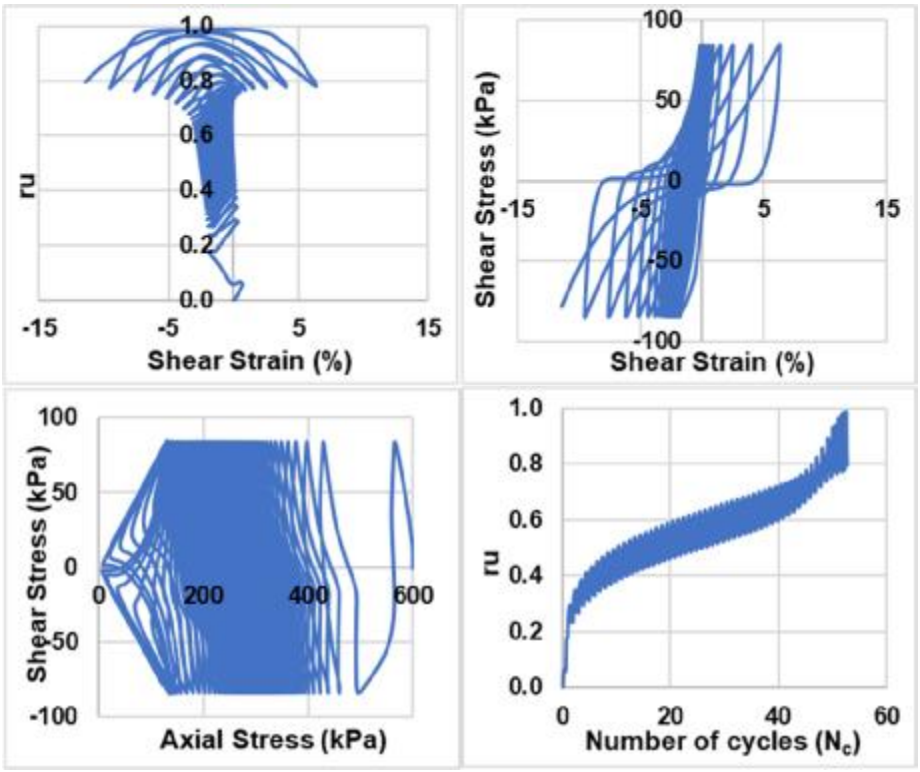


Monodirectional; $D_{rc}$ = 45%; $\sigma'_{vc}$ = 600 kPa; CSR = 0.14 (Re-liquefaction)

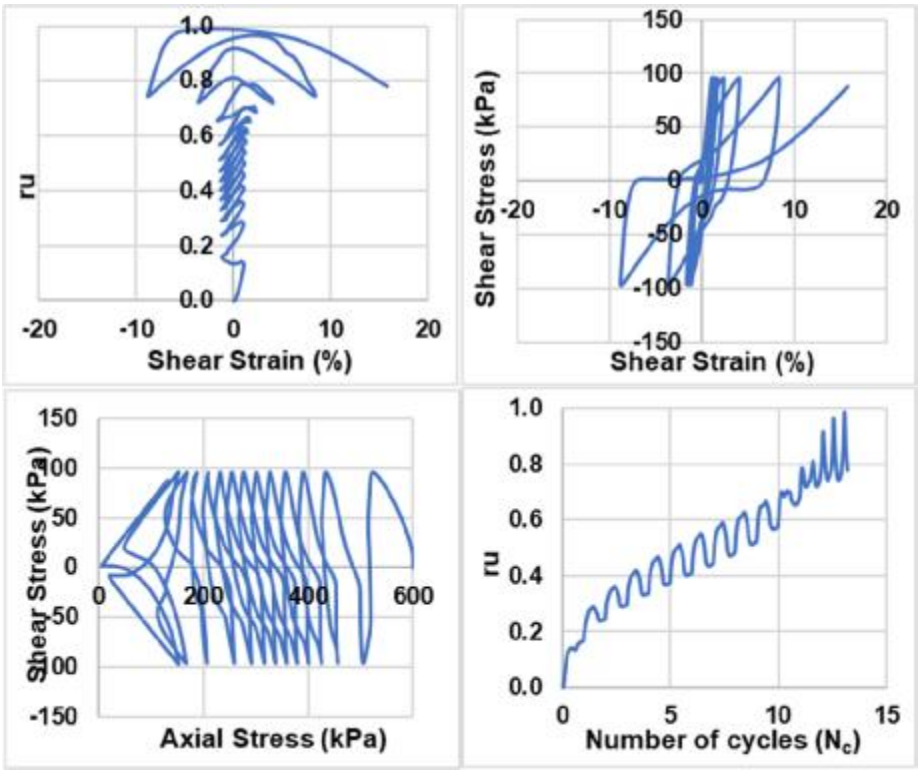


Monodirectional; $D_{rc}$ = 45%; $\sigma'_{vc}$ = 600 kPa; CSR = 0.16 (Liquefaction)

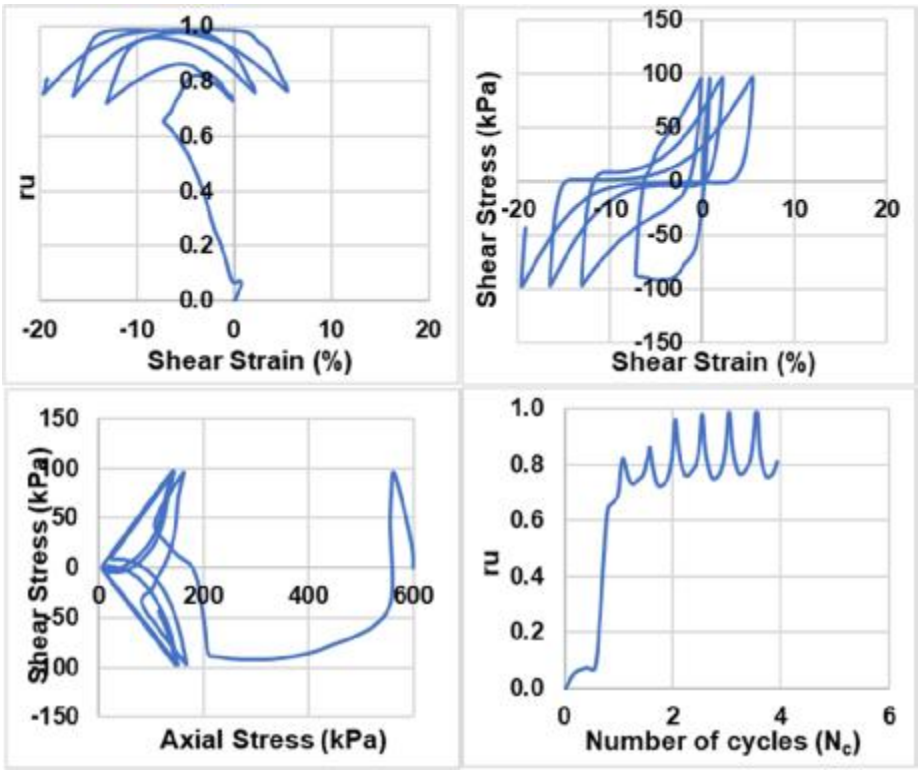


Monodirectional; $D_{rc}$ = 45%; $\sigma'_{vc}$ = 600 kPa; CSR = 0.16 (Re-liquefaction)

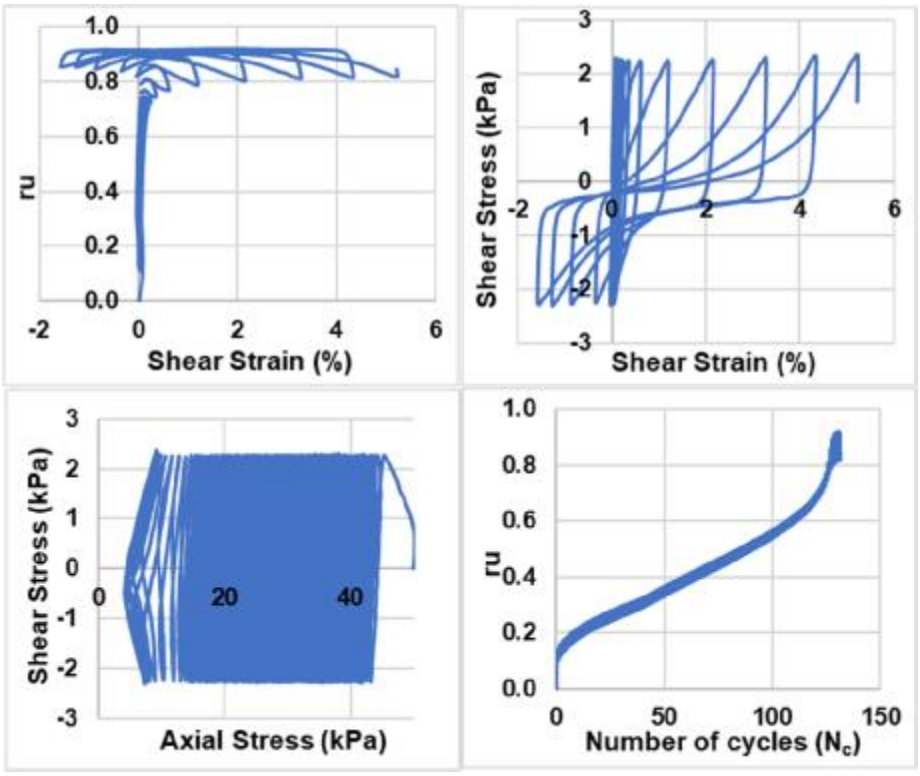


Monodirectional; $D_{rc}$ = 65%; $\sigma'_{vc}$ = 50 kPa; CSR = 0.045 (Liquefaction)

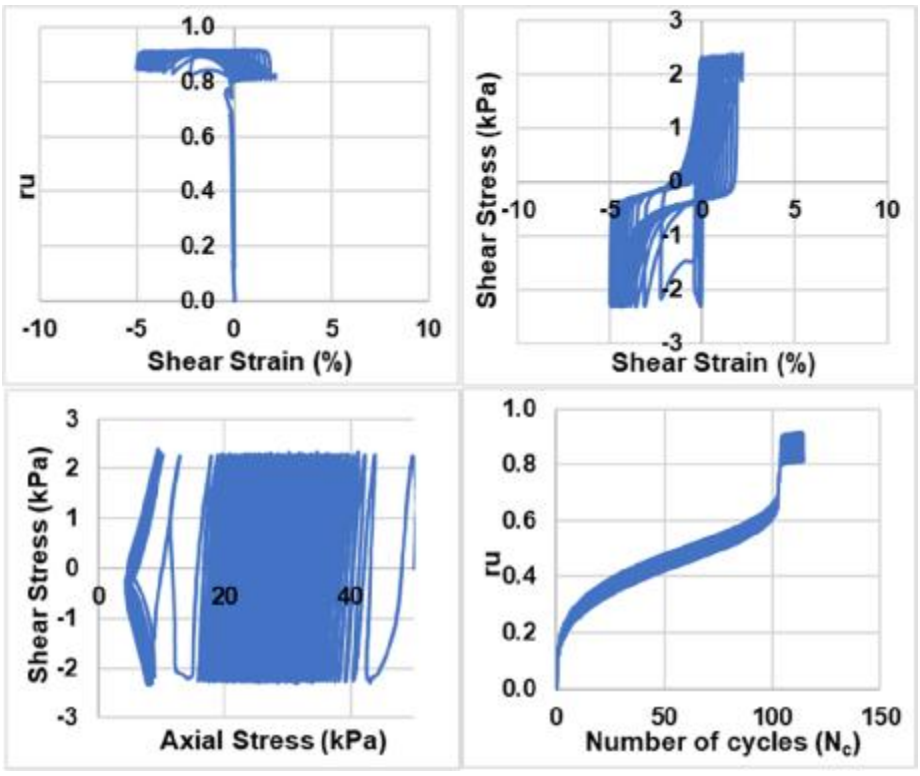


Monodirectional; $D_{rc}$ = 65%; $\sigma'_{vc}$ = 50 kPa; CSR = 0.045 (Re-liquefaction)

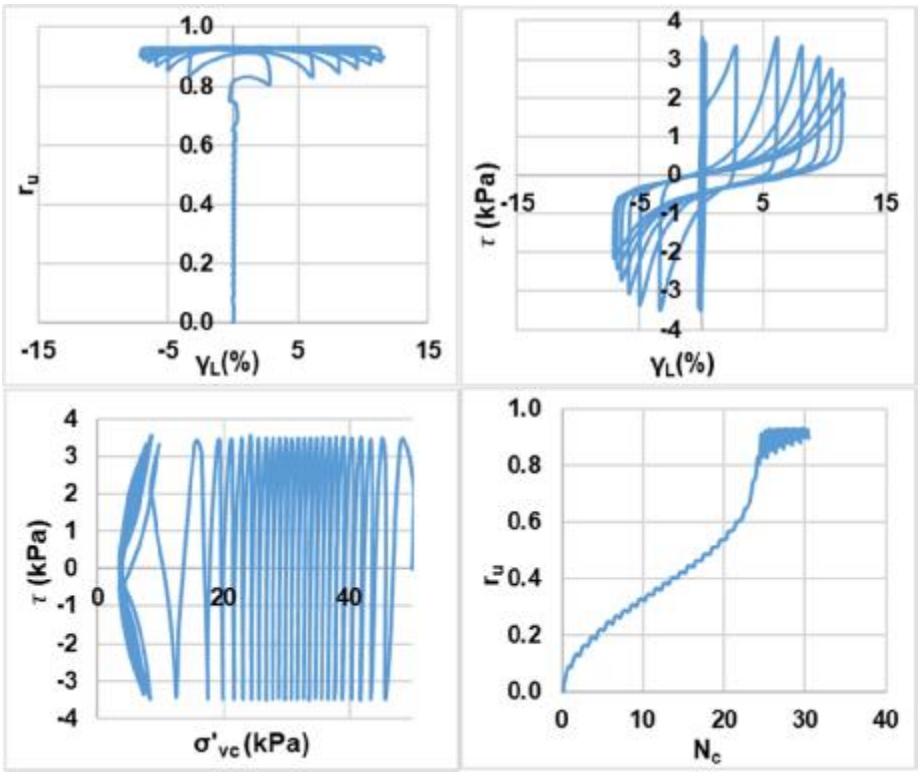


Monodirectional; $D_{rc}$ = 65%; $\sigma'_{vc}$ = 50 kPa; CSR = 0.07 (Liquefaction)

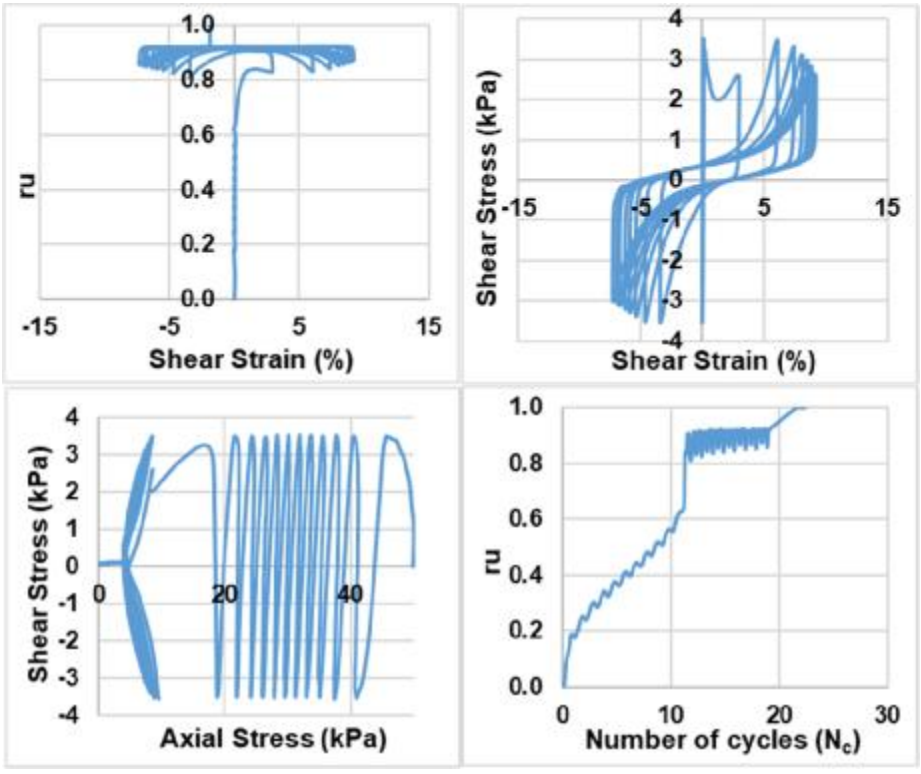


Monodirectional; $D_{rc}$ = 65%; $\sigma'_{vc}$ = 50 kPa; CSR = 0.07 (Re-liquefaction)

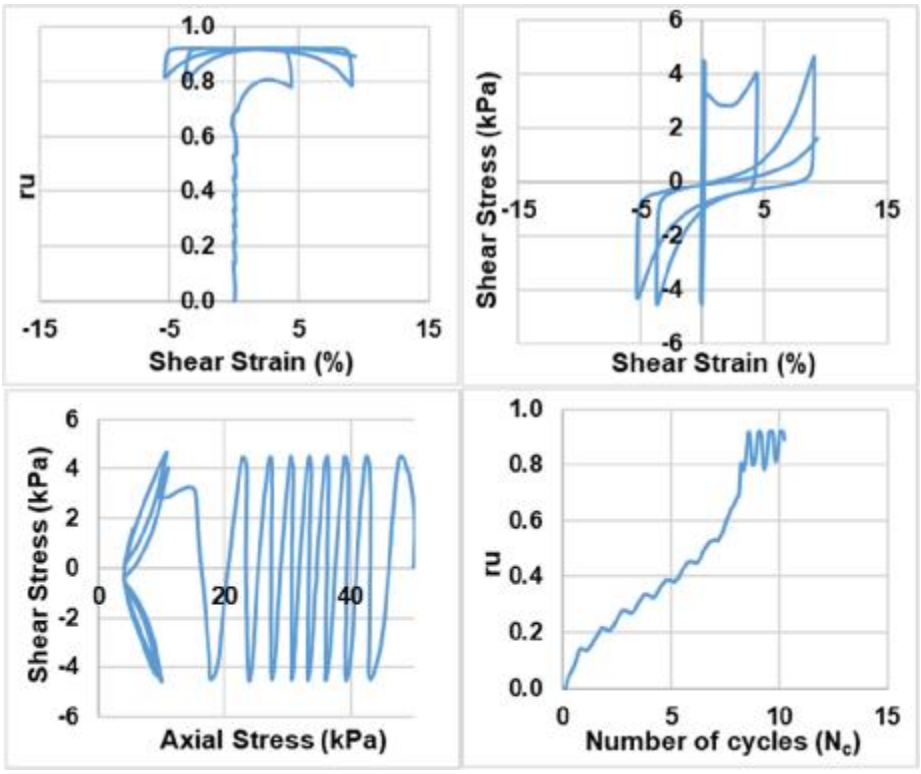


Monodirectional; $D_{rc}$ = 65%; $\sigma'_{vc}$ = 50 kPa; CSR = 0.09 (Liquefaction)

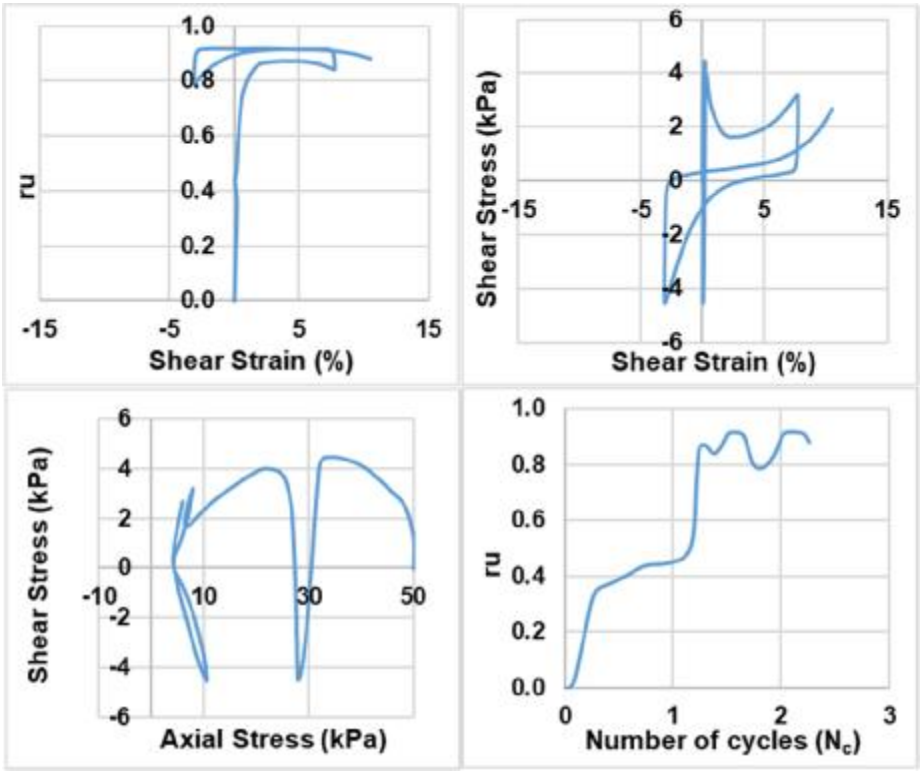


Monodirectional; $D_{rc}$ = 65%; $\sigma'_{vc}$ = 50 kPa; CSR = 0.09 (Re-liquefaction)

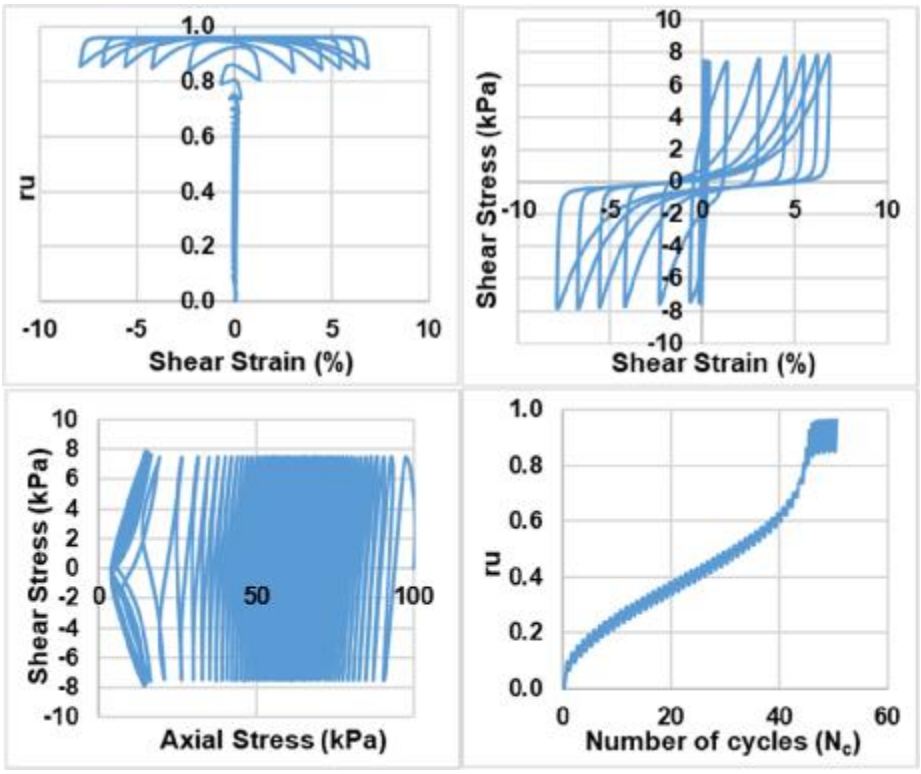


Monodirectional; $D_{rc}$ = 65%; $\sigma'_{vc}$ = 100 kPa; CSR = 0.075 (Liquefaction)

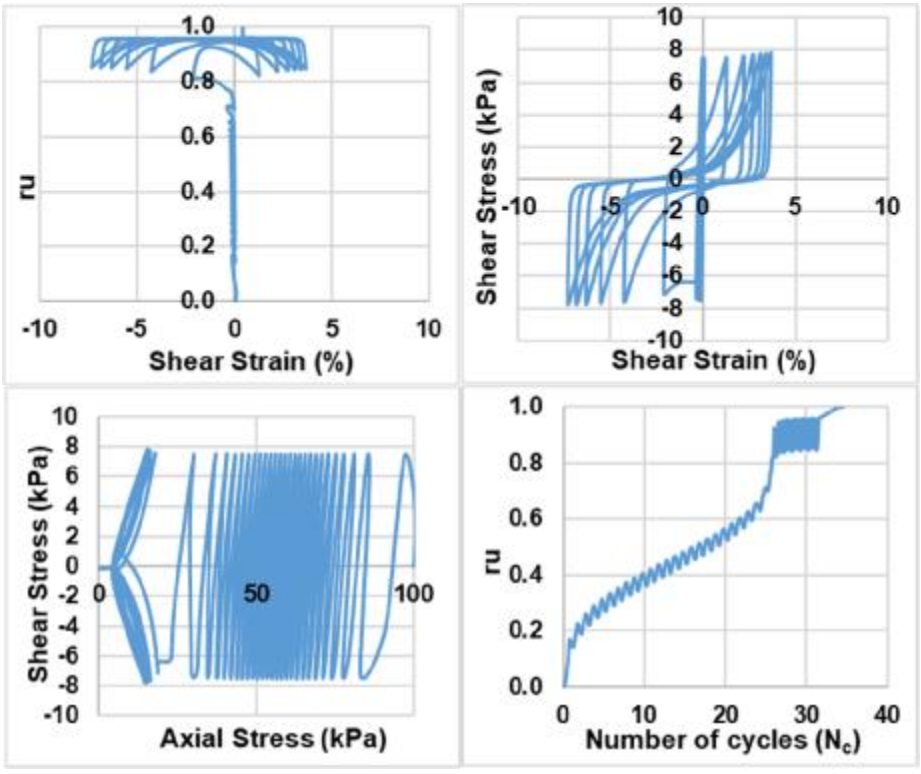


Monodirectional; $D_{rc}$ = 65%; $\sigma'_{vc}$ = 100 kPa; CSR = 0.075 (Re-liquefaction)

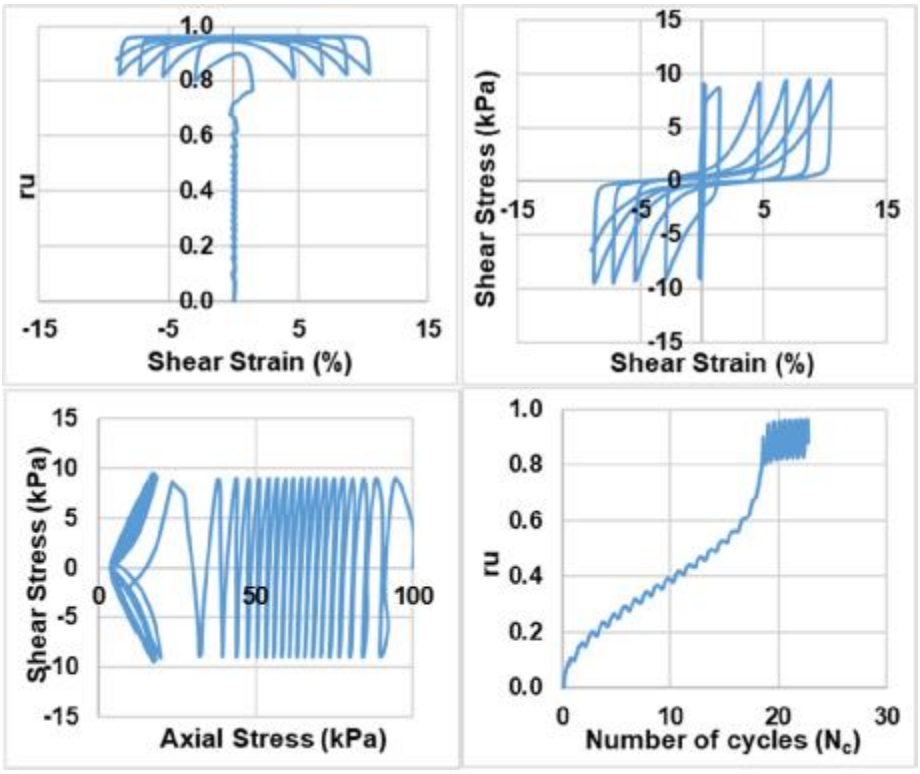


Monodirectional; $D_{rc}$ = 65%; $\sigma'_{vc}$ = 100 kPa; CSR = 0.09 (Liquefaction)

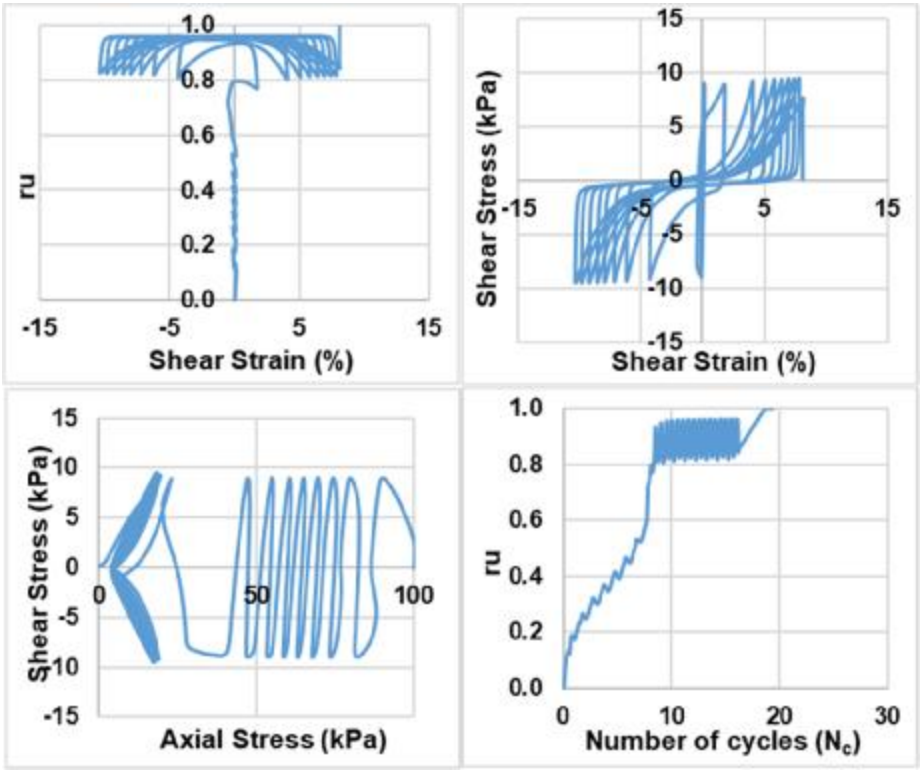


Monodirectional; $D_{rc}$ = 65%; $\sigma'_{vc}$ = 100 kPa; CSR = 0.09 (Re-liquefaction)

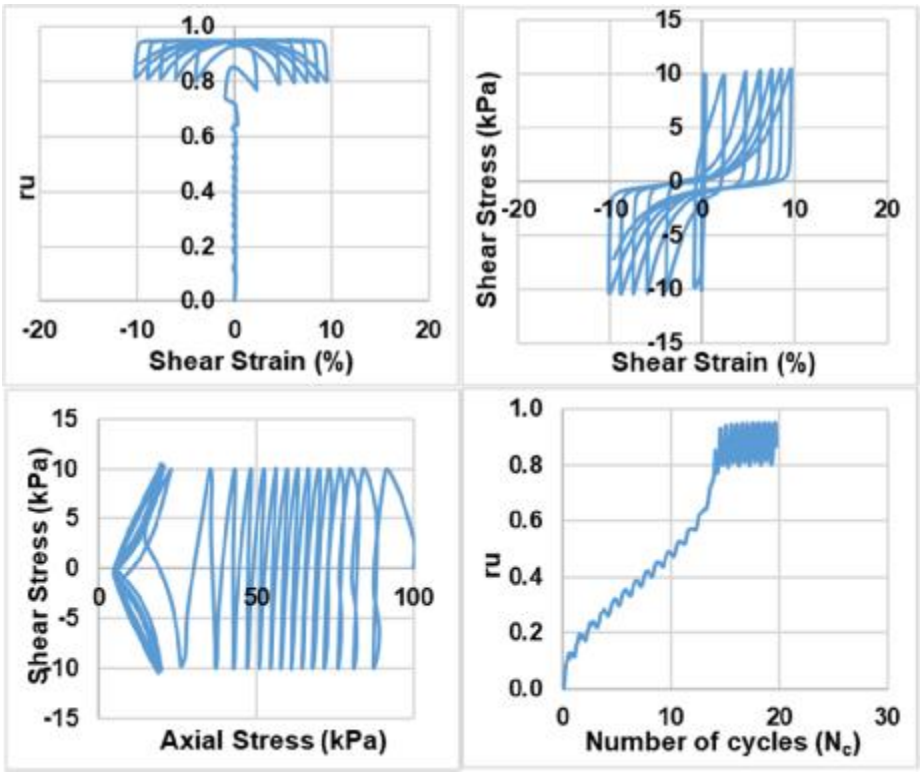


Monodirectional; $D_{rc}$ = 65%; $\sigma'_{vc}$ = 100 kPa; CSR = 0.1 (Liquefaction)

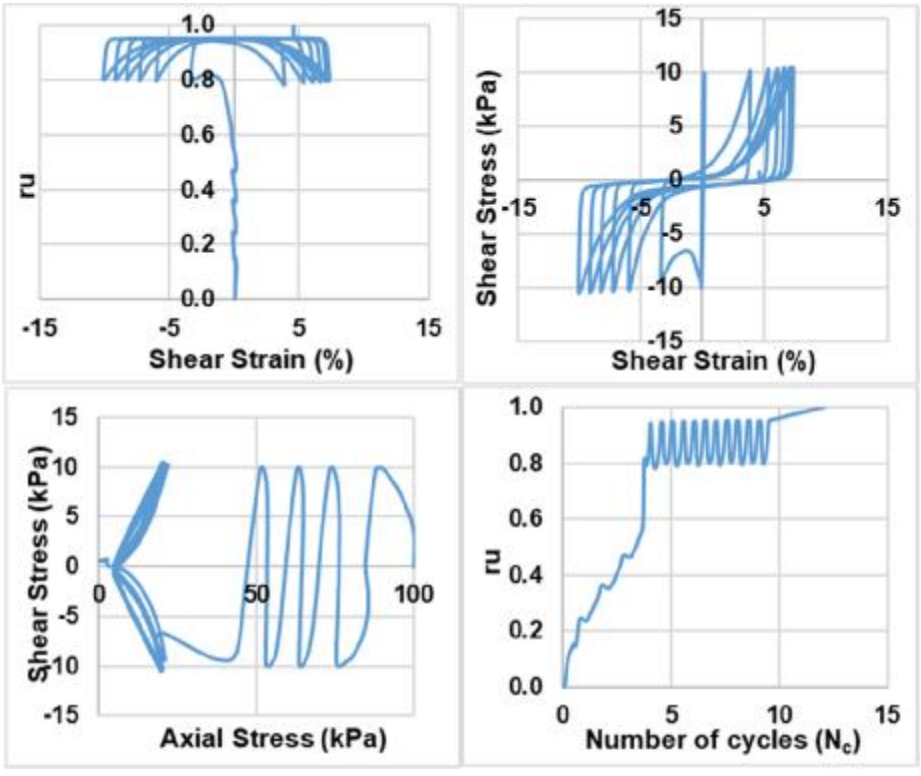


Monodirectional; $D_{rc}$ = 65%; $\sigma'_{vc}$ = 100 kPa; CSR = 0.1 (Re-liquefaction)

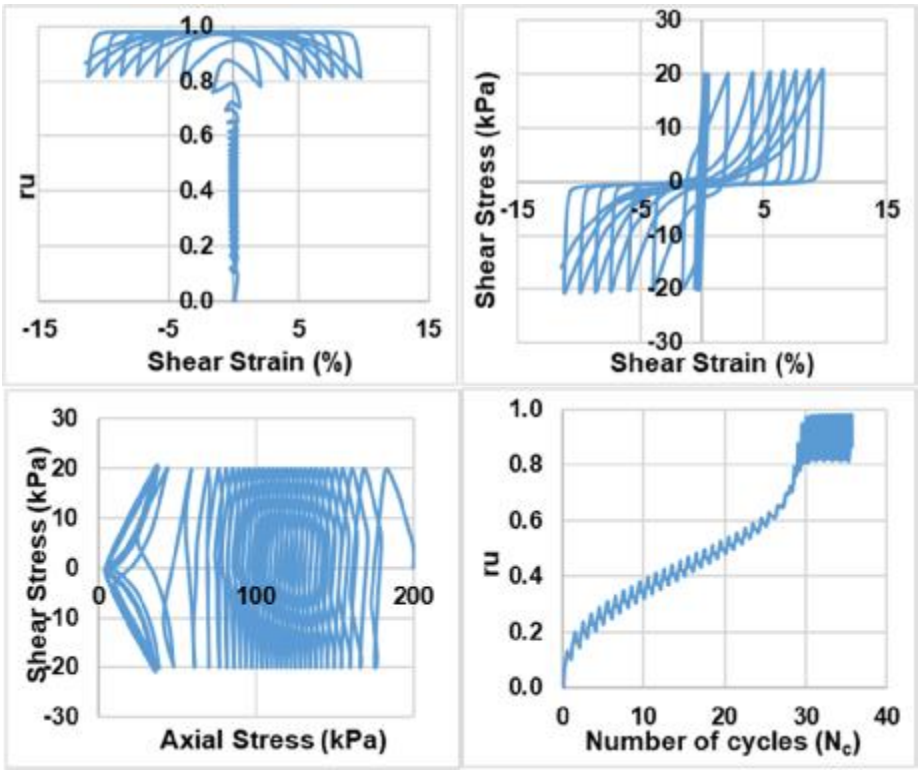


Monodirectional; $D_{rc}$ = 65%; $\sigma'_{vc}$ = 200 kPa; CSR = 0.1 (Liquefaction)

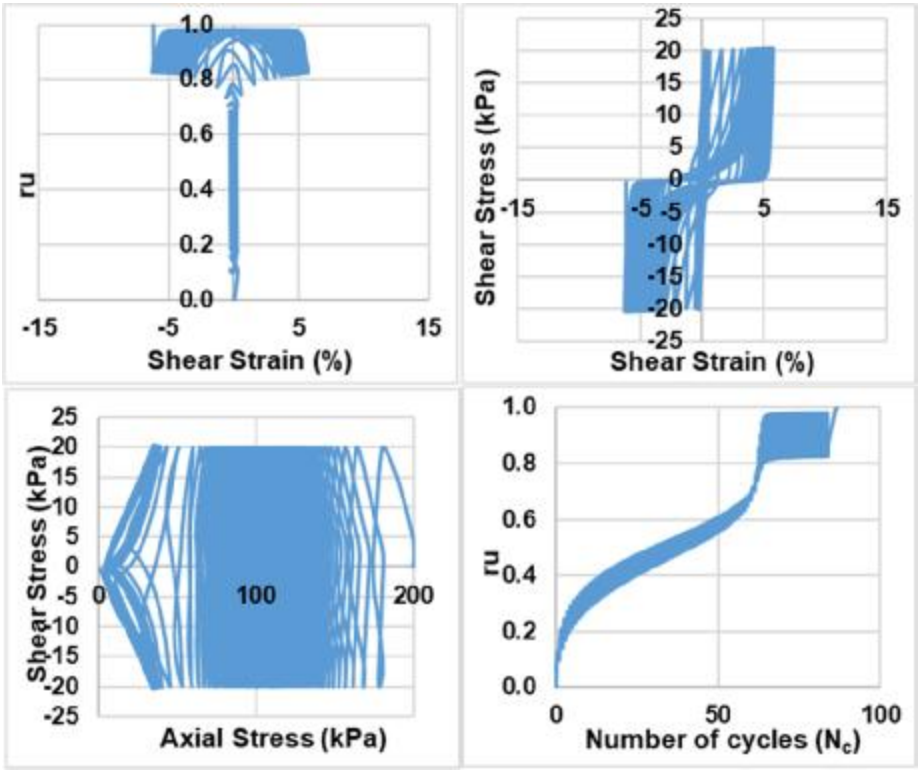


Monodirectional; $D_{rc}$ = 65%; $\sigma'_{vc}$ = 200 kPa; CSR = 0.1 (Re-liquefaction)

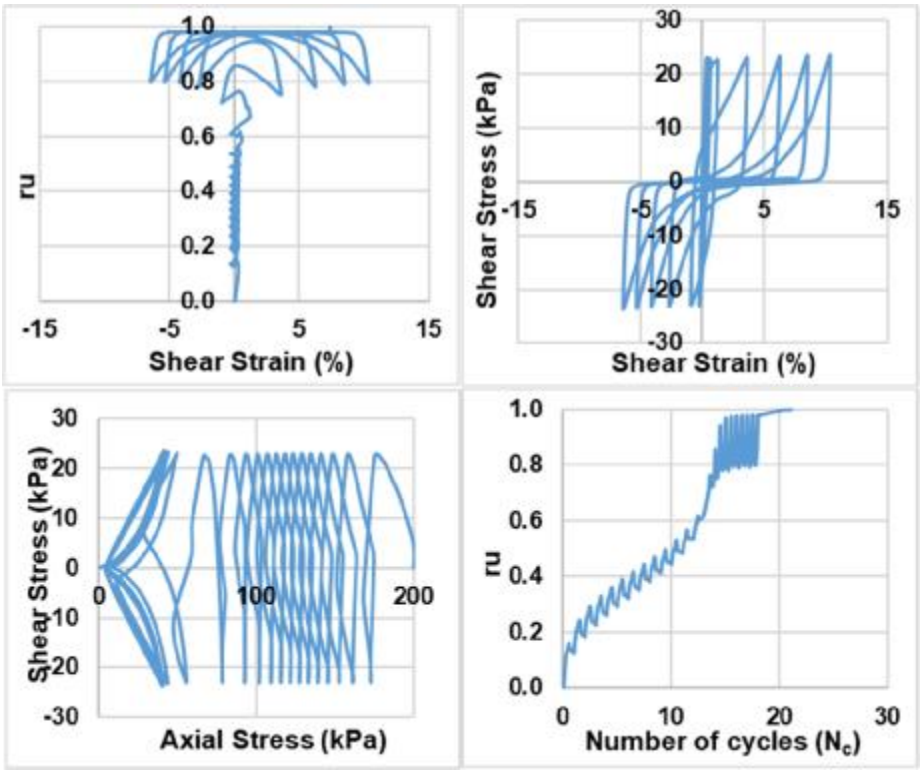


Monodirectional; $D_{rc}$ = 65%; $\sigma'_{vc}$ = 200 kPa; CSR = 0.115 (Liquefaction)

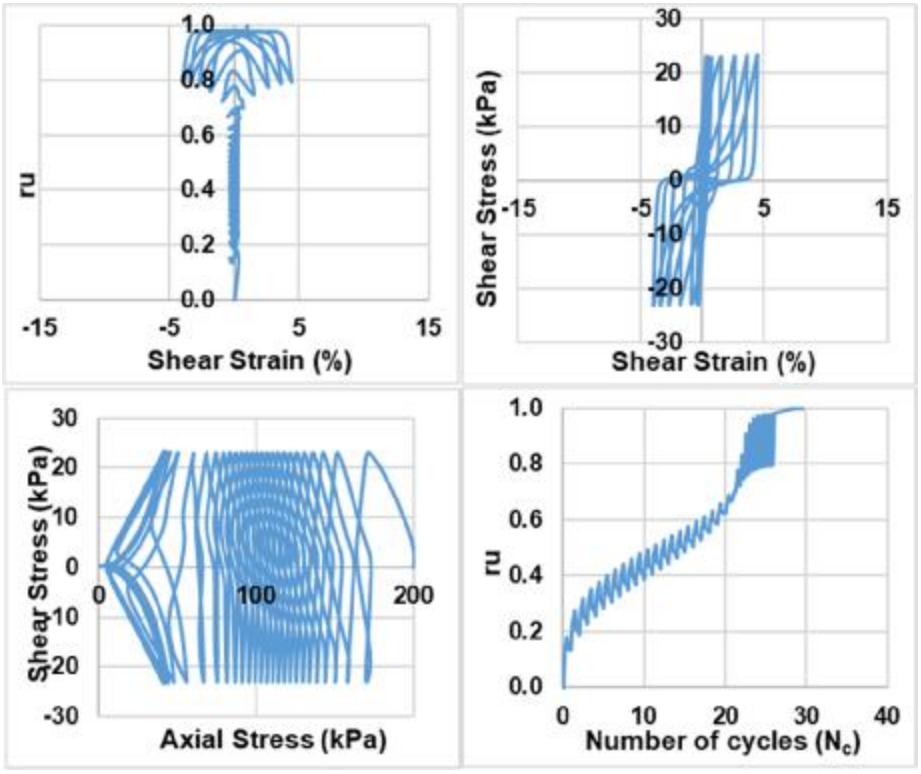


Monodirectional; $D_{rc}$ = 65%; $\sigma'_{vc}$ = 200 kPa; CSR = 0.115 (Re-liquefaction)

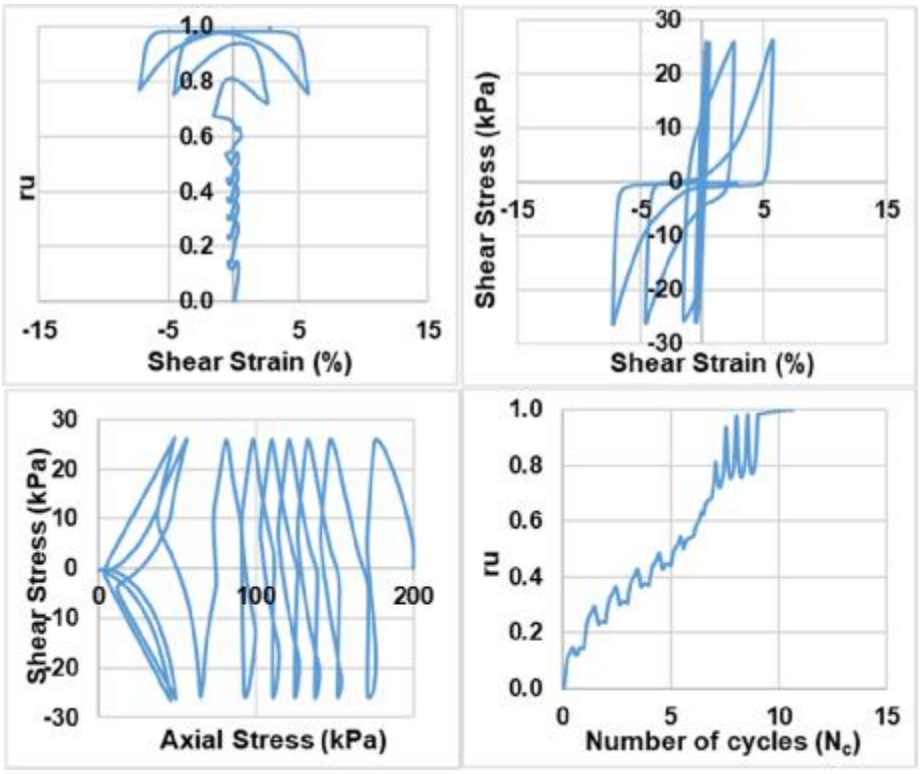


Monodirectional; $D_{rc}$ = 65%; $\sigma'_{vc}$ = 200 kPa; CSR = 0.13 (Liquefaction)

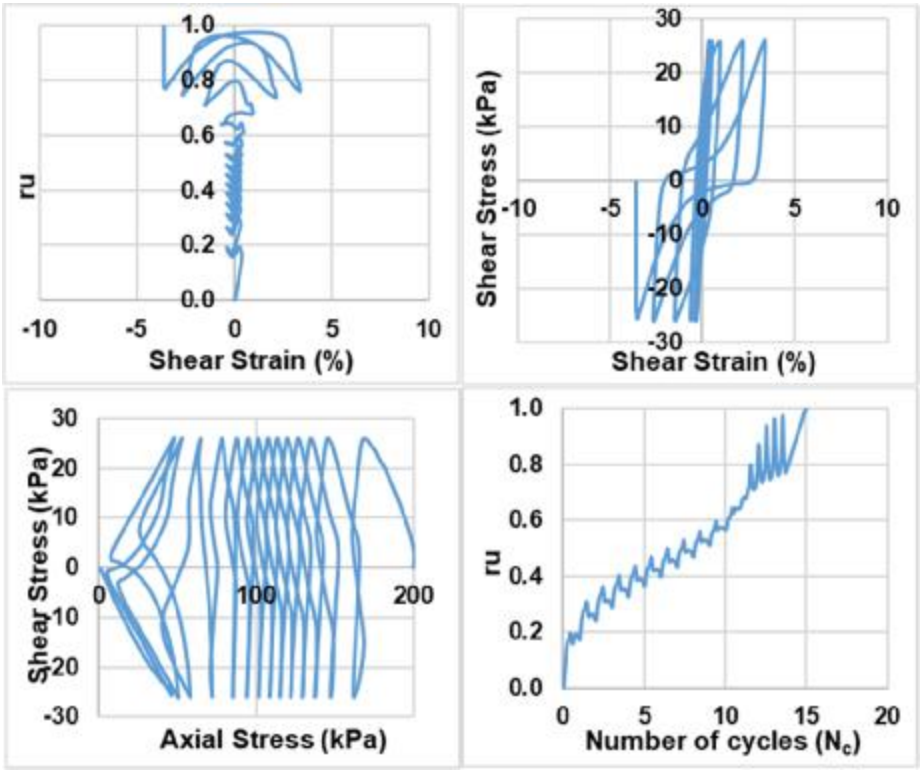


Monodirectional; $D_{rc}$ = 65%; $\sigma'_{vc}$ = 200 kPa; CSR = 0.13 (Re-liquefaction)

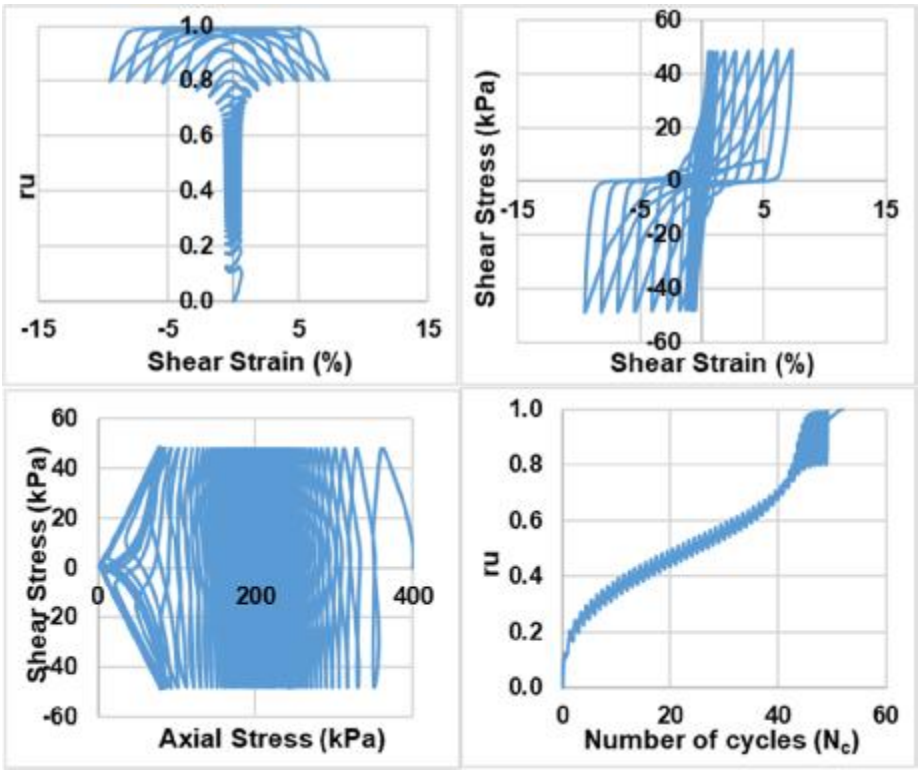


Monodirectional; $D_{rc}$ = 65%; $\sigma'_{vc}$ = 400 kPa; CSR = 0.12 (Liquefaction)

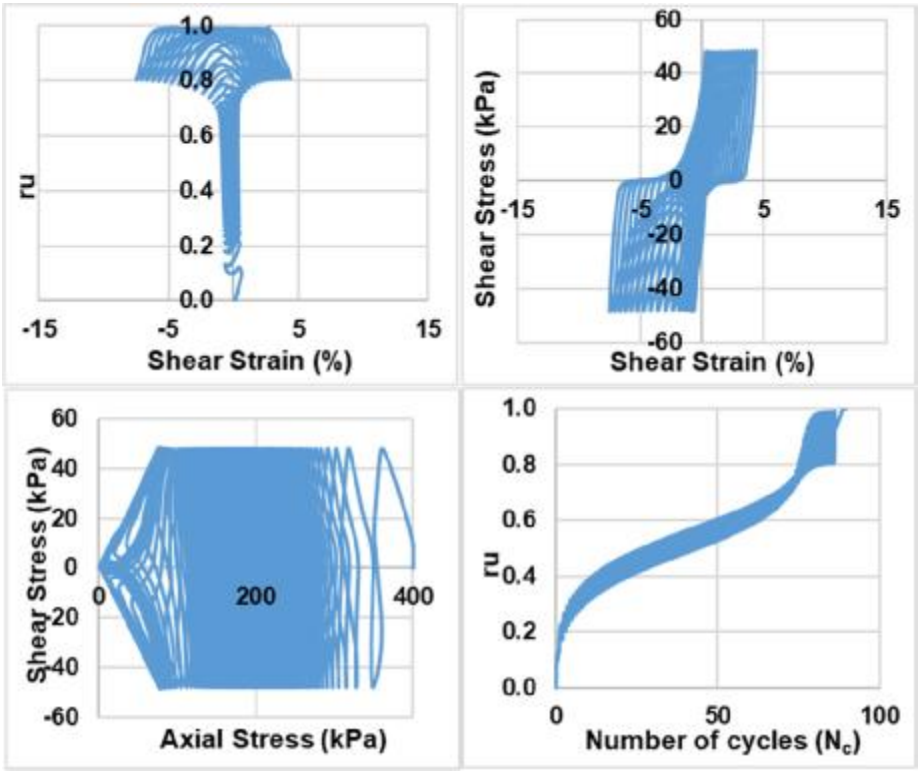


Monodirectional; $D_{rc}$ = 65%; $\sigma'_{vc}$ = 400 kPa; CSR = 0.12 (Re-liquefaction)

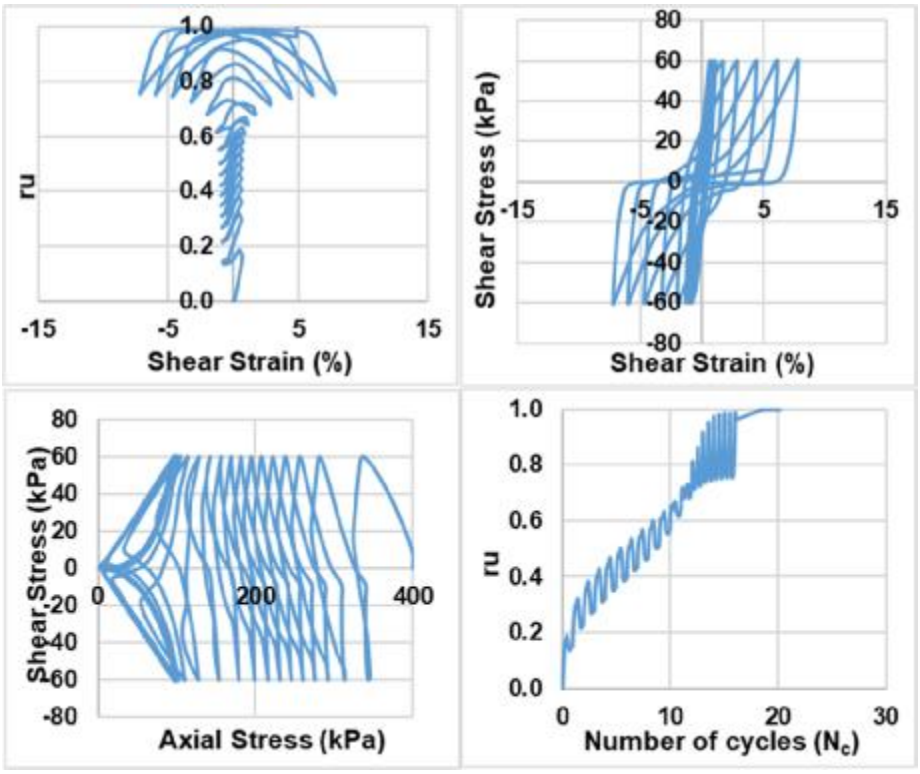


Monodirectional; $D_{rc}$ = 65%; $\sigma'_{vc}$ = 400 kPa; CSR = 0.15 (Liquefaction)

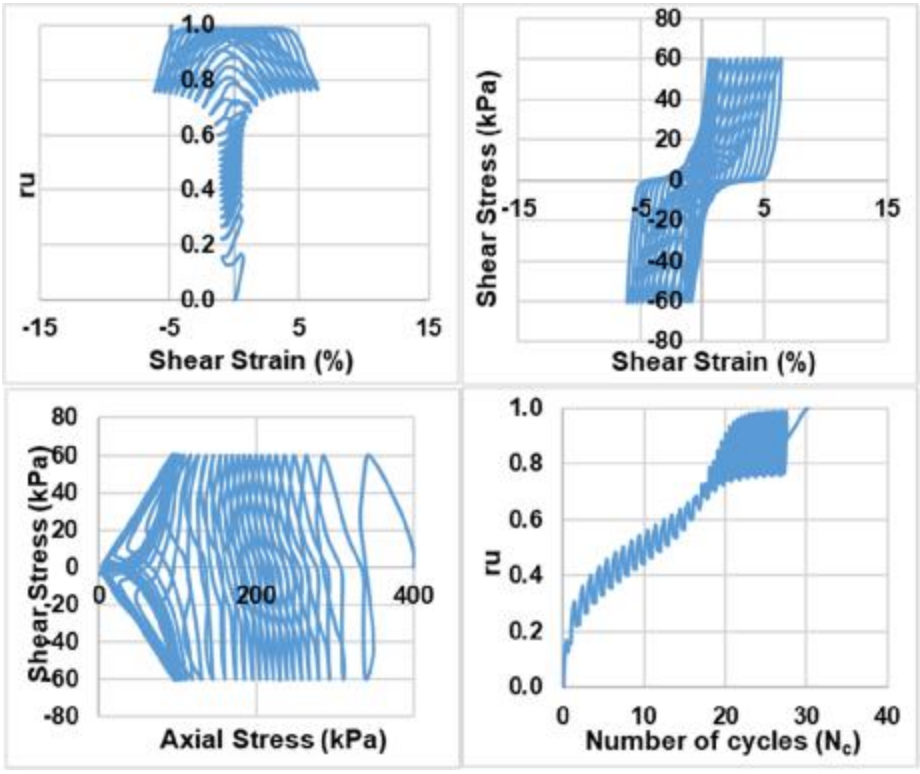


Monodirectional; $D_{rc}$ = 65%; $\sigma'_{vc}$ = 400 kPa; CSR = 0.15 (Re-liquefaction)

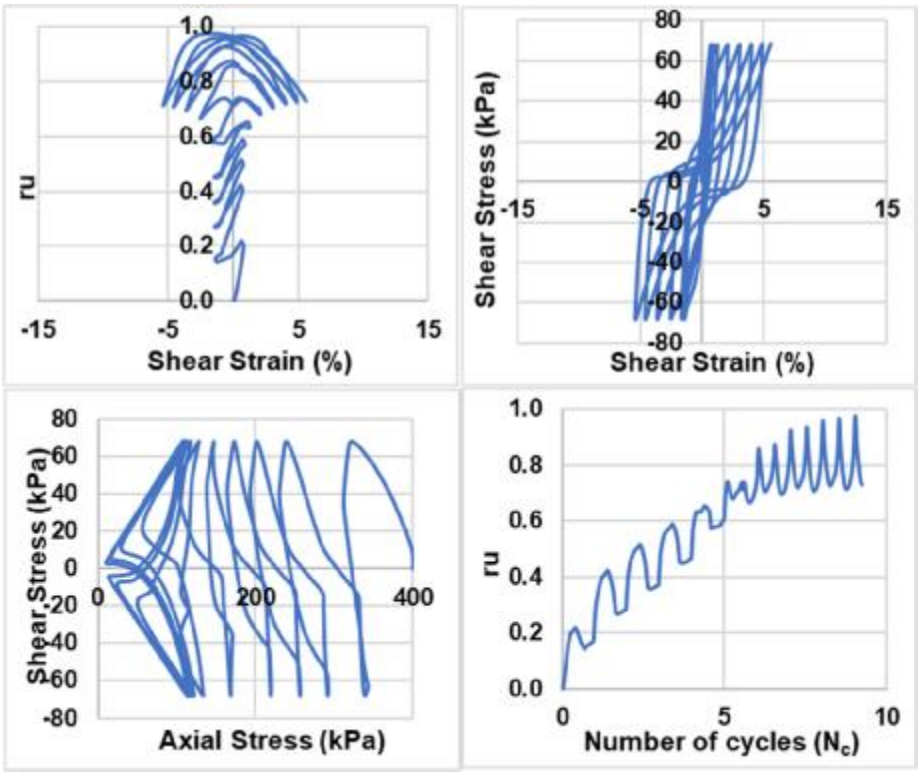


Monodirectional; $D_{rc}$ = 65%; $\sigma'_{vc}$ = 400 kPa; CSR = 0.17 (Liquefaction)

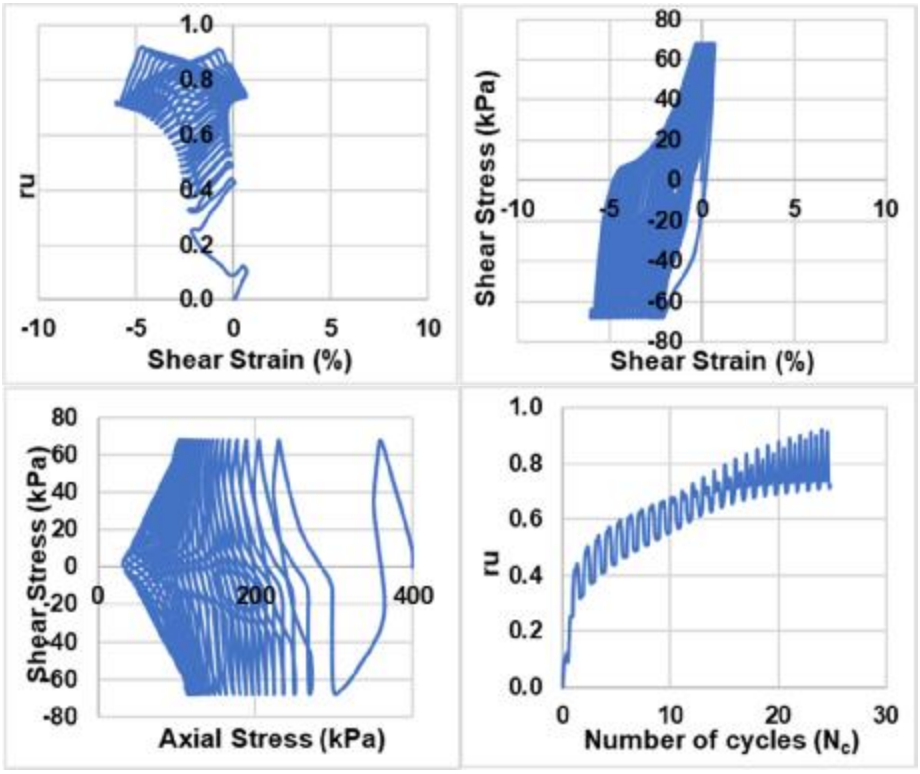


Monodirectional; $D_{rc}$ = 65%; $\sigma'_{vc}$ = 400 kPa; CSR = 0.17 (Re-liquefaction)

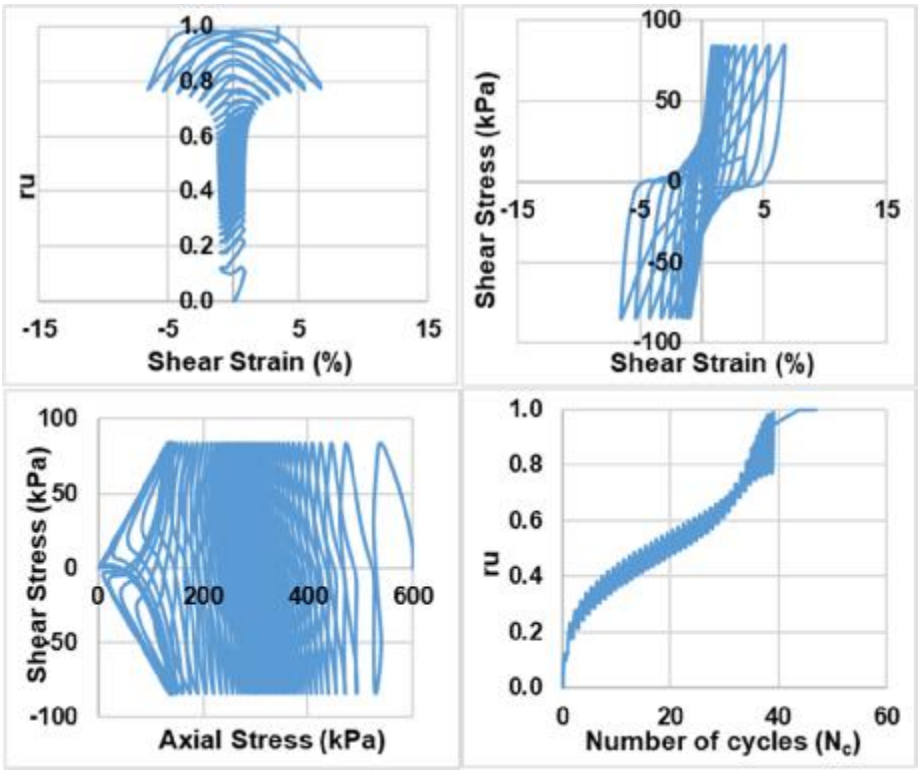


Monodirectional; $D_{rc}$ = 65%; $\sigma'_{vc}$ = 600 kPa; CSR = 0.14 (Liquefaction)

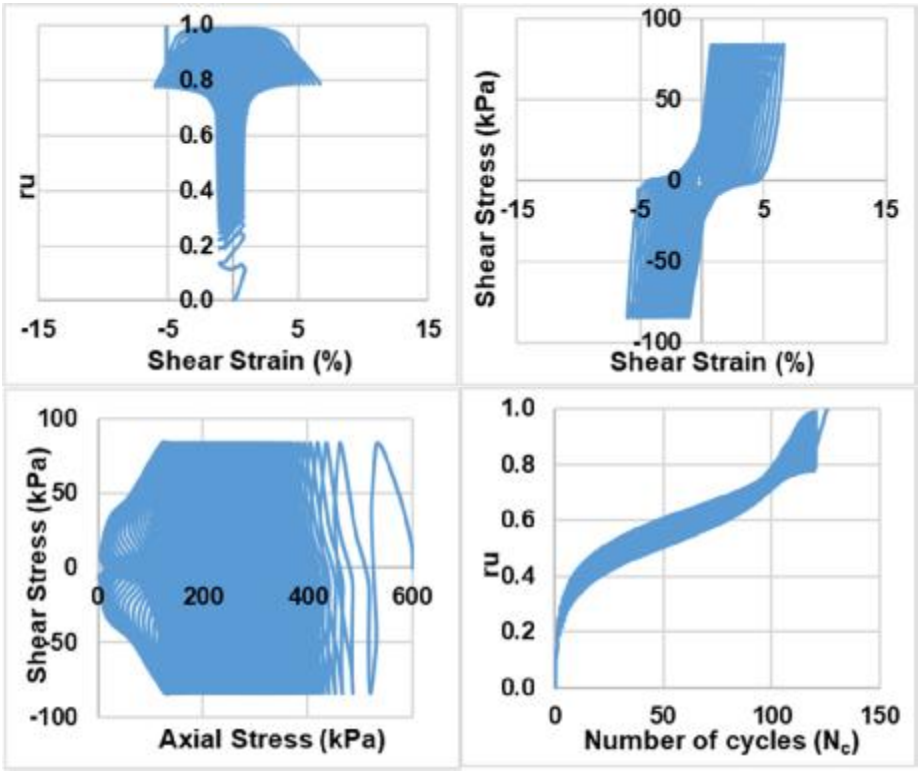


Monodirectional; $D_{rc}$ = 65%; $\sigma'_{vc}$ = 600 kPa; CSR = 0.14 (Re-liquefaction)

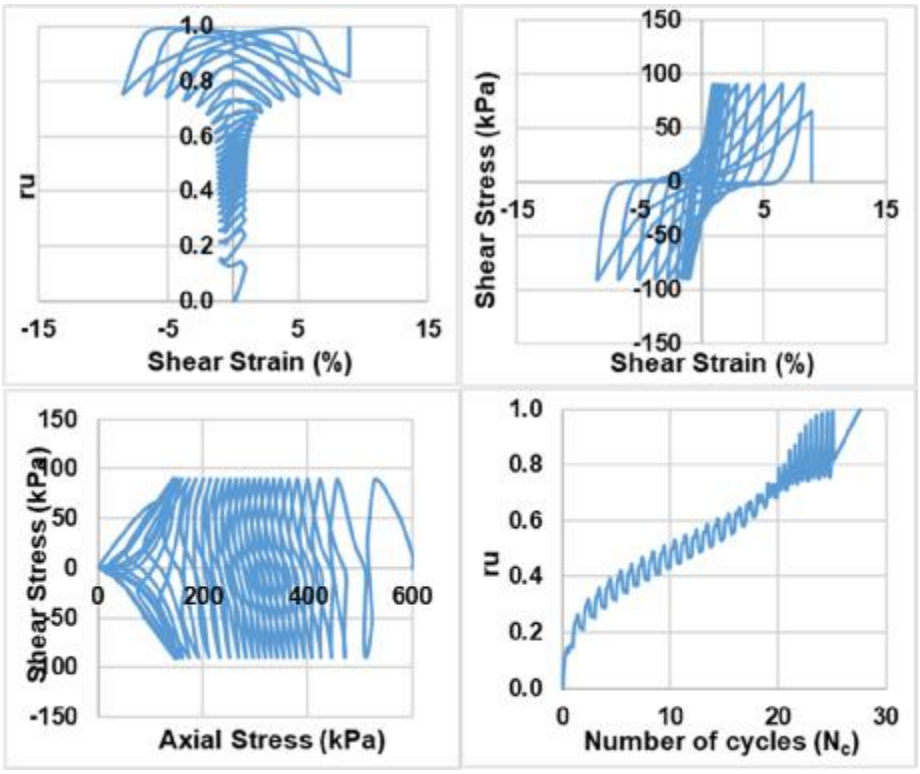


Monodirectional; $D_{rc}$ = 65%; $\sigma'_{vc}$ = 600 kPa; CSR = 0.15 (Liquefaction)

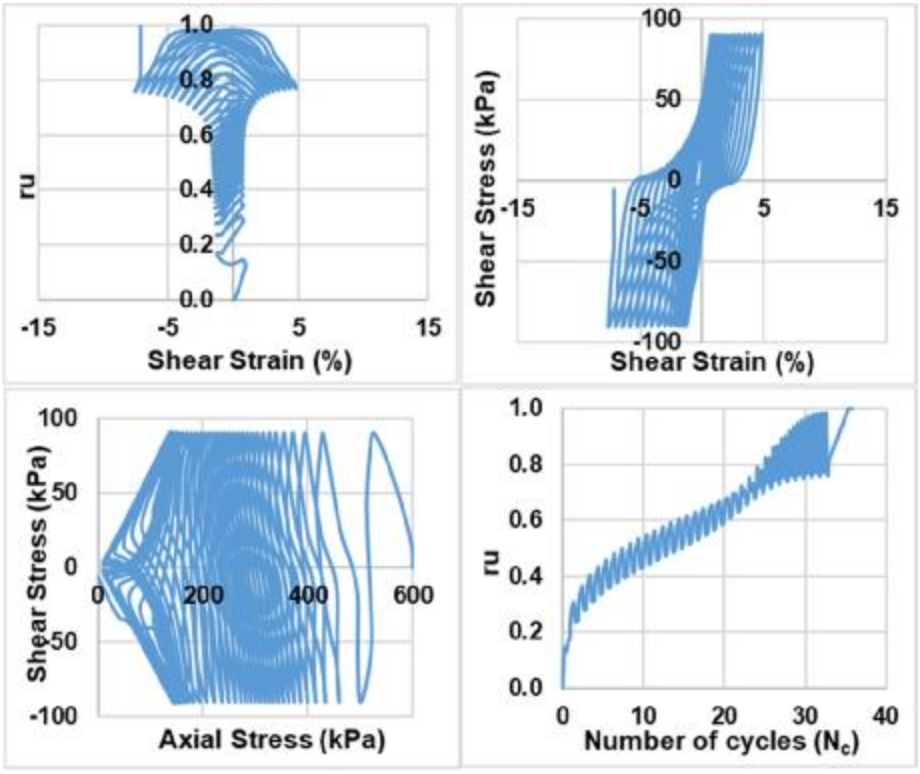


Monodirectional; $D_{rc}$ = 65%; $\sigma'_{vc}$ = 600 kPa; CSR = 0.15 (Re-liquefaction)

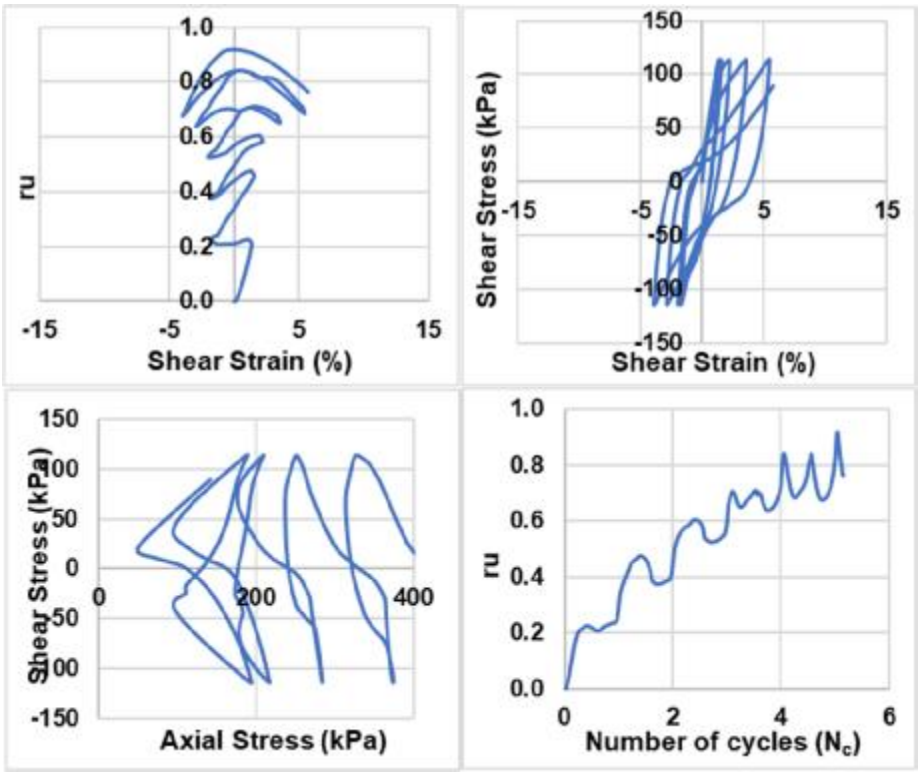


Monodirectional; $D_{rc}$ = 65%; $\sigma'_{vc}$ = 600 kPa; CSR = 0.19 (Liquefaction)

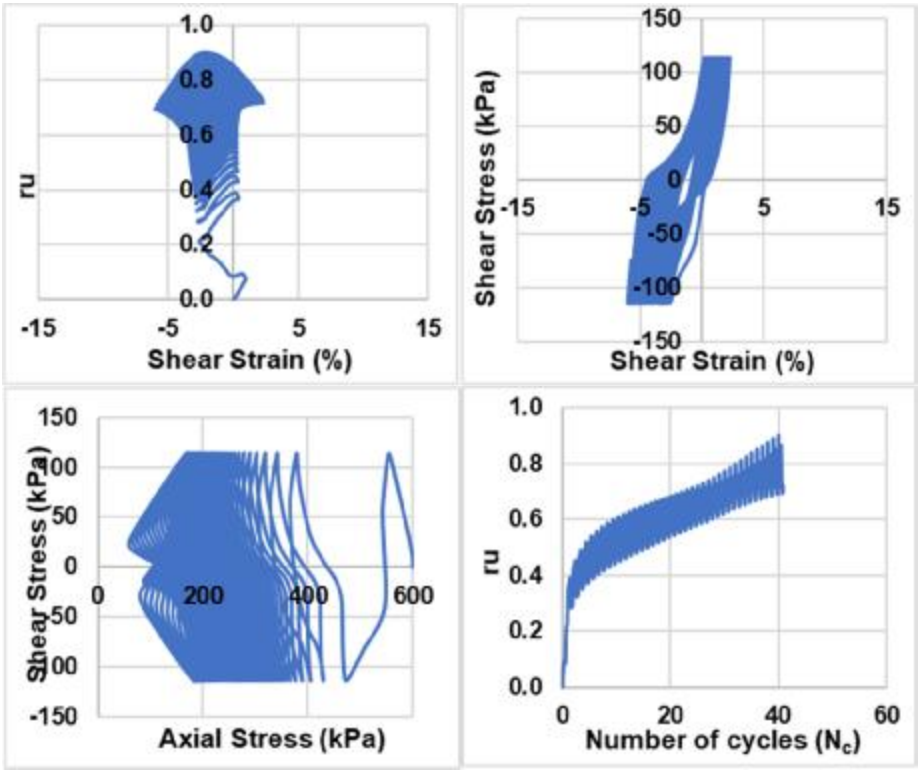


Monodirectional; $D_{rc}$ = 65%; $\sigma'_{vc}$ = 600 kPa; CSR = 0.19 (Re-liquefaction)

# Appendix 2

Bi-directional / Circular Cyclic Simple Shear Test Results

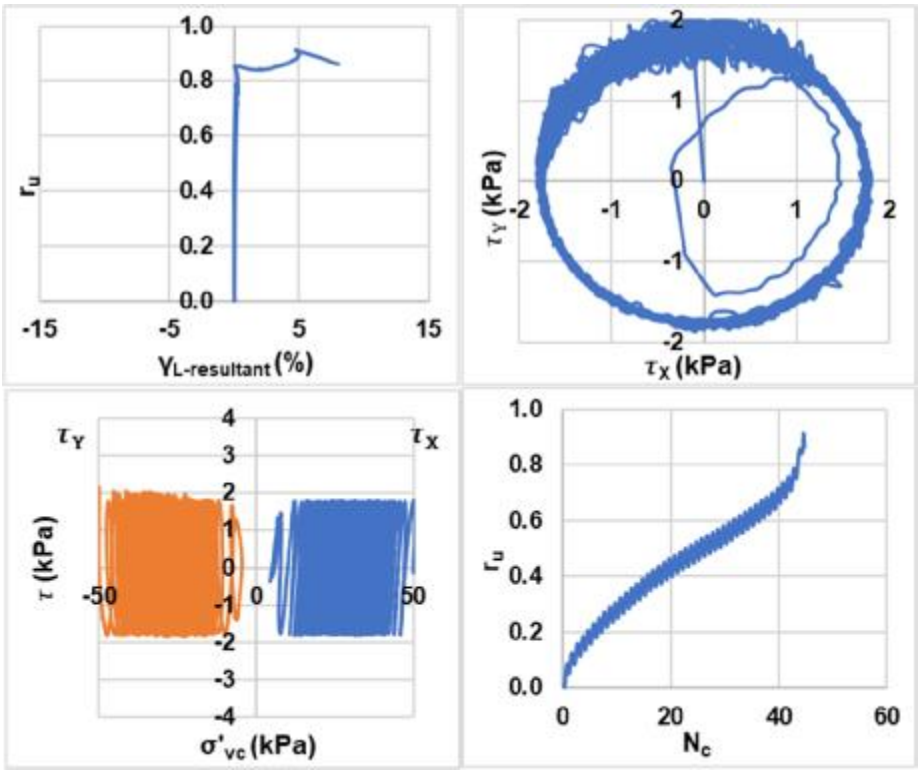


Bi-directional (Circular); $D_{rc}$ = 25%; $\sigma'_{vc}$ = 50 kPa; CSR = 0.04 (Liquefaction)

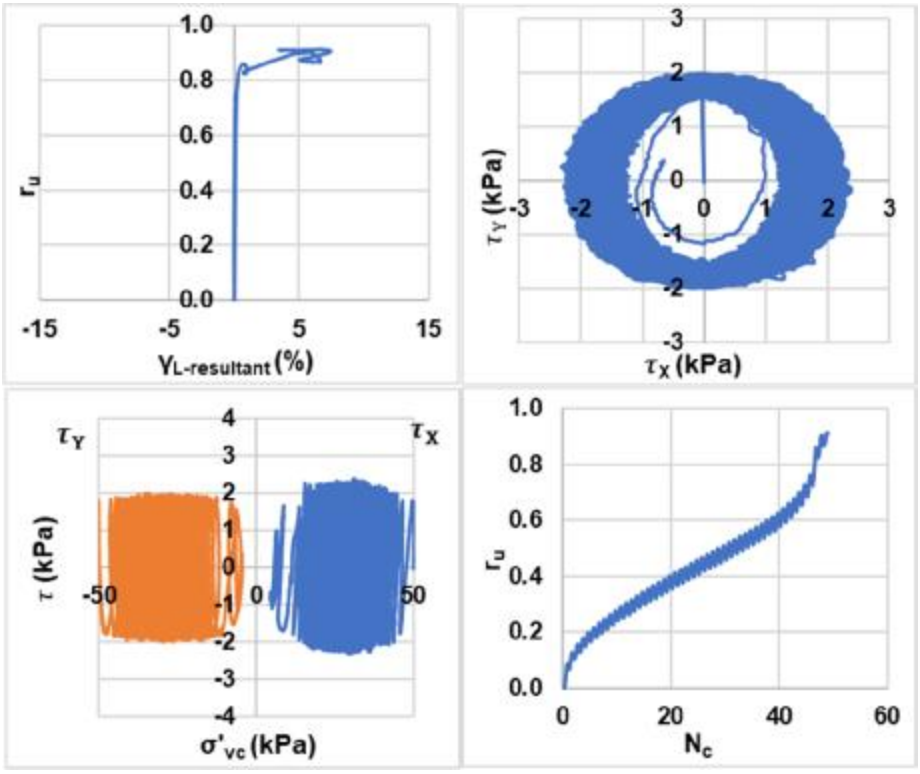


Bi-directional (Circular); $D_{rc}$ = 25%; $\sigma'_{vc}$ = 50 kPa; CSR = 0.04 (Re-liquefaction)

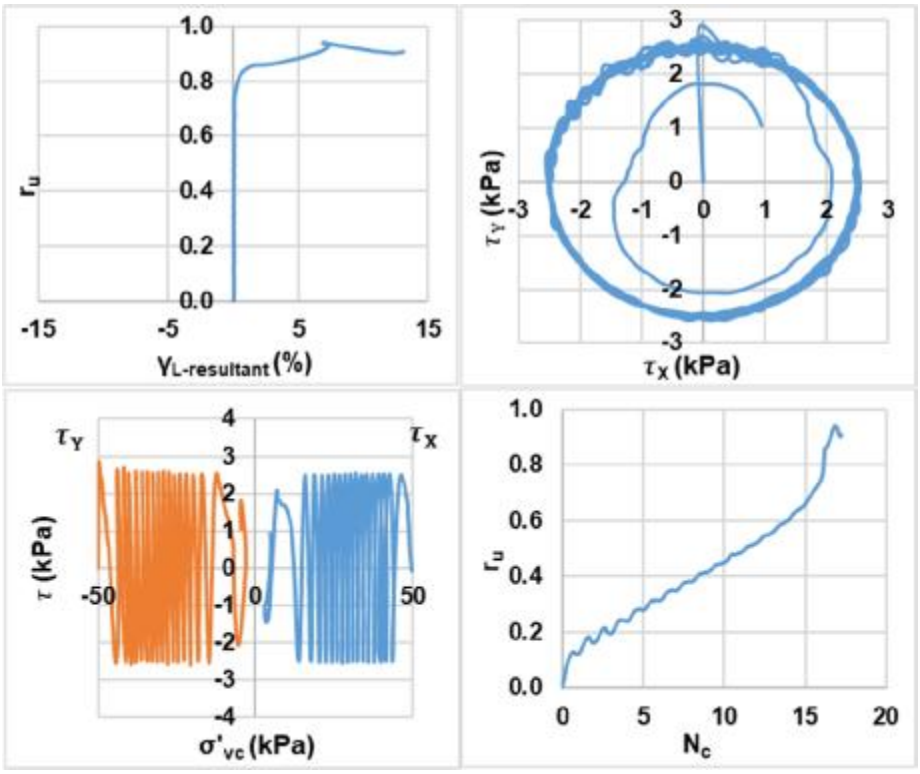


Bi-directional (Circular); $D_{rc}$ = 25%; $\sigma'_{vc}$ = 50 kPa; CSR = 0.05 (Liquefaction)

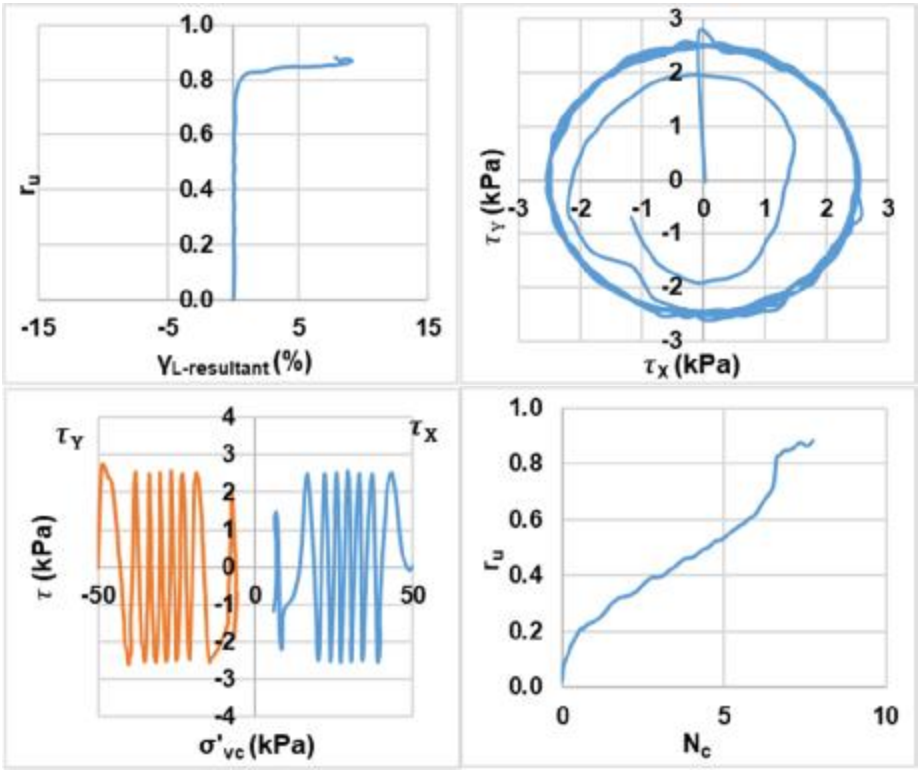


Bi-directional (Circular); $D_{rc}$ = 25%; $\sigma'_{vc}$ = 50 kPa; CSR = 0.05 (Re-liquefaction)

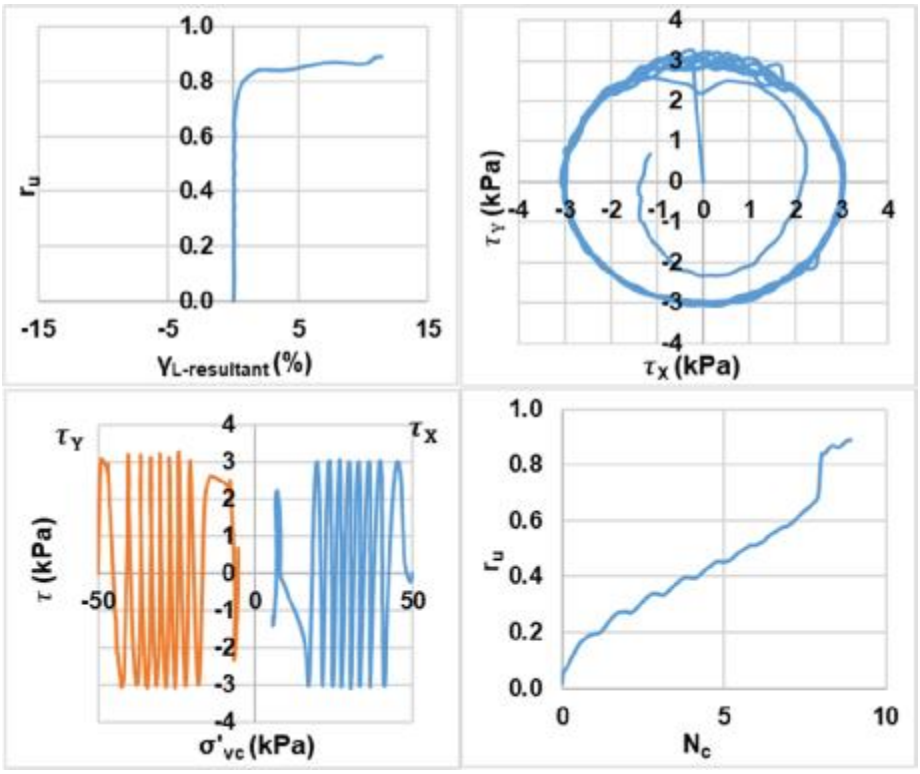


Bi-directional (Circular); $D_{rc}$ = 25%; $\sigma'_{vc}$ = 50 kPa; CSR = 0.06 (Liquefaction)

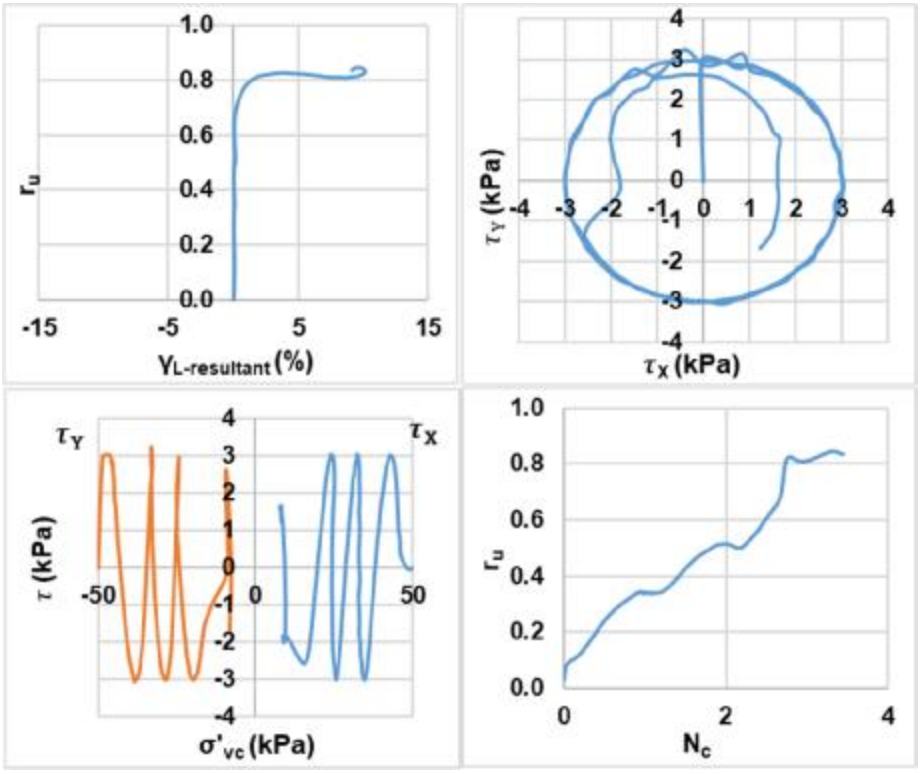


Bi-directional (Circular); $D_{rc}$ = 25%; $\sigma'_{vc}$ = 50 kPa; CSR = 0.06 (Re-liquefaction)

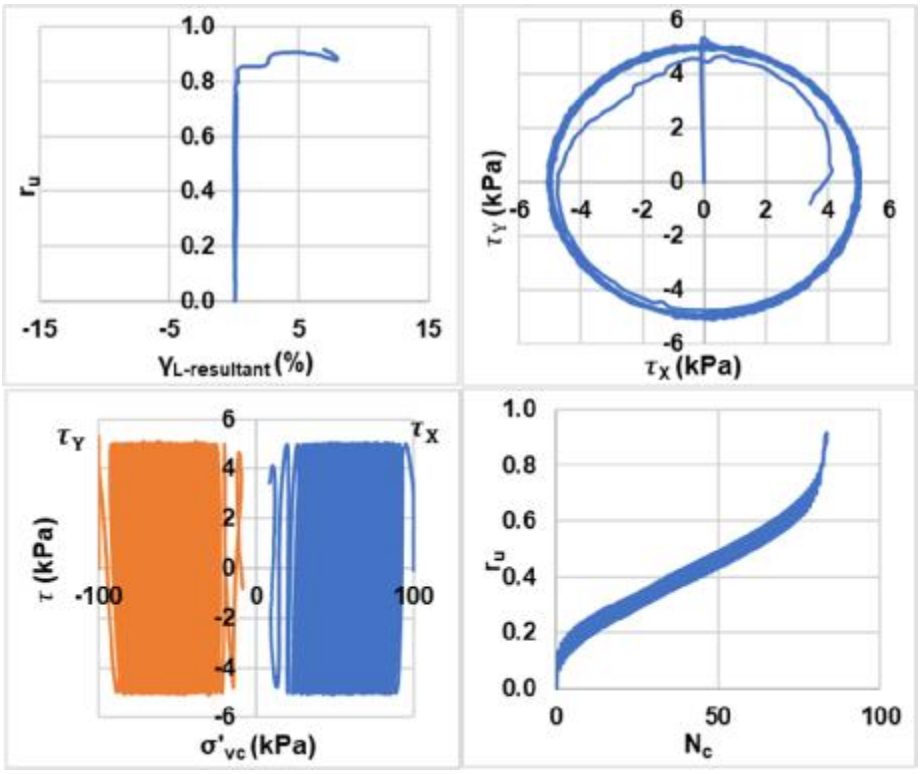


Bi-directional (Circular); $D_{rc}$ = 25%; $\sigma'_{vc}$ = 100 kPa; CSR = 0.05 (Liquefaction)

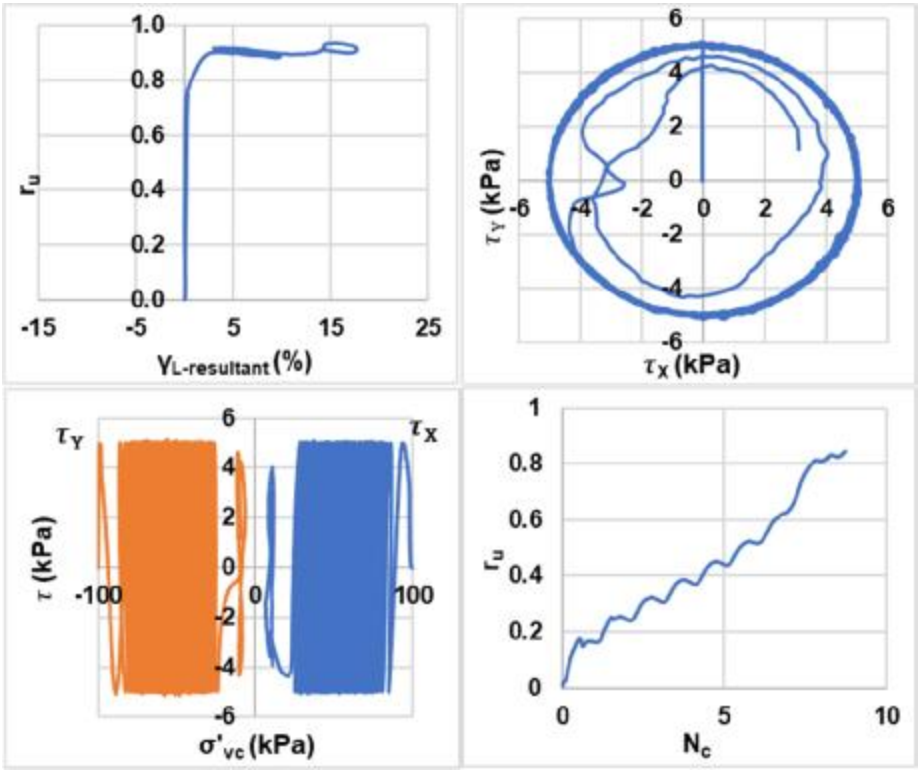


Bi-directional (Circular); $D_{rc}$ = 25%; $\sigma'_{vc}$ = 100 kPa; CSR = 0.05 (Re-liquefaction)

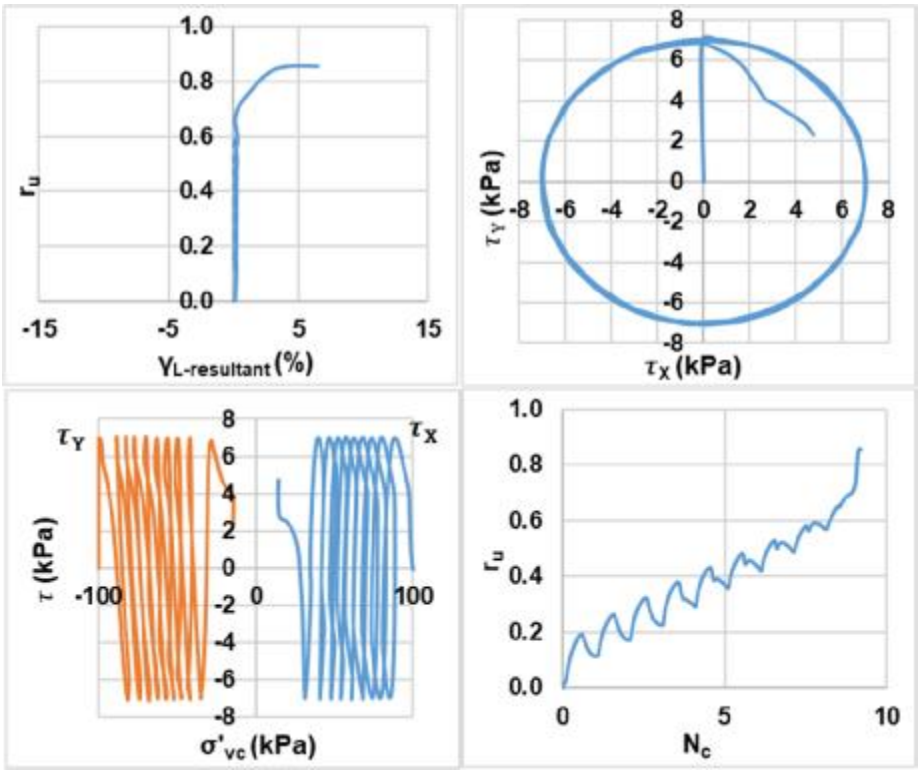


Bi-directional (Circular); $D_{rc}$ = 25%; $\sigma'_{vc}$ = 100 kPa; CSR = 0.07 (Liquefaction)

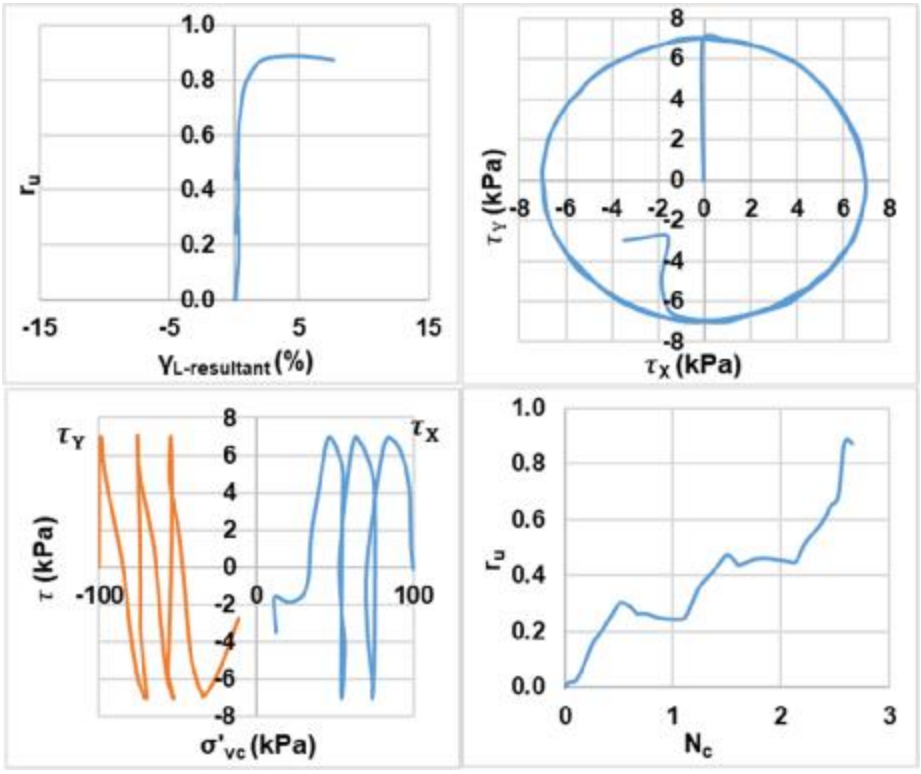


Bi-directional (Circular); $D_{rc}$ = 25%; $\sigma'_{vc}$ = 100 kPa; CSR = 0.07 (Re-liquefaction)

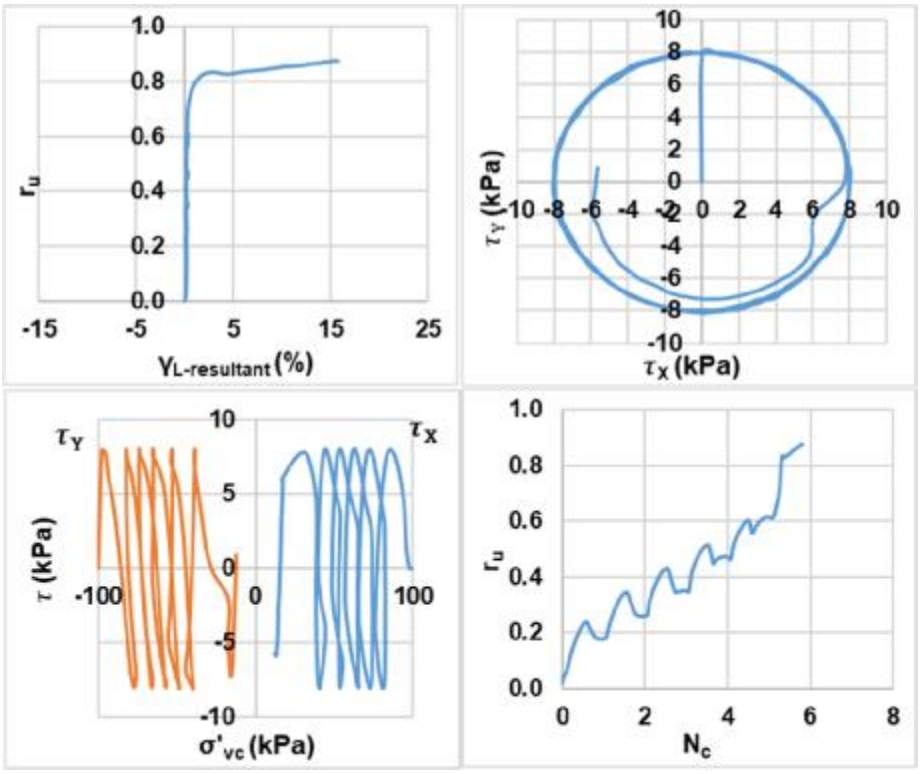


Bi-directional (Circular); $D_{rc}$ = 25%; $\sigma'_{vc}$ = 100 kPa; CSR = 0.08 (Liquefaction)

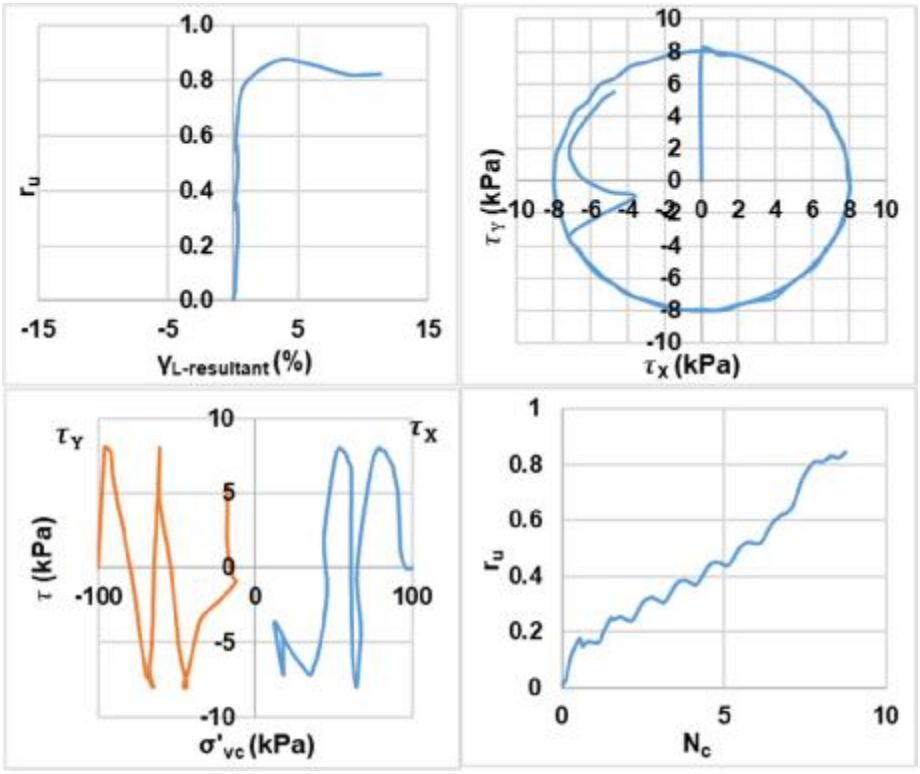


Bi-directional (Circular); $D_{rc}$ = 25%; $\sigma'_{vc}$ = 100 kPa; CSR = 0.08 (Re-liquefaction)

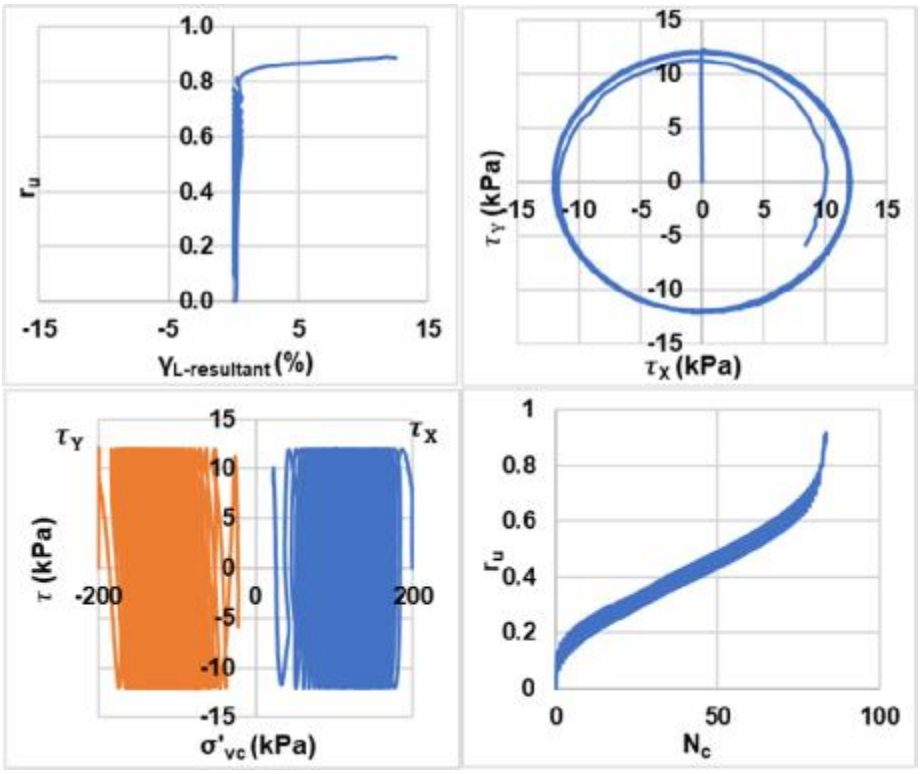


Bi-directional (Circular); $D_{rc}$ = 25%; $\sigma'_{vc}$ = 200 kPa; CSR = 0.06 (Liquefaction)

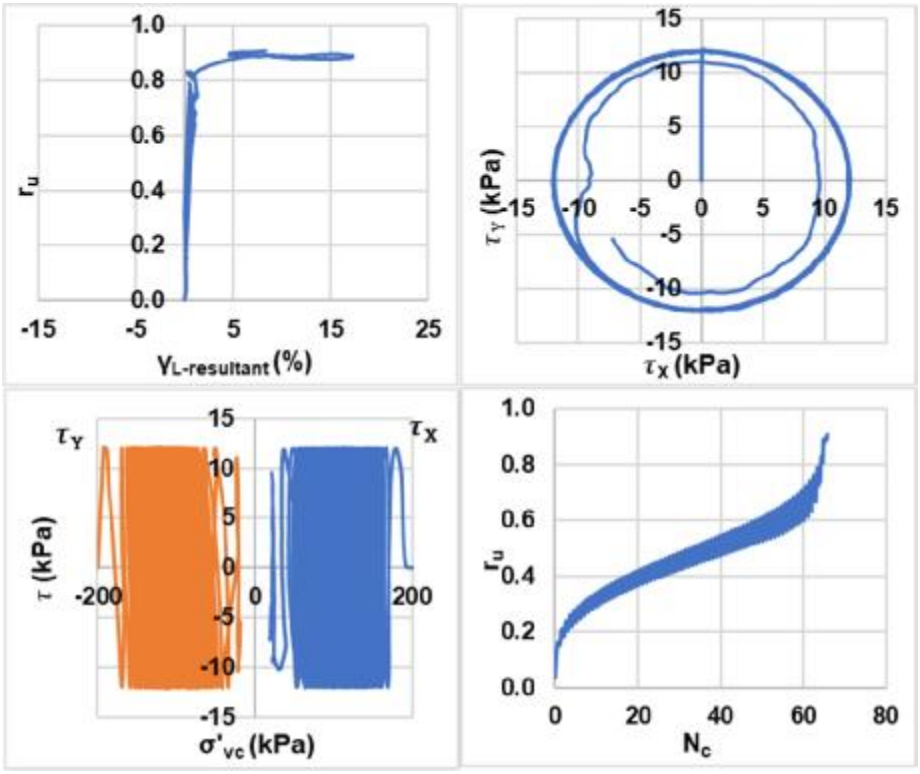


Bi-directional (Circular); $D_{rc}$ = 25%; $\sigma'_{vc}$ = 200 kPa; CSR = 0.06 (Re-liquefaction)

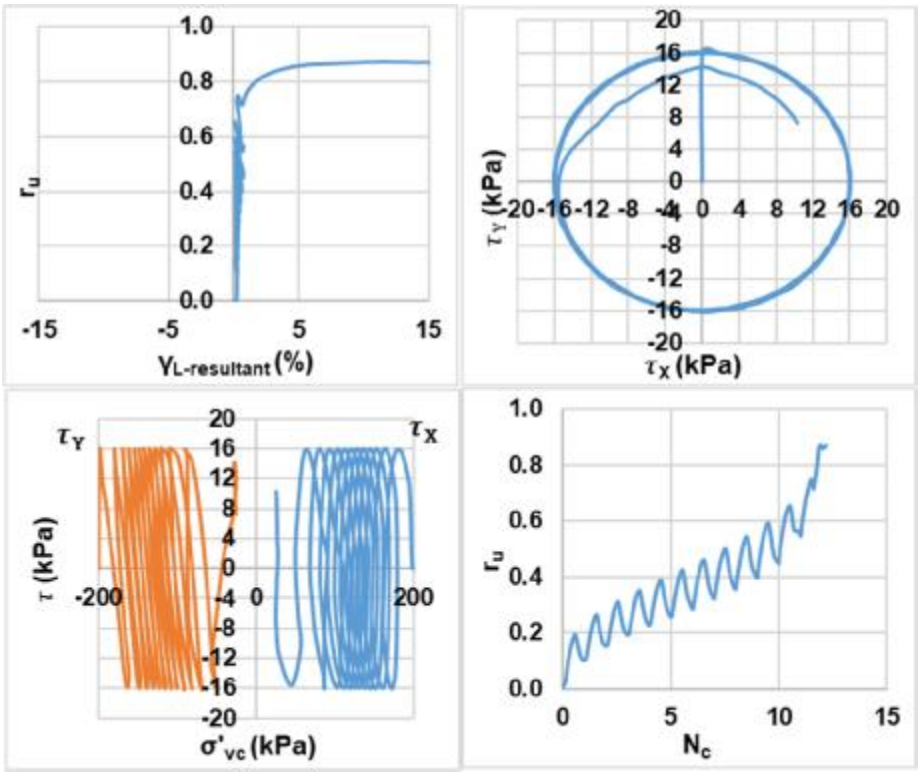


Bi-directional (Circular); $D_{rc}$ = 25%; $\sigma'_{vc}$ = 200 kPa; CSR = 0.08 (Liquefaction)

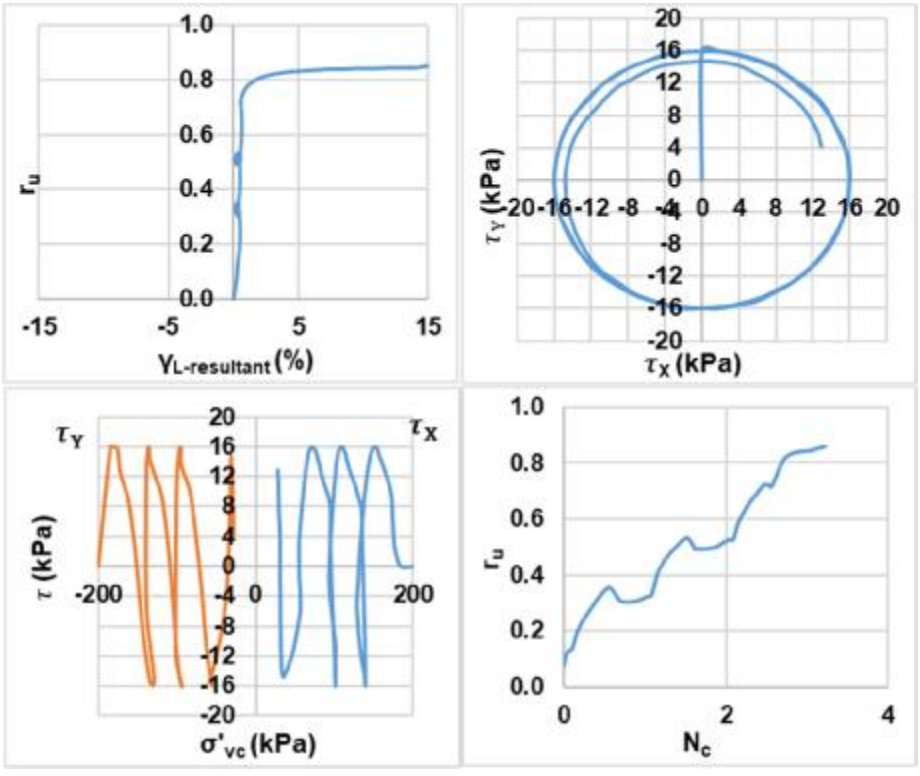


Bi-directional (Circular); $D_{rc}$ = 25%; $\sigma'_{vc}$ = 200 kPa; CSR = 0.08 (Re-liquefaction)

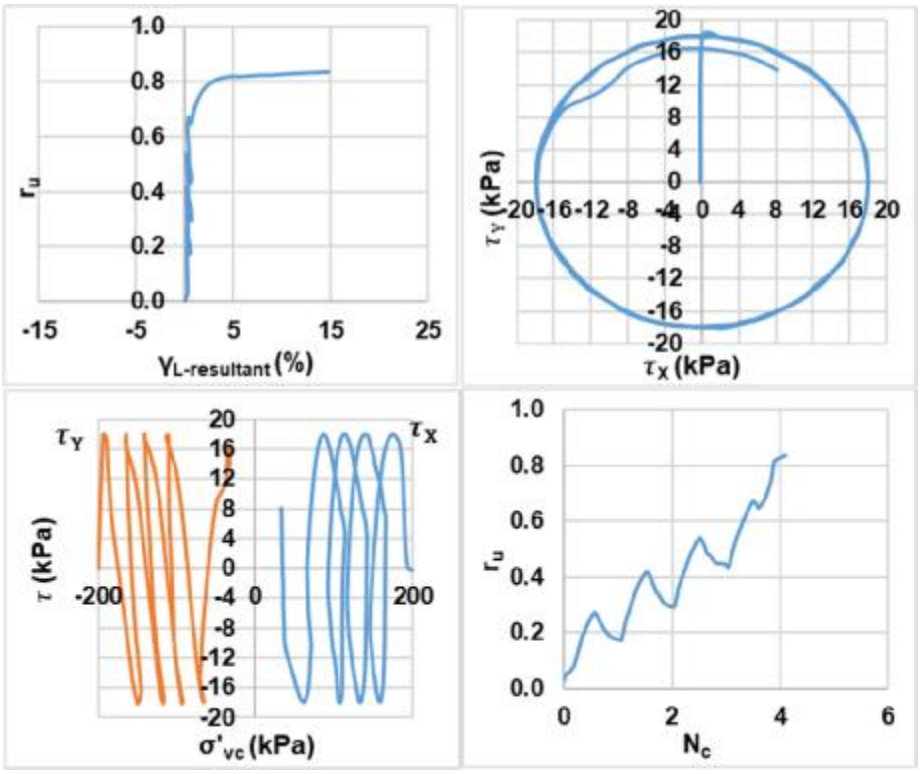


Bi-directional (Circular); $D_{rc}$ = 25%; $\sigma'_{vc}$ = 200 kPa; CSR = 0.09 (Liquefaction)

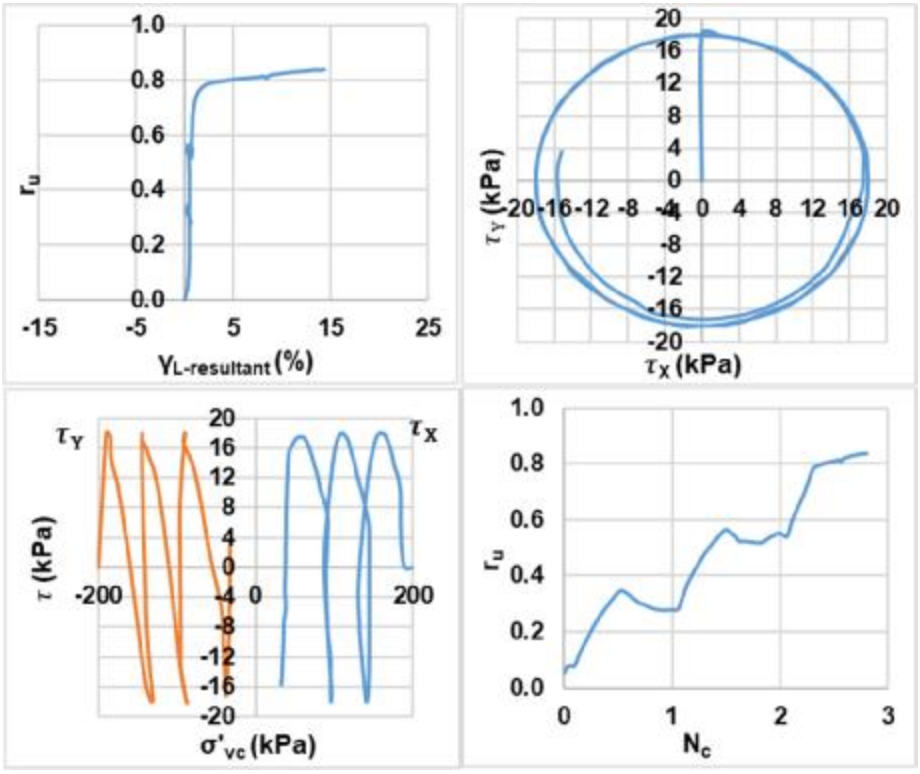


Bi-directional (Circular); $D_{rc}$ = 25%; $\sigma'_{vc}$ = 200 kPa; CSR = 0.09 (Re-liquefaction)

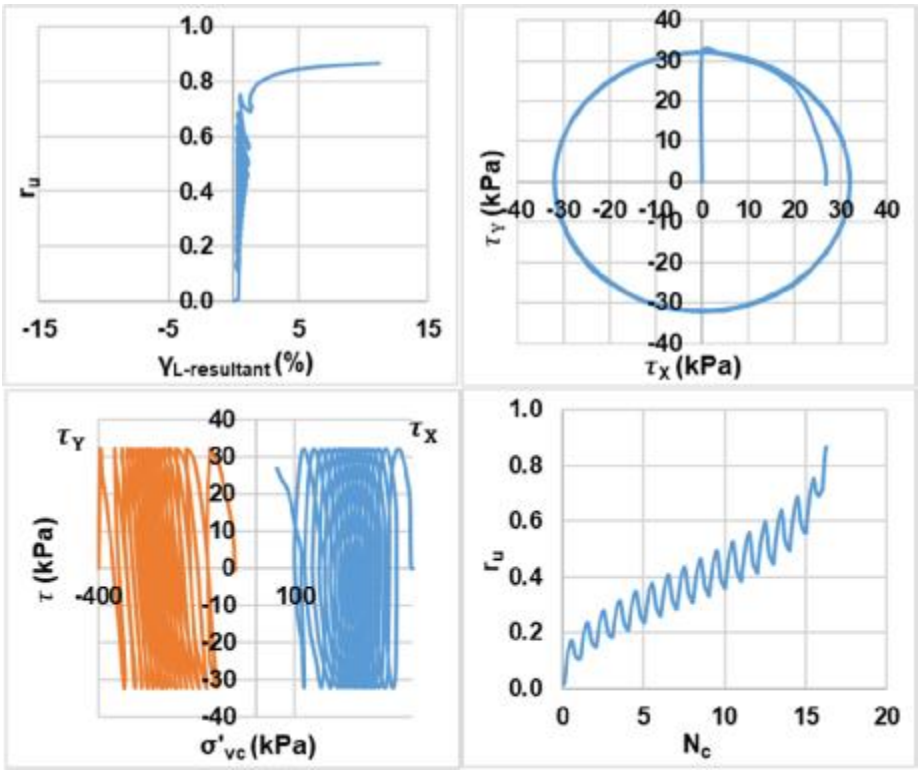


Bi-directional (Circular); $D_{rc}$ = 25%; $\sigma'_{vc}$ = 400 kPa; CSR = 0.08 (Liquefaction)

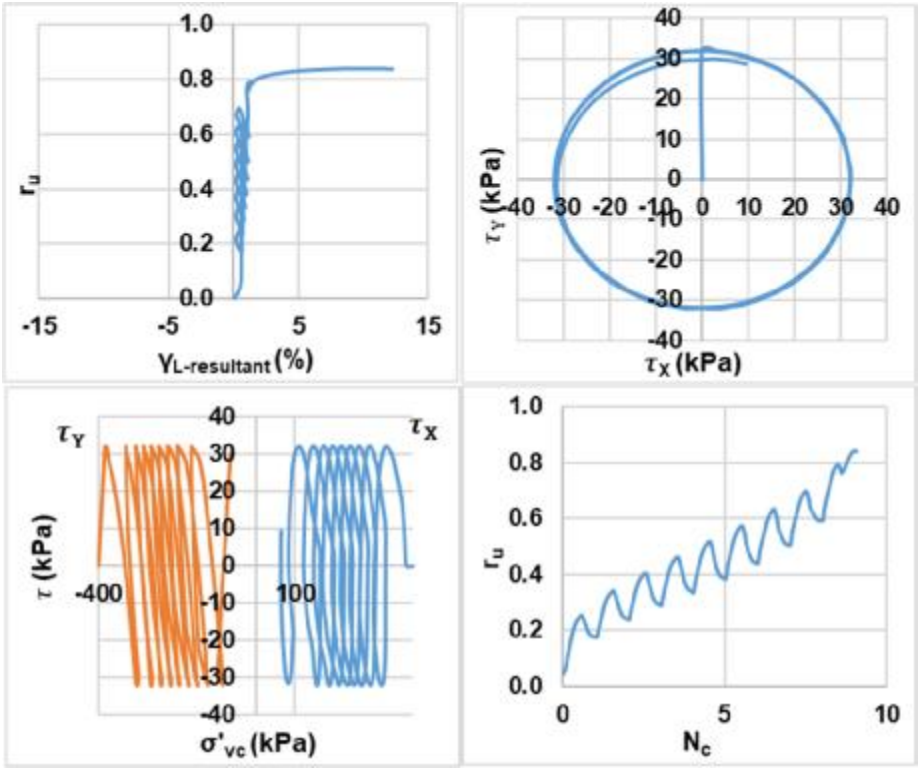


Bi-directional (Circular); $D_{rc}$ = 25%; $\sigma'_{vc}$ = 400 kPa; CSR = 0.08 (Re-liquefaction)

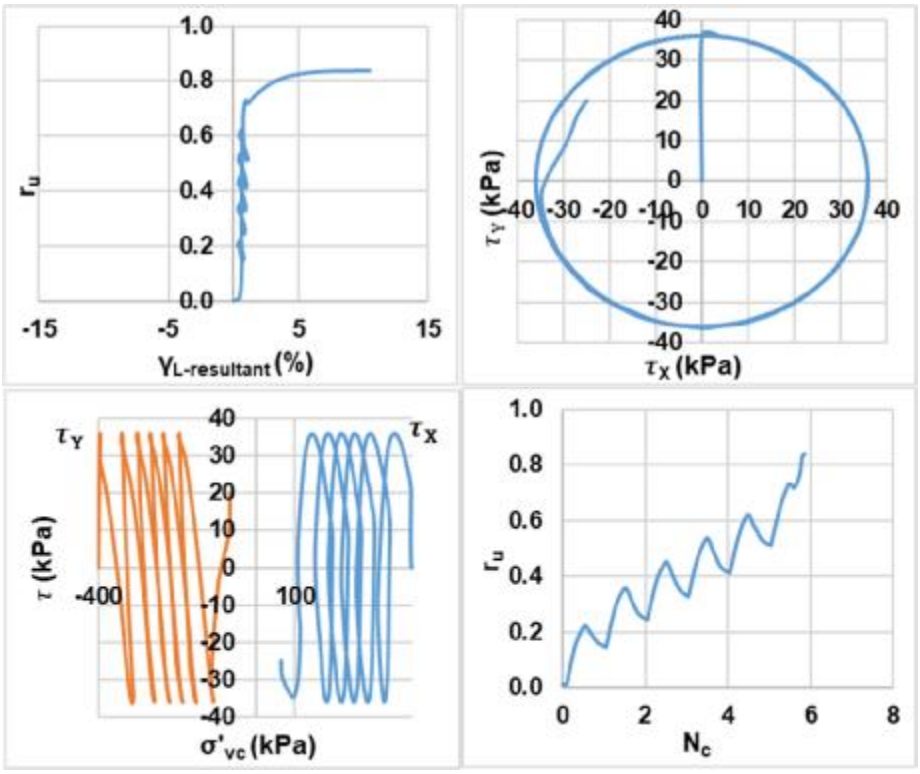


Bi-directional (Circular); $D_{rc}$ = 25%; $\sigma'_{vc}$ = 400 kPa; CSR = 0.09 (Liquefaction)

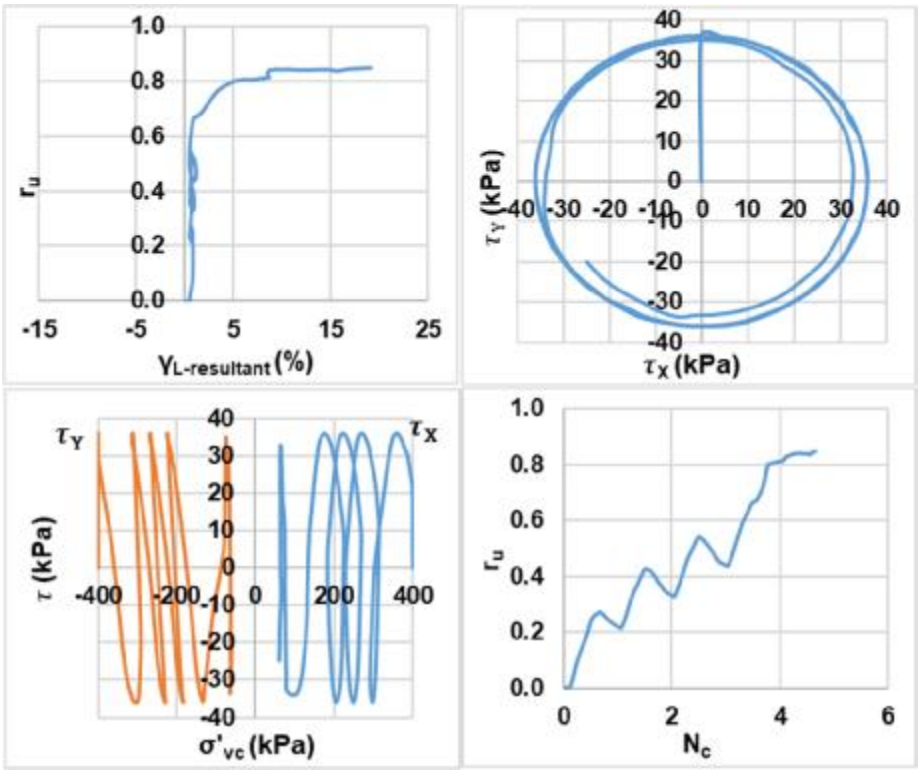


Bi-directional (Circular); $D_{rc}$ = 25%; $\sigma'_{vc}$ = 400 kPa; CSR = 0.09 (Re-liquefaction)

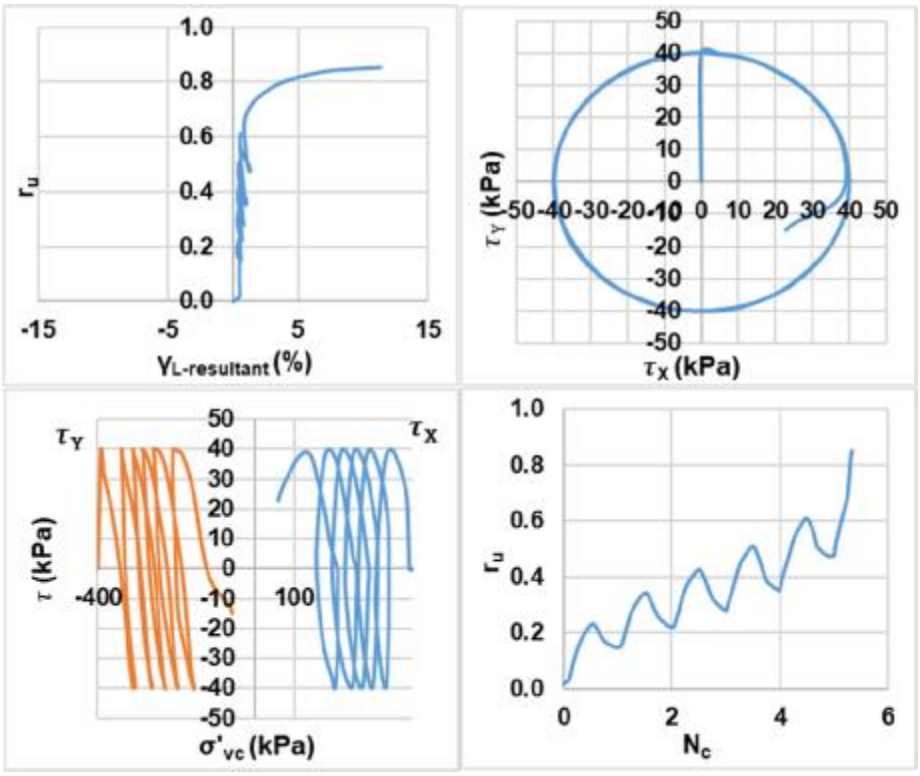


Bi-directional (Circular); $D_{rc}$ = 25%; $\sigma'_{vc}$ = 400 kPa; CSR = 0.1 (Liquefaction)

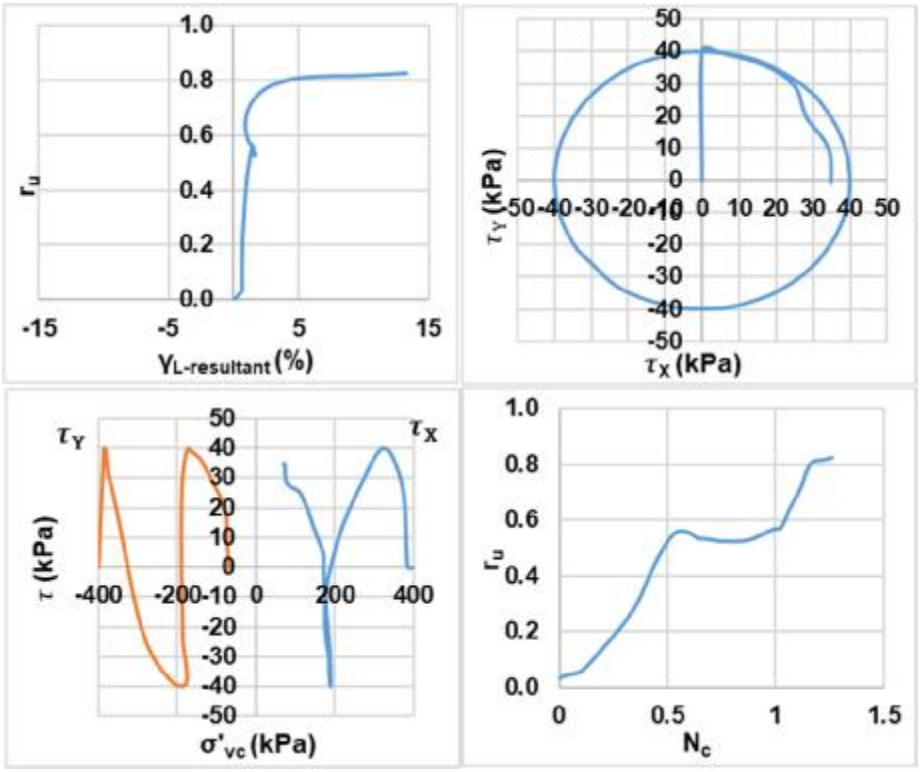


Bi-directional (Circular); $D_{rc}$ = 25%; $\sigma'_{vc}$ = 400 kPa; CSR = 0.1 (Re-liquefaction)

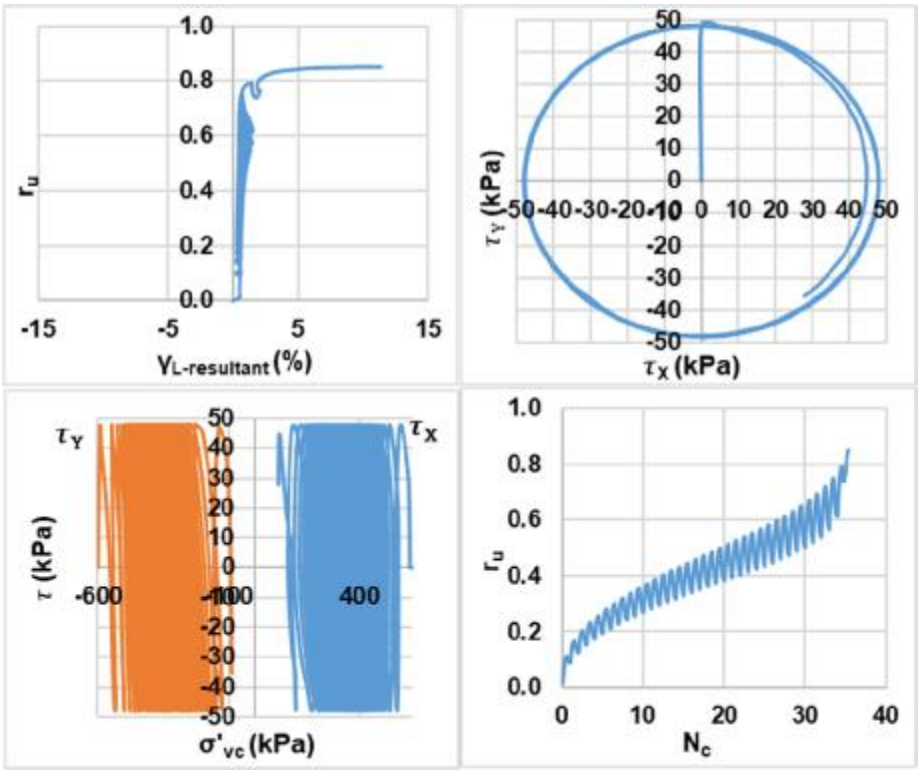


Bi-directional (Circular); $D_{rc}$ = 25%; $\sigma'_{vc}$ = 600 kPa; CSR = 0.08 (Liquefaction)

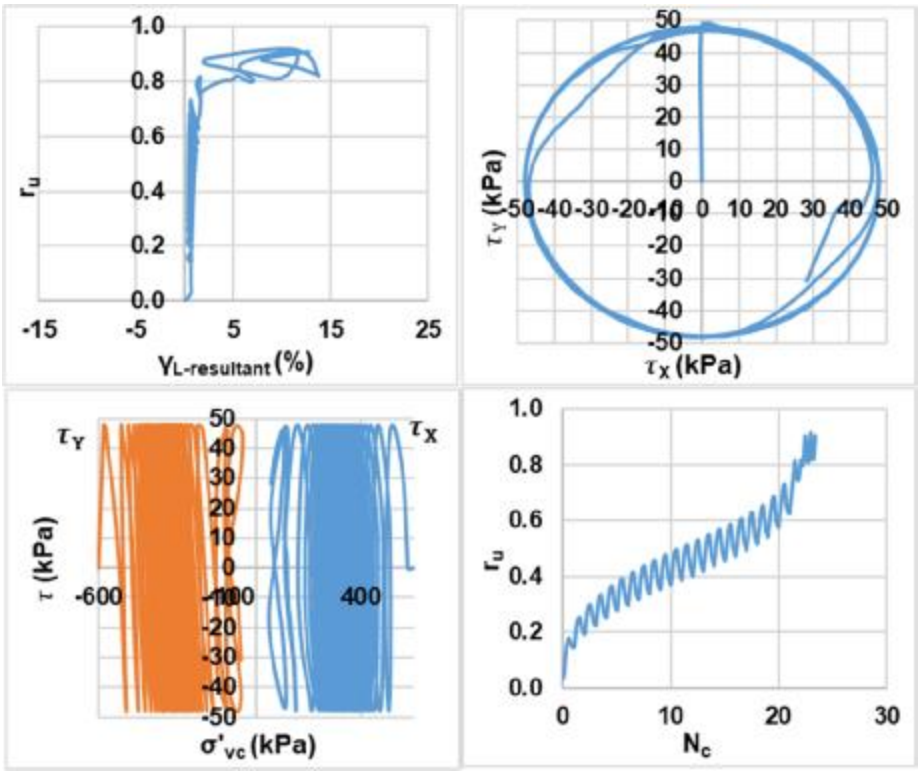


Bi-directional (Circular); $D_{rc}$ = 25%; $\sigma'_{vc}$ = 600 kPa; CSR = 0.08 (Re-liquefaction)

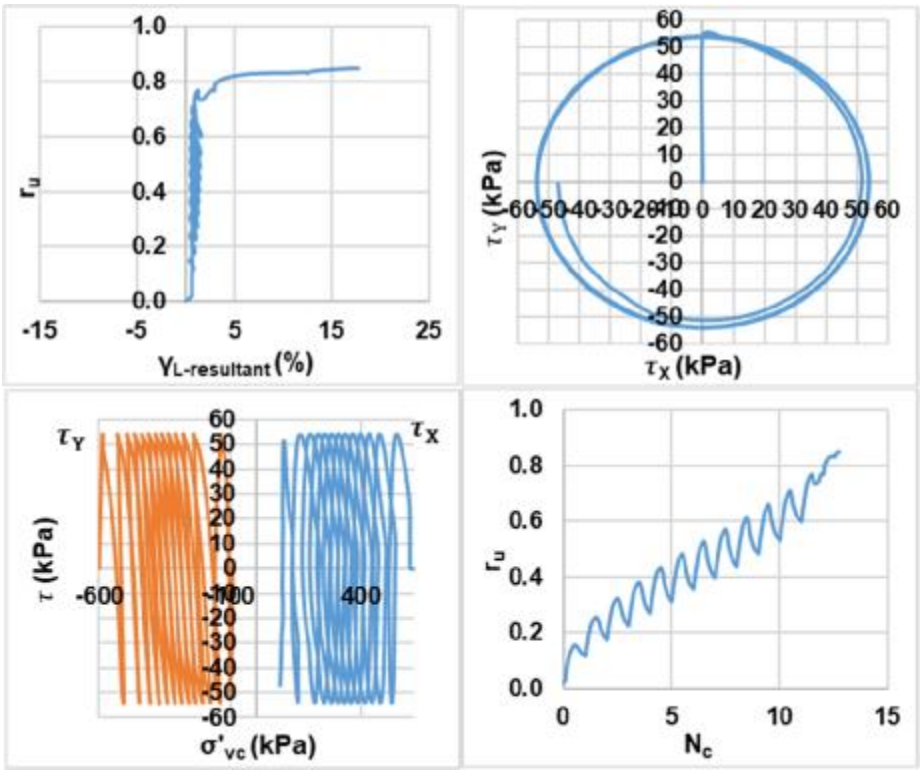


Bi-directional (Circular); $D_{rc}$ = 25%; $\sigma'_{vc}$ = 600 kPa; CSR = 0.09 (Liquefaction)

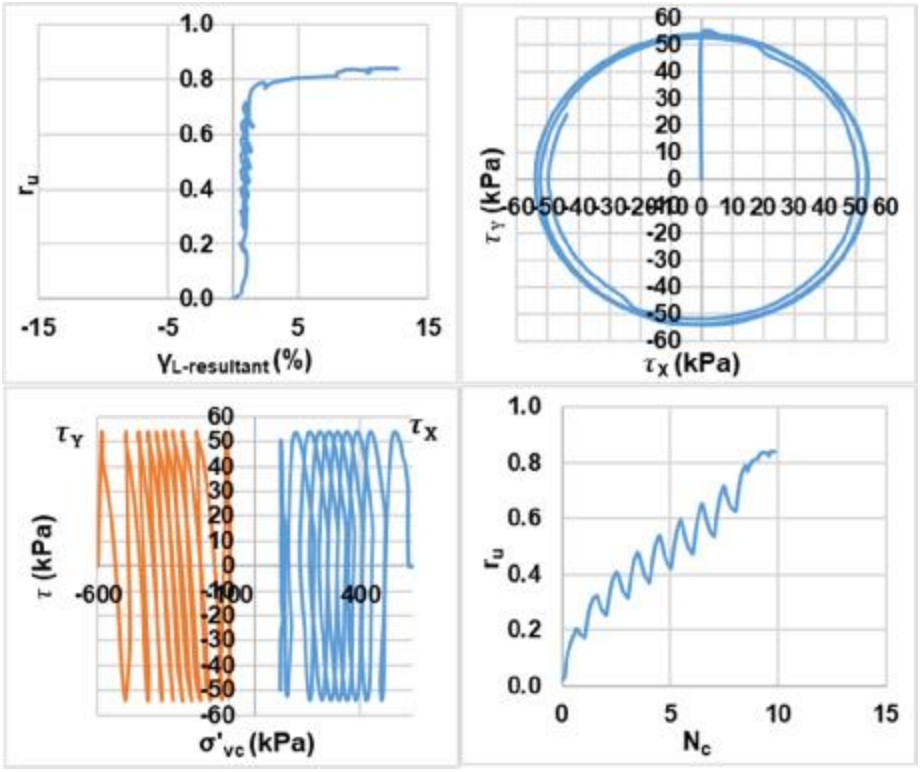


Bi-directional (Circular); $D_{rc}$ = 25%; $\sigma'_{vc}$ = 600 kPa; CSR = 0.09 (Re-liquefaction)

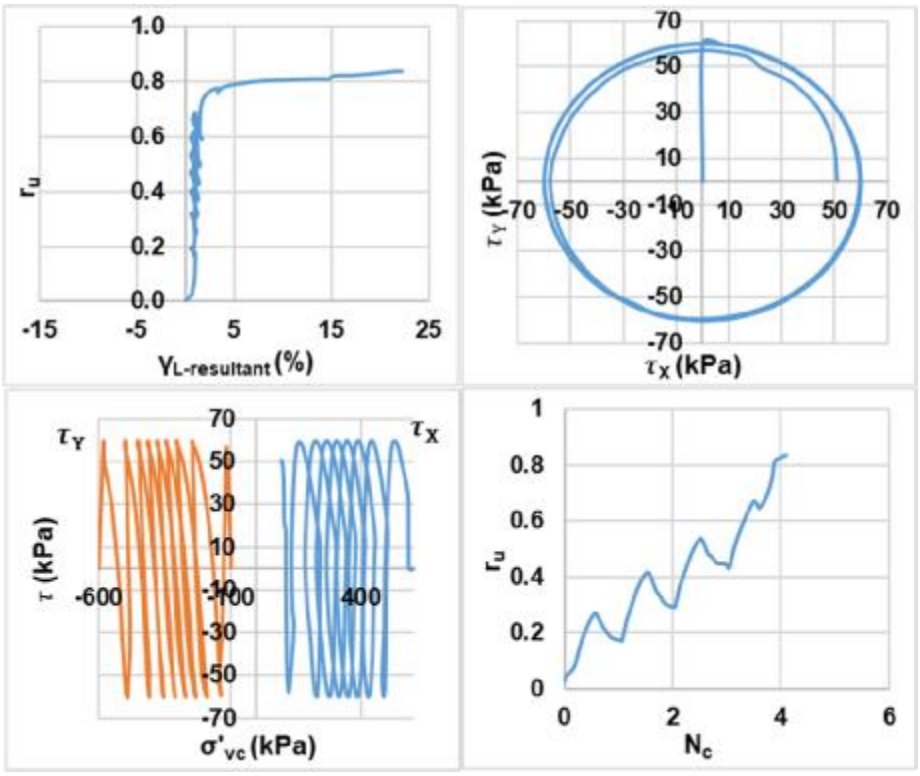


Bi-directional (Circular); $D_{rc}$ = 25%; $\sigma'_{vc}$ = 600 kPa; CSR = 0.1 (Liquefaction)

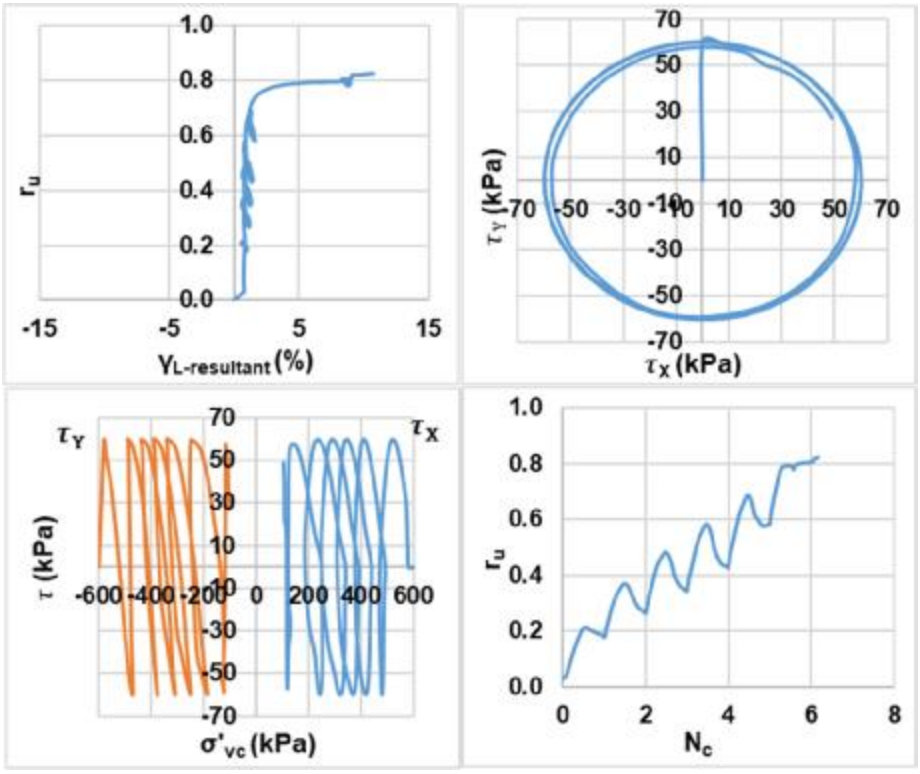


Bi-directional (Circular); $D_{rc}$ = 25%; $\sigma'_{vc}$ = 600 kPa; CSR = 0.1 (Re-liquefaction)

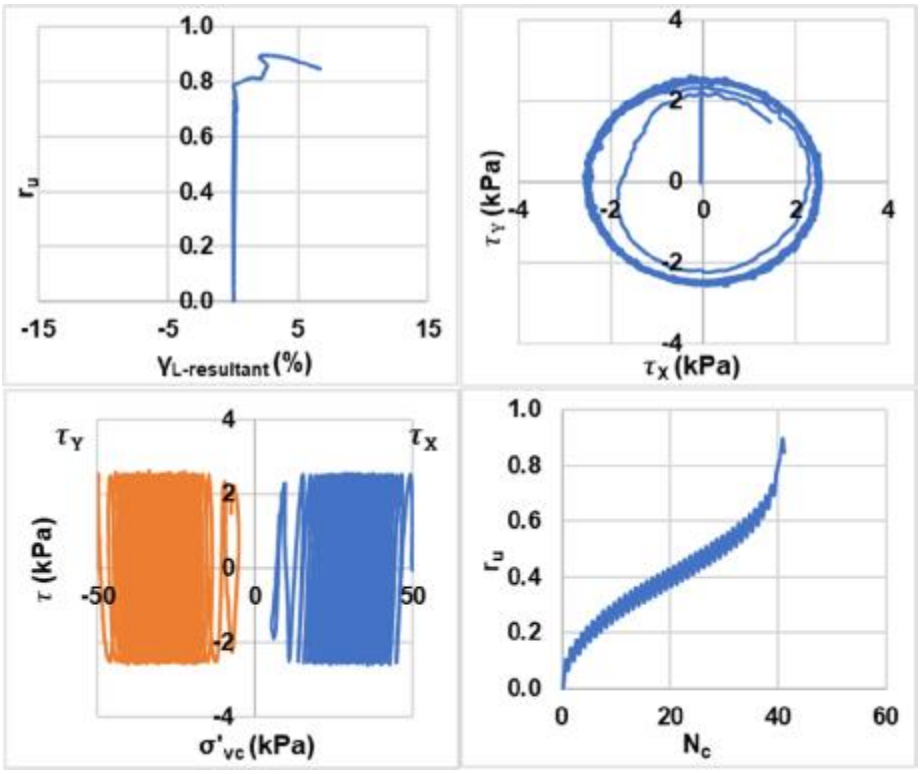


Bi-directional (Circular); $D_{rc}$ = 45%; $\sigma'_{vc}$ = 50 kPa; CSR = 0.05 (Liquefaction)

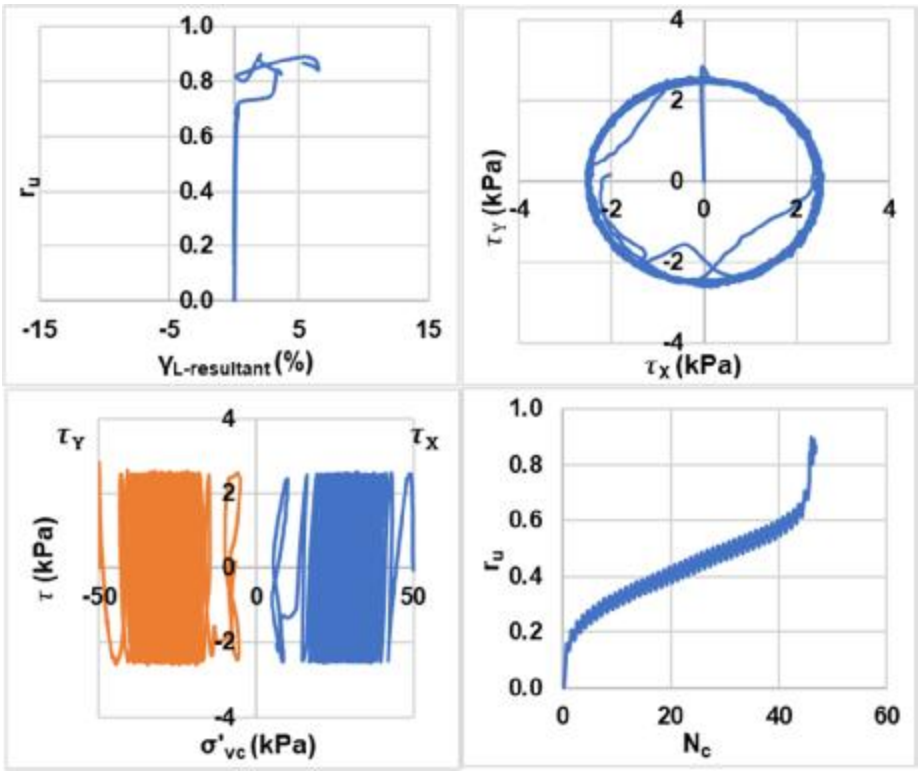


Bi-directional (Circular); $D_{rc}$ = 45%; $\sigma'_{vc}$ = 50 kPa; CSR = 0.05 (Re-liquefaction)

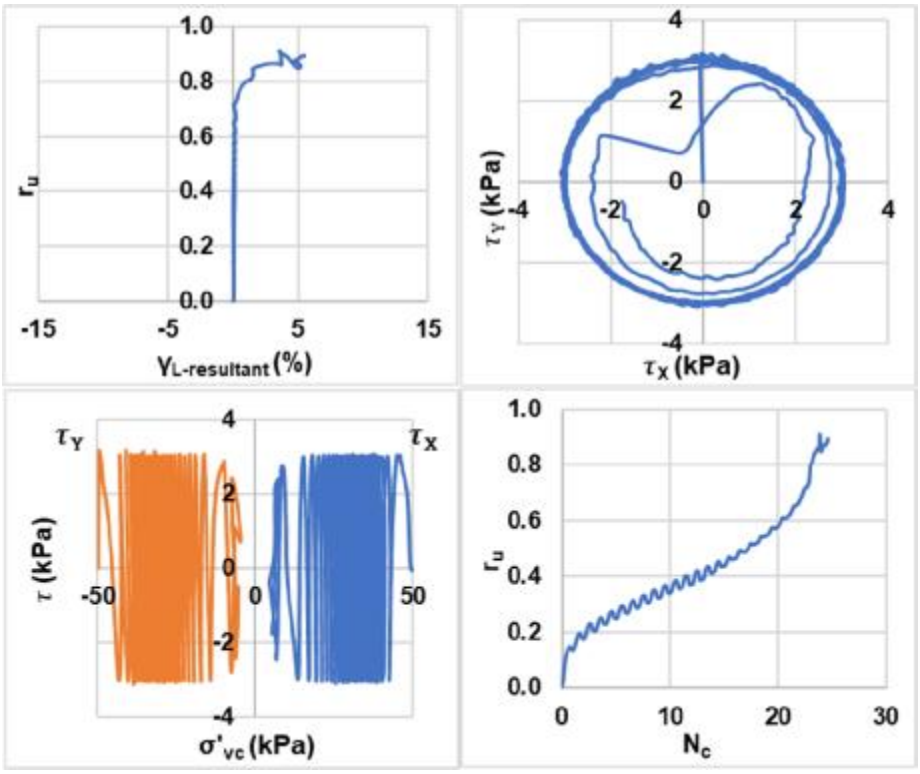


Bi-directional (Circular); $D_{rc}$ = 45%; $\sigma'_{vc}$ = 50 kPa; CSR = 0.06 (Liquefaction)

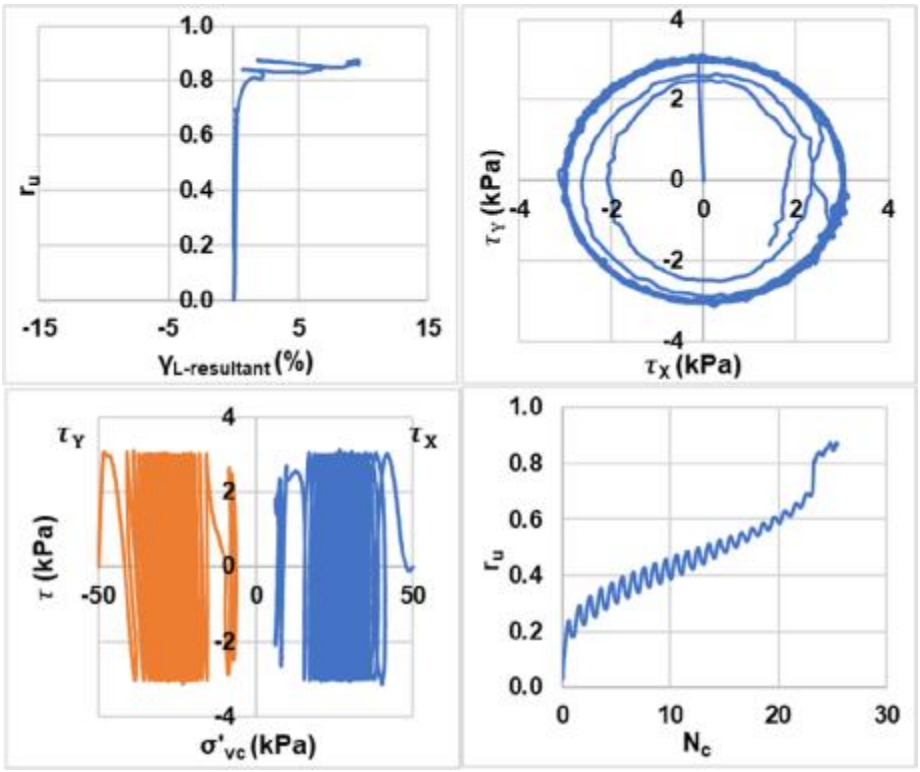


Bi-directional (Circular); $D_{rc}$ = 45%; $\sigma'_{vc}$ = 50 kPa; CSR = 0.06 (Re-liquefaction)

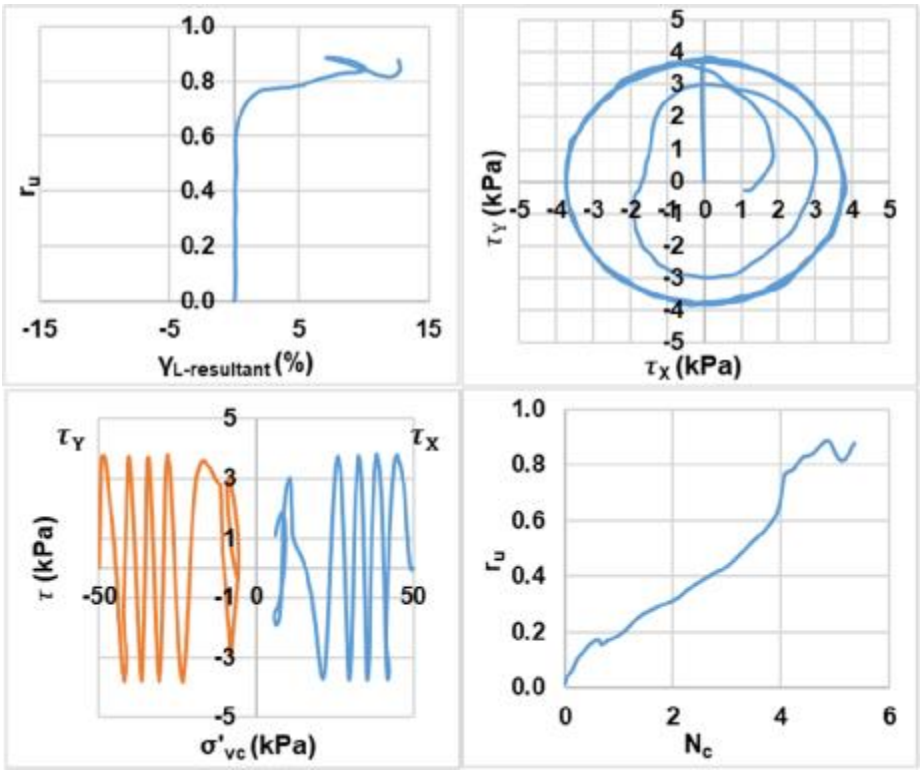


Bi-directional (Circular); $D_{rc}$ = 45%; $\sigma'_{vc}$ = 50 kPa; CSR = 0.075 (Liquefaction)

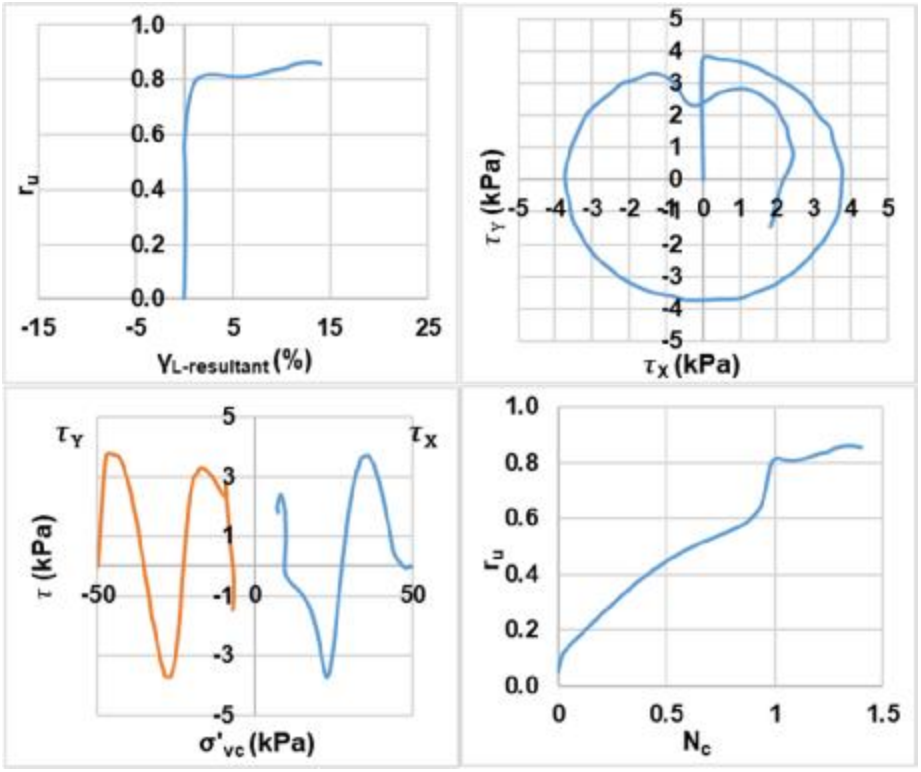


Bi-directional (Circular); $D_{rc}$ = 45%; $\sigma'_{vc}$ = 50 kPa; CSR = 0.075 (Re-liquefaction)

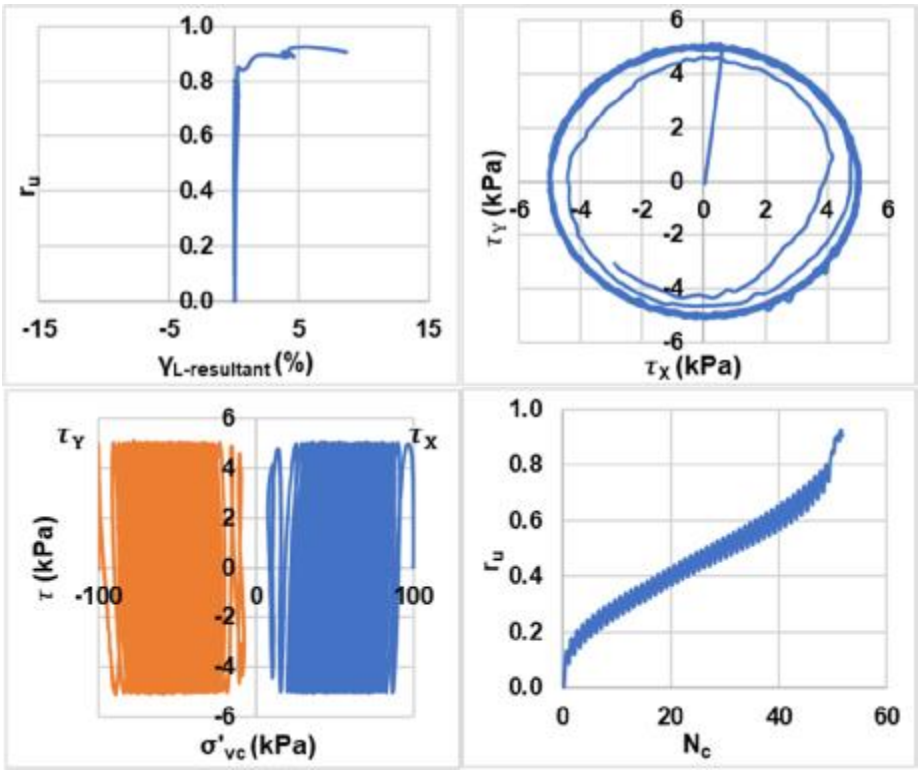


Bi-directional (Circular); $D_{rc}$ = 45%; $\sigma'_{vc}$ = 100 kPa; CSR = 0.05 (Liquefaction)

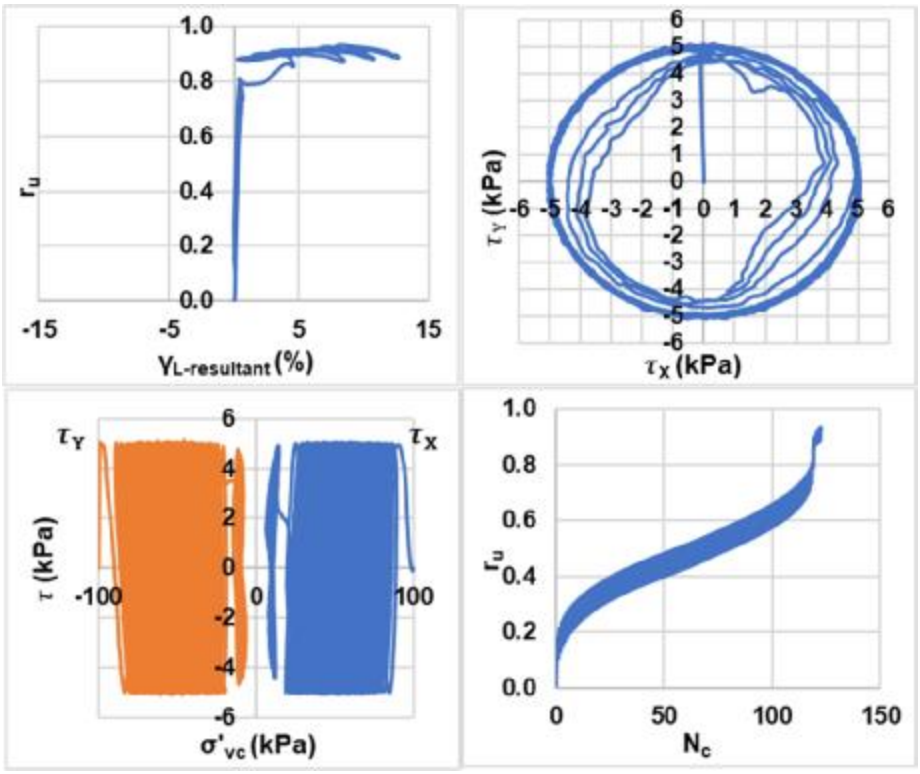


Bi-directional (Circular); $D_{rc}$ = 45%; $\sigma'_{vc}$ = 100 kPa; CSR = 0.05 (Re-liquefaction)

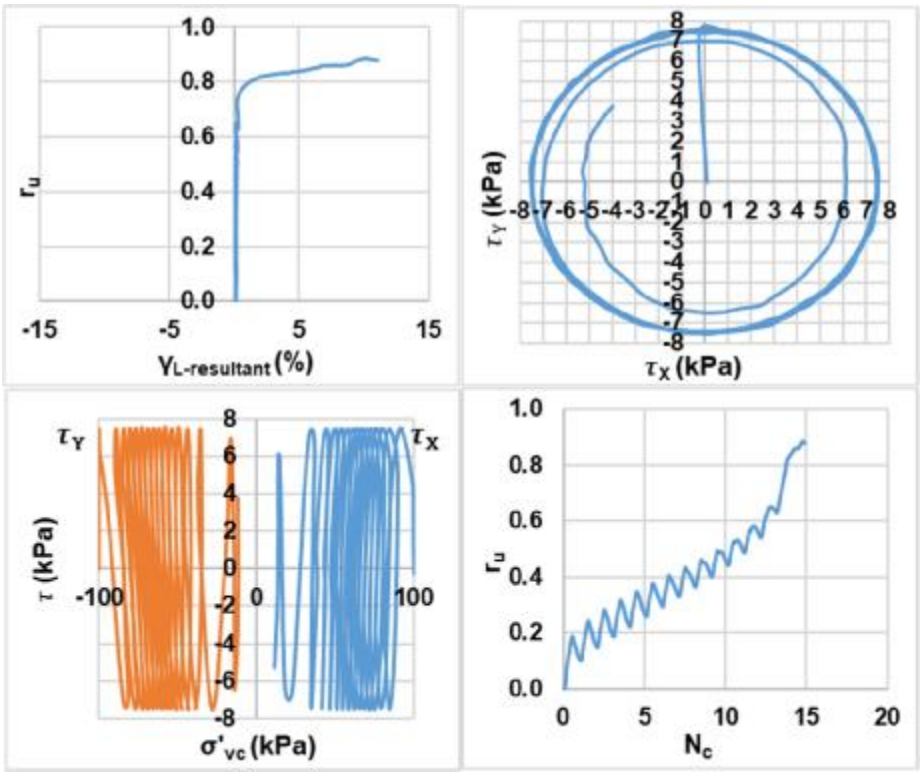


Bi-directional (Circular); $D_{rc}$ = 45%; $\sigma'_{vc}$ = 100 kPa; CSR = 0.075 (Liquefaction)

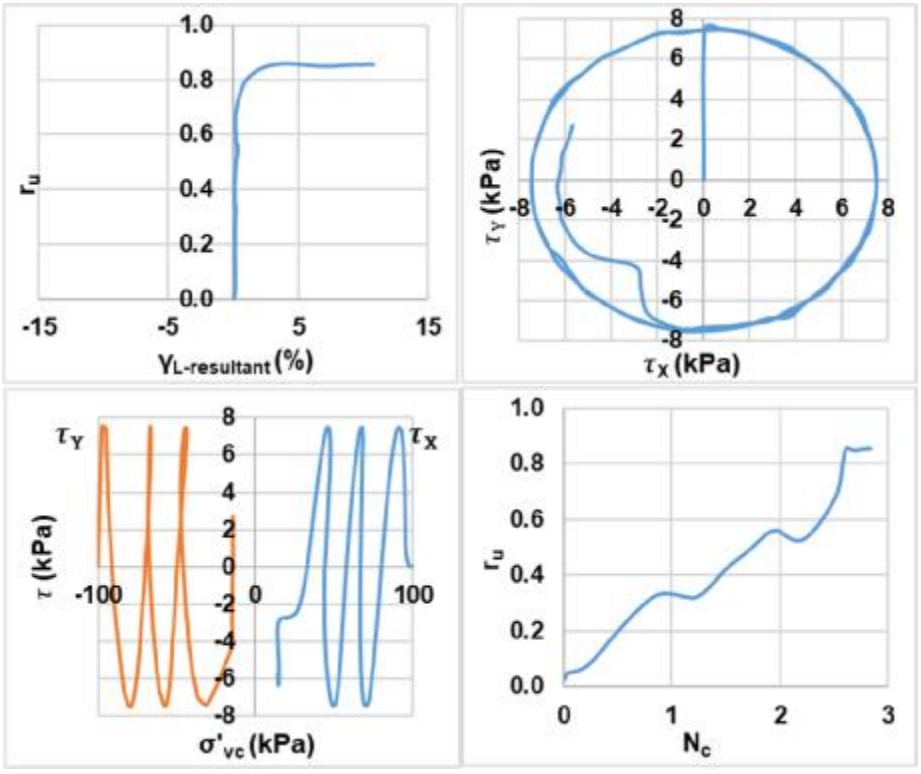


Bi-directional (Circular); $D_{rc}$ = 45%; $\sigma'_{vc}$ = 100 kPa; CSR = 0.075 (Re-liquefaction)

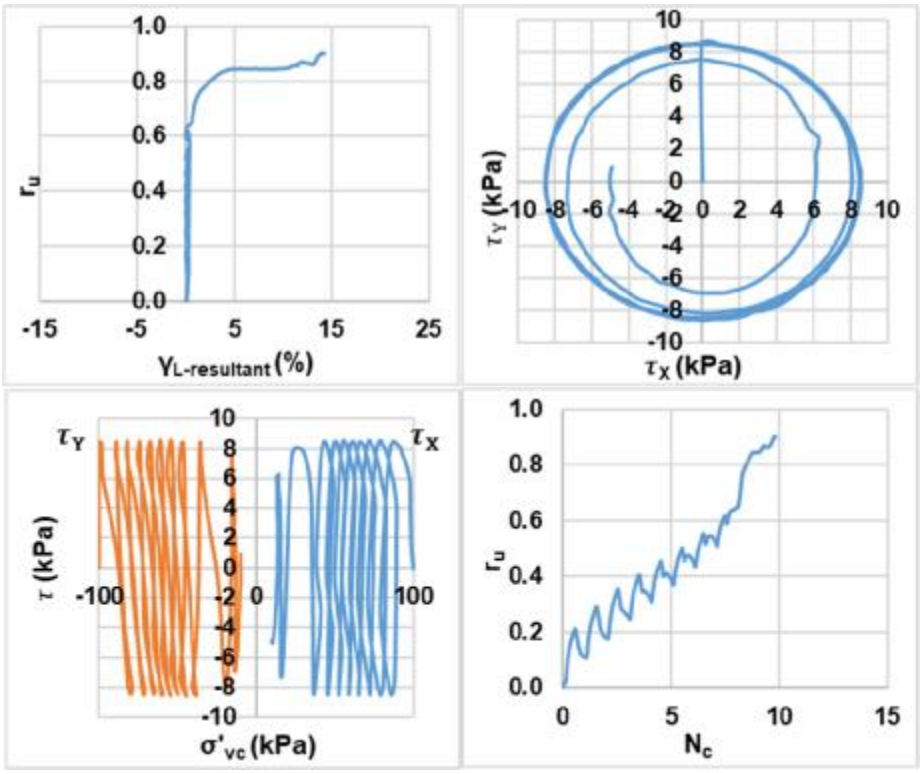


Bi-directional (Circular); $D_{rc}$ = 45%; $\sigma'_{vc}$ = 100 kPa; CSR = 0.085 (Liquefaction)

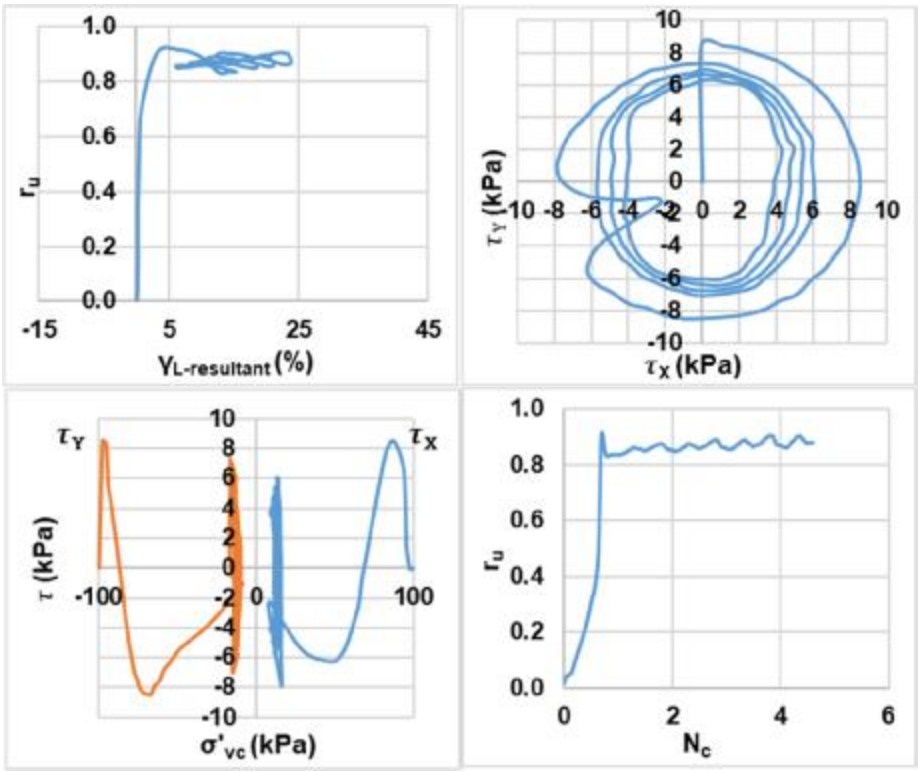


Bi-directional (Circular); $D_{rc}$ = 45%; $\sigma'_{vc}$ = 100 kPa; CSR = 0.085 (Re-liquefaction)

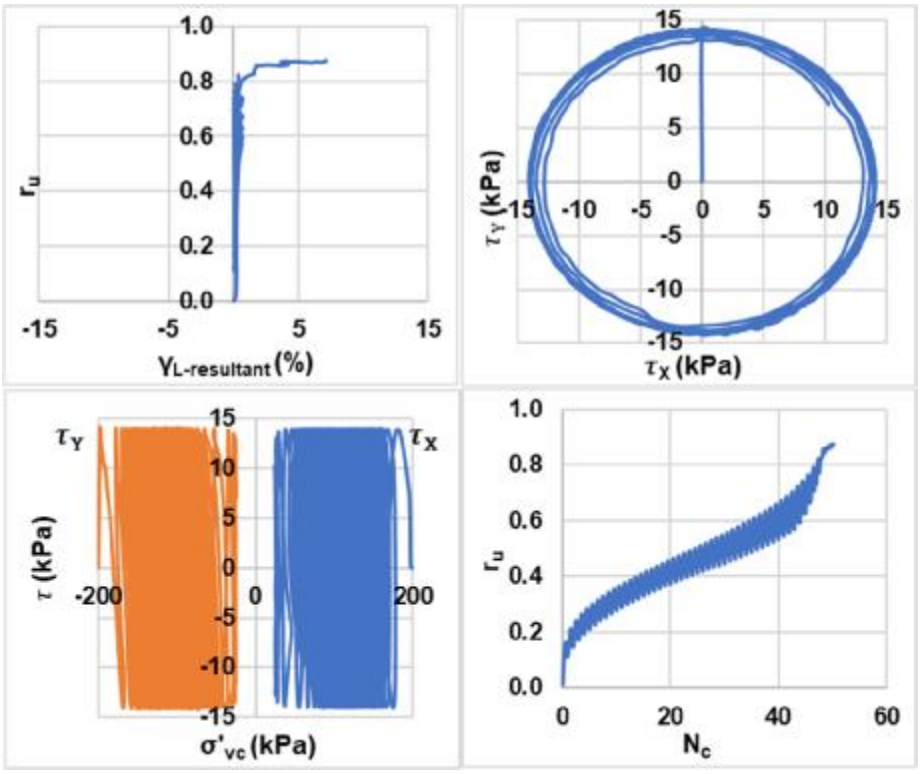


Bi-directional (Circular); $D_{rc}$ = 45%; $\sigma'_{vc}$ = 200 kPa; CSR = 0.07 (Liquefaction)

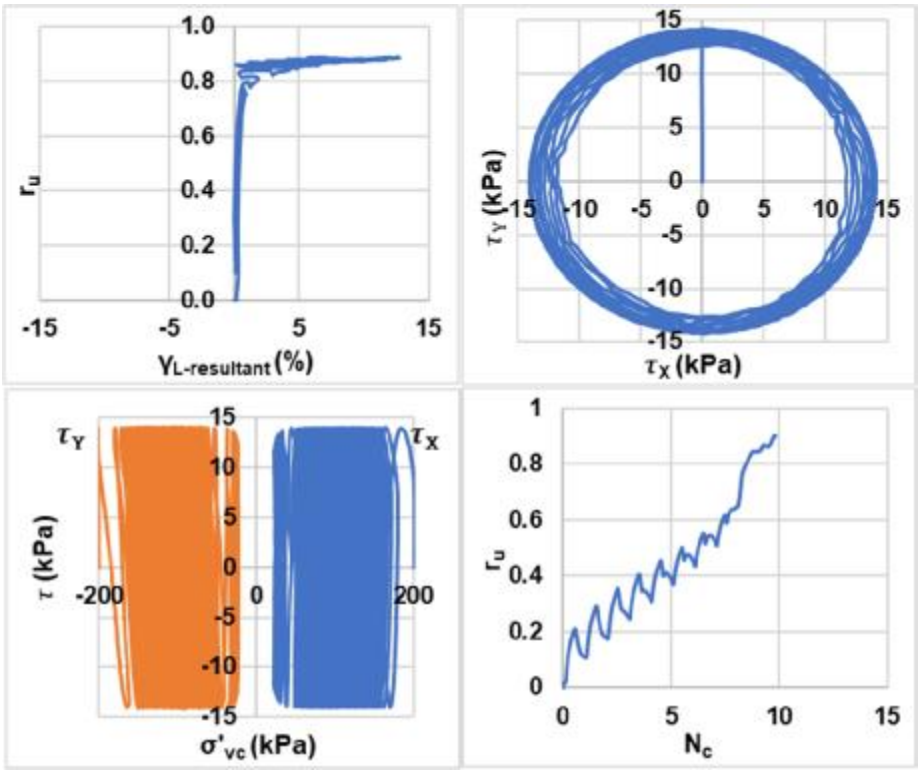


Bi-directional (Circular); $D_{rc}$ = 45%; $\sigma'_{vc}$ = 200 kPa; CSR = 0.07 (Re-liquefaction)

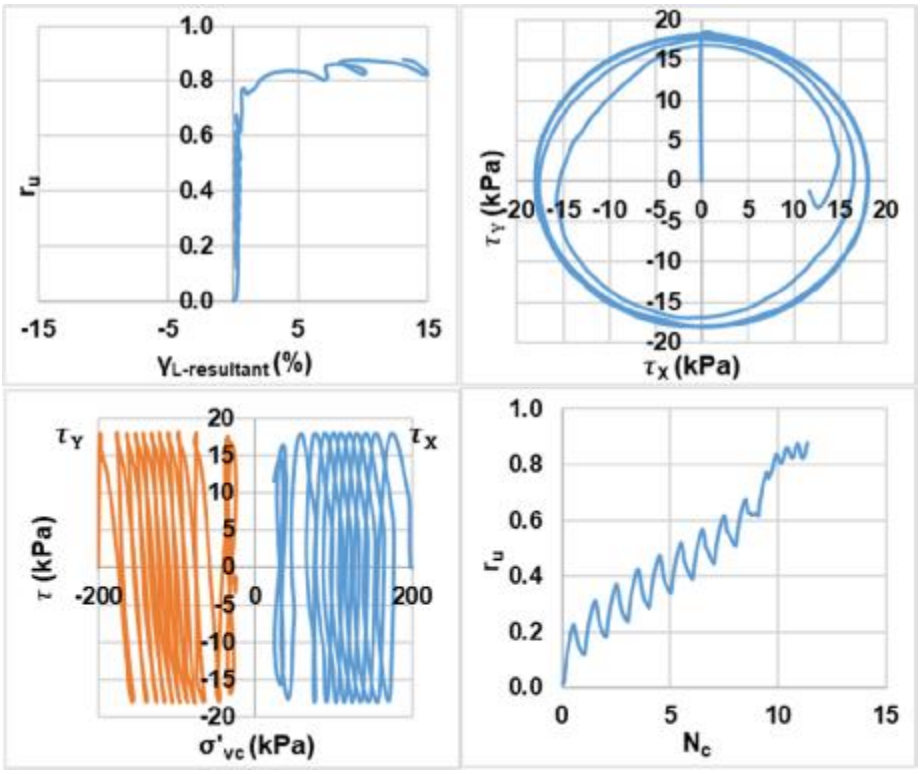


Bi-directional (Circular); $D_{rc}$ = 45%; $\sigma'_{vc}$ = 200 kPa; CSR = 0.09 (Liquefaction)

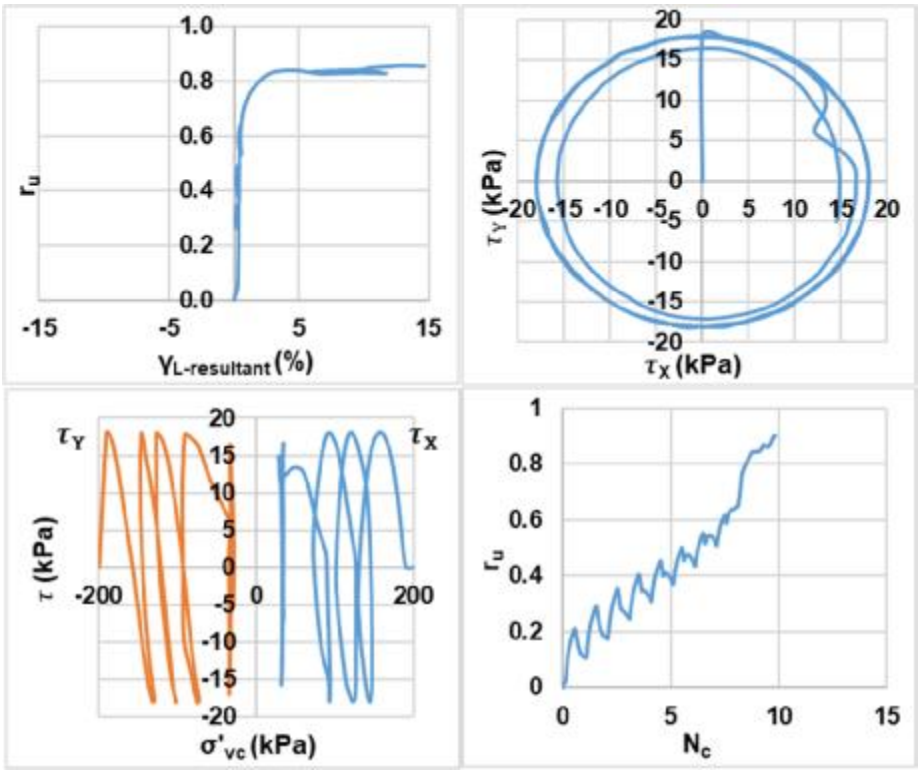


Bi-directional (Circular); $D_{rc}$ = 45%; $\sigma'_{vc}$ = 200 kPa; CSR = 0.09 (Re-liquefaction)

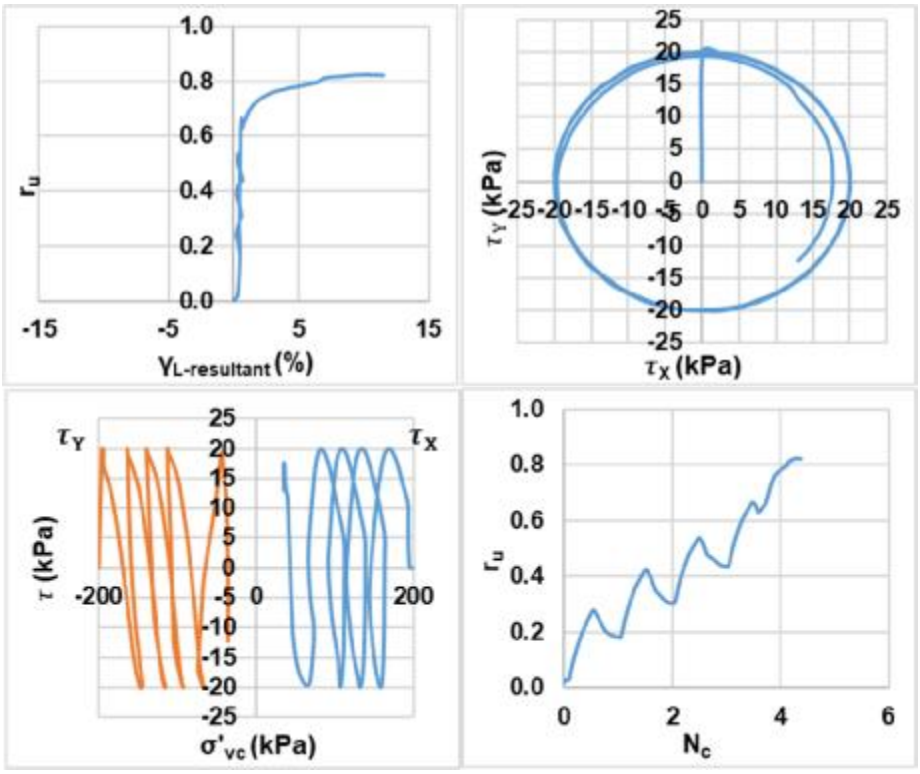


Bi-directional (Circular); $D_{rc}$ = 45%; $\sigma'_{vc}$ = 200 kPa; CSR = 0.1 (Liquefaction)

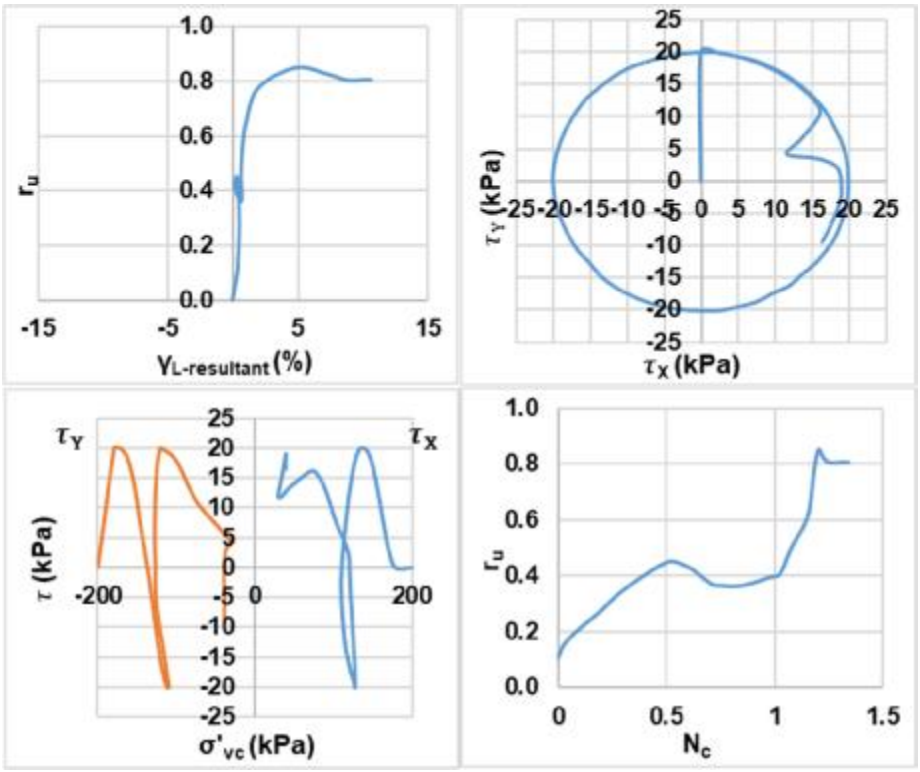


Bi-directional (Circular); $D_{rc}$ = 45%; $\sigma'_{vc}$ = 200 kPa; CSR = 0.1 (Re-liquefaction)

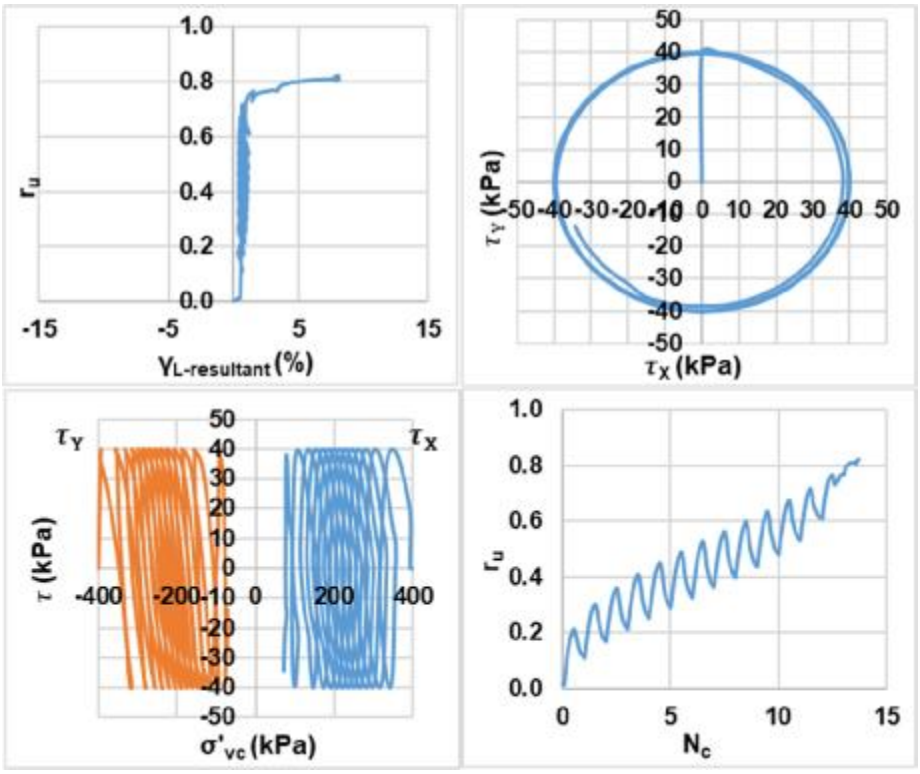


Bi-directional (Circular); $D_{rc}$ = 45%; $\sigma'_{vc}$ = 400 kPa; CSR = 0.1 (Liquefaction)

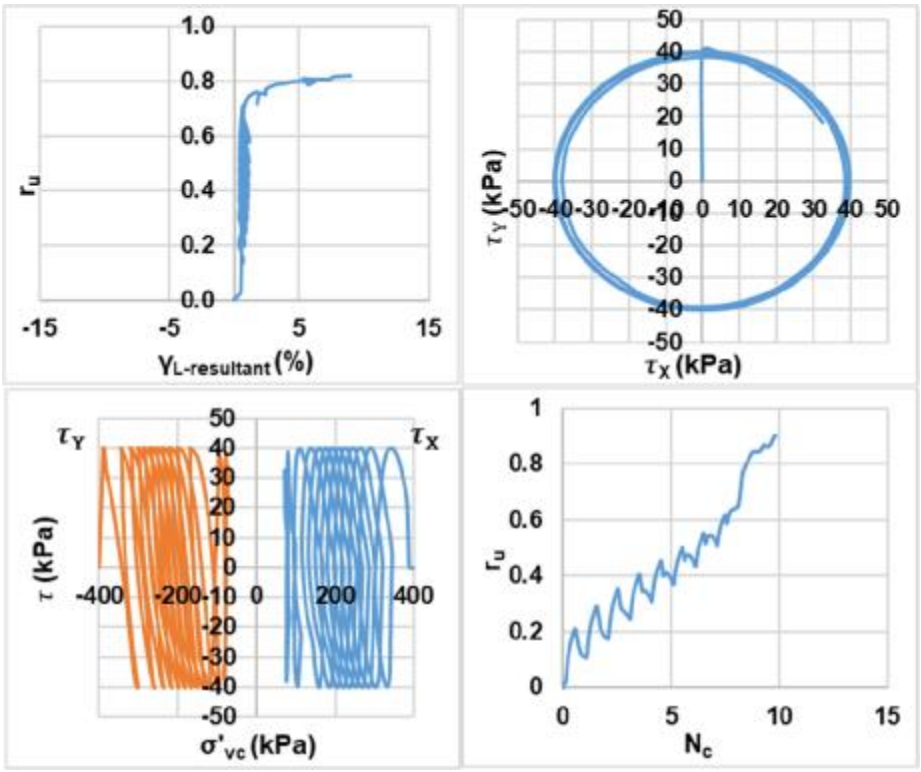


Bi-directional (Circular); $D_{rc}$ = 45%; $\sigma'_{vc}$ = 400 kPa; CSR = 0.1 (Re-liquefaction)

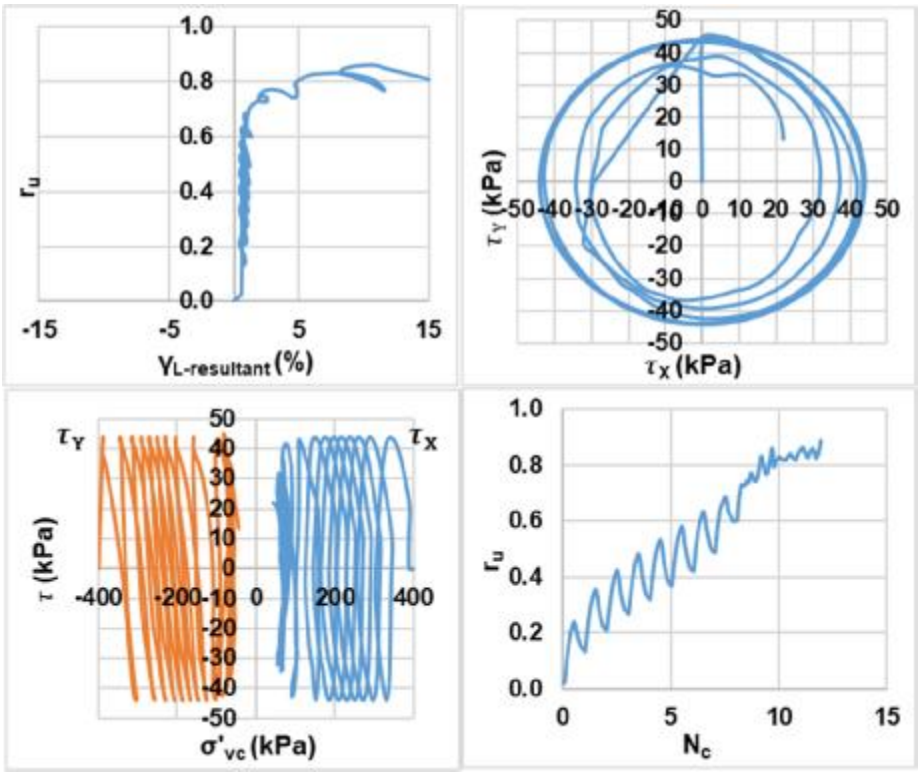


Bi-directional (Circular); $D_{rc}$ = 45%; $\sigma'_{vc}$ = 400 kPa; CSR = 0.11 (Liquefaction)

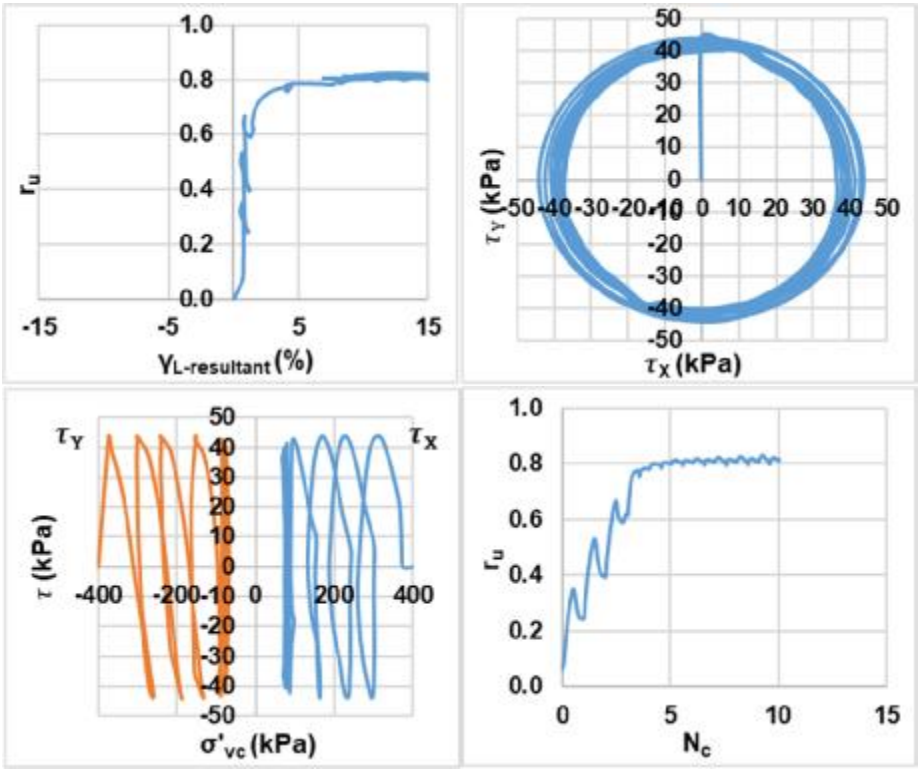


Bi-directional (Circular); $D_{rc}$ = 45%; $\sigma'_{vc}$ = 400 kPa; CSR = 0.11 (Re-liquefaction)

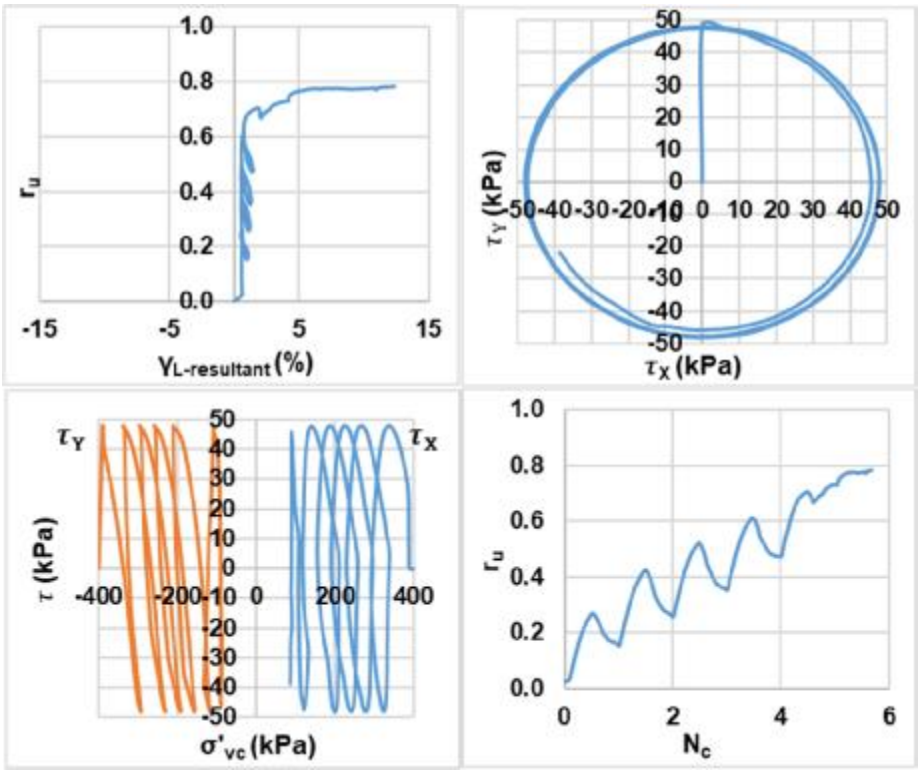


Bi-directional (Circular); $D_{rc}$ = 45%; $\sigma'_{vc}$ = 400 kPa; CSR = 0.12 (Liquefaction)

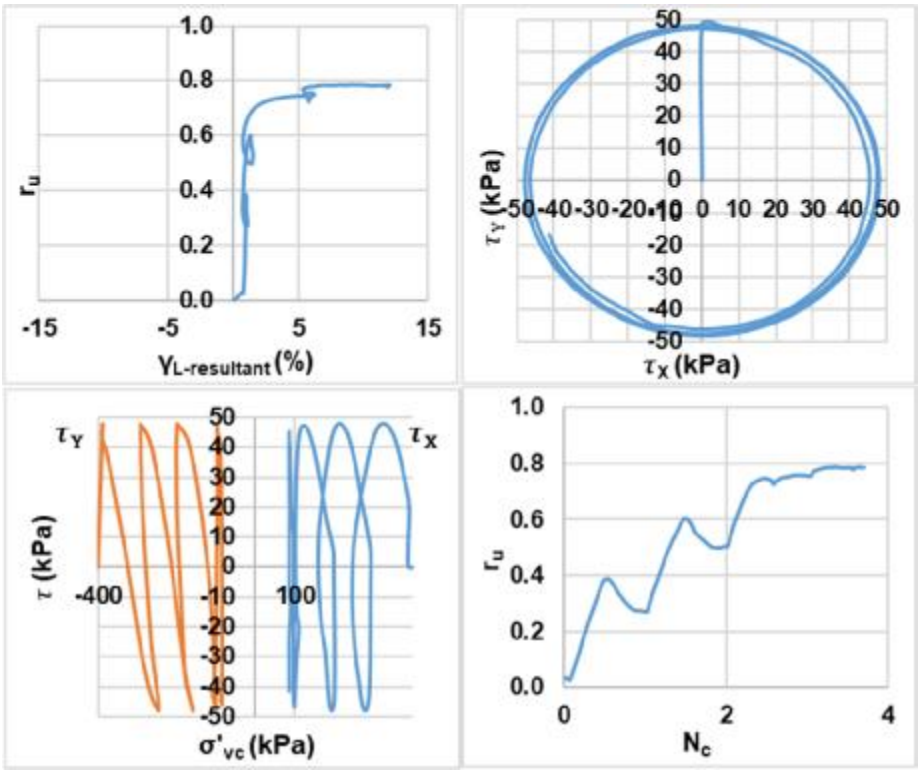


Bi-directional (Circular); $D_{rc}$ = 45%; $\sigma'_{vc}$ = 400 kPa; CSR = 0.12 (Re-liquefaction)

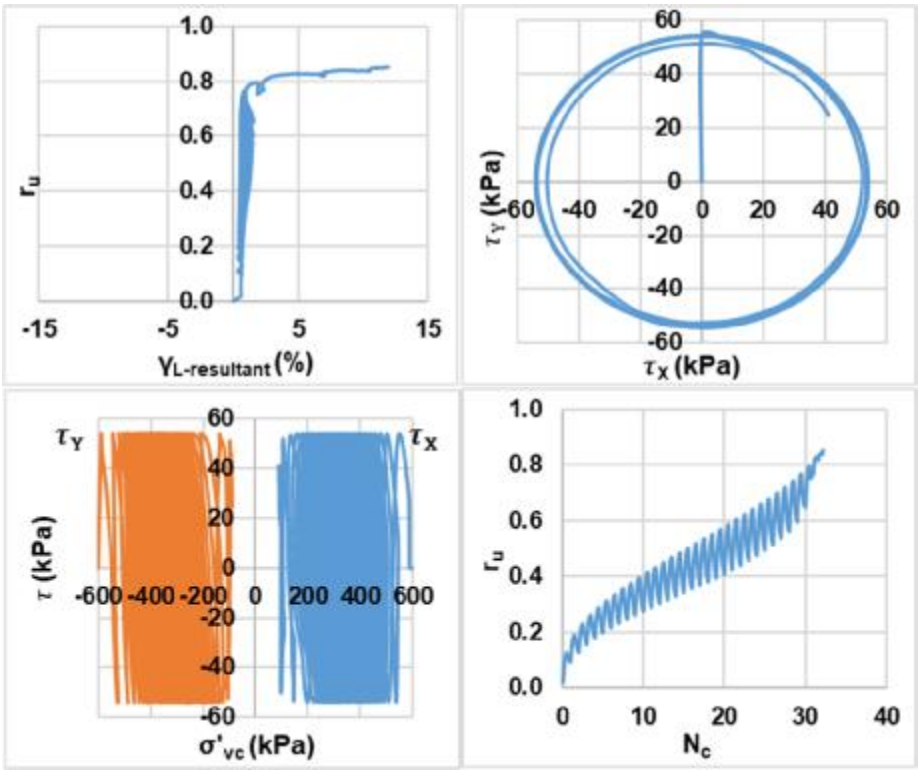


Bi-directional (Circular); $D_{rc}$ = 45%; $\sigma'_{vc}$ = 600 kPa; CSR = 0.09 (Liquefaction)

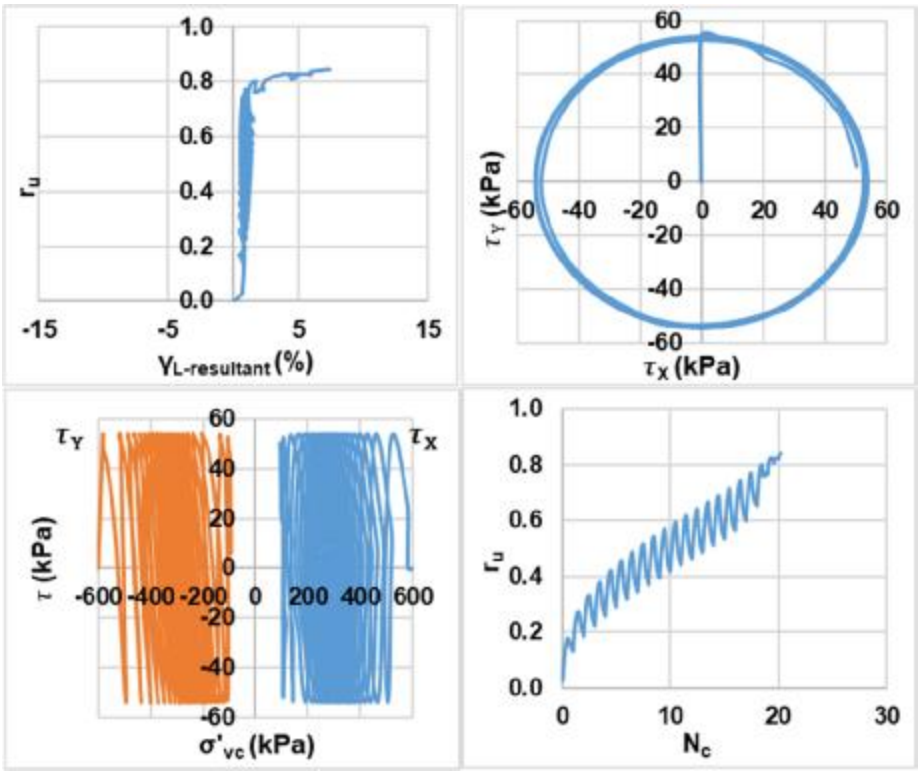


Bi-directional (Circular); $D_{rc}$ = 45%; $\sigma'_{vc}$ = 600 kPa; CSR = 0.09 (Re-liquefaction)

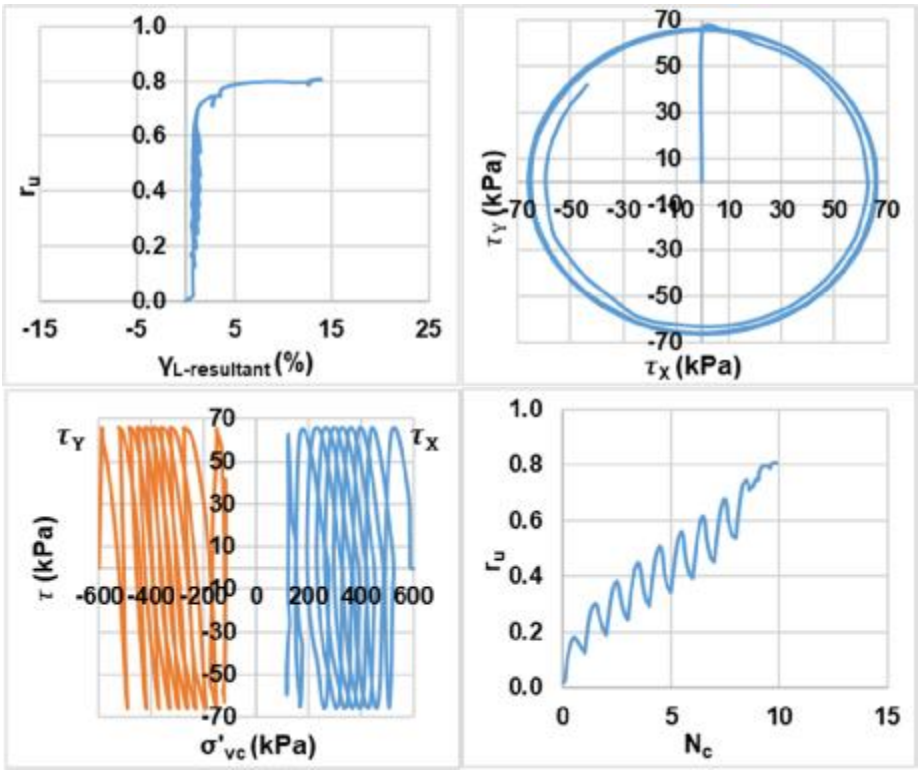


Bi-directional (Circular); $D_{rc}$ = 45%; $\sigma'_{vc}$ = 600 kPa; CSR = 0.11 (Liquefaction)

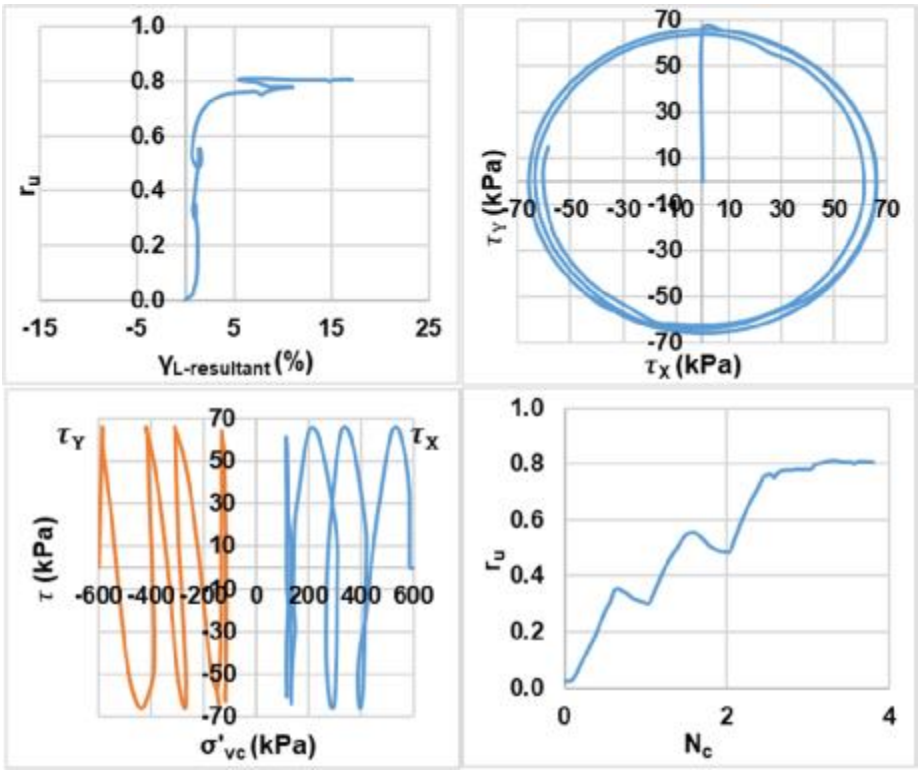


Bi-directional (Circular); $D_{rc}$ = 45%; $\sigma'_{vc}$ = 600 kPa; CSR = 0.11 (Re-liquefaction)

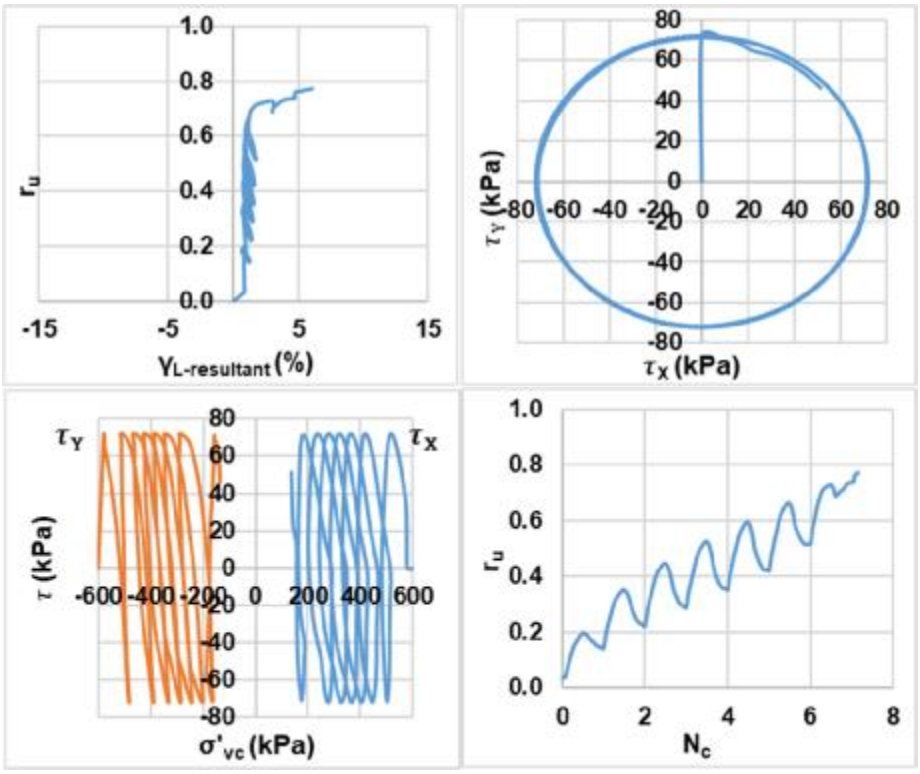


Bi-directional (Circular); $D_{rc}$ = 45%; $\sigma'_{vc}$ = 600 kPa; CSR = 0.12 (Liquefaction)

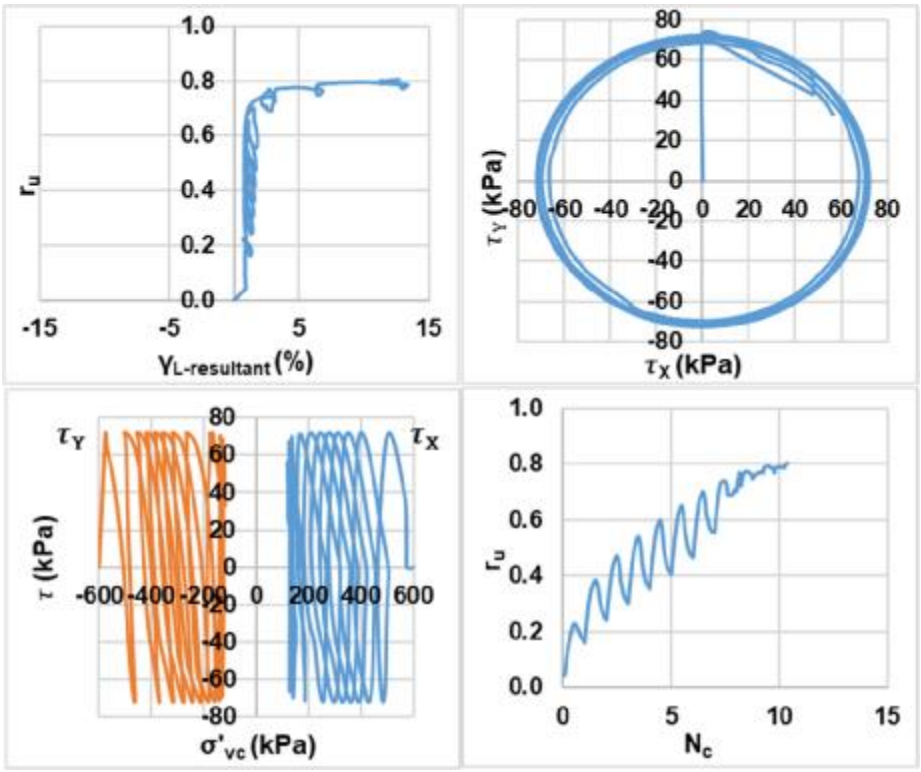


Bi-directional (Circular); $D_{rc}$ = 45%; $\sigma'_{vc}$ = 600 kPa; CSR = 0.12 (Re-liquefaction)

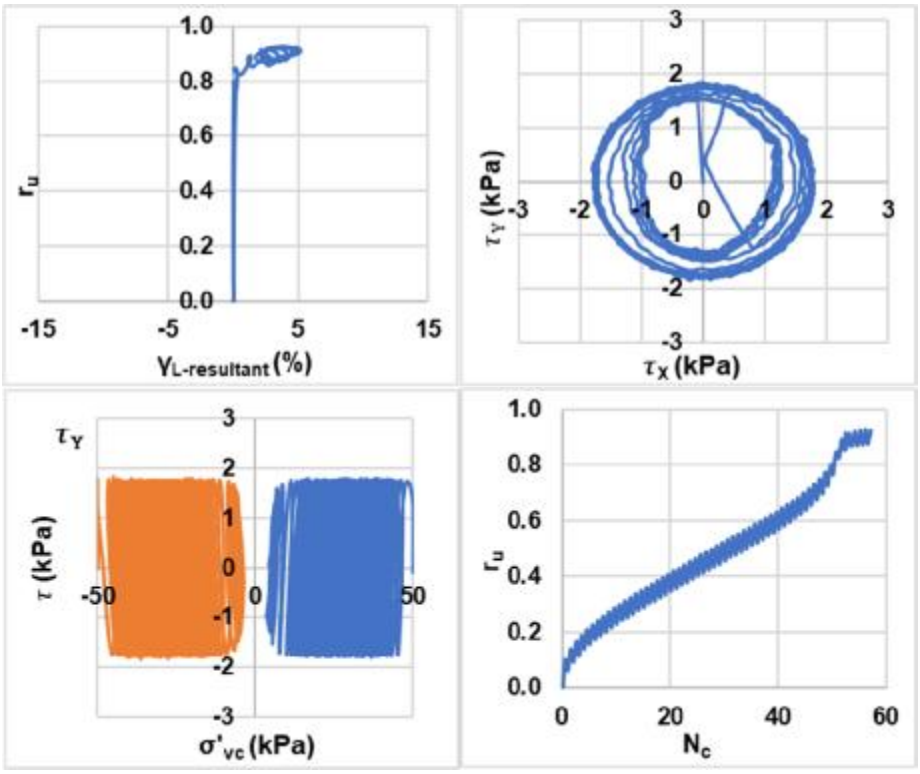


Bi-directional (Circular); $D_{rc}$ = 65%; $\sigma'_{vc}$ = 50 kPa; CSR = 0.035 (Liquefaction)

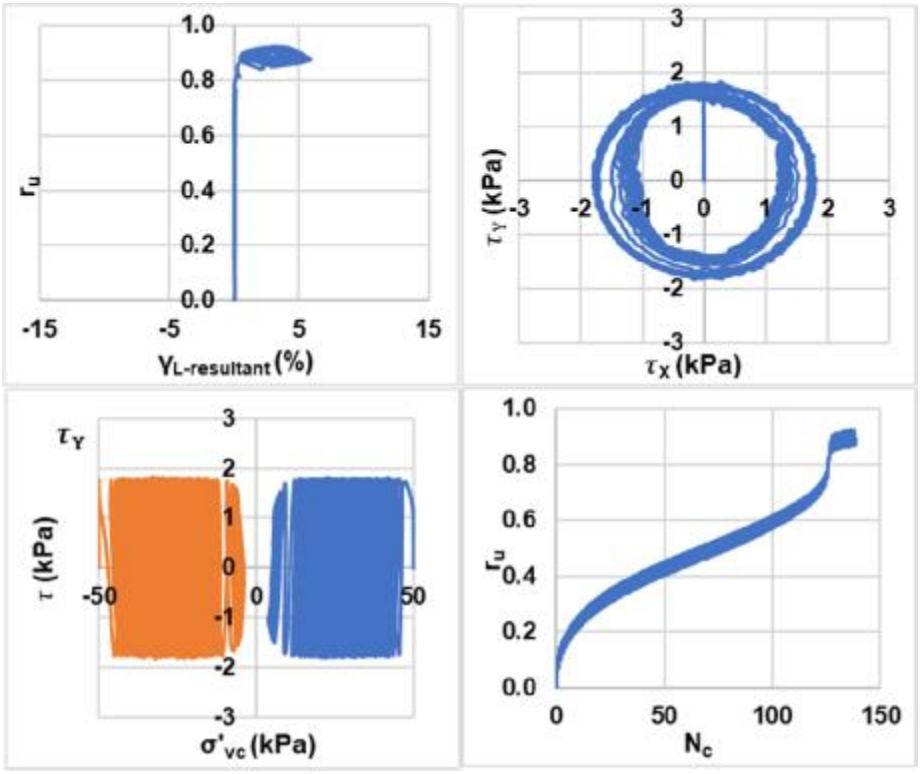


Bi-directional (Circular); $D_{rc}$ = 65%; $\sigma'_{vc}$ = 50 kPa; CSR = 0.035 (Re-liquefaction)

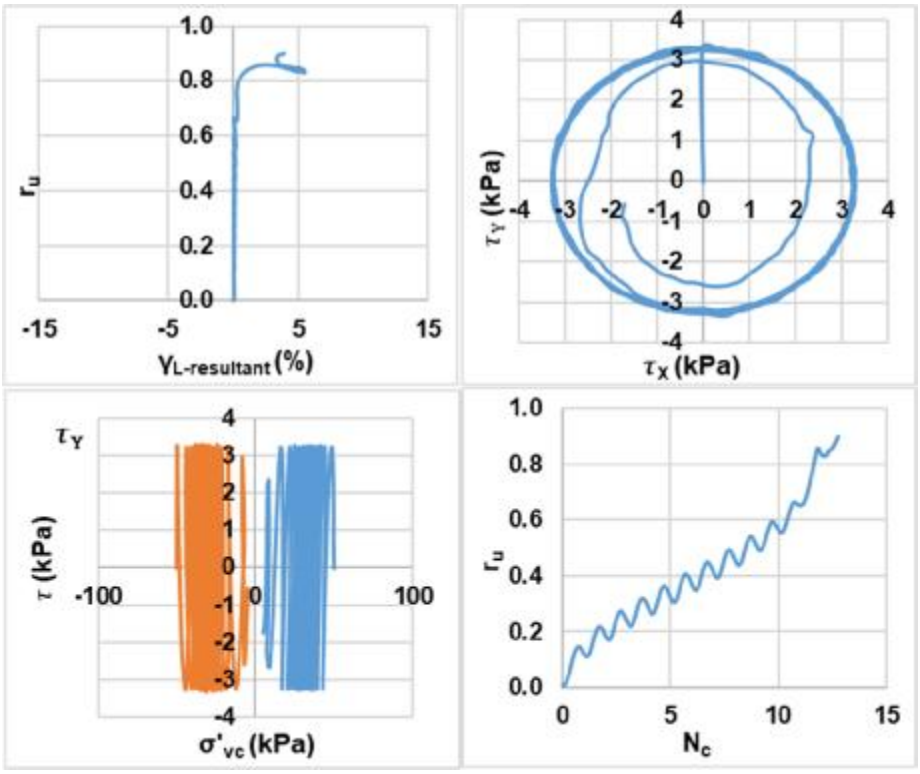


Bi-directional (Circular); $D_{rc}$ = 65%; $\sigma'_{vc}$ = 50 kPa; CSR = 0.065 (Liquefaction)

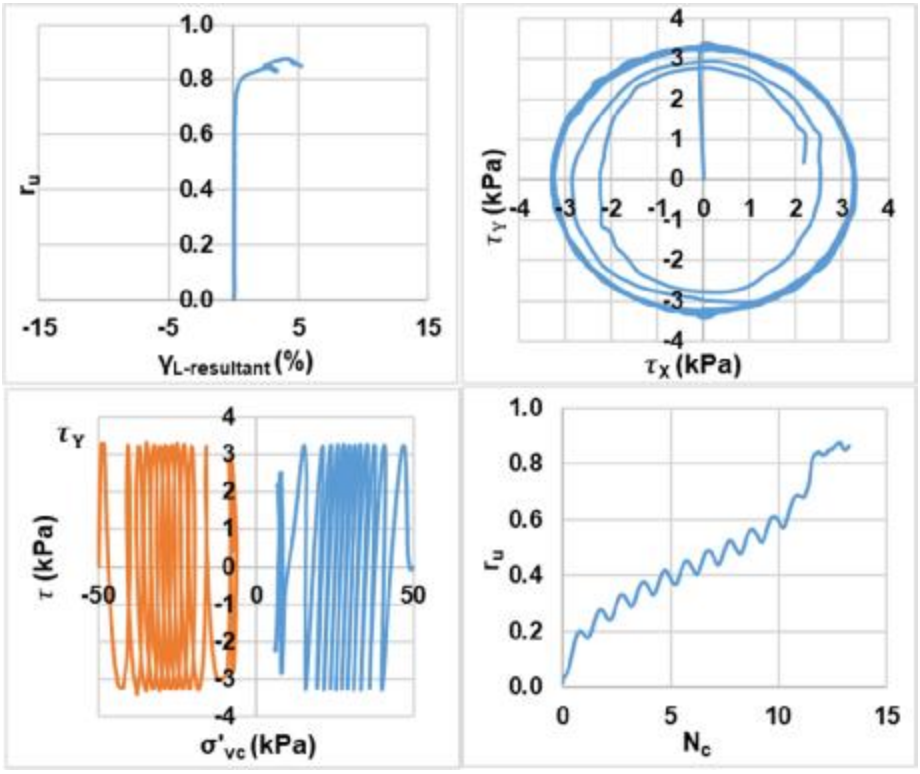


Bi-directional (Circular); $D_{rc}$ = 65%; $\sigma'_{vc}$ = 50 kPa; CSR = 0.065 (Re-liquefaction)

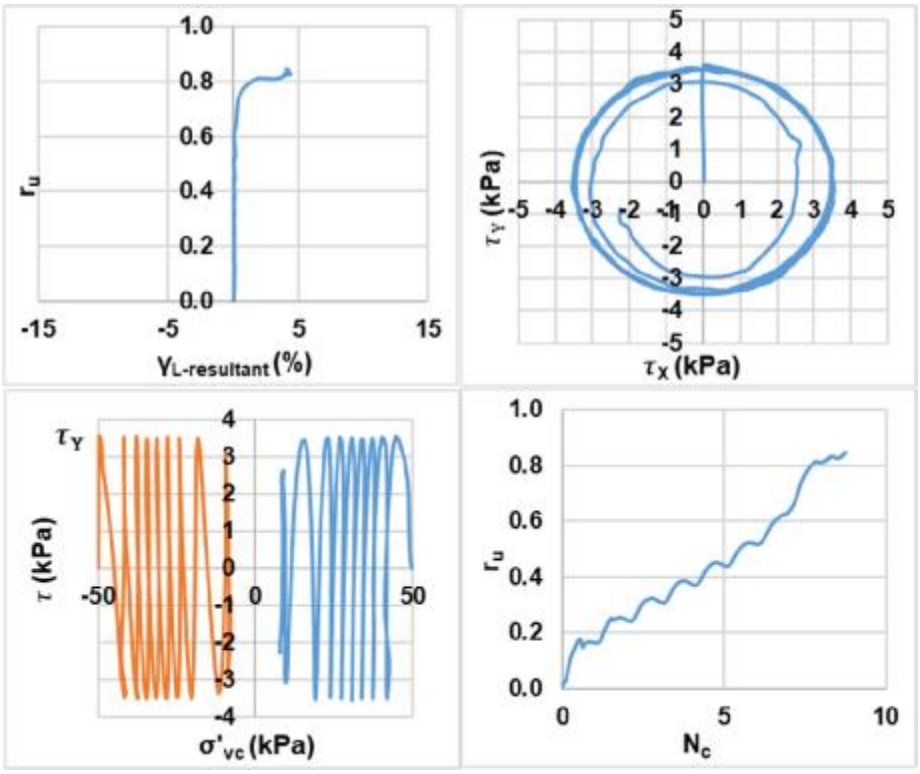


Bi-directional (Circular); $D_{rc}$ = 65%; $\sigma'_{vc}$ = 50 kPa; CSR = 0.07 (Liquefaction)

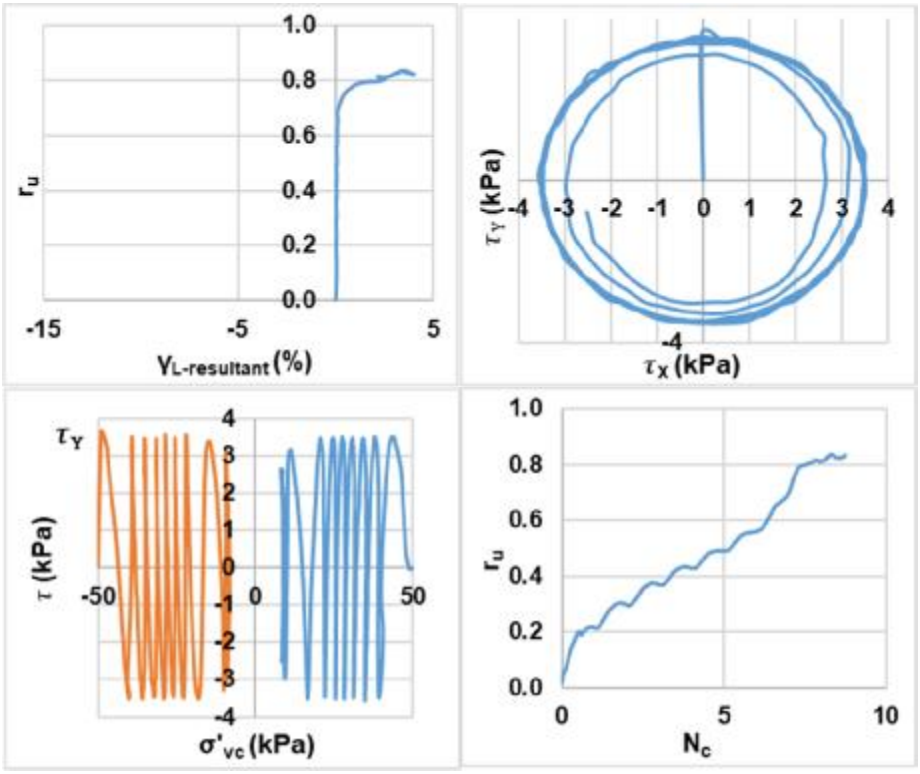


Bi-directional (Circular); $D_{rc}$ = 65%; $\sigma'_{vc}$ = 50 kPa; CSR = 0.07 (Re-liquefaction)

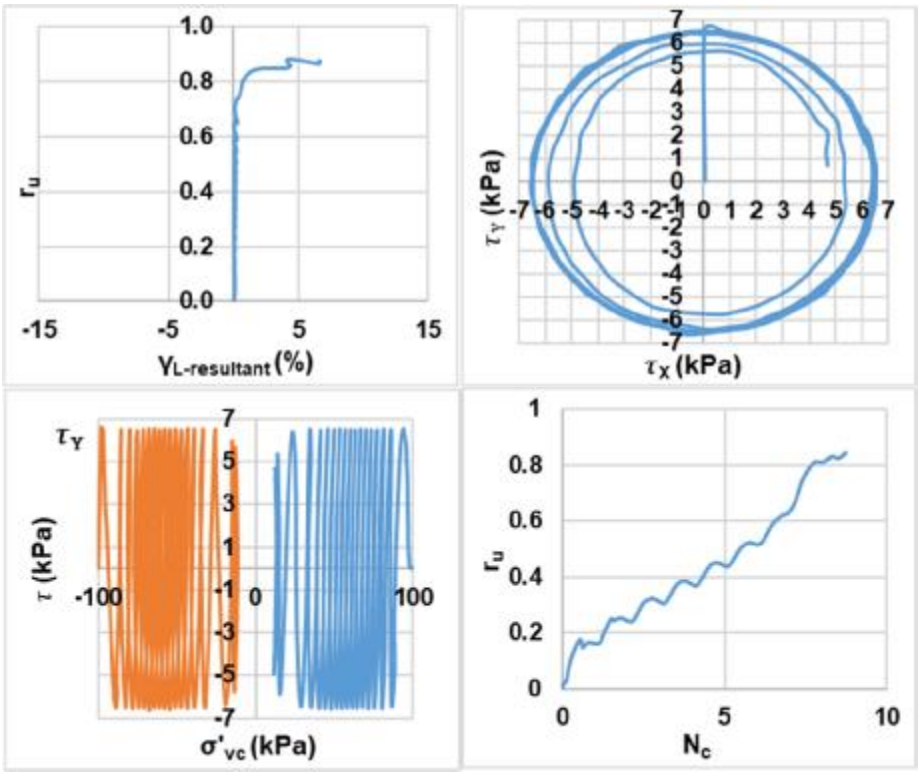


Bi-directional (Circular); $D_{rc}$ = 65%; $\sigma'_{vc}$ = 100 kPa; CSR = 0.065 (Liquefaction)

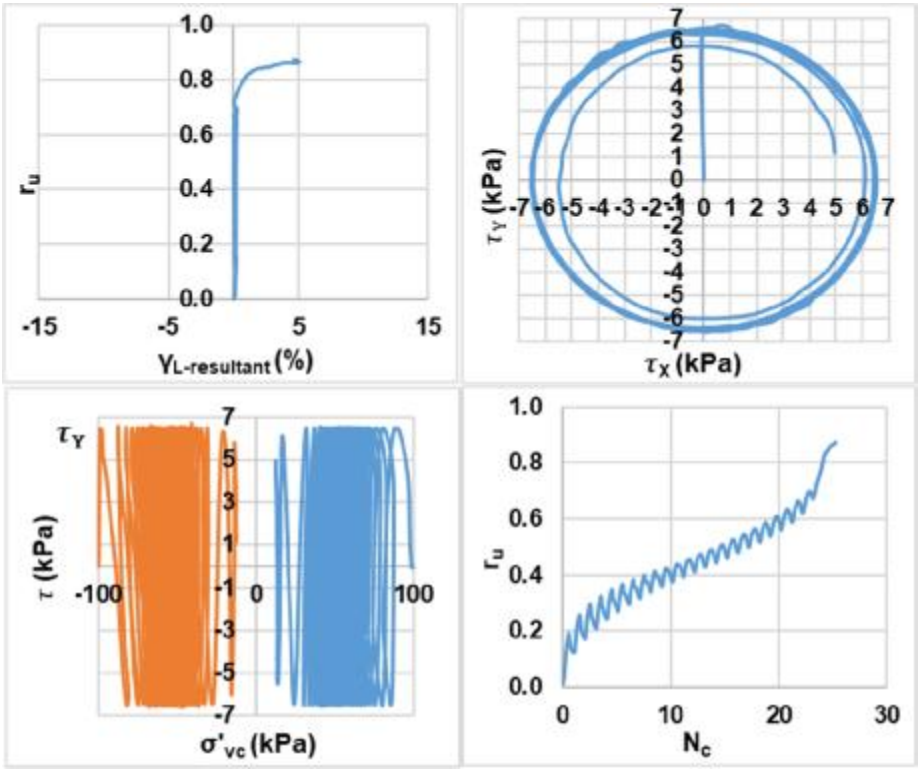


Bi-directional (Circular); $D_{rc}$ = 65%; $\sigma'_{vc}$ = 100 kPa; CSR = 0.065 (Re-liquefaction)

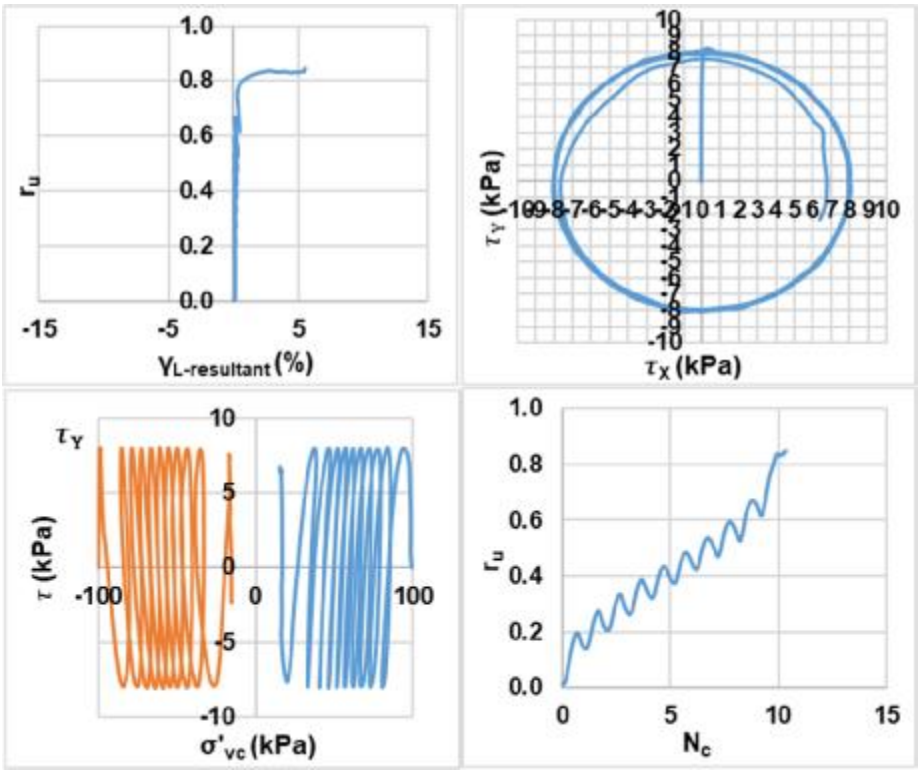


Bi-directional (Circular); $D_{rc}$ = 65%; $\sigma'_{vc}$ = 100 kPa; CSR = 0.08 (Liquefaction)

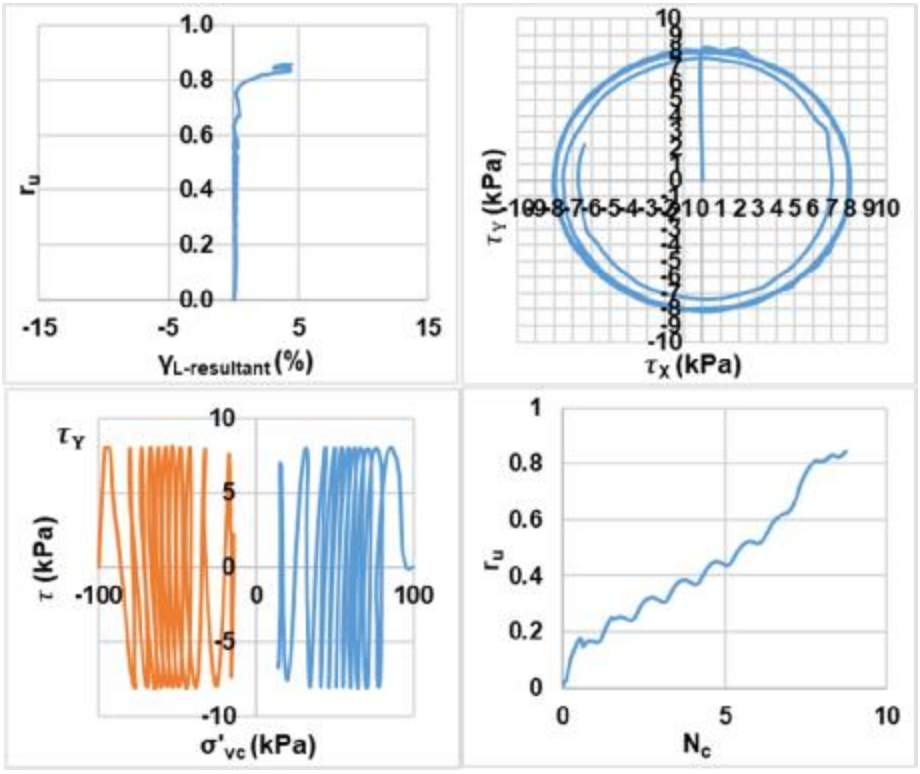


Bi-directional (Circular); $D_{rc}$ = 65%; $\sigma'_{vc}$ = 100 kPa; CSR = 0.08 (Re-liquefaction)

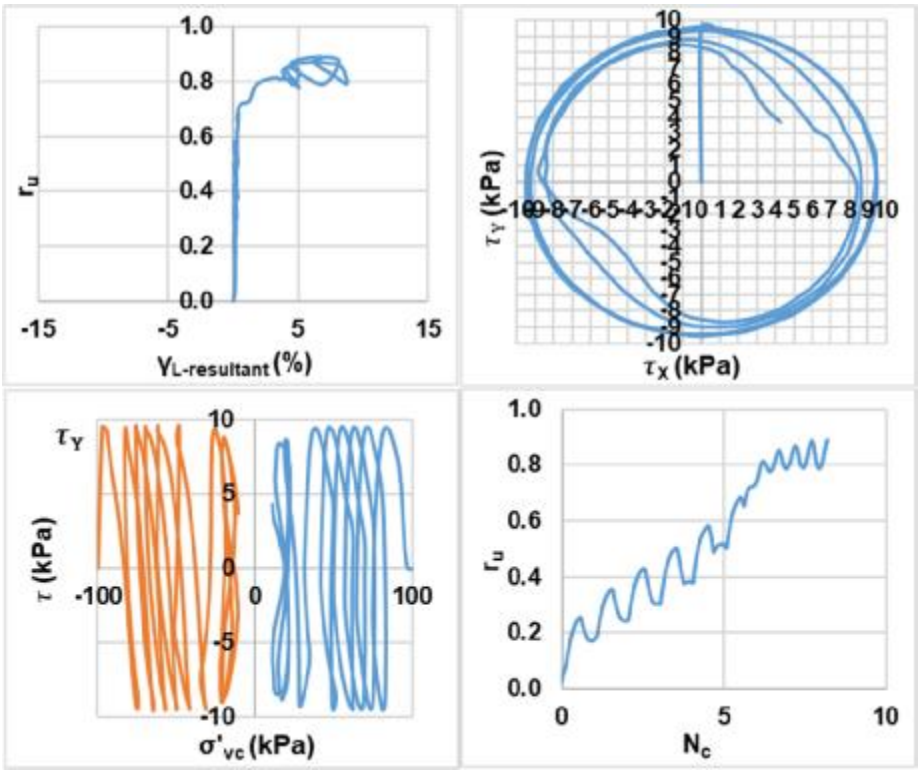


Bi-directional (Circular); $D_{rc}$ = 65%; $\sigma'_{vc}$ = 100 kPa; CSR = 0.095 (Liquefaction)

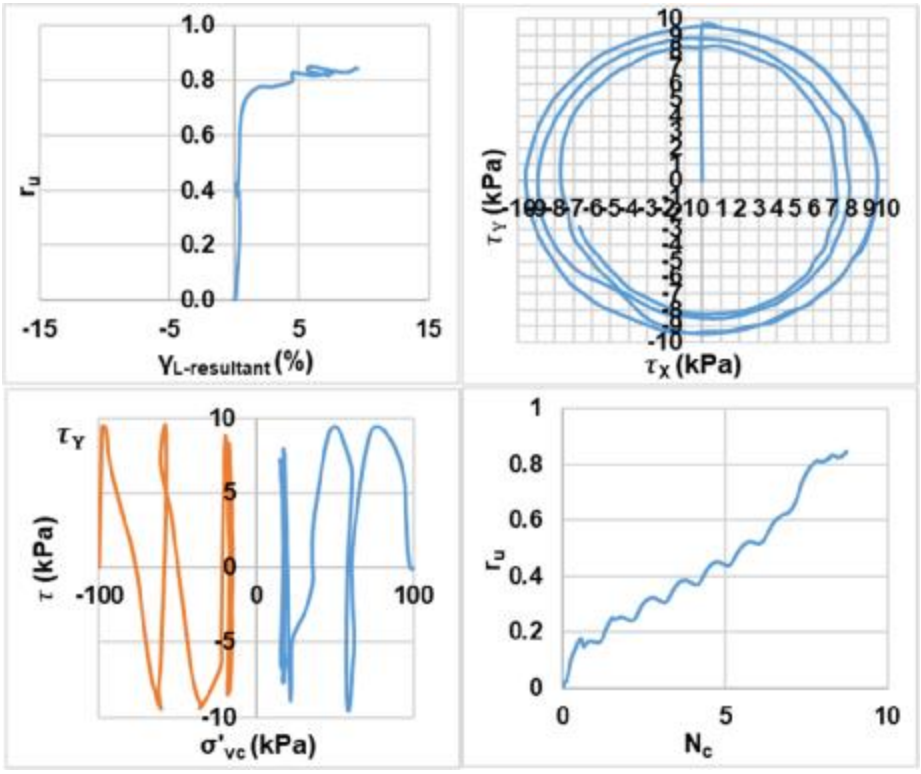


Bi-directional (Circular); $D_{rc}$ = 65%; $\sigma'_{vc}$ = 100 kPa; CSR = 0.095 (Re-liquefaction)

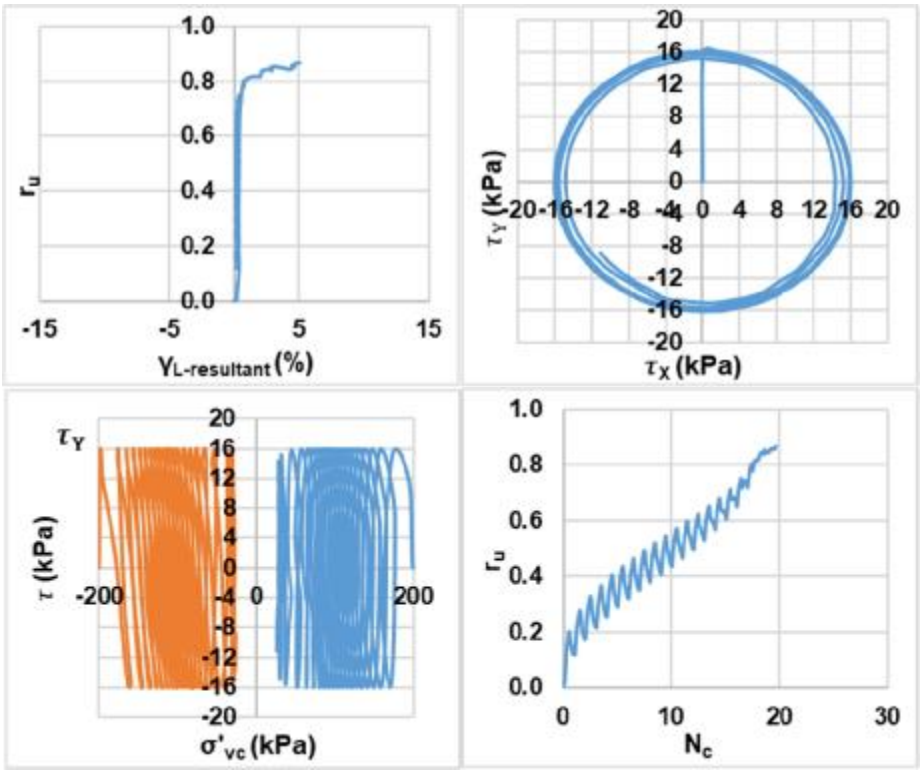


Bi-directional (Circular); $D_{rc}$ = 65%; $\sigma'_{vc}$ = 200 kPa; CSR = 0.08 (Liquefaction)

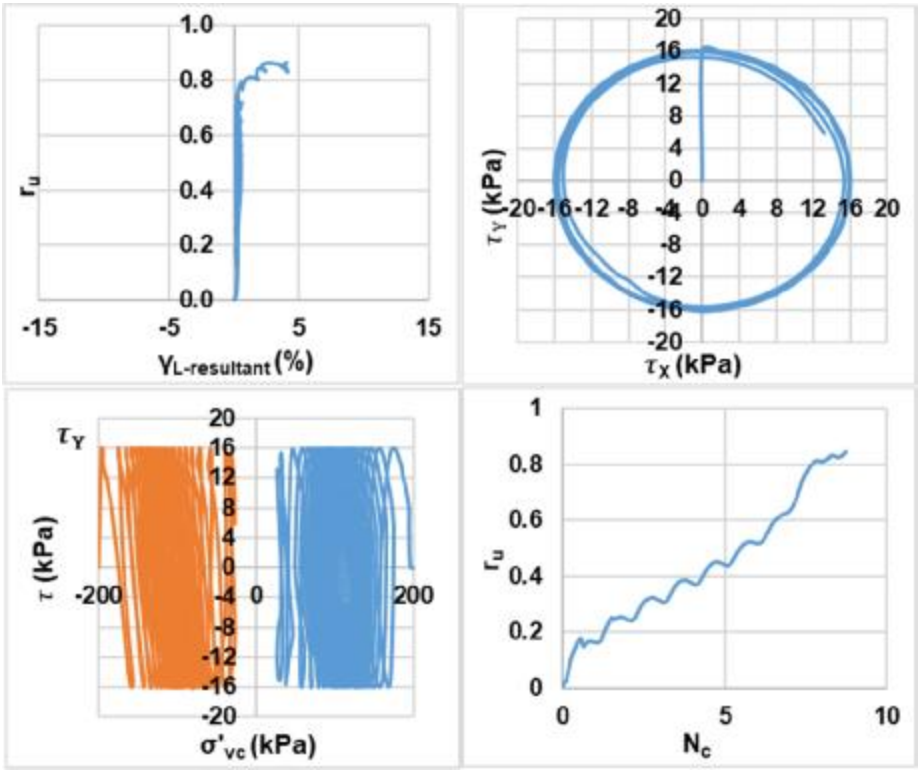


Bi-directional (Circular); $D_{rc}$ = 65%; $\sigma'_{vc}$ = 200 kPa; CSR = 0.08 (Re-liquefaction)

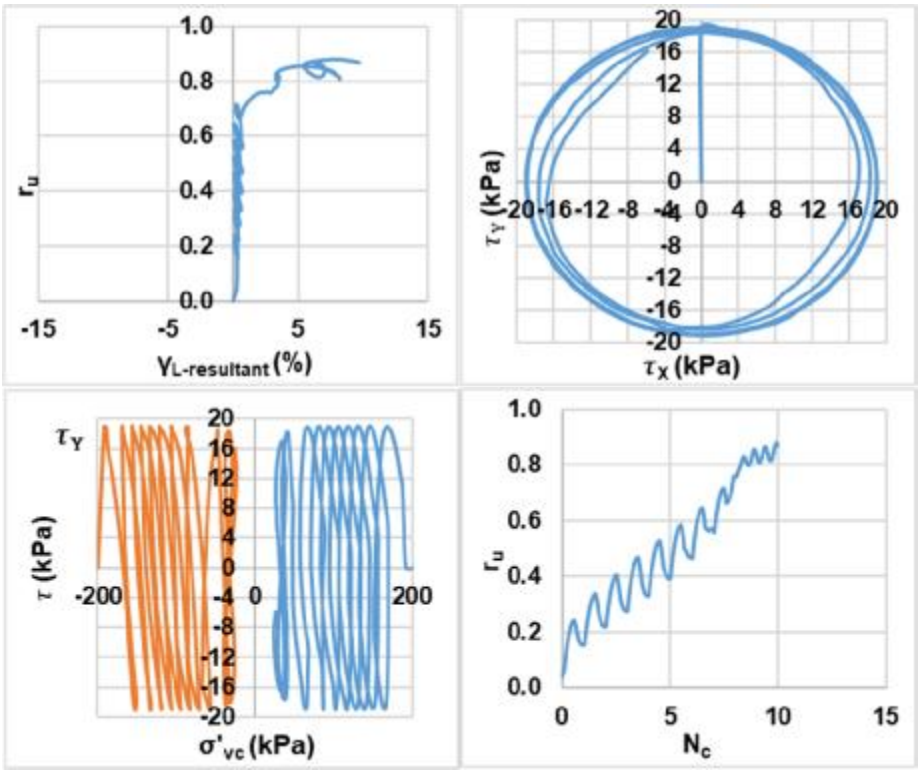


Bi-directional (Circular); $D_{rc}$ = 65%; $\sigma'_{vc}$ = 200 kPa; CSR = 0.095 (Liquefaction)

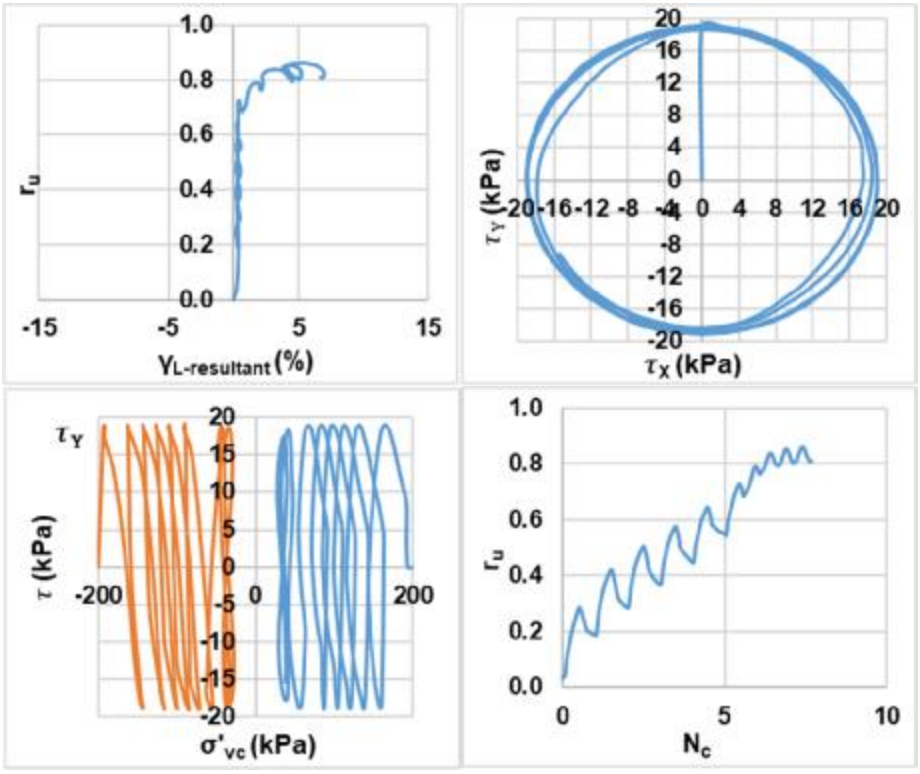


Bi-directional (Circular); $D_{rc}$ = 65%; $\sigma'_{vc}$ = 200 kPa; CSR = 0.095 (Re-liquefaction)

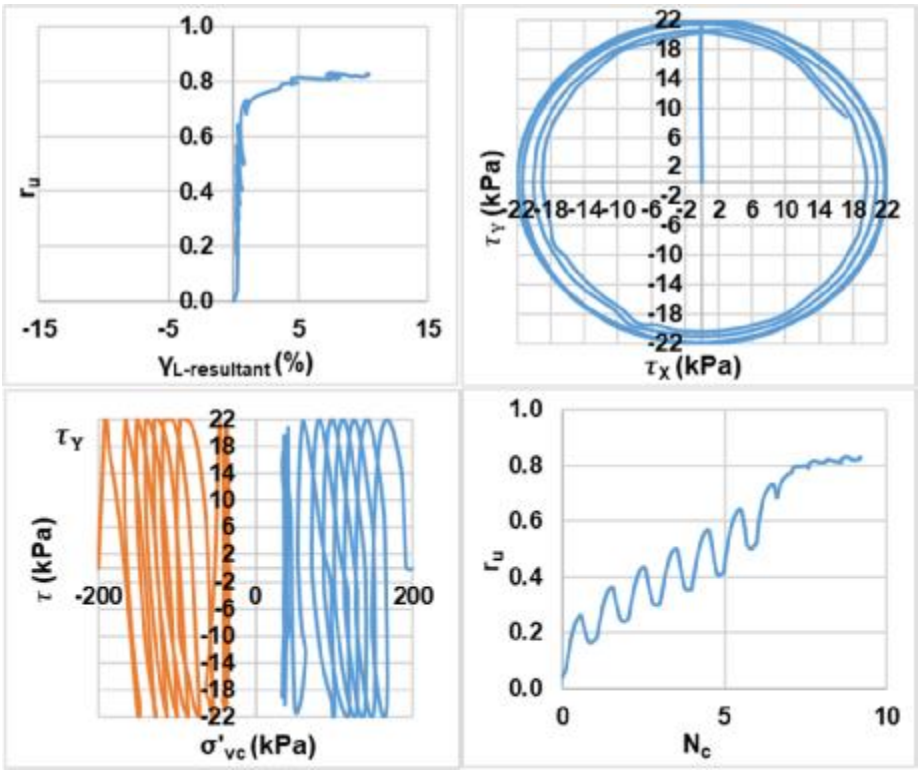


Bi-directional (Circular); $D_{rc}$ = 65%; $\sigma'_{vc}$ = 200 kPa; CSR = 0.11 (Liquefaction)

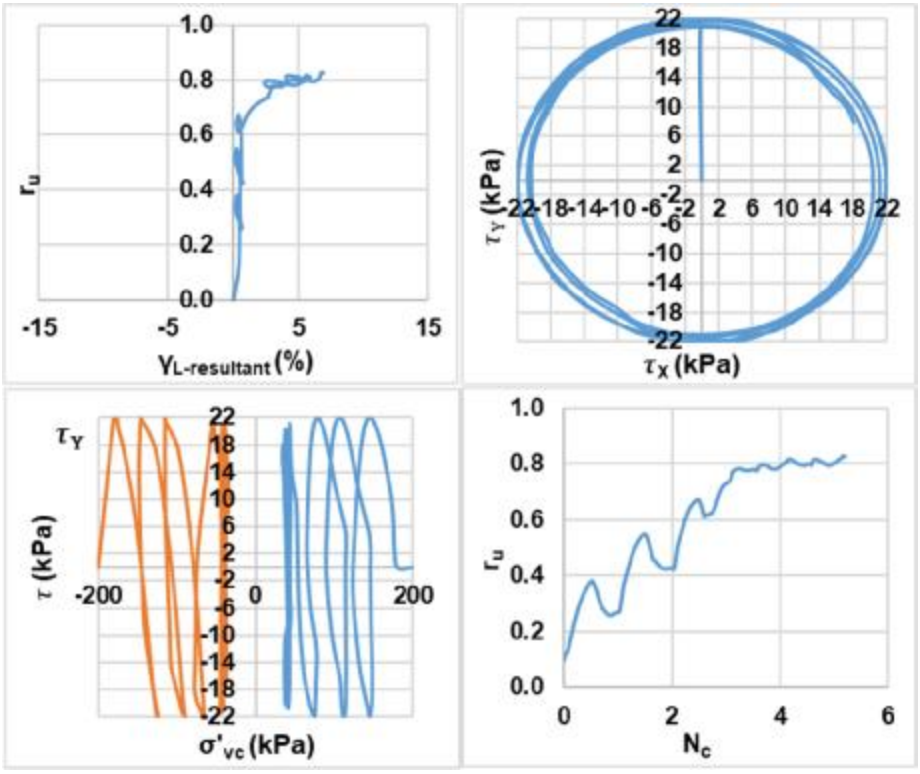


Bi-directional (Circular); $D_{rc}$ = 65%; $\sigma'_{vc}$ = 200 kPa; CSR = 0.11 (Re-liquefaction)

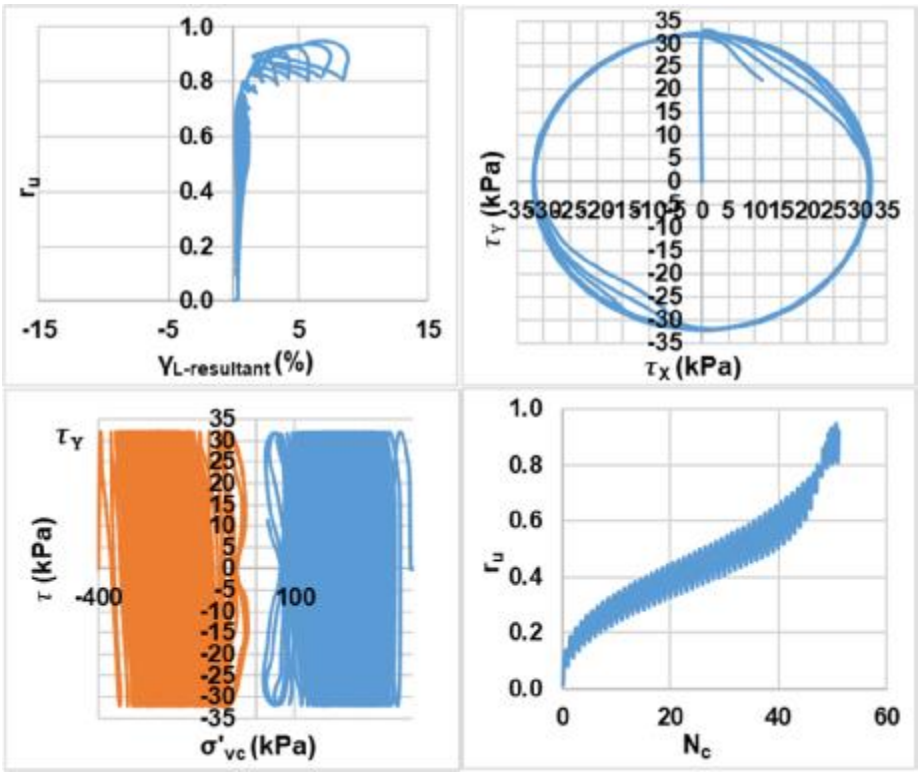


Bi-directional (Circular); $D_{rc}$ = 65%; $\sigma'_{vc}$ = 400 kPa; CSR = 0.08 (Liquefaction)

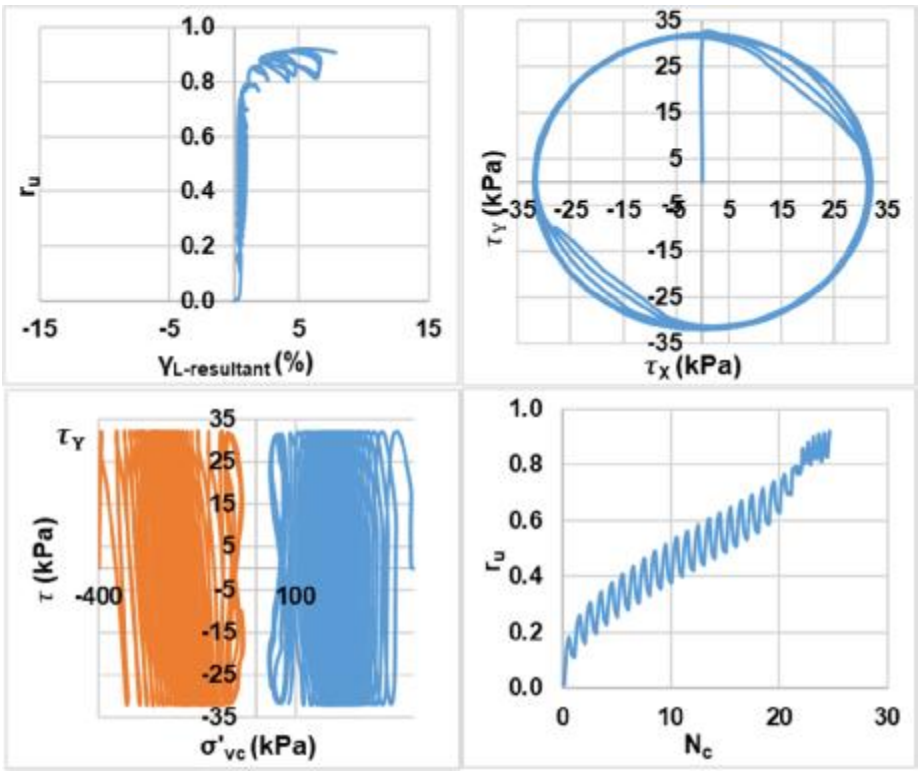


Bi-directional (Circular); $D_{rc}$ = 65%; $\sigma'_{vc}$ = 400 kPa; CSR = 0.08 (Re-liquefaction)

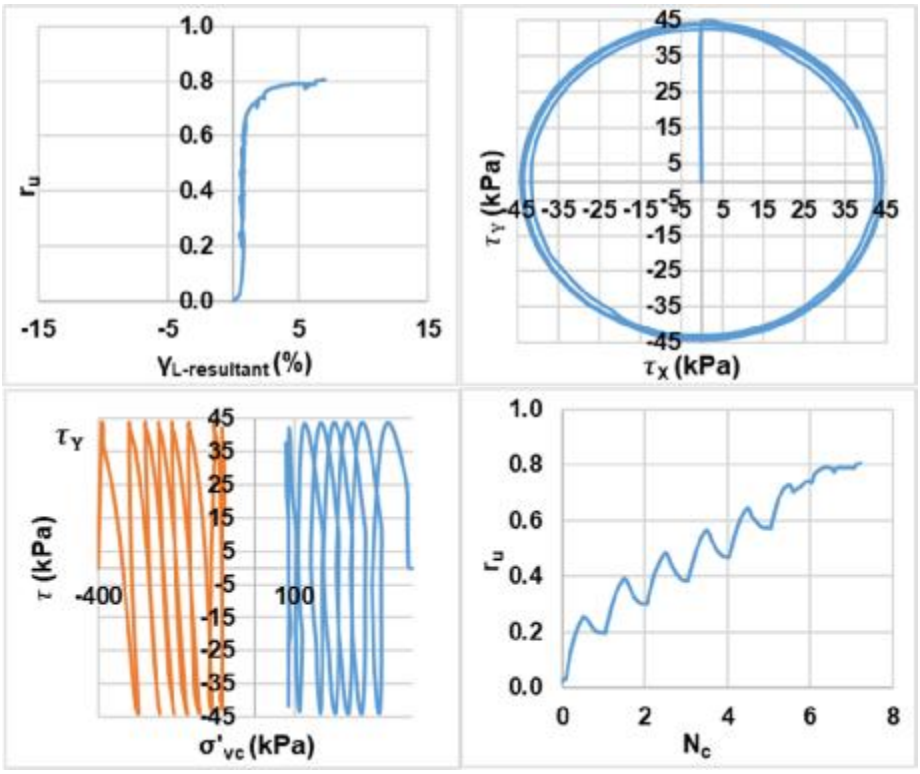


Bi-directional (Circular); $D_{rc}$ = 65%; $\sigma'_{vc}$ = 400 kPa; CSR = 0.11 (Liquefaction)

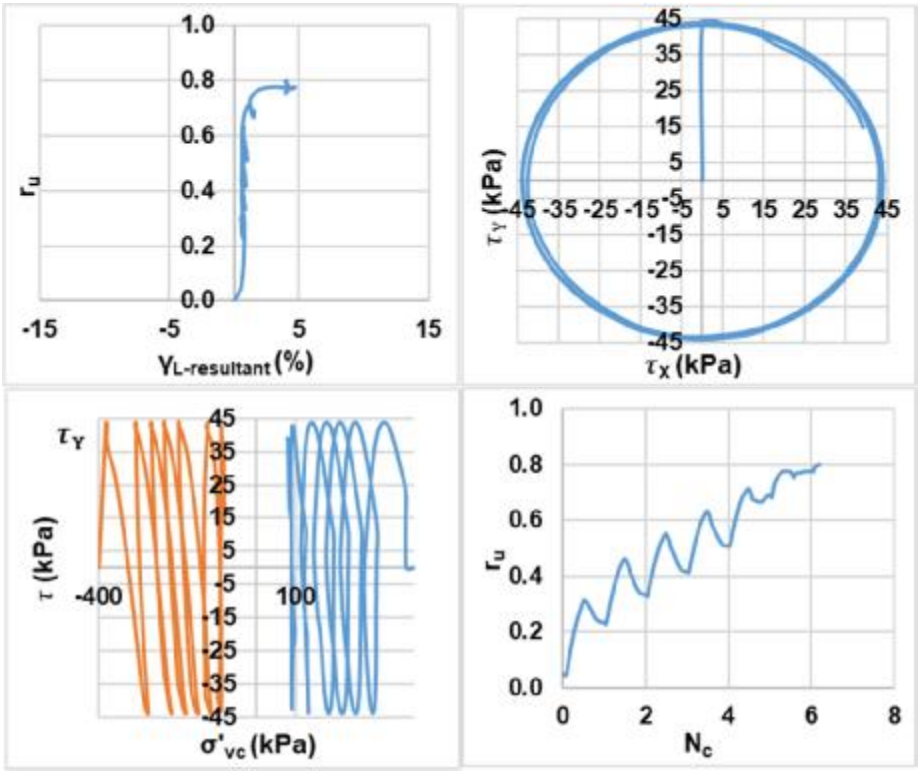


Bi-directional (Circular); $D_{rc}$ = 65%; $\sigma'_{vc}$ = 400 kPa; CSR = 0.11 (Re-liquefaction)

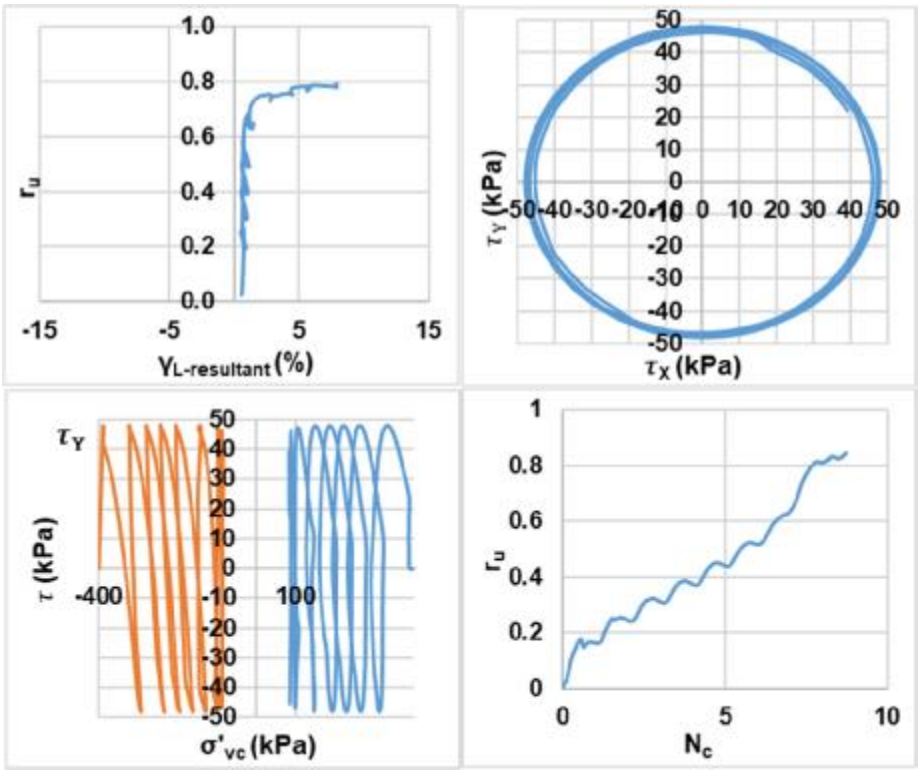


Bi-directional (Circular); $D_{rc}$ = 65%; $\sigma'_{vc}$ = 400 kPa; CSR = 0.12 (Liquefaction)

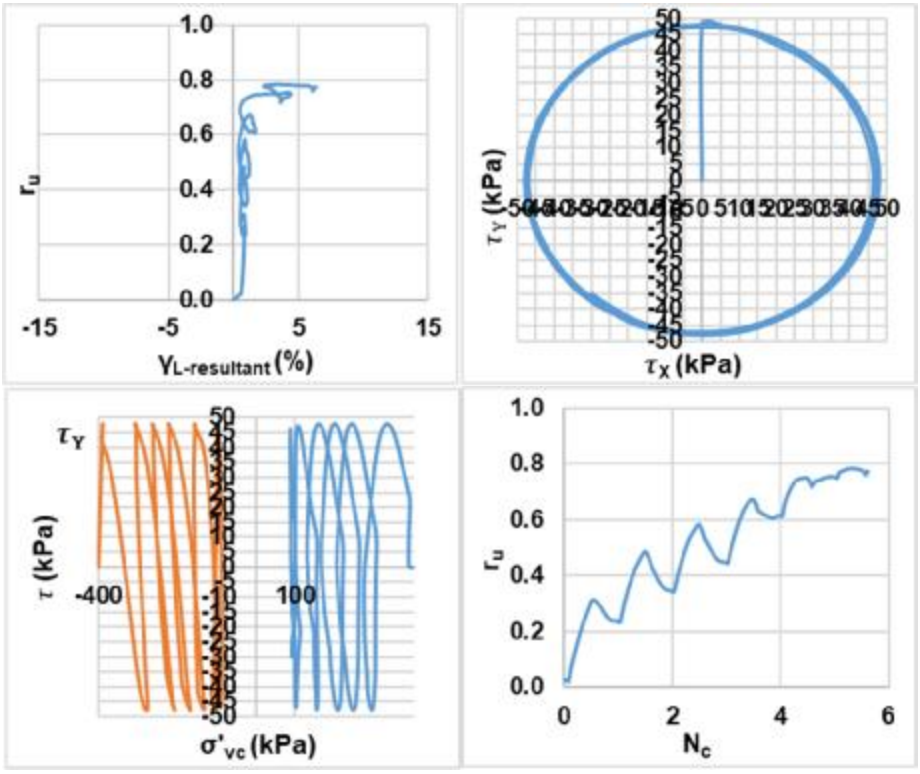


Bi-directional (Circular); $D_{rc}$ = 65%; $\sigma'_{vc}$ = 400 kPa; CSR = 0.12 (Re-liquefaction)

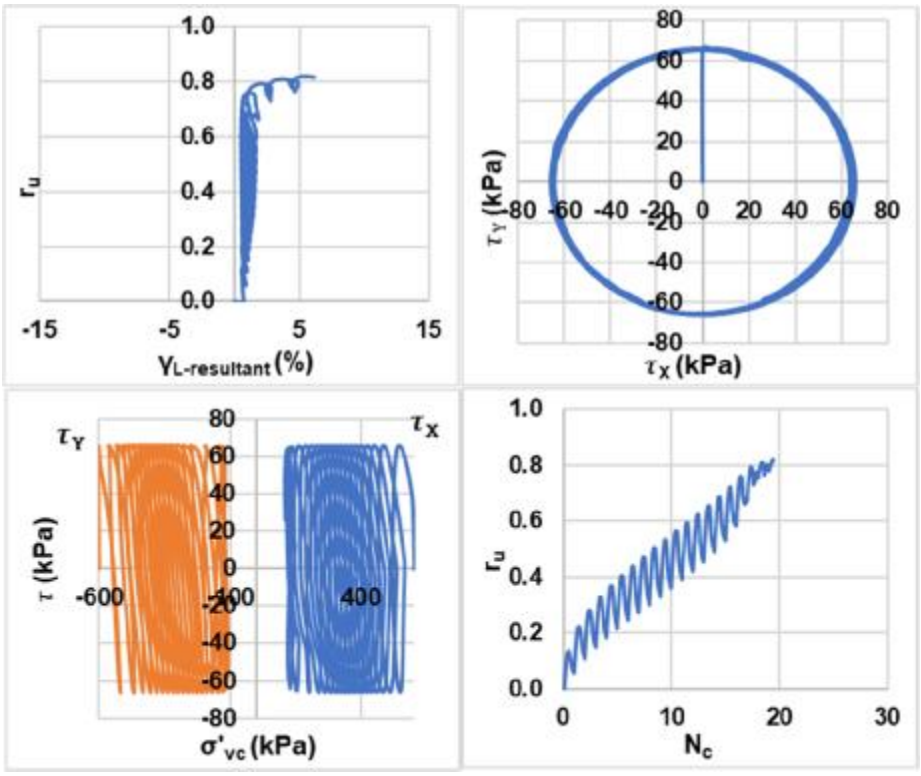


Bi-directional (Circular); $D_{rc}$ = 65%; $\sigma'_{vc}$ = 600 kPa; CSR = 0.11 (Liquefaction)

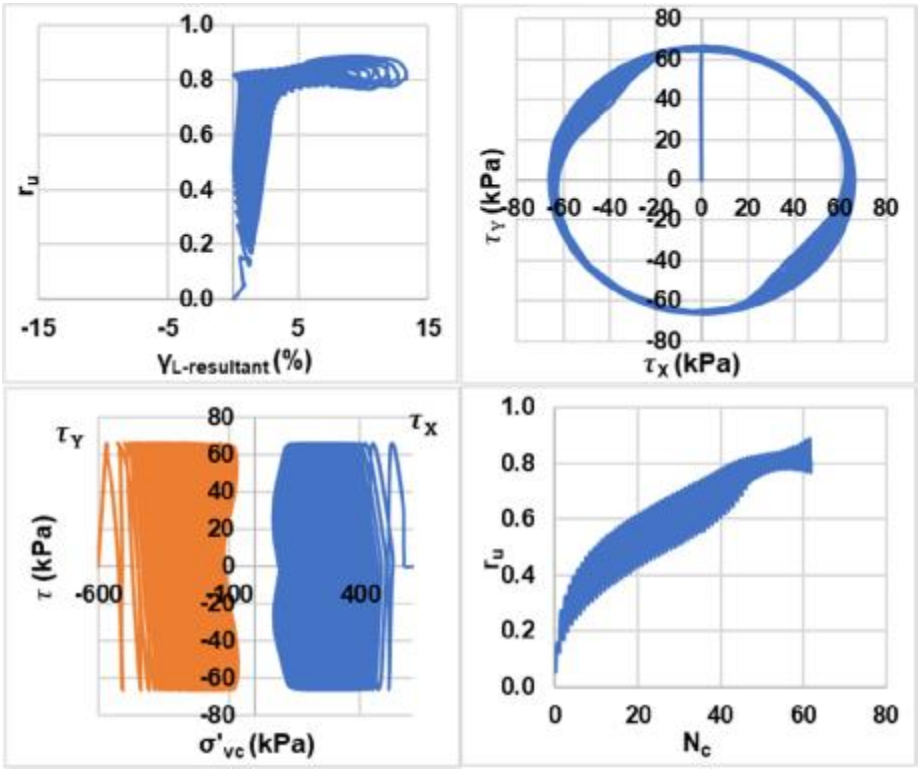


Bi-directional (Circular); $D_{rc}$ = 65%; $\sigma'_{vc}$ = 600 kPa; CSR = 0.11 (Re-liquefaction)

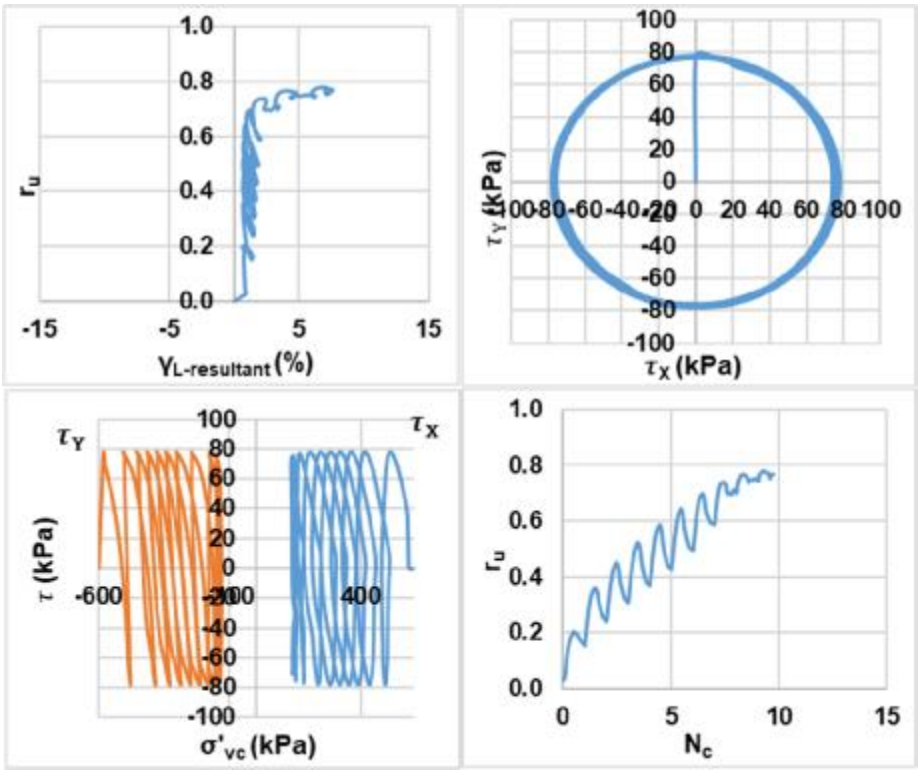


Bi-directional (Circular); $D_{rc}$ = 65%; $\sigma'_{vc}$ = 600 kPa; CSR = 0.13 (Liquefaction)

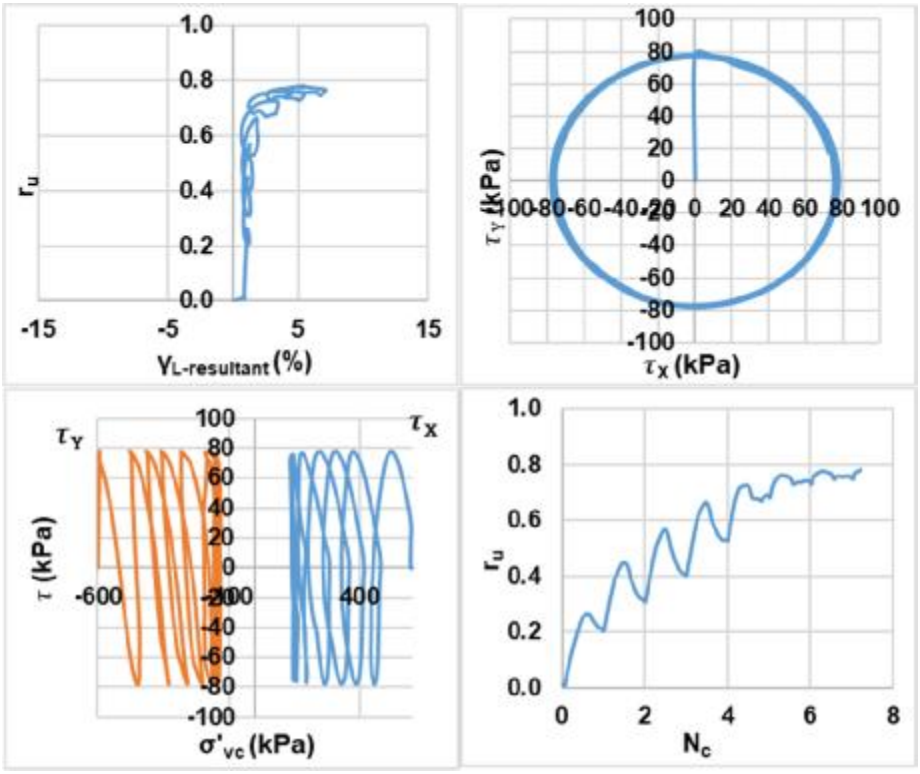


Bi-directional (Circular); $D_{rc}$ = 65%; $\sigma'_{vc}$ = 600 kPa; CSR = 0.13 (Re-liquefaction)

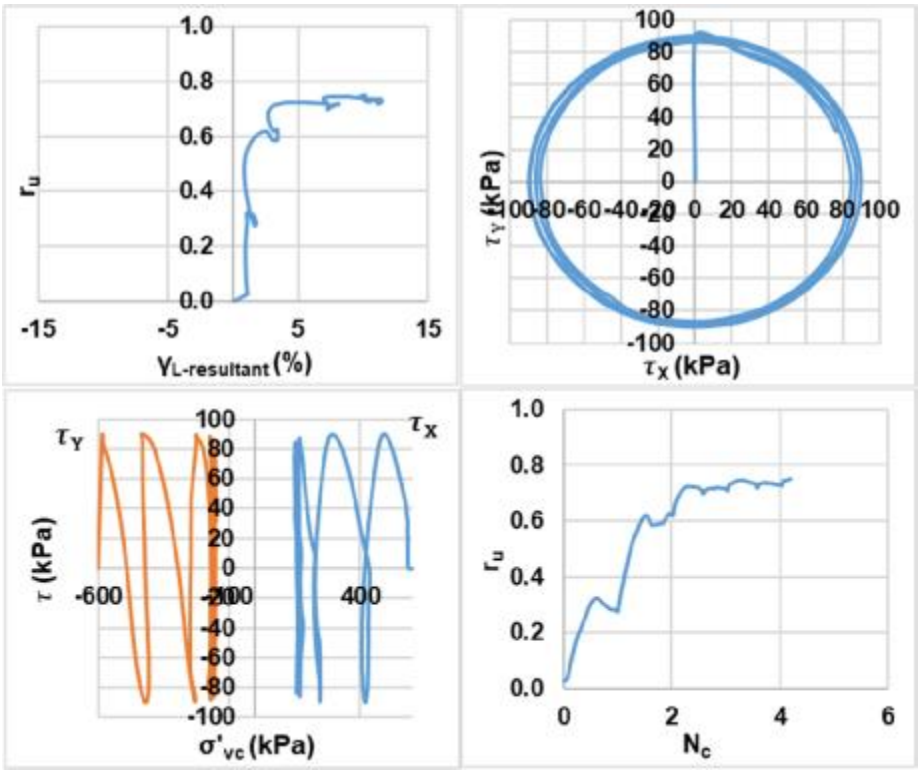


Bi-directional (Circular); $D_{rc}$ = 65%; $\sigma'_{vc}$ = 600 kPa; CSR = 0.15 (Liquefaction)

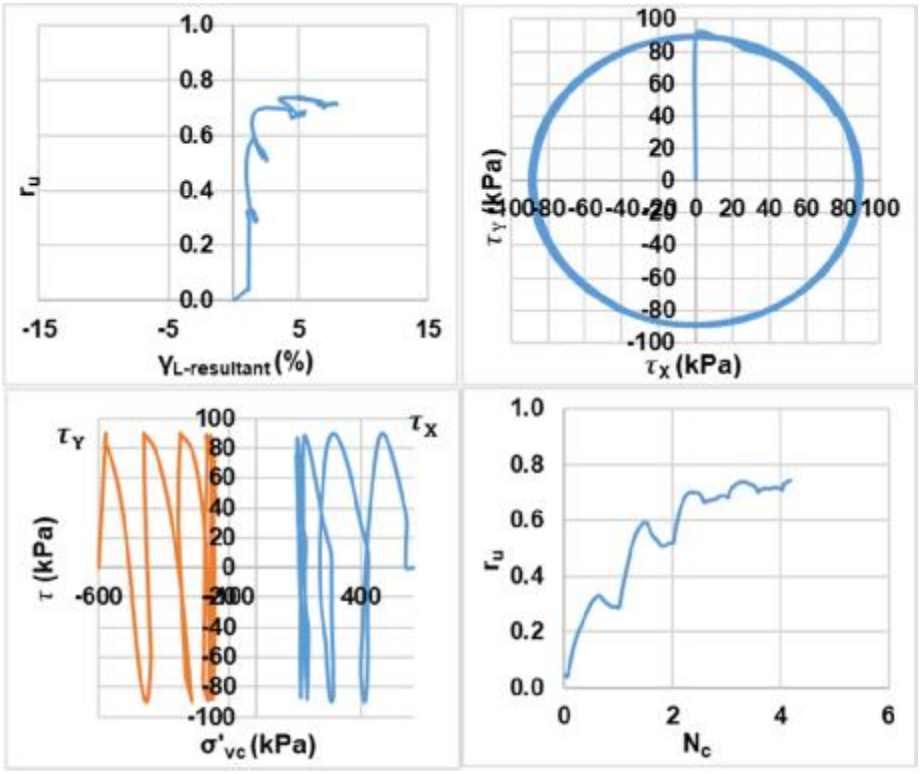


Bi-directional (Circular); $D_{rc}$ = 65%; $\sigma'_{vc}$ = 600 kPa; CSR = 0.15 (Re-liquefaction)

# Appendix 3

Bi-directional / Elliptical Cyclic Simple Shear Test Results

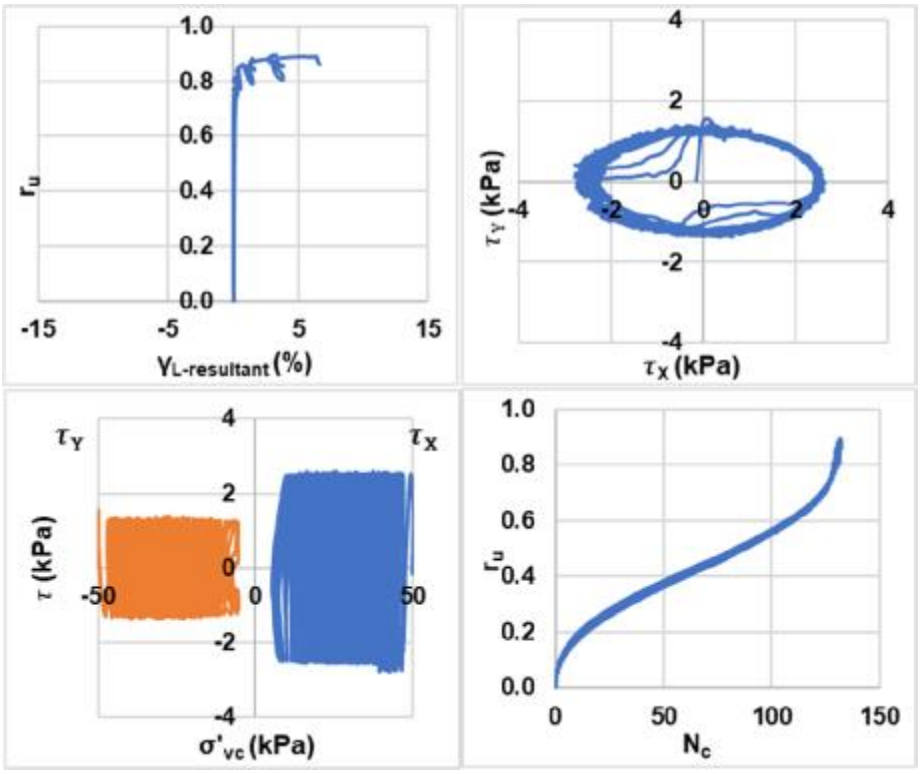


Bi-directional (Elliptical); $D_{rc}$ = 25%; $\sigma'_{vc}$ = 50 kPa; CSR = 0.05 (Liquefaction)

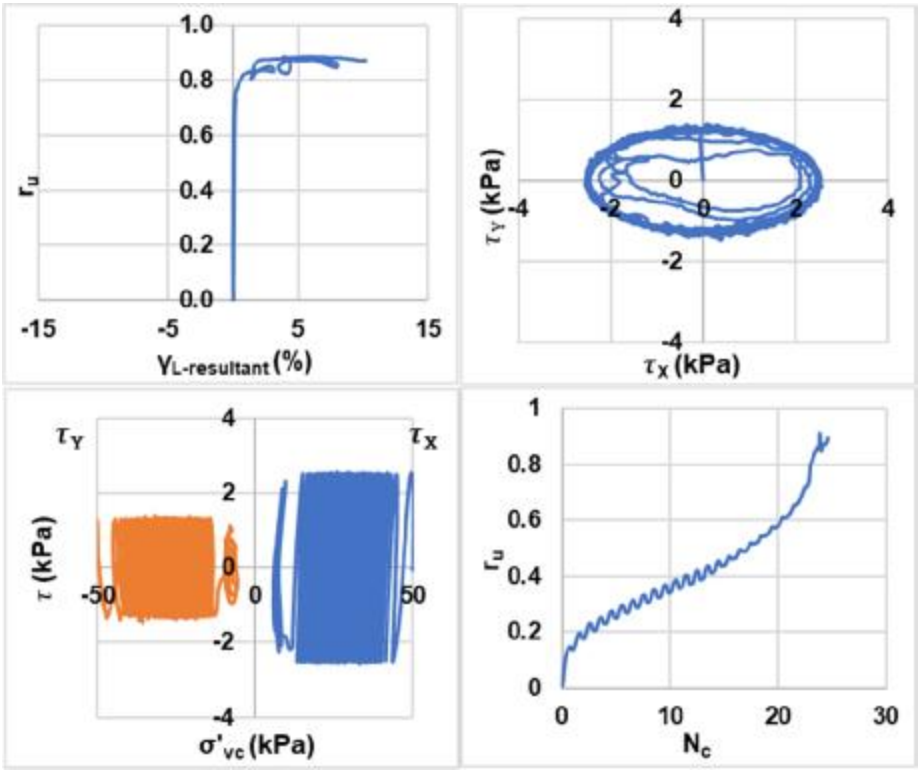


Bi-directional (Elliptical); $D_{rc}$ = 25%; $\sigma'_{vc}$ = 50 kPa; CSR = 0.05 (Re-liquefaction)

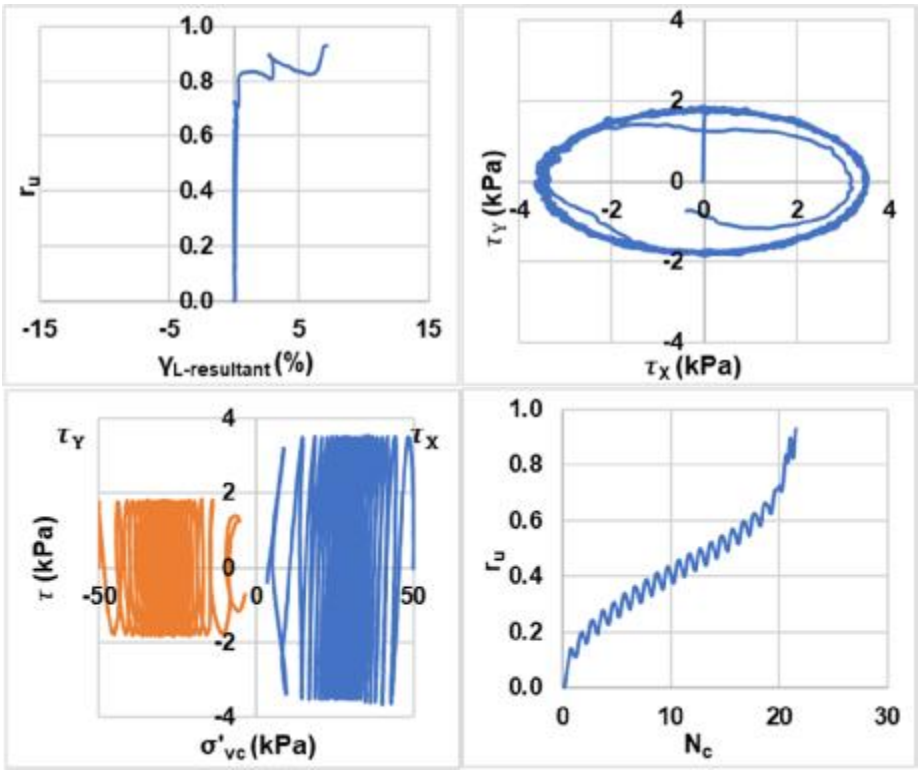


Bi-directional (Elliptical); $D_{rc}$ = 25%; $\sigma'_{vc}$ = 50 kPa; CSR = 0.07 (Liquefaction)

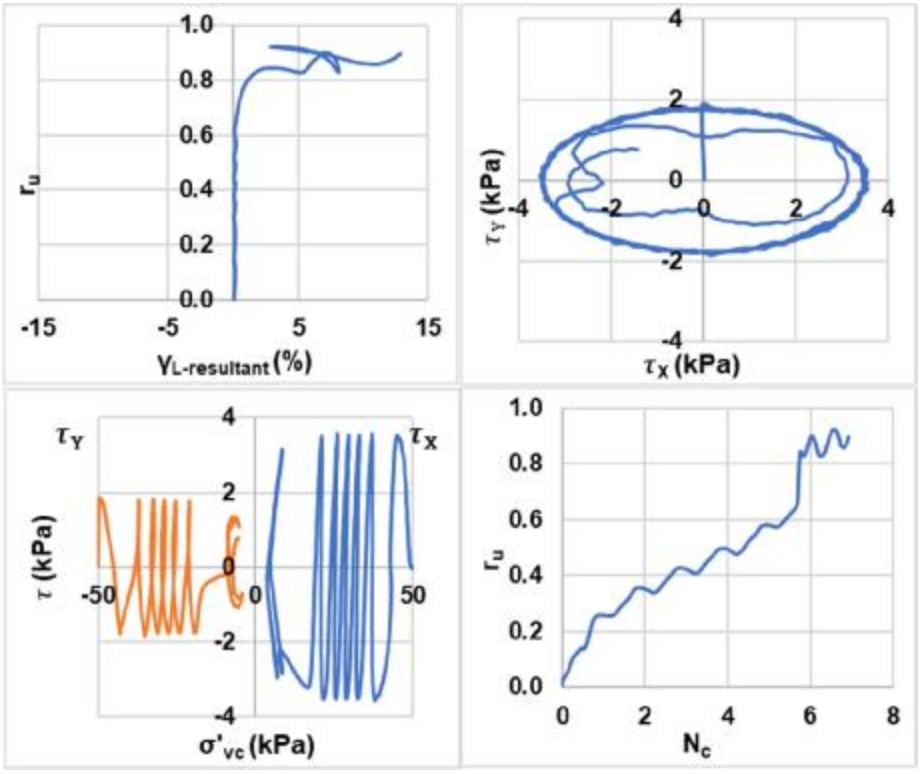


Bi-directional (Elliptical); $D_{rc}$ = 25%; $\sigma'_{vc}$ = 50 kPa; CSR = 0.07 (Re-liquefaction)

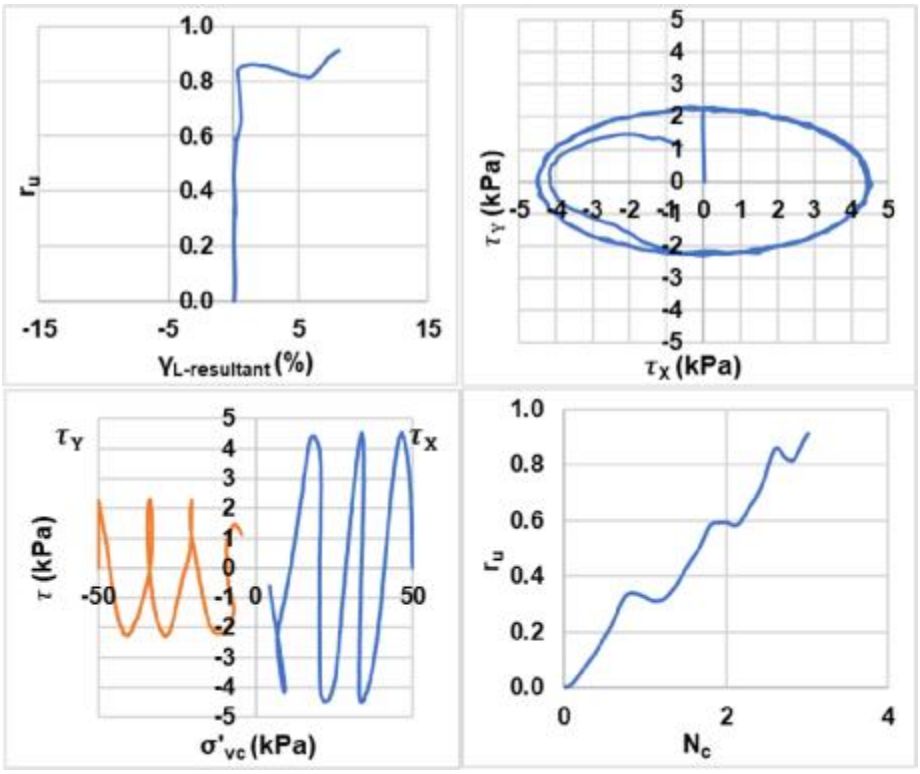


Bi-directional (Elliptical); $D_{rc}$ = 25%; $\sigma'_{vc}$ = 50 kPa; CSR = 0.09 (Liquefaction)

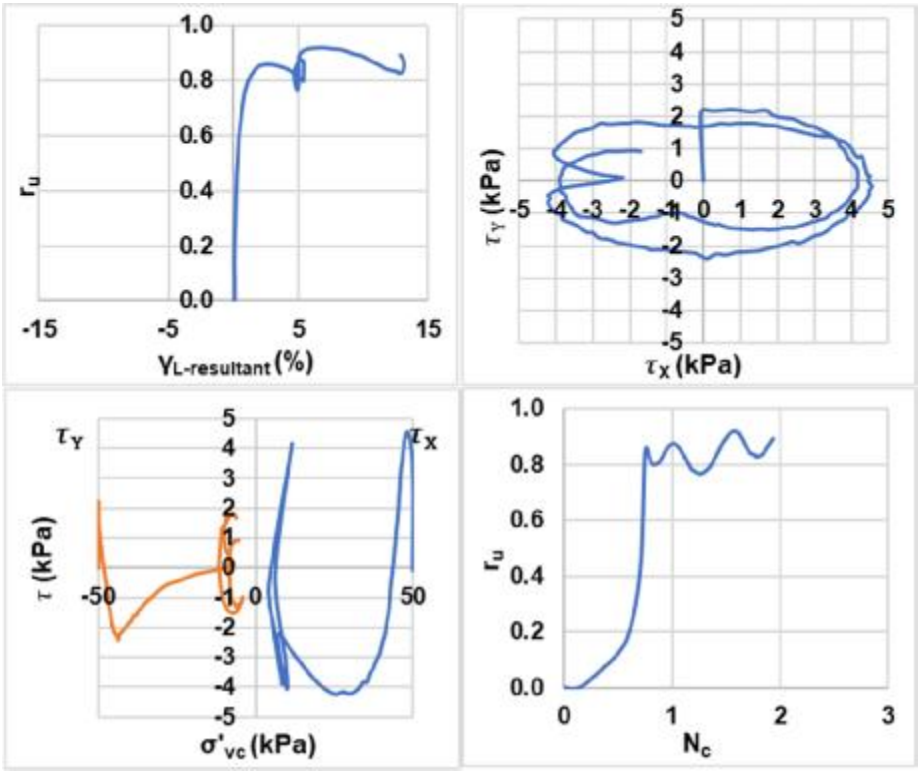


Bi-directional (Elliptical); $D_{rc}$ = 25%; $\sigma'_{vc}$ = 50 kPa; CSR = 0.09 (Re-liquefaction)

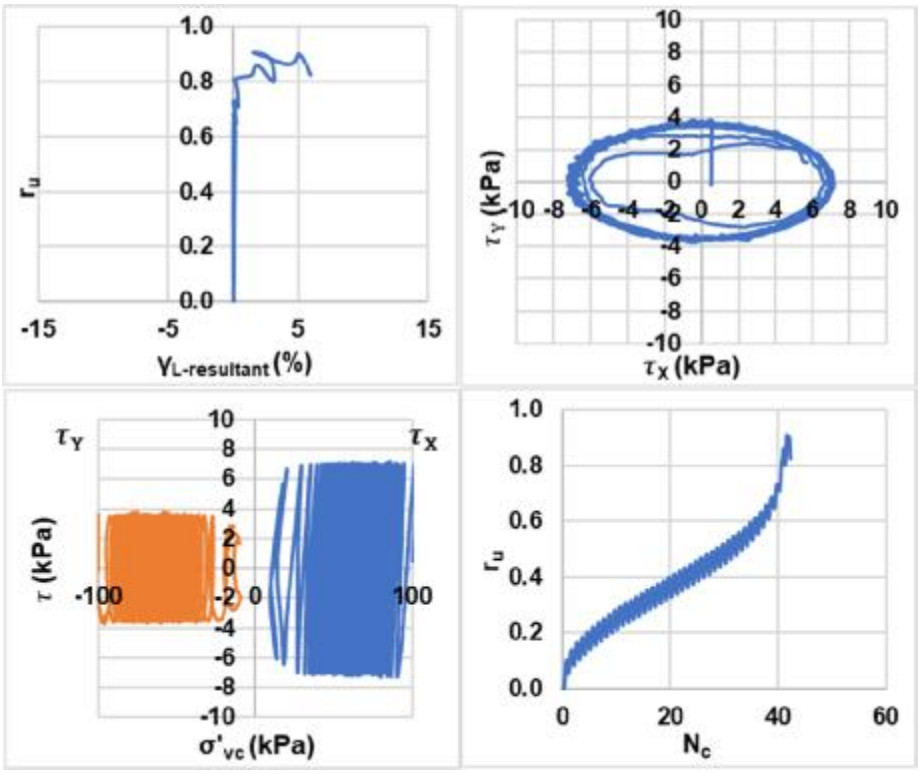


Bi-directional (Elliptical); $D_{rc}$ = 25%; $\sigma'_{vc}$ = 100 kPa; CSR = 0.07 (Liquefaction)

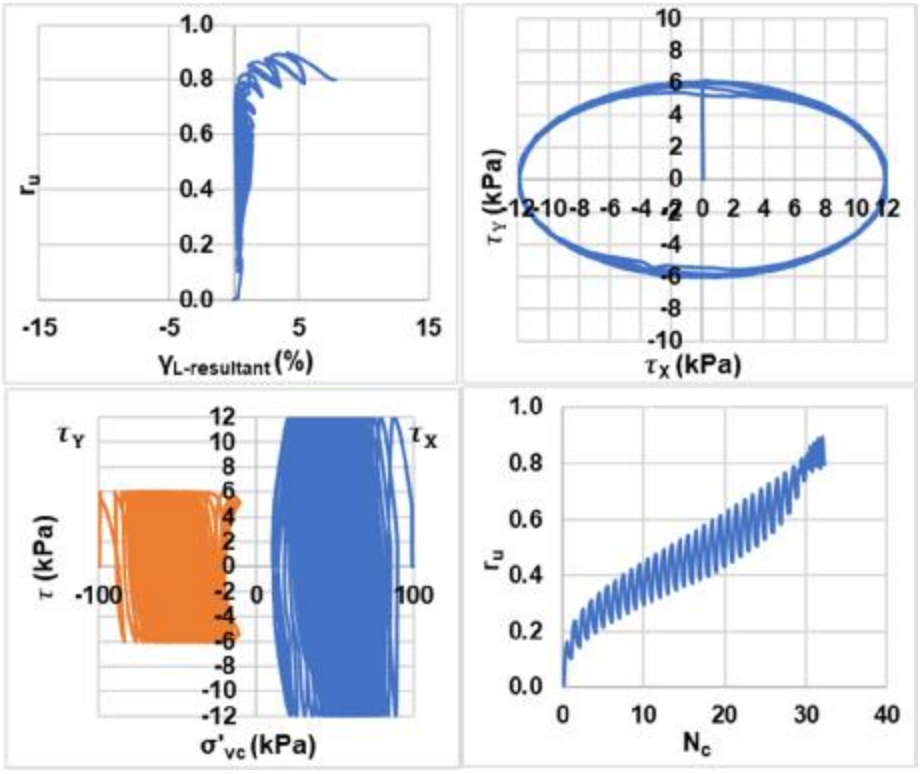


Bi-directional (Elliptical); $D_{rc}$ = 25%; $\sigma'_{vc}$ = 100 kPa; CSR = 0.07 (Re-liquefaction)

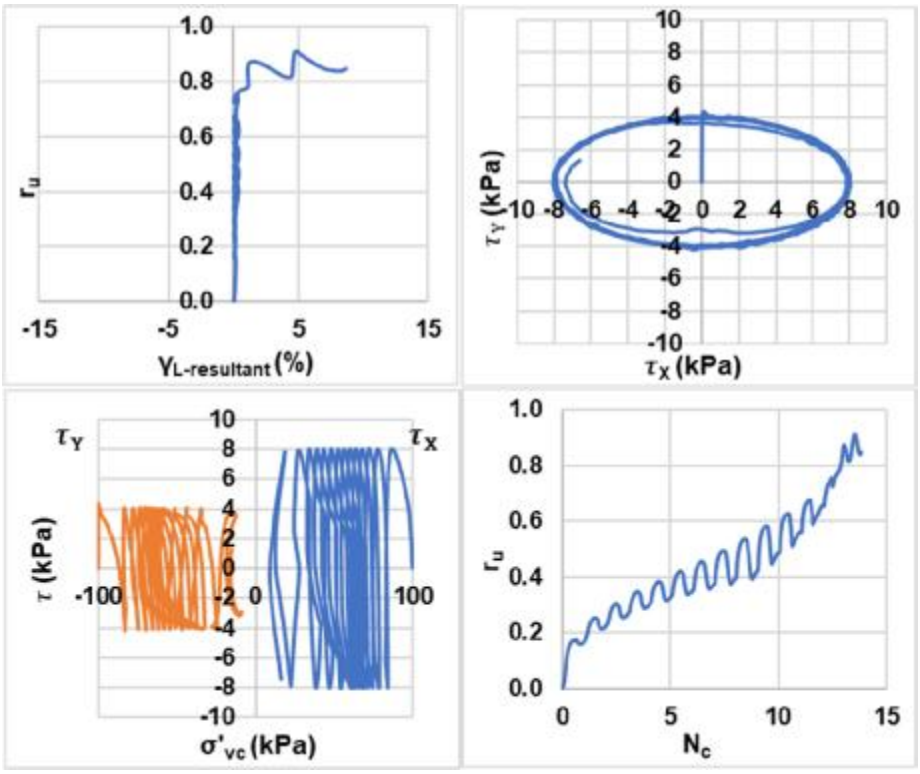


Bi-directional (Elliptical); $D_{rc}$ = 25%; $\sigma'_{vc}$ = 100 kPa; CSR = 0.08 (Liquefaction)

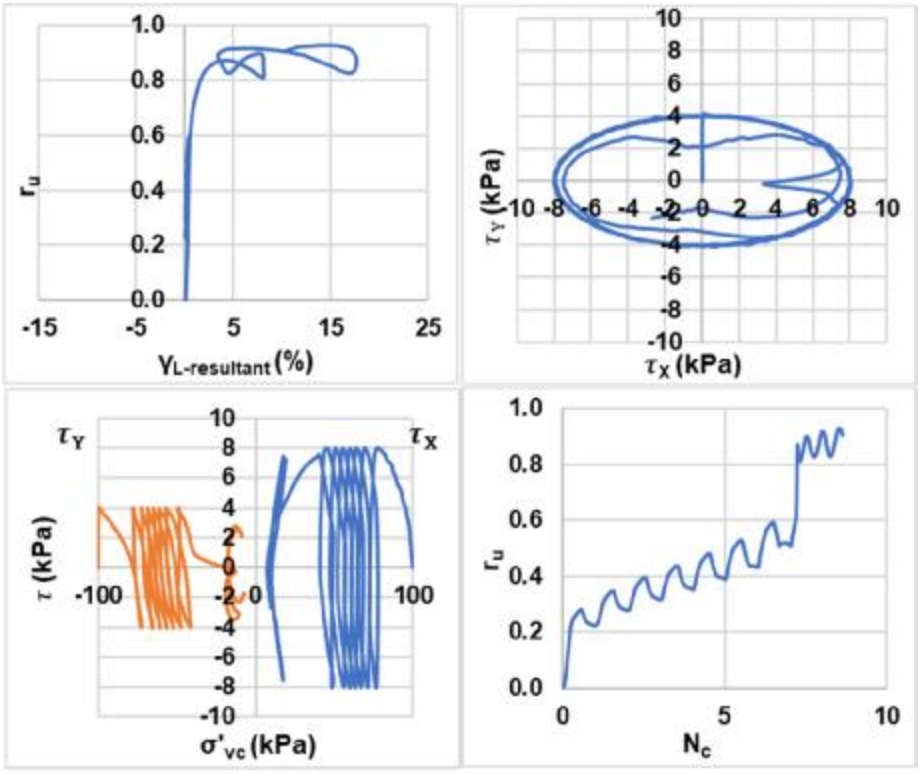


Bi-directional (Elliptical); $D_{rc}$ = 25%; $\sigma'_{vc}$ = 100 kPa; CSR = 0.08 (Re-liquefaction)

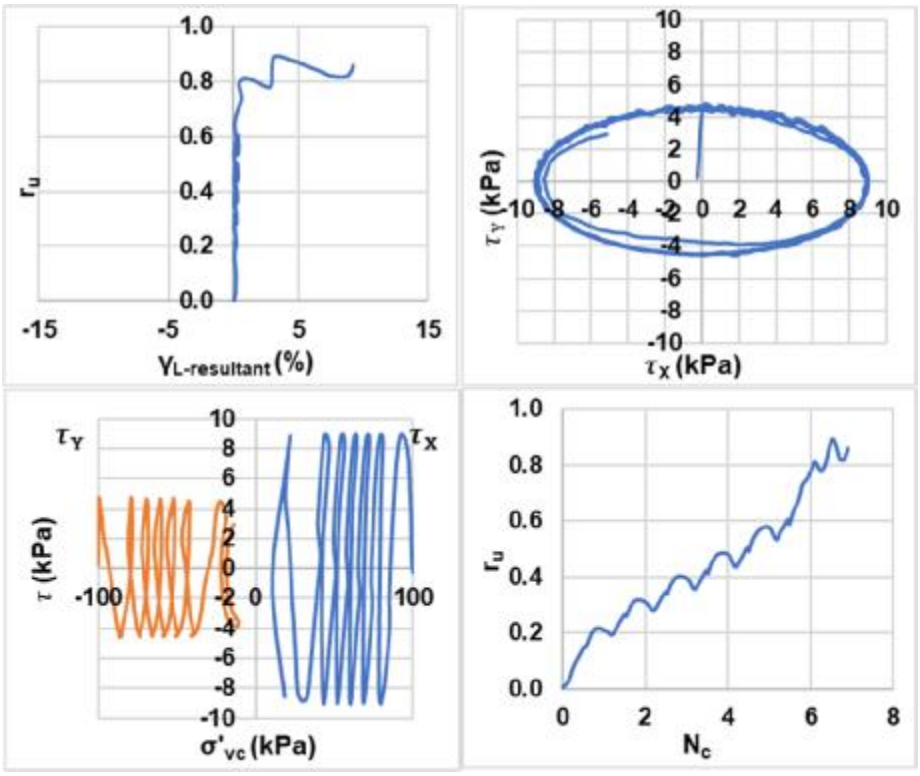


Bi-directional (Elliptical); $D_{rc}$ = 25%; $\sigma'_{vc}$ = 100 kPa; CSR = 0.09 (Liquefaction)

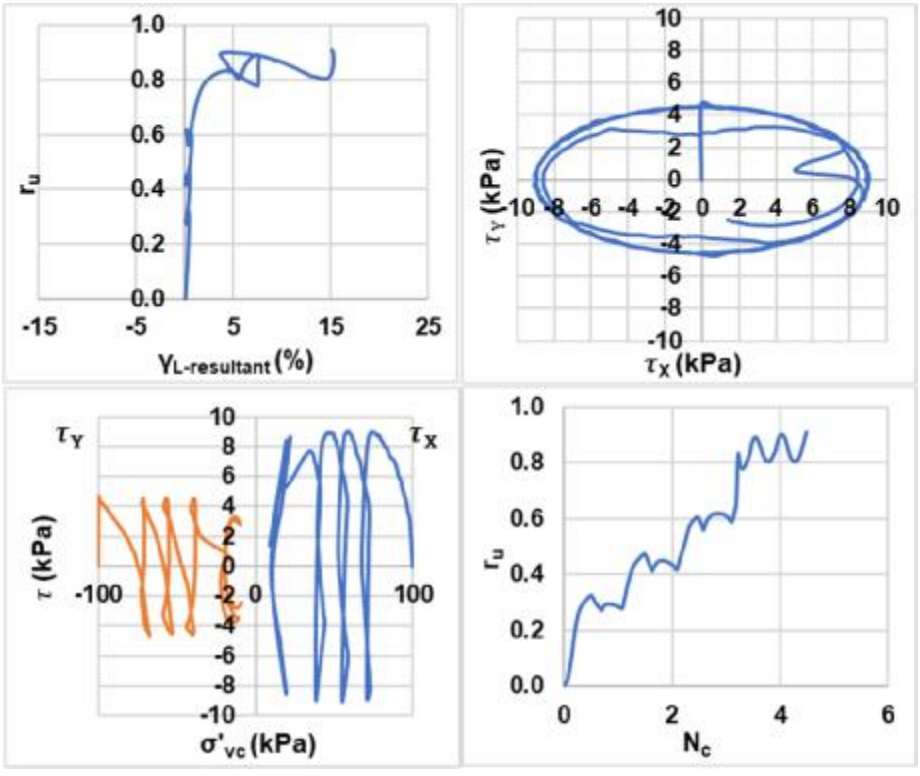


Bi-directional (Elliptical); $D_{rc}$ = 25%; $\sigma'_{vc}$ = 100 kPa; CSR = 0.09 (Re-liquefaction)

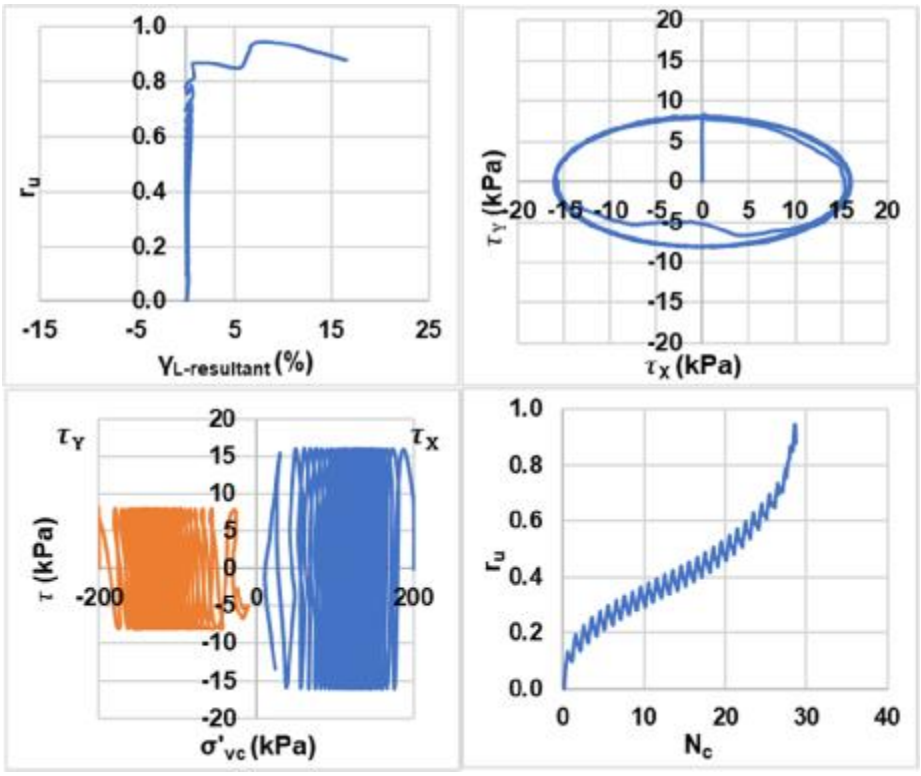


Bi-directional (Elliptical); $D_{rc}$ = 25%; $\sigma'_{vc}$ = 200 kPa; CSR = 0.08 (Liquefaction)

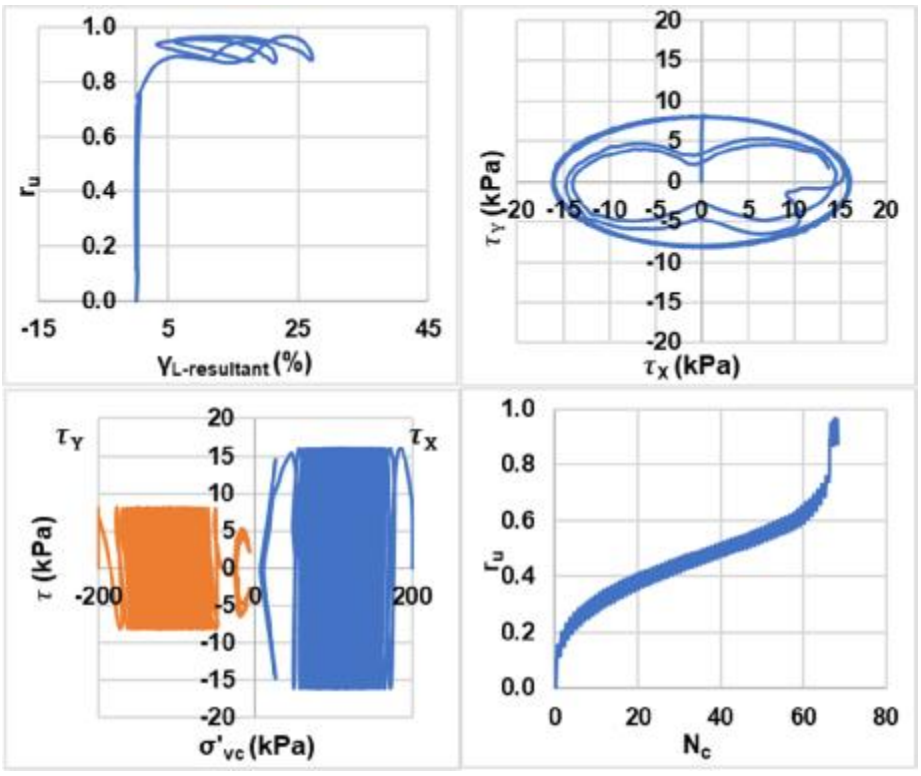


Bi-directional (Elliptical); $D_{rc}$ = 25%; $\sigma'_{vc}$ = 200 kPa; CSR = 0.08 (Re-liquefaction)

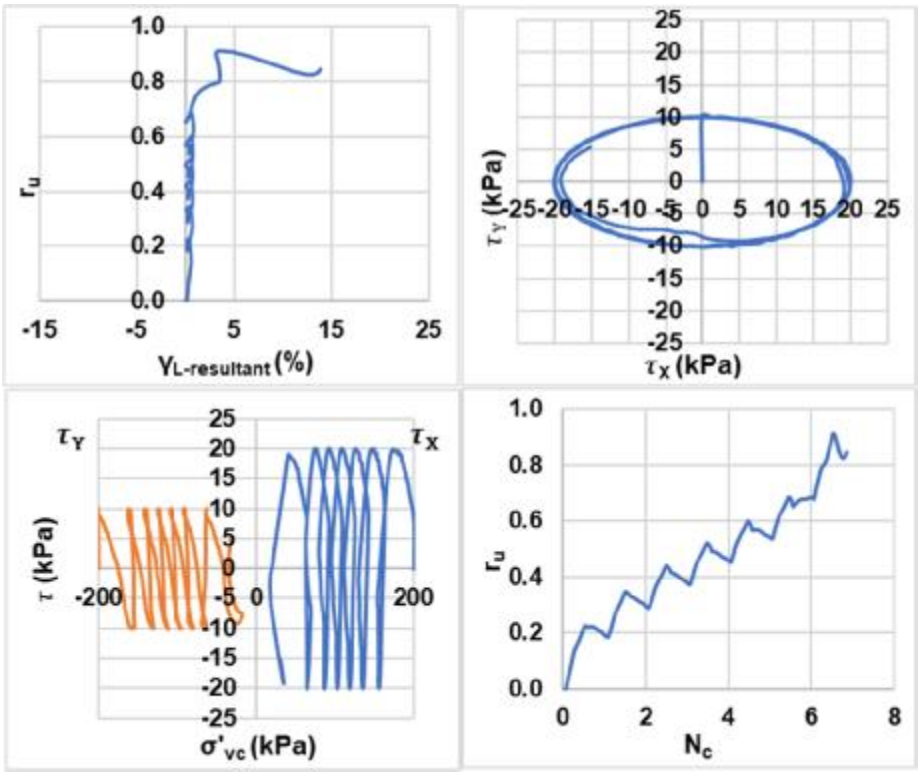


Bi-directional (Elliptical); $D_{rc}$ = 25%; $\sigma'_{vc}$ = 200 kPa; CSR = 0.1 (Liquefaction)

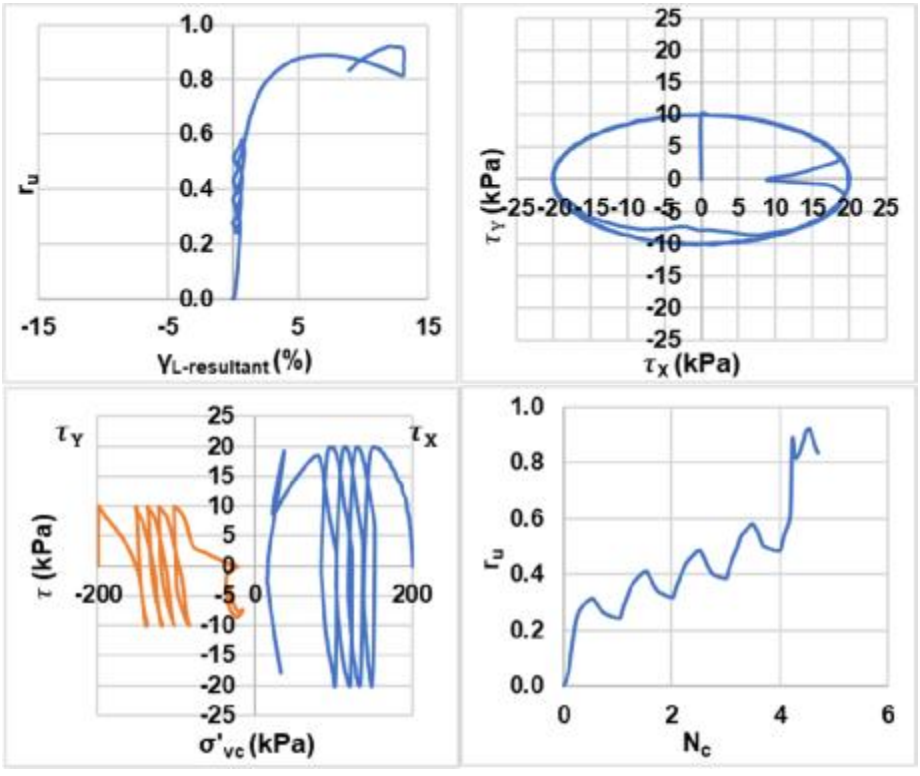


Bi-directional (Elliptical); $D_{rc}$ = 25%; $\sigma'_{vc}$ = 200 kPa; CSR = 0.1 (Re-liquefaction)

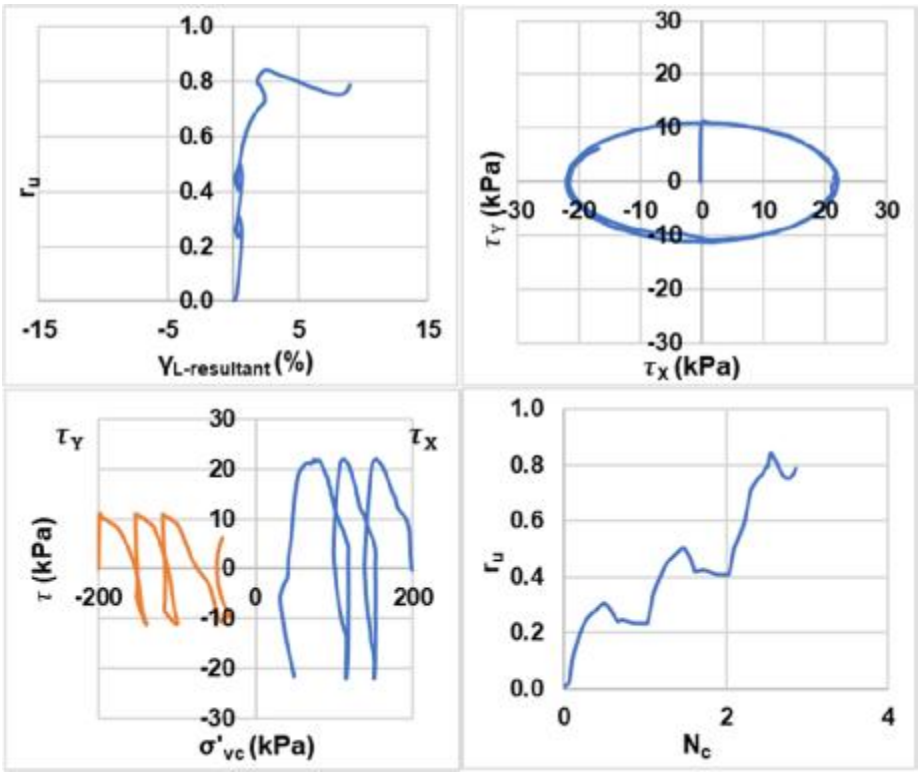


Bi-directional (Elliptical); $D_{rc}$ = 25%; $\sigma'_{vc}$ = 200 kPa; CSR = 0.11 (Liquefaction)

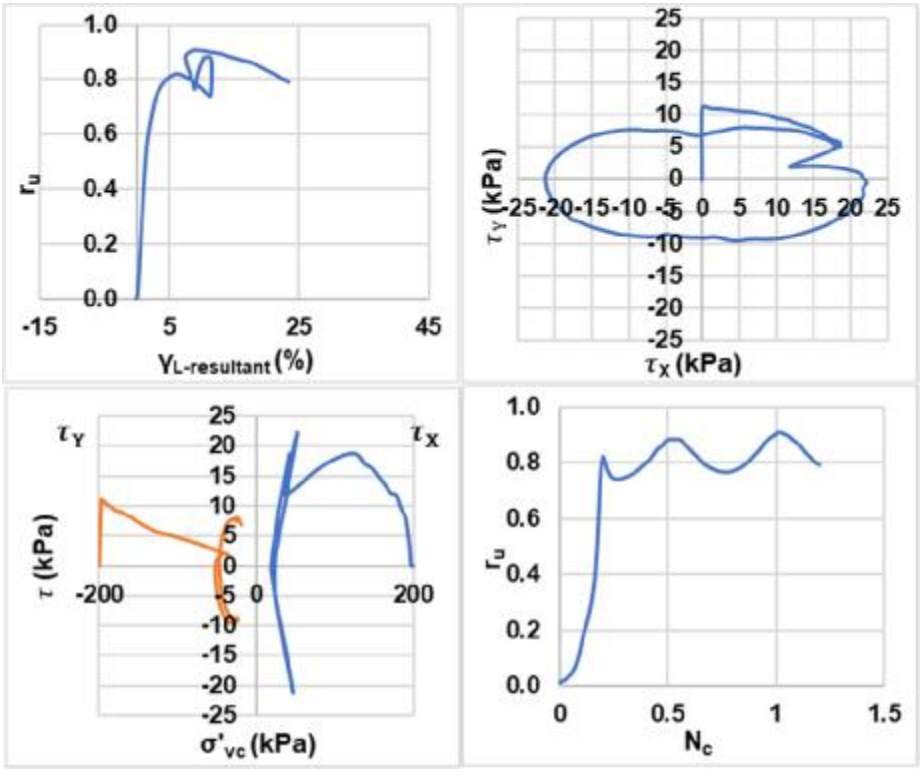


Bi-directional (Elliptical); $D_{rc}$ = 25%; $\sigma'_{vc}$ = 200 kPa; CSR = 0.11 (Re-liquefaction)

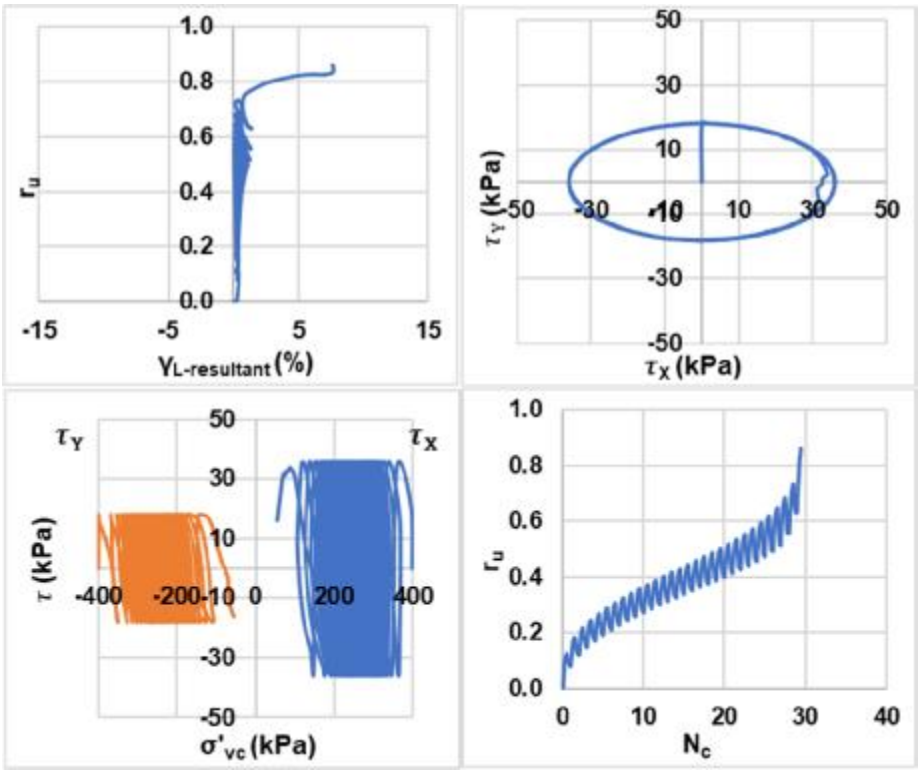


Bi-directional (Elliptical); $D_{rc}$ = 25%; $\sigma'_{vc}$ = 400 kPa; CSR = 0.09 (Liquefaction)

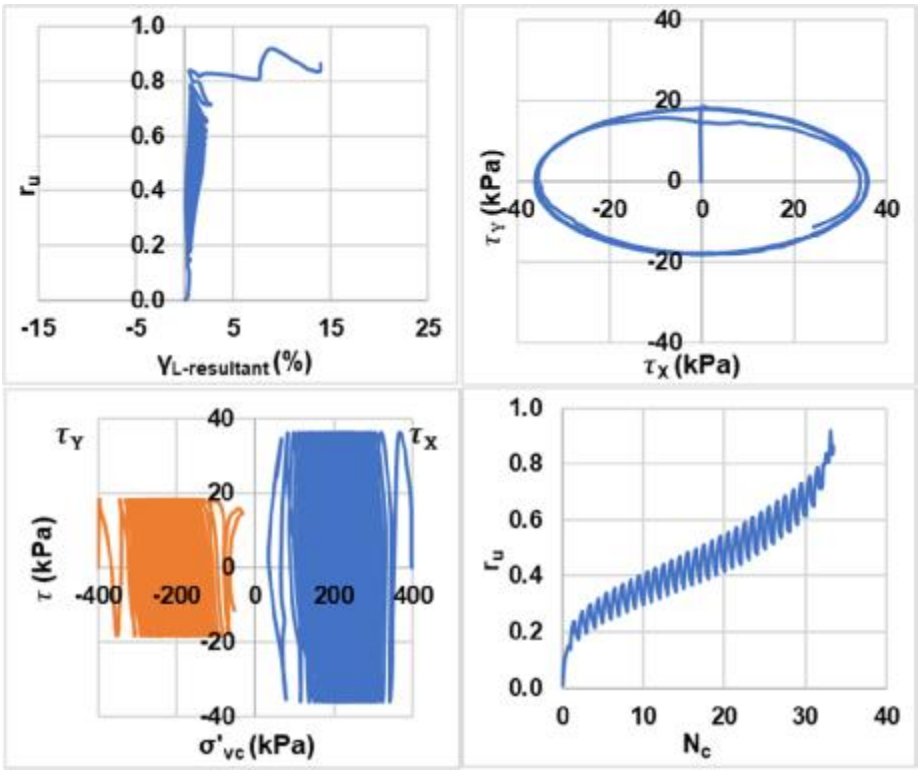


Bi-directional (Elliptical); $D_{rc}$ = 25%; $\sigma'_{vc}$ = 400 kPa; CSR = 0.09 (Re-liquefaction)

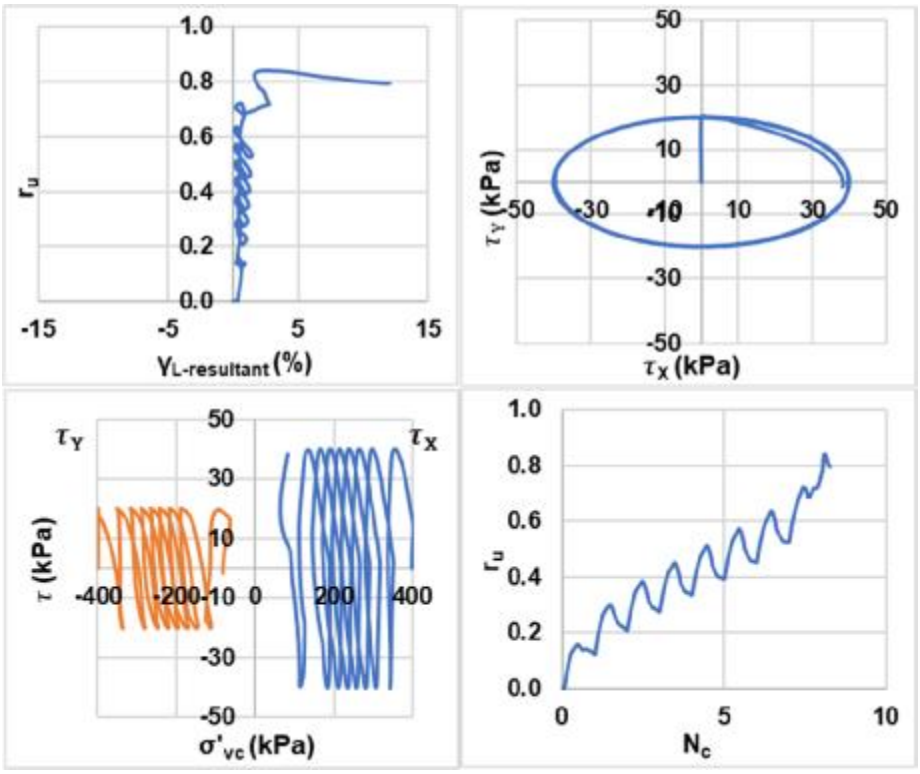


Bi-directional (Elliptical); $D_{rc}$ = 25%; $\sigma'_{vc}$ = 400 kPa; CSR = 0.1 (Liquefaction)

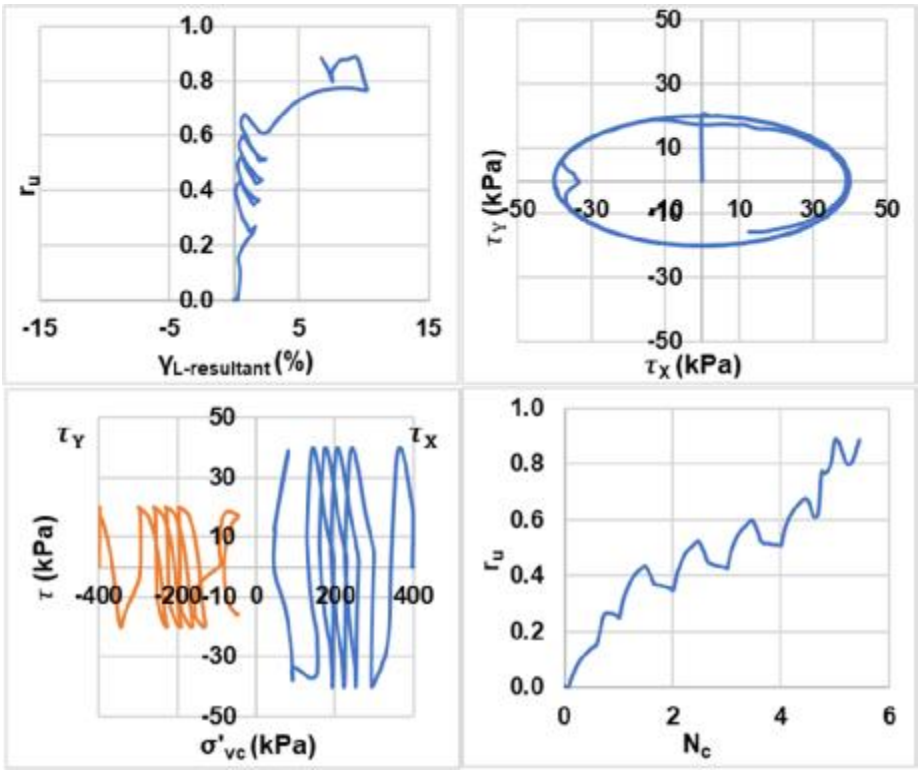


Bi-directional (Elliptical); $D_{rc}$ = 25%; $\sigma'_{vc}$ = 400 kPa; CSR = 0.1 (Re-liquefaction)

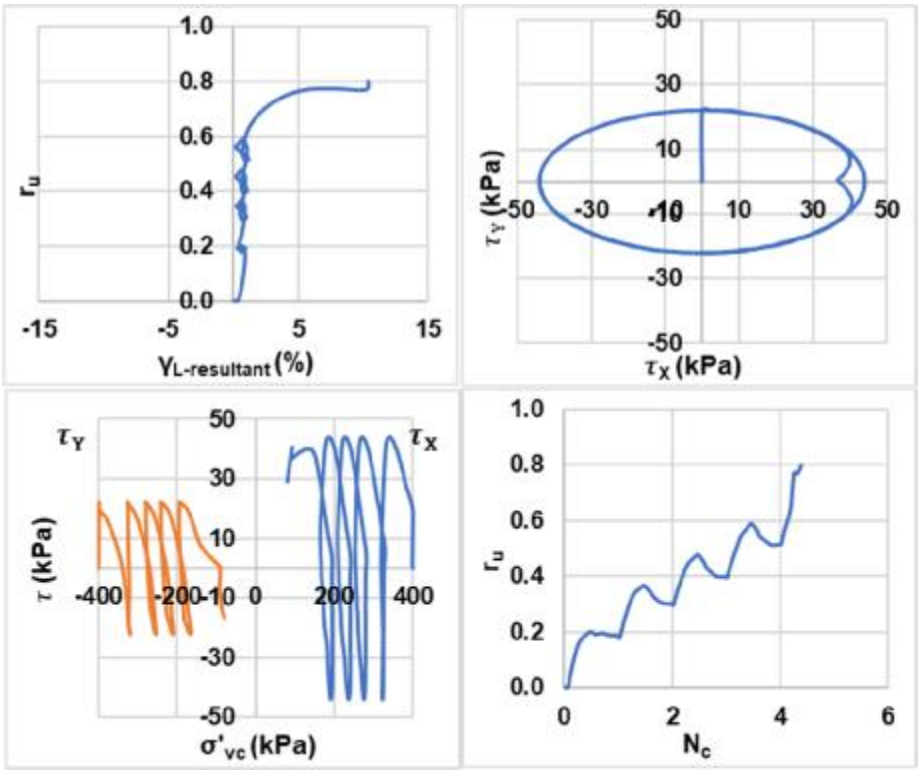


Bi-directional (Elliptical); $D_{rc}$ = 25%; $\sigma'_{vc}$ = 400 kPa; CSR = 0.11 (Liquefaction)

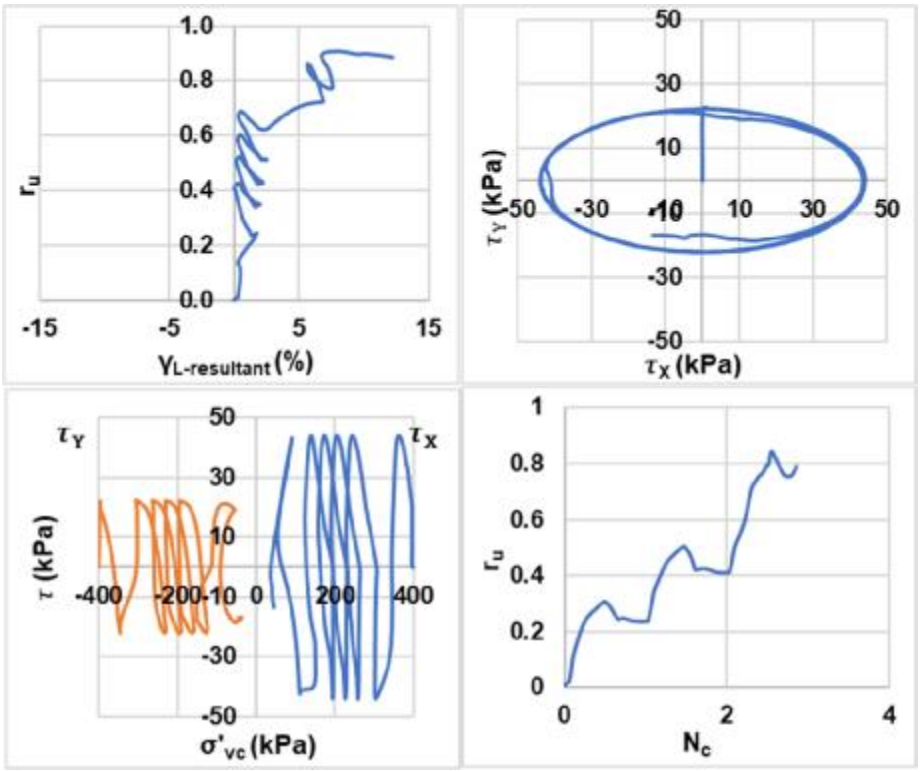


Bi-directional (Elliptical); $D_{rc}$ = 25%; $\sigma'_{vc}$ = 400 kPa; CSR = 0.11 (Re-liquefaction)

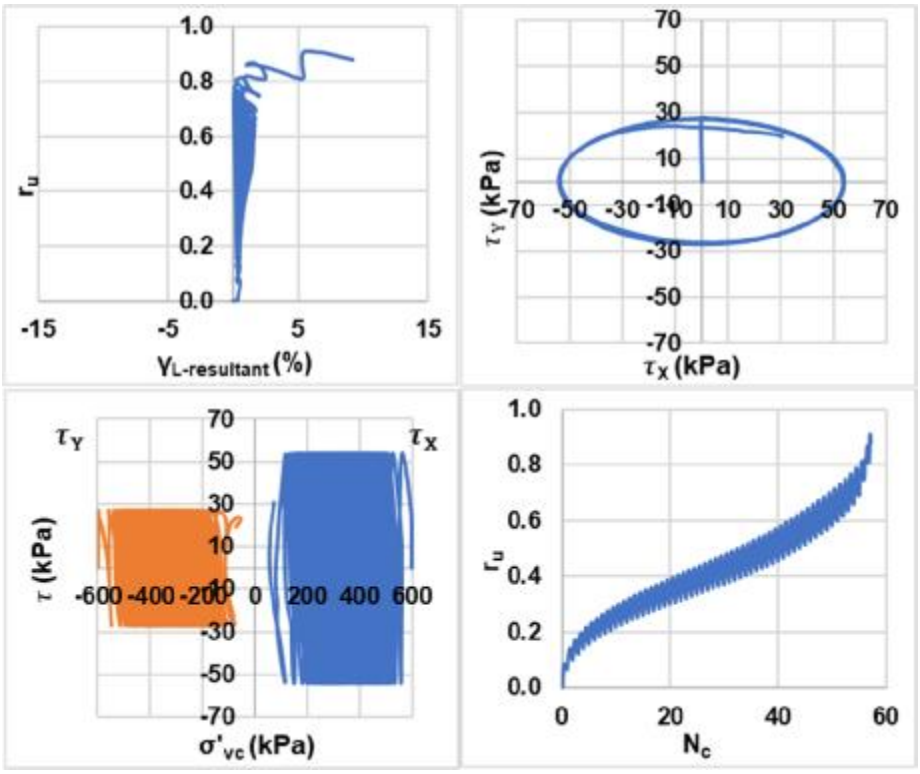


Bi-directional (Elliptical); $D_{rc}$ = 25%; $\sigma'_{vc}$ = 600 kPa; CSR = 0.09 (Liquefaction)

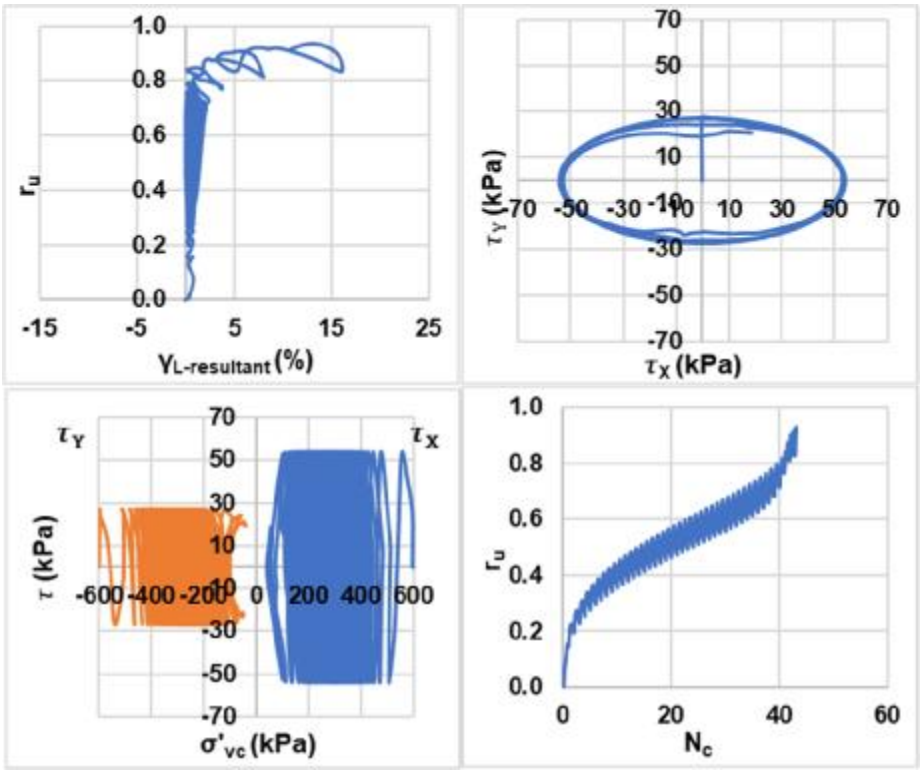


Bi-directional (Elliptical); $D_{rc}$ = 25%; $\sigma'_{vc}$ = 600 kPa; CSR = 0.09 (Re-liquefaction)

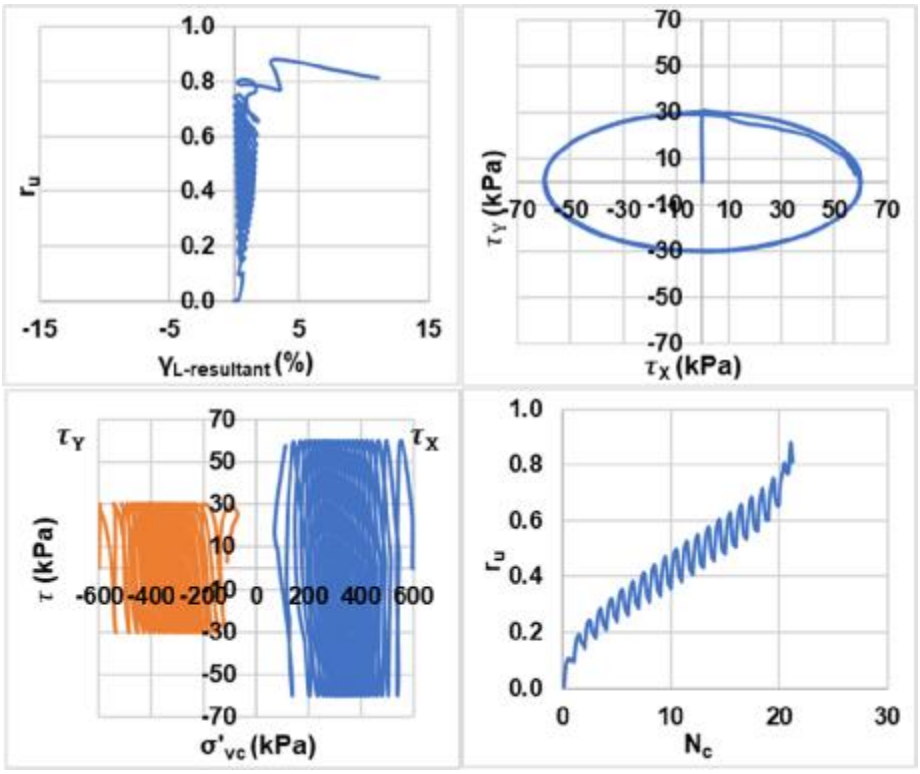


Bi-directional (Elliptical); $D_{rc}$ = 25%; $\sigma'_{vc}$ = 600 kPa; CSR = 0.1 (Liquefaction)

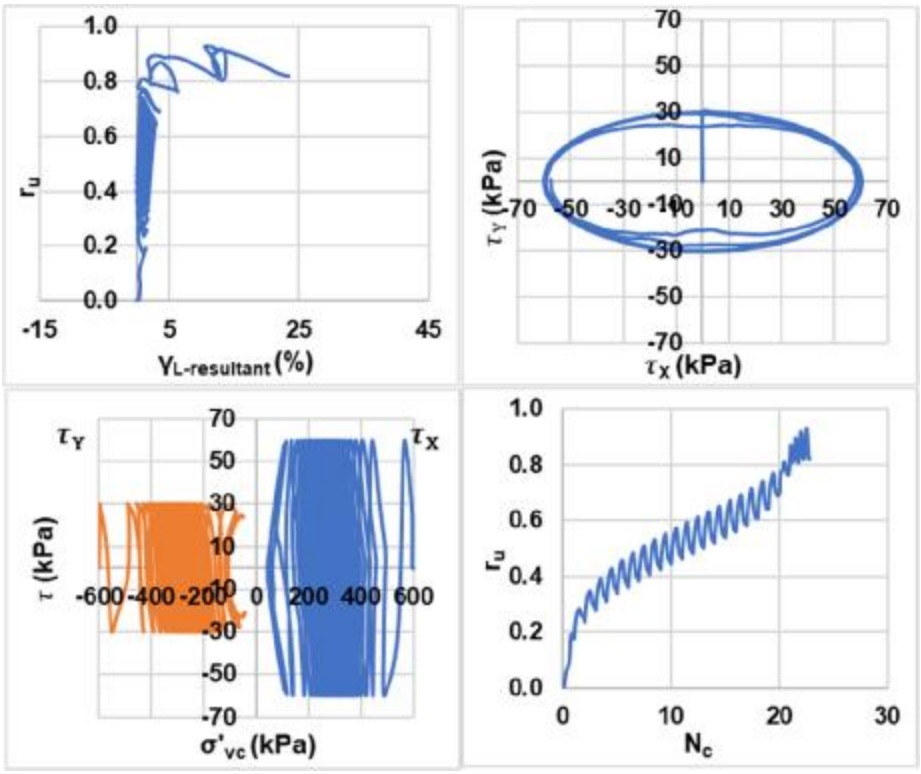


Bi-directional (Elliptical); $D_{rc}$ = 25%; $\sigma'_{vc}$ = 600 kPa; CSR = 0.1 (Re-liquefaction)

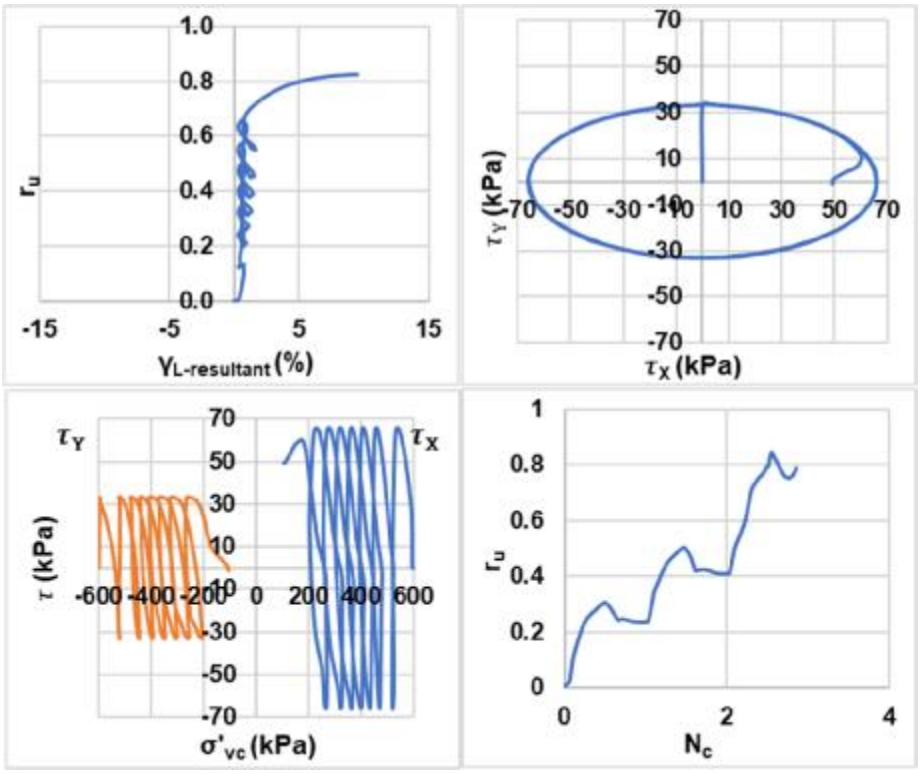


Bi-directional (Elliptical); $D_{rc}$ = 25%; $\sigma'_{vc}$ = 600 kPa; CSR = 0.11 (Liquefaction)

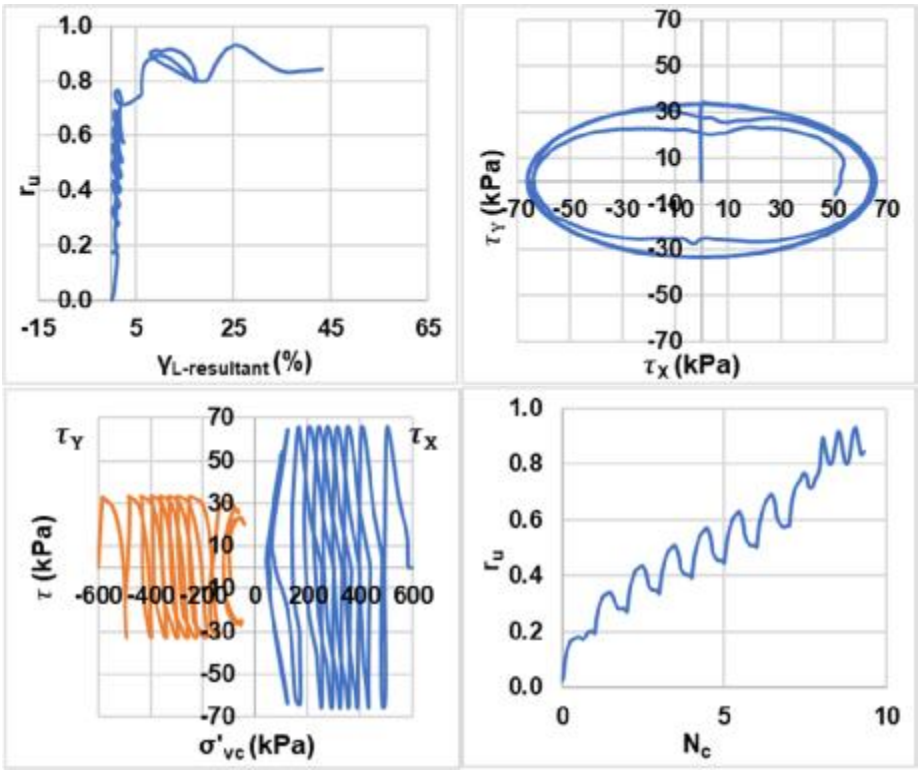


Bi-directional (Elliptical); $D_{rc}$ = 25%; $\sigma'_{vc}$ = 600 kPa; CSR = 0.11 (Re-liquefaction)

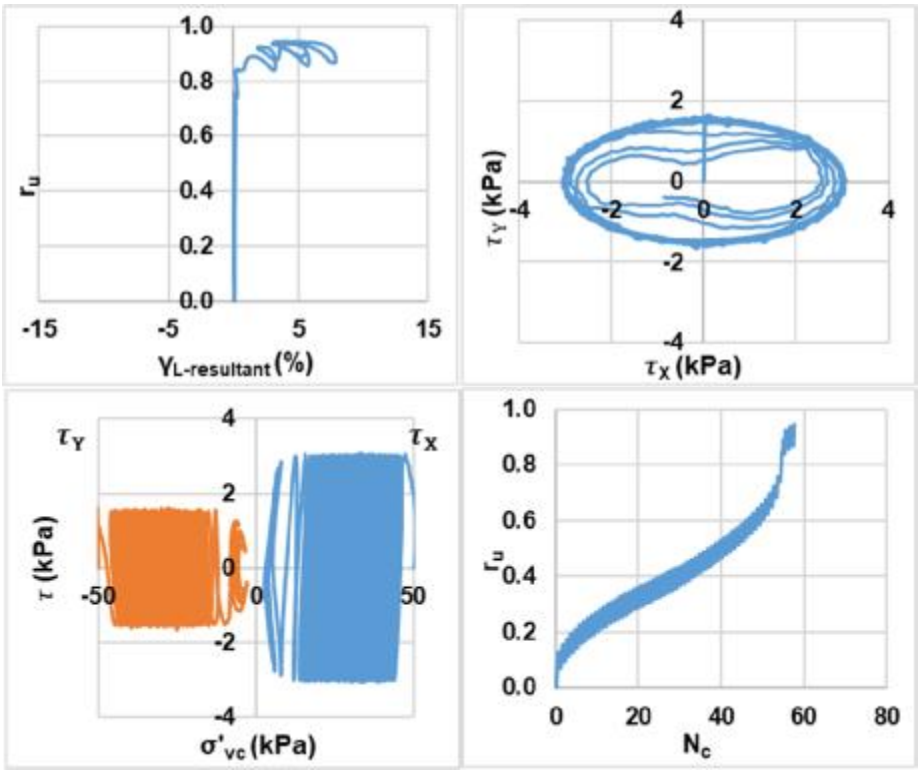


Bi-directional (Elliptical); $D_{rc}$ = 45%; $\sigma'_{vc}$ = 50 kPa; CSR = 0.06 (Liquefaction)

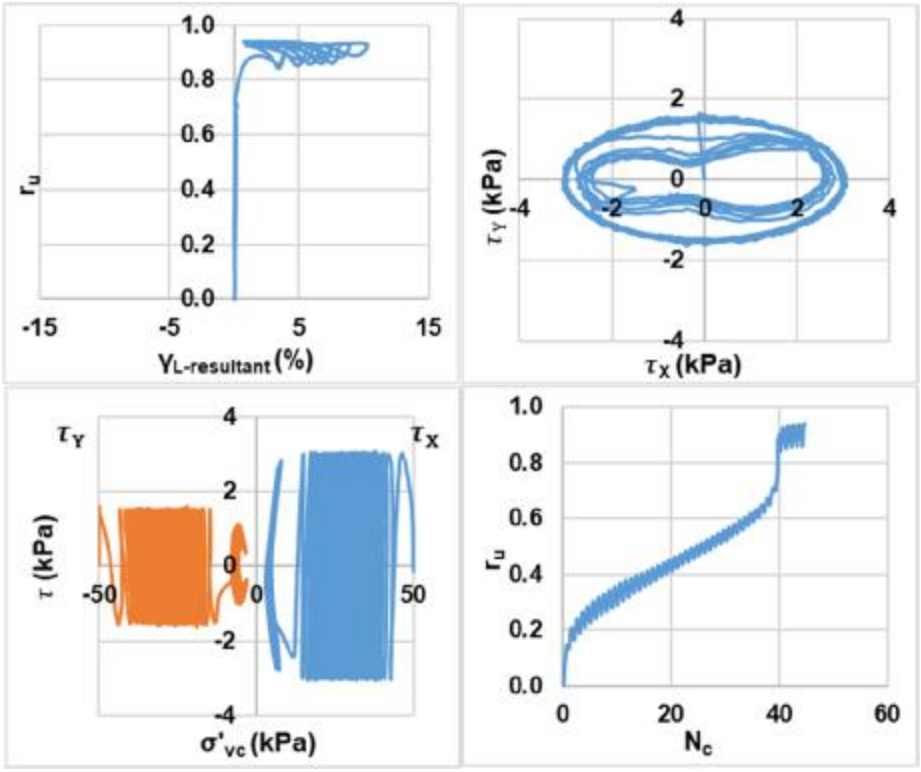


Bi-directional (Elliptical); $D_{rc}$ = 45%; $\sigma'_{vc}$ = 50 kPa; CSR = 0.06 (Re-liquefaction)

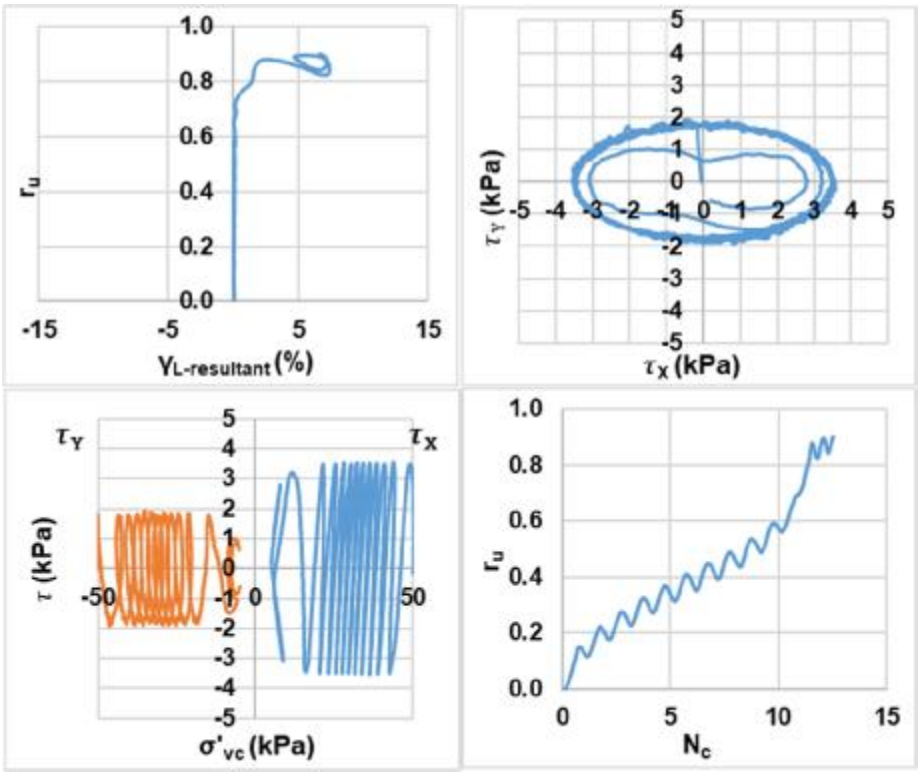


Bi-directional (Elliptical); $D_{rc}$ = 45%; $\sigma'_{vc}$ = 50 kPa; CSR = 0.07 (Liquefaction)

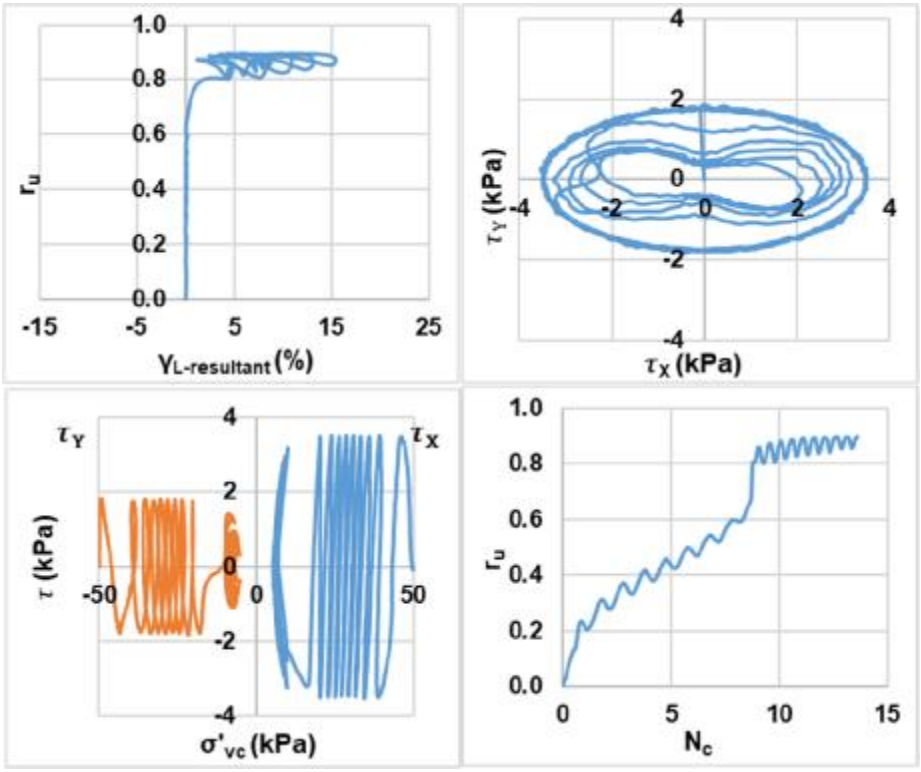


Bi-directional (Elliptical); $D_{rc}$ = 45%; $\sigma'_{vc}$ = 50 kPa; CSR = 0.07 (Re-liquefaction)

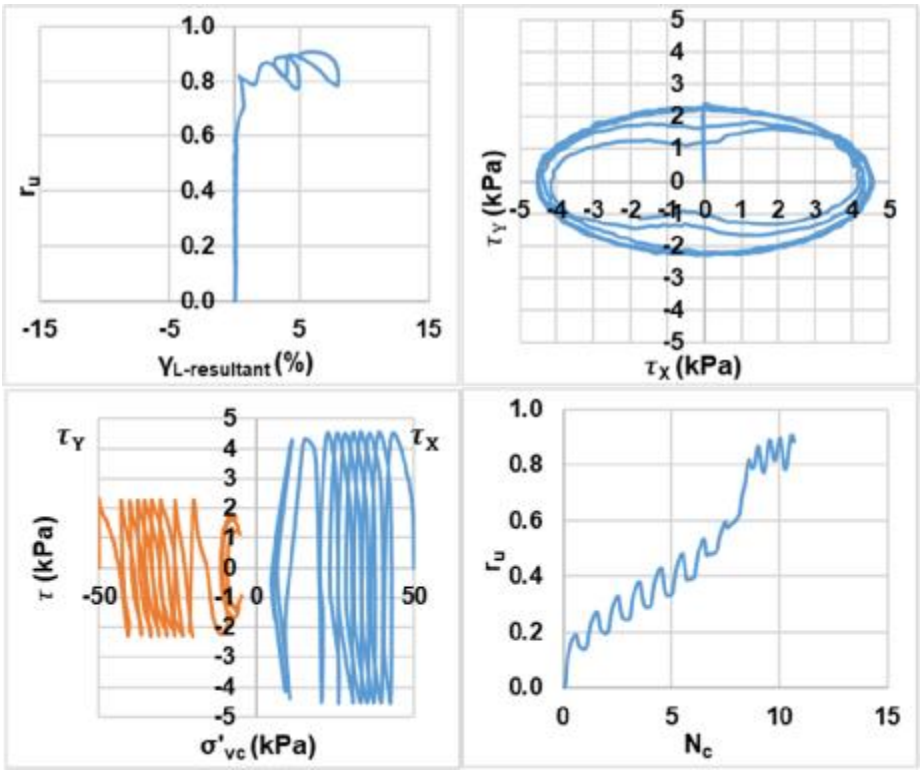


Bi-directional (Elliptical); $D_{rc}$ = 45%; $\sigma'_{vc}$ = 50 kPa; CSR = 0.09 (Liquefaction)

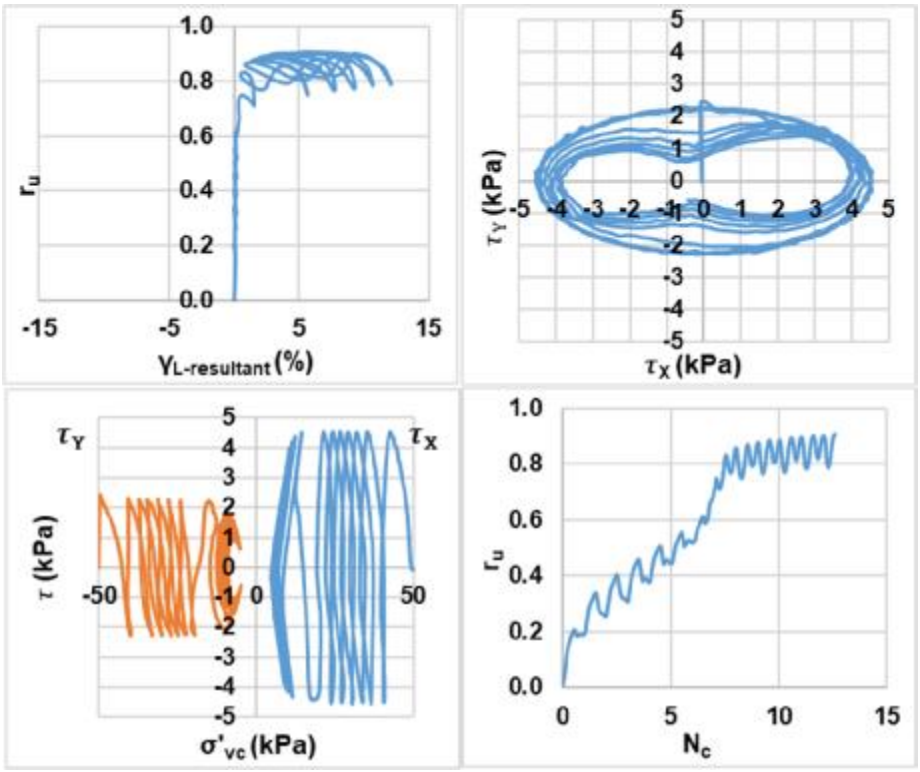


Bi-directional (Elliptical); $D_{rc}$ = 45%; $\sigma'_{vc}$ = 50 kPa; CSR = 0.09 (Re-liquefaction)

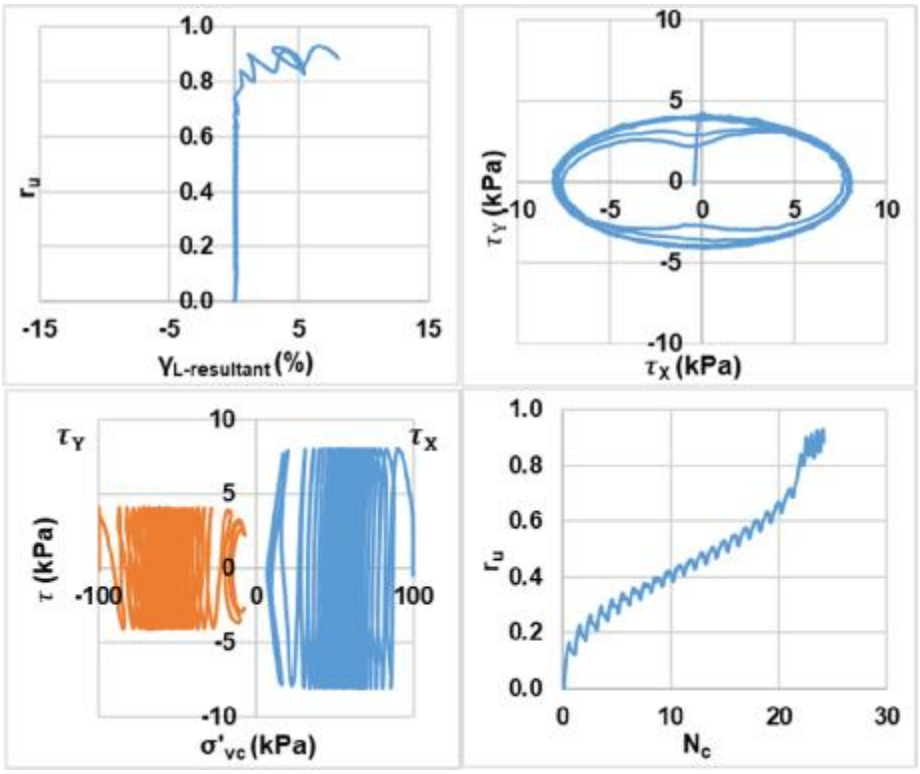


Bi-directional (Elliptical); $D_{rc}$ = 45%; $\sigma'_{vc}$ = 100 kPa; CSR = 0.08 (Liquefaction)

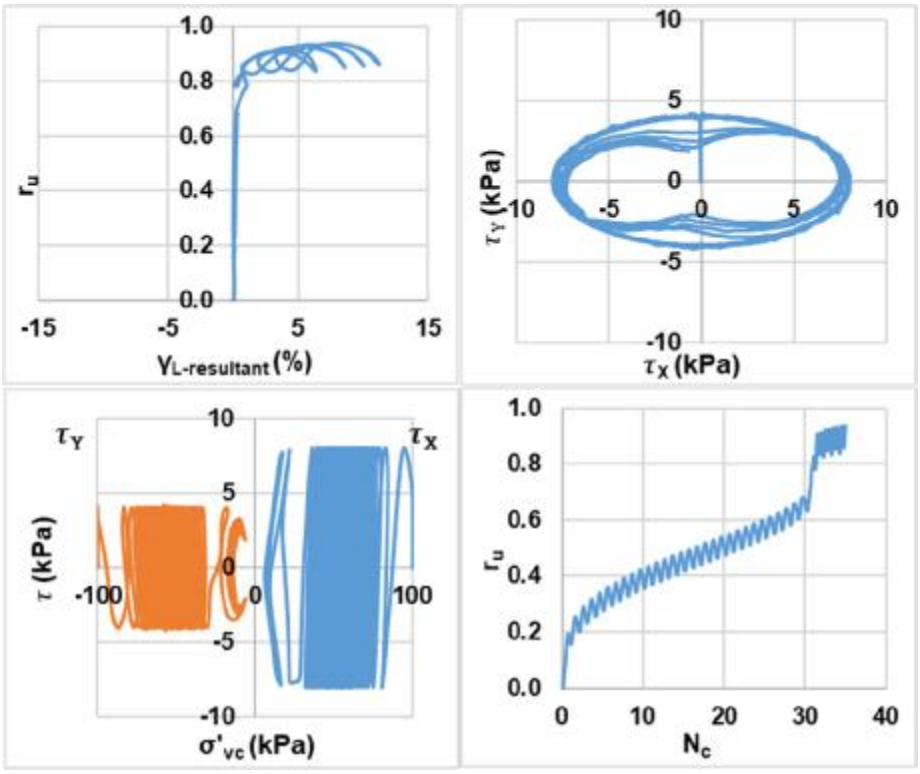


Bi-directional (Elliptical); $D_{rc}$ = 45%; $\sigma'_{vc}$ = 100 kPa; CSR = 0.08 (Re-liquefaction)

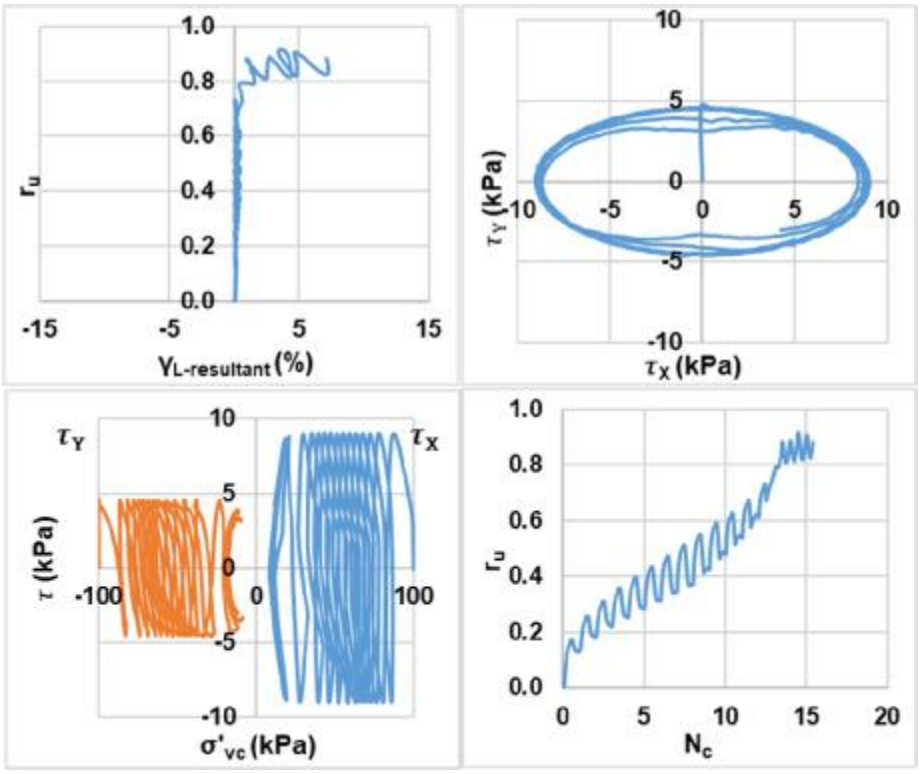


Bi-directional (Elliptical); $D_{rc}$ = 45%; $\sigma'_{vc}$ = 100 kPa; CSR = 0.09 (Liquefaction)

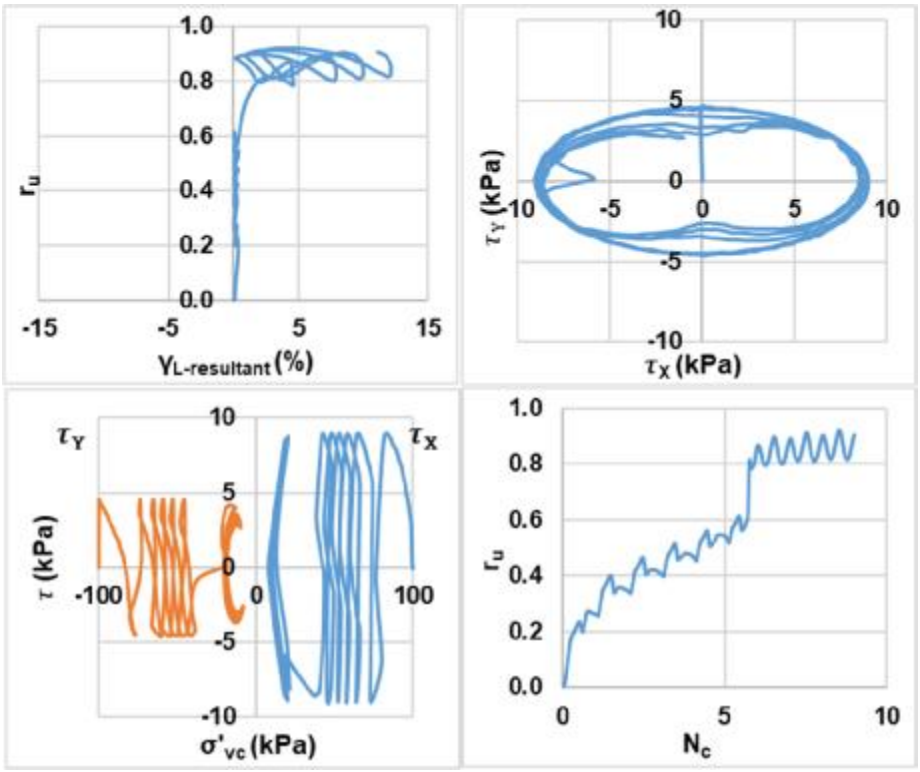


Bi-directional (Elliptical); $D_{rc}$ = 45%; $\sigma'_{vc}$ = 100 kPa; CSR = 0.09 (Re-liquefaction)

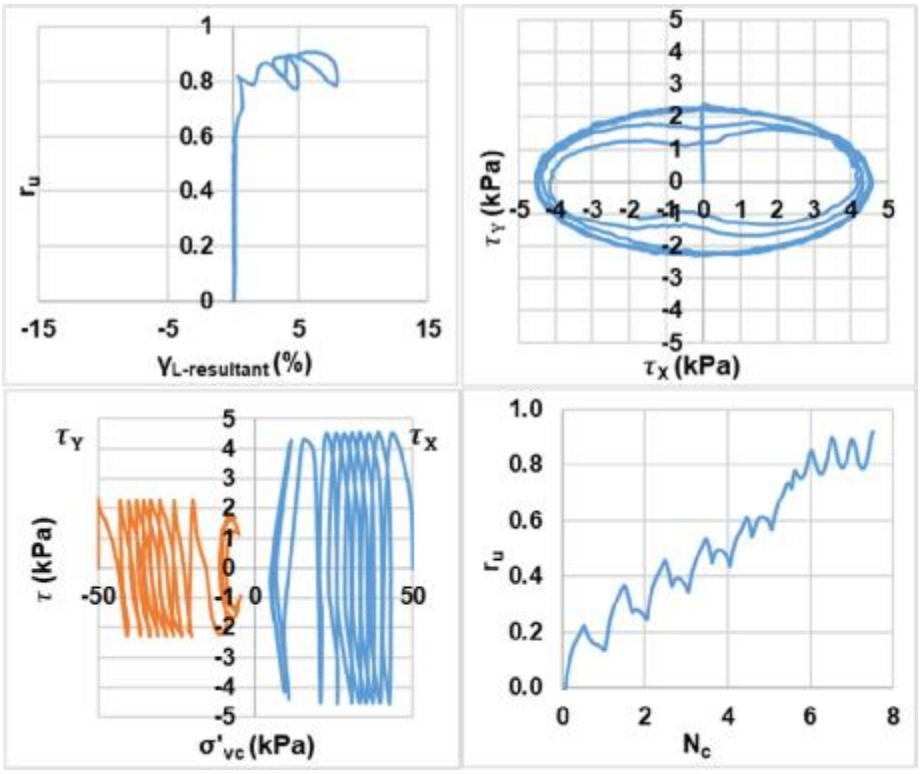


Bi-directional (Elliptical); $D_{rc}$ = 45%; $\sigma'_{vc}$ = 100 kPa; CSR = 0.11 (Liquefaction)

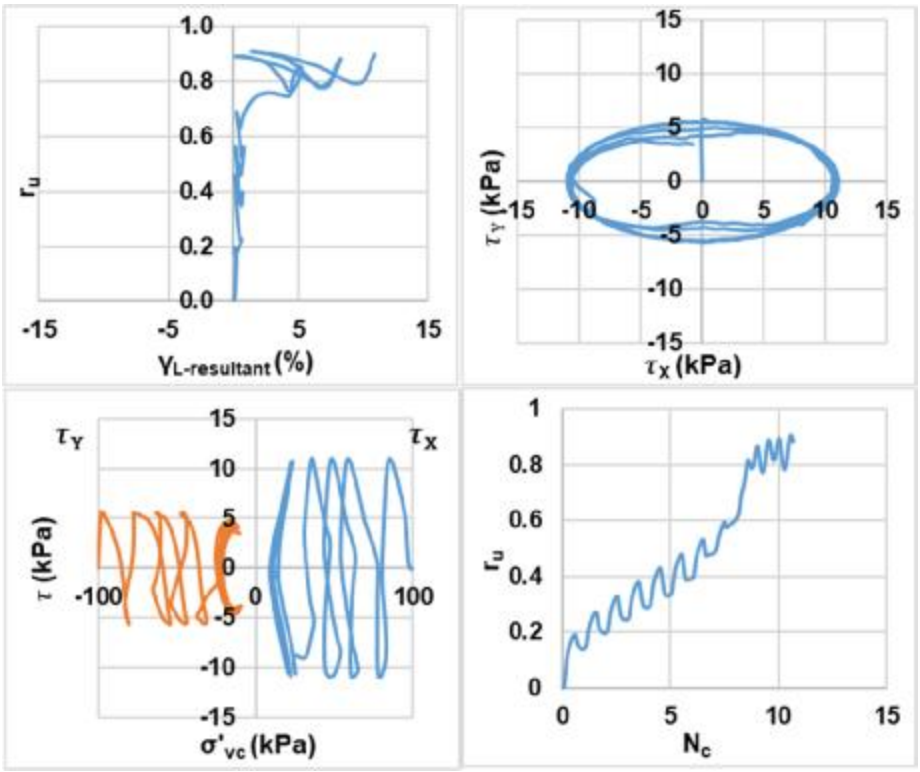


Bi-directional (Elliptical); $D_{rc}$ = 45%; $\sigma'_{vc}$ = 100 kPa; CSR = 0.11 (Re-liquefaction)

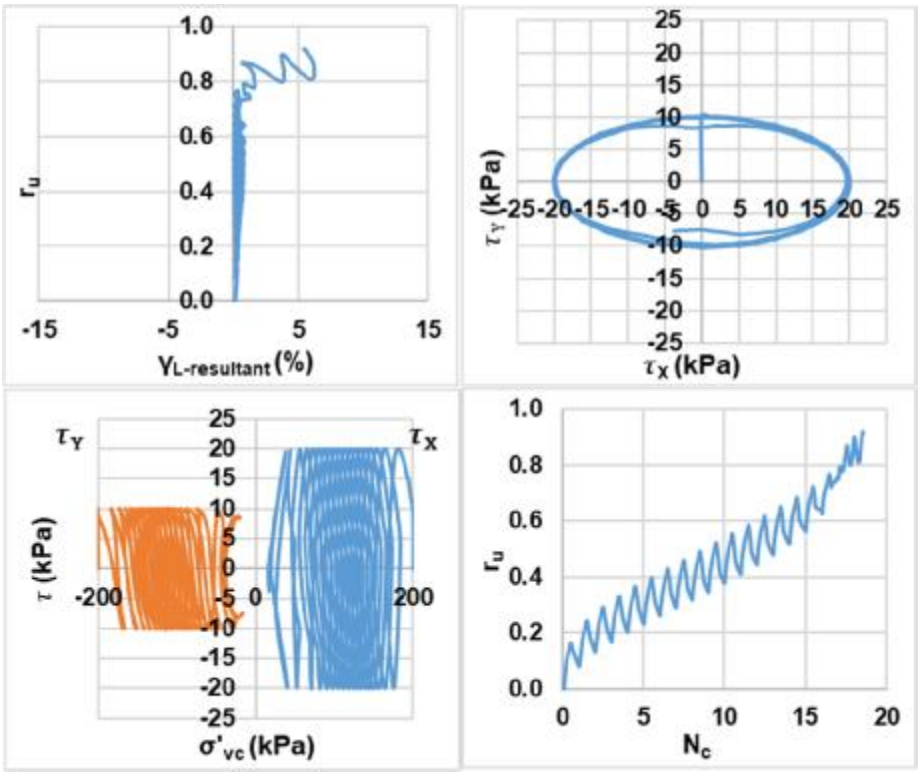


Bi-directional (Elliptical); $D_{rc}$ = 45%; $\sigma'_{vc}$ = 200 kPa; CSR = 0.1 (Liquefaction)

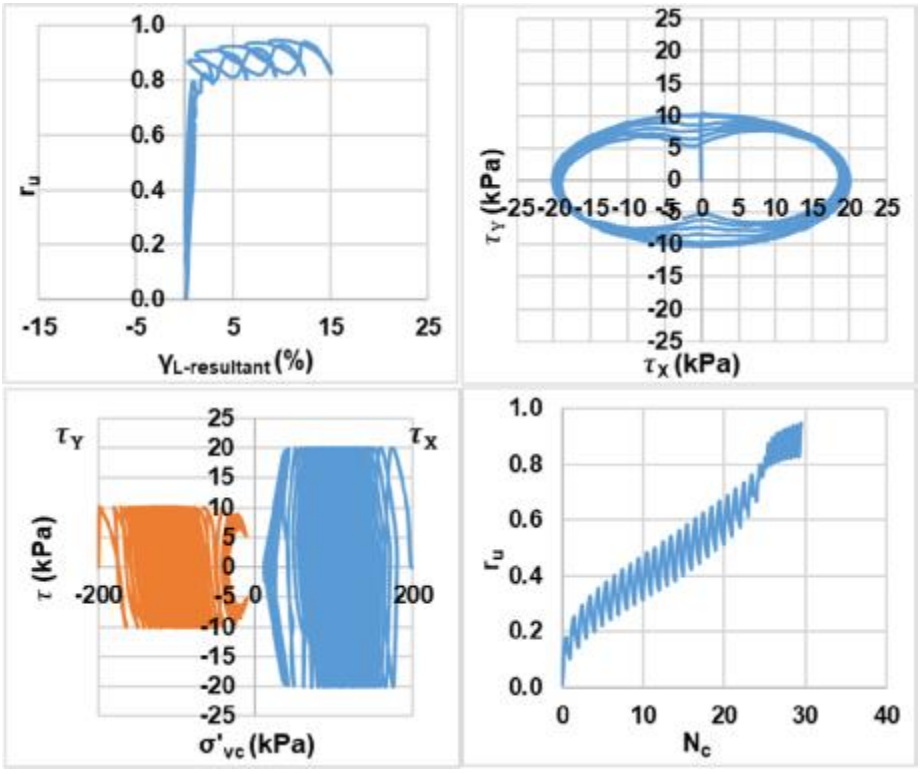


Bi-directional (Elliptical); $D_{rc}$ = 45%; $\sigma'_{vc}$ = 200 kPa; CSR = 0.1 (Re-liquefaction)

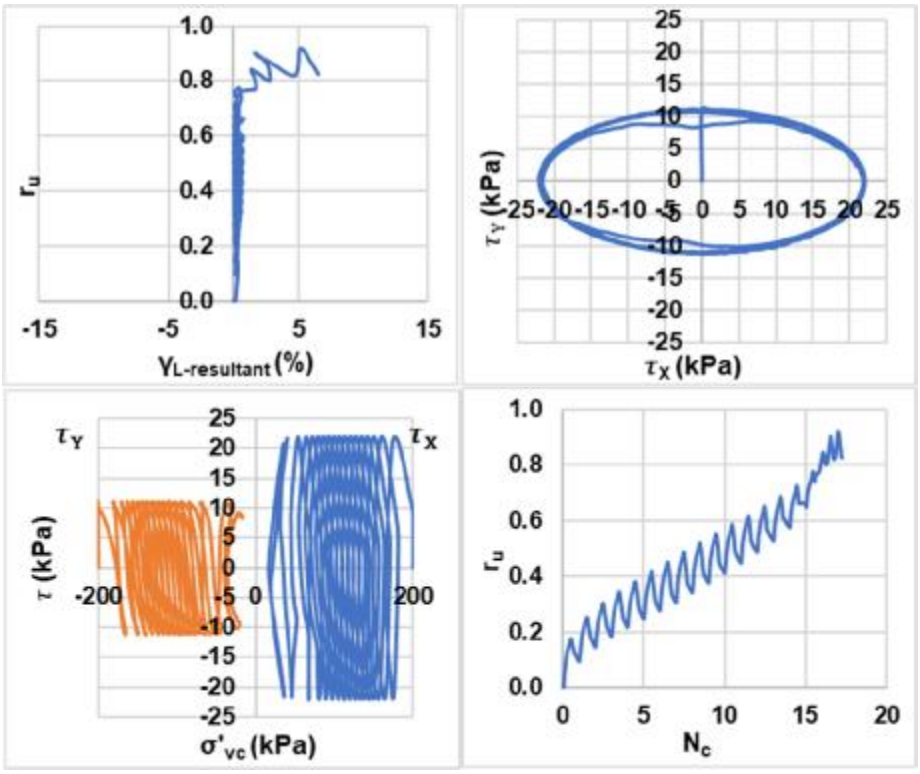


Bi-directional (Elliptical); $D_{rc}$ = 45%; $\sigma'_{vc}$ = 200 kPa; CSR = 0.11 (Liquefaction)

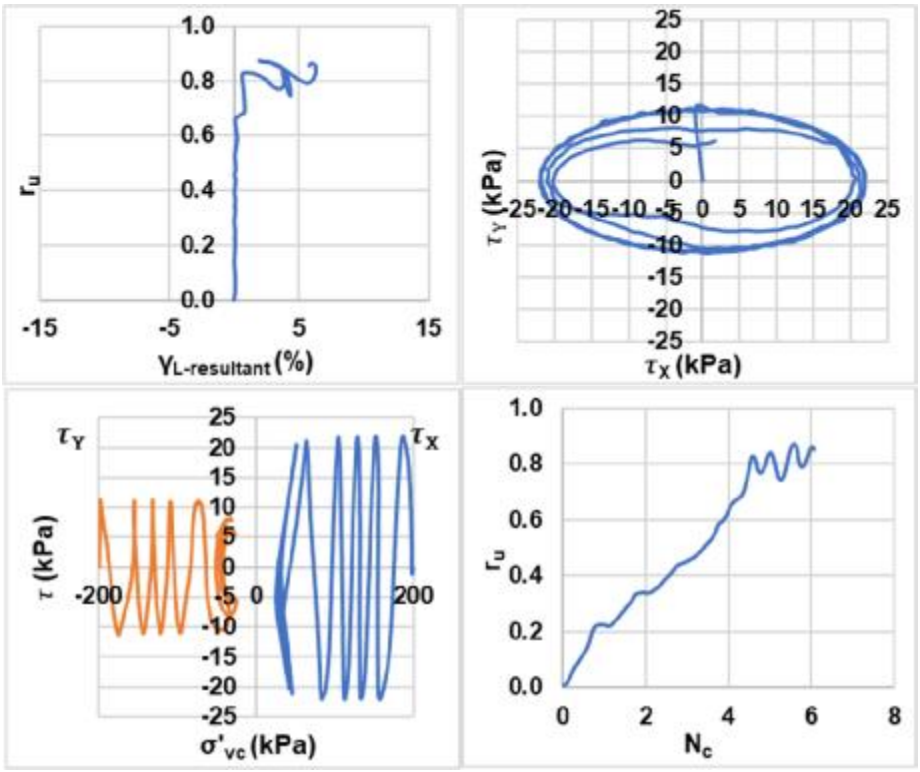


Bi-directional (Elliptical); $D_{rc}$ = 45%; $\sigma'_{vc}$ = 200 kPa; CSR = 0.11 (Re-liquefaction)

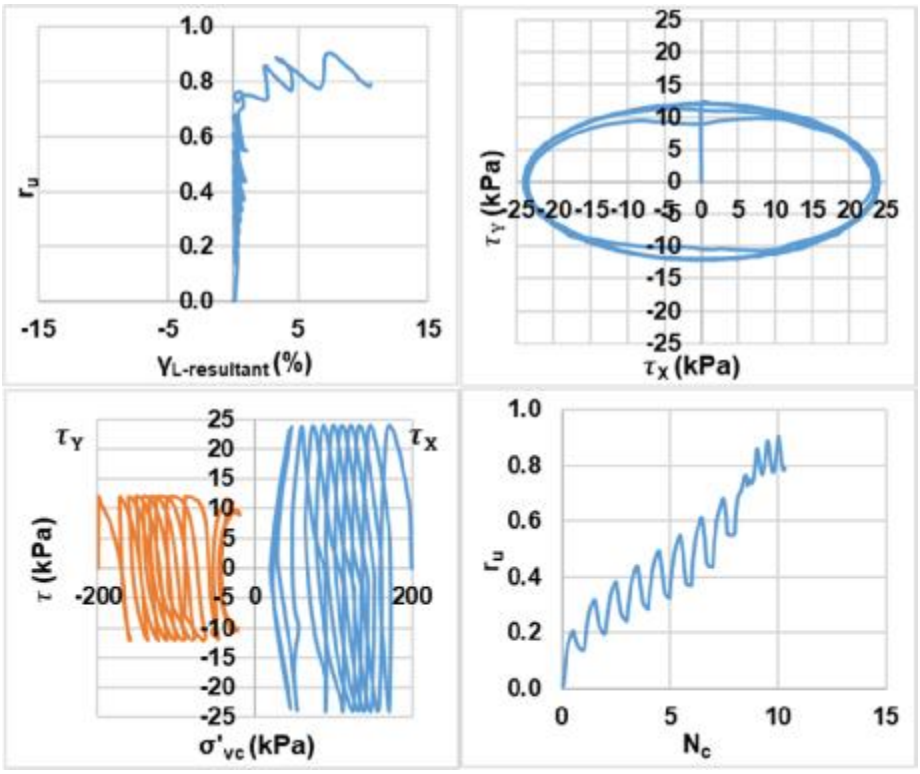


Bi-directional (Elliptical); $D_{rc}$ = 45%; $\sigma'_{vc}$ = 200 kPa; CSR = 0.12 (Liquefaction)

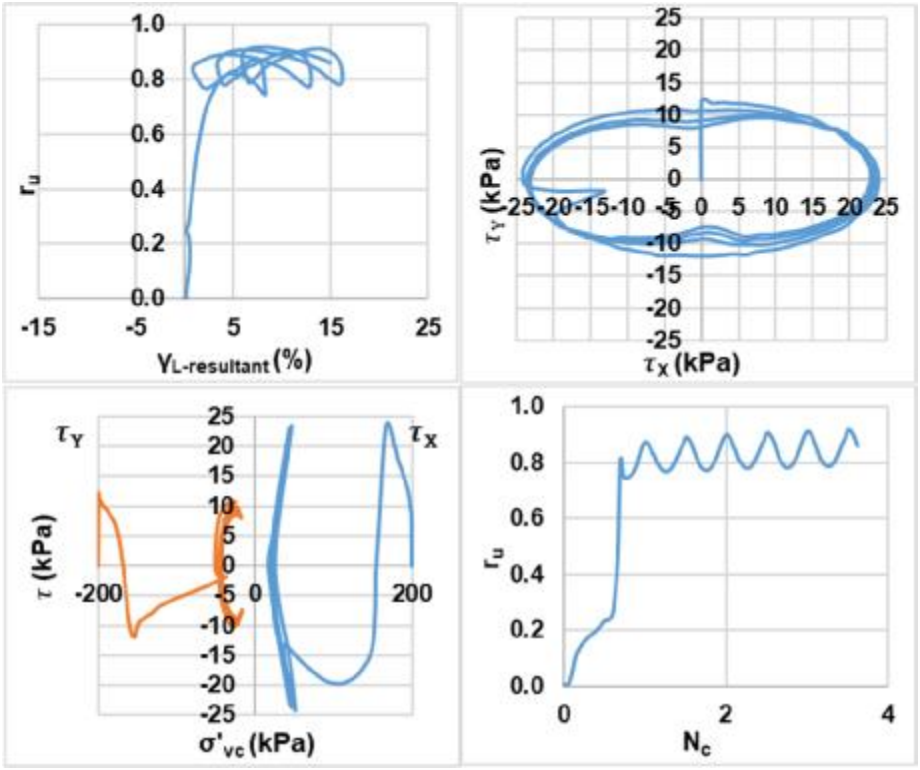


Bi-directional (Elliptical); $D_{rc}$ = 45%; $\sigma'_{vc}$ = 200 kPa; CSR = 0.12 (Re-liquefaction)

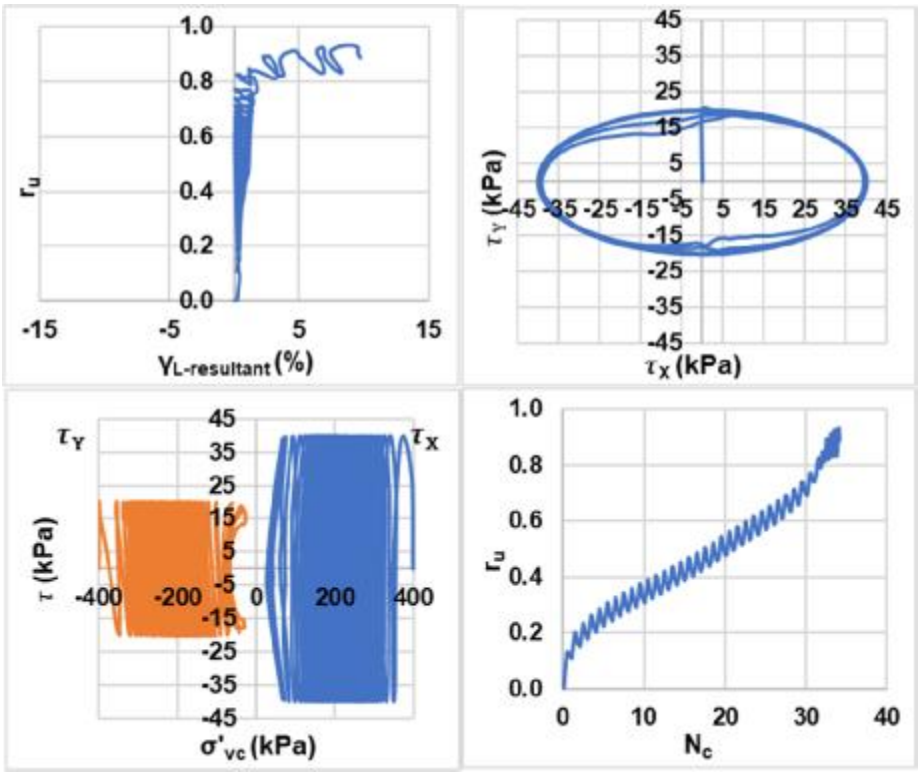


Bi-directional (Elliptical); $D_{rc}$ = 45%; $\sigma'_{vc}$ = 400 kPa; CSR = 0.1 (Liquefaction)

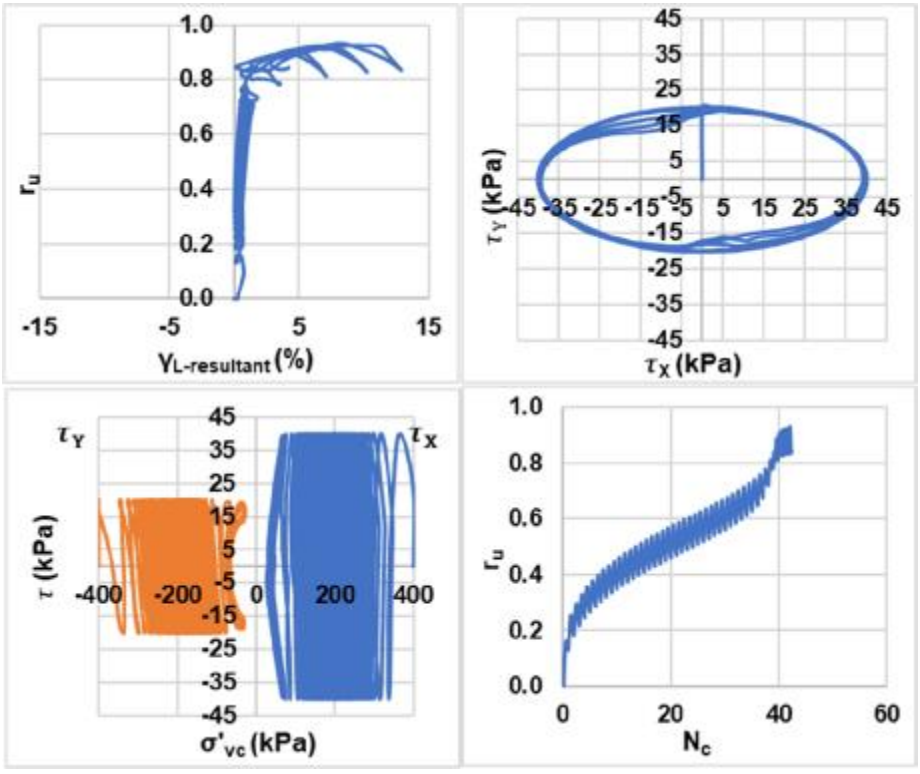


Bi-directional (Elliptical); $D_{rc}$ = 45%; $\sigma'_{vc}$ = 400 kPa; CSR = 0.1 (Re-liquefaction)

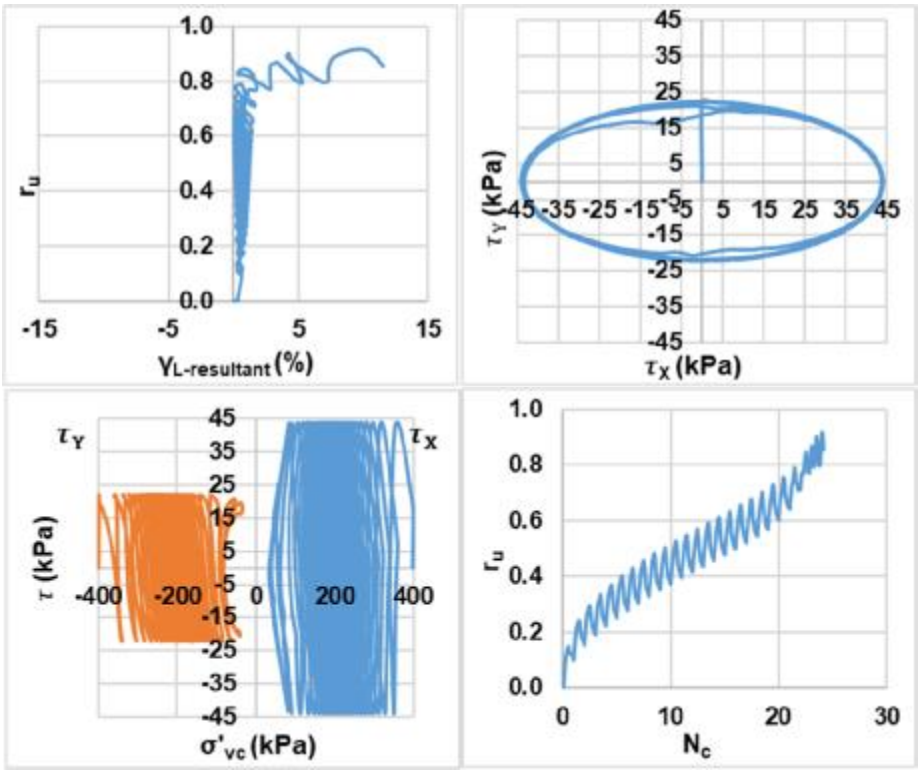


Bi-directional (Elliptical); $D_{rc}$ = 45%; $\sigma'_{vc}$ = 400 kPa; CSR = 0.11 (Liquefaction)

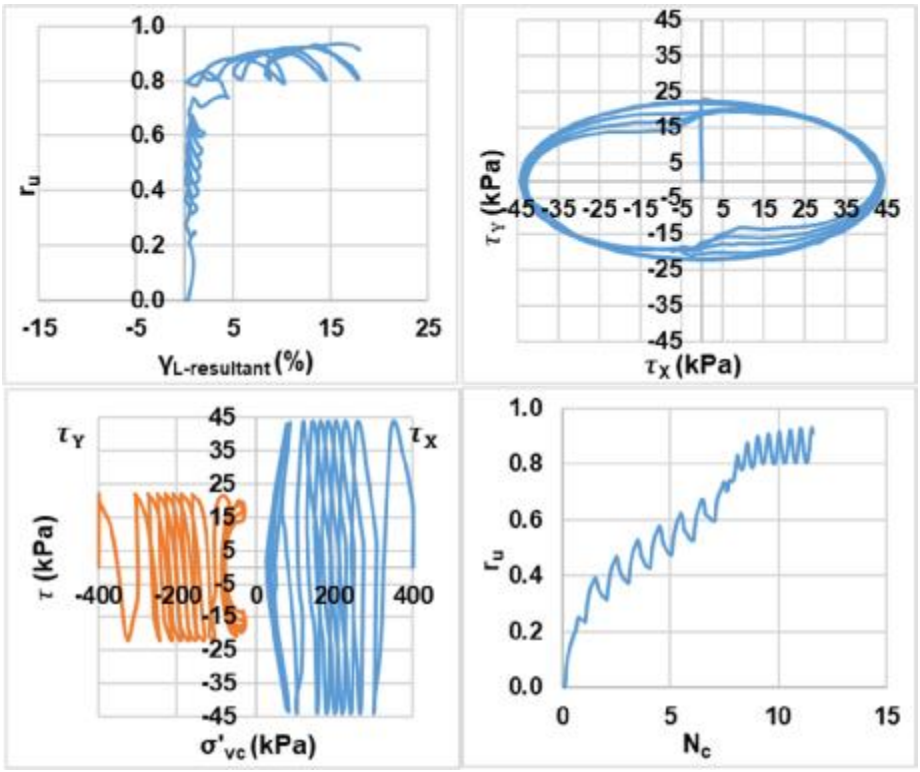


Bi-directional (Elliptical); $D_{rc}$ = 45%; $\sigma'_{vc}$ = 400 kPa; CSR = 0.11 (Re-liquefaction)

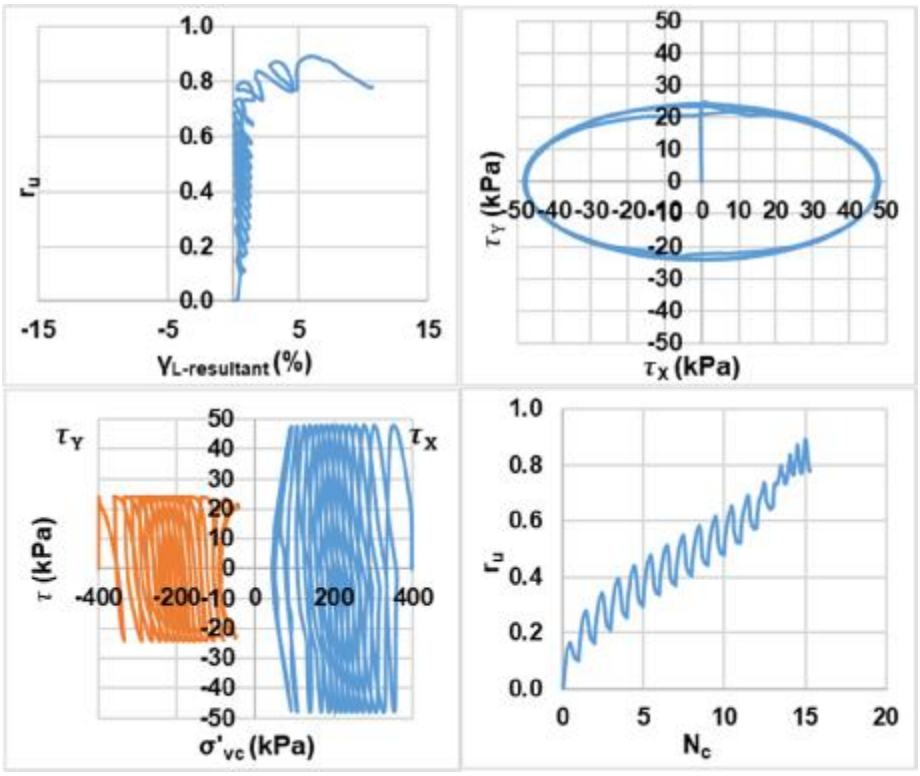


Bi-directional (Elliptical); $D_{rc}$ = 45%; $\sigma'_{vc}$ = 400 kPa; CSR = 0.12 (Liquefaction)

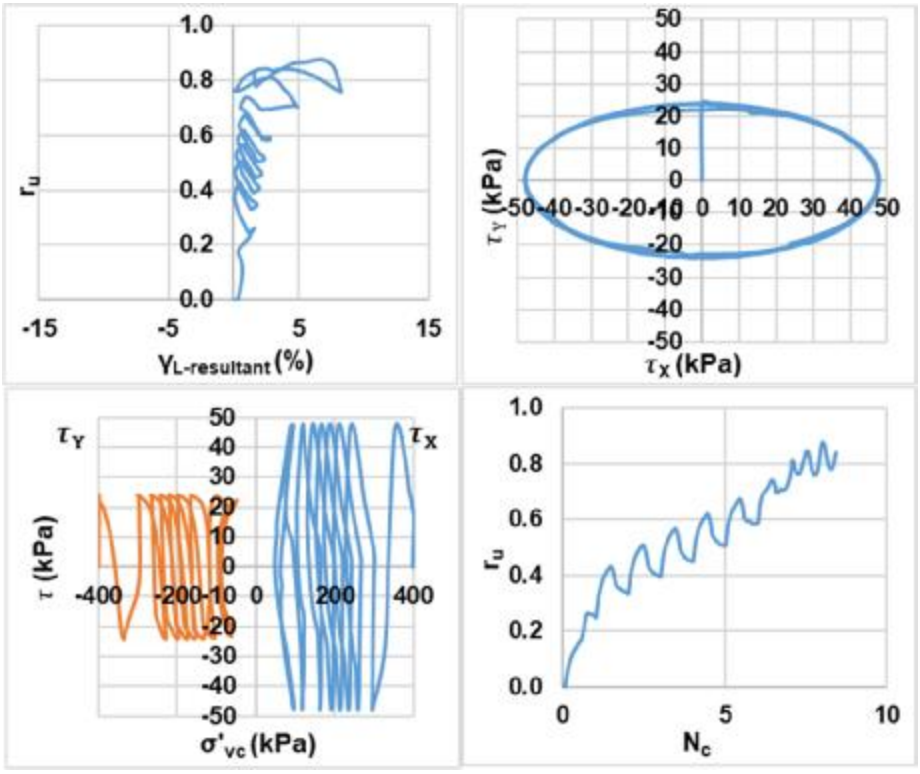


Bi-directional (Elliptical); $D_{rc}$ = 45%; $\sigma'_{vc}$ = 400 kPa; CSR = 0.12 (Re-liquefaction)

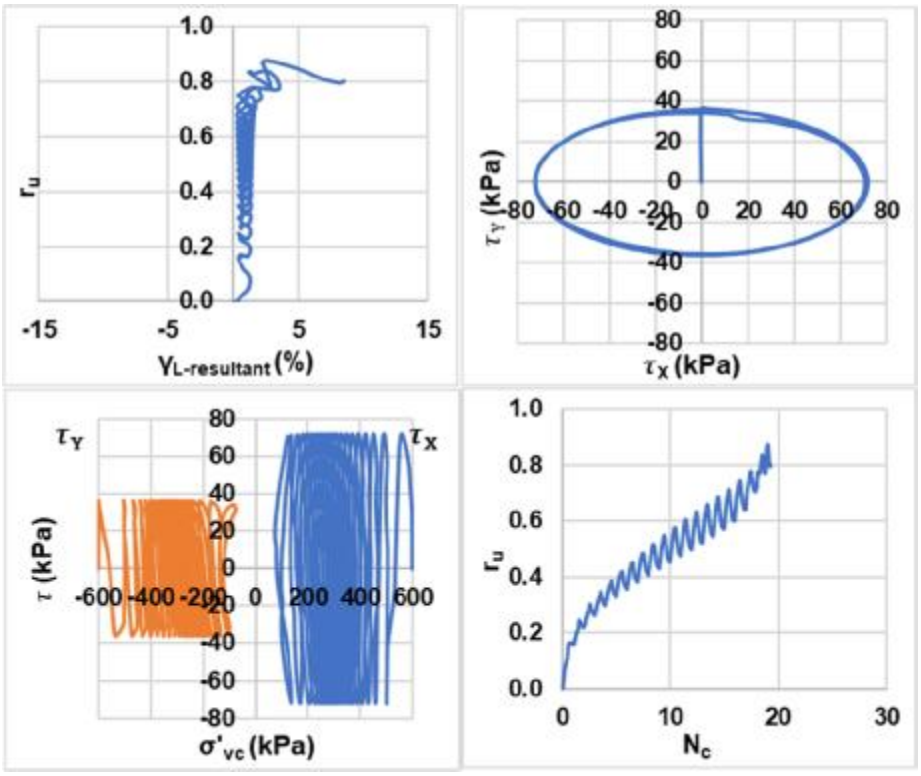


Bi-directional (Elliptical); $D_{rc}$ = 45%; $\sigma'_{vc}$ = 600 kPa; CSR = 0.12 (Liquefaction)

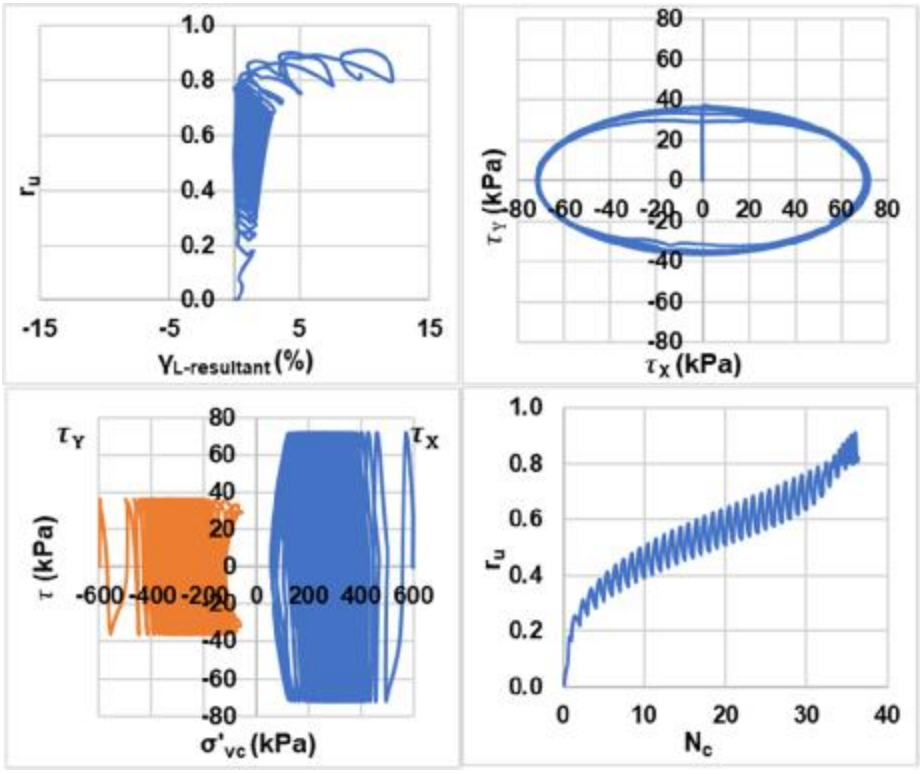


Bi-directional (Elliptical); $D_{rc}$ = 45%; $\sigma'_{vc}$ = 600 kPa; CSR = 0.12 (Re-liquefaction)

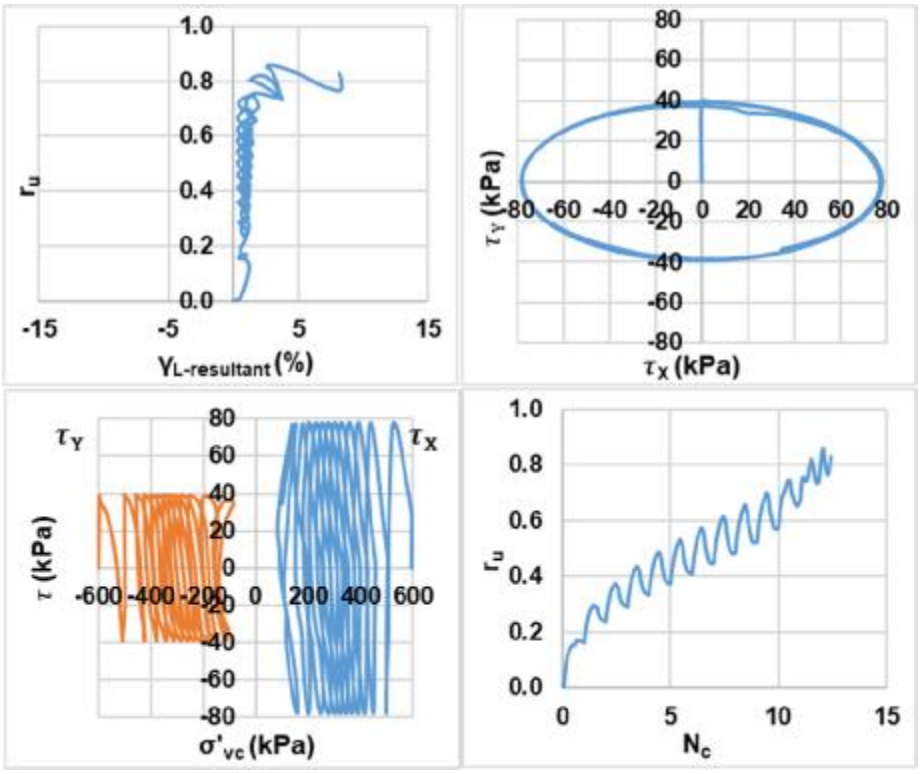


Bi-directional (Elliptical); $D_{rc}$ = 45%; $\sigma'_{vc}$ = 600 kPa; CSR = 0.13 (Liquefaction)

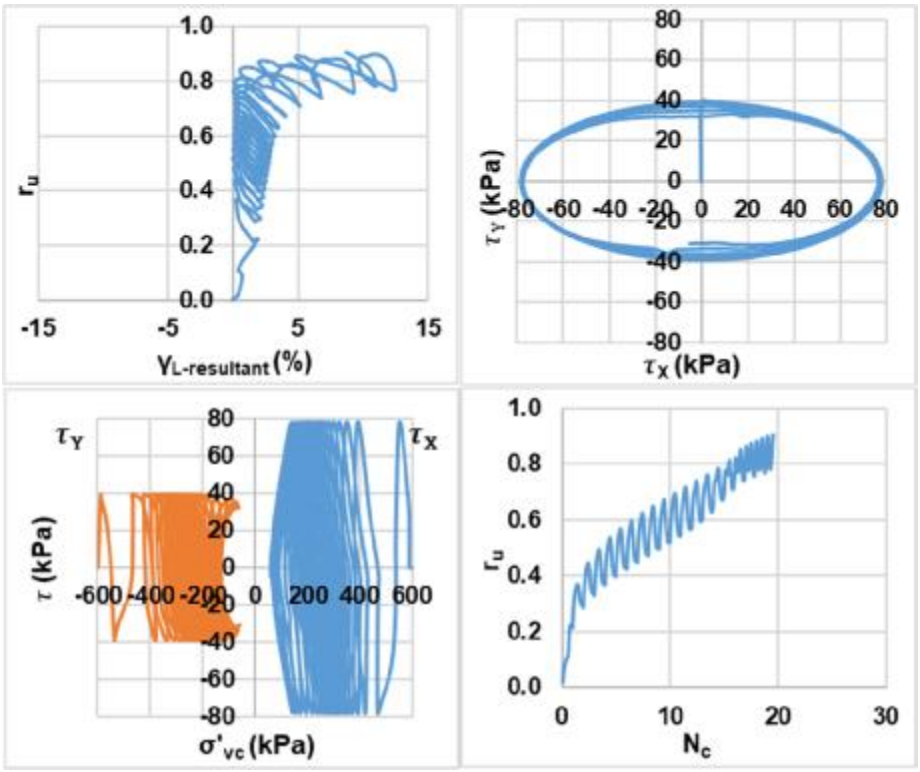


Bi-directional (Elliptical); $D_{rc}$ = 45%; $\sigma'_{vc}$ = 600 kPa; CSR = 0.13 (Re-liquefaction)

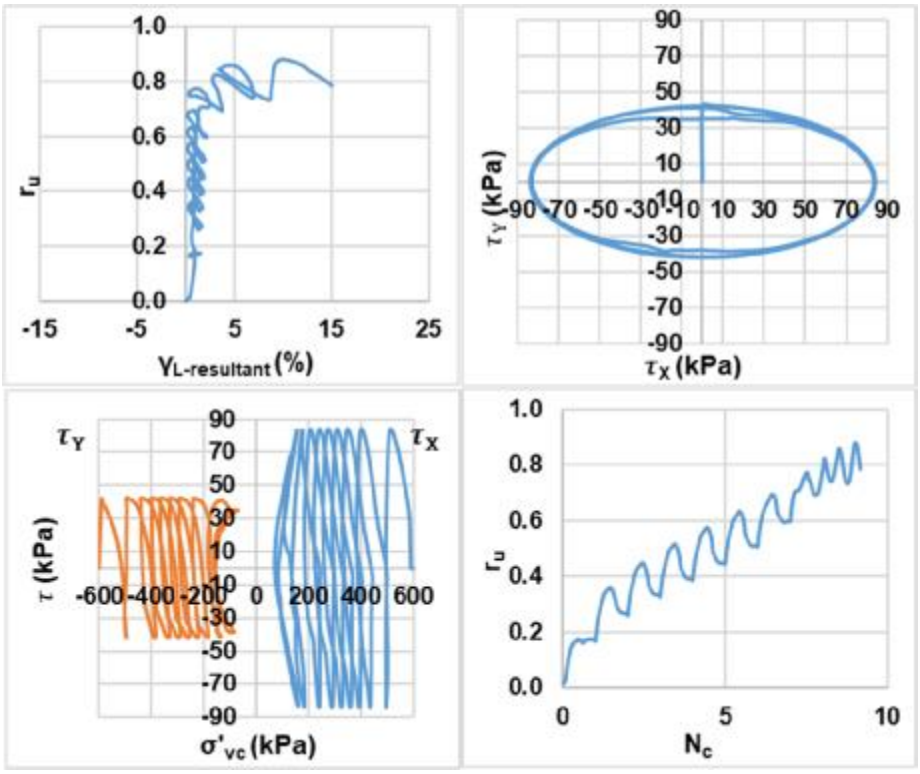


Bi-directional (Elliptical); $D_{rc}$ = 45%; $\sigma'_{vc}$ = 600 kPa; CSR = 0.14 (Liquefaction)

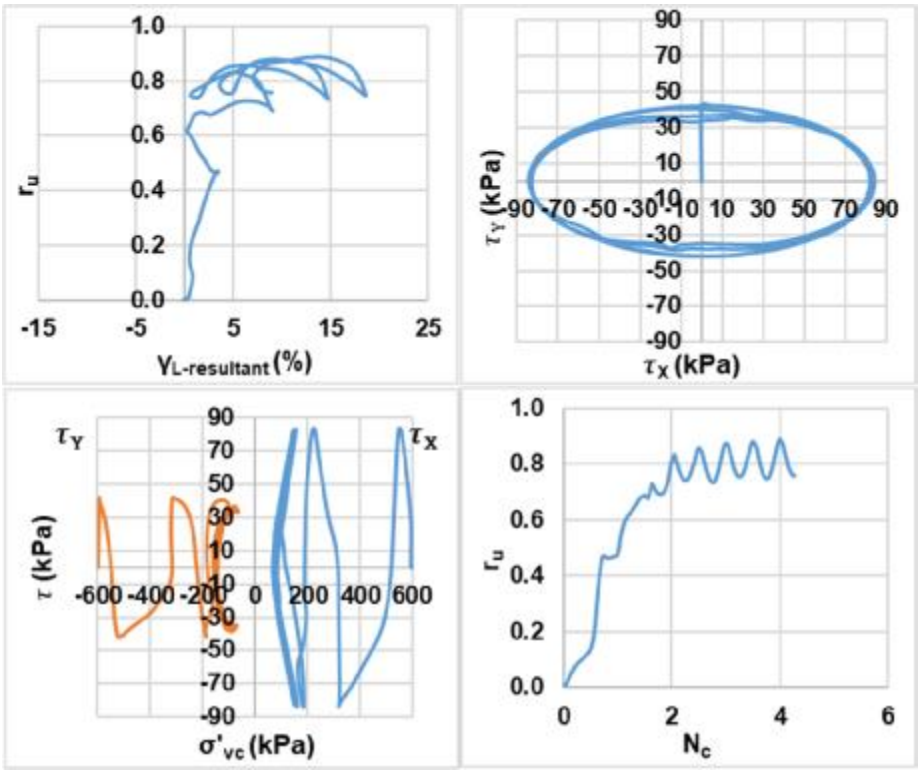


Bi-directional (Elliptical); $D_{rc}$ = 45%; $\sigma'_{vc}$ = 600 kPa; CSR = 0.14 (Re-liquefaction)

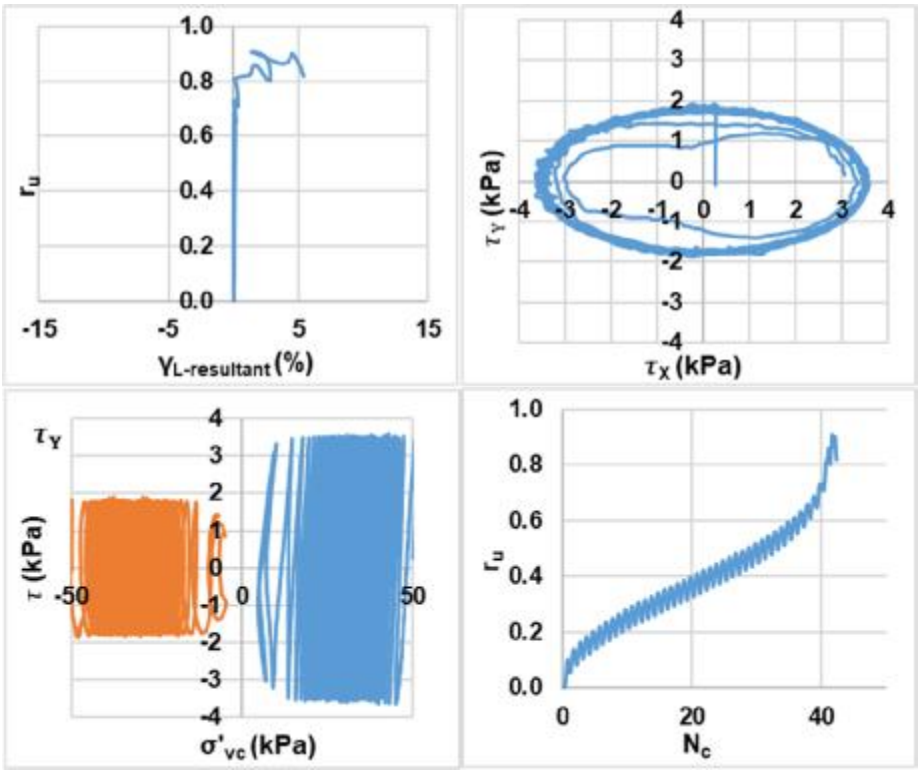


Bi-directional (Elliptical); $D_{rc}$ = 65%; $\sigma'_{vc}$ = 50 kPa; CSR = 0.07 (Liquefaction)

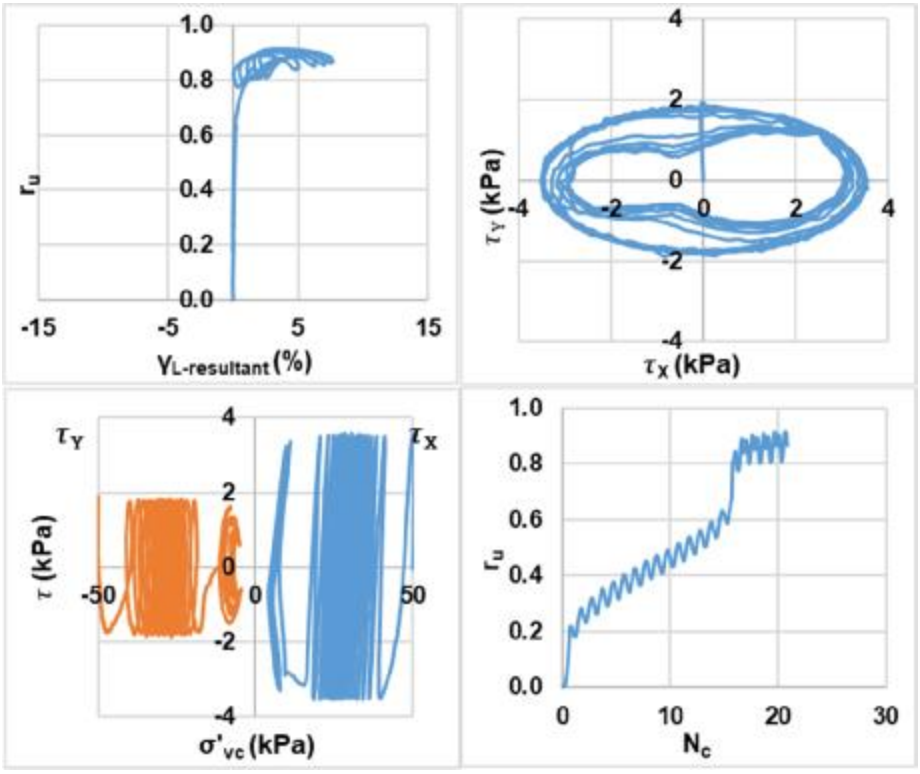


Bi-directional (Elliptical); $D_{rc}$ = 65%; $\sigma'_{vc}$ = 50 kPa; CSR = 0.07 (Re-liquefaction)

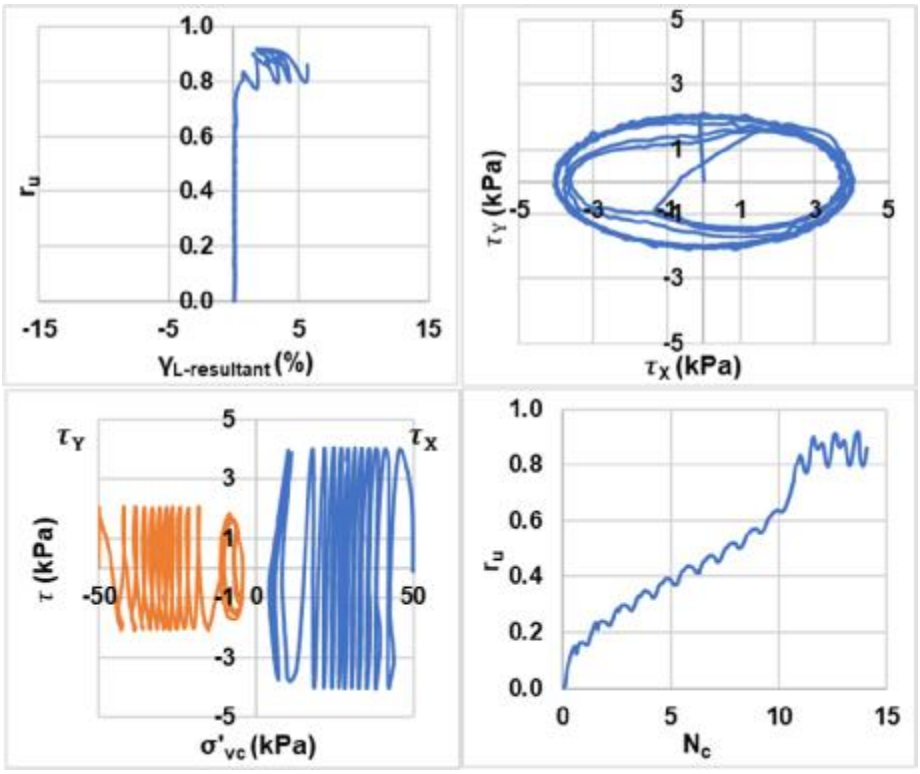


Bi-directional (Elliptical); $D_{rc}$ = 65%; $\sigma'_{vc}$ = 50 kPa; CSR = 0.08 (Liquefaction)

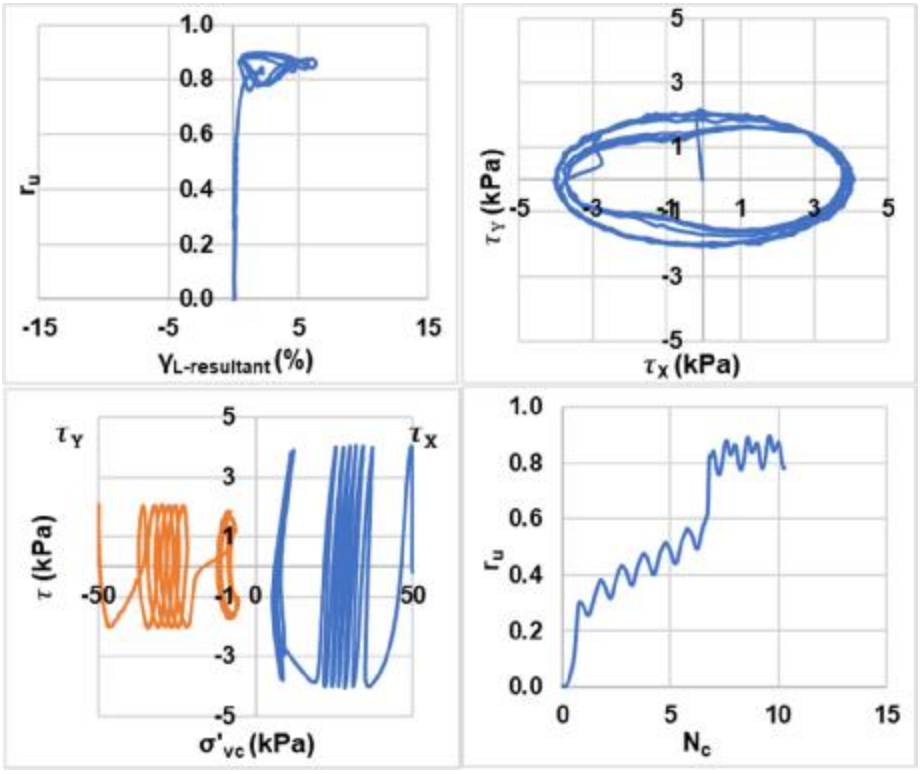


Bi-directional (Elliptical); $D_{rc}$ = 65%; $\sigma'_{vc}$ = 50 kPa; CSR = 0.08 (Re-liquefaction)

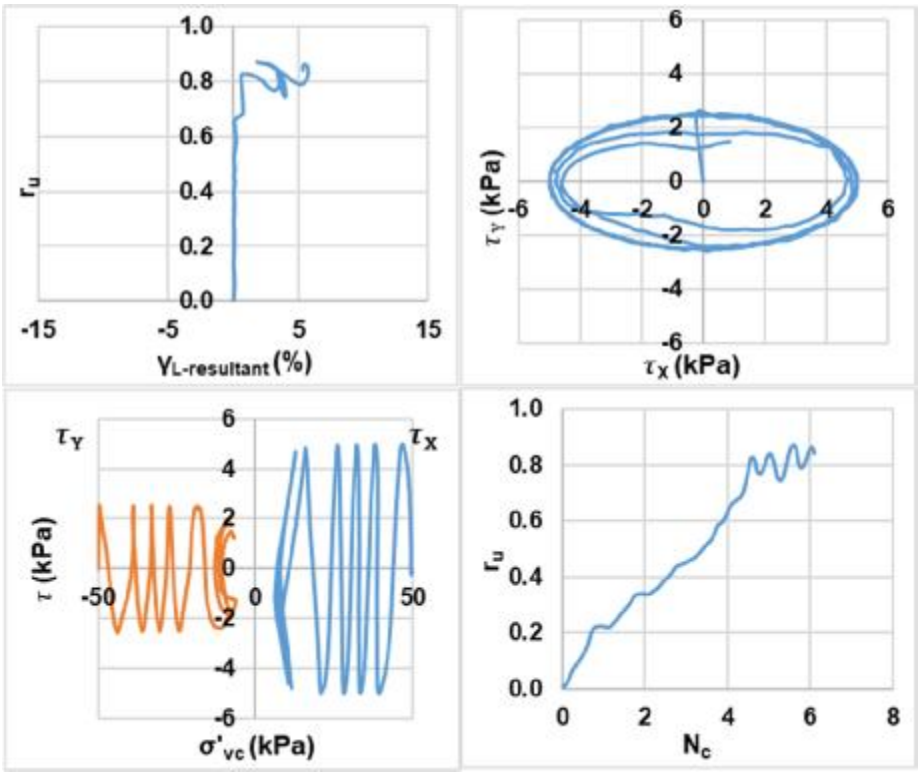


Bi-directional (Elliptical); $D_{rc}$ = 65%; $\sigma'_{vc}$ = 50 kPa; CSR = 0.1 (Liquefaction)

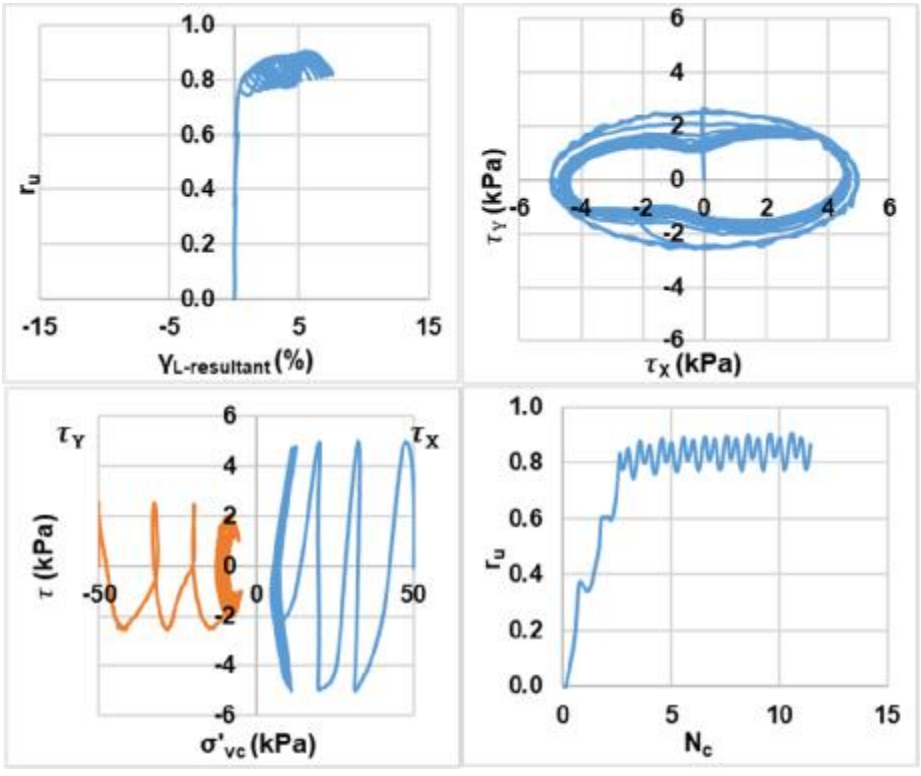


Bi-directional (Elliptical); $D_{rc}$ = 65%; $\sigma'_{vc}$ = 50 kPa; CSR = 0.1 (Re-liquefaction)

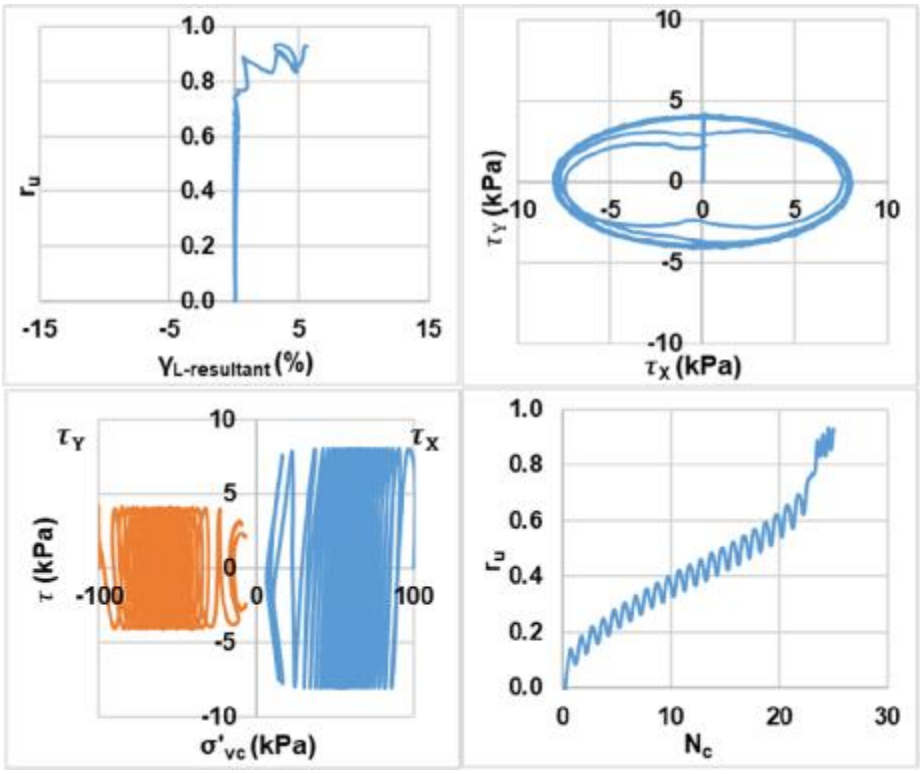


Bi-directional (Elliptical); $D_{rc}$ = 65%; $\sigma'_{vc}$ = 100 kPa; CSR = 0.08 (Liquefaction)

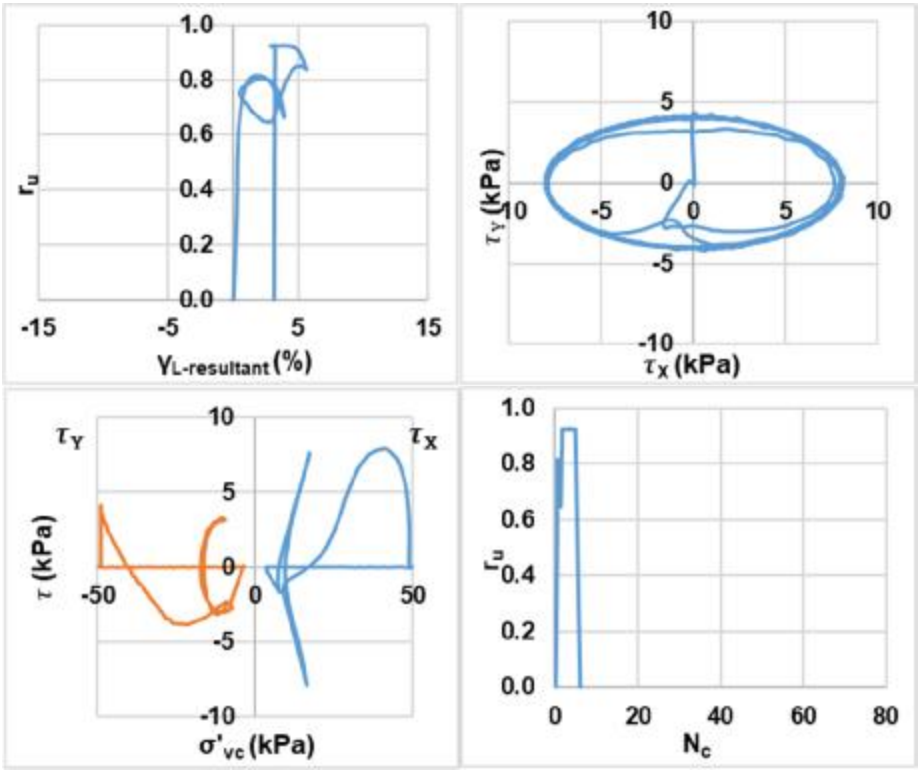


Bi-directional (Elliptical); $D_{rc}$ = 65%; $\sigma'_{vc}$ = 100 kPa; CSR = 0.08 (Re-liquefaction)

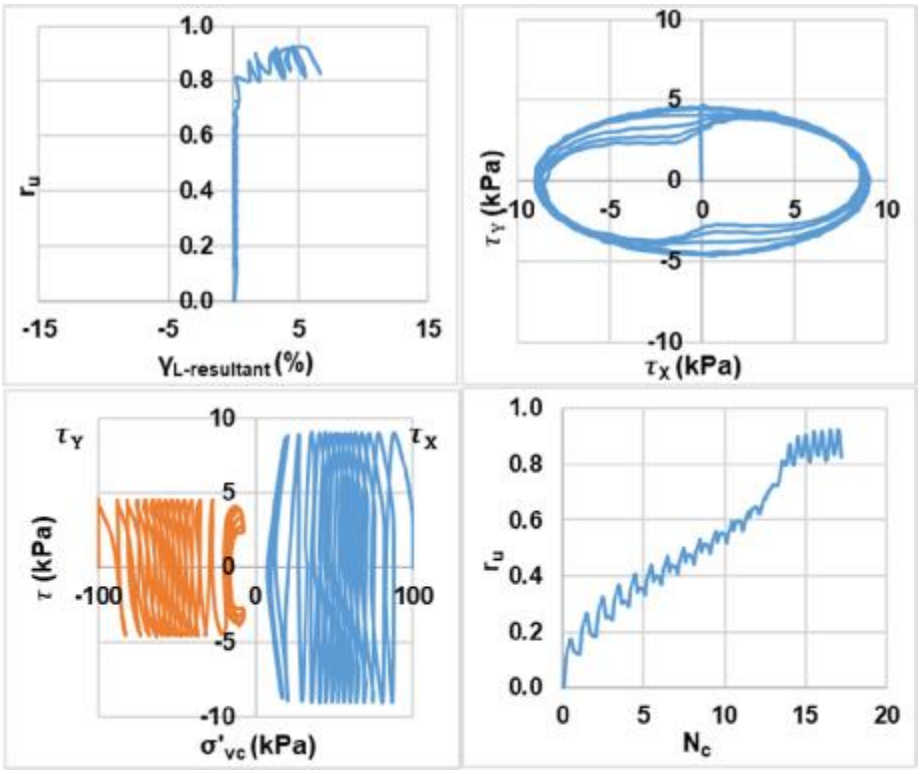


Bi-directional (Elliptical); $D_{rc}$ = 65%; $\sigma'_{vc}$ = 100 kPa; CSR = 0.09 (Liquefaction)

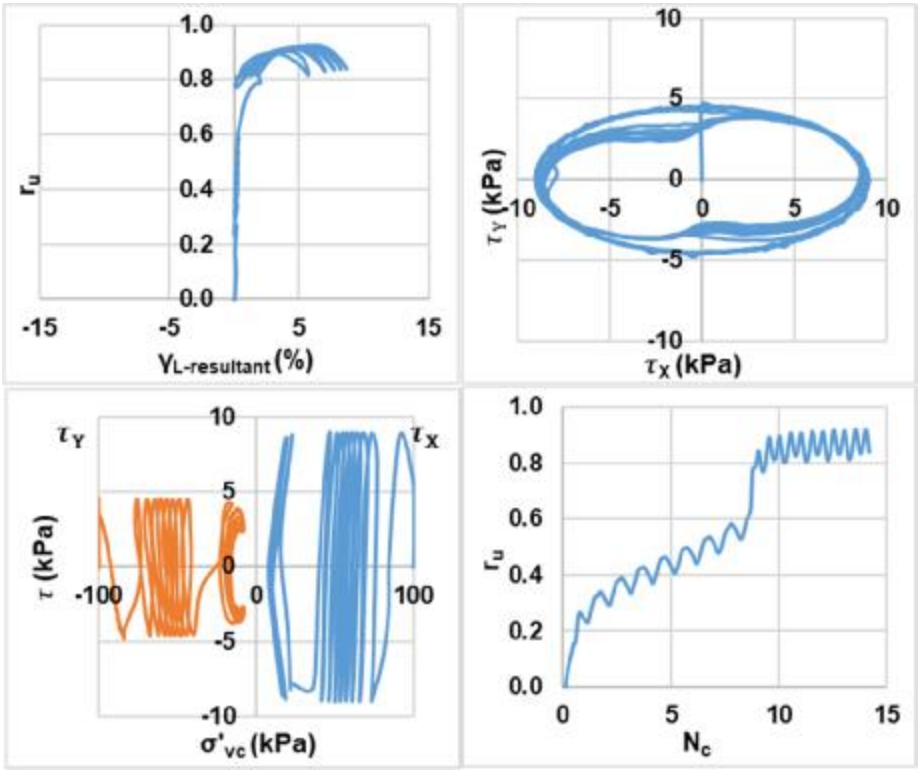


Bi-directional (Elliptical); $D_{rc}$ = 65%; $\sigma'_{vc}$ = 100 kPa; CSR = 0.09 (Re-liquefaction)

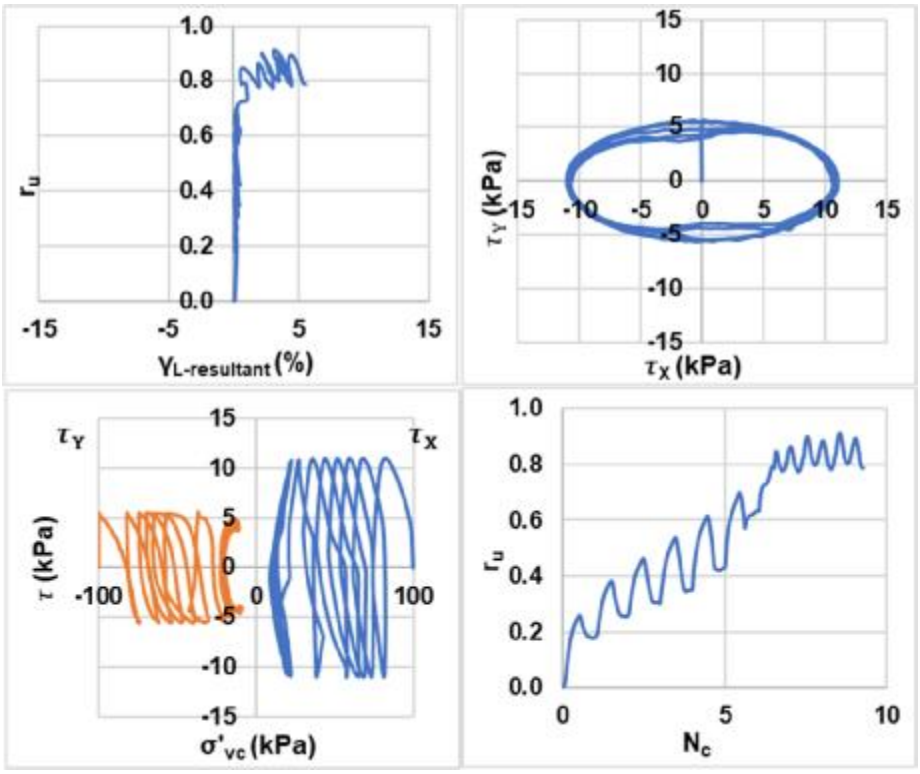


Bi-directional (Elliptical); $D_{rc}$ = 65%; $\sigma'_{vc}$ = 100 kPa; CSR = 0.11 (Liquefaction)

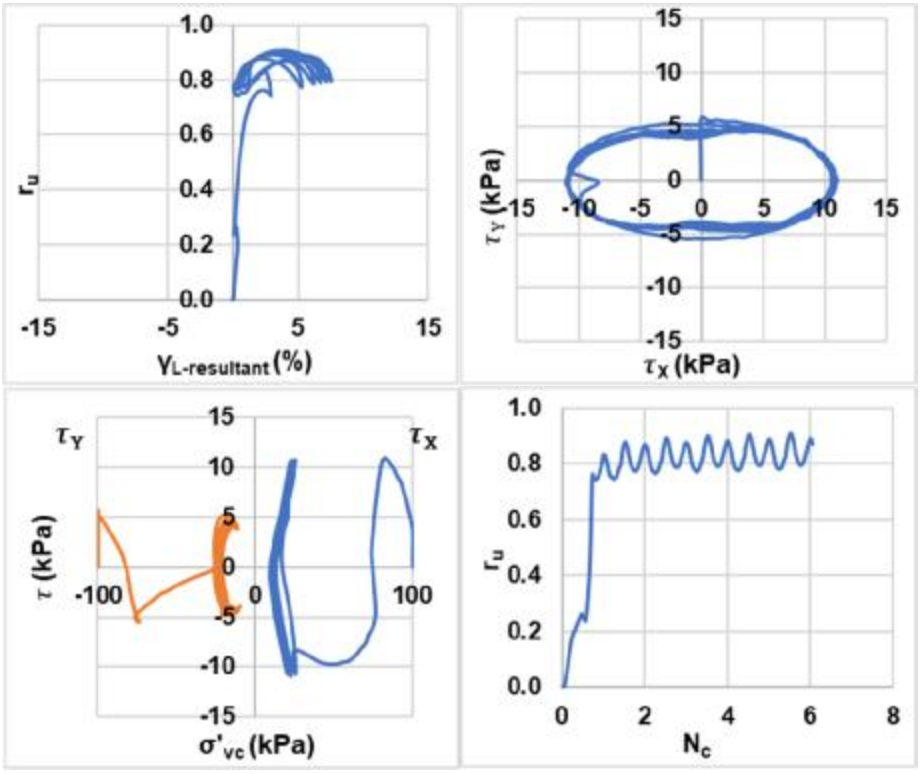


Bi-directional (Elliptical); $D_{rc}$ = 65%; $\sigma'_{vc}$ = 100 kPa; CSR = 0.11 (Re-liquefaction)

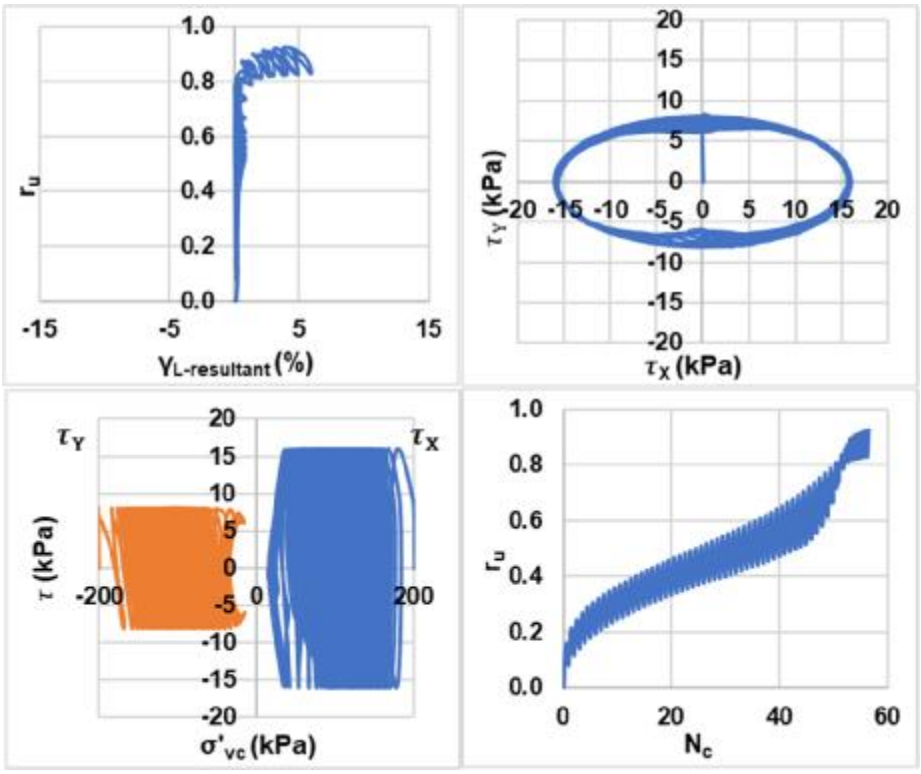


Bi-directional (Elliptical); $D_{rc}$ = 65%; $\sigma'_{vc}$ = 200 kPa; CSR = 0.08 (Liquefaction)

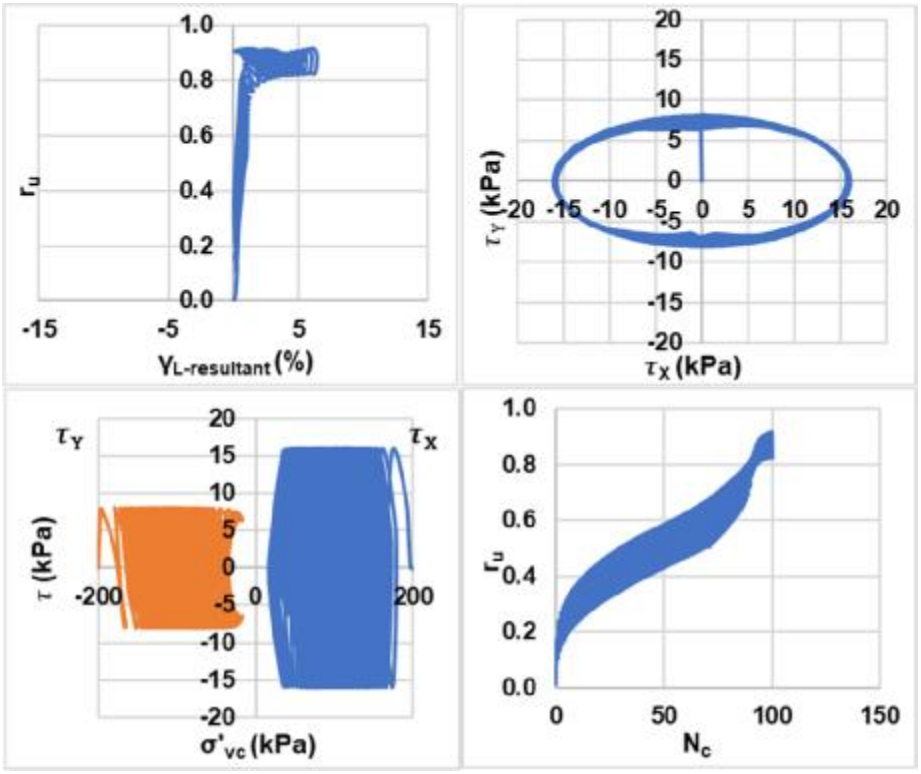


Bi-directional (Elliptical); $D_{rc}$ = 65%; $\sigma'_{vc}$ = 200 kPa; CSR = 0.08 (Re-liquefaction)

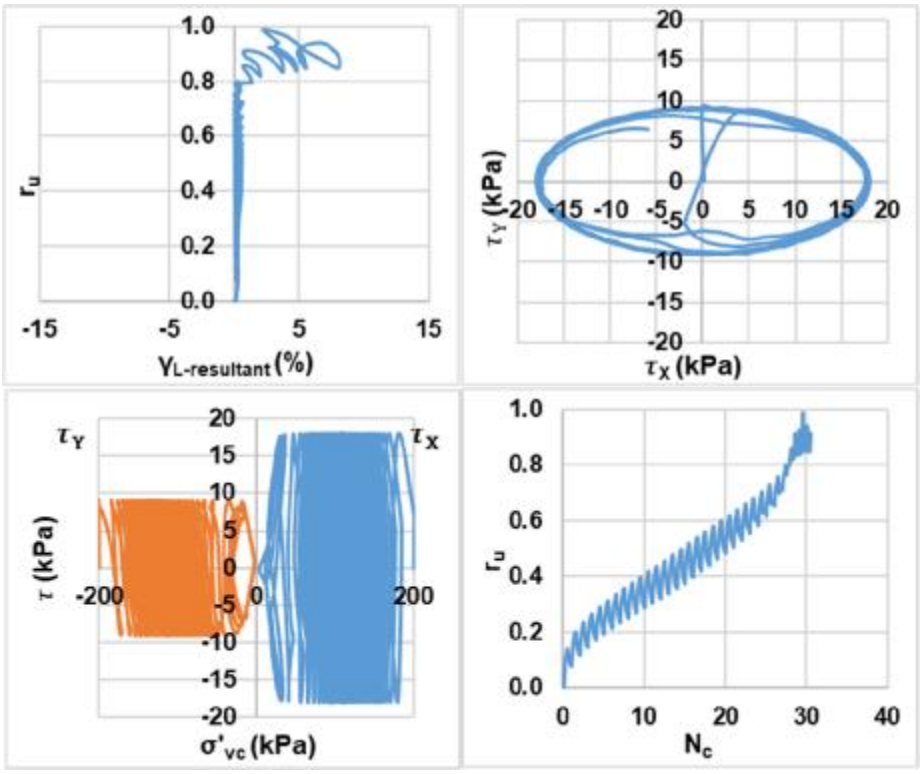


Bi-directional (Elliptical); $D_{rc}$ = 65%; $\sigma'_{vc}$ = 200 kPa; CSR = 0.09 (Liquefaction)

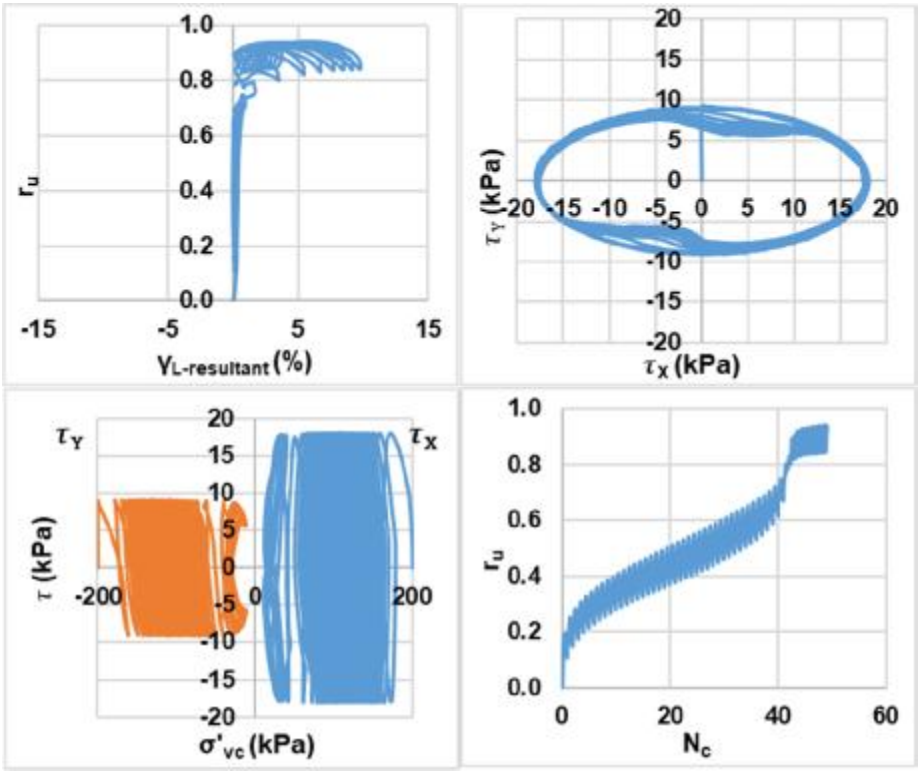


Bi-directional (Elliptical); $D_{rc}$ = 65%; $\sigma'_{vc}$ = 200 kPa; CSR = 0.09 (Re-liquefaction)

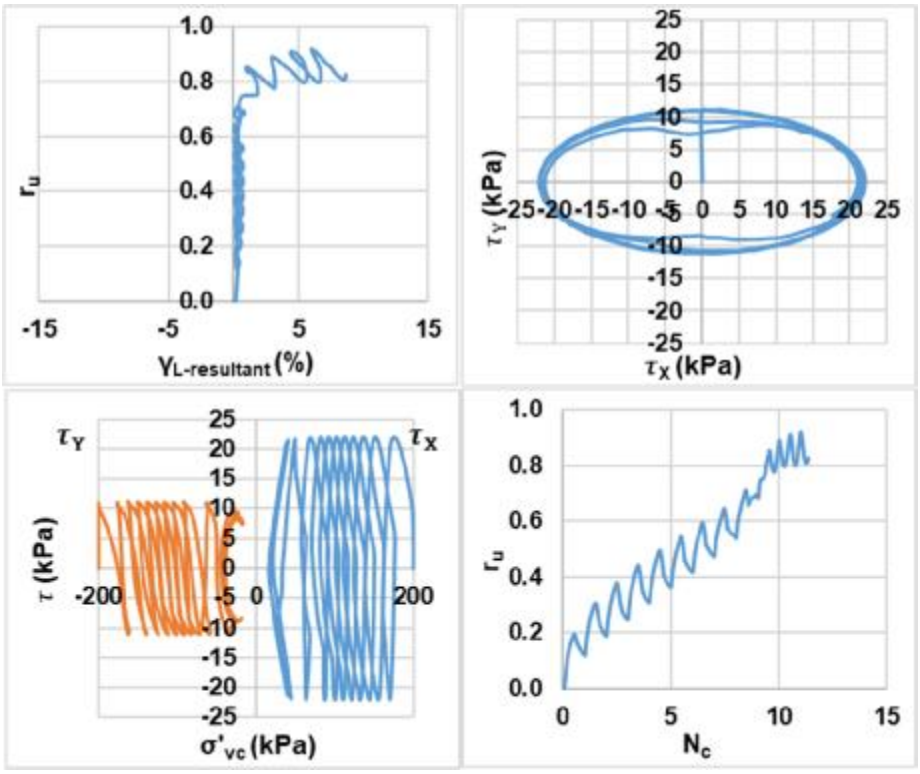


Bi-directional (Elliptical); $D_{rc}$ = 65%; $\sigma'_{vc}$ = 200 kPa; CSR = 0.11 (Liquefaction)

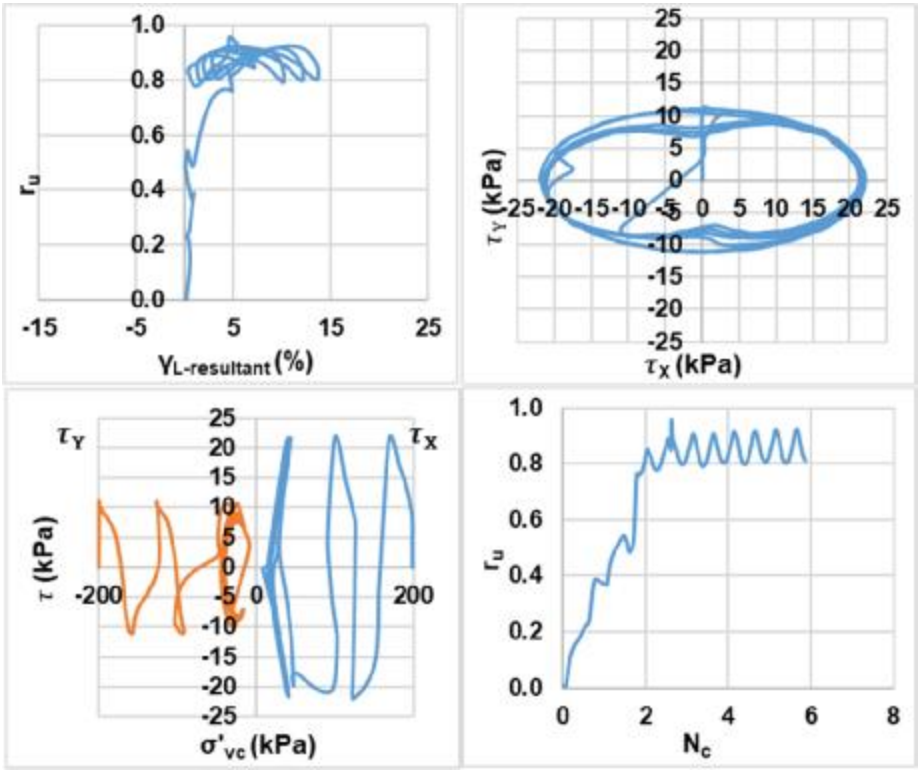


Bi-directional (Elliptical); $D_{rc}$ = 65%; $\sigma'_{vc}$ = 200 kPa; CSR = 0.11 (Re-liquefaction)

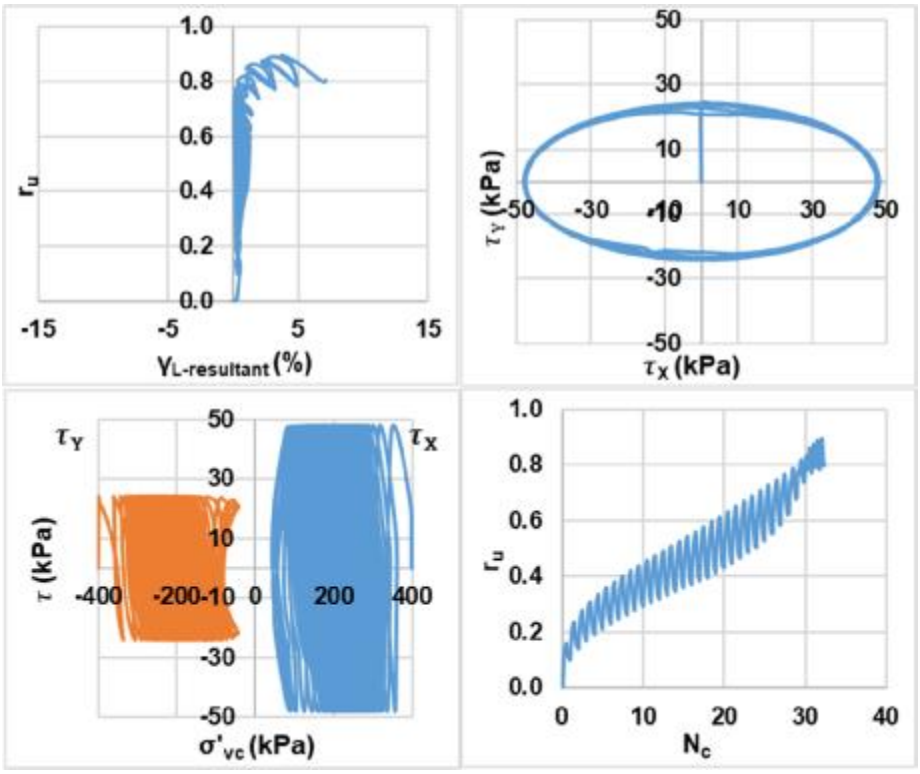


Bi-directional (Elliptical); $D_{rc}$ = 65%; $\sigma'_{vc}$ = 400 kPa; CSR = 0.12 (Liquefaction)

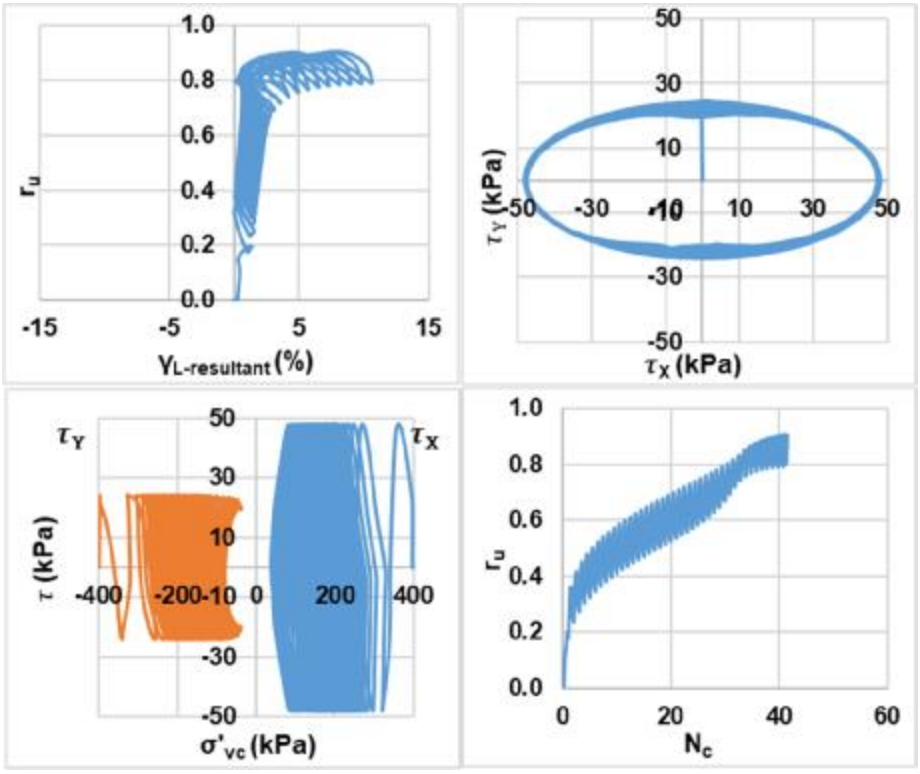


Bi-directional (Elliptical); $D_{rc}$ = 65%; $\sigma'_{vc}$ = 400 kPa; CSR = 0.12 (Re-liquefaction)

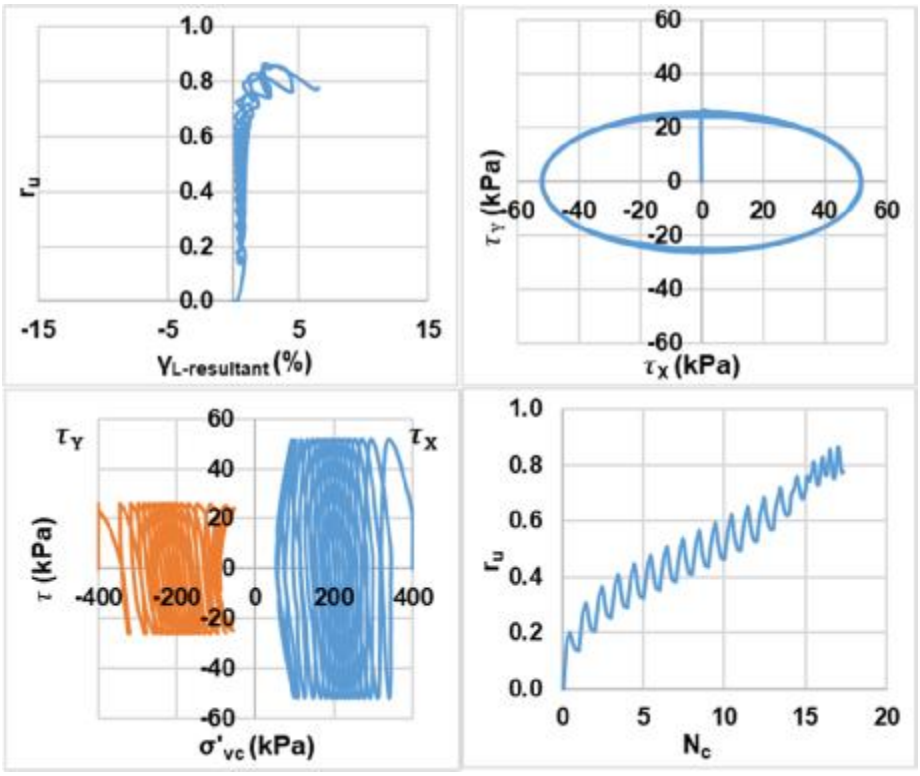


Bi-directional (Elliptical); $D_{rc}$ = 65%; $\sigma'_{vc}$ = 400 kPa; CSR = 0.13 (Liquefaction)

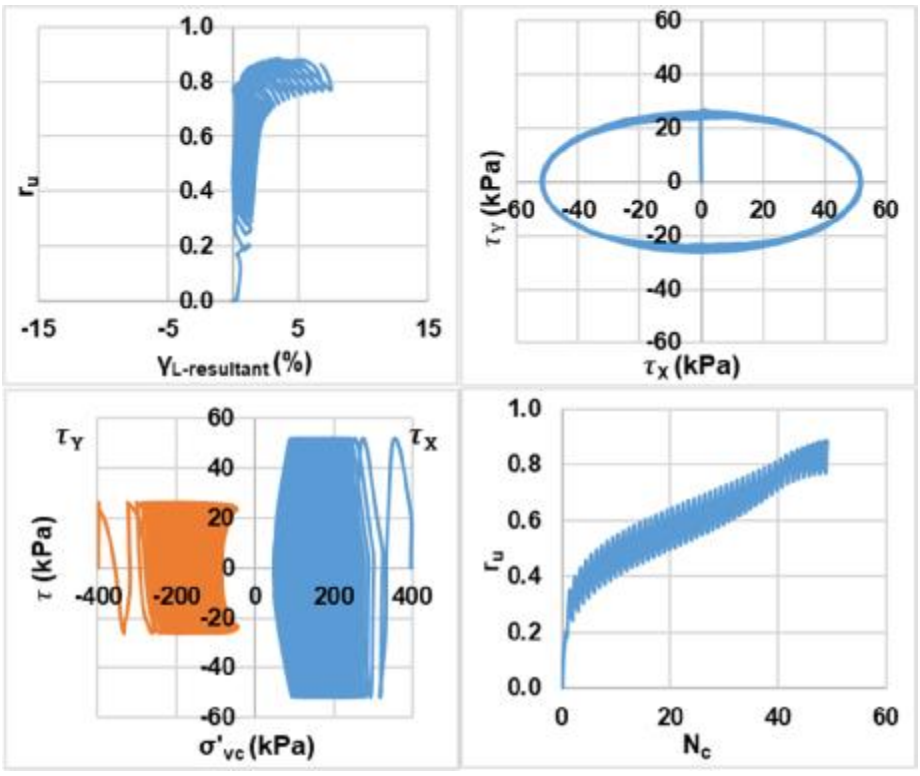


Bi-directional (Elliptical); $D_{rc}$ = 65%; $\sigma'_{vc}$ = 400 kPa; CSR = 0.13 (Re-liquefaction)

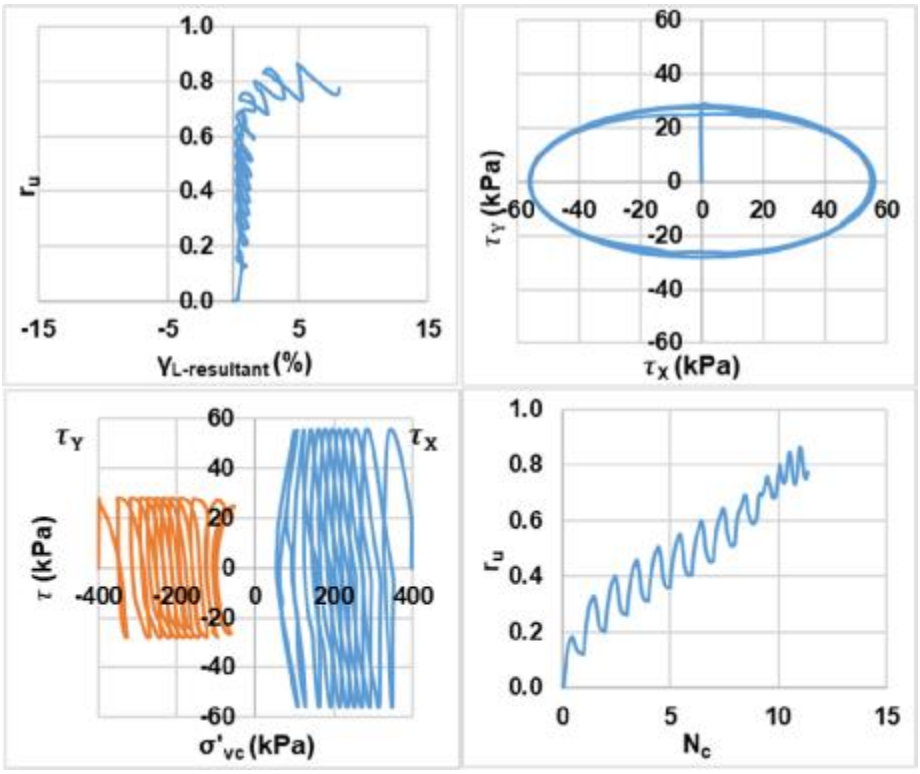


Bi-directional (Elliptical); $D_{rc}$ = 65%; $\sigma'_{vc}$ = 400 kPa; CSR = 0.14 (Liquefaction)

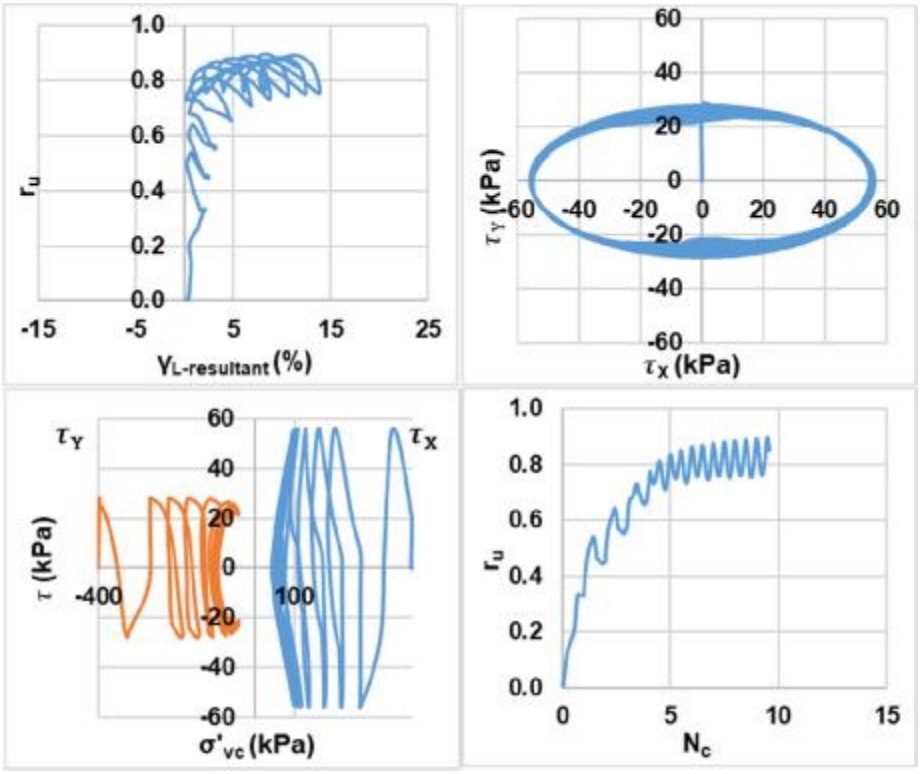


Bi-directional (Elliptical); $D_{rc}$ = 65%; $\sigma'_{vc}$ = 400 kPa; CSR = 0.14 (Re-liquefaction)

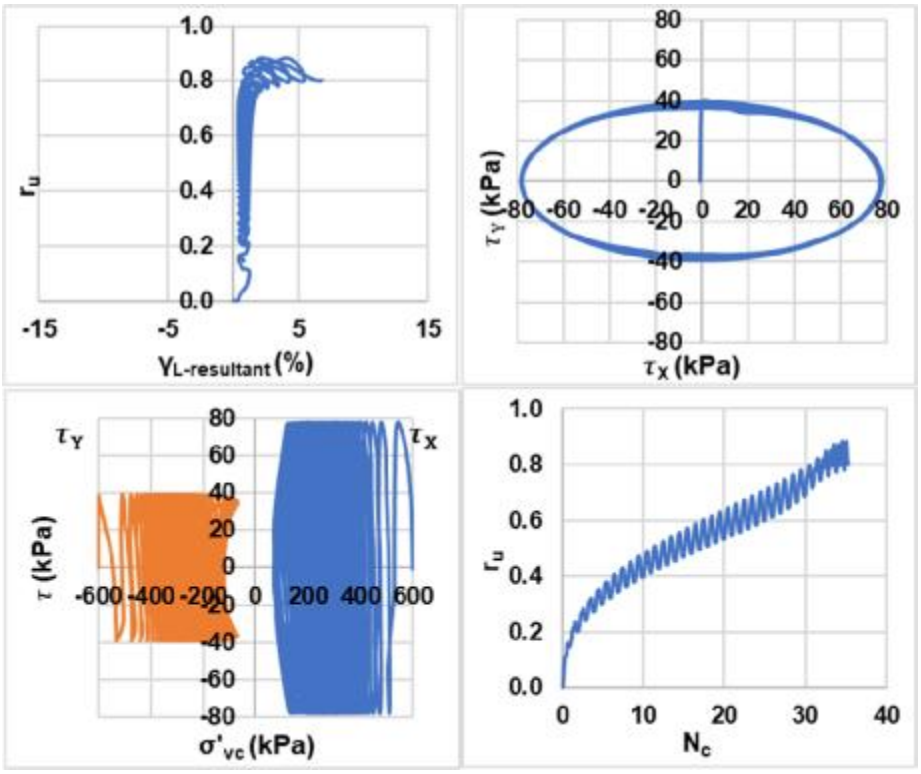


Bi-directional (Elliptical); $D_{rc}$ = 65%; $\sigma'_{vc}$ = 600 kPa; CSR = 0.13 (Liquefaction)

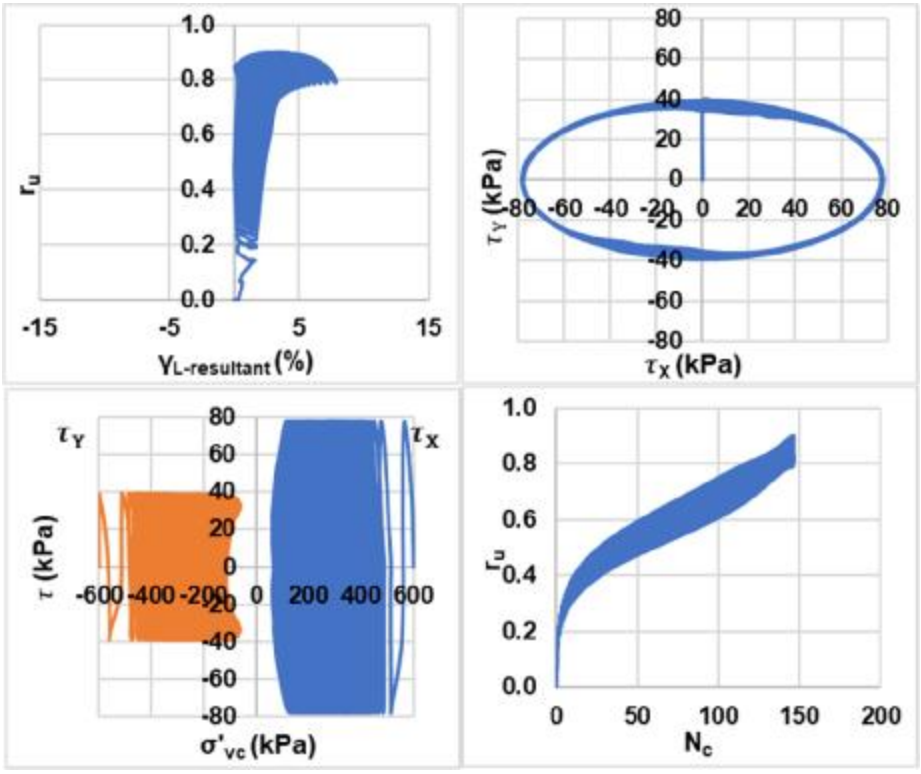


Bi-directional (Elliptical); $D_{rc}$ = 65%; $\sigma'_{vc}$ = 600 kPa; CSR = 0.13 (Re-liquefaction)

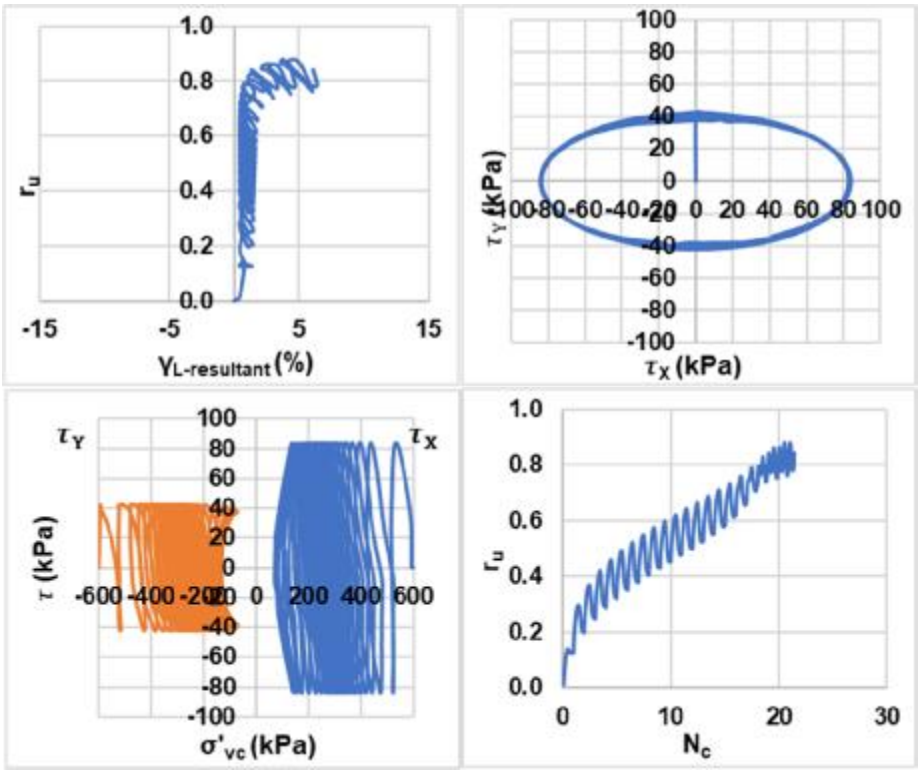


Bi-directional (Elliptical); $D_{rc}$ = 65%; $\sigma'_{vc}$ = 600 kPa; CSR = 0.14 (Liquefaction)

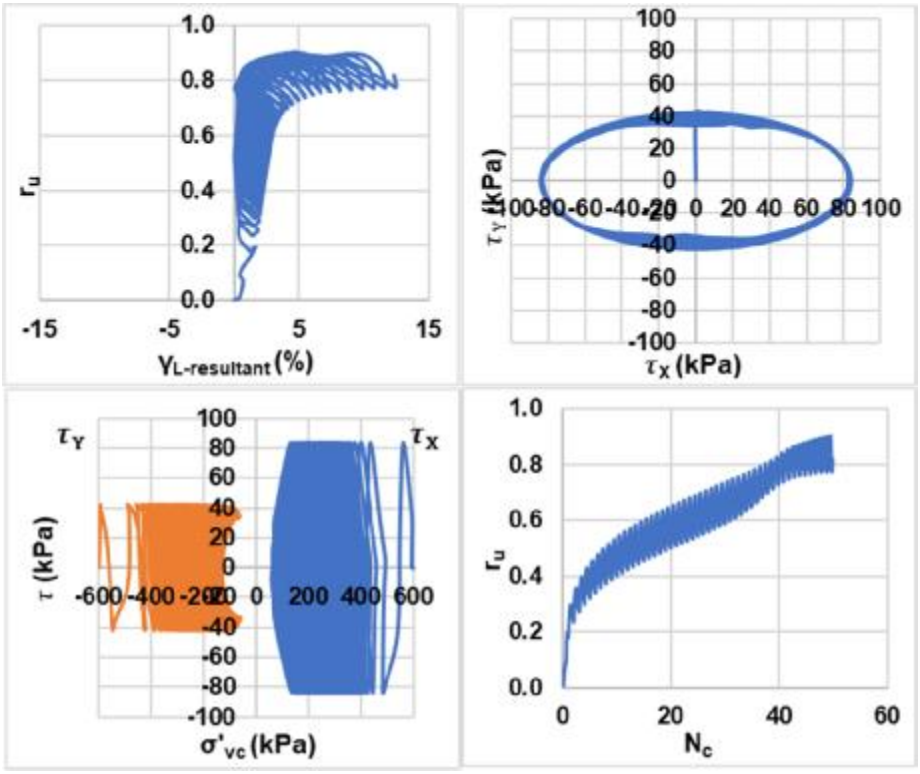


Bi-directional (Elliptical); $D_{rc}$ = 65%; $\sigma'_{vc}$ = 600 kPa; CSR = 0.14 (Re-liquefaction)

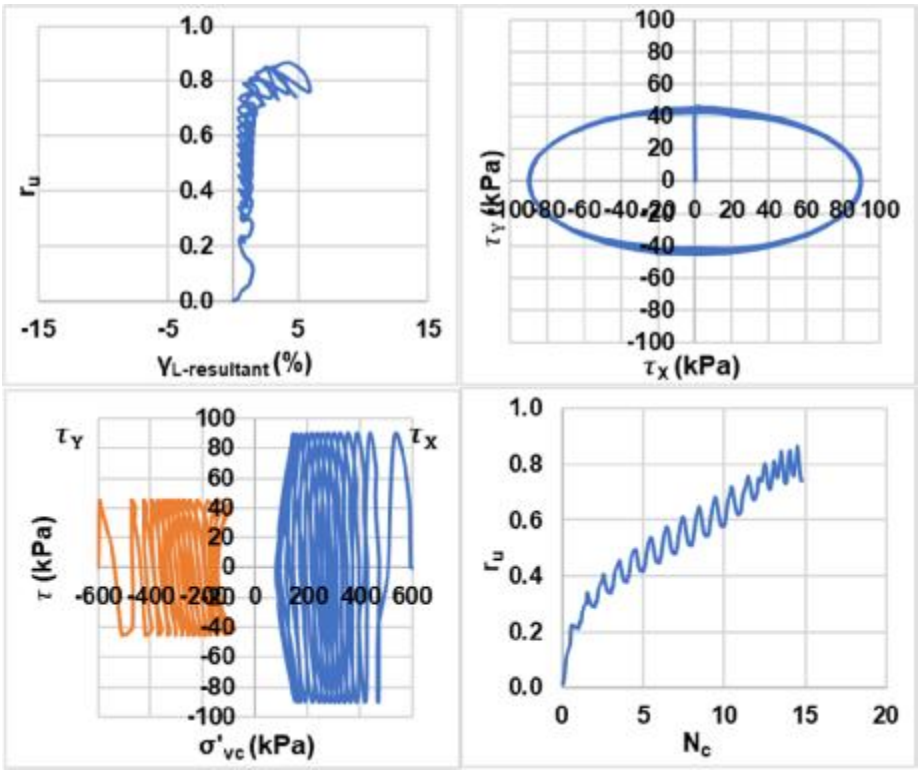


Bi-directional (Elliptical); $D_{rc}$ = 65%; $\sigma'_{vc}$ = 600 kPa; CSR = 0.15 (Liquefaction)

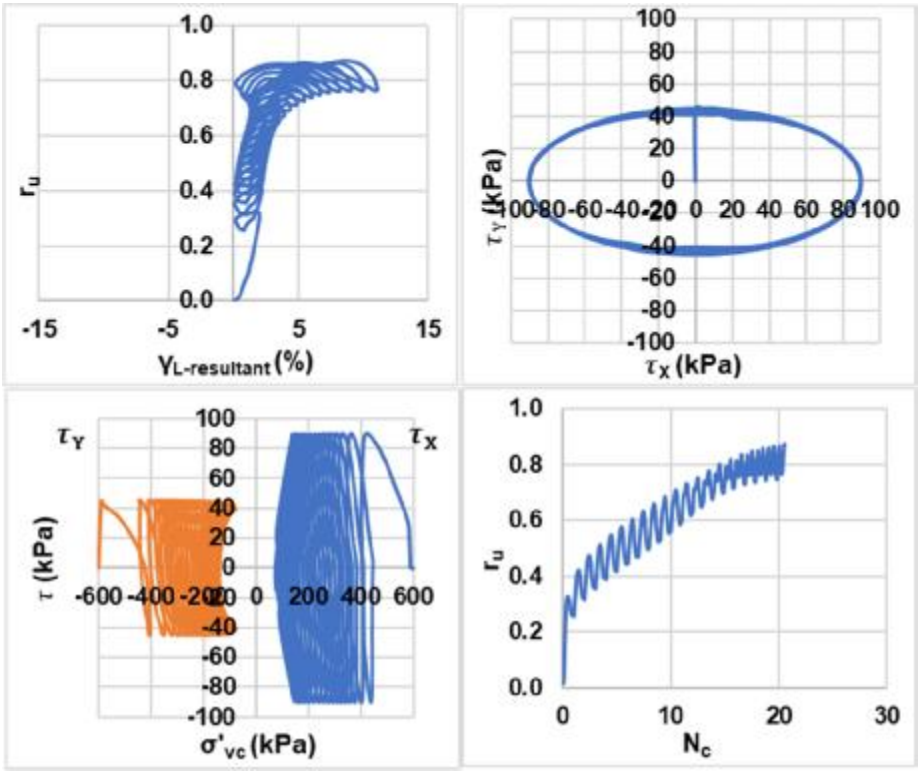


Bi-directional (Elliptical); $D_{rc}$ = 65%; $\sigma'_{vc}$ = 600 kPa; CSR = 0.15 (Re-liquefaction)

# Appendix 4

Bi-directional / Figure-8 Cyclic Simple Shear Test Results

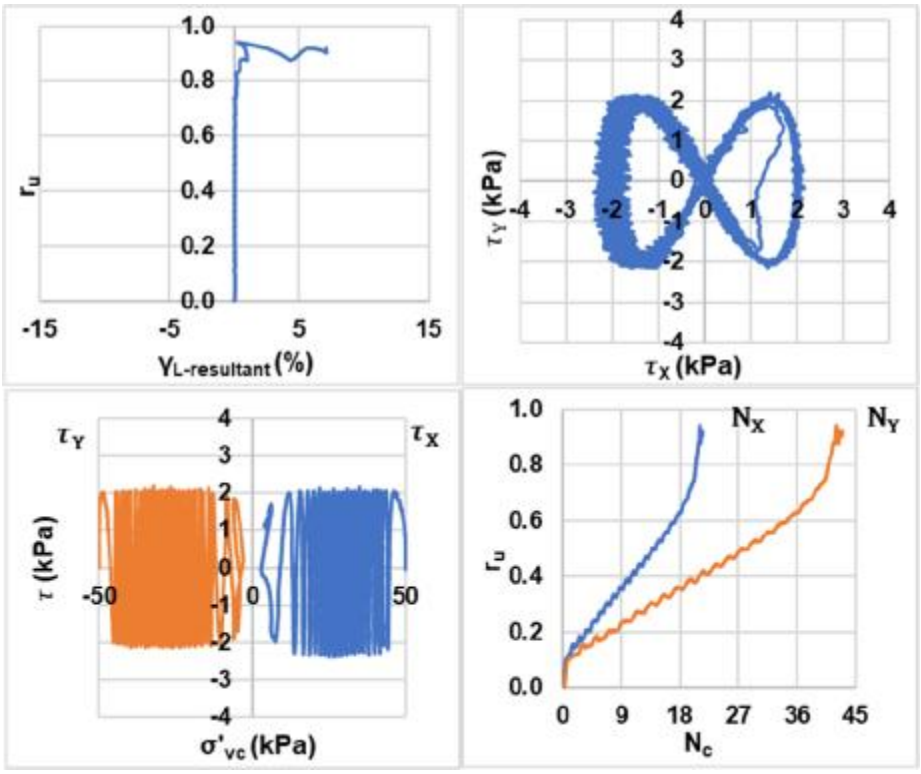


Bi-directional (Figure-8); $D_{rc}$ = 25%; $\sigma'_{vc}$ = 50 kPa; CSR = 0.04 (Liquefaction)

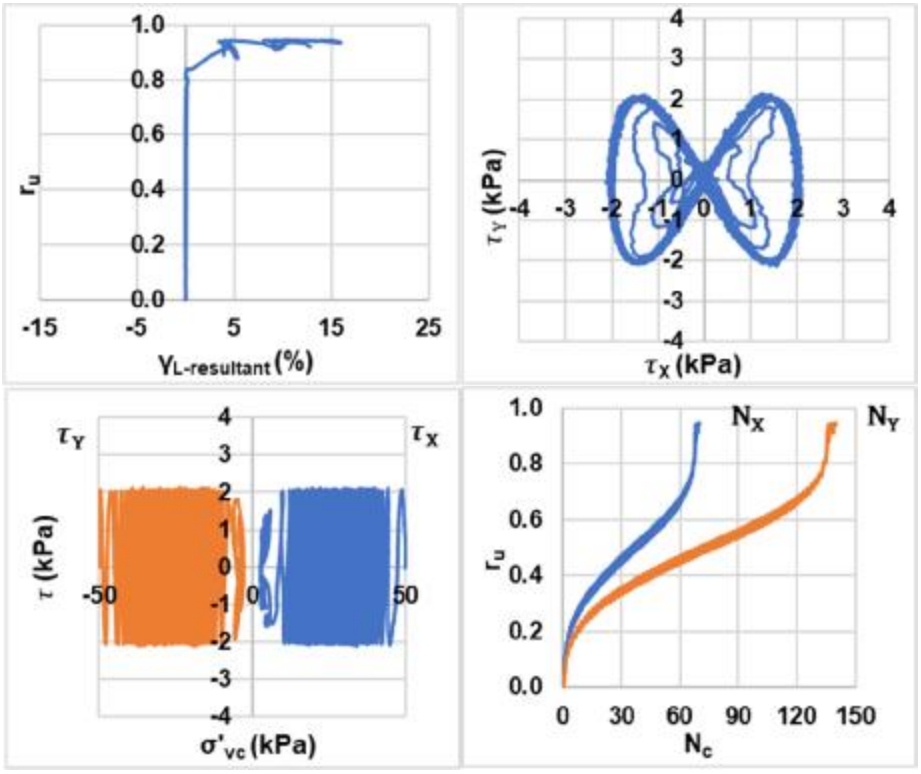


Bi-directional (Figure-8); $D_{rc}$ = 25%; $\sigma'_{vc}$ = 50 kPa; CSR = 0.04 (Re-liquefaction)

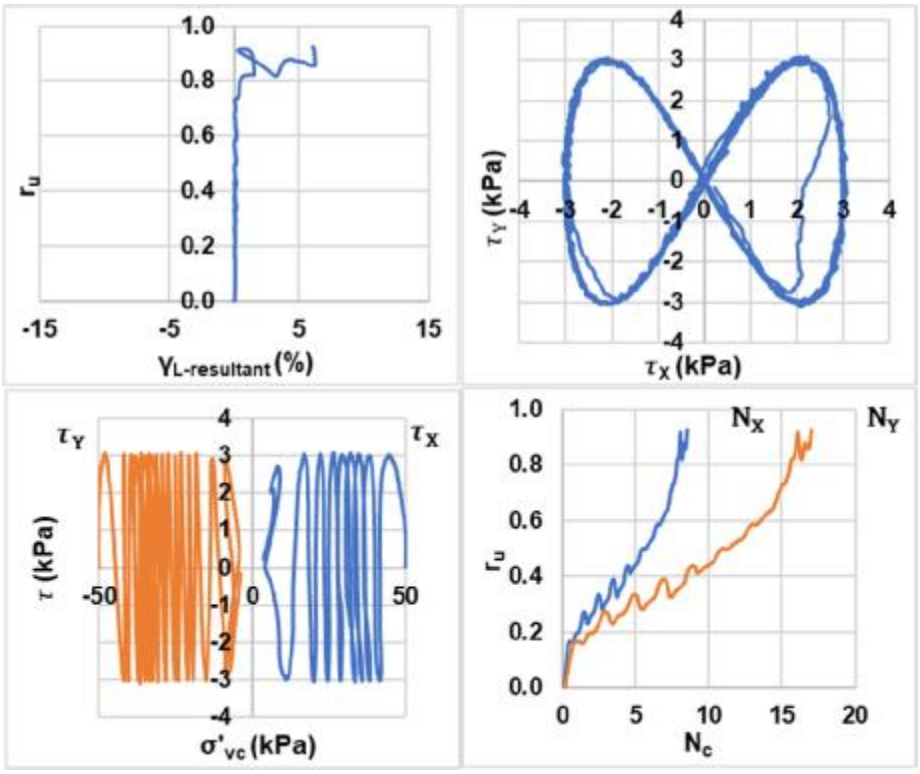


Bi-directional (Figure-8); $D_{rc}$ = 25%; $\sigma'_{vc}$ = 50 kPa; CSR = 0.06 (Liquefaction)

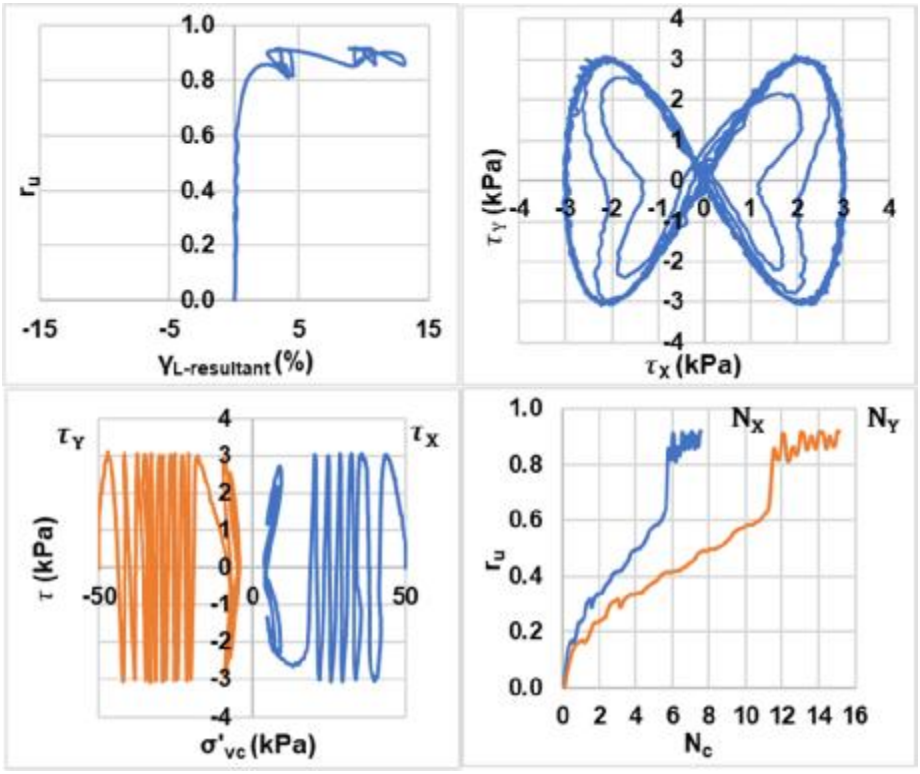


Bi-directional (Figure-8); $D_{rc}$ = 25%; $\sigma'_{vc}$ = 50 kPa; CSR = 0.06 (Re-liquefaction)

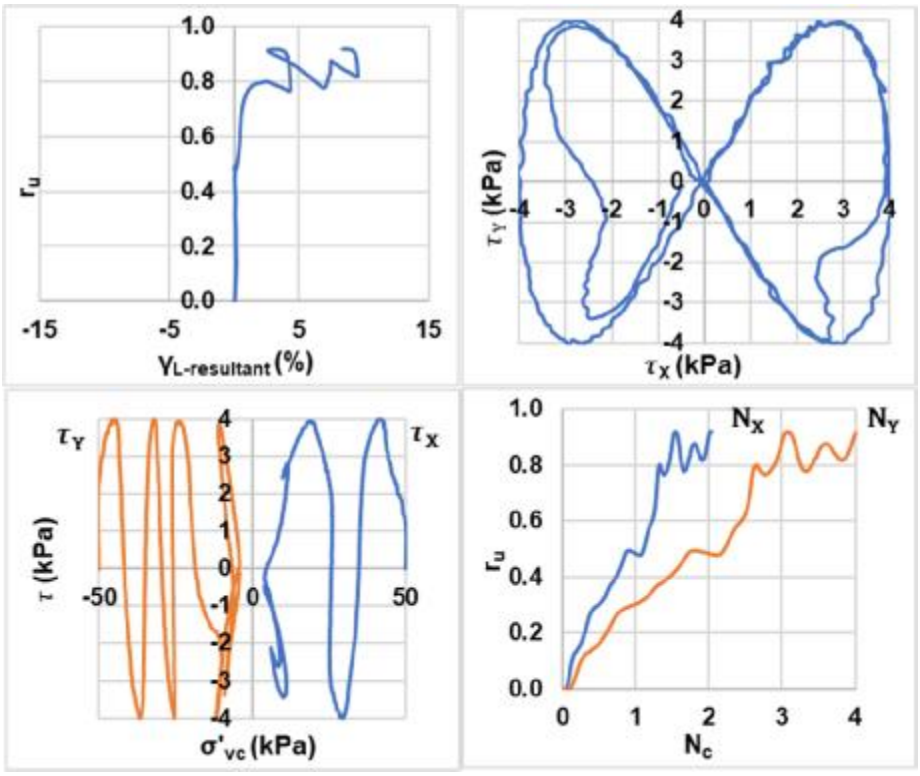


Bi-directional (Figure-8); $D_{rc}$ = 25%; $\sigma'_{vc}$ = 50 kPa; CSR = 0.08 (Liquefaction)

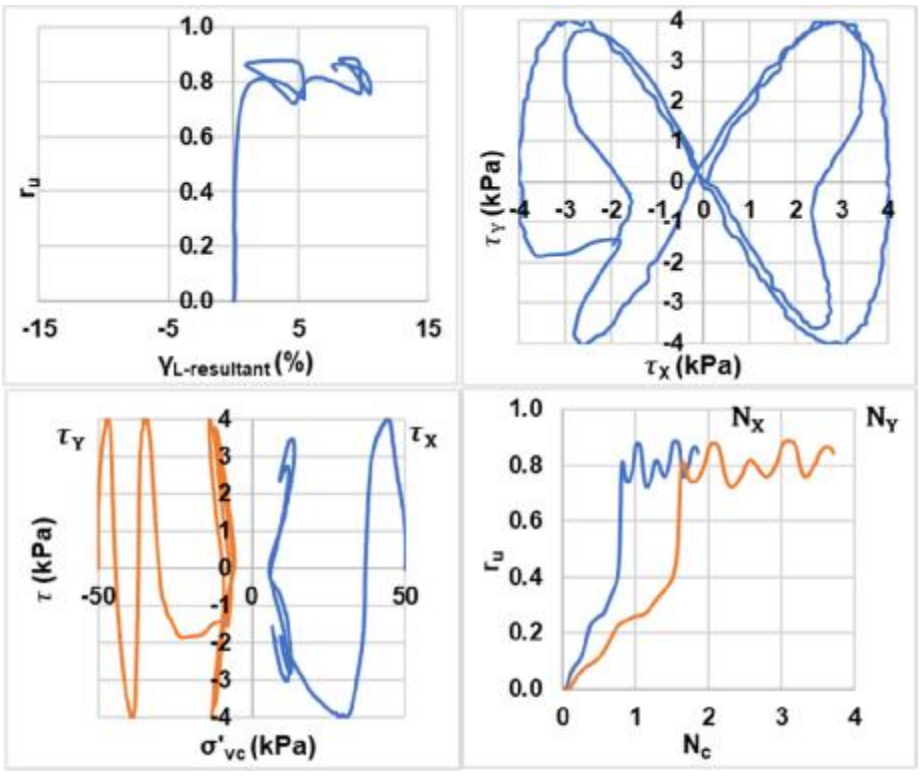


Bi-directional (Figure-8); $D_{rc}$ = 25%; $\sigma'_{vc}$ = 50 kPa; CSR = 0.08 (Re-liquefaction)

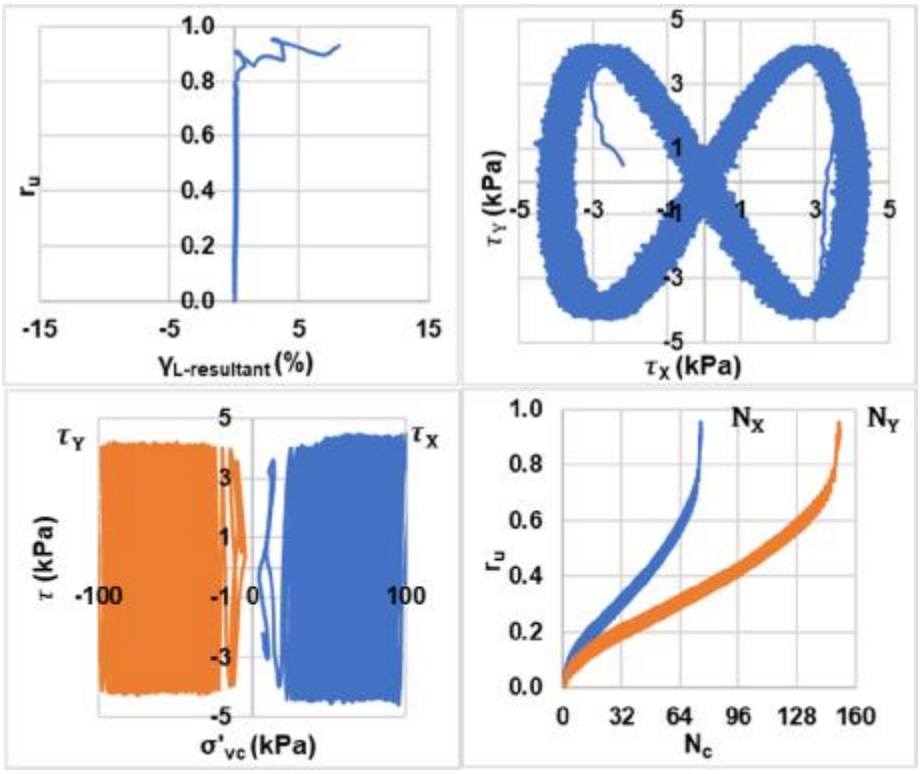


Bi-directional (Figure-8); $D_{rc}$ = 25%; $\sigma'_{vc}$ = 100 kPa; CSR = 0.04 (Liquefaction)

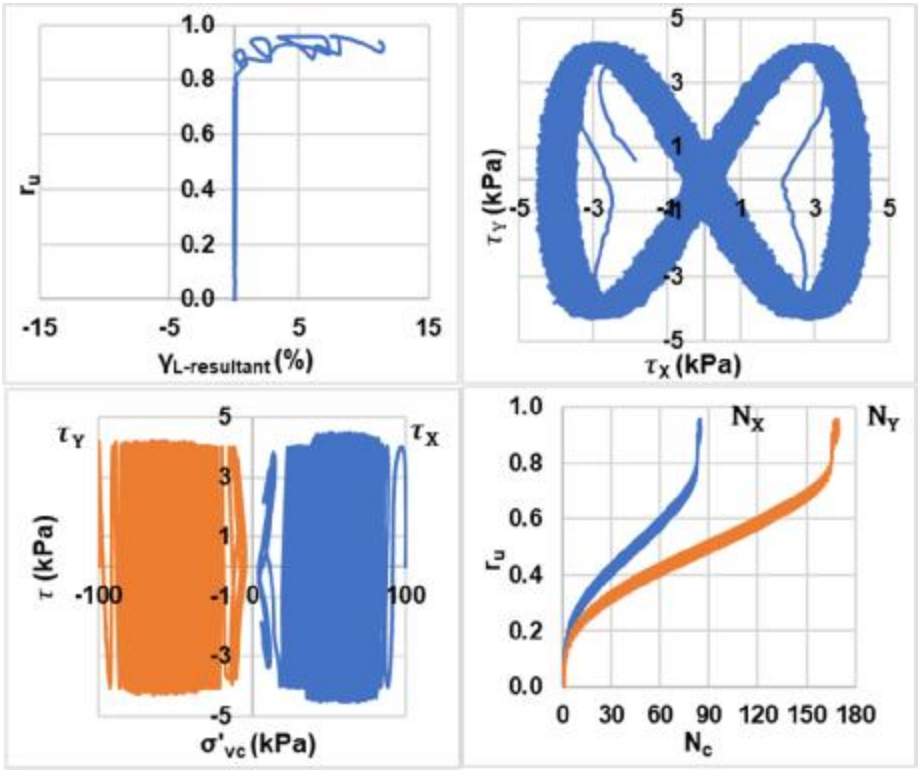


Bi-directional (Figure-8); $D_{rc}$ = 25%; $\sigma'_{vc}$ = 100 kPa; CSR = 0.04 (Re-liquefaction)

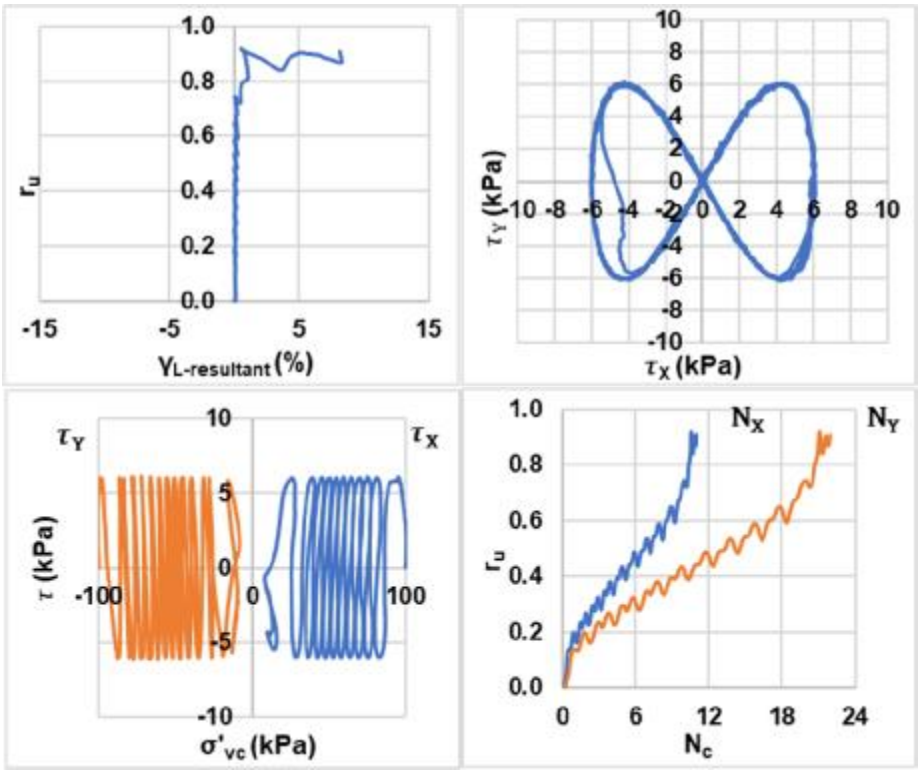


Bi-directional (Figure-8); $D_{rc}$ = 25%; $\sigma'_{vc}$ = 100 kPa; CSR = 0.06 (Liquefaction)

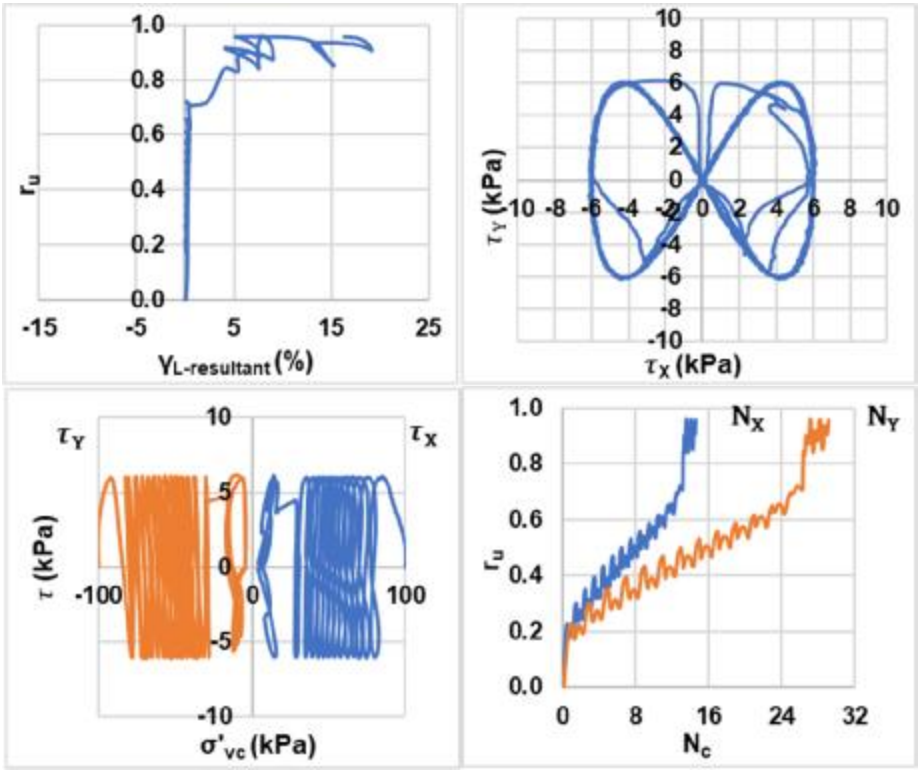


Bi-directional (Figure-8); $D_{rc}$ = 25%; $\sigma'_{vc}$ = 100 kPa; CSR = 0.06 (Re-liquefaction)

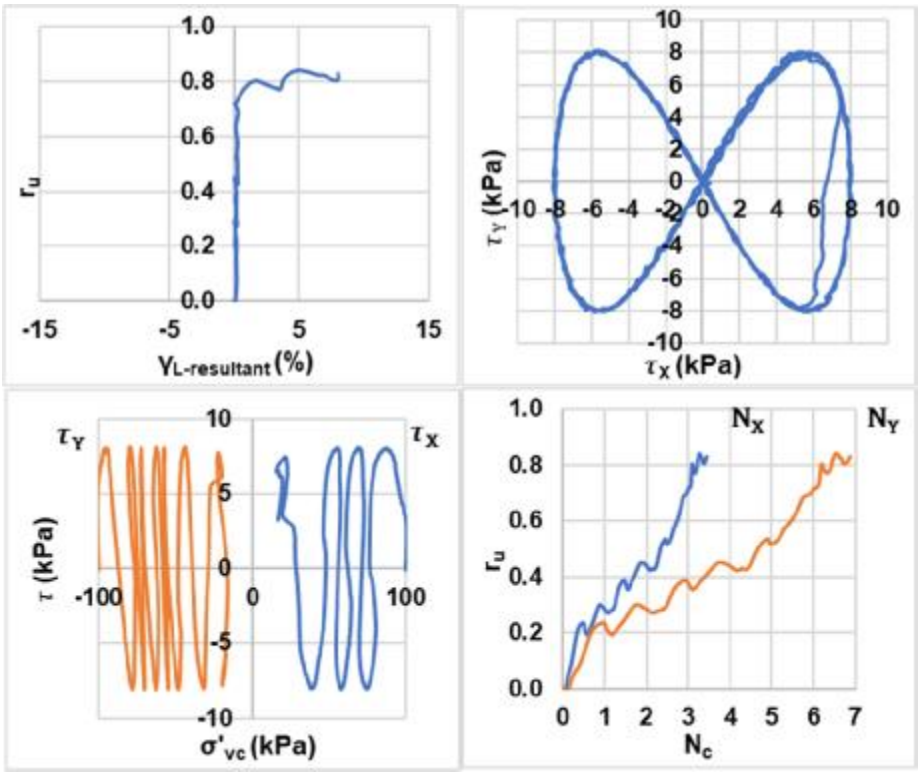


Bi-directional (Figure-8); $D_{rc}$ = 25%; $\sigma'_{vc}$ = 100 kPa; CSR = 0.08 (Liquefaction)

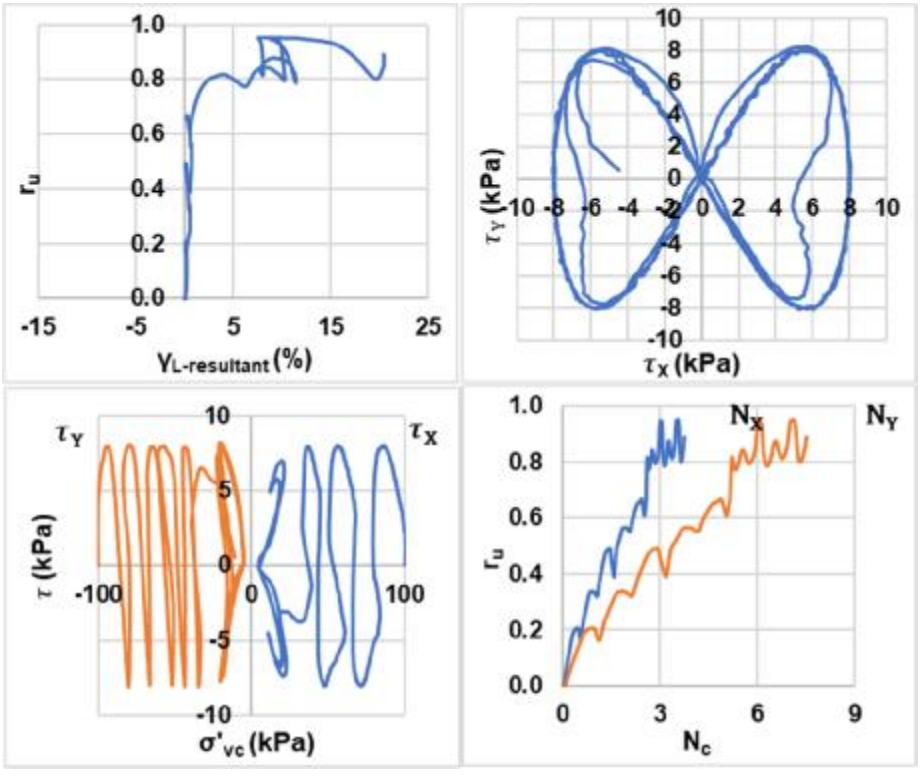


Bi-directional (Figure-8); $D_{rc}$ = 25%; $\sigma'_{vc}$ = 100 kPa; CSR = 0.08 (Re-liquefaction)

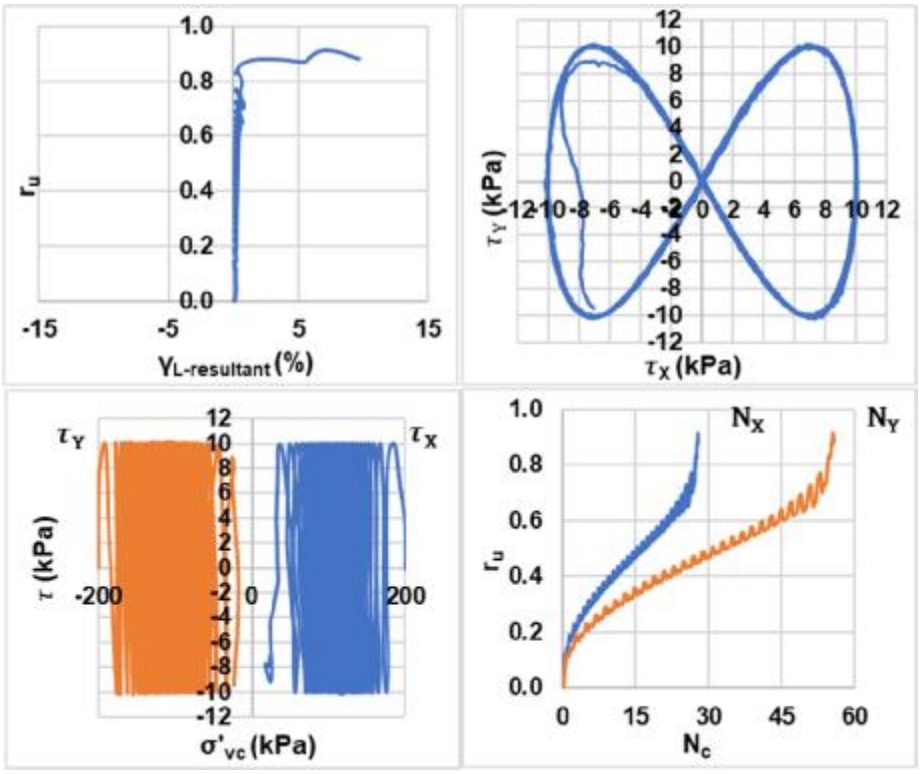


Bi-directional (Figure-8); $D_{rc}$ = 25%; $\sigma'_{vc}$ = 200 kPa; CSR = 0.05 (Liquefaction)

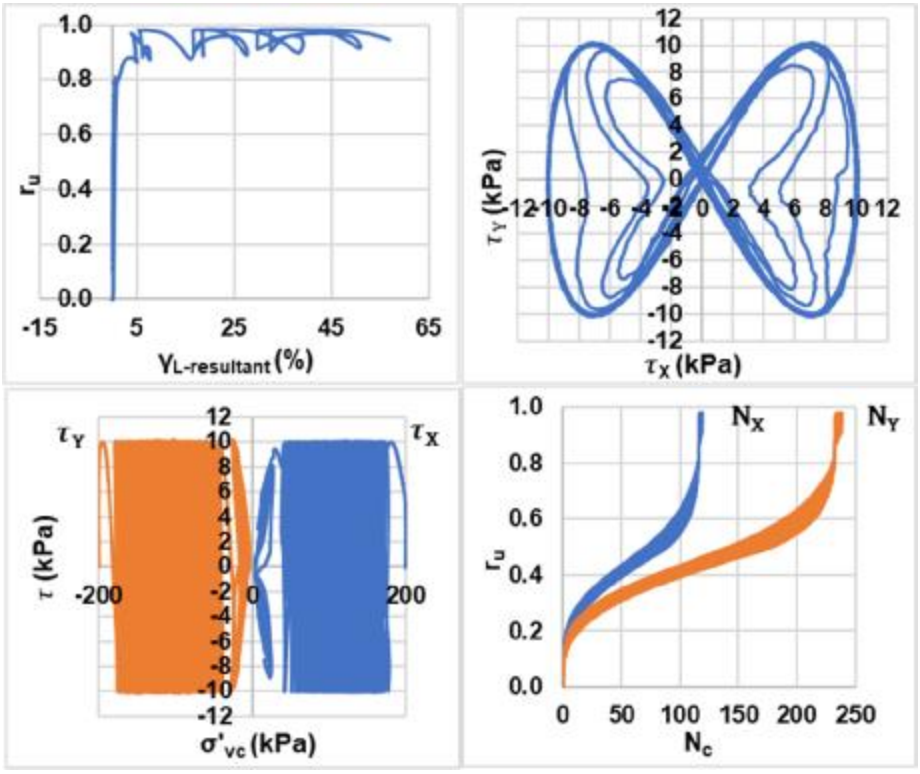


Bi-directional (Figure-8); $D_{rc}$ = 25%; $\sigma'_{vc}$ = 200 kPa; CSR = 0.05 (Re-liquefaction)

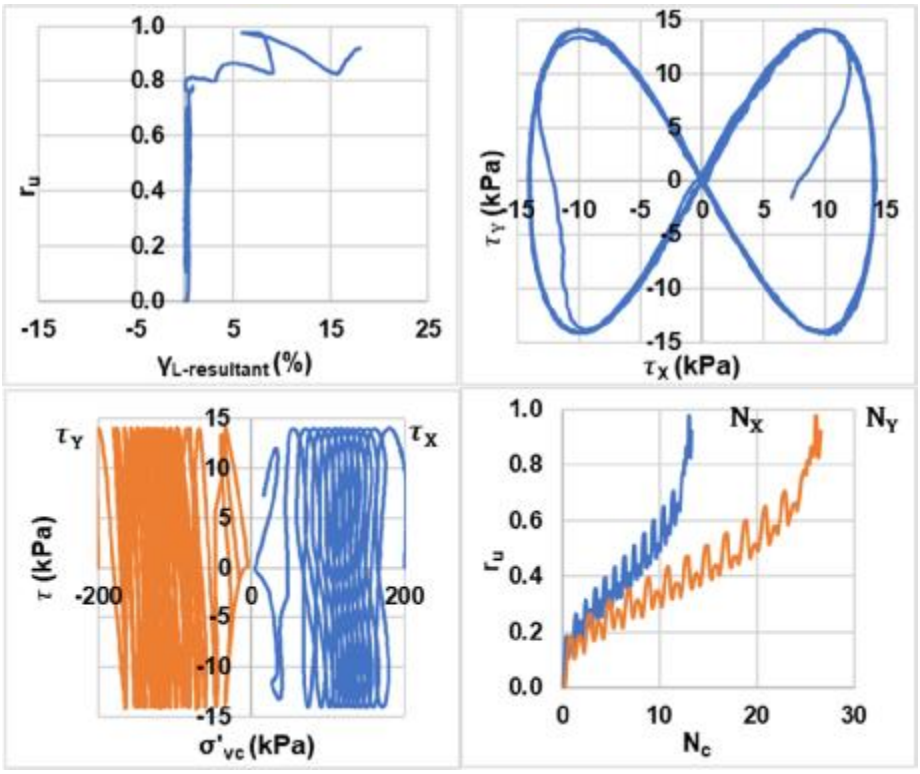


Bi-directional (Figure-8); $D_{rc}$ = 25%; $\sigma'_{vc}$ = 200 kPa; CSR = 0.07 (Liquefaction)

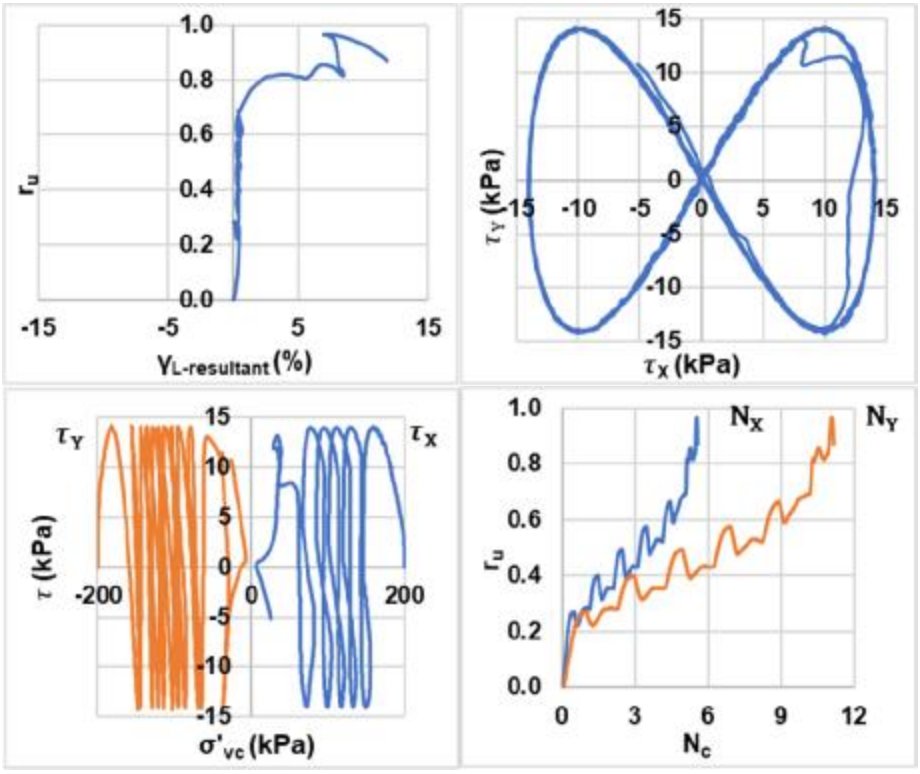


Bi-directional (Figure-8); $D_{rc}$ = 25%; $\sigma'_{vc}$ = 200 kPa; CSR = 0.07 (Re-liquefaction)

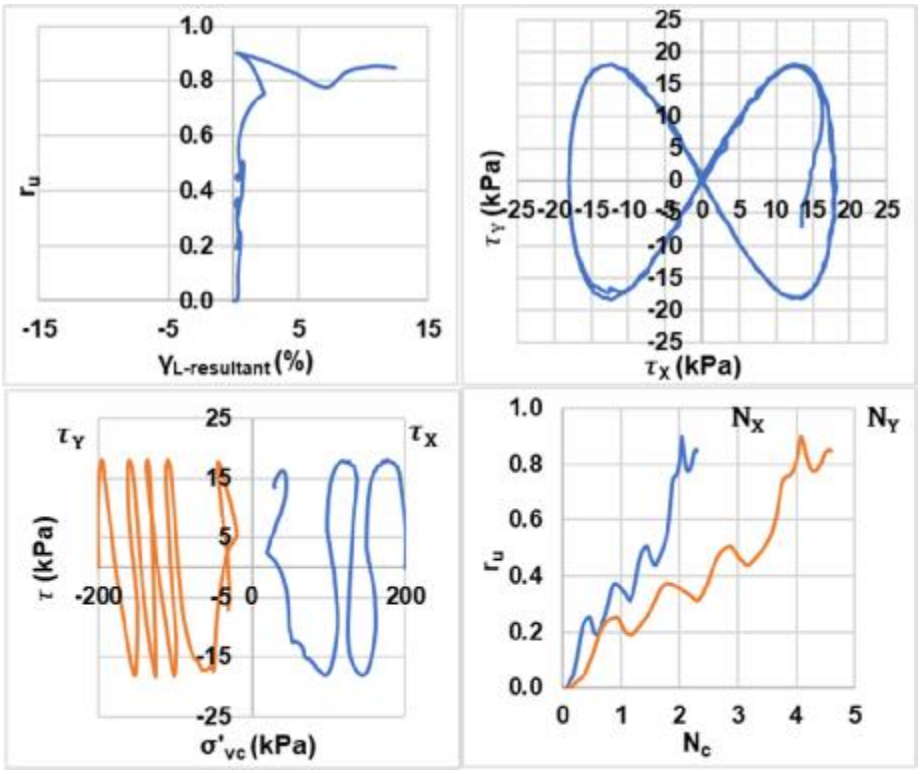


Bi-directional (Figure-8); $D_{rc}$ = 25%; $\sigma'_{vc}$ = 200 kPa; CSR = 0.09 (Liquefaction)

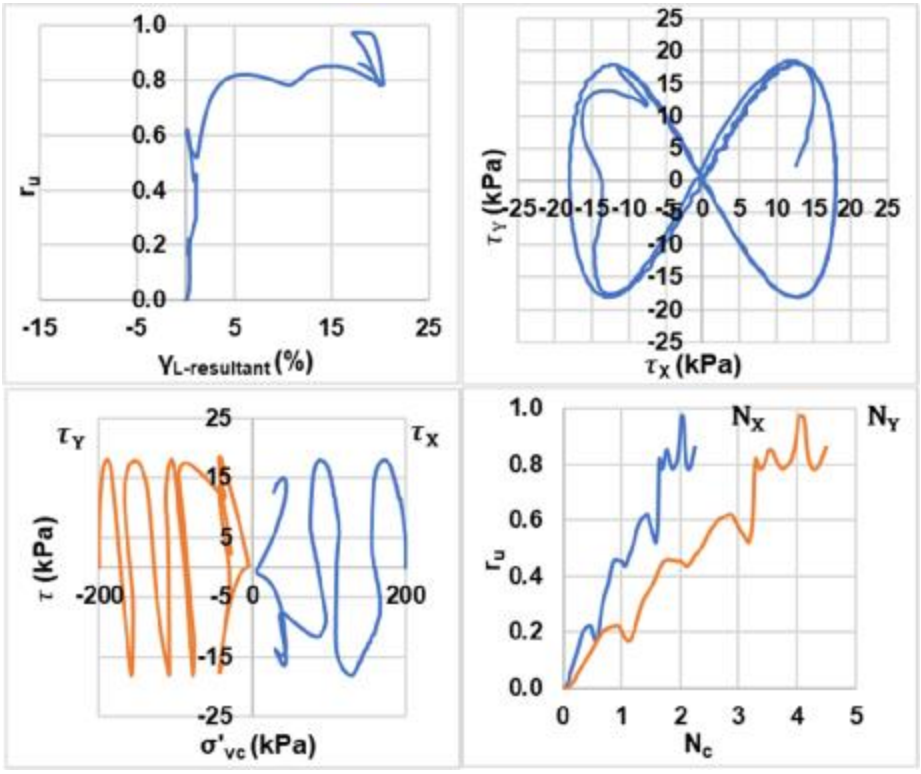


Bi-directional (Figure-8); $D_{rc}$ = 25%; $\sigma'_{vc}$ = 200 kPa; CSR = 0.09 (Re-liquefaction)

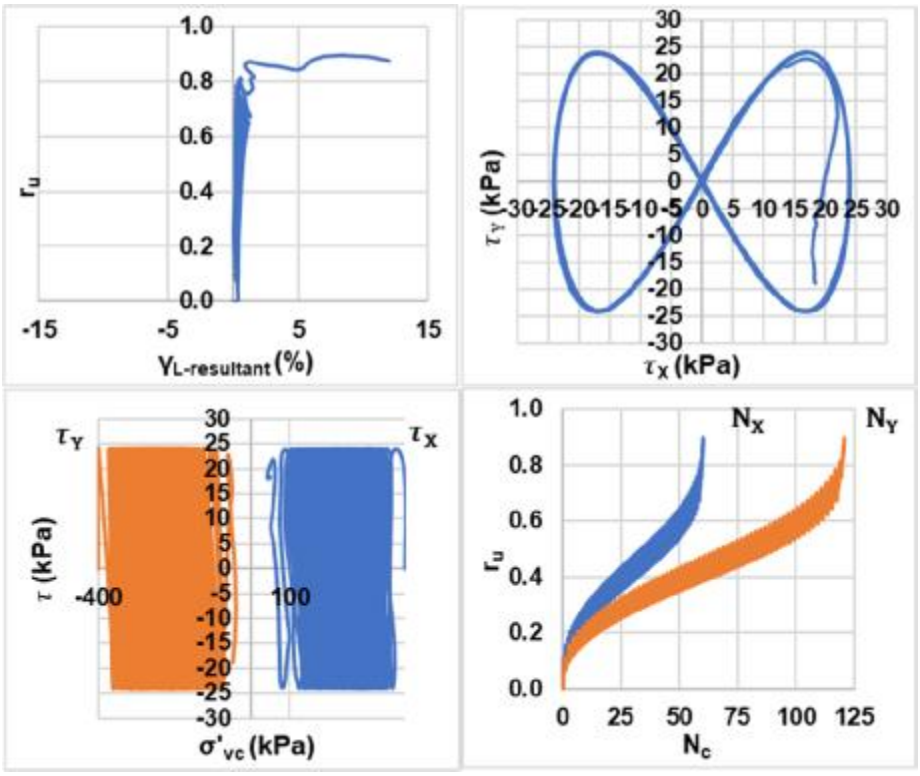


Bi-directional (Figure-8); $D_{rc}$ = 25%; $\sigma'_{vc}$ = 400 kPa; CSR = 0.06 (Liquefaction)

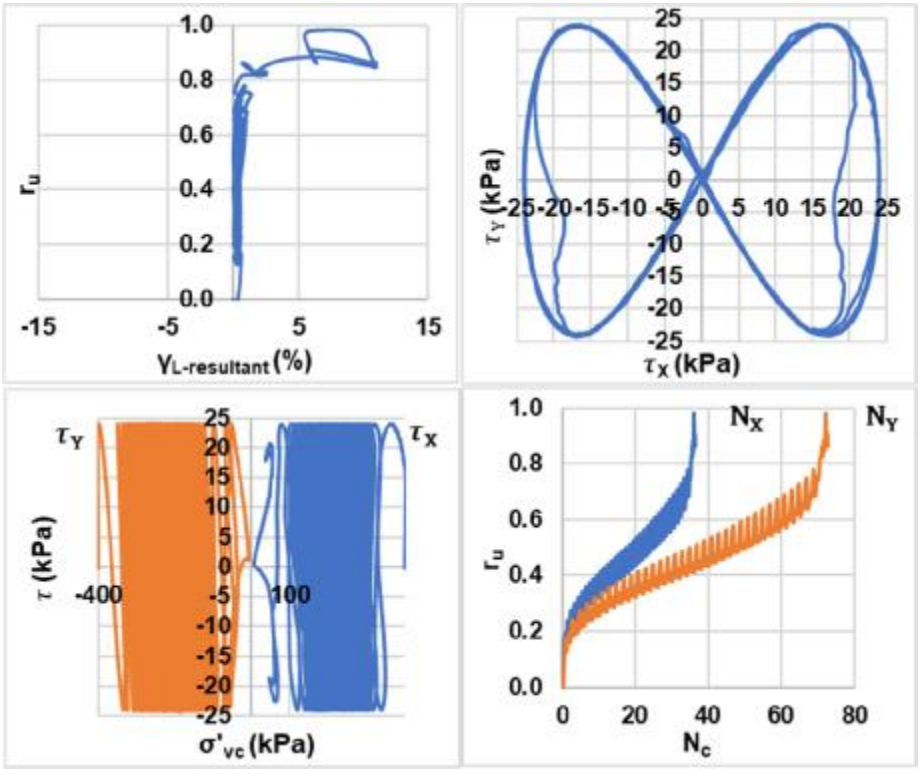


Bi-directional (Figure-8); $D_{rc}$ = 25%; $\sigma'_{vc}$ = 400 kPa; CSR = 0.06 (Re-liquefaction)

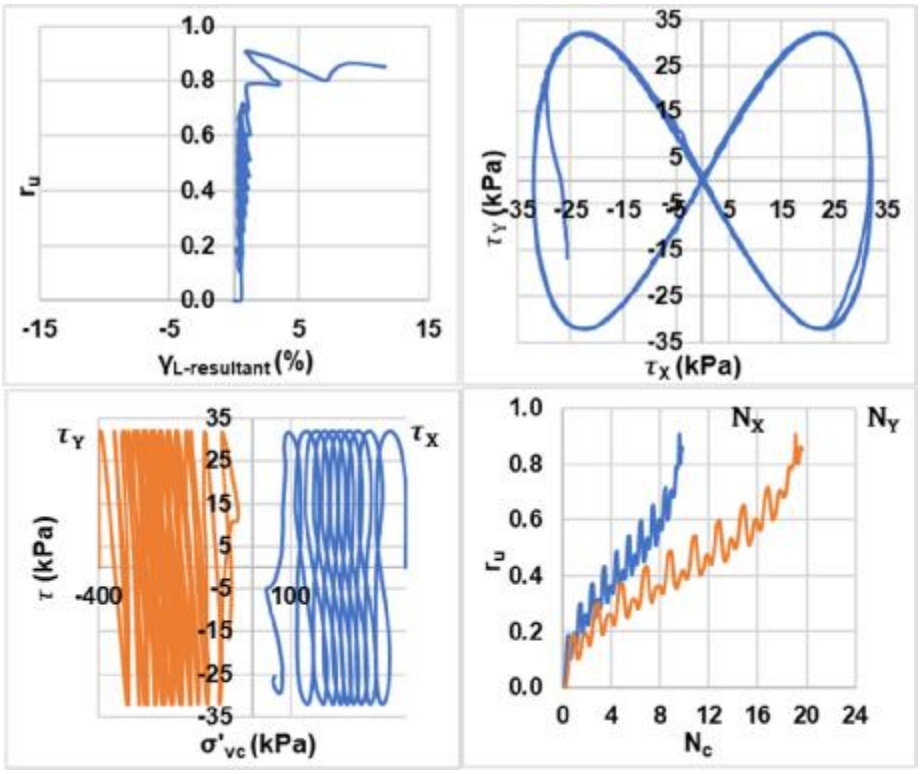


Bi-directional (Figure-8); $D_{rc}$ = 25%; $\sigma'_{vc}$ = 400 kPa; CSR = 0.08 (Liquefaction)

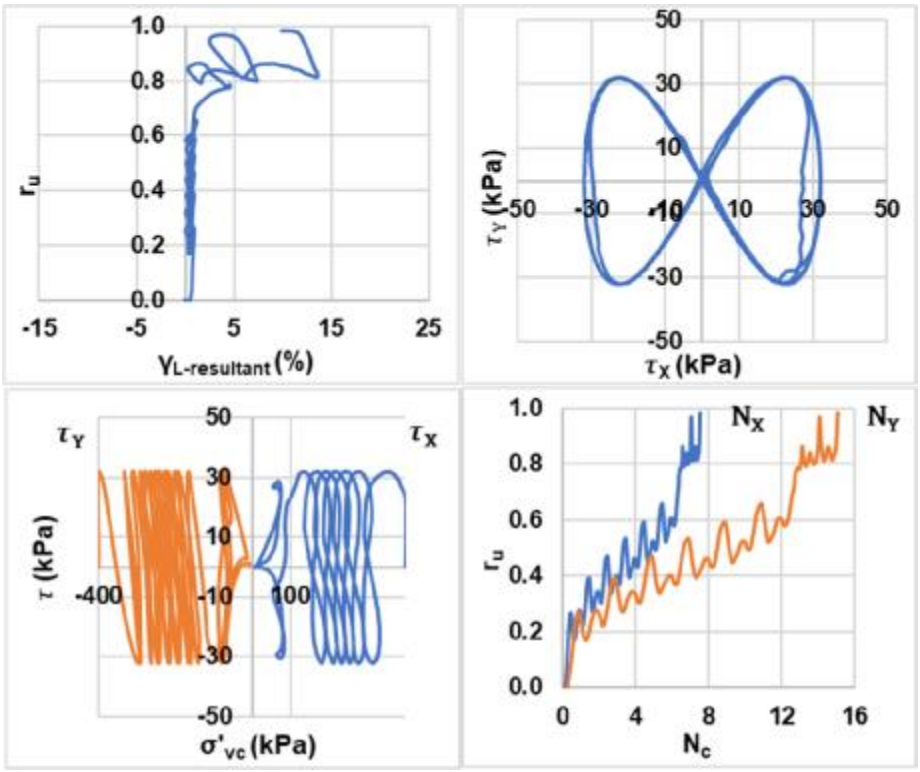


Bi-directional (Figure-8); $D_{rc}$ = 25%; $\sigma'_{vc}$ = 400 kPa; CSR = 0.08 (Re-liquefaction)

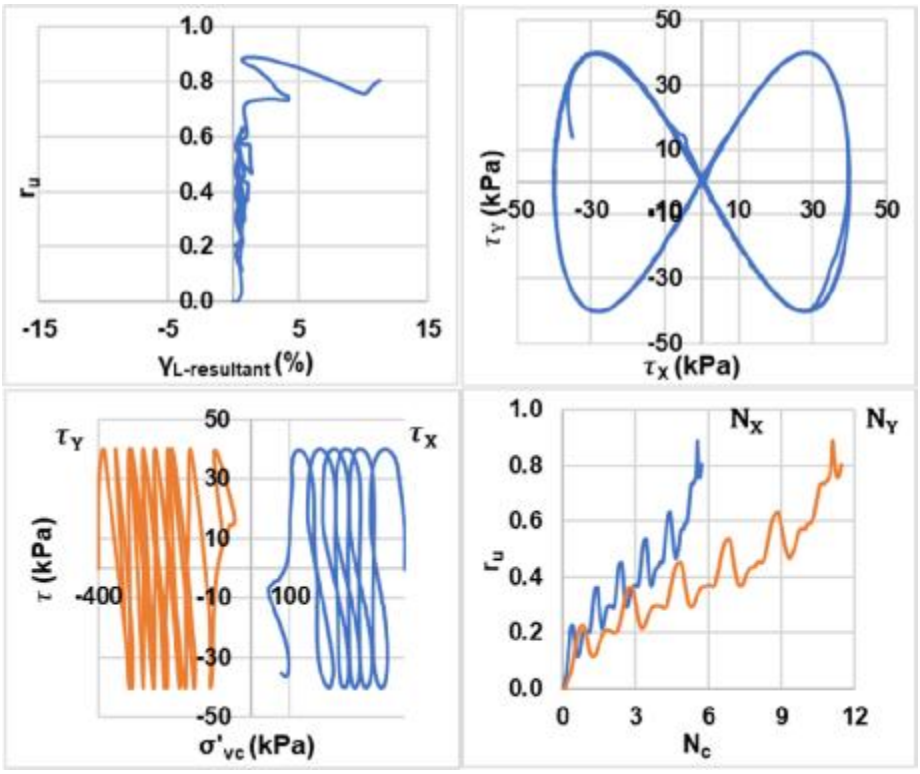


Bi-directional (Figure-8); $D_{rc}$ = 25%; $\sigma'_{vc}$ = 400 kPa; CSR = 0.1 (Liquefaction)

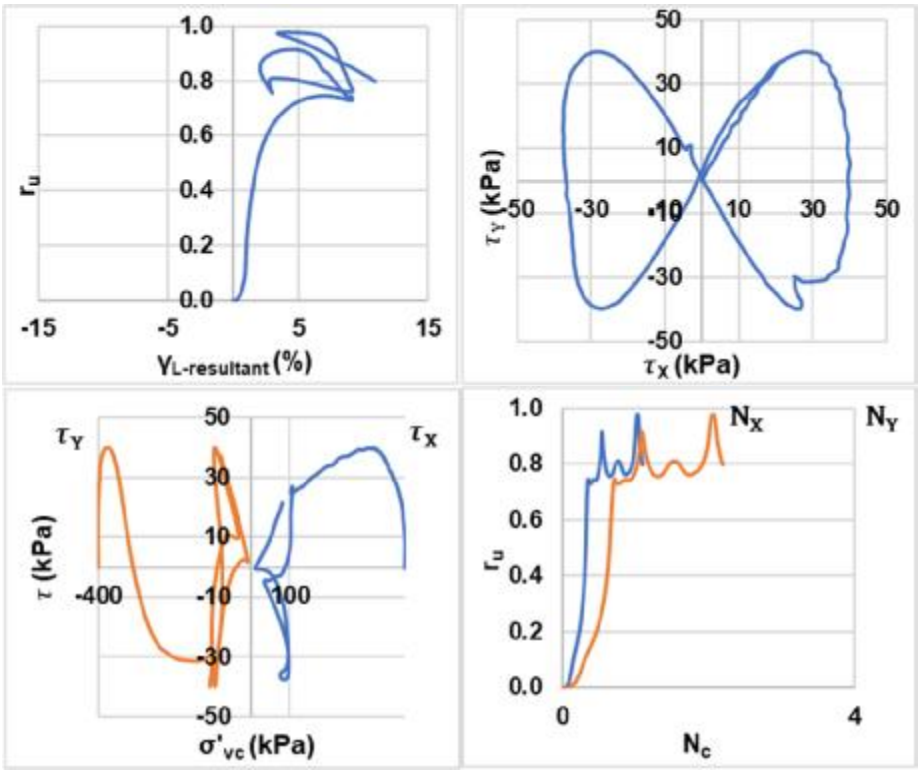


Bi-directional (Figure-8); $D_{rc}$ = 25%; $\sigma'_{vc}$ = 400 kPa; CSR = 0.1 (Re-liquefaction)

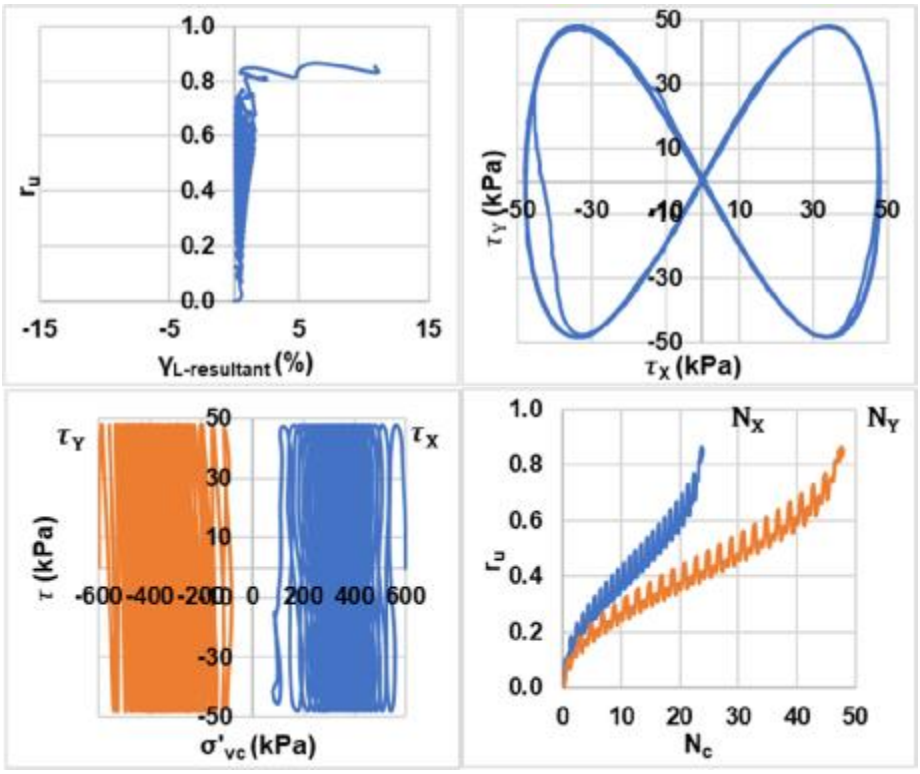


Bi-directional (Figure-8); $D_{rc}$ = 25%; $\sigma'_{vc}$ = 600 kPa; CSR = 0.08 (Liquefaction)

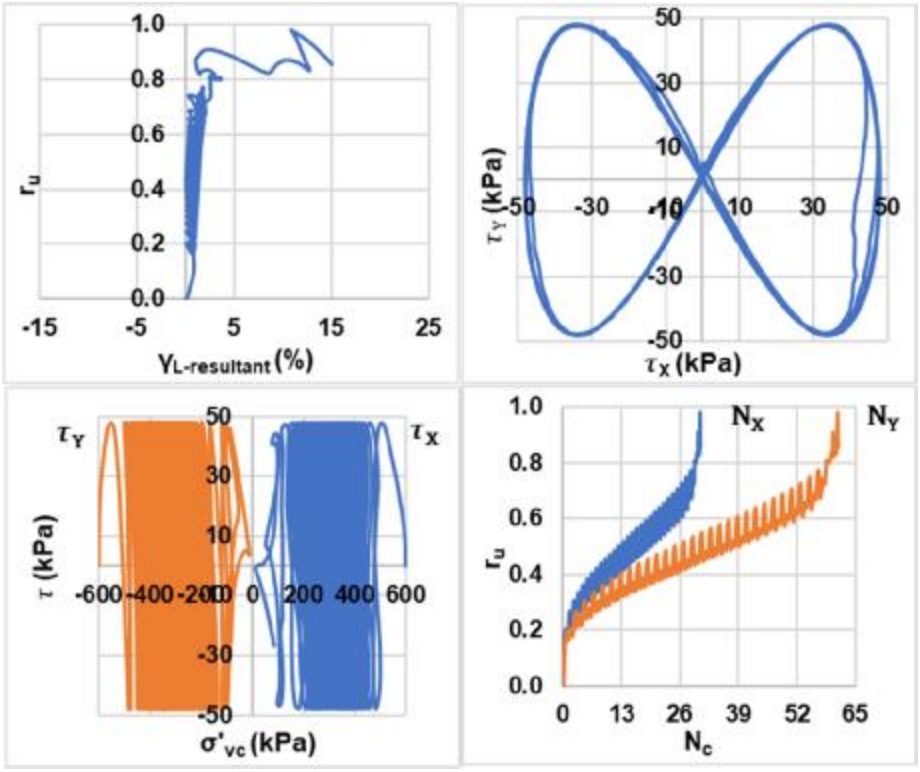


Bi-directional (Figure-8); $D_{rc}$ = 25%; $\sigma'_{vc}$ = 600 kPa; CSR = 0.08 (Re-liquefaction)

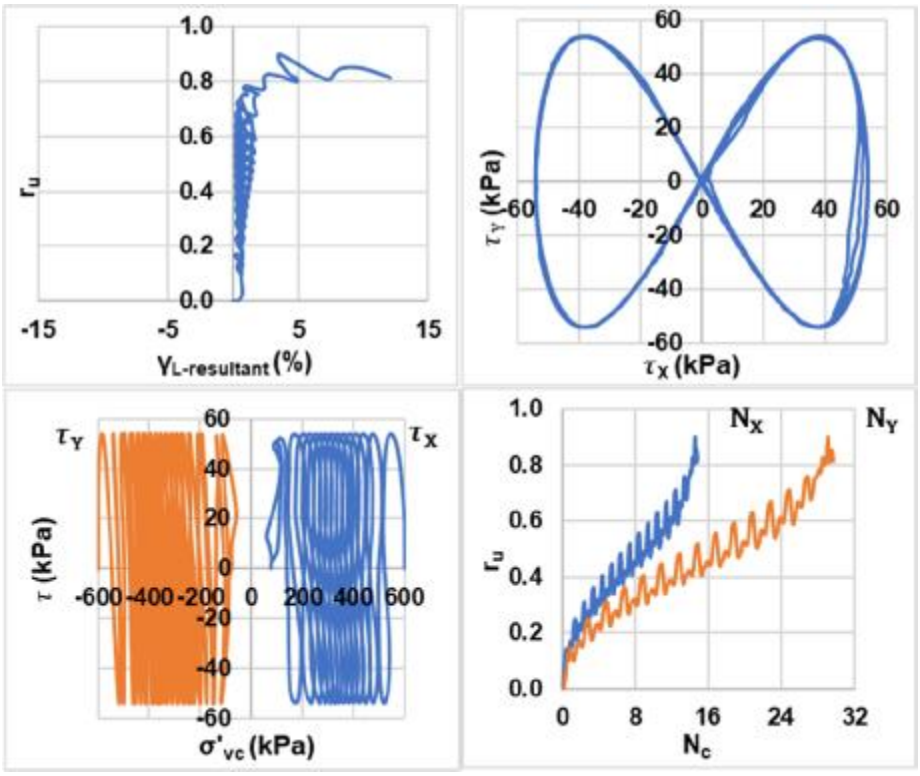


Bi-directional (Figure-8); $D_{rc}$ = 25%; $\sigma'_{vc}$ = 600 kPa; CSR = 0.09 (Liquefaction)

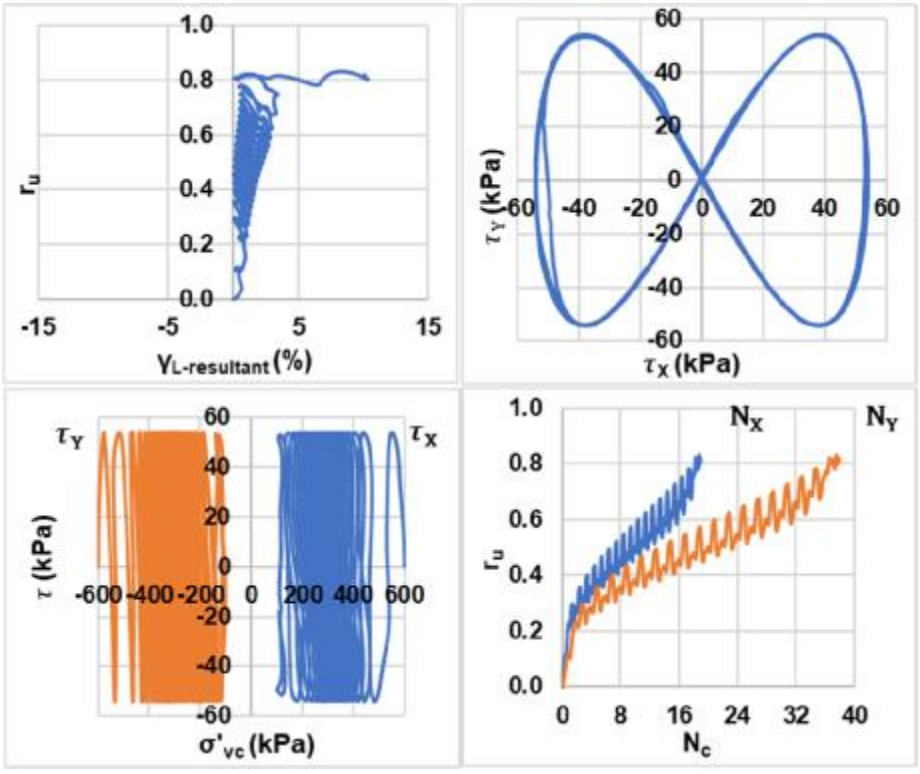


Bi-directional (Figure-8); $D_{rc}$ = 25%; $\sigma'_{vc}$ = 600 kPa; CSR = 0.09 (Re-liquefaction)

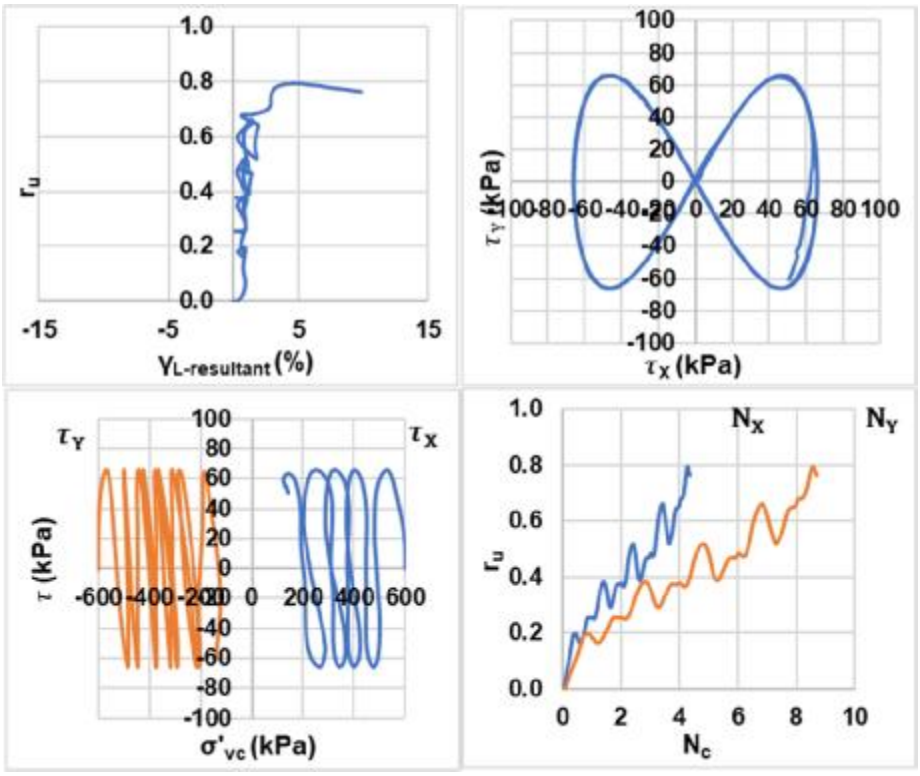


Bi-directional (Figure-8); $D_{rc}$ = 25%; $\sigma'_{vc}$ = 600 kPa; CSR = 0.11 (Liquefaction)

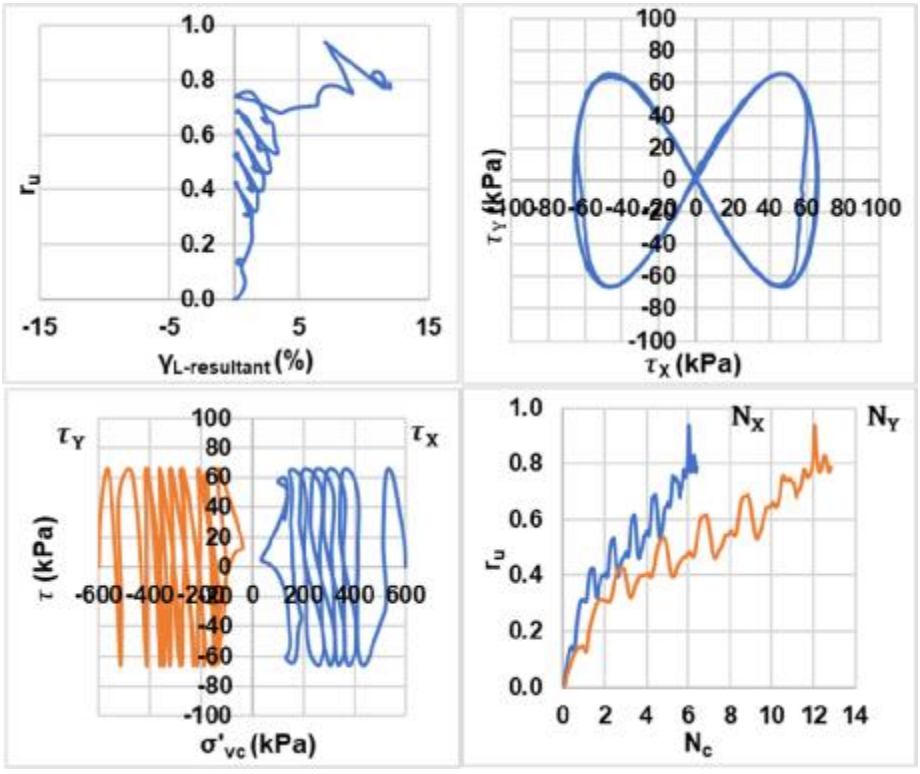


Bi-directional (Figure-8); $D_{rc}$ = 25%; $\sigma'_{vc}$ = 600 kPa; CSR = 0.11 (Re-liquefaction)

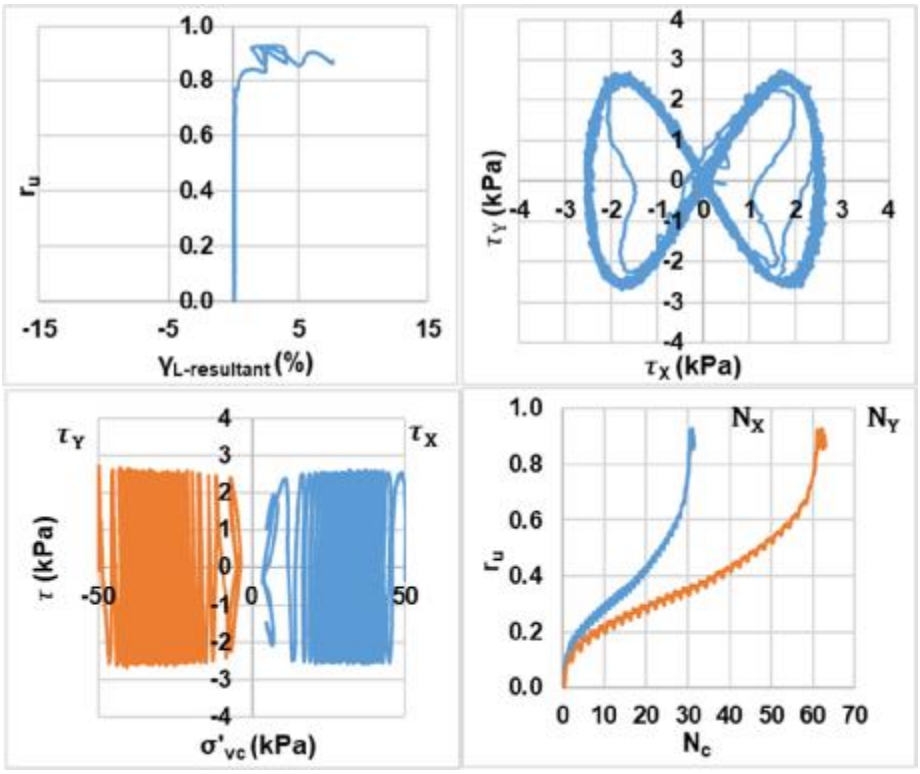


Bi-directional (Figure-8); $D_{rc}$ = 45%; $\sigma'_{vc}$ = 50 kPa; CSR = 0.05 (Liquefaction)

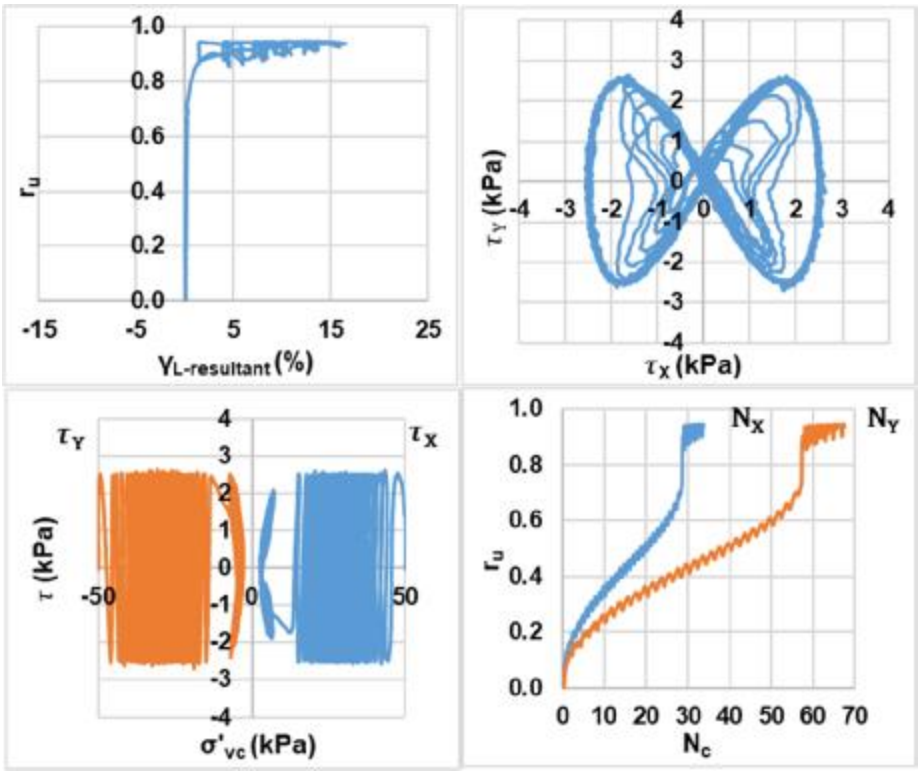


Bi-directional (Figure-8); $D_{rc}$ = 45%; $\sigma'_{vc}$ = 50 kPa; CSR = 0.05 (Re-liquefaction)

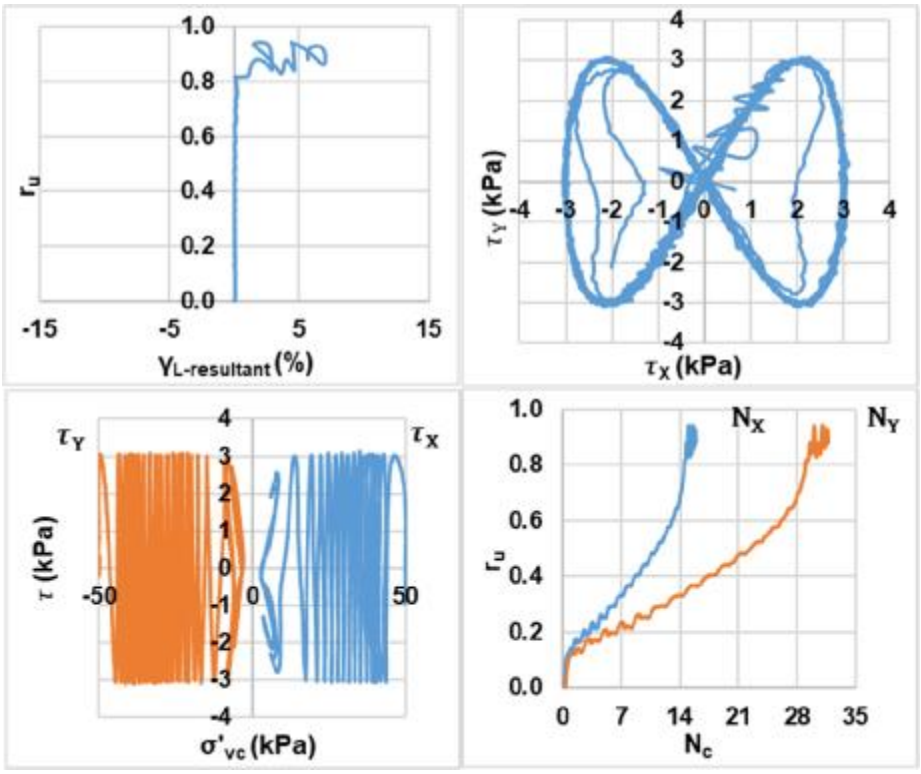


Bi-directional (Figure-8); $D_{rc}$ = 45%; $\sigma'_{vc}$ = 50 kPa; CSR = 0.06 (Liquefaction)

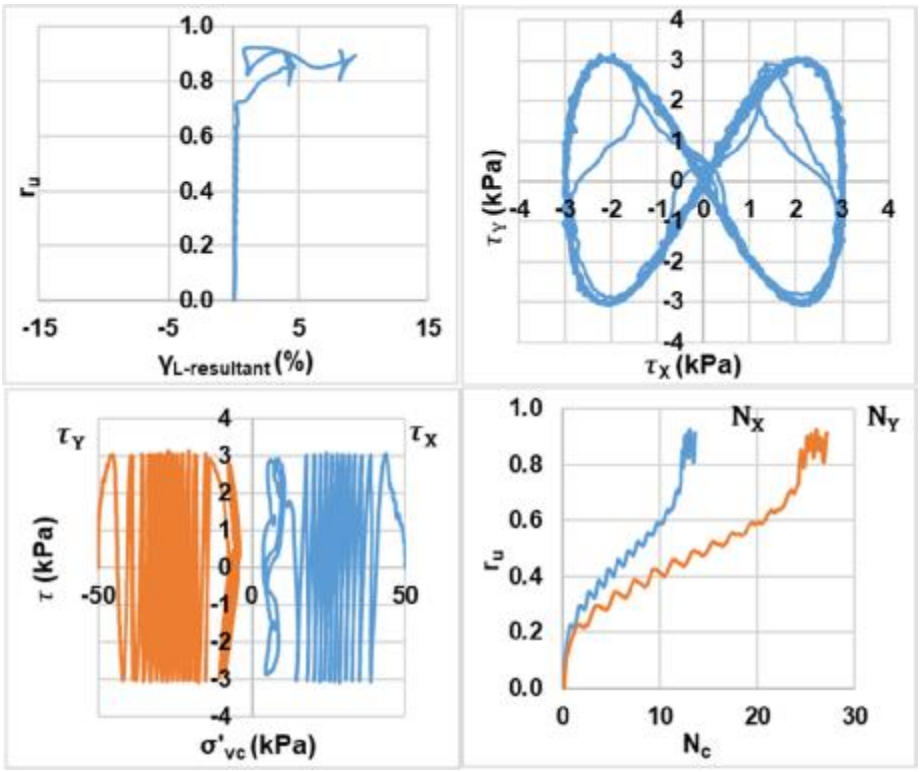


Bi-directional (Figure-8); $D_{rc}$ = 45%; $\sigma'_{vc}$ = 50 kPa; CSR = 0.06 (Re-liquefaction)

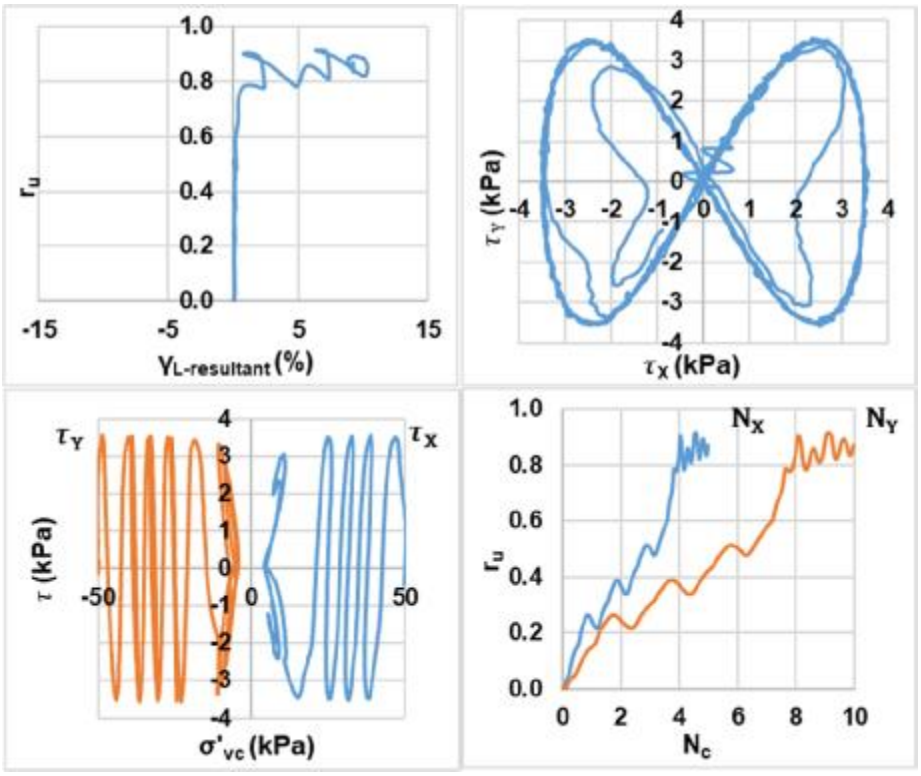


Bi-directional (Figure-8); $D_{rc}$ = 45%; $\sigma'_{vc}$ = 50 kPa; CSR = 0.07 (Liquefaction)

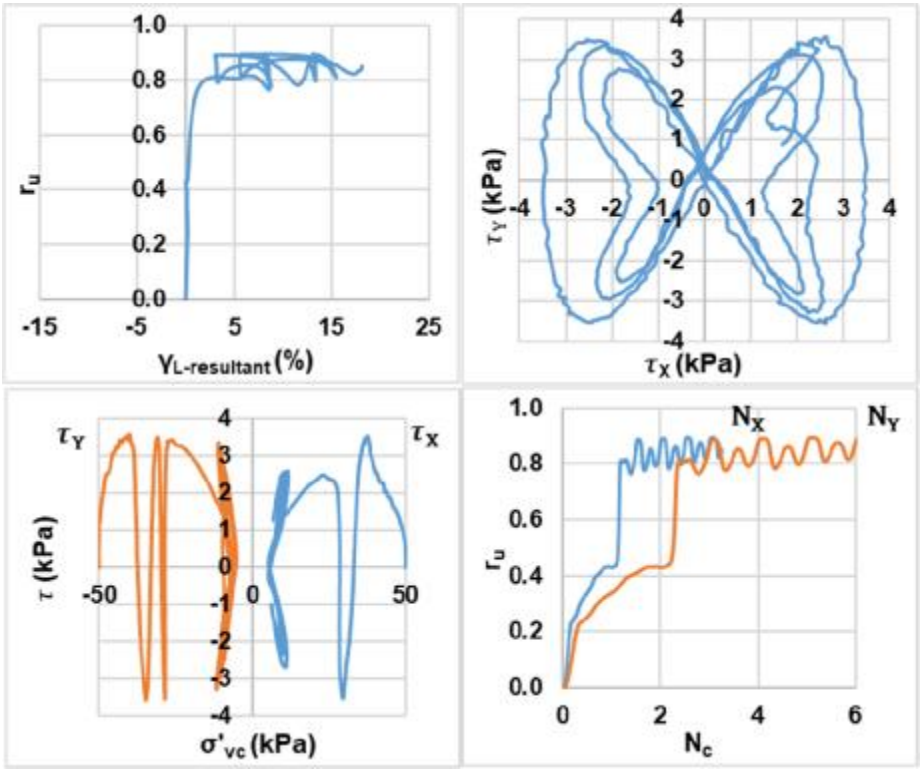


Bi-directional (Figure-8); $D_{rc}$ = 45%; $\sigma'_{vc}$ = 50 kPa; CSR = 0.07 (Re-liquefaction)

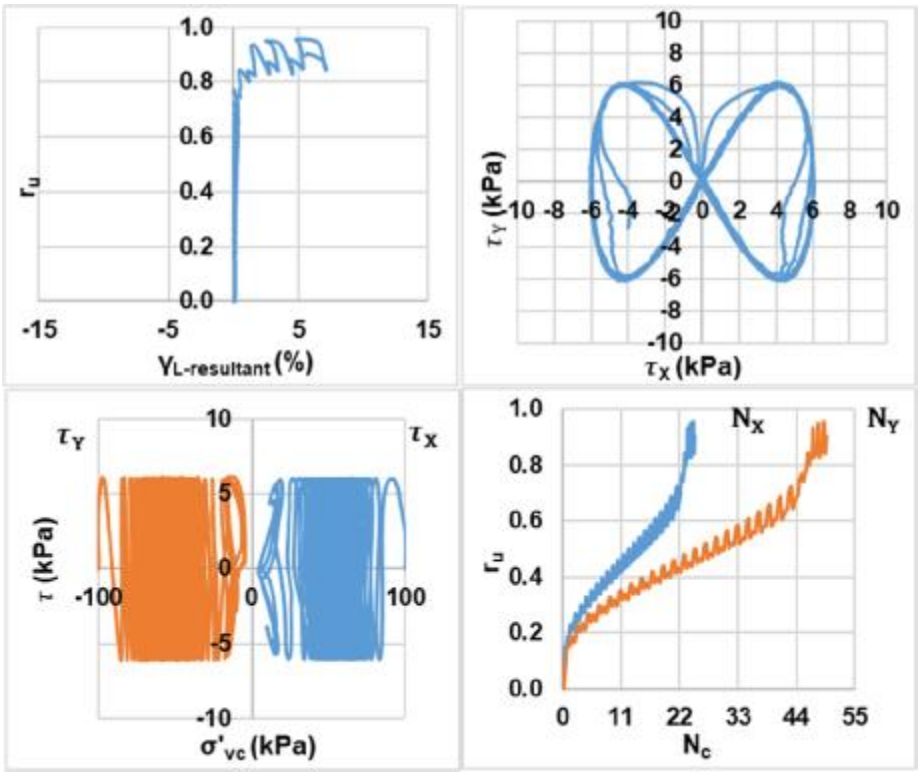


Bi-directional (Figure-8); $D_{rc}$ = 45%; $\sigma'_{vc}$ = 100 kPa; CSR = 0.06 (Liquefaction)

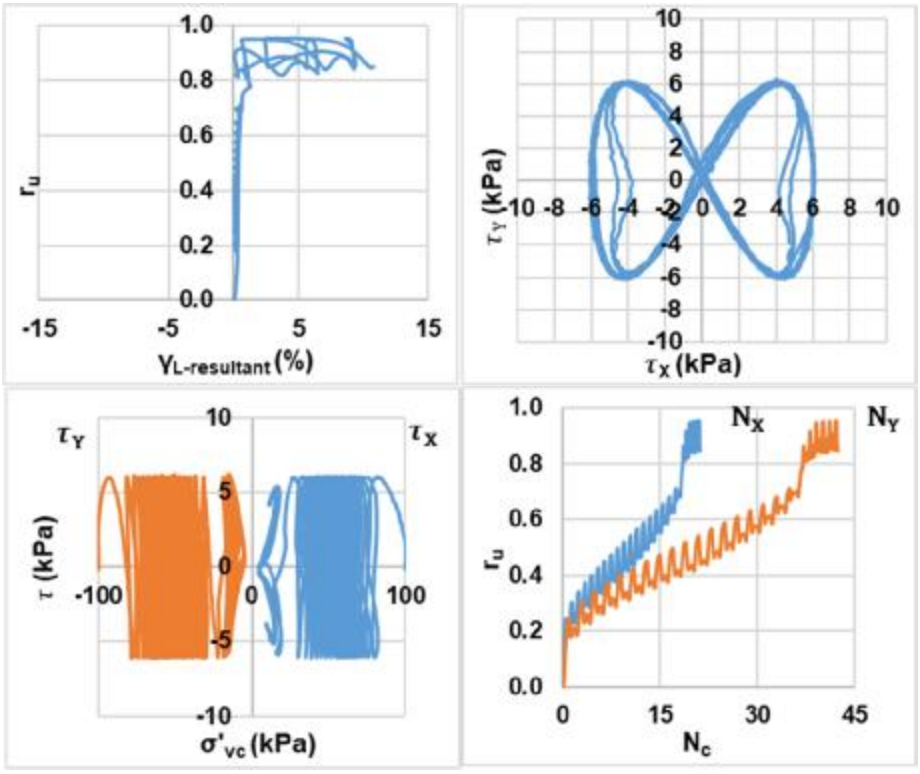


Bi-directional (Figure-8); $D_{rc}$ = 45%; $\sigma'_{vc}$ = 100 kPa; CSR = 0.06 (Re-liquefaction)

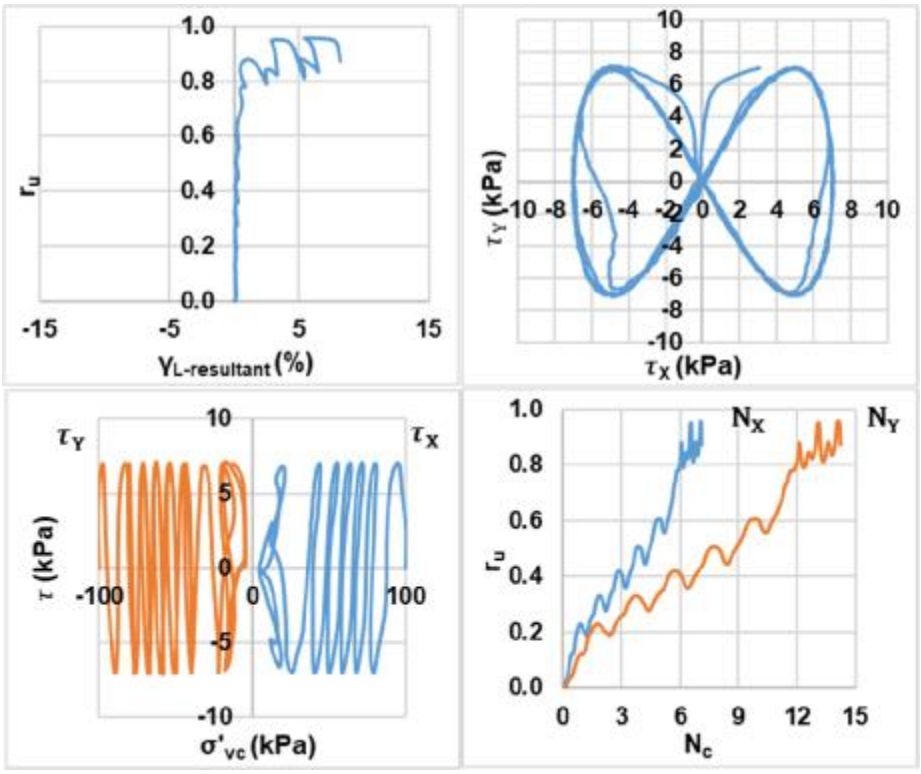


Bi-directional (Figure-8); $D_{rc}$ = 45%; $\sigma'_{vc}$ = 100 kPa; CSR = 0.07 (Liquefaction)

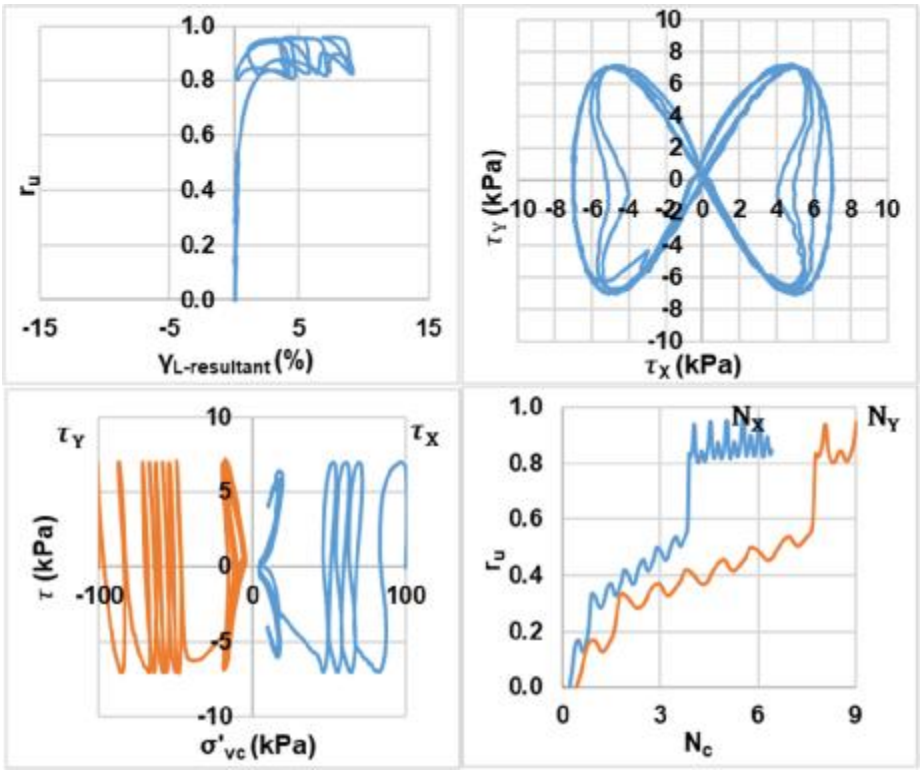


Bi-directional (Figure-8); $D_{rc}$ = 45%; $\sigma'_{vc}$ = 100 kPa; CSR = 0.07 (Re-liquefaction)

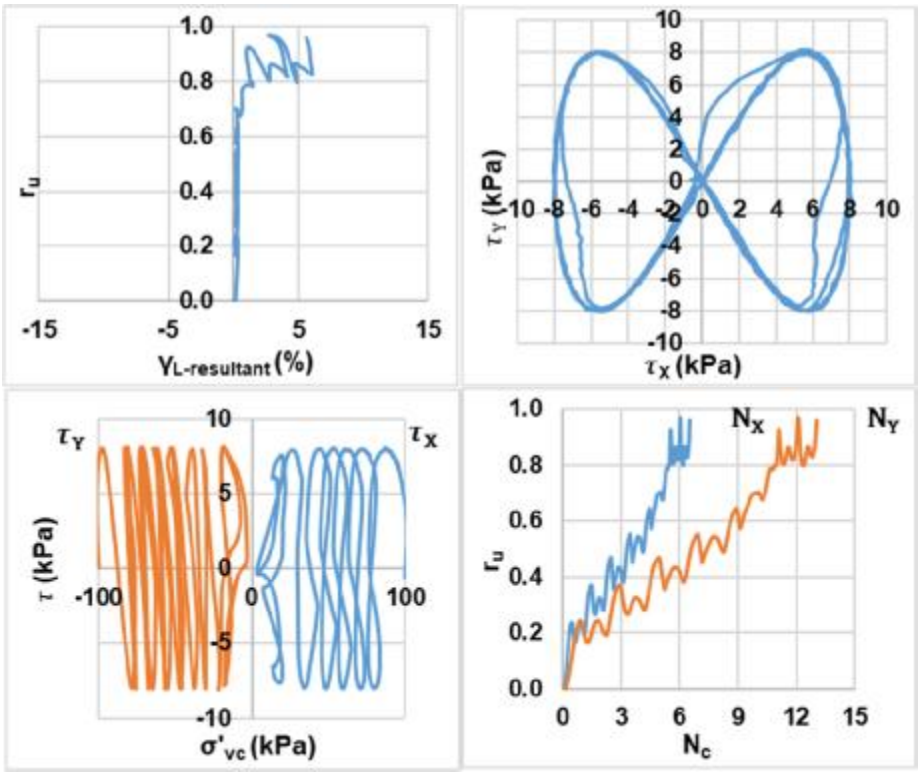


Bi-directional (Figure-8); $D_{rc}$ = 45%; $\sigma'_{vc}$ = 100 kPa; CSR = 0.08 (Liquefaction)

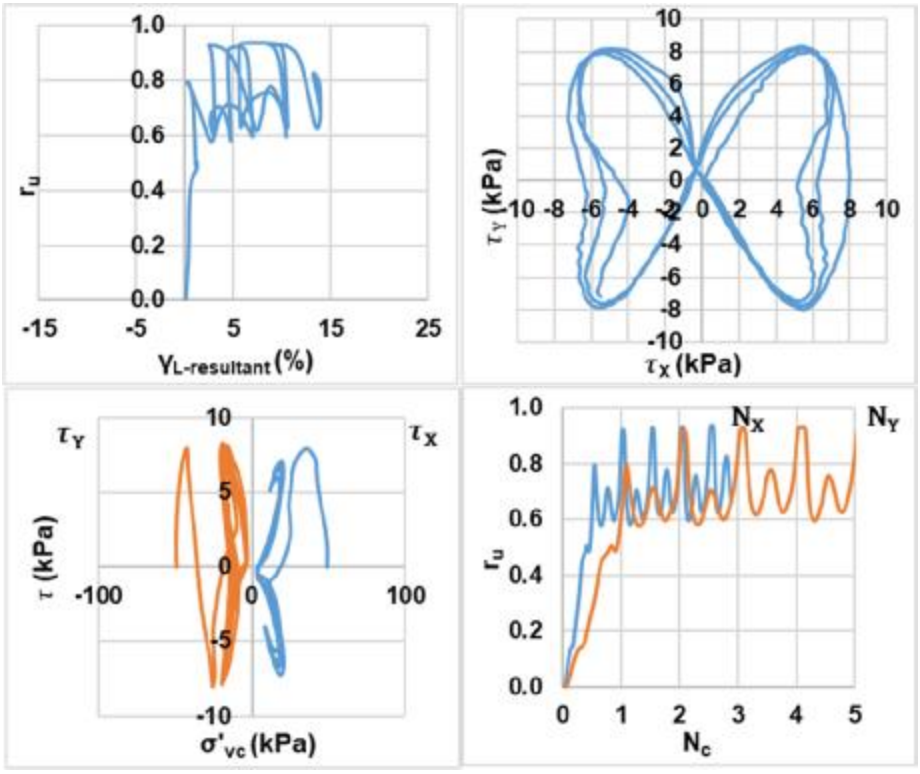


Bi-directional (Figure-8); $D_{rc}$ = 45%; $\sigma'_{vc}$ = 100 kPa; CSR = 0.08 (Re-liquefaction)

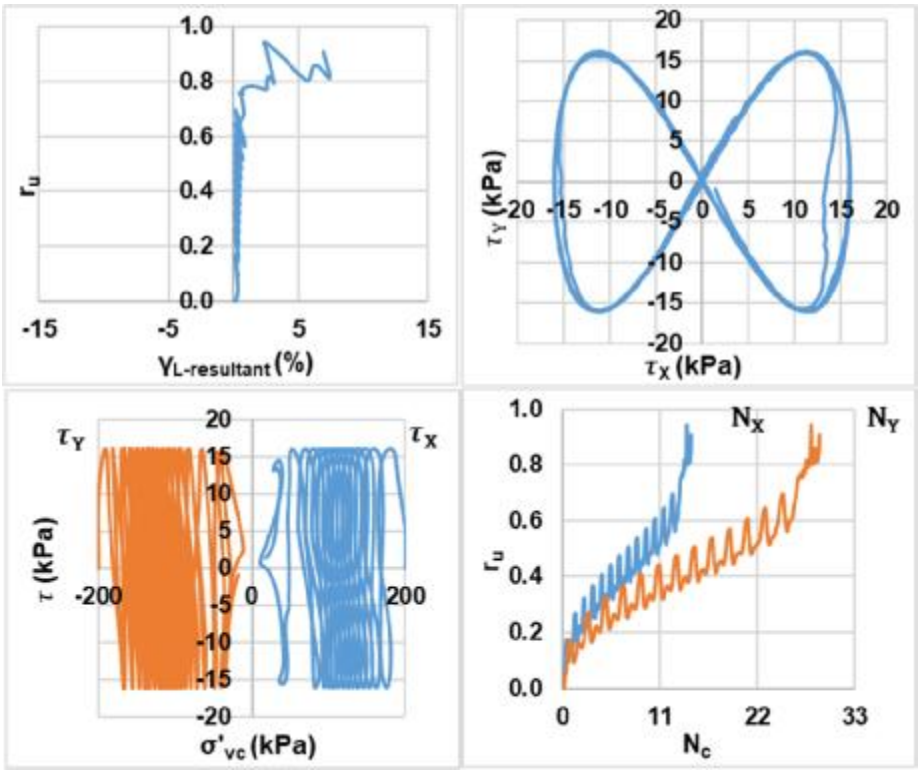


Bi-directional (Figure-8); $D_{rc}$ = 45%; $\sigma'_{vc}$ = 200 kPa; CSR = 0.08 (Liquefaction)

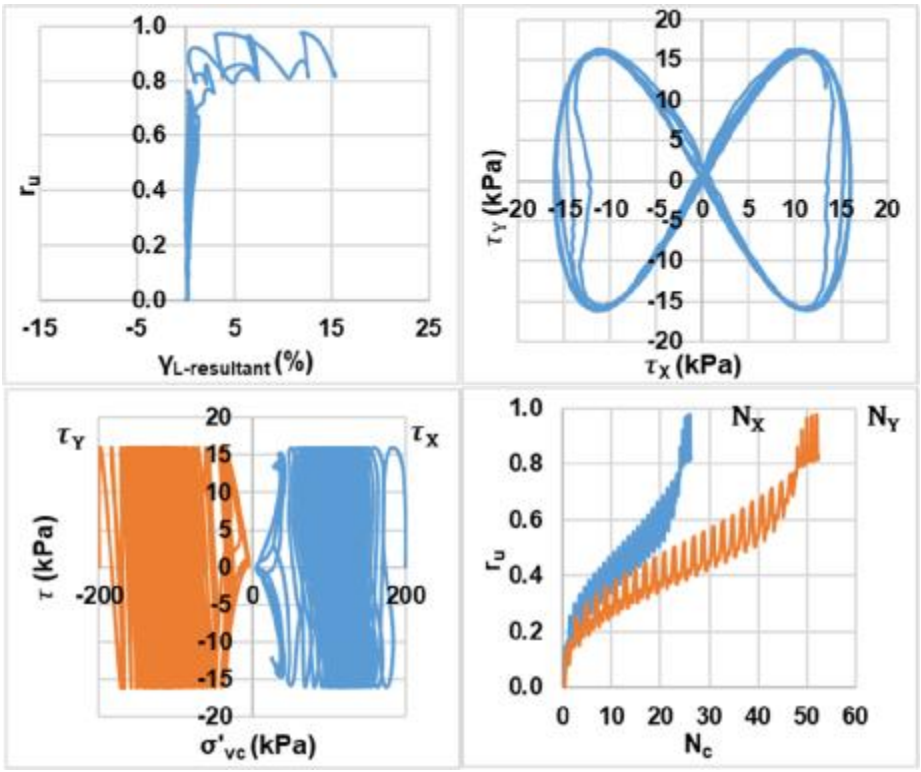


Bi-directional (Figure-8); $D_{rc}$ = 45%; $\sigma'_{vc}$ = 200 kPa; CSR = 0.08 (Re-liquefaction)

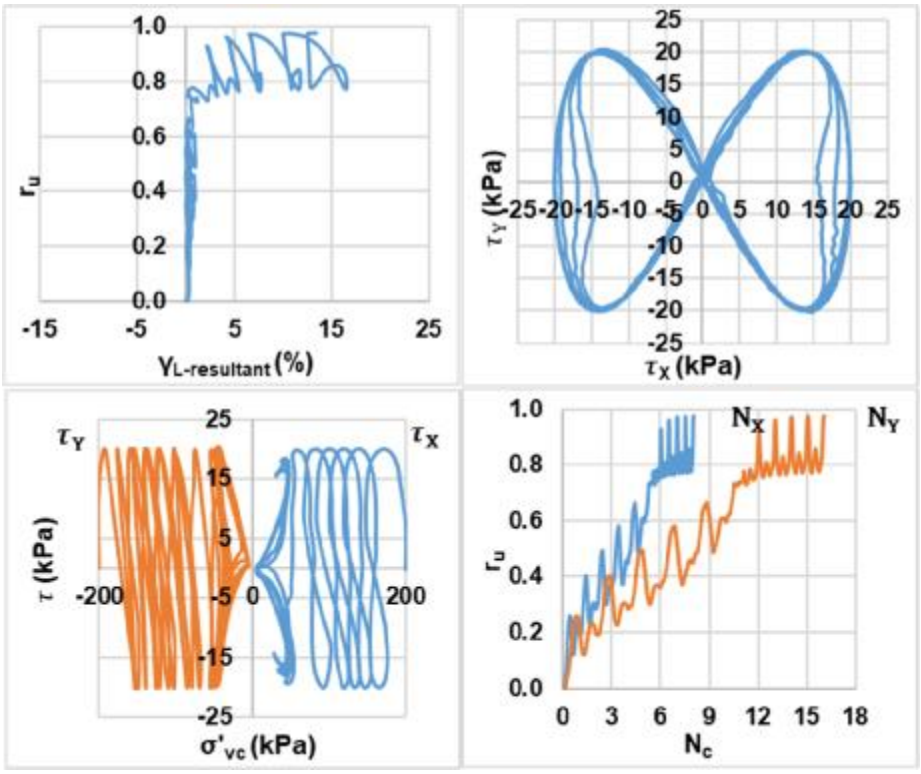


Bi-directional (Figure-8); $D_{rc}$ = 45%; $\sigma'_{vc}$ = 200 kPa; CSR = 0.1 (Liquefaction)

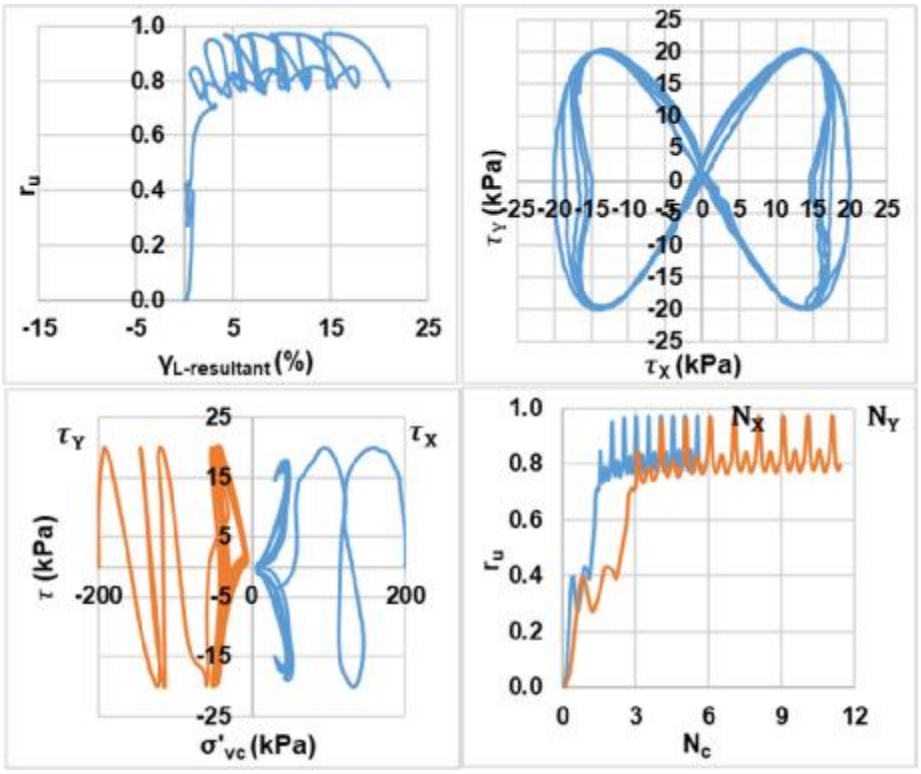


Bi-directional (Figure-8); $D_{rc}$ = 45%; $\sigma'_{vc}$ = 200 kPa; CSR = 0.1 (Re-liquefaction)

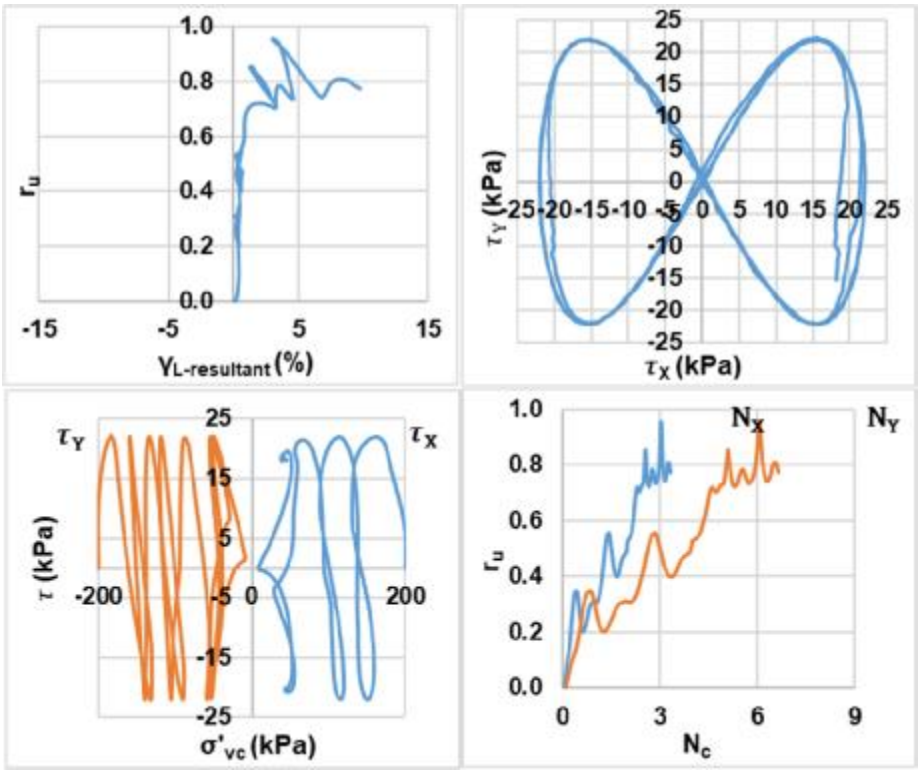


Bi-directional (Figure-8); $D_{rc}$ = 45%; $\sigma'_{vc}$ = 200 kPa; CSR = 0.11 (Liquefaction)

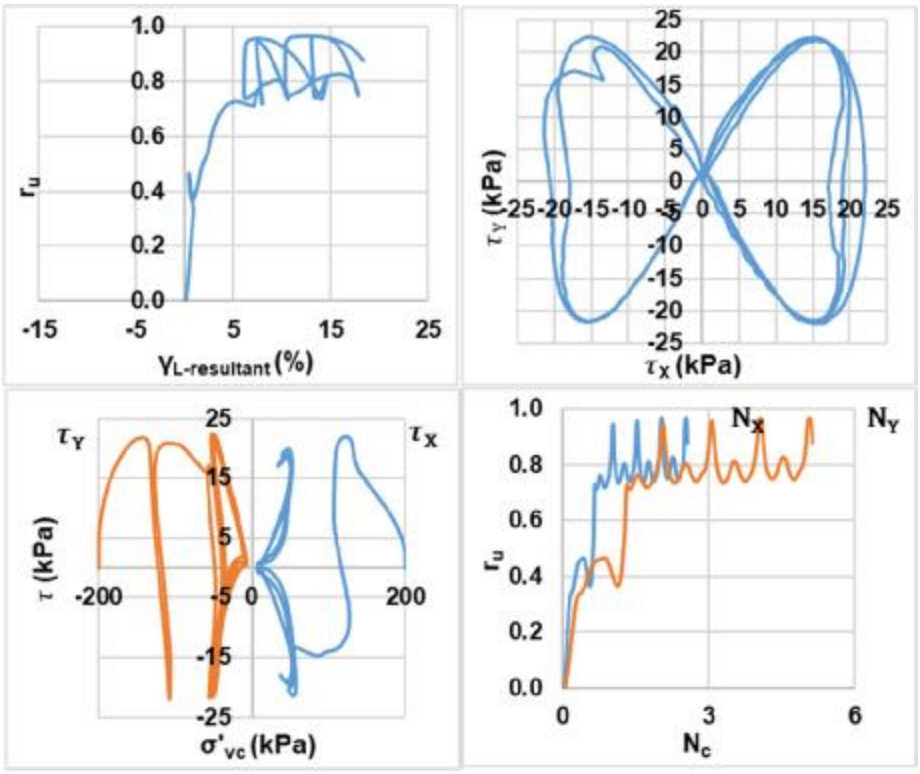


Bi-directional (Figure-8); $D_{rc}$ = 45%; $\sigma'_{vc}$ = 200 kPa; CSR = 0.11 (Re-liquefaction)

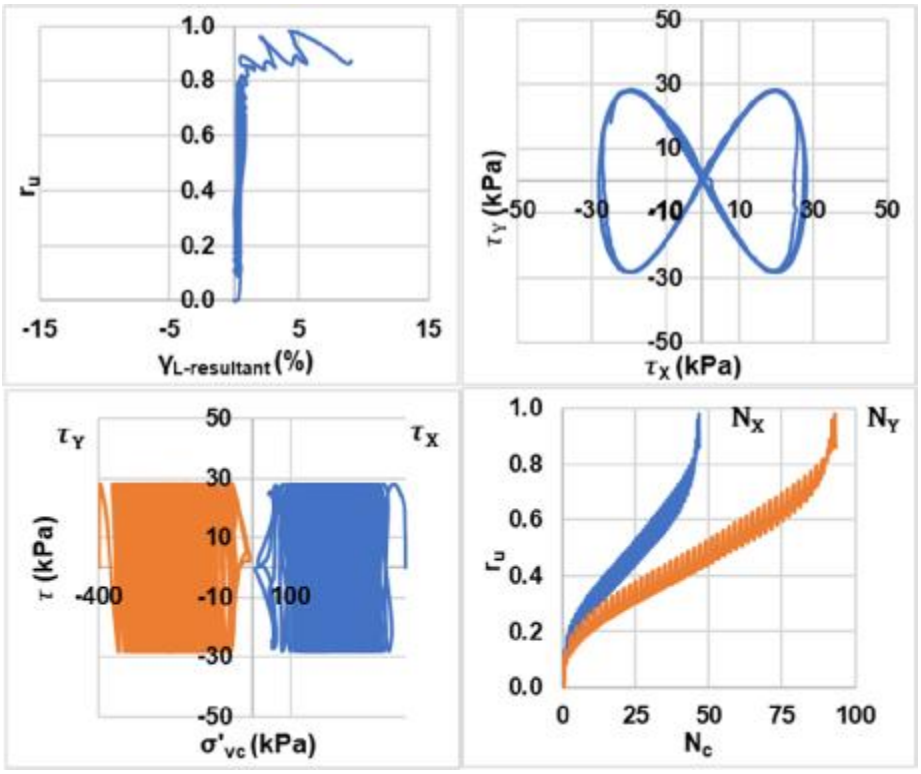


Bi-directional (Figure-8); $D_{rc}$ = 45%; $\sigma'_{vc}$ = 400 kPa; CSR = 0.07 (Liquefaction)

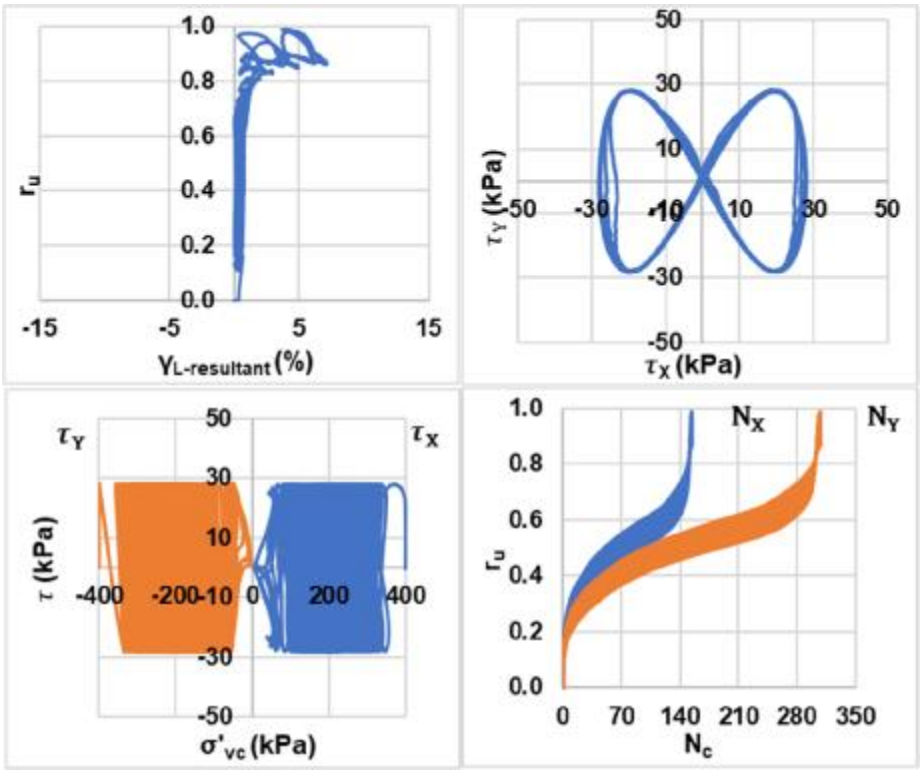


Bi-directional (Figure-8); $D_{rc}$ = 45%; $\sigma'_{vc}$ = 400 kPa; CSR = 0.07 (Re-liquefaction)

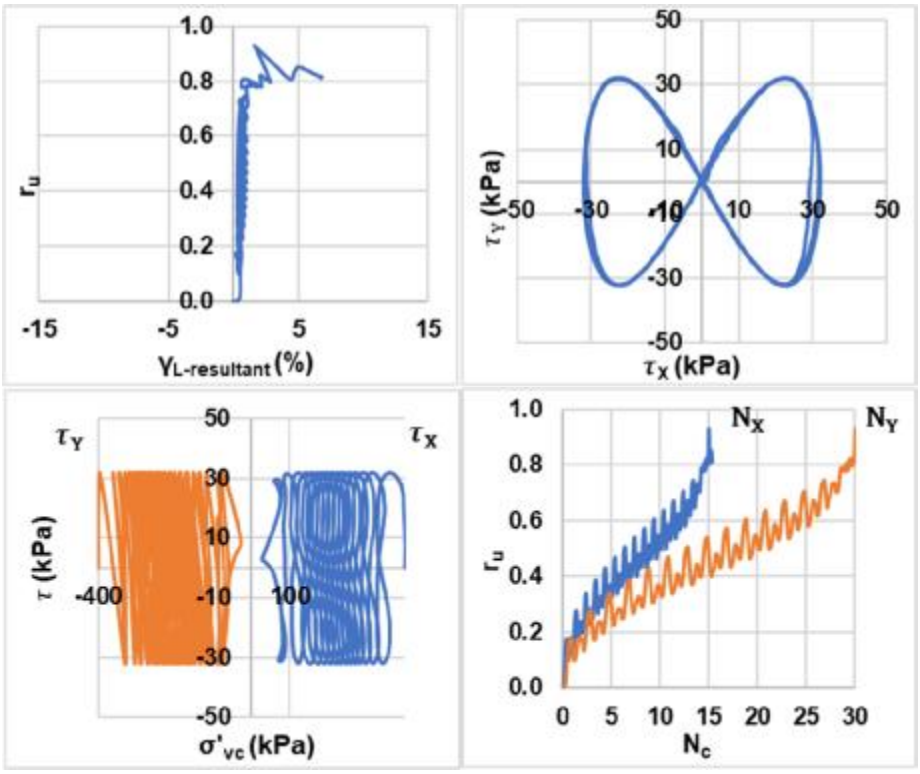


Bi-directional (Figure-8); $D_{rc}$ = 45%; $\sigma'_{vc}$ = 400 kPa; CSR = 0.08 (Liquefaction)

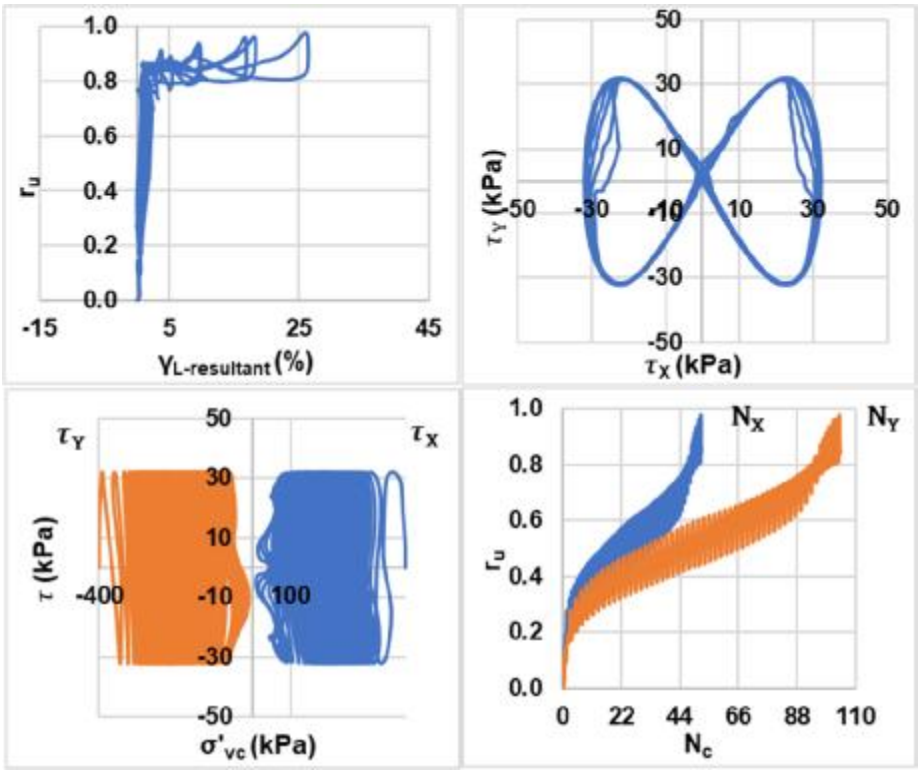


Bi-directional (Figure-8); $D_{rc}$ = 45%; $\sigma'_{vc}$ = 400 kPa; CSR = 0.08 (Re-liquefaction)

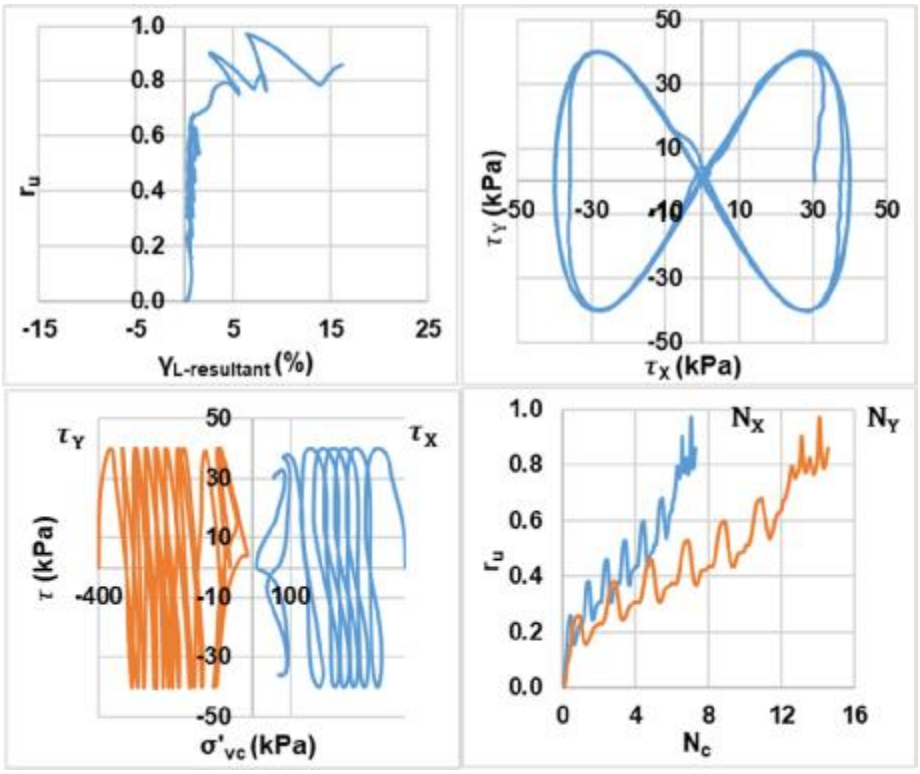


Bi-directional (Figure-8); $D_{rc}$ = 45%; $\sigma'_{vc}$ = 400 kPa; CSR = 0.1 (Liquefaction)

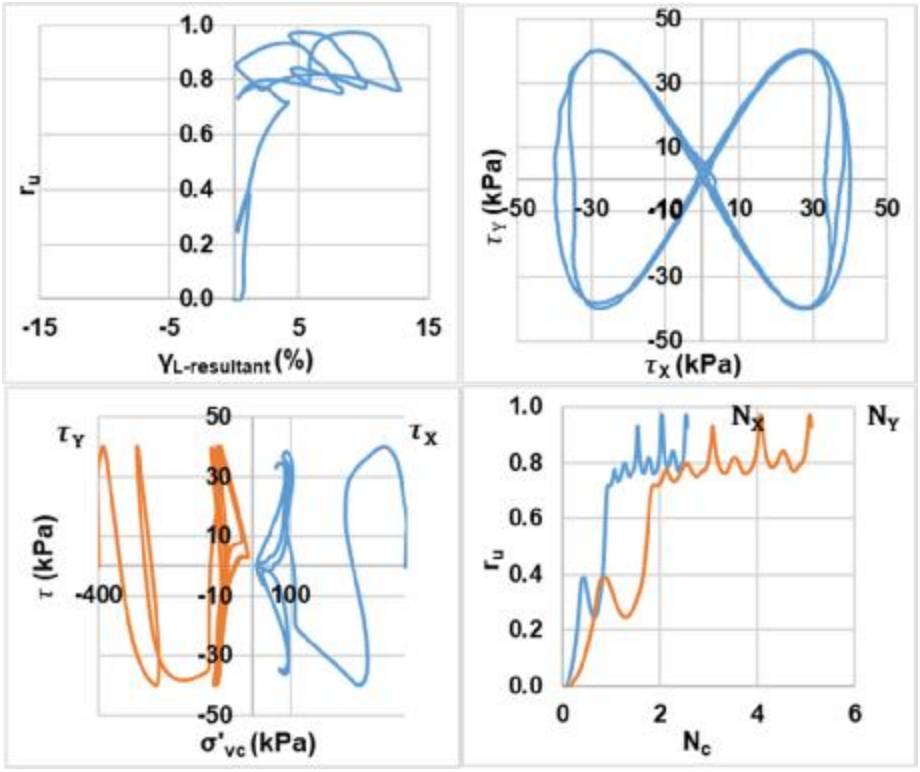


Bi-directional (Figure-8); $D_{rc}$ = 45%; $\sigma'_{vc}$ = 400 kPa; CSR = 0.1 (Re-liquefaction)

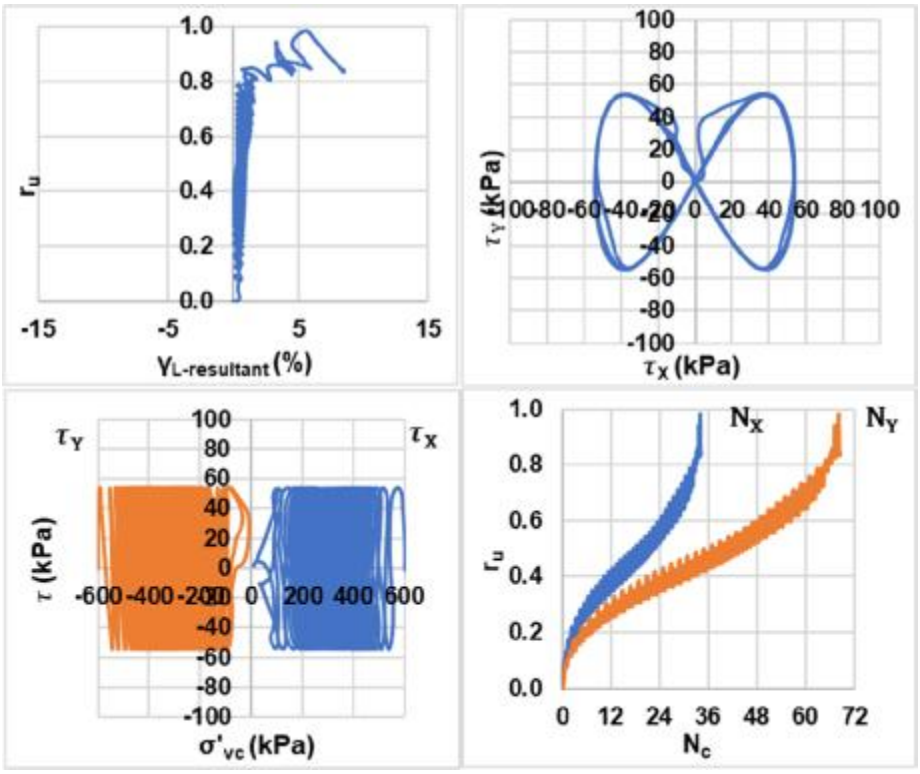


Bi-directional (Figure-8); $D_{rc}$ = 45%; $\sigma'_{vc}$ = 600 kPa; CSR = 0.09 (Liquefaction)

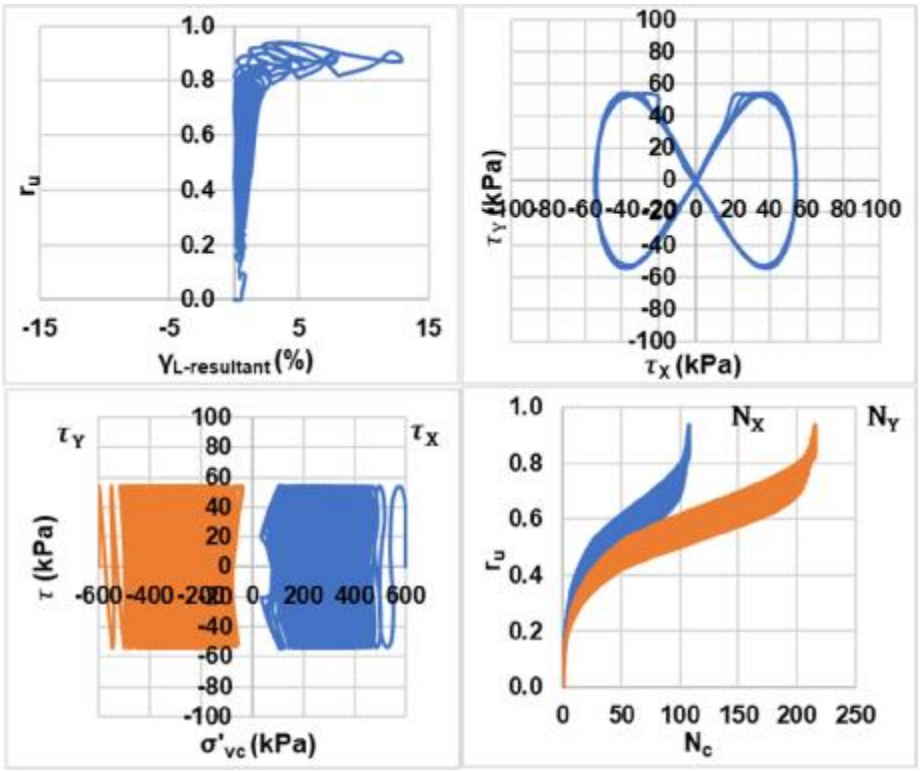


Bi-directional (Figure-8); $D_{rc}$ = 45%; $\sigma'_{vc}$ = 600 kPa; CSR = 0.09 (Re-liquefaction)

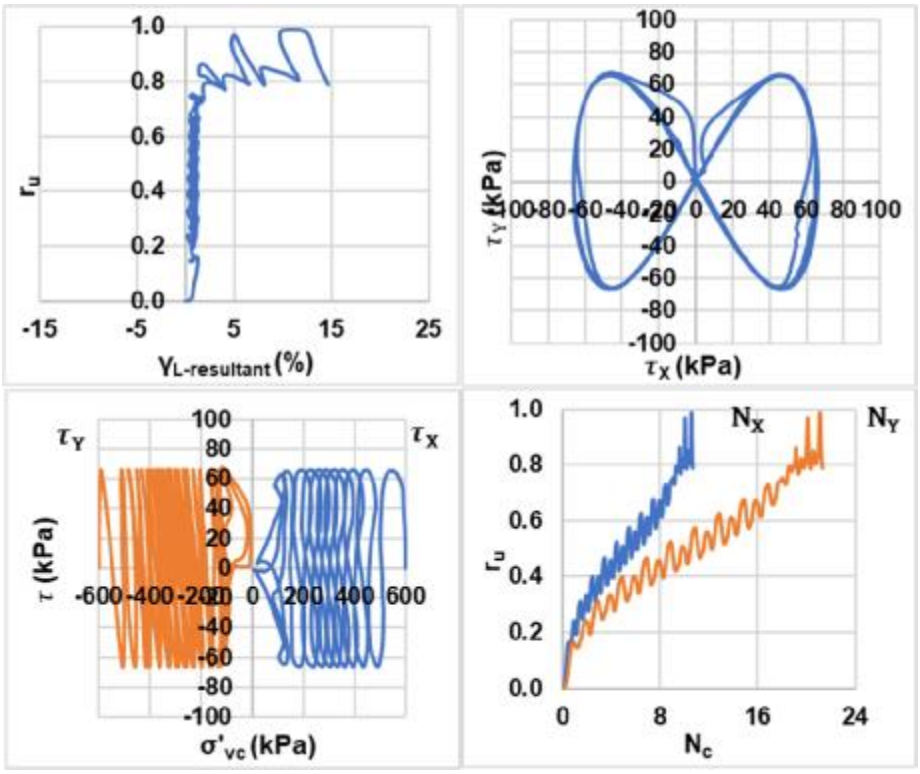


Bi-directional (Figure-8); $D_{rc}$ = 45%; $\sigma'_{vc}$ = 600 kPa; CSR = 0.11 (Liquefaction)

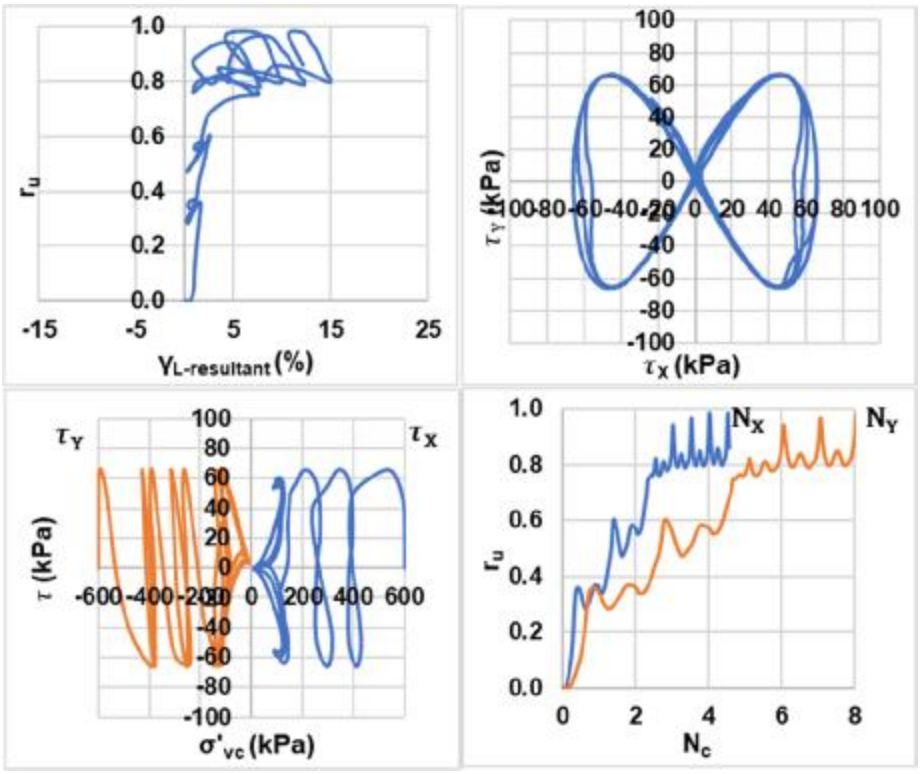


Bi-directional (Figure-8); $D_{rc}$ = 45%; $\sigma'_{vc}$ = 600 kPa; CSR = 0.11 (Re-liquefaction)

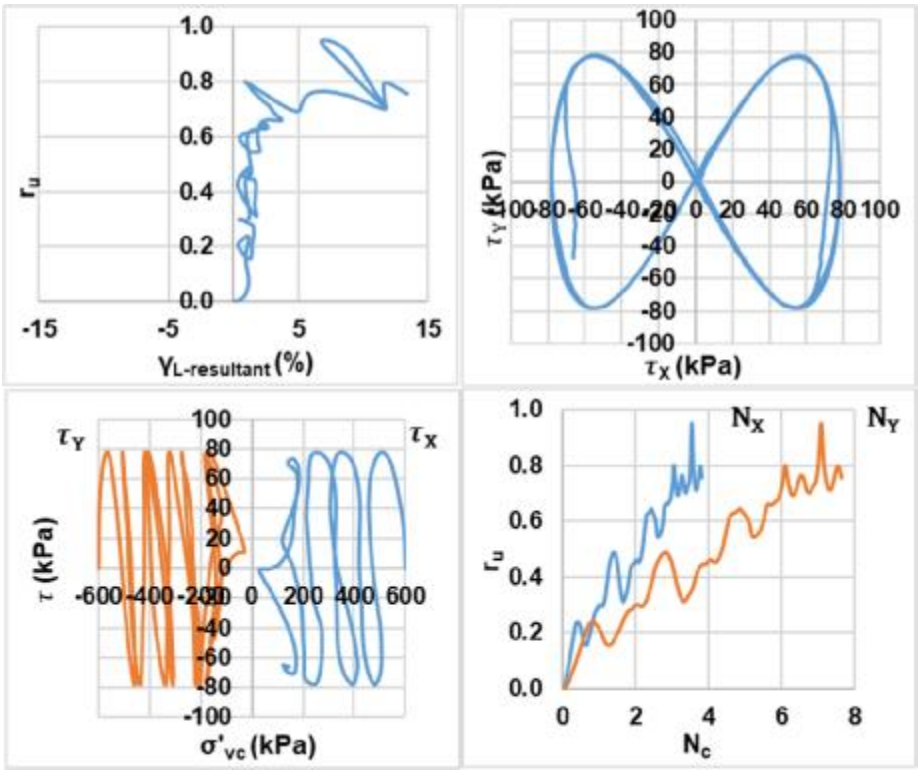


Bi-directional (Figure-8); $D_{rc}$ = 45%; $\sigma'_{vc}$ = 600 kPa; CSR = 0.13 (Liquefaction)

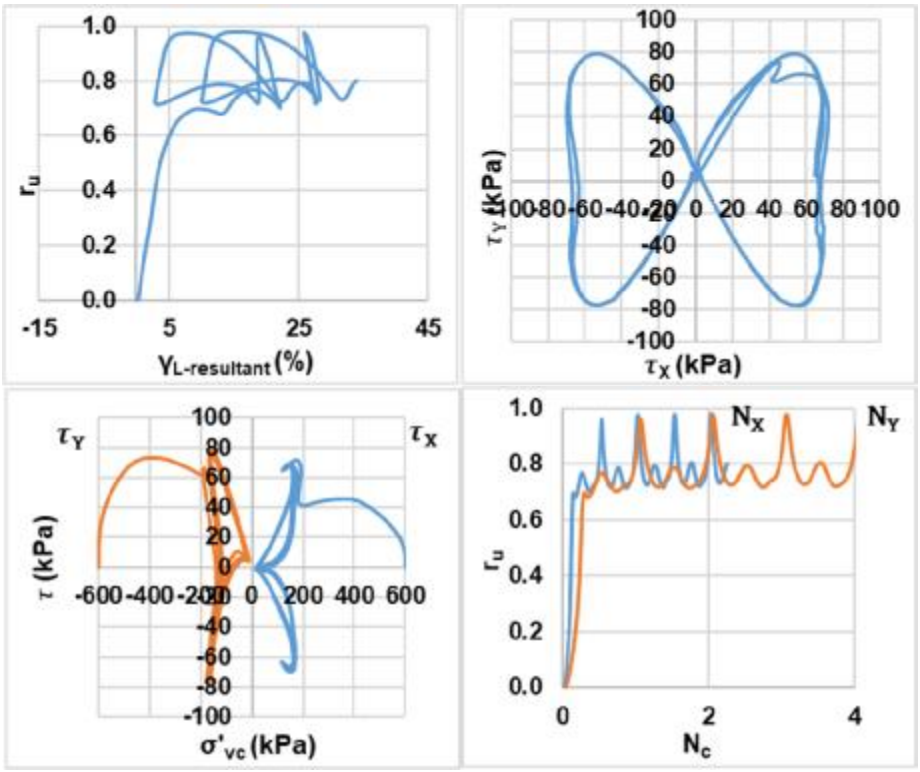


Bi-directional (Figure-8); $D_{rc}$ = 45%; $\sigma'_{vc}$ = 600 kPa; CSR = 0.13 (Re-liquefaction)

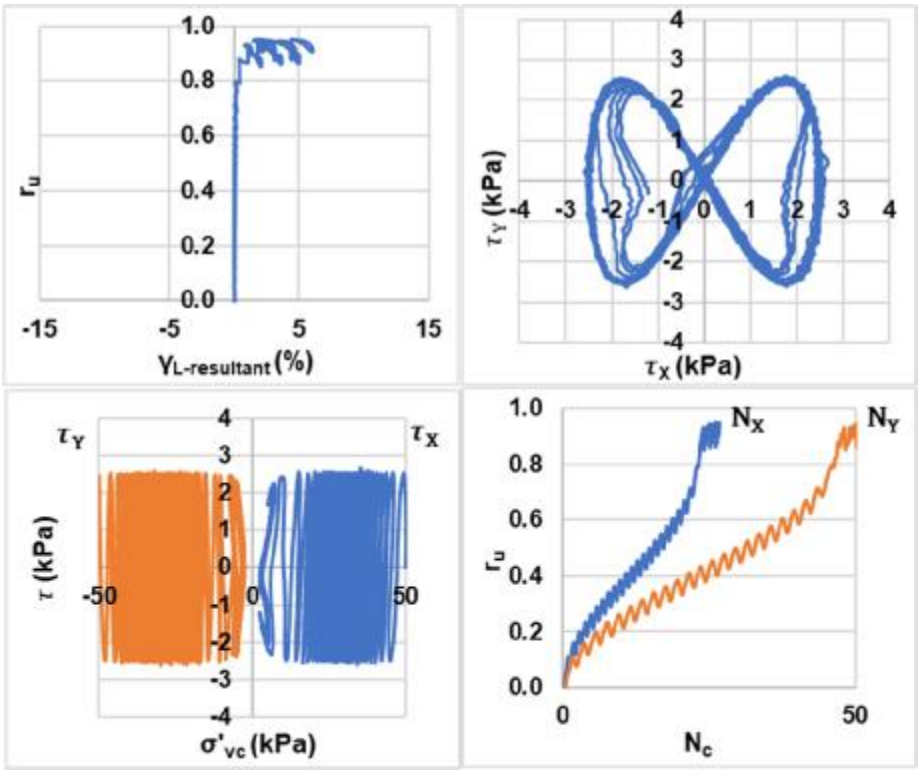


Bi-directional (Figure-8); $D_{rc}$ = 65%; $\sigma'_{vc}$ = 50 kPa; CSR = 0.05 (Liquefaction)

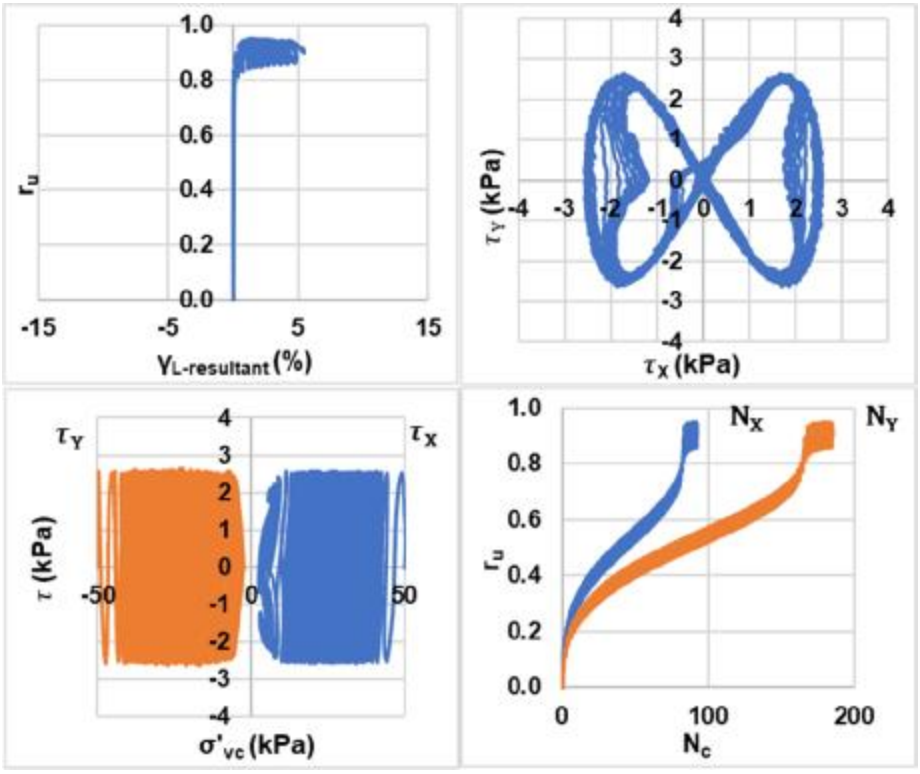


Bi-directional (Figure-8); $D_{rc}$ = 65%; $\sigma'_{vc}$ = 50 kPa; CSR = 0.05 (Re-liquefaction)

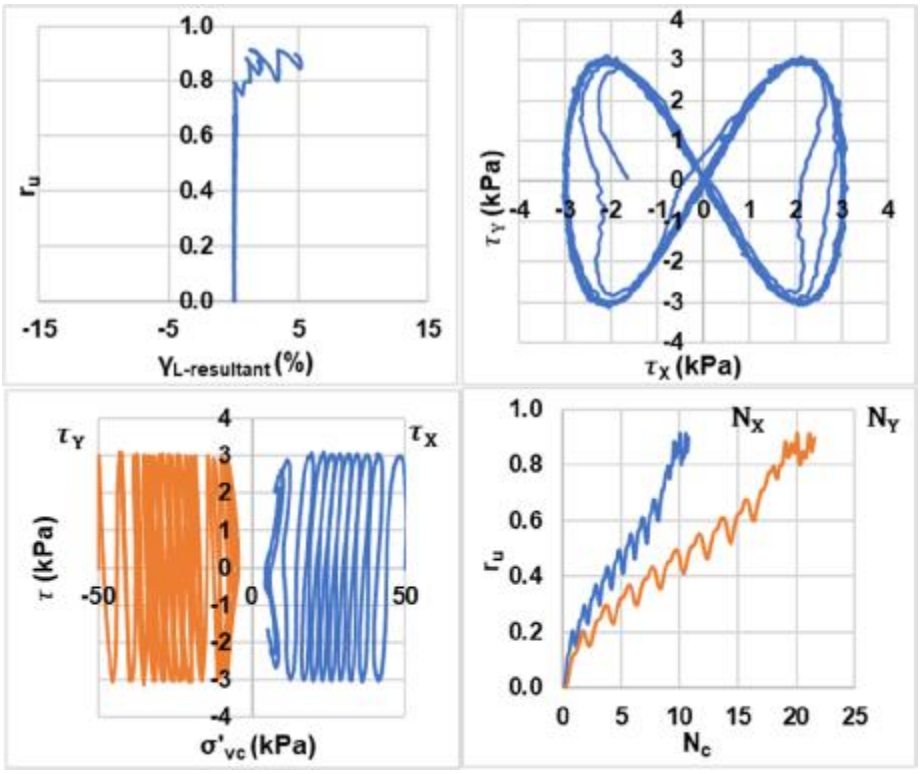


Bi-directional (Figure-8); $D_{rc}$ = 65%; $\sigma'_{vc}$ = 50 kPa; CSR = 0.06 (Liquefaction)

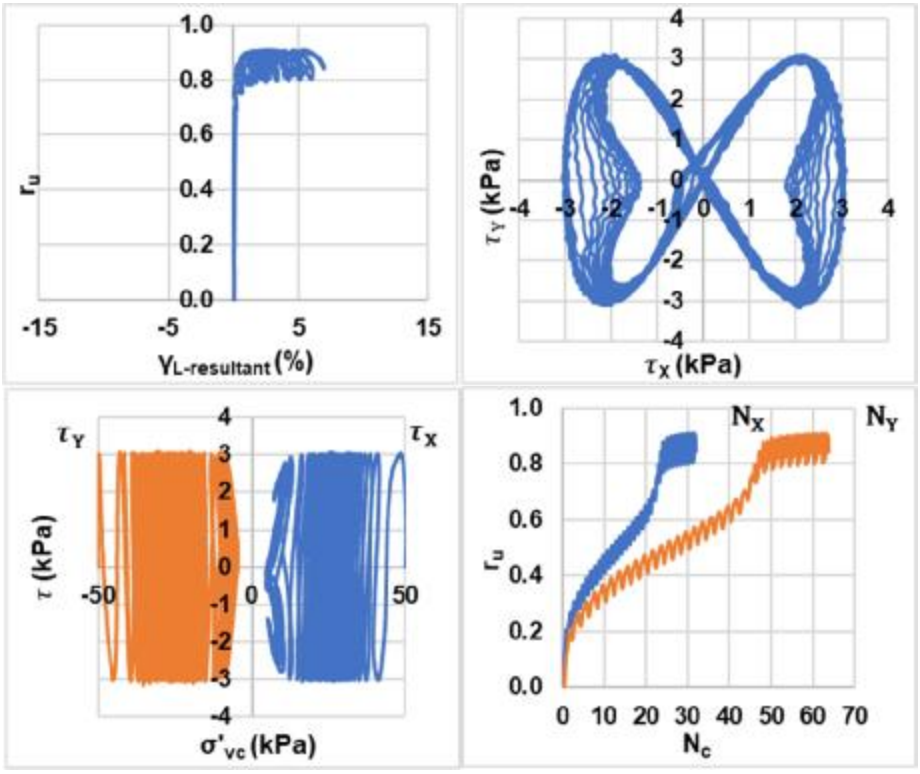


Bi-directional (Figure-8); $D_{rc}$ = 65%; $\sigma'_{vc}$ = 50 kPa; CSR = 0.06 (Re-liquefaction)

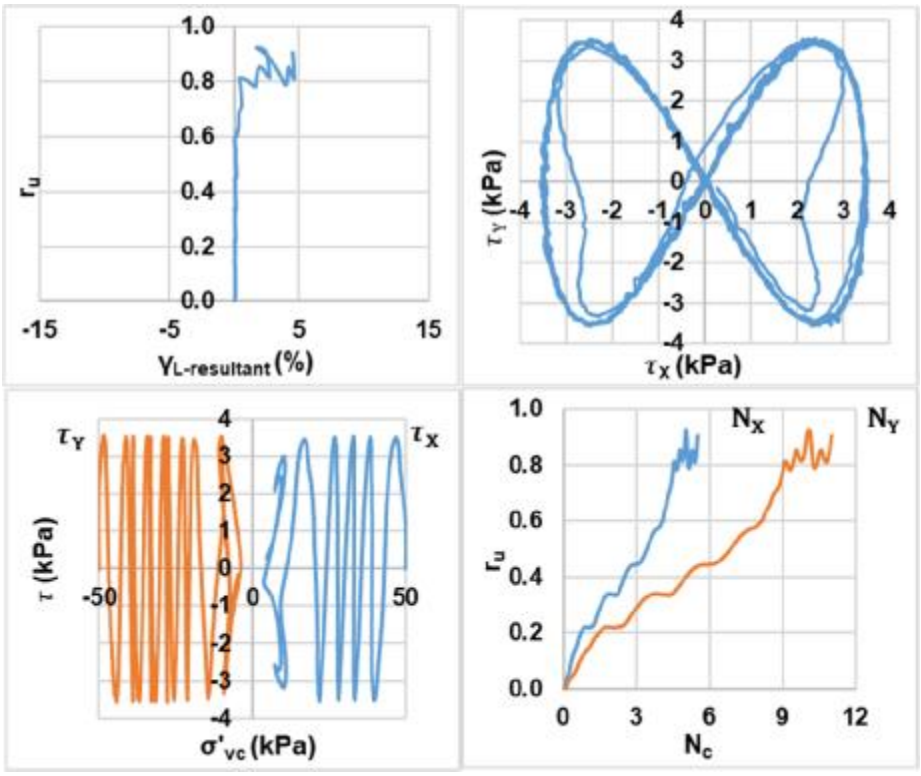


Bi-directional (Figure-8); $D_{rc}$ = 65%; $\sigma'_{vc}$ = 50 kPa; CSR = 0.07 (Liquefaction)

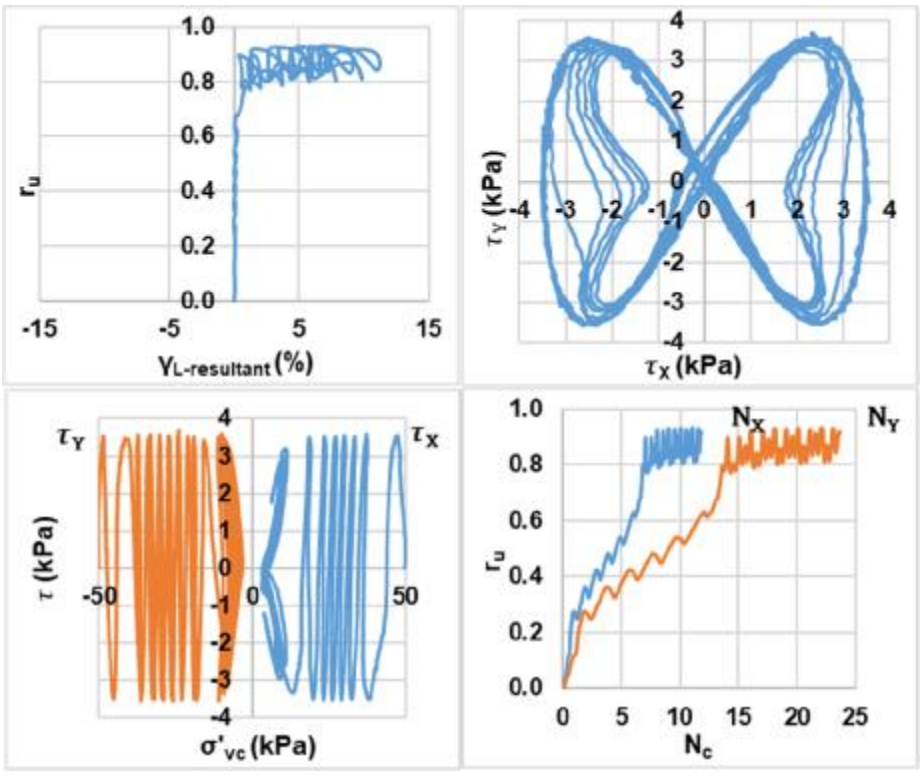


Bi-directional (Figure-8); $D_{rc}$ = 65%; $\sigma'_{vc}$ = 50 kPa; CSR = 0.07 (Re-liquefaction)

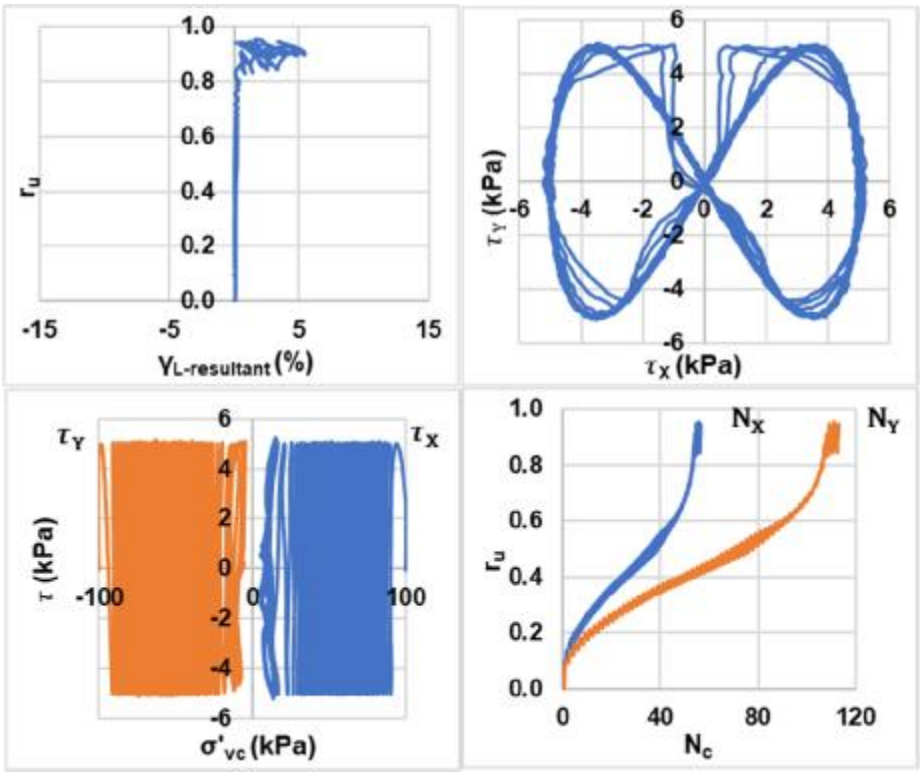


Bi-directional (Figure-8); $D_{rc}$ = 65%; $\sigma'_{vc}$ = 100 kPa; CSR = 0.05 (Liquefaction)

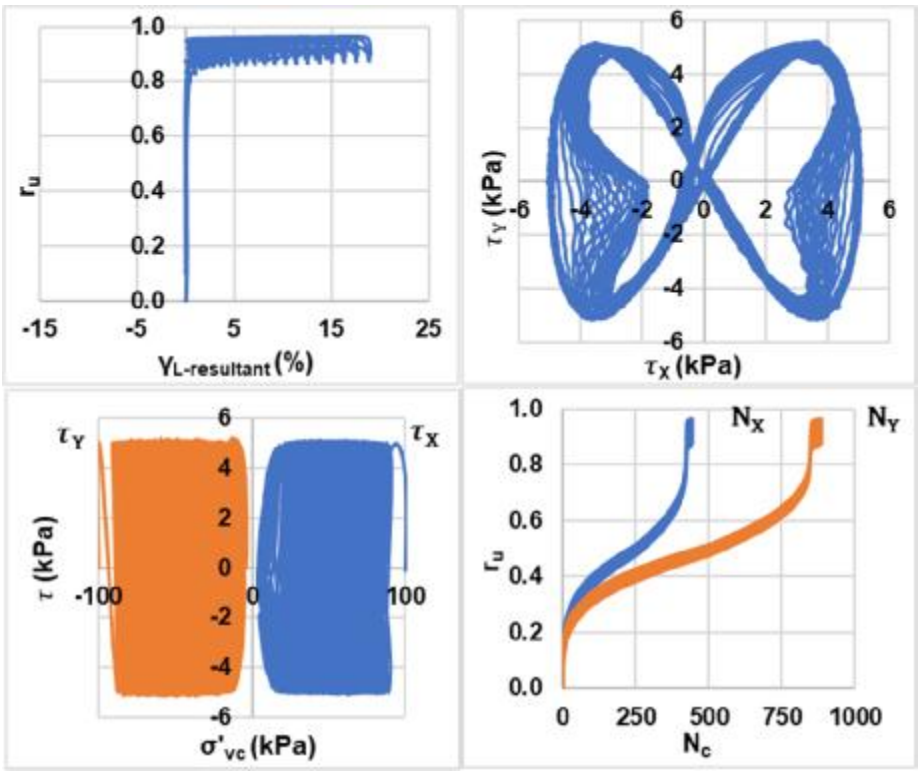


Bi-directional (Figure-8); $D_{rc}$ = 65%; $\sigma'_{vc}$ = 100 kPa; CSR = 0.05 (Re-liquefaction)

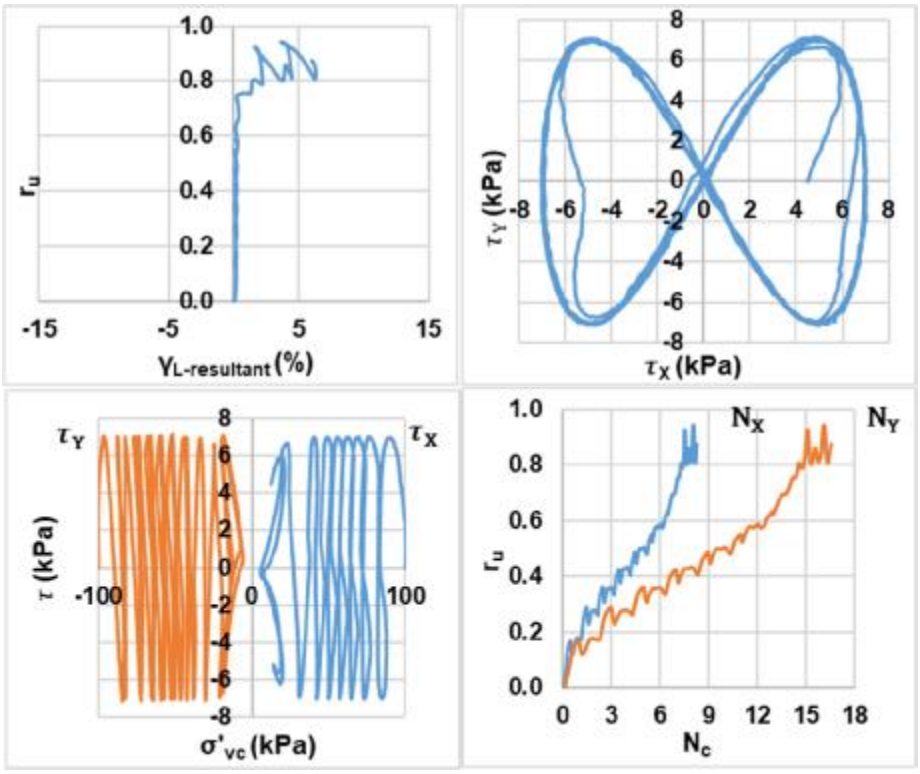


Bi-directional (Figure-8); $D_{rc}$ = 65%; $\sigma'_{vc}$ = 100 kPa; CSR = 0.07 (Liquefaction)

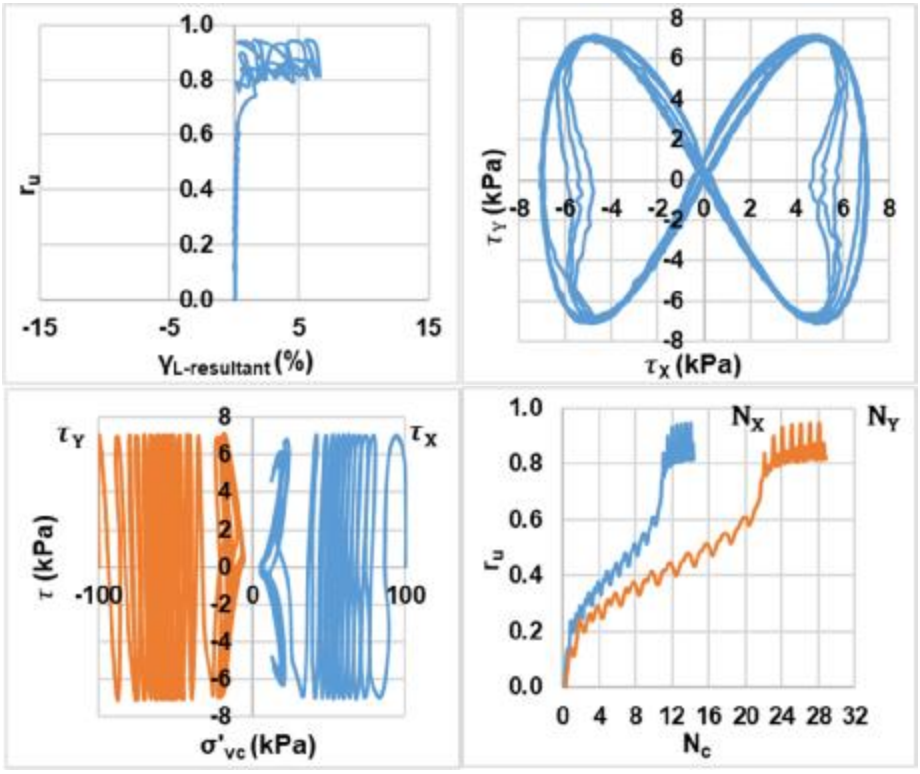


Bi-directional (Figure-8); $D_{rc}$ = 65%; $\sigma'_{vc}$ = 100 kPa; CSR = 0.07 (Re-liquefaction)

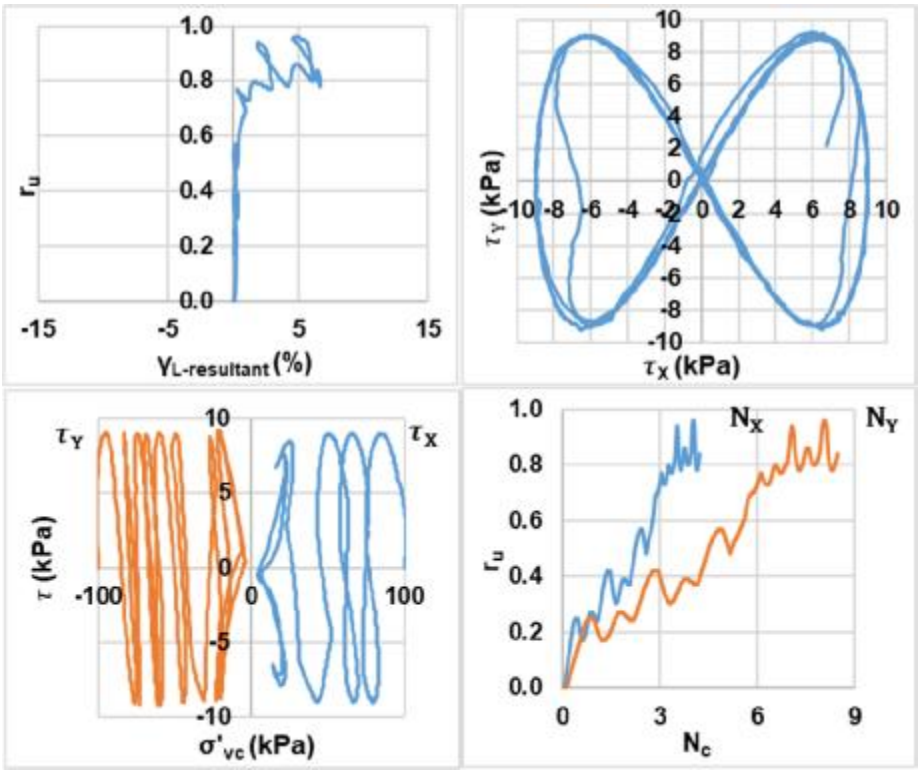


Bi-directional (Figure-8); $D_{rc}$ = 65%; $\sigma'_{vc}$ = 100 kPa; CSR = 0.09 (Liquefaction)

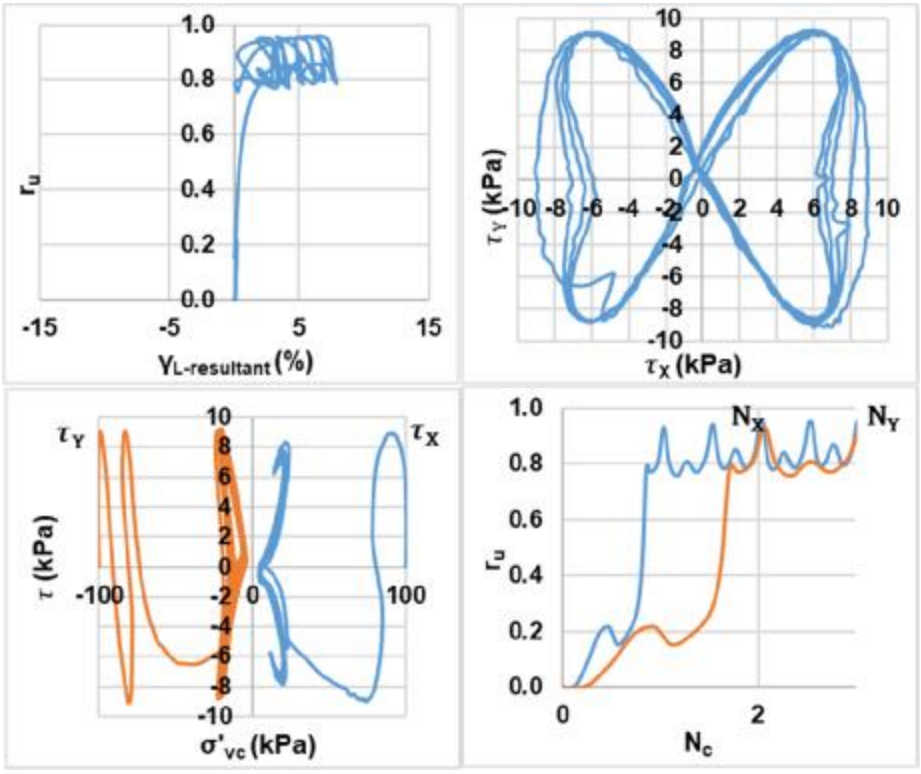


Bi-directional (Figure-8); $D_{rc}$ = 65%; $\sigma'_{vc}$ = 100 kPa; CSR = 0.09 (Re-liquefaction)

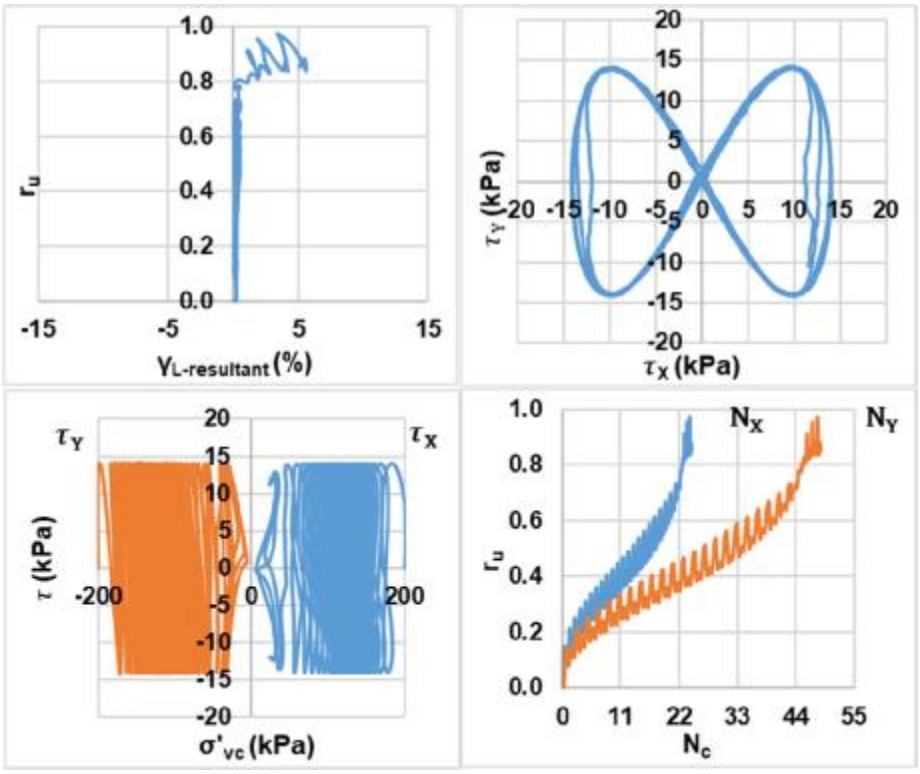


Bi-directional (Figure-8); $D_{rc}$ = 65%; $\sigma'_{vc}$ = 200 kPa; CSR = 0.07 (Liquefaction)

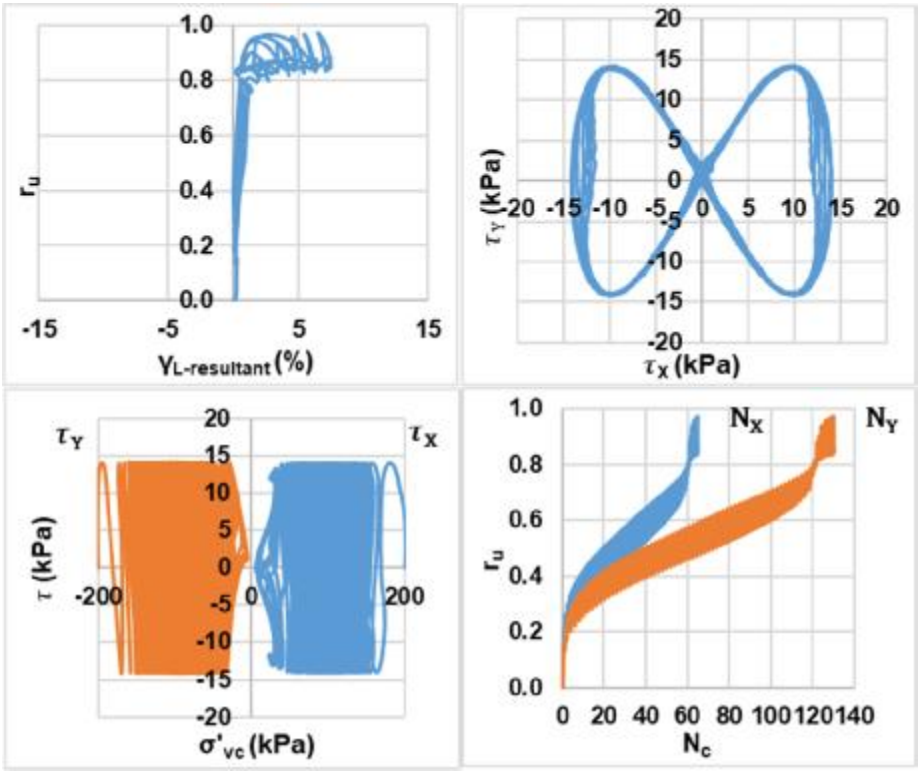


Bi-directional (Figure-8); $D_{rc}$ = 65%; $\sigma'_{vc}$ = 200 kPa; CSR = 0.07 (Re-liquefaction)

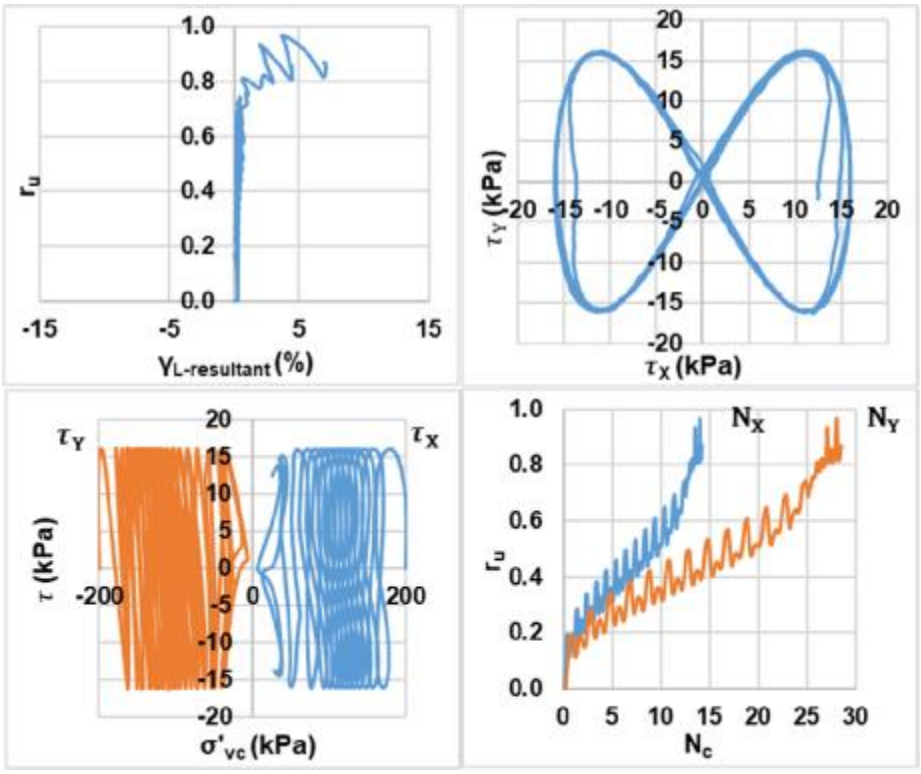


Bi-directional (Figure-8); $D_{rc}$ = 65%; $\sigma'_{vc}$ = 200 kPa; CSR = 0.08 (Liquefaction)

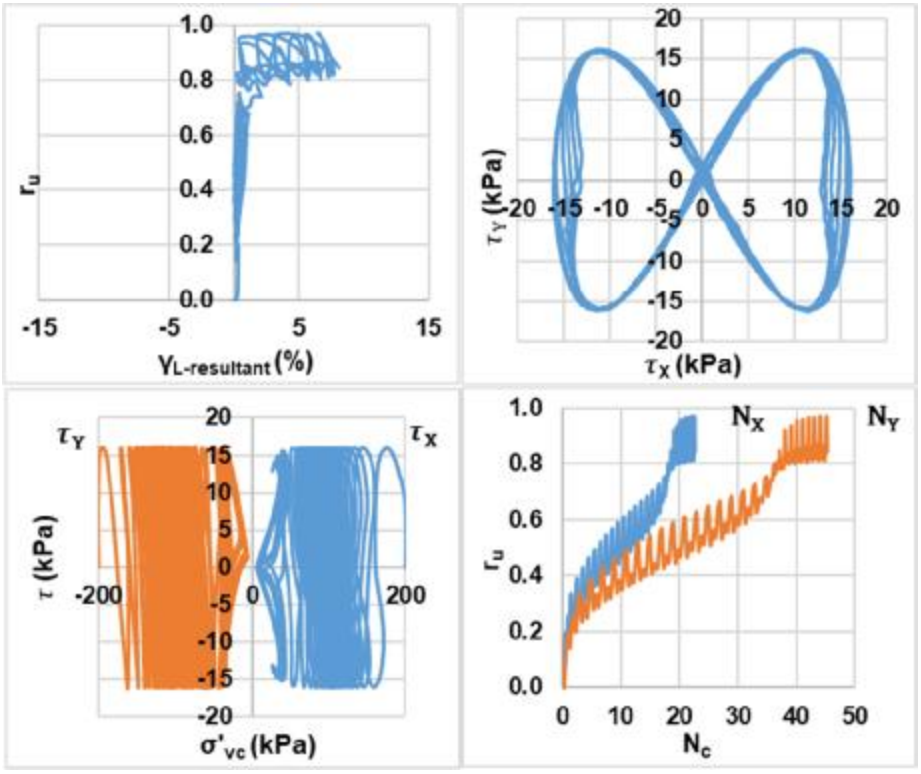


Bi-directional (Figure-8); $D_{rc}$ = 65%; $\sigma'_{vc}$ = 200 kPa; CSR = 0.08 (Re-liquefaction)

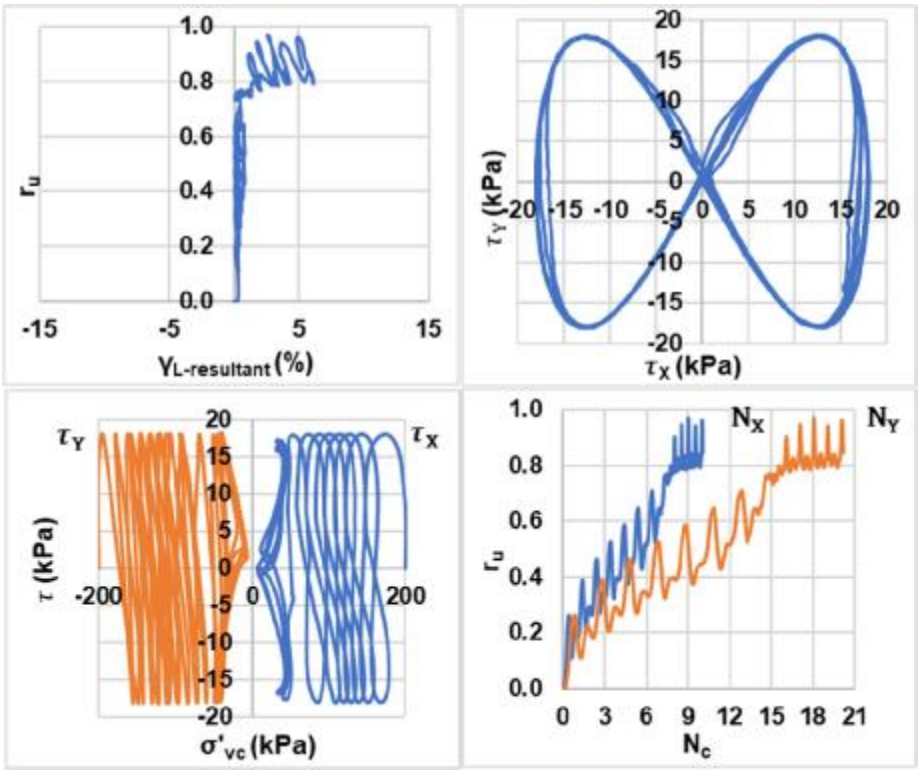


Bi-directional (Figure-8); $D_{rc}$ = 65%; $\sigma'_{vc}$ = 200 kPa; CSR = 0.09 (Liquefaction)

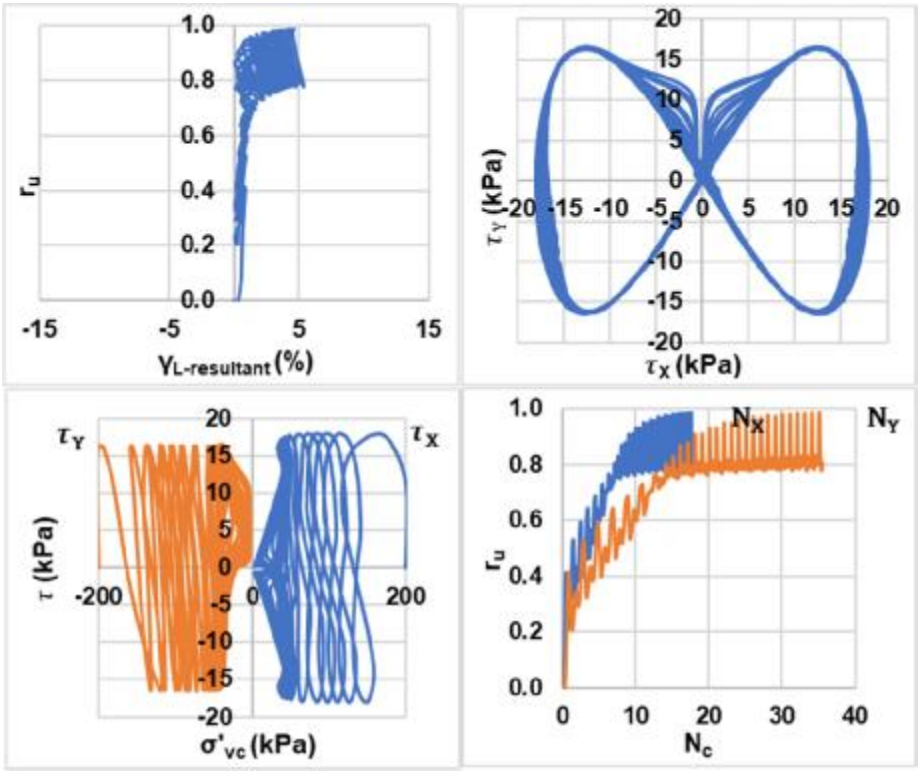


Bi-directional (Figure-8); $D_{rc}$ = 65%; $\sigma'_{vc}$ = 200 kPa; CSR = 0.09 (Re-liquefaction)

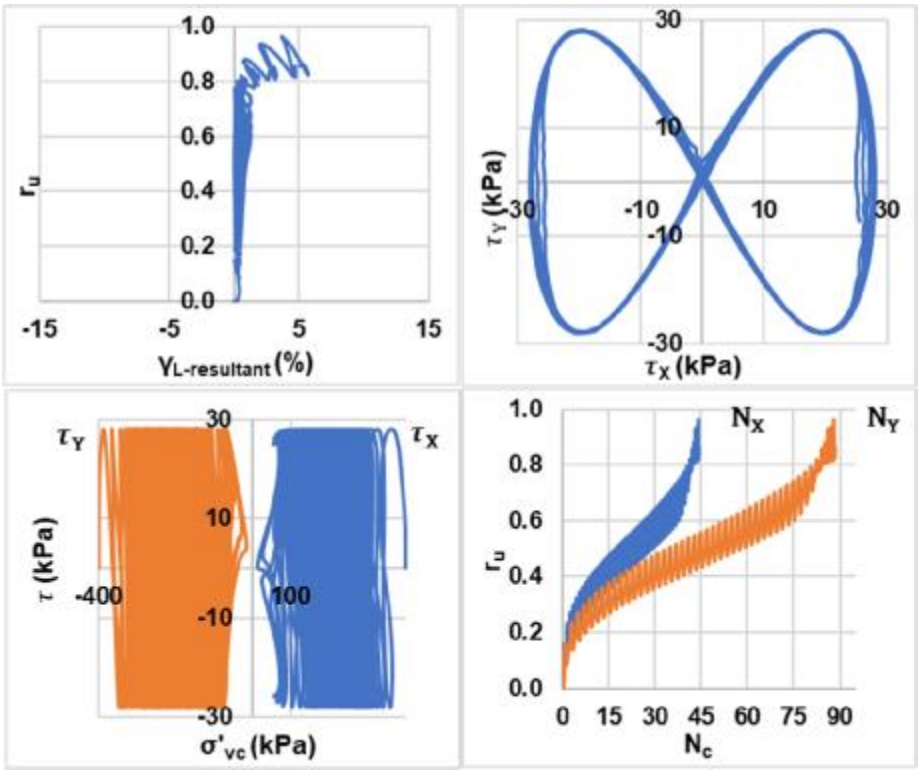


Bi-directional (Figure-8); $D_{rc}$ = 65%; $\sigma'_{vc}$ = 400 kPa; CSR = 0.07 (Liquefaction)

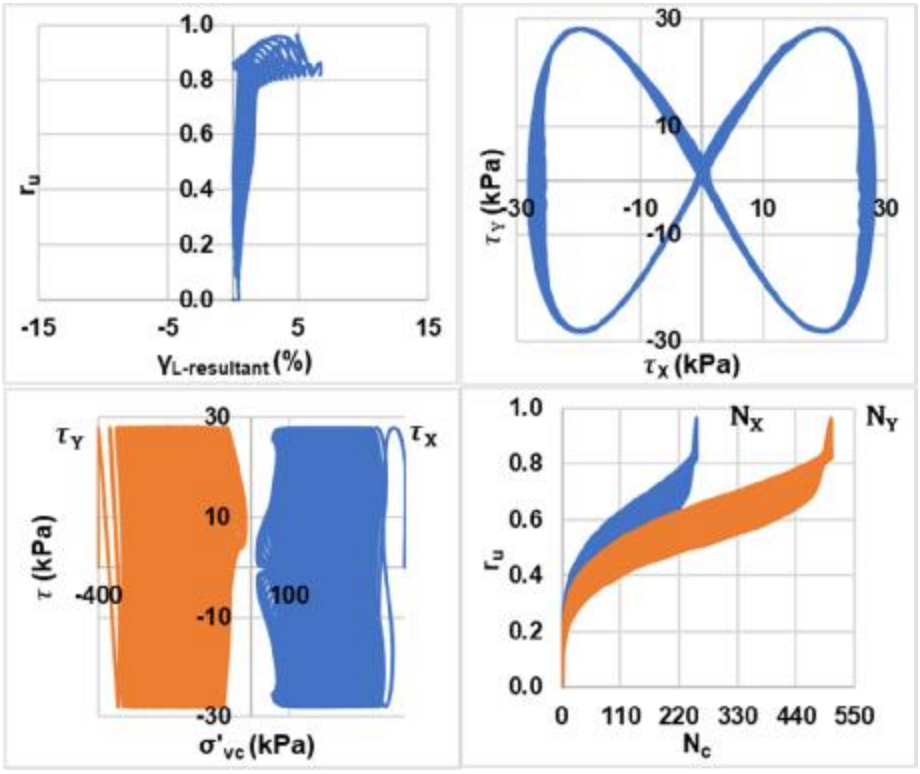


Bi-directional (Figure-8); $D_{rc}$ = 65%; $\sigma'_{vc}$ = 400 kPa; CSR = 0.07 (Re-liquefaction)

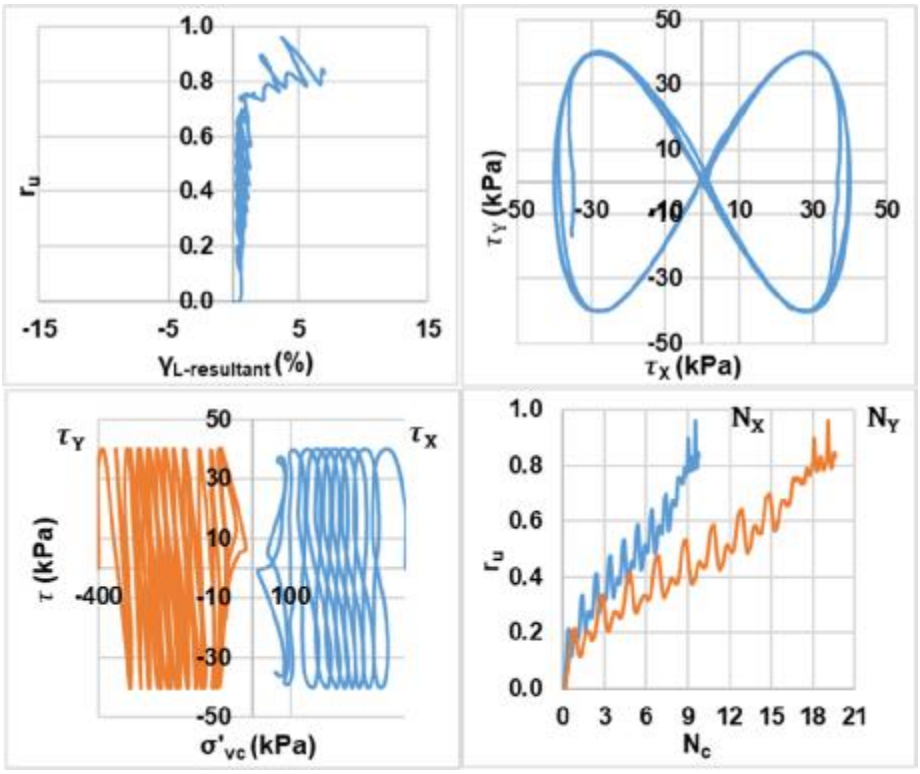


Bi-directional (Figure-8); $D_{rc}$ = 65%; $\sigma'_{vc}$ = 400 kPa; CSR = 0.1 (Liquefaction)

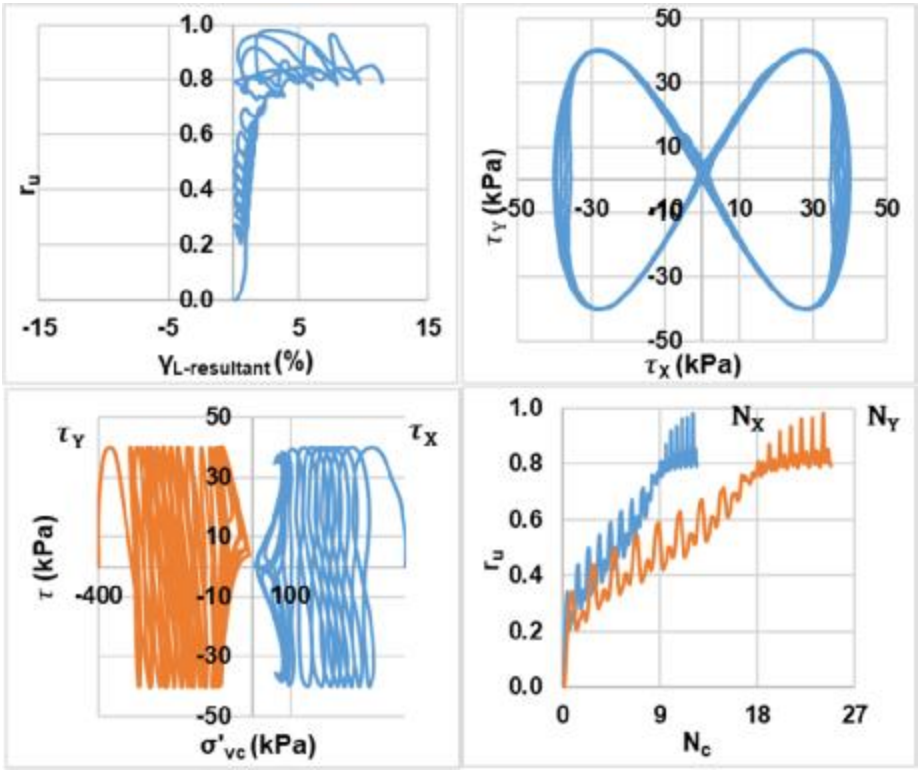


Bi-directional (Figure-8); $D_{rc}$ = 65%; $\sigma'_{vc}$ = 400 kPa; CSR = 0.1 (Re-liquefaction)

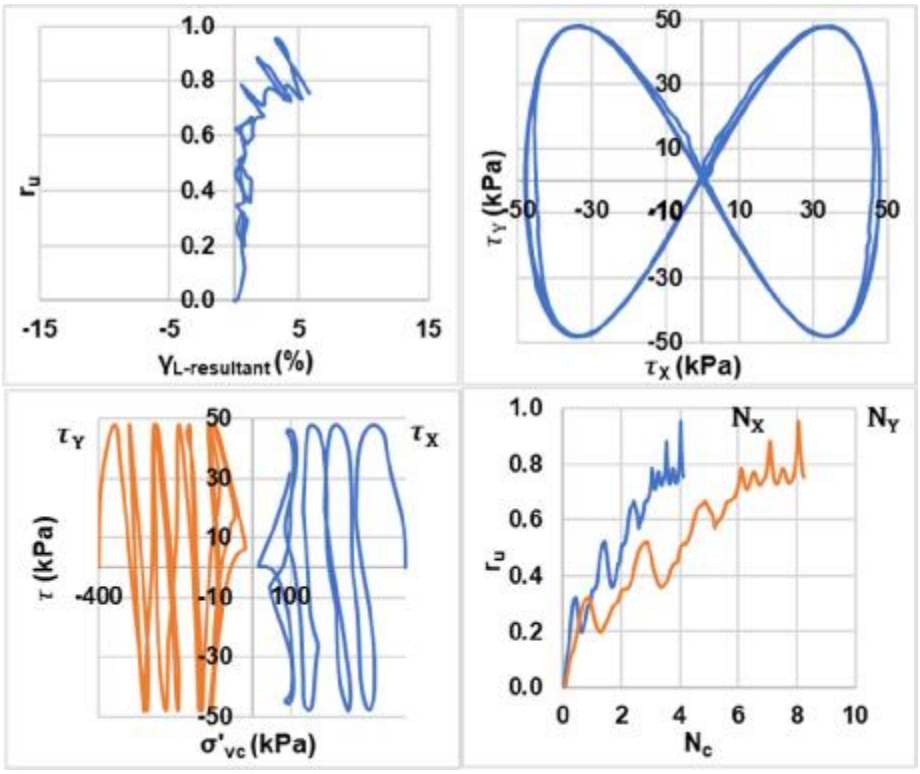


Bi-directional (Figure-8); $D_{rc}$ = 65%; $\sigma'_{vc}$ = 400 kPa; CSR = 0.12 (Liquefaction)

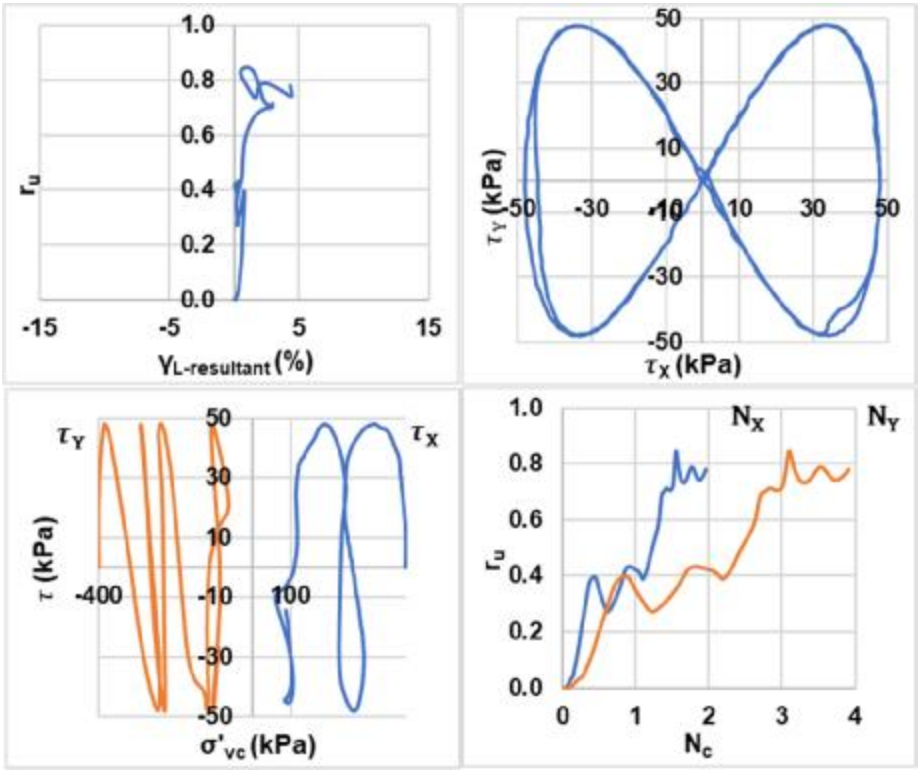


Bi-directional (Figure-8); $D_{rc}$ = 65%; $\sigma'_{vc}$ = 400 kPa; CSR = 0.12 (Re-liquefaction)

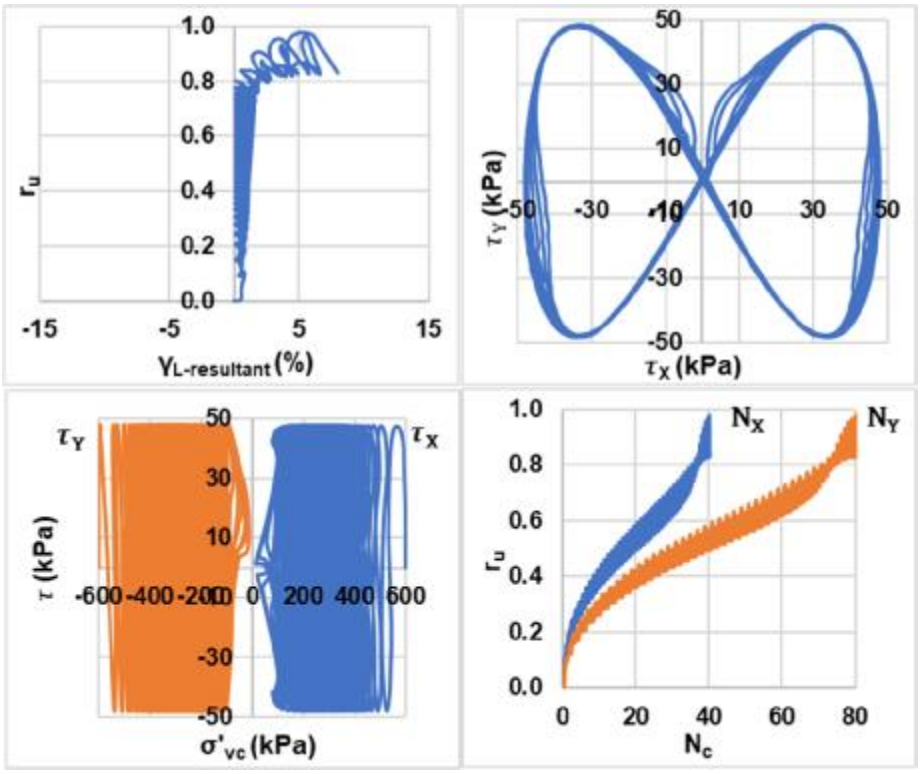


Bi-directional (Figure-8); $D_{rc}$ = 65%; $\sigma'_{vc}$ = 600 kPa; CSR = 0.08 (Liquefaction)

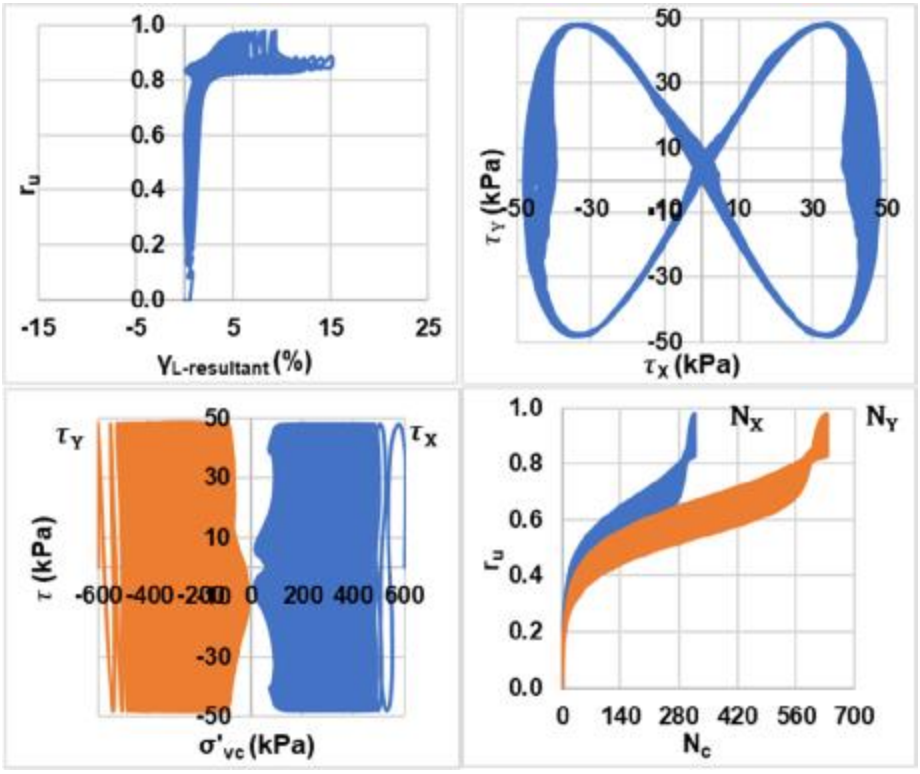


Bi-directional (Figure-8); $D_{rc}$ = 65%; $\sigma'_{vc}$ = 600 kPa; CSR = 0.08 (Re-liquefaction)

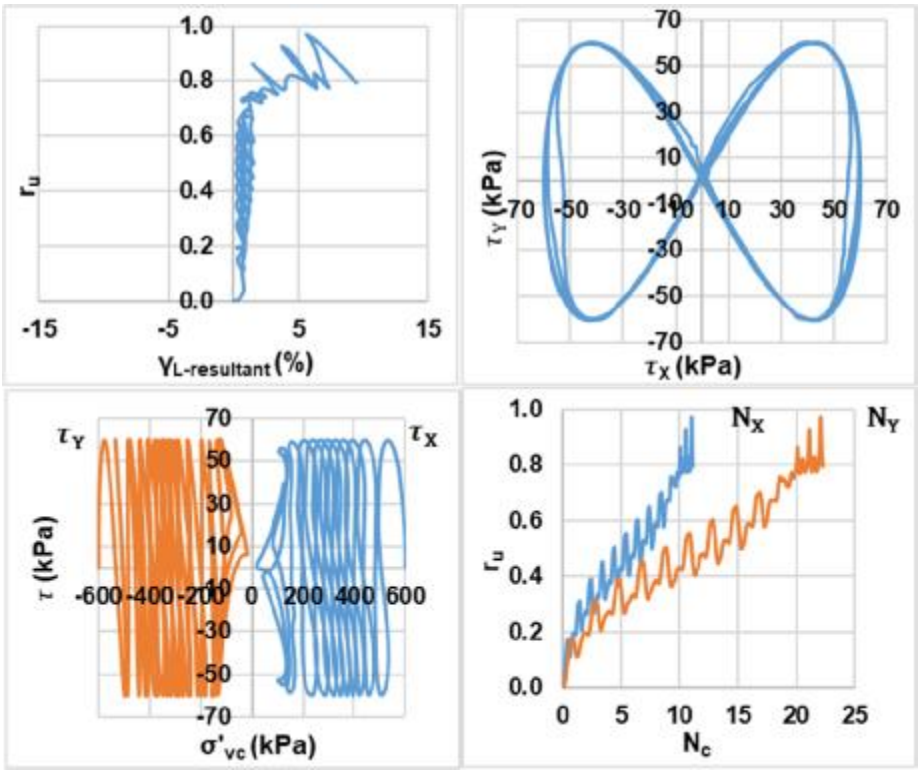


Bi-directional (Figure-8); $D_{rc}$ = 65%; $\sigma'_{vc}$ = 600 kPa; CSR = 0.1 (Liquefaction)

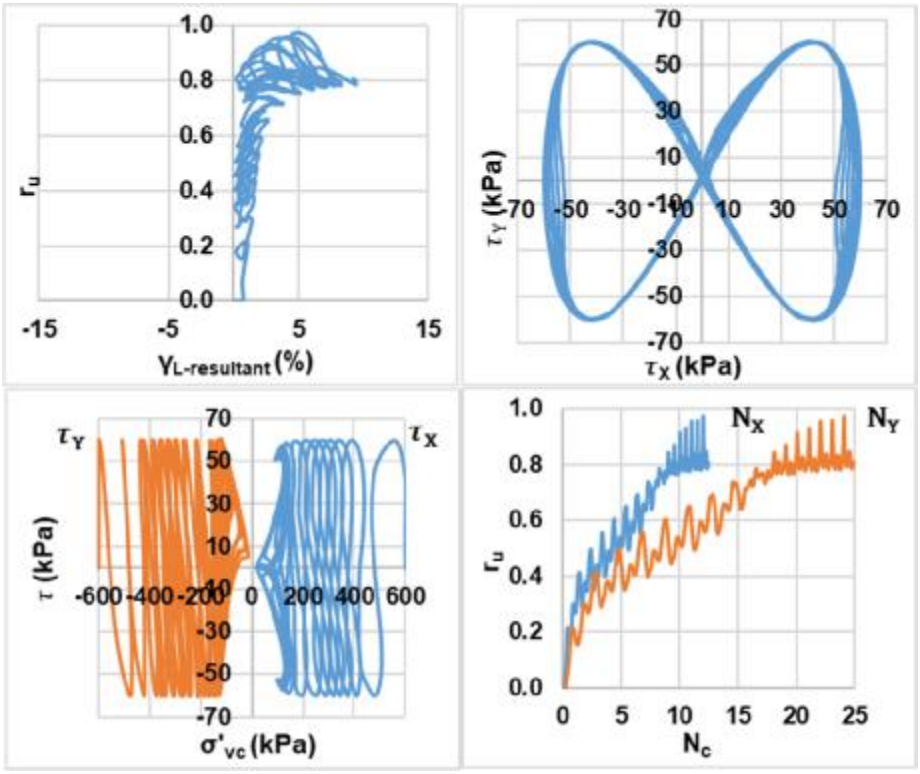


Bi-directional (Figure-8); $D_{rc}$ = 65%; $\sigma'_{vc}$ = 600 kPa; CSR = 0.1 (Re-liquefaction)

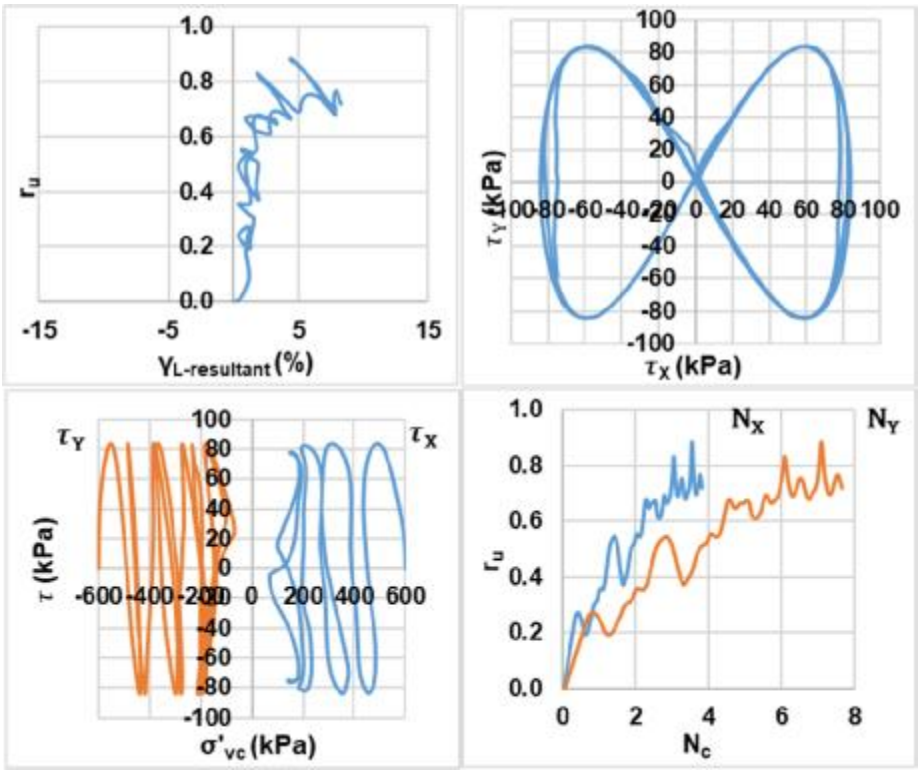


Bi-directional (Figure-8); $D_{rc}$ = 65%; $\sigma'_{vc}$ = 600 kPa; CSR = 0.14 (Liquefaction)

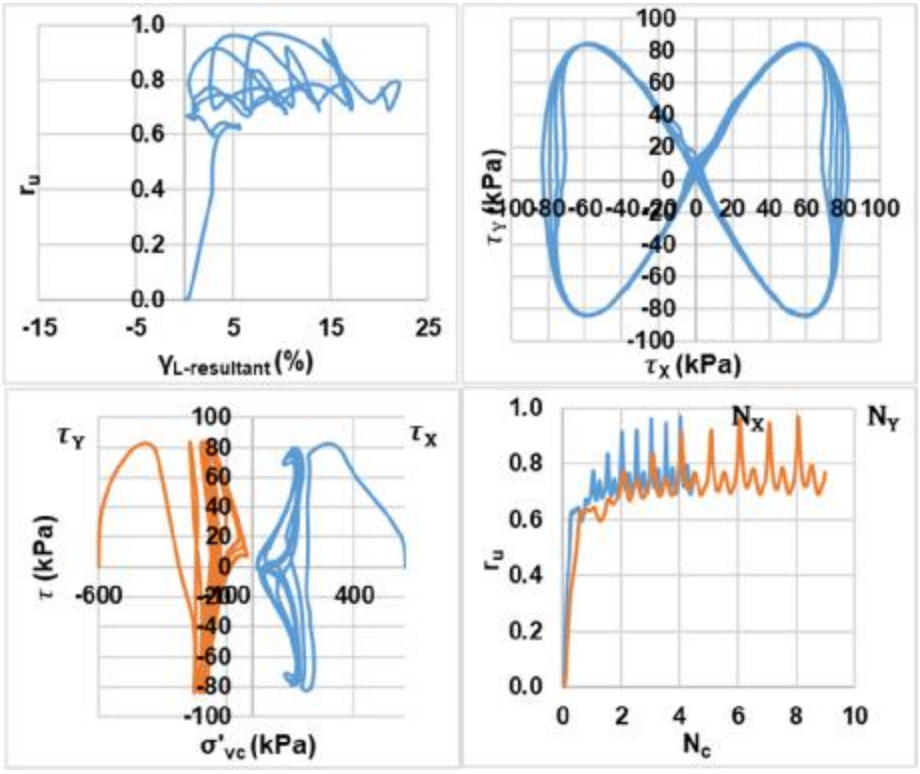


Bi-directional (Figure-8); $D_{rc}$ = 65%; $\sigma'_{vc}$ = 600 kPa; CSR = 0.14 (Re-liquefaction)

# Keyvan Mirbaha curriculum vitae (CV)

## EDUCATION

- Master of Science in Geotechnical Eng. – Uni. of Westrn Ontario - GPA 92% (A+) — London, Canada, 2015-2017
- Master of Science in Structural Eng. - Amir Kabir Uni. of Technology - GPA 82% (A) — Tehran, Iran, 2004-2007
- Bachelor of Science in Civil Eng. - University of Tehran - GPA 74% (B) — Tehran, Iran, 2000-2004

## THESIS, RESEARCHES and PUBLICATION ACTIVITIES

### Thesis Title:

"Bi-directional cyclic behaviour and liquefaction analysis of a silica-carbonate sand" Fall 2017, Western University, Department of Civil and Environmental Engineering - Advisor: Dr Abouzar Sadrekarimi

### Article Title:

"Characterization of a Silica-Carbonate Sand Based on Shear Wave Velocity Measurement and Cyclic Simple Shear Tests" Conference on Performance Based Design in Earthquake Geotechnical Engineering (PBD III), Vancouver, 2017

### Thesis Title:

"Effect of different steel yield stresses in strength and ductility of steel plate shear walls" Fall 2006, Amir Kabir University of Technology, Department of Civil and Environmental Engineering - Advisor: Dr. Ardeshir Deilami

## PROFESSIONAL EXPERIENCE

Geostructural Engineer — Oct. 2017 – current
SITE Canada, Micropiles Anchors and Grouting; — Toronto, Canada

- Analyzed (finite element) shoring systems with soldier piles and timber lagging or shotcretes
- Calculated anchoring systems with grouting to sustain tensile forces for deep excavations and shorings
- Designed micropiles for load bearing (deep) foundations, ground and rock improvements
- Prepared tender documents, proposals and conducted material quantity take off and cost estimations
- Reviewed various geotechnical reports and design specifications for extracting required data

Structural Design Engineer – Lead Engineer — 2009 – 2015
Fakoor Sanat Tehran Co. — Tehran, Iran

- Effectively designed diverse steel / concrete structures for mineral processing / metal manufacturing industry from conceptual to detailed design which led to more than 30% savings compared to traditional methods
- Oversaw thermal, buckling, seismic, vibration, fatigue, hydraulic and geo technical analysis / design
- Prepared guidelines through intensive research to provide technical instruction / design spreadsheets
- Organized field / site reviews of construction or fabrication and prepared technical reports
- Coordinated with electrical, mechanical, architectural and other disciplines for the smooth design and execution of projects according to project scope, cost limit and time schedule
- Led an engineering team of about 20 members to develop structural design activities (during last year)

# Keyvan Mirbaha curriculum vitae (CV)

Structural Design Engineer – Technical Adviser (Project Based) 2012 – 2014
Arme Tarh Kaveh Co. Tehran, Iran

- Completed seismic design or rehabilitation of existing structures, utilizing base isolators / dampers
- Effectively designed mid-rise to high-rise residential, institutional and industrial structures (Concrete and steel)
- Designed shallow / deep (pile) foundations and proposals for excavation and construction sequences
- Developed design procedures for several industrial structures of Abyek Cement Factory

Seismic Engineer (Part time) 2007 – 2009
Permayon Advanced Strengthening Co. Tehran, Iran

- Developed design procedures for the rehabilitation and retrofitting of 10 school buildings (existing)
- Calculated and developed designs by retrofitting methods according to specifications, codes and standards
- Recommended the most economical solution for seismic rehabilitating of structures after a feasibility study
- Ensured projects met time schedules based on a project control program and stayed within budget

Civil Engineer 2007 – 2008
Engineering Department, Military Service Tehran, Iran

- Prepared calculations for steel/concrete residential buildings (3-6 stories) mostly constructed as typical blocks in residential complexes according to relevant engineering standards and procedures
- Studied different architectural drawings for compatibility of structure and proper loading of model
- Reviewed, checked, and utilized geotechnical and surveying reports especially for foundation design

Junior Civil Engineer (part time – project based) 2004 – 2007
The House of Seven Moons Co. Tehran, Iran

- Performed civil and structural design procedures for diverse residential and some commercial buildings
- Efficiently assisted CAD technicians with 2D/3D software tools to prepare executive / shop drawings
- Developed the design of an oval shaped art gallery for the Iranian Artists Center in Tehran
- Studied different architectural drawings and coordinated with architects for compatibility of the design

## INSTRUCTING EXPERIENCE

Instructor (Part Time) 2005 – 2007
Azad University of Varamin Tehran, Iran

- Taught courses such as statics, strength of materials, and structural analysis to undergraduate students and also courses for finite element software programs including ETABS, SAFE and SAP2000
- Developed instructional materials according to the industry requirements
- Provided coaching and guidance to the students for their career advancement and for making connections